université de BORDEAUX

Année Universitaire : 2022-2023

MEMOIRE D'HABILITATION A DIRIGER LES RECHERCHES

Ecole Doctorale des Sciences de la Vie et de la Santé

Spécialité : Sciences de la Vie et de la Santé

Discipline : Immunologie

Soutenue publiquement le 5 Juin 2023 par

Vanja SISIRAK

Chargé de Recherche de classe normale CNRS

UMR CNRS 5164 – Immunoconcept, Université de Bordeaux.

The role of dendritic cells and their ability to regulate endogenous DNA sensing in cancer immunity and autoimmunity

Devant le jury composé de :

Dr. Lucile Capuron	DR-INRAE (HDR), NeutriNeuro, Bordeaux, France	Présidente
Dr. Nadine Laguette	DR-CNRS (HDR), IGMM, Montpellier, France	Rapporteure
Pr. Alexandre Belot	PU-PH (HDR), CHU de Lyon, CIRI, Lyon, France	Rapporteur
Pr. Georg Gasteiger	PU (HDR), Université de Würzburg, Allemagne	Rapporteur
Dr. Nathalie Bendriss-Vermare	CR-INSERM (HDR), CRCL, Lyon, France	Examinatrice
Dr. Yenkel Grinberg-Bleyer	CR-INSERM (HDR), CRCL, Lyon, France	Examinateur
Pr. Patrick Blanco	PU-PH (HDR), CHU de Bordeaux, France	Membre Invité

"Every day is a gift, it's just, does it have to be a pair of socks?"

Tony Soprano, Sopranos, Season 6 - Episode 9

AKNOWLEDGEMENTS

To the member of the jury,

I would like to first thank Dr. Nadine Laguette, Pr. Alexandre Belot and Pr. Georg Gasteiger who kindly accepted to evaluate my work. I am certain that your comments and opinions are going to make progress my research projects.

Thank you as well to Dr. Nathalie Bendriss-Vermare, Pr. Patrick Blanco and Dr. Yenkel Grinberg-Bleyer for agreeing to take part in this jury. You have been by my side at different stages of my research career and your guidance has been instrumental in the making of the scientist who I have become.

I am really grateful to Dr. Lucile Capuron for accepting to preside this jury. Thank you very much for accepting this role as an “outsider” of the field of immunology. Your expertise in obesity has been key in the advancement of our project and I can’t wait for your insightful comments regarding this work.

To my mentors (in chronologic order),

Thanks again to Dr. Nathalie Bendriss-Vermare but also to Dr. Chistophe Caux who together supervised me during my PhD. You both desensitized me from my allergy to the various CD molecules and transferred to me your love and passion of the field of immunology. Working by your side has thought me scientific rigor, critical thinking and has greatly contributed to my will to continue to do academic research.

I am very grateful to Dr. Boris Reizis who gave me the opportunity to join his lab in New York. Thank you for your trust and for taking the risk to hire a person with no published work in his pocket. I have learned a lot by your side, particularly how to use mouse genetic models to answer fundamental questions in immunology. You also gave me a lot of freedom which has enormously helped me to gain confidence in my own ideas and experimental approaches to explore them. This confidence that you instilled in myself has paved the way for the development of my independent career.

Thank you Dr. Dechanet-Merville and Pr. Patrick Blanco who have kindly opened to me the gates of the Immunoconcept research department. You have provided fundamental support and critical advice to the establishment of my own research group. Thank you very much for your availability, for taking to time to address my doubt and questions as well as for sharing with the entire department your relentless motivation.

To my colleagues, collaborators and students (et al.),

Over the years I have worked with a lot of colleagues, collaborators, students and research assistants who have immensely contributed to my work, scientific fulfillment, scientific enlightenment, well-being, etc. There are way too many of them to cite them all without forgetting some. Therefore, I will just use the term *et al.* which is commonly used in science to thank them for their help, support, availability, insights, advice, critics and their unique personalities. Even though this term *et al.* is generic, without all the *et al*, there won't be any completed projects nor fun in doing research.

To the team members,

Thank you to all the current and past team members. All of you were instrumental in setting our laboratory in Bordeaux and are the main driving force in conducting our current and future projects. You create an environment that is lovely making it a real pleasure to come to work every day. Your team spirit, availability, honesty, scientific rigor and critical thinking, gives me a lot of confidence into future successes of our team.

To the family,

Thanks to my entire family ("belle où pas belle"). I am grateful to my parents who provided to me what Pierre Bourdieu calls the "*habitus*", which has allowed me to freely and comfortably pursue my path. Thanks to my two brothers for their encouragements, unconformity and their occasional disbelief in science that has motivated me a lot. Thanks to my dear wife Katie who decided to undertake with me this new journey in Bordeaux. Thank you for your daily support and your countless hours of reading and providing critical feedback to my proposals, papers and my HDR manuscript. Finally, thank you to Sid and Sana, our two little monsters, who brighten my days with their smiles, curiosity, enthusiasm and unlimited energy.

ABBREVIATION LIST

AAV : Adeno-associated virus
AIM-2 : Absent in Melanoma-2
ANR : agence nationale de la recherche
Ag : antigen
ALAT : alanine aminotransferase
ARC : association pour la recherche sur le cancer
AT : adipose tissue
BM : bone morrow
BDCA : blood dendritic cell antigen
CCR : C-C motif chemokine receptors
CCL : chemokine (C-C motif) ligand
cDC : conventional dendritic cell
cGAMP : 2′3′-Cyclic GMP-AMP
cGAS : cyclic GMP-AMP synthase
CFCD: club francophone des cellules dendritiques
cfDNA : cell-free DNA
CNRS : centre national de recherche scientifique
CRCL : cancer research center in Lyon
CRI : cancer research institute
CTACK : cutaneous T cell-attracting chemokine
CT : chemotherapy
CTL : cytotoxic T lymphocytes
CXCL10 : C-X-C motif chemokine ligand 10
DAMP : damage associated molecular pattern
DC : dendritic cell
DKO : double knock out
DNASE : deoxyribonuclease
DSS : dextran sodium sulfate
ER : estrogen receptor
FoxP3: forkhead box P3
FRM: fondation pour la recherche médicale
Flow-FISH : flow cytometry-based fluorescence in situ hybridization
gDNA : genomic DNA
GC : germinal center
Her 2: human epidermal growth factor receptor 2
HFD : high fat diet
HMGB1 : high mobility group box 1
HOCl : hypochlorous acid
H3cit : citrullinated histone H3
IBD : inflammatory bowel diseases
ICOS-L : inducible T cell costimulator ligand
IFN-I : type I interferons
IFNAR : interferon alpha receptor
Ig : immunoglobulin
IL : interleukin
ILT-7 : immunoglobulin-like transcript 7
INSERM : institut national de la santé et de la recherche
IRF : interferon regulatory factor
IR : insulin resistance
IP-10 : interferon gamma-induced protein 10
ISG : interferon stimulated genes
KO : knock out
MEC : mucosae-associated epithelial chemokine
Mip-3 : macrophage inflammatory protein-3
MPs : microparticles
MRI : magnetic resonance imaging
mtDNA : mitochondrial DNA
MyD88 : myeloid differentiation primary response 88
NAFLD : non-alcoholic fatty liver disease
ND : normal diet
NETs : neutrophil extracellular traps
NK : natural killer cell
Ova: ovalbumin
PBMC : peripheral blood mononuclear cell
pDC : plasmacytoid dendritic cell
PDL-1 : programed death ligand-1
PR : progesterone receptor
PRR : pathogen recognition receptors
PTPRS : protein tyrosine phosphatase s receptor
q-PCR : quantitative polymerase chain reaction
Rag1 : recombination activating gene 1
RT: radiotherapy
Runx2 : runt-related transcription factor 2
SLE : systemic lupus erythematosus
SLO : secondary lymphoid organs
SSc : systemic sclerosis
STING : stimulator of interferon genes
SVF : stromal vascular fraction
TApDC : tumor-associated pDCs
TGF-β : transforming growth factor-β
TKO : tripe knock out
TLR : toll like receptors
TLR7.1Tg : TLR7 transgenic mice
Treg : regulatory CD4 T cell
TREX1 : three prime repair exonuclease 1
TNF-α : tumor necrosis factor-α
T2D : type 2 diabetes
TRT : targeted radionuclide therapy
WASP : Wiskott-Aldrich syndrome protein
WAT: white adipose tissue
WT : wild type

TABLE OF CONTENTS

LIST OF FIGURES

I. CURRICULUM VITAE

Vanja Sisirak, Ph.D

ORCID: 0000-0003-3070-653

SCOPUS: 15119416000

Born: 15th of July 1982 in Mostar, Bosnia and Herzegovina

Nationality: French

Address: CNRS UMR 5164 - Immunoconcept, Université de Bordeaux, Bâtiment 1B, 146 rue Léo Saignat, 33076 Bordeaux, France.

☎ +33 5 57 57 92 75, 💻 vsisirak@immuconcept.org & vanja.sisirak@u-bordeaux.fr

Laboratory web site: https://immunoconcept.cnrs.fr/axes/dna-sensing/

1. EDUCATION

- 2006-2010: PhD in Immunology Université Claude Bernard, Lyon, France (Supervisors: Dr. Christophe Caux and Dr. Nathalie Bendriss-Vermare), Cancer Research Center of Lyon (CRCL)
  Title: Functional characterization of plasmacytoid dendritic cells in human breast tumors and identification of their migratory capacities during inflammation
- 2004-2006: M.Sc, Molecular and Cellular Biology, Ecole Normale Supérieure of Lyon, France
- 2003-2004: B.Sc, Molecular and Cellular Biology, Ecole Normale Supérieure of Lyon, France

2. CURRENT POSITION

- 2018-present: Chargé de Recherche de Classe Normale (CRCN, equivalent of a tenured associate professor), Centre National de la recherche Scientifique (CNRS), UMR CNRS 5164 – Immunoconcept, Université de Bordeaux, France
  Research project: Regulation of DNA sensing in cancer immunosurveillance, autoimmune syndromes and inflammatory disorders.

3. PREVIOUS POSITION

- 2017-2018: Junior Group Leader (IdEx junior chair - “recruitment of high-level young researchers”) UMR CNRS 5164 – Immunoconcept, Université de Bordeaux, France
  Research project: Regulation of DNA sensing in cancer immunosurveillance, autoimmune syndromes and inflammatory disorders.
- 2015-2017: Associate research scientist (Supervisor: Dr. Boris Reizis)
  Department of Medicine and Pathology, New York University, New York, USA

Research project: Study of tolerance break mechanisms to self-DNA in systemic lupus erythematosus (SLE)

- 2010-2015: Postdoctoral fellow (Supervisor: Dr. Boris Reizis)
  Department of Microbiology and Immunology, Columbia University, New York, USA
  Research project: Characterization of a novel monogenic model of SLE

4. TEACHING ACTIVITIES

- 2020-present: Tutoring for the Master 2 Cancer Biology, University of Bordeaux, France
  Supervision: Design of interdisciplinary research projects combing mathematical modeling and cancer immunology (10h/year)
- 2020-present: Tutoring for the Master Microbiology & Immunology, University of Bordeaux, France
  Supervision: Identification and description of novel therapeutic approaches harnessing the immune system to treat diseases (2h/year)
- 2019-present: Lecturer for the École Santé-Science, University of Bordeaux, France
  Lecture: DNA sensing in Systemic Lupus Erythematosus (4h/year)
- 2018-present: Lecturer for the Master 1 Cancer Biology, University of Bordeaux, France
  Lecture: Immunogenic and tolerogenic cancer cell death (4h/year)
- 2018-present: Lecturer for the Master 2 Cell Biology, University of Bordeaux, France
  Lecture: Harnessing the immune system to treat cancer (4h/year)
- 2015-2016: Lecturer for Medical Degree students, New York University, USA.
  Lecture: Immunological mechanisms of hypersensitivity (4h/year)
- 2008-2009: Lecturer for Medical Degree students, Cours Galien, Lyon, France.
  Lecture: Basics in Cellular biology (24h/year)
- 2007-2008: Lecturer for the Professional Master program of the Faculté Catholique, Lyon, France
  Lecture: Initiation to tumor immunology (20h/year)

5. SUPERVISION ACTIVITY

- 01/2023-present: Master 2 Student, Anissa El Mammeri, University of Bordeaux, France.
- 01/2021-present: PhD Student, Anaïs Roubertie, University of Bordeaux, France.
- 05/2020-present: Associate Professor, Dorothée Duluc, University of Bordeaux, France.
- 05/2020-present: Permanent Research Engineer, Séverine Loizon, CNRS, France.
- 01/2019-present: Pauline Santa, PhD student, University of Bordeaux, France.
- 11/2018-12/2022: MD-PhD student, Amandine Ferriere, University of Bordeaux, France.
- 12/2022-10/2023: Master 2 Student, Maxime Dubois. University of Bordeaux, France
- 2018-2021: Dr. Anne Garreau, postdoctoral research scientist, University of de Bordeaux, France.
  Currently project manager in a private company, France
- 2010-2017: I supervised 6 graduate students and 2 Master students as a Postdoc.

Currently they are all pursuing scientific careers, with 3 of them in industry and 5 of them in academic research (3 PhD Students, 1 Postdoc, 1 Independent group leader)

6. FELLOWSHIPS AND AWARDS

- 2015: Scholarship, Keystone symposia (Autoimmunity &Tolerance), Keystone, USA.
- 2013: Award for postdoctoral research, Phillippe Foundation, New York, USA.
- 2012: Postdoctoral fellowship (3 years), Cancer Research institute (CRI), New York, USA
- 2011: Postdoctoral fellowship (1 year), Fondation pour la Recherche Médicale (FRM), France
- 2010: Doctoral fellowship (1 year), Association pour la Recherche sur le Cancer (ARC), France
- 2009: Scholarship, Keystone symposia (Biology of Dendritic Cells), Banff, Canada.
- 2008: Best communication, European Association for Cancer Research symposium, Lyon, France
- 2007: Best communication, French Dendritic Cell Society (CFCD)symposium, Paris, France
- 2006: Doctoral fellowship (3 years), Région Rhône-Alpes, France

7. ORGANIZATION OF SCIENTIFIC MEETINGS

- 12/2023: Co-organizer of the French Dendritic Cell Society (CFCD), biennial international symposium "Development, metabolism and function of dendritic cells and macrophages in health and disease", University of Bordeaux, France
  Role: speaker invitation, abstract selection, fundraising, communication and session chair.
- 01/2023: Co-organizer of the Bordeaux "Oncosphere" international meeting.
  Role: speaker invitation and session chair. (250 participants)
- 03/2022: Co-organizer of a Franco-Indian online workshop on "Obesity mediated inflammation"
  Role: speaker invitation, communication and session chair. (80 participants)
- 12/2021: Co-organizer of the French Dendritic Cell Society (CFCD), biennial international symposium "DC-phering mononuclear phagocyte biology in health and disease", Institut Necker enfants maladies, Paris, France
  Role: speaker invitation, abstract selection, communication and session chair. (120 participants)
- 09/2019: Co-Organizer of the joint meeting between the French Dendritic Cell Society (CFCD) and European Macrophage and Dendritic cell Society (EMDS) on "The mononuclear phagocyte system in development, immunity and cancer", World Trade Center, Marseille, France.
  Role: speaker invitation, abstract selection, and session chair. (410 participants)

8. INSTITUTIONAL RESPONSIBILITIES

- Since 2022: Elected researcher representative**,** Council of the Research unit CNRS UMR 5164 – Immunoconcept, University of Bordeaux, France.

Role: Discussion on the departmental life quality and future scientific directions.

- Since 2022: Jury Member, Master Microbiology and Immunology, University of Bordeaux, France
  Role: Master 2 reports and oral presentations evaluation.
- Since 2019: Jury Member, Ecole Doctorale SVS, University of Bordeaux, France
  Role: selection of PhD students to receive French Ministry funding for their research projects.
- Since 2019: Ethical committee member, University of Bordeaux, France
  Role: Evaluation of experimental animal protocols (10 protocols annually)
- Since 2020: Member, Sustainable development group, University of Bordeaux, France
  Role: Development of strategies to reduce laboratory waste and carbon footprint.
- Since 2020**:** Resource person, Sustainable development, CNRS UMR 5164 – Immunoconcept
  Role: Awareness of department members to strategies to reduce laboratory waste and carbon footprint.

9. REVIEWING ACTIVITIES

- Since 2020: Guest Editor, Methods in Molecular Biology on « Dendritic cells protocols »
  Role: Coordination of a book of 23 chapters, author invitation, reviewing and editing. The book was published in March 2023.
- Since 2019: Review Editor**,** Frontiers Immunology (Antigen presenting cells, Mechanisms of Lupus, Inflammation, Translational immunology)
- Since 2018: Reviewer for Journal of Immunology Research, Cellular Immunology, Annals of Rheumatic Diseases, Apoptosis, Biomaterials and Frontiers in Immunology
- Since 2018: Grant evaluation for the French Society of Dermatology, IdEx program of Strasbourg University, Arthritis Fondation Courtin and the Canceropôle Nord-Ouest
- Committee (Jury) member

2023: Assistant Professor Recruitment, Université de Strasbourg, France
2022: Assistant Professor Recruitment, Université de Strasbourg, France
2022: HDR-Tenure Defense, Dr. J. Visentin, Université de Bordeaux, France
2021: HDR-Tenure Defense, Dr. Y Grinberg-Bleyer, Cancer Research Center of Lyon, France
2023: PhD Defense, Candice Sakref, Cancer Research Center of Lyon, France
2022: PhD Defense, Miquel Charles-Henry, Toulouse INFINITY, France
2019: PhD Defense, Abdenour Abbas. Centre d'Immunologie Marseille-Luminy, France
2018: PhD Defense, Margaux Hubert, Cancer Research Center of Lyon, France

10. MEMBERSHIP TO SCIENTIFIC SOCIETIES

- 2019-present: Member of the Société Française d'Immunologie (SFI)
- 2018-present: Board member of Club Francophone des Cellules Dendritiques (CFCD)

11. MAJOR COLLABORATIONS

- **International** Dr. Boris Reizis, New York University School of Medicine, New York USA
  Functional characterization of DNASEs in systemic lupus erythematous (SLE)
  Dr. Dipyaman Ganguly, CSIR-Indian Institute of Chemical Biology, Kolkata, India
  Role of DNASEs in the regulation of obesity mediated metaflammation
  Dr. David Santamaria, Centro de Investigación del Cáncer, Salamanca, Spain
  Impact of ageing on lung cancer immunosurveillance

- **National** Pr. Blanco Patrick, UMR CNRS 5164 - Immunoconcept, Univeristy of Bordeaux
  Study of platelets-derived microparticles & B cell inhibitory peptide in SLE pathogenesis
  Dr. J.P Pouget, Institut de Recherche en Cancerologie, Montpelier, France
  Impact of DNASEs on targeted and conventional radiotherapy efficacy in cancer
  Dr. Lucille Capuron, NeutriNeuro - INRA, University of Bordeaux, France
  Role of DNASEs in the regulation of obesity mediated metaflammation
  Dr. Daniela Cota, NeuroCentre Magendie, University of Bordeaux, France
  Role of DNASEs in the regulation of obesity mediated metaflammation

12. INVITED PRESENTATIONS

- 2023: 8th International Conference on Molecular Signaling and 4th CeSin Symposium: Signaling in Disease Management and Diagnostics (ICMSCS-SDMD-2023), Kolkata, India
  Title: Role of extracellular DNASE1L3 in the control of chemotherapy induced anti-tumor immunity.
- 2023: IICB-Translational Research Unit of Excellence (IICB-TRUE), CSIR-Indian Institute of Chemical Biology, Kolkata, India
  Title: DNASE1L3 function in the regulation of autoimmunity and metaflammation.
- 2023: Oncosphere international meeting, University of Bordeaux, France
  Title: Role of extracellular DNASE1L3 in the control of chemotherapy induced anti-tumor immunity.
- 2021: French Dendritic Cell Society (CFCD), international symposium, Paris, France
  Title: Plasmacytoid dendritic cells promote DNA autoreactivity
- 2021: Annual Symposium of the ITMO I3M, Marseille, France
- 2021: Infectious Diseases Research Federation (Feri) Scientific Days, Tours, France
  Title: Cellular and molecular mechanisms of anti-DNA autoreactivity
- 2020: Third Philosophy of Cancer Biology Workshop (PhilInBioMed), Bordeaux, France
  Title: Regulation of tumor DNA potential to activate anti-tumor immunity by DNASEs
- 2020: Centre de Recherche en Transplantation en Immunologie (CRTI), Nantes, France
- 2020: Centre International de Recherche en Infectiologie (CIRI), Lyon, France
  Title: Cellular and molecular mechanisms of self-DNA autoreactivity

- 2019: Bordeaux Cell Biology Gathering (BCBG), Bordeaux, France
- 2018: EULAR course on immunology, Lisbon, Portugal
- 2018: Centre de Physiopathologie Toulouse-Purpan (CPTP), Toulouse, France
  Title: Cellular and molecular immunological mechanisms contributing to SLE pathogenesis.
- 2016: Bristol-Myers Squibb, Lawrence Township, New Jersey, USA
  Title: Dendritic cell functions in cancer and autoimmune syndromes.
- 2016: Centre d'Immunologie Marseille-Luminy (CIML), France
- 2016: Cancer Research Center of Lyon (CRCL), Lyon, France
  Title: Function and regulation of tumor DNA in the establishment of anti-tumor immunity.

13. SELECTED PRESENTATIONS

- 2019: Annual meeting of the Cancéropôle Grand Sud-Ouest, Arcachon, France
  Title: Regulation of tumor DNA potential to activate anti-tumor immunity by DNASE1L
- 2017: Annual meeting of the French Society of Immunology (SFI), Reims, France
  Title: *Cellular and molecular mechanisms involved in SLE pathogenesis induced by Dnase1L3 deficiency.*
- 2009: Keystone symposium on dendritic cells, Banff, Canada
- 2008: European Association for Cancer Research (EACR) symposium, Lyon, France
- 2007: Annual meeting of the French Society of Immunology (SFI), Lyon, France
  Title: Breast tumor microenvironment alters plasmacytoid dendritic cell (pDCs) functions.
- 2007: French Dendritic Cell Society (CFCD) international symposium, Paris, France
  Title: CCR6 and CCR10 orchestrate pDCs recruitment during pathogen invasion.
- 2006: French Dendritic Cell Society (CFCD) international symposium, Paris, France
  Title: Humanized mouse model to study breast tumor impact on pDCs functions.

14. FUNDING

- **International**

2021-2023: Indo-French Centre for Promotion of Advanced Research (IFCPAR), India and France, (Co-PI with Dr. Dipyaman Ganaguly) 200k€
Title: Exploring the role of Dnase1L3 in the development of obesity associated metabolic syndrome.
2018-2021: CLIP Program, Cancer Research Institute (CRI), New York, USA, (PI), 163k€
Title: In vivo study of mechanisms that regulate tumor DNA immunogenicity during cancer immunosurveillance.

- **National**

2023-2027: Institut National du Cancer (InCa PLBio) (Co-PI with Dr. Jean-Pierre Pouget) 576K€
Title: Functions of extracellular DNASEs in the regulation of anti-tumor immunity.

2021-2024: Agence Nationale de la Recherche, (ANR JCJC), (PI) 326k€

Title: DNASE1L3 role in obesity-mediated inflammation and metabolic syndrome (DOMINO).

- **Local**

2019-2021: Cancéropôle Grand Sud-Ouest (GSO), France, (PI) 20k€

Title: Study of the role of gut-derived T cells in cancer immunosurveillance.

2017-2021: IdEx Junior Chair award, Bordeaux University, France, (PI), 300K€

Title: Study of Dnase1L3 as a novel regulator of tumor-derived microparticles processing and immunogenicity

- **Foundations**

2022-2024: Association des Sclérodermique de France (ASF), France (PI) 25K€

Title: Study of the role of type I interferon in systemic sclerosis.

2019-2021: Fondation Bordeaux Université, France, (PI) 20k€

Title: Exploring the role of DNASE1L3 in the development of obesity associated metabolic syndromes.

2019-2021: Fondation Bristol-Myers Squibb, France, (PI), 50k€

Title: Impact of extracellular DNASEs deficiency on the efficacy of immune checkpoint inhibitors.

2017-2021: Fondation pour la Recherche Médicale (FRM), Labéllisation, (Partner) Collaborative project with Pr. Patrick Blanco as PI, 393k€ / 4 years

Title: Microparticle functions in systemic autoimmune diseases syndromes

15. OUTREACH AND MEDIA COVERAGE

- 2021-2023: Participation to seminar “Introduction to trades to industry” at the University of Bordeaux in order to sensitize Cancer Biology graduate students to professional paths in academia and industry.
- 2020: “SIRIC BRIO Bright Days” Panelist on the theme of neo-adjuvant therapies and immunotherapies for cancer patients, Palais de la Bourse, Bordeaux, France.
- 2018: “Round Table” Panelist on theme cancer immunotherapy at the 3rd anniversary of the Fondation Bristol-Myers Squibb, at the Maison de la recherche, Paris, France.
- 2018: “Soirée grand public” Panelist on the theme “Cancer: is the response within us”, Station Ausone Bordeaux, France.
- 2017: Scientist the human, podcast on postdoctoral work on DNASE1L3 on lupus pathogenesis

16. PUBLICATION LIST

a. *Peer reviewed research articles*

1. *Elevated levels of circulatory follicular T helper cells in chronic lymphocytic leukemia contribute to B cell expansion*
   Le Saos--Patrinos C, Loizon S, Zouine A, Turpin D, Dilhuydy M.S, Blanco P, Sisirak V, Forcade E, and Duluc D. ***Journal of Leukocyte Biology***. 2023 Mar 1;113(3):305-314

2. *Selectins impair regulatory T cell function and contribute to systemic lupus erythematosus pathogenesis*
   Scherlinger M, Guillotin V, Douchet I, Vacher P, Boizard A, Guegan J.P, Garreau A, Merillon N, Vermorel A, Ribeiro E, Machelart I, Lazaro E, Couzi L, Duffau P, Barnetche T, Pellegrin J.L, Viallard J.F, Saleh M, Schaeverbeke T, Truchetet M.E, Contin-Bordes C, Legembre P, **Sisirak V**, Richez C* and Blanco P*. ***Sci Transl Med***. 2021 Jun 30;13(600):eabi4994 (*co-corresponding authors)

3. *Autoantibody-mediated impairment of DNASE1L3 activity in sporadic systemic lupus erythematosus* Hartl J, Serpas L, Wang Y, Rashidfarrokhi A, Perez OA, Sally B, **Sisirak V**, Soni C, Khodadadi-Jamayran A, Tsirigos A, Caiello I, Bracaglia C, Volpi S, Ghiggeri GM, Chida AS, Sanz I, Kim MY, Belmont HM, Silverman GJ, Clancy RM, Izmirly PM, Buyon JP, Reizis B, ***J Exp Med***. 2021 May 3;218(5):e20201138.

4. *Elevated Circulatory Levels of Microparticles Are Associated to Lung Fibrosis and Vasculopathy During Systemic Sclerosis*
   Leleu D, Levionnois E, Laurent P, Lazaro E, Richez C, Duffau P, Blanco P, **Sisirak V**, Contin-Bordes C, Truchetet M-E, ***Front Immunol***. 2020 Oct 23;11:532177

5. *Plasma DNA Profile Associated with DNASE1L3 Gene Mutations: Clinical Observations, Relationships to Nuclease Substrate Preference, and In Vivo Correction*
   Chan RWY, Serpas L, Ni M, Volpi S, Hiraki LT, Tam LS, Rashidfarrokhi A, Wong PCH, Tam LHP, Wang Y, Jiang P, Cheng ASH, Peng W, Han DSC, Tse PPP, Lau PK, Lee WS, Magnasco A, Buti E, **Sisirak V**, AlMutairi N, Chan KCA, Chiu RWK, Reizis B, Lo YMD, ***Am J Hum Genet***. 2020 Nov 5;107(5):882-894.

6. *Plasmacytoid dendritic cells promote extrafollicular anti-DNA responses in lupus through type I interferon*

Soni C, Perez O.A, Woss W.A, Serpas L, Mehl J, Goike J, Georgiou G, Ippolito G.C, **Sisirak V*** and Reizis B*, ***Immunity***. 2020 May 19:S1074-7613(20)30173-4. (*co-corresponding authors).

7. *Dnase1l3 deletion causes aberrations in length and end-motif frequencies in plasma DNA*
   Serpas L, Chan RWY, Jiang P, Ni M, Sun K, Rashidfarrokhi A, Soni C, **Sisirak V**, Lee WS, Cheng SH, Peng W, Chan KCA, Chiu RWK, Reizis B, Lo YMD, ***Proc Natl Acad Sci USA***. 2019 Jan 8;116(2):641-649.

8. *Plasmacytoid dendritic cells are largely dispensable for the pathogenesis of experimental inflammatory bowel disease*
   Sawai CM, Serpas L, Neto AG, Jang G, Rashidfarrokhi A, Kolbeck R, Sanjuan MA, Reizis B* and **Sisirak V***, ***Front Immunol***. 2018 Oct 25;9:2475. (*co-corresponding authors)

9. *Digestion of Chromatin in Apoptotic Cell Microparticles Prevents Autoimmunity*
   Sisirak V*, Sally B*, D'Agati V, Martinez-Ortiz W, Özçakar ZB, David J, Rashidfarrokhi A, Yeste A, Panea C, Chida AS, Bogunovic M, Ivanov II, Quintana FJ, Sanz I, Elkon KB, Tekin M, Yalçınkaya F, Cardozo TJ, Clancy RM, Buyon JP, Reizis B, ***Cell***. 2016 Jun 30;166(1):88-101. (*co-first authors)
   Highlights: Onuora, S. DNASE1L3 prevents anti-DNA responses. Nat Rev Rheumatol 12, 437, 2016

10. *A novel regulation of PD-1 ligands on mesenchymal stromal cells through MMP-mediated proteolytic cleavage*
    Dezutter-Dambuyant C, Durand I, Alberti L, Bendriss-Vermare N, Valladeau-Guilemond J, Duc A, Magron A, Morel AP, **Sisirak V**, Rodriguez C, Cox D, Olive D, Caux C, ***Oncoimmunology***. 2015 Oct 29;5(3):e1091146.

11. *Plasmacytoid dendritic cells are dispensable for noninfectious intestinal IgA responses in vivo*
    Moro-Sibilot L, This S, Blanc P, Sanlaville A, **Sisirak V**, Bardel E, Boschetti G, Bendriss-Vermare N, Defrance T, Dubois B, Kaiserlian D, ***Eur J Immunol***. 2016 Feb;46(2):354-9.

12. *Protein Tyrosine Phosphatase PTPRS Is an Inhibitory Receptor on Human and Murine Plasmacytoid Dendritic Cells*
    Bunin A, **Sisirak V**, Ghosh HS, Grajkowska LT, Hou ZE, Miron M, Yang C, Ceribelli M, Uetani N, Chaperot L, Plumas J, Hendriks W, Tremblay ML, Häcker H, Staudt LM, Green PH, Bhagat G, Reizis B, ***Immunity***. 2015 Aug 18;43(2):277-88.

13. *Genetic evidence for the role of plasmacytoid dendritic cells in systemic lupus erythematosus*

Sisirak V*, Ganguly D*, Lewis KL, Couillault C, Tanaka L, Bolland S, D'Agati V, Elkon KB, Reizis B. ***J Exp Med***. 2014 Sep 22;211(10):1969-76. (*co-first author)

Highlights: Onuora, S. Depleting plasmacytoid dendritic cells: a new therapeutic approach in SLE? Nat Rev Rheumatol 10, 573, 2014

14. *Transcription factor Runx2 controls the development and migration of plasmacytoid dendritic cells*
    Sawai CM, **Sisirak V**, Ghosh HS, Hou EZ, Ceribelli M, Staudt LM, Reizis B, ***J Exp Med***. 2013 Oct 21;210(11):2151-9.

15. *Tumor promotion by intratumoral plasmacytoid dendritic cells is reversed by TLR7L treatment*
    Le Mercier I, Poujol D, Sanlaville A, **Sisirak V**, Gobert M, Durand I, Dubois B, Treilleux I, Marvel J, Vlach J, Blay JY, Bendriss Vermare N, Caux C, Puisieux I, Goutagny N, ***Cancer Res***. 2013 Aug 1;73(15):4629-40.

16. *Breast cancer-derived transforming growth factor-β and tumor necrosis factor-α compromise interferon-α production by tumor-associated plasmacytoid dendritic cells*
    Sisirak V, Vey N, Goutagny N, Renaudineau S, Malfroy M, Thys S, Treilleux I, Labidi-Galy SI, Bachelot T, Dezutter-Dambuyant C, Ménétrier-Caux C, Blay JY, Caux C, Bendriss-Vermare N, ***Int J Cancer***. 2013 Aug 1;133(3):771-8.

17. *Impaired IFN-α production by plasmacytoid dendritic cells favors regulatory T-cell expansion that may contribute to breast cancer progression*
    Sisirak V*, Faget J*, Gobert M, Goutagny N, Vey N, Treilleux I, Renaudineau S, Poyet G, Labidi-Galy SI, Goddard-Leon S, Durand I, Le Mercier I, Bajard A, Bachelot T, Puisieux A, Puisieux I, Blay JY, Ménétrier-Caux C, Caux C, Bendriss-Vermare N, ***Cancer Res***. 2012 Oct 15;72(20):5188-97. (*co-first authors)

18. *Gene expression profiling identifies sST2 as an effector of ErbB2-driven breast carcinoma cell motility, associated with metastasis*
    Gillibert-Duplantier J, Duthey B, **Sisirak V**, Salaün D, Gargi T, Trédan O, Finetti P, Bertucci F, Birnbaum D, Bendriss-Vermare N, Badache A, ***Oncogene***. 2012 Jul 26;31(30):3516-24.

19. *CCR6/CCR10-mediated plasmacytoid dendritic cell recruitment to inflamed epithelia after instruction in lymphoid tissues*
    Sisirak V, Vey N, Vanbervliet B, Duhen T, Puisieux I, Homey B, Bowman EP, Trinchieri G, Dubois B, Kaiserlian D, Lira SA, Puisieux A, Blay JY, Caux C, Bendriss-Vermare N, ***Blood***. 2011 Nov 10;118(19):5130-40.

20. *Quantitative and functional alterations of plasmacytoid dendritic cells contribute to immune tolerance in ovarian cancer*
    Labidi-Galy SI, **Sisirak V**, Meeus P, Gobert M, Treilleux I, Bajard A, Combes JD, Faget J, Mithieux F, Cassignol A, Tredan O, Durand I, Ménétrier-Caux C, Caux C, Blay JY, Ray-Coquard I, Bendriss-Vermare N, ***Cancer Res***. 2011 Aug 15;71(16):5423-34.

21. *Human Langerhans cells express a specific TLR profile and differentially respond to viruses and Gram-positive bacteria*
    Flacher V, Bouschbacher M, Verronèse E, Massacrier C, **Sisirak V**, Berthier-Vergnes O, de Saint-Vis B, Caux C, Dezutter-Dambuyant C, Lebecque S, Valladeau J, ***J Immunol***. 2006 Dec 1;177(11):7959-67.

b. Peer reviewed review articles

1. *The role of nucleases and nucleic acid editing enzymes in the regulation of self-nucleic acid sensing* Santa P, Garreau A, Serpas L, Ferriere A, Blanco P, Soni C* and **Sisirak V***, ***Front Immunol***. 2021 Fev 26, 12:629922. (*co-corresponding authors)

2. *Self-nucleic acid sensing: a novel crucial pathway involved in obesity-mediated metaflammation and metabolic syndrome*
   Ferriere A, Santa P, Garreau A, Bandopadhyay P, Blanco P, Ganguly D and **Sisirak V**, ***Front Immunol***. 2021 Jan 26;11:624256.

3. *HIV protease inhibitors and autoimmunity: an odd, but promising idea.*
   Galli G, Poissonnier A, Guégan J.P, Charrier M, **Sisirak V**, Lazaro E, Truchetet M.E, Richez C, Legembre P, Blanco P. ***Autoimmun Rev***. 2019 Oct;18(10):102370.

4. *Innate Immunity in Systemic Sclerosis Fibrosis: Recent Advances*
   Laurent P*, **Sisirak V***, Lazaro E, Richez C, Duffau P, Blanco P, Truchetet ME, Contin-Bordes C, ***Front Immunol***. 2018 Jul 23;9:1702. (*co-first authors)

5. *Systemic lupus erythematosus and systemic sclerosis: All roads lead to platelets*
   Scherlinger M, Guillotin V, Truchetet ME, Contin-Bordes C, **Sisirak V**, Duffau P, Lazaro E, Richez C, Blanco P, ***Autoimmun Rev***. 2018 Jun;17(6):625-635.

6. *New Insights on Platelets and Platelet-Derived Microparticles in Systemic Lupus Erythematosus*

Scherlinger M, **Sisirak V**, Richez C, Lazaro E, Duffau P, Blanco P, ***Curr Rheumatol Rep***. 2017 Aug;19(8):48.

7. *The role of dendritic cells in autoimmunity*
   Ganguly D, Haak S, **Sisirak V**, Reizis B, ***Nat Rev Immunol***. 2013 Aug;13(8):566-77.

8. *Plasmacytoid dendritic cells: recent progress and open questions*
   Reizis B, Bunin A, Ghosh HS, Lewis KL, **Sisirak V**, ***Annu Rev Immunol***. 2011;29:163-83. Review.

c. Invited comments

1. *ICOS is associated with poor prognosis in breast cancer as it promotes the amplification of immunosuppressive CD4+ T cells by plasmacytoid dendritic cells*
   Faget J, **Sisirak V**, Blay JY, Caux C, Bendriss-Vermare N, Ménétrier-Caux C, ***Oncoimmunology***. 2013 Mar 1;2(3):e23185

2. *Plasmacytoid dendritic cells deficient in IFN-alpha production promote the amplification of FOXP3+ regulatory T cells and are associated with poor prognosis in breast cancer patients*
   Sisirak V, Faget J, Vey N, Blay JY, Ménétrier-Caux C, Caux C, Bendriss-Vermare N, ***Oncoimmunology***. 2013 Jan 1;2(1):e22338.

d. Book chapters

1. *Origin, phenotype and function of mouse dendritic cell subsets*
   Duluc D* and **Sisirak V***, ***Methods in Molecular Biology***, Dendritic Cell Methods and Protocols, 2023;2618:3-16, (*co-corresponding authors)

2. *Enrichment of large numbers of splenic mouse dendritic cells after injection of Flt3L-producing tumor cells*
   Santa P, Garreau A, Ferriere A, Roubertie A, Loizon S, Duluc D* and **Sisirak V***, ***Methods in Molecular Biology***, Dendritic Cell Methods and Protocols, 2023;2618:173-186 (*co-corresponding authors)

17. RESEARCH SUMMARY

As a PhD student, I joined Dr. Caux's and Dr. Bendriss-Vermare's laboratory at the Cancer Research Center of Lyon, France in 2006 to work on cancer immunology. I was awarded competitive funding from the French government and a cancer research foundation (ARC). I identified a novel deleterious

function of plasmacytoid dendritic cells (pDCs) in breast cancer patients leading to tumor tolerance, particularly through the ability to promote regulatory T cell functions. This work resulted in 3 first author publications (Cancer Research, Blood and International Journal of Cancer) and provided me with a strong foundation in cancer immunology.

After my PhD, which was focused on human immunology, I wanted to master mouse genetic models to explore dendritic cell (DC) functions *in vivo*. Therefore, in 2010 I joined the laboratory of Dr. Reizis (Columbia University, USA), who is a world leader in the establishment of innovative murine models to study the biology of DCs. I led and contributed to multiple projects characterizing the development of DCs and their role in autoimmune and inflammatory diseases (Sisirak et al. Journal of Experimental Medicine, 2014; Sawai, Sisirak et al, Journal of Experimental Medicine; 2013, Bunin, Sisirak et al. Immunity, 2016). In addition, I developed a novel and independent research project, for which I obtained a prestigious fellowship from the Cancer Research Institute (CRI) that led to the characterization of DNASE1L3 as a key enzyme that enforces tolerance to endogenous DNA released by apoptotic cells and consequently prevents the development of autoimmunity (Sisirak et al, Cell, 2016). Thus, during my postdoc, I gained a unique expertise in DNASE biology. I also supervised numerous graduate students who contributed to the publication and overall success of my work.

Awarded the Junior Chair position from the selective IdEx program of Bordeaux University meant to "recruit high-level young researchers", I started my group in 2017 in the Immunoconcept research department (UMR CNRS 5164). In 2018 I was tenured by the CNRS and secured competitive funding, which has enabled me to initiate my independent projects and build my research team. As an independent scientist, I established and analyzed multiple novel mouse models that were critical in the identification of the cellular and molecular mechanisms involved in the autoimmunity driven by *Dnase1l3* deficiency (Soni et al, Immunity, 2020, co-corresponding author). I also supervised a project developed in a partnership with industry (MedImmune) in order to evaluate the therapeutic potential of pDC targeting in experimental models of inflammatory bowel disease (Sawai et al, Frontiers in Immunology, 2019, co-corresponding author). In addition, I collaborated with Pr. Blanco (University of Bordeaux) by providing the "proof-of-concept" that P-selectin blockade ameliorates lupus pathogenesis in *Dnase1l3*-deficient mice (Scherlinger et al, Science Translational Medicine, 2021). These early career achievements attest to my capacity to lead and supervise independent projects.

My group is currently exploring the function of DNASE1L3 beyond its role in autoimmunity. Two PhD students (A. Ferriere and A. Roubertie) who I directly supervise, have identified a key role for DNASE1L3 in limiting obesity-induced metabolic tissue inflammation. Collaboration with Dr. Ganguly

(India) and Dr. Capuron (France) has enabled us to address the relevance of our findings in obese individuals, and this work is currently being finalized for publication. Building on my dual expertise in cancer immunology and DNASE biology, I also initiated with a postdoctoral fellow (Dr. A. Garreau) and another PhD student (P. Santa) a project to study the function of DNASE1L3 in the regulation of anti-tumor immunity. Our results indicate that DNASE1L3 is required for the therapeutic efficacy of cytotoxic treatments inducing an immunogenic tumor cell death. These counterintuitive results suggest that DNASE1L3 likely promotes the immunogenic potential of tumor DNA to activate anti-tumor immunity. The main hypothesis is that DNASEs do not simply mediate the “waste management” of apoptotic DNA, but rather are crucial enzymes that regulate tolerance versus reactivity to endogenous DNA depending on the modality of cell death, which is likely different at the steady state and in pathological contexts such as cancer.

II. FOREWORD

My interest in science lies in the study of the immune system. One important function of the immune system is to protect organisms against microbial threats such as bacteria and viruses. It also plays an essential role in controlling and preventing the development of cancers. The function of the immune system is mediated by white blood cells. My main focus was centered on dendritic cells (DCs), which are subset of white blood cells bridging innate and adaptive immune responses. DCs are considered as immune sentinels through their ability to sense pathogens and nascent tumor cells and consequently instruct adaptive immune responses against such threats. They are classically subdivided in two main subsets, including conventional DCs (cDCs) and plasmacytoid DCs (pDCs). cDCs capture and present microbial and tumor antigens to both CD4 and CD8 T cells to activate specific adaptive immune responses, whereas pDCs are specialized in the production of type I Interferons (IFN-I), cytokines that are essential for the activation of anti-viral immune responses, upon virus encounter. The function of the immune system must be tightly regulated. In healthy individuals, DCs are also crucial in maintaining the balance of immune function, both promoting immune responses during pathogen infection or cancer development and preventing the immune system from turning against our body's own (self) molecules. Any deregulation in this balance initiates the development of pathology. Indeed, an aberrant activation of the immune system causes autoimmune syndromes while poor immune function favors tumor development and susceptibility to microbial infection. During my career, I worked on both aspects of such unbalanced systems to understand the immunological mechanisms that contribute to the development of cancer and autoimmune syndromes. This dual expertise paved the way for my current research projects which aim at studying the mechanisms that are involved in the activation of aberrant immune responses and autoimmunity in the contexts of cancer immunosurveillance and aberrant inflammation induced by obesity.

III. PREVIOUS SCIENTIFIC ACHIEVEMENTS

1. DOCTORAL WORK (2006-2010)

I joined Dr. Caux's laboratory (UMR INSERM 1052 CNRS 5286) at the Cancer Research Center in Lyon (CRCL) in 2006 as a graduate student, and I worked under the supervision of Dr. Bendriss-Vermare**.** For the completion of my PhD I was awarded two competitive grants, one from the Région Rhône Alpes (Allocation Doctorale de Recherche) and one from the Association pour la Recherche sur le Cancer (ARC). During the 3.5 years of my graduate studies I was interested in understanding the function of pDCs in the immunosurveillance of human tumors and their migratory properties in

inflammatory settings. pDCs are DC subset specialized in the sensing of viruses through the recognition of their nucleic acids by pathogen recognition receptors (PRR) such as Toll like receptors (TLR)-7 and 9 *(Reizis, 2019)*. In response to such stimuli, interferon regulatory factor (IRF)-7, a master regulator of IFN-I genes, is activated, subsequently translocated to the nucleus where it induces the expression and ultimately the production of massive amounts of IFN-I by pDCs *(Reizis, 2019)*. IFN-I is an essential cytokine for the induction of anti-viral immunity and was also shown to be required for the initiation of antitumor immune responses *(Zitvogel et al., 2015)*. Indeed, IFN-I can activate the expression of numerous genes involved in antiviral defenses (interferon stimulated genes (ISG)) and a variety of immune cells such as cytotoxic T lymphocytes (CTLs) which can subsequently acquire the capacity to kill infected and/or transformed cells *(Zitvogel et al., 2015)*.

a. *pDC migration into inflamed epithelia is controlled by CCR6 and CCR10*

CCR6/CCR10-mediated plasmacytoid dendritic cells recruitment to inflamed epithelia after instruction in lymphoid tissues
Sisirak V, Vey N, Vanbervliet B, Duhen T, Puisieux I, Homey B, Bowman EP, Trinchieri G, Dubois B, Kaiserlian D, Lira SA, Puisieux A, Blay JY, Caux C, Bendriss-Vermare N, **Blood,** 2011 Nov 10;118(19):5130-40.

The development of pDCs takes place in the bone morrow (BM). Unlike cDCs which exit the BM at a precursor state and terminate their specification in tissues, pDCs fully differentiate from hematopoietic stem cells in the BM *(Reizis, 2019)*. The developmental path and origin of pDCs is still unclear and remains actively debated. Indeed, pDCs were described to share common ancestry with cDCs and thus to develop from common DC progenitors, which themselves derive from common myeloid progenitors (CMP) *(Feng et al., 2022; Reizis, 2019)*. However, this common developmental path between cDCs and pDCs was recently challenged by observations indicating that pDCs originate from common lymphoid progenitors (CLP) which do not give rise to cDCs *(Dress et al., 2019; Rodrigues et al., 2018)*. As these findings indicate a distinct developmental path of pDCs from cDC, the authors suggested to consider pDCs as innate lymphoid cells specialized in IFN-I production *(Dress et al., 2019)*. Therefore, the development of pDCs requires further studies to delineate their lymphoid *versus* myeloid origins and to assess whether heterogeneity may exist within this DC subset. Upon their development in the BM, mature pDCs are redistributed through the circulation into secondary lymphoid organs (SLO) where they typically comprise 0.1% to 0.5% of total nucleated cells *(Reizis, 2019)*. Unlike cDCs they have a round morphology closely resembling secretory plasmocytes, express low-level of major histocompatibility complex (MHC)-II molecules and are poorly represented in peripheral epithelial tissues at steady state. As a consequence of viral infections or sterile inflammation (*e.g.* psoriasis) pDCs accumulate in the affected epithelial tissues where they seem to contribute to local inflammation through their production of IFN-I *(Kohrgruber et al., 2004; Nestle et al., 2005)*. **However, the regulation of pDCs migration into inflamed epithelial**

tissues remained uncharacterized.

We were particularly interested in C-C motif chemokine receptors (CCR)-6 and CCR10 whose ligands were previously shown to be highly expressed in inflamed epithelia and described to contribute to the recruitment of cDCs *(Vanbervliet et al., 2002)* and T cells *(Homey et al., 2002)*, respectively. We first analyzed by flow cytometry the expression of these chemokine receptors on pDCs and observed that contrary to blood pDCs, a subset of inflamed tonsil pDCs expressed CCR6 and CCR10. Accordingly, tonsil pDCs migrated in response to CCR6 ligand chemokine (C-C motif) ligand (CCL)-20 (Mip-3α) and CCR10 ligand CCL27 (CTACK) in trans-well experiments *in vitro*, while blood pDCs did not. By immunohistochemistry we observed that pDCs co-localized with CCR6 ligand (CCL20) and CCR10 ligand (CCL28 or MEC) in psoriatic skin and virally induced verrucae vulgaris skin lesions. This was specific to inflamed skin, since CCL20 and CCL28 were only marginally expressed in normal skin, where pDCs were not detected. To further evaluate the role of CCR6-CCL20 axis in pDC migration *in vivo* we used *Ccr6* deficient mice that we obtained through a collaboration with Dr. Dominique Kaiserlian (International Center for Infectiology Research (CIRI), Lyon) and Dr. Bertrand Dubois (UMR INSERM 1052 CNRS 5286, Cancer Research Center of Lyon). After induction of inflammation in skin tumors by topical treatment with synthetic TLR7 agonist (Imiquimod) *(van der Fits et al., 2009)*, we observed a significant reduction of pDC recruitment in *Ccr6*-deficient animals. In addition, adoptively transferred *Ccr6*-deficient pDCs poorly migrated into inflamed tumors compared to control pDCs, further strengthening a cell-intrinsic role for CCR6 in the migration of pDCs into inflamed tissues *in vivo*. Of note, we did not have access at that time to *Ccr10*-deficient mice and could not study the contribution of this chemokine receptor to pDCs migration into inflamed tissues *in vivo*. We next observed that CCR6 and CCR10 expression can be induced on human blood pDCs after

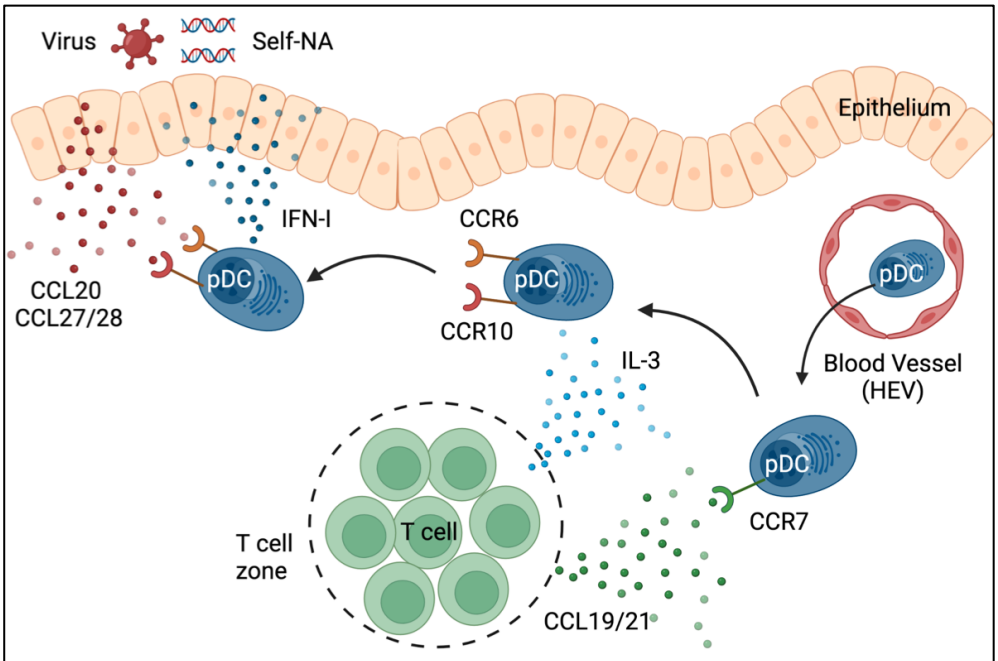

Figure 1. Model for pDC recruitment into inflamed epithelial sites.
On their recruitment into lymphoid organs in a manner that involves CCR7, pDCs are instructed through IL-3 released by local T cells to express CCR6 and CCR10. Such instructed pDCs then respond to CCL20 and CCL27/CCL28 mediating their migration into epithelial areas of mucosa or skin where they can sense viruses or self nucleic acids (NA) and produce IFN-I participating in viral clearance or inflammatory reactions.

their exposure to interleukin (IL)-3. Induction of CCR6 and CCR10 on blood pDCs allowed their migration in response to their respective ligands *in vitro*. CCR6- and CCR10-expressing pDCs were functional after their migration as reflected by their ability to produce IFN-I after TLR7 or 9 stimulation. Given that blood pDCs constitutively express CCR7, known to control their homing into SLO expressing its ligand CCL19 (Mip-3β**)** (*Seth et al., 2011*), we suggested the model depicted in **Fig. 1** to explain pDCs migration into inflamed tissues. After their constitutive recruitment to SLO in a CCR7-dependent manner, pDCs are instructed by IL-3, which is locally produced by T cells to express CCR6 and CCR10. $CCR6^+$ and $CCR10^+$ pDCs consequently migrate into inflamed epithelia producing high levels of their respective ligands CCL20 and CCL27/28. Once in inflamed sites pDCs produce IFN-I to clear viral infections or participate to chronic inflammation in pathologies such as psoriasis *(Sisirak et al., 2011)*. I had the opportunity to present this work at the French Dendritic Cell Society (CFCD) international annual meeting in Paris (2007) where I was awarded a prize for the best oral communication.

b. Functionally impaired pDCs in breast tumors contribute to tumor-immune escape

Impaired IFN-α production by plasmacytoid dendritic cells favors regulatory T-cell expansion that may contribute to breast cancer progression
Sisirak V*, Faget J*, Gobert M, Goutagny N, Vey N, Treilleux I, Renaudineau S, Poyet G, Labidi-Galy S.I, Goddard-Leon S, Durand I, Le Mercier I, Bajard A, Bachelot T, Puisieux A, Puisieux I, Blay J.Y, Ménétrier-Caux C, Caux C, and Bendriss-Vermare N, **Cancer Research**, 2012 Oct 15;72(20):5188-97. (*equal contribution) (*See **Annex 1***)
Breast cancer-derived TGF-ß and TNF-α compromise IFN-α production by tumor-associated plasmacytoid dendritic cells
Sisirak V, Vey N, Goutagny N, Renaudineau S, Malfroy M, Thys S, Treilleux I, Labidi-Galy S.I, Bachelot T, Ménétrier-Caux C, Blay J.Y, Caux C, and Bendriss-Vermare N, **International Journal of Cancer**, 2013 Aug 1;133(3):771-8.
Quantitative and functional alterations of plasmacytoid dendritic cells contribute to immune tolerance in ovarian cancer
Labidi-Galy SI, Sisirak V, Meeus P, Gobert M, Treilleux I, Bajard A, Combes JD, Faget J, Mithieux F, Cassignol A, Tredan O, Durand I, Ménétrier-Caux C, Caux C, Blay JY, Ray-Coquard I, Bendriss-Vermare N, **Cancer Research,** 2011 Aug 15;71(16):5423-34

Numerous human tumors were shown to be infiltrated by pDCs *(Vermi et al., 2011)*. However, the role of such tumor-associated pDCs (TApDCs) in cancer immunosurveillance remained controversial and poorly characterized. A retroprospective analysis of a cohort of 152 metastatic breast cancer patients from our laboratory in Lyon (CRCL) has demonstrated that pDC infiltration in breast tumors was associated with a poor clinical outcome for patients *(Treilleux et al., 2004)*. Indeed, breast cancer patients with high numbers of infiltrating pDCs (identified as $CD123^+$ (IL3Rα)) were more prone to relapse and exhibited a decreased survival *(Treilleux et al., 2004)*. **These results suggested that pDCs might contribute to tumor growth and/or immune escape, but the mechanisms involved**

in this process remained unknown.

To understand the function of pDCs within breast tumors we initiated a prospective study on a new cohort of 60 breast cancer patients. We observed that pDCs are significantly more represented in breast tumors with an aggressive phenotype, including tumors with a high mitotic index and the so-called triple negative tumors (human epidermal growth factor receptor 2 $(Her2)^-$, estrogen receptor $(ER)^-$ and progesterone receptor $(PR)^-$). These observations were in accordance with the previous results indicating that pDCs infiltration in breast tumors was associated with an adverse clinical outcome *(Treilleux et al., 2004)*. We further characterized their phenotype by flow cytometry and observed that TApDCs, compared to healthy donor blood and tonsil pDCs, exhibited a partially activated phenotype, expressing high levels of co-stimulatory molecules CD80 and CD86. After their isolation, TApDCs induced similar levels of proliferation of allogeneic naïve CD4 T cells as compared to healthy donor pDCs, while their ability to produce IFN-I after TLR7 and TLR9 stimulation was strongly inhibited. These results indicated that TApDCs capacity to activate T cell proliferation remained intact while their ability to produce IFN-I was impaired in tumors. This inhibition was specific to IFN-I and to the tumor site, since TApDCs produced normal level of other inflammatory cytokines such as C-X-C motif chemokine ligand (CXCL)-10 (IP-10) and breast tumor patients' blood pDCs produced similar levels of IFN-I as healthy blood pDCs in response to TLR7 and TLR9 stimulation. We observed on breast tumor tissue sections that TApDCs were located in close contact with suppressive regulatory CD4 T cells (Tregs) expressing the transcription factor forkhead box P3 (FoxP3). The infiltration of pDCs within breast tumors significantly correlated with the presence of Tregs, particularly in triple negative aggressive breast tumors. Importantly, isolated TApDCs were able to induce the proliferation of Tregs *in vitro* while healthy donor pDCs failed to do so. This immunosuppressive property of TApDCs was inhibited in the presence of IFN-I. These results suggested that the selective inhibition of TApDC production of IFN-I enables them to promote tumor immune escape through the induction of the proliferation of suppressive Tregs (**Fig. 2**) *(Sisirak et al., 2012)*. This process was

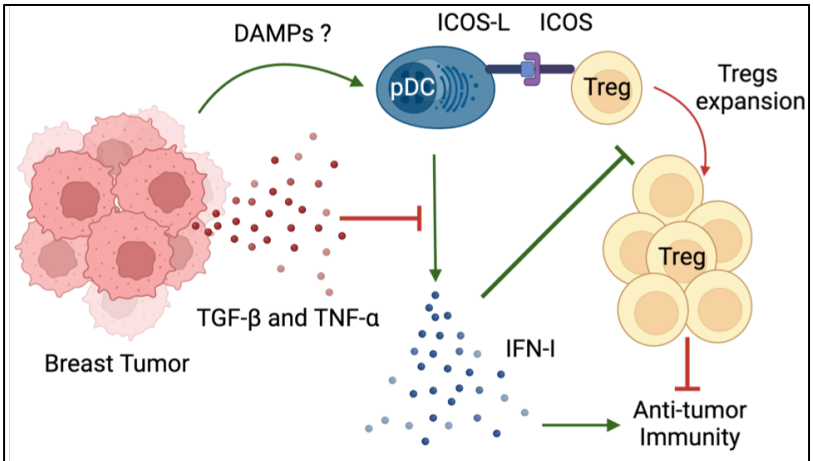

Figure 2. Model for tumor-associated pDC function in tumor immune suppression. TGF-β and TNF-α produced by the tumor microenvironment inhibit the production of IFN-I by tumor-associated pDCs (TApDCs) that may be activated by endogenous signals (DAMPs). Such functionally impaired TApDCs support the proliferation of tumor-associated Tregs (TATreg) through ICOS-L-ICOS interaction, establishing an immunosuppressive environment. This enables breast tumors to escape immunosurveillance and grow. As the proliferation of TATregs is strongly inhibited by exogenous IFN-I, our data collectively suggested that restoring IFN-I production by TApDCs may favor antitumor immunity in breast cancer.

subsequently shown by our laboratory to depend on the interaction between the inducible T cell co-stimulator ligand (ICOS-L) on pDCs and ICOS on Tregs *(Faget et al., 2012)*, and observed in patients with ovarian carcinoma as well *(Conrad et al., 2012*), further strengthening our observations.

To decipher the mechanisms involved in the inhibition of IFN-I production by TApDC, we established an *in vitro* model of pDC interaction with the breast tumor environment. To model the soluble tumor microenvironment, we generated breast tumor-derived supernatants. These supernatants, obtained after a 48h culture of primary breast tumors-derived single cell suspensions, were next cultured in the presence of healthy donor pDCs during 16h prior to their activation with TLR7 and TLR9 ligands. We observed that 25 out of 33 independent primary breast tumor supernatants specifically inhibited pDC production of IFN-I without affecting their ability to produce CXCL10, reproducing our results observed *ex vivo* with TApDCs. We then identified factors produced by the tumor environment that block pDCs production of IFN-I. These factors included the transforming growth factor (TGF)-β and the tumor necrosis factor (TNF)-α. Indeed, blocking antibodies directed against TGF-β and TNF-α restored pDCs' ability to produce IFN-I after TLR7 and TLR9 stimulations in the presence of breast tumor-derived supernatants (**Fig. 2**). TGF-β and TNF-α were found to work synergistically by reducing both the expression of IRF7 and its nuclear translocation upon pDC stimulation thus preventing its ability to activate IFN-I expression upon TLR7 and 9 stimulation. We also observed by fluorescent microscopy on breast tumor sections that TApDCs show elevated levels of phosphorylated Smad2 protein in their nuclei, which is indicative of TGF-β activity within human breast tumors *in vivo (Sisirak et al., 2013)*. I assisted an MD-PhD student (Intidhar Labidi-Galy) who studied in parallel the function of pDCs in human ovarian carcinomas. We observed that similar phenomena occur in ovarian cancer, where pDCs are impaired in their capacity to produce IFN-I and promote immunosuppressive responses *(Labidi-Galy et al., 2011)*. I had the opportunity to present these contributions to the understanding of pDC functions in cancer at several national (French Dendritic Cell Society (CFCD), Société Française d' Immunologie) and international (European Association for Cancer Research, Keystone Symposia on DCs) meetings, where I received multiple scholarships and prizes for best communication as outlined in my CV. In addition to the primary research articles, these studies led to the publication of two following comments in Oncoimmunology.

Plasmacytoid dendritic cells deficient in IFN-α production in breast cancer promotes amplification of FoxP3+ regulatory T cells and are associated with poor prognosis
Sisirak V, Faget J, Vey N, Blay J.Y, Ménétrier-Caux C, Caux C, and Bendriss-Vermare N, ***Oncoimmunology***, 2013 Jan 1;2(1):e22338.
ICOS is associated with poor prognosis in breast cancer as it promotes the amplification of immunosuppressive CD4+ T cells by plasmacytoid dendritic cells
Faget J, Sisirak V, Blay J.Y, Caux C, Bendriss-Vermare N and Ménétrier-Caux C, ***Oncoimmunology***, 2013 Mar 1;2(3):e23185.

c. *Collaborative studies: pDCs and beyond*

Tumor promotion by intratumoral plasmacytoid dendritic cells is reversed by TLR7 ligand treatment.
Le Mercier I, Poujol D, Sanlaville A, Sisirak V, Gobert M, Durand I, Dubois B, Treilleux I, Marvel J, Vlach J, Blay JY, Bendriss-Vermare N, Caux C, Puisieux I, Goutagny N. ***Cancer Research***. 2013 Aug 1;73(15):4629-40.
Human Langerhans cells express a specific TLR profile and differentially respond to viruses and Gram-positive bacteria.
Flacher V, Bouschbacher M, Verronèse E, Massacrier C, Sisirak V, Berthier-Vergnes O, de Saint-Vis B, Caux C, Dezutter-Dambuyant C, Lebecque S, Valladeau J. ***Journal of Immunology***. 2006 Dec 1;177(11):7959-67.
Gene expression profiling identifies sST2 as an effector of ErbB2-driven breast carcinoma cell motility, associated with metastasis.
Gillibert-Duplantier J, Duthey B, Sisirak V, Salaün D, Gargi T, Trédan O, Finetti P, Bertucci F, Birnbaum D, Bendriss-Vermare N, Badache A. ***Oncogene***. 2012 Jul 26;31(30):3516-24.
A novel regulation of PD-1 ligands on mesenchymal stromal cells through MMP-mediated proteolytic cleavage.
Dezutter-Dambuyant C, Durand I, Alberti L, Bendriss-Vermare N, Valladeau-Guilemond J, Duc A, Magron A, Morel AP, Sisirak V, Rodriguez C, Cox D, Olive D, Caux C. ***Oncoimmunology***. 2015 Oct 29;5(3):e1091146

In collaboration with the group of Dr. Isabelle Puisieux (UMR INSERM 1052 CNRS 5286, CRCL) we addressed the relevance of pDC function in breast tumor immunosurveillance *in vivo* and whether TApDC targeting may be an effective therapeutic strategy to restore breast tumor immunity. Using an orthotopic murine mammary tumor model that mimics the human pathology we observed that TApDCs were inhibited in their ability to produce IFN-I in response to TLR9 stimulation while their ability to respond to TLR7 ligands was not affected. These results were in accordance with our observation obtained in breast tumor patients with the exception that IFN-I production by human TApDCs was also inhibited in response to TLR7 stimulation, although less severely than in response to TLR9 stimulation. Depletion of pDCs in this murine model reduced the tumor growth and increased the overall survival of animals, indicating that as in human TApDCs seem to promote tumor growth and/or immune escape. Targeting TApDCs with a synthetic TLR7 agonist induced their production of IFN-I *in vivo*, which resulted in the inhibition of the tumor growth *(Le Mercier et al., 2013)*. These results indicated that therapeutic targeting of TApDCs may restore their production of IFN-I and ultimately lead to anti-tumor immunity and tumor regression. I was also involved in multiple collaborations beyond the function of pDCs. I participated in the (i) characterization of the TLR expression profile and responsiveness of a subset of skin DCs, called Langerhans cells *(Flacher et al., 2006)*, in the (ii) identification of the soluble ST2 molecule as important factor associated with breast cancer metastasis *(Gillibert-Duplantier et al., 2012)* as well as in the (iii) discovery of a novel enzymatic regulation of the expression of programed death ligand (PDL)-1 on cancer associated fibroblast, shown to contribute to cancer immune escape *(Dezutter-Dambuyant et al., 2016)*.

d. Conclusions and significance

During my doctoral work we have identified a novel migratory pathway involving CCR6-CLL20 and CCR10-CCL27/28 axes in the control of pDCs recruitment into inflamed tissues. Once in epithelial sites pDCs contribute to local inflammation by producing elevated levels of IFN-I. While during viral infection IFN-I-derived from pDCs is beneficial to the host and participate to viral clearance, in sterile conditions it may exacerbate local inflammation and contribute to inflammatory syndromes such as psoriasis. Therefore, preventing pDCs recruitment into inflamed epithelial sites by blocking CCR6 and/or CCR10 may be an attractive therapeutic approach to limit their capacity to further fuel inflammation. The recruitment of pDCs was further observed in epithelial areas of the tonsil upon bacterial infection *(Michea et al., 2013)*. In addition, inflammation found in allergic asthma *(Bratke et al., 2013)* and ankylosing spondylitis *(Liu et al., 2020)* was shown to upregulate CCR6 and CCR10 expression by pDCs, which in turn contributed to pDCs recruitment in inflamed sites. Nevertheless, a recent study has reported a population of cells co-expressing markers of pDCs ($CD123^+$, blood dendritic cell antigen (BDCA)-2^+) and cDC ($CD1a^+$) in inflamed human skin. When transcriptionally analyzed, these cells did not correspond to *bona-fide* pDCs but rather to activated cDCs *(Chen et al., 2019)*. These observations warrant further investigations to specifically delineate pDC recruitment and function during skin inflammation.

We have also identified the mechanisms leading to pDCs' deleterious impact on breast cancers patients' clinical outcomes. pDCs that infiltrate breast tumors were shown to be impaired in their production of IFN-I and instead induce a "tolerogenic" environment by promoting Tregs' proliferation, and consequently, the tumor immune escape. This functional alteration of pDCs that we have observed in breast tumors was generalized to lung cancer, head and neck squamous cell carcinoma, liver cancer, ovarian carcinoma and myeloid leukemia *(Ganguly, 2022)*. However, in colorectal cancer pDC infiltration was associated with a favorable prognosis for patients *(Kießler et al., 2021)*. In colorectal carcinoma TApDC production of IFN-I by the tumor environment appeared unaffected, indicating that pDCs assume the role of a favorable immune cell for anti-cancer immunity when their IFN-I production is maintained. This understanding of pDCs function in cancer paved the way for the development of therapeutic strategies, that restore pDCs IFN-I production and have shown efficacy in murine breast tumor models *(Le Mercier et al., 2013).* There are multiple questions that remained unanswered, particularly what may trigger IFN-I production by pDCs in breast tumors? Several lines of evidence indicate that tumors release immunostimulatory molecules called damage associated molecular pattern (DAMPs) that can activate various PRR *(Galluzzi et al., 2017)*. Tumor-derived DNA represents an important DAMP that was shown to activate DNA sensing PRR, including TLR9 *(Kang et al., 2019)*. IFN-I production resulting from such activation was shown to contribute to anti-tumor immune response and to boost the efficacy of current immunotherapies *(Woo et al., 2015)*. Therefore, DNA derived from breast tumors may trigger IFN-I production by TApDCs, so to avoid

the attacks from the immune system initiated by IFN-I, multiple tumors may have adopted strategies to block its production.

2. POSTDOCTORAL WORK (2010-2017)

The role of dendritic cells in autoimmunity.
Ganguly D, Haak S, Sisirak V, Reizis B. **Nature Reviews Immunology**. 2013 Aug;13(8):566-77.
Plasmacytoid dendritic cells: recent progress and open questions.
Reizis B, Bunin A, Ghosh HS, Lewis KL, Sisirak V. **Annual Review of Immunology**. 2011;29:163-83.

After completing my PhD, I joined the laboratory of Dr. Reizis at Columbia University in New York as a postdoctoral fellow in 2010. After 4 years the team moved to New York University Langone Medical Center where I was promoted to an associate research scientist. During my postdoctoral experience, I was awarded a fellowship from the Fondation Pour la Recherche Médicale (FRM) providing one year of funding as well as a grant from the Cancer Research Institute (CRI) that funded my salary for 3 years. My main motivation in joining Dr. Reizis's laboratory was to master mouse genetic models developed by his team that allow a deeper understanding of pDC function during steady state and pathological conditions *in vivo*. My initial achievement was to take part in the writing of an overview about pDC functions *(Reizis et al., 2011)* and DC roles in autoimmunity *(Ganguly et al., 2013)* for the Annual Review of Immunology and Nature Reviews Immunology, respectively. During the literature review process, we were particularly intrigued by multiple works suggesting that pDC-derived IFN-I contributes to autoimmune syndromes such as systemic lupus erythematosus (SLE). SLE is an autoimmune disorder characterized by an aberrant production of autoantibodies against self-nucleic acids *(Tsokos et al., 2016)*. Such autoantibodies together with self-nucleic acids form immune complexes that are deposited in various tissues such as the kidney where they cause inflammation (nephritis) and ultimately the destruction of the tissue. Immune complexes as well as self-nucleic acids were shown to activate pDC production of IFN-I *via* TLR7 and TLR9, which was further suggested to participate in the pathogenic loop of SLE *(Garcia-Romo et al., 2011; Lande et al., 2011; Means et al., 2005)*. **However, these observations were obtained primarily from *in vitro* or *ex vivo* studied and there was no clear evidence for pDCs contribution to SLE pathogenesis *in vivo*.**

a. pDCs exacerbate SLE pathogenesis in vivo

Genetic evidence for the role of plasmacytoid dendritic cells in systemic lupus erythematosus.
Sisirak V*, Ganguly D*, Lewis KL, Couillault C, Tanaka L, Bolland S, D'Agati V, Elkon KB, Reizis B. ***Journal of Experimental Medicine***. 2014 Sep 22;211(10):1969-76. (* equal contribution) (*See **Annex 2***)

To establish genetic evidence for pDC involvement in SLE we used mice haplodeficient for the transcription factor E2-2 (encoded by *Tcf4* the gene), which is the master regulator of pDC fate *(Cisse et al., 2008; Ghosh et al., 2010)*. Mice that are haplodeficient for *Tcf4* display reduced pDC numbers and are unable to produce IFN-I after TLR9 stimulation *in vivo*, indicating an overall impairment of their function *(Cisse et al., 2008)*. These mice were crossed with *Tlr7* transgenic (*Tlr7.1Tg*) ones, which contain multiples copies of the *Tlr7* gene on the Y chromosome, and are thus prone to develop SLE *(Deane et al., 2007)*. *Tfc4* haplodeficiency increased the survival of *Tlr7.1Tg* mice and reduced the systemic immune activation that occurs with time in these mice. *Tcf4* expression is also found at a minimal level in B cells. Therefore, to avoid any confounding impact of *Tcf4* haplodeficiency on B cells we generated mice with a specific haplodeficiency of *Tcf4* in pDCs using a CD11c (*Igax*) Cre deleter strain and one "floxed" allele of *Tcf4*. This pDC-specific haplodeficiency of *Tcf4* in *Tlr7.1Tg* mice also ameliorated SLE by reducing the production of anti-RNA autoantibodies and the kidney inflammation as evaluated by immunoglobulin (Ig) deposition and the overall kidney pathological score, further confirming the deleterious impact of pDCs on SLE pathogenesis. *Tlr7.1Tg* mice do not fully recapitulate all features of human SLE, including the multigenic nature of the disease, the female bias, and the production of anti-DNA antibodies. We thus crossed *Tcf4* haplodeficient mice with B6;NZM *Sle1.Sle3* animals that carry quantitative traits loci (*Sle1* and *Sle3* derived from the NZM2410 strain) that confers susceptibility to SLE development in a manner that closely mimics the human disease *(Morel et al., 2000)*. *Tcf4* haplodeficiency in B6;NZM *Sle1.Sle3* animals prevented the production of anti-nuclear antibodies, anti-DNA antibodies and the development of glomerulonephritis (**Fig. 3A-C**), underlining the role of pDCs in SLE pathogenesis in yet another model of the disease. Finally, to investigate the molecular mechanisms involved in the deleterious impact of pDCs in SLE development, we performed a transcriptomic analysis (microarray) of splenocytes from B6;NZM *Sle1.Sle3* animals and compared to those that were haplodeficient for *Tcf4*. We did not observe any IFN-I signature (ISG expression) in either group and could not connect the deleterious impact of pDCs on SLE to their IFN-I production. However, we observed a reduction in the expression of genes involved in the germinal center (GC) reaction. The GC reaction is at the basis of T cell-dependent B cell immunity against foreign pathogens and plays an important role in the proliferation of autoreactive B cells and their production of autoantibodies *(Victora and Nussenzweig, 2022)*. During the GC reaction B cells undergo class-switching, somatic hypermutation and differentiate into long-lived plasma cells that produce high affinity antibodies *(Victora and Nussenzweig, 2022)*. We further observed that SLE-prone animals develop a spontaneous GC reaction *in vivo,* a process that was prevented in *Tcf4*-haplodeficient SLE-prone mice (**Fig. 3D**). Thus, our results indicated that pDCs play an essential role in experimental SLE, most likely through their ability to promote the GC reaction *(Sisirak et al., 2014).* The results from our study were highlighted in Nature Reviews in Rheumatology *(Onuora, 2014)*,

and I was awarded a scholarship and presented this work at the 2015 Keystone Symposium on autoimmunity.

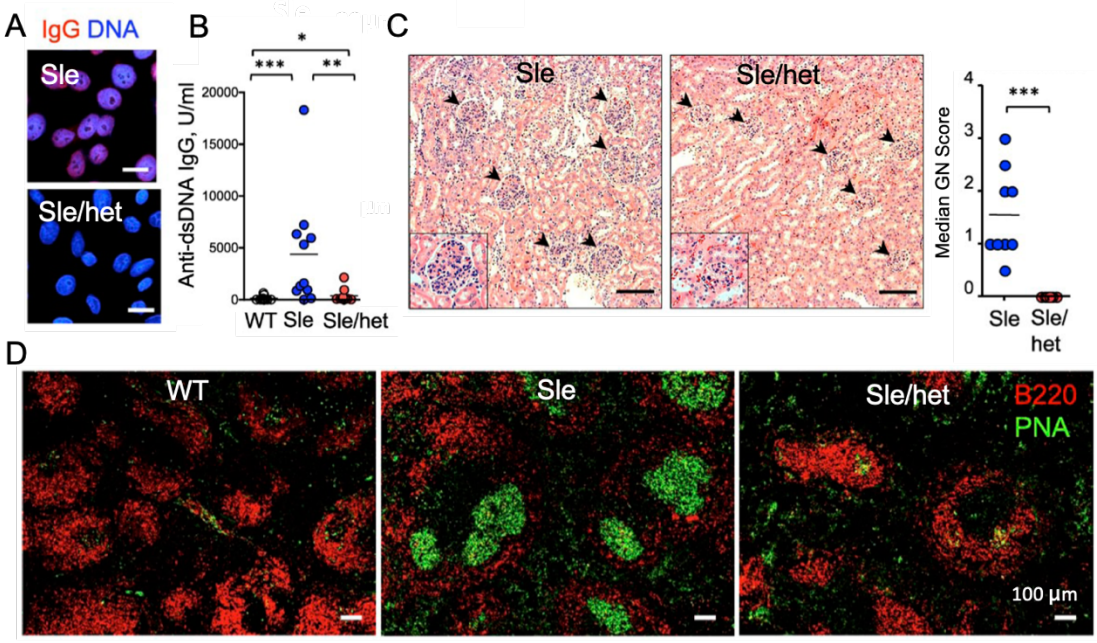

Figure 3. ***Tcf4 haplodeficiency ameliorates SLE in B6;NZM Sle1.Sle3 mice.***
30-week-old B6;NZM*Sle1.Sle3* mice (Sle) or their *Tcf4* haplodeficient littermates (Sle/het) were analyzed along with WT controls. (**A**) Fixed Hep2 cells were incubated with sera from Sle mice, stained for IgG (red) and DNA (blue), and analyzed by fluorescence microscopy (bars, 20 µm). (**B**) Levels of anti-dsDNA in the sera of indicated animals were measured by ELISA. (**C**) Kidney paraffin sections from indicated mice were stained with H&E and analyzed by microscopy (bars, 100 µm). Arrows show kidney glomeruli, with a representative glomerulus on the inset. Median glomerulonephritis (GN) histopathological scores were quantified in the indicated animals. (**D**) Spleen sections from indicated mice were stained for total B cells (B220, red) and GC B cells (PNA, green). Horizontal bars indicate mean. *, P ≤ 0.05; **, P ≤ 0.01; ***, P ≤ 0.001.

b. DNASE1L3: a novel endonuclease preventing SLE development

Digestion of Chromatin in Apoptotic Cell Microparticles Prevents Autoimmunity.
Sisirak V*, Sally B*, D'Agati V, Martinez-Ortiz W, Özçakar ZB, David J, Rashidfarrokhi A, Yeste A, Panea C, Chida AS, Bogunovic M, Ivanov II, Quintana FJ, Sanz I, Elkon KB, Tekin M, Yalçınkaya F, Cardozo TJ, Clancy RM, Buyon JP, Reizis B. ***Cell***. 2016 Jun 30;166(1):88-101 (*equal contribution) (*See **Annex 3***)

As we have previously discussed, the immune system is capable of detecting microbial nucleic acids via PRR in order to mount anti-microbial immune responses. PRR ability to detect microbial genetic material confers an advantage to the host by enabling the activation of the immune system against a broad range of microbes *(Barbalat et al., 2011; Crowl et al., 2017)*. However, this specificity of PRRs comes with an eminent risk, as PRRs sensing DNA do not robustly discriminate between self and foreign DNA and can thus be activated by DNA that arises from the natural turnover of cells, or the release of genomic DNA (gDNA) and mitochondrial DNA (mtDNA) into the cytosol *(Barbalat et al., 2011; Crowl et al., 2017)*. Self-DNA immune recognition can consequently lead to the aberrant activation of immune responses and ultimately to the development autoimmune diseases such as

SLE. Therefore, endogenous or self-DNA availability and immunostimulatory potential must be tightly regulated. Multiple safeguard mechanisms have evolved to limit self-DNA ability to stimulate abnormal immune responses. These include sequestration of DNA in cellular compartments as well as specific chemical and structural properties that prevent its recognition by PRRs *(Bartok and Hartmann, 2020)*. In addition, a system of intracellular and extracellular deoxyribonucleases (DNASEs) is critical for disposing of endogenous DNA and limiting its immunostimulatory potential. Cell-intrinsic DNASEs such as DNASE2A *(Kawane et al., 2006; Rodero et al., 2017; Yoshida et al., 2005)* and three prime repair exonuclease (TREX)-1 *(Crow et al., 2006; Stetson et al., 2008)* were extensively studied and shown to dispose of intracellular DNA to prevent fatal autoinflammatory diseases. Indeed, both in mice and humans, deficiency of individual cell-intrinsic DNASEs leads to the activation of the intracellular DNA sensor cyclic GMP-AMP synthase (cGAS) which induces the production of IFN-I through the activation of the stimulator of interferon genes (STING) adaptor protein, ultimately causing disease *(Ablasser et al., 2014; Ahn et al., 2012)*. Conversely, extracellular DNASEs functions remains poorly characterized. Extracellular DNASEs comprise DNASE1 and three homologous enzymes (DNASE1-like (L) 1, DNASE1L2 and DNASE1L3). While DNASE1L1 and DNASE1L2 are specifically expressed in muscular tissue and skin epidermis respectively, DNASE1 and DNASE1L3 are responsible for most of the DNASE activity detected in the circulation (serum) *(Keyel, 2017)*. DNASE1 specifically digests "naked" DNA and has been proposed to prevent the development of SLE *(Napirei et al., 2005, 2000)*. These results were challenged since *Dnase1*-deficiency in mice on pure genetic background did not cause SLE and *DNASE1* mutations were not found in large cohorts of SLE patients *(Santa et al., 2021)*. DNASE1 function may therefore be compensated by other extracellular DNASEs. We were particularly interested in the function of DNASE1L3. Null mutations in *DNASE1L3* were described to lead to the

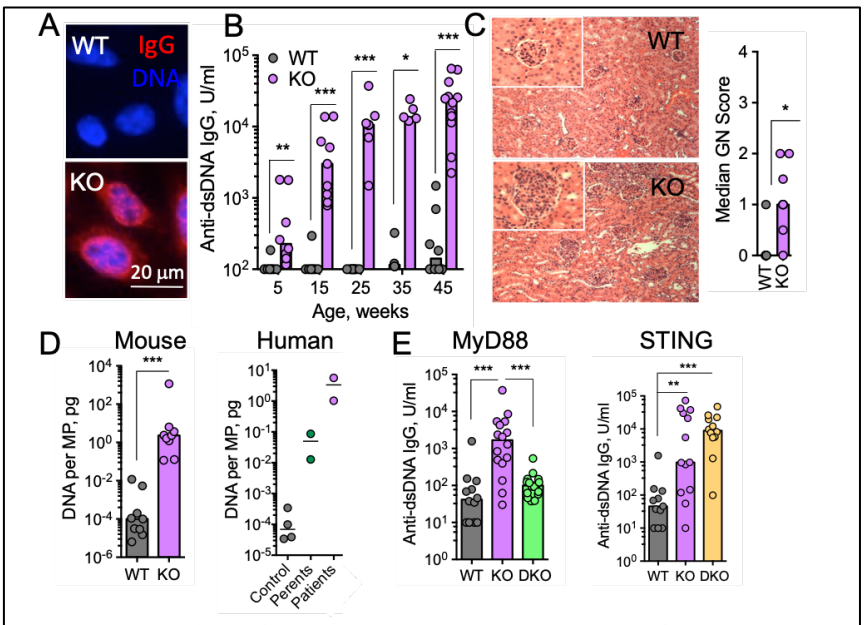

Figure 4. ***Dnase1l3* deficiency causes MyD88 dependent SLE like disease.** (**A**) Fixed Hep2 cells were incubated with sera from WT and *Dnase1l3* KO mice, stained for IgG (red) and DNA (blue), and analyzed by fluorescence microscopy. (**B**) Levels of anti-dsDNA in the sera of indicated mice were measured by ELISA. (**C**) Kidney paraffin sections from WT and *Dnase1l3* KO mice were stained with H&E and analyzed by microscopy with a representative glomerulus in the inset. Glomerulonephritis (GN) scores were quantified. (**D**) DNA levels as measured by Q-PCR in circulatory microparticles (MPs) of WT and *Dnase1l3* KO mice and control, *DNASE1L3*$^{+/-}$ (parents) *and DNASE1L3*$^{-/-}$ (patients) humans. (**E**) Anti-dsDNA in the sera of WT, *Dnase1l3* KO (KO), *Dnase1l3-Myd88* double KO (DKO) and *Dnase1l3-Sting DKO mice* were measured by ELISA. Horizontal bars indicate mean. *, P ≤ 0.05; **, P ≤ 0.01; ***, P ≤ 0.001.

development of a severe familial form of SLE with Mendelian inheritance *(Al-Mayouf et al., 2011)*. In addition, polymorphisms in the *DNASE1L3* locus were associated with sporadic forms of SLE *(Coke et al., 2021)*. DNASE1L3 was previously described to exhibit unique functions compared to DNASE1 such as digesting lipid-encapsulated *(Wilber et al., 2002)* and nucleosomal DNA *(Napirei et al., 2005)* without any helper proteases. **However, the mechanisms of action of DNASE1L3 in SLE pathogenesis remained unknown**.

To further understand its function, we acquired *Dnase1l3* deficient mice. We observed that, as they age these mice develop all the cardinal features of SLE, including anti-nuclear antibodies, anti-DNA antibodies, anti-nucleosome antibodies, overall immune activation and a mild glomerulonephritis (**Fig. 4A-C**). The phenotype induced by *Dnase1l3* deficiency in mice was milder than in humans and did not result in lethality. This difference is likely due to the housing of *Dnase1l3* KO mice in specific pathogen free facilities, since treatment with exogenous IFN-I significantly accelerated/exacerbated SLE pathogenesis and induced lethality in these mice. SLE development also occurred when wild type (WT) recipient mice were transplanted with *Dnase1l3*-deficient BM cells but not with WT BM cells, indicating that the main source of DNASE1L3 resides within the hematopoietic system. We consequently identified that DCs and macrophages express the highest levels of *Dnase1l3*. Furthermore, specific depletion of DCs and macrophages reduced circulatory DNASE1L3 activity by ~70% and ~30% respectively, indicating that myeloid cells are the main source of DNASE1L3 in mice. Available expression data in human, showed that *DNASE1L3* is mostly expressed in DCs and macrophages as well but also in liver endothelial cells. From a mechanistic standpoint, we observed that *Dnase1l3* deficient mice and humans accumulate DNA, particularly in circulatory microparticles (MPs) derived from apoptotic cells (**Fig. 4D**), suggesting that the *in vivo* function of DNASE1L3 is to dispose of DNA present in MPs originating from dying cells. In addition, we observed that humans and mice deficient for DNASE1L3 display high levels of serum autoantibodies that target MPs derived from apoptotic cells further emphasizing their role as a major antigenic source. The binding of autoantibodies to MPs could be prevented by their treatment with DNASE1L3. Finally, to address how the DNA within MPs leads to SLE development, we crossed *Dnase1l3* deficient mice to animals

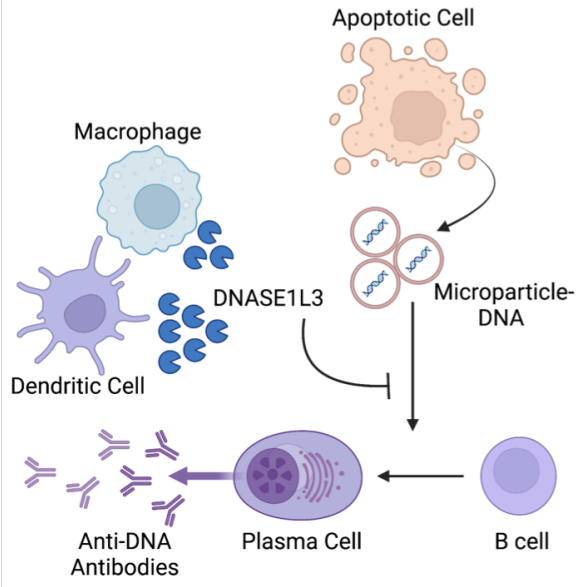

Figure 5. ***Model for DNASE1L3 function in preventing DNA-mediated autoreactivity.*** DNASE1L3 produced by dendritic cells and macrophages dispose of DNA associated to microparticles released by dying cells and prevent thus its ability to activate autoreactive B cells transition into anti-DNA producing plasma cells

deficient for STING (encoded by the gene *Tmem173*) and myeloid differentiation primary response 88 (*Myd88*). STING and MyD88 are adaptor molecules that are required for the signaling of the intracellular DNA sensor cGAS and most of the TLRs except TLR3, respectively. While *Tmem173* deficiency did not have a major impact on the disease in *Dnase1l3*-deficient mice, *Myd88* deficiency prevented SLE development, suggesting that TLR-mediated recognition of DNA associated to MPs drives SLE pathogenesis in *Dnase1l3*-deficient animals (**Fig. 4E**). Thus, our study uncovered a novel cell-extrinsic mechanism of tolerance to self-DNA that involves DNASE1L3 selectively produced by DCs and macrophages *(Sisirak et al., 2016)*. DNASE1L3 regulates the availability of immunogenic DNA on MPs derived from apoptotic cells and thus limits its capacity to aberrantly activate autoreactive B cells (**Fig. 5**). These results were highlighted in Nature Reviews in Rheumatology *(Onuora, 2016)* and presented at the annual meeting of the French Society of Immunology (SFI, 2018) and during multiple invited seminars as described in my curriculum vitae.

c. Collaborative studies: regulation of pDC development and function

Protein Tyrosine Phosphatase PTPRS Is an Inhibitory Receptor on Human and Murine Plasmacytoid Dendritic Cells.
Bunin A, Sisirak V, Ghosh HS, Grajkowska LT, Hou ZE, Miron M, Yang C, Ceribelli M, Uetani N, Chaperot L, Plumas J, Hendriks W, Tremblay ML, Häcker H, Staudt LM, Green PH, Bhagat G, Reizis B. **Immunity**. 2015 Aug 18;43(2):277-88.
Transcription factor Runx2 controls the development and migration of plasmacytoid dendritic cells.
Sawai CM, Sisirak V, Ghosh HS, Hou EZ, Ceribelli M, Staudt LM, Reizis B. **Journal of Experimental Medicine**. 2013 Oct 21;210(11):2151-9.
Plasmacytoid dendritic cells are dispensable for noninfectious intestinal IgA responses in vivo.
Moro-Sibilot L, This S, Blanc P, Sanlaville A, Sisirak V, Bardel E, Boschetti G, Bendriss-Vermare N, Defrance T, Dubois B, Kaiserlian D. **European Journal of Immunology**. 2016 Feb;46(2):354-9.

During my postdoctoral experience, we initiated collaborations with clinical teams, notably with Dr. Jill Buyon and Dr. Robert Clancy (Department of Rheumatology, New Your University Langone Medical Center) to understand DNASE1L3 function in sporadic SLE patients. We have observed in a small cohort of ~60 SLE patients, that 60% of them show autoreactivity to *in vitro* generated MPs. Among patients showing autoreactivity to MPs, in half of them this autoreactivity could be prevented upon pretreatment of MPs with exogenous DNASE1L3, indicating that DNASE1L3 activity is likely negatively regulated in sporadic SLE patients as well. These results were included in the previously described publication. Furthermore, I collaborated with postdoctoral fellows within Dr. Reizis's laboratory, to study the regulation of pDC function and development. With Dr. Anna Bunin, we identified a novel inhibitory receptor called protein tyrosine phosphatase S receptor (PTPRS) that is specifically expressed on pDCs and restrains their ability to produce IFN-I and thus prevents the development of colitis *(Bunin et al., 2015)*. In collaboration with Dr. Catherine Sawai, we found that the runt-related transcription factor 2 (Runx2) regulates pDC egress from the BM to the SLO by

controlling the expression of chemokine receptors CCR2 and CCR5 *(Sawai et al., 2013)*. Finally, in a collaborative work with Dr. Bertrand Dubois (CRCL, Lyon, France), we have shown, using *Tcf4* haplodeficient mice, that pDCs are not involved in the production of intestinal IgA, contrary to what was previously suggested *(Moro-Sibilot et al., 2016)*.

d. Conclusions and significance

Our results have shown that pDCs play a pathogenic role in SLE. While we could not associate this pathogenic pDC function in SLE to their production of IFN-I, we observed that pDCs exacerbate SLE by promoting the GC reaction and ultimately the activation of B cells' production of anti-DNA antibodies. These results were further confirmed by two independent teams using different approaches to deplete pDCs in two additional experimental SLE models *(Davison and Jørgensen, 2015; Rowland et al., 2014)*. These studies have led to the development of therapeutic approaches to deplete and block pDC function for SLE patients *(Pellerin et al., 2015)*. Recently, pDCs depletion *via* the targeting of pDC-specific marker immunoglobulin-like transcript 7 (ILT-7) *(Karnell et al., 2021)* and pDC-specific inhibition of IFN-I production *via* the targeting of BDCA-2 *(Furie et al., 2019; Werth et al., 2022)* have shown therapeutic efficacy in clinical trials in patient with cutaneous SLE.
In addition, we have functionally characterized DNASE1L3 as a novel enzyme enforcing tolerance to self-DNA by preventing the systemic accumulation of endogenous DNA originating from apoptotic cells. In the absence of DNASE1L3, extracellular DNA accumulates, particularly in MPs, and stimulates DNA-specific autoreactive responses in a MyD88-dependent manner (**Fig. 5**). The results suggested that endogenous nucleic acid recognition by TLRs likely contribute to SLE pathogenesis in *DNASE1L3* null patients and thus provided further rationale for the use of hydroxychloroquine for their treatment through its ability to impair endosomal TLR function. SLE development was also recently reported in an additional strain of *Dnase1l3*-deficient mice *(Weisenburger et al., 2018),* and since our study, multiple *DNASE1L3* null patients developing early onset SLE and SLE-associated diseases were described *(Carbonella et al., 2017; Kisla Ekinci et al., 2021; Ozçakar et al., 2013; Paç Kisaarslan et al., 2020; Tusseau et al., 2022)*, emphasizing the human relevance of our findings. In addition, DNASE1L3 together with DNASE1, was shown to degrade DNA present in neutrophil extracellular traps (NETs) and thus to prevent the occurrence of vascular occlusion during sterile neutrophilia or septicemia, underlining yet-another essential function of DNASE1L3 in the clearance of pathogenic forms of DNA *(Jiménez-Alcázar et al., 2017)*.

3. ***INDEPENDENT CAREER (2018-2023)***

Systemic lupus erythematosus and systemic sclerosis: All roads lead to platelets
Scherlinger M, Guillotin V, Truchetet ME, Contin-Bordes C, Sisirak V, Duffau P, Lazaro E, Richez C, Blanco P, **Autoimmun Rev**. 2018 Jun;17(6):625-635.

New Insights on Platelets and Platelet-Derived Microparticles in Systemic Lupus Erythematosus
Scherlinger M, Sisirak V, Richez C, Lazaro E, Duffau P, Blanco P, **Curr Rheumatol Rep**. 2017 Aug;19(8):48.

After being awarded a Junior Chair by the IdEx program of the University of Bordeaux, I joined the Immunoconcept (UMR CNRS 5164) research department in 2017 as an independent scientist. In 2018 I was tenured by the Centre National de la Recherche Scientifique (CNRS) and secured competitive funding from the Cancer Research Institute (CLIP investigator) and the Bristol-Myers Squibb Foundation, which has enabled me to initiate my independent projects and build my research team. My initial achievement was to take part in the writing of reviews on innate immune mechanisms involved in SLE pathogenesis and particularly the role of platelets in this process *(Scherlinger et al., 2018, 2017)*. I also continued my work on the study of pDCs function in disease and on the characterization of the cellular and molecular mechanisms involved in SLE induced by *Dnase1l3* deficiency. Furthermore, I also developed a novel project in order to study DNASE1L3 function in other pathological contexts beyond SLE.

a. pDCs are dispensable in inflammatory bowel disease pathogenesis

Plasmacytoid dendritic cells are dispensable for inflammatory bowel disease pathogenesis.
Sawai CM, Serpas L, Neto AG, Jang G, Rashidfarrokhi A, Kolbeck R, Sanjuan MA, Reizis B[#], Sisirak V[#], **Frontiers in Immunology**. 2018 Oct 25;9:2475 ([#]co-corresponding authors) (*See **Annex 4***)

Initially we pursued our work on the contribution of pDCs to inflammatory and autoimmune diseases. In addition to SLE, pDCs were also shown to be involved in the pathogenesis of inflammatory bowel diseases (IBD). IBD, including ulcerative colitis and Crohn's disease, is a chronic and recurrent inflammatory disease that mainly relates to the intestinal tract *(Abraham and Cho, 2009)*. pDCs were detected in the inflamed epithelial colonic mucosa *(Baumgart et al., 2005)*, and conflicting roles for their IFN-I producing properties were described in IBD, either preventing *(Yang et al., 2016)* or exacerbating the disease *(Prete et al., 2013)*. **Nevertheless, there was no clear evidence for pDC function in IBD pathogenesis**.

To study the function of pDCs in IBD pathogenesis we adopted a similar approach to the one conducted to understand their function in SLE. We established as previously described a *Tcf4* haplodeficiency in Wiskott-Aldrich syndrome protein (*Was*) deficient mice and a conditional deletion (CKO) of *Tcf4* specifically in pDCs in IL-10 (*Il10*) deficient mice. WAS KO humans and mice show major immune dysregulation, including systemic autoimmunity and IBD *(Prete et al., 2013)*. Both in human and mice, pDC overproduction of IFN-I was suggested to exacerbate autoimmunity and IBD pathogenesis mediated by WAS deficiency *(Prete et al., 2013)*. Genetic studies associated *IL10* to human IBD and mice deficient for *Il10* develop a severe colitis *(Kühn et al., 1993)*. IL-10 is an anti-

inflammatory and regulatory cytokine preventing aberrant immune responses, and its production, in particular by macrophages in the gut, plays a crucial role in suppressing the overt immune activation induced by the microbiota and consequently the development of IBD *(Ip et al., 2017; Zigmond et al., 2014)*. We observed that *Tcf4* haplodeficiency or CKO reduced pDC numbers and abrogated their function in both disease models. However, the overall autoimmunity in *Was* KO mice and the development of colitis in both *Was* and *Il10* deficient mice was not impacted by *Tcf4* haplodeficiency or pDC-specific CKO, respectively. Indeed, mice lacking or not pDCs exhibited a colon shortening and a profound colonic inflammation as reflected by a massive infiltration of immune cells in the colonic mucosa. These results indicated that pDCs are dispensable for the IBD pathogenesis *(Sawai et al., 2018)* and were in contradiction with a study claiming that pDCs exacerbate colitis *(Arimura et al., 2017)*. These conflicting results likely rely on the use of Siglec H-DTR mice in the latter study which not only deplete pDCs after diphtheria toxin treatment but also a population of intestinal macrophages that may be important in IBD pathogenesis *(Swiecki et al., 2014)*. In addition, the use of a colitis induced by dextran sodium sulfate (DSS) treatment differ greatly from the genetic models of colitis used in our study. DSS-induced colitis mostly depends on the disruption of the intestinal barrier while in *Was* and *Il10* KO mice colitis is due do dysregulations of immune cells functions *(Kiesler et al., 2015)*. Nevertheless, our study indicates that contrary to SLE, IBD patients may not benefit from therapies targeting specifically pDCs. This project was funded by the company MedImmune, developed in collaboration with Dr. Reizis and performed by 3 graduate students (Serpas Lee, Jang Guenhyo and Rashidfarrokhi Ali) that I directly supervised.

b. *Cellular and molecular mechanisms of SLE caused by Dnase1l3 deficiency*

Plasmacytoid dendritic cells promote extrafollicular anti-DNA responses in lupus through type I interferon
Soni C, Perez O.A, Woss W.A, Serpas L, Mehl J, Goike J, Georgiou G, Ippolito G.C, Sisirak V* and Reizis B*, **Immunity**. 2020 May 19:S1074-7613(20)30173-4. (*co-corresponding authors). (*See **Annex 5***)

As discussed previously, we have shown that *Dnase1l3* deficiency causes SLE as manifested by that production of anti-DNA and anti-nucleosome antibodies and ultimately a glomerulonephritis (**Fig. 4A-C**). The development of SLE in these mice was dependent of MyD88 signaling and independent of intracellular DNA sensors cGAS and absent in melanoma (AIM)-2 *(Sisirak et al., 2016)*. These observations suggested that SLE development in *Dnase1l3*-deficient mice relied on TLRs that are involved in nucleic acid sensing. We therefore crossed *Dnase1l3* KO mice with those that are deficient for *Tlr9*, which is a endolysosomal PRR specialized in the recognition of DNA *(Bauer et al., 2001; Hemmi et al., 2000)*. *Dnase1l3-Tlr9* double KO (DKO) mice developed autoreactivity directed against DNA and nucleosomes and also displayed mild glomerulonephritis, indicating that TLR9 did not play a major role in SLE pathogenesis induced by *Dnase1l3* deficiency.

TLR7 is another endolysosomal nucleic acid sensor that in addition to single stranded RNA *(Diebold et al., 2004)* was recently reported to recognize nucleic acid degradation products (including deoxyguanosines) *(Shibata et al., 2016)*. We therefore established KO mice for both *Dnase1l3* and *Tlr7*, and observed that these mice developed as well all the cardinal features of SLE. To address whether TLR7 and TLR9 share redundant functions we established tripe KO (TKO) animals for *Dnase1l3* and both *Tlr7* and *Tlr9*. These TKO mice were protected from SLE development and were a phenocopy of *Dnase1l3-Myd88* DKO mice, indicating that both TLR7 and TLR9 play a crucial role in SLE pathogenesis induced by *Dnase1l3* deficiency. We next wanted to assess B cell-specific endosomal TLR contribution to SLE pathogenesis *in vivo*. For that purpose, we developed *Dnase1l3* deficiency on recombination activating gene 1 (*Rag1*) KO background. RAG1 is an essential enzyme that is responsible for T cell receptor (TCR) and B cell receptor (BCR) recombination, and thus its deficiency abolishes the development of the adaptive branch of the immune system including T cells and B cells *(Mombaerts et al., 1992)*. We transferred WT and *Dnase1l3* KO lymphocytes in *Dnase1l3-Rag1* DKO mice as well as in *Rag1* single KO mice and observed that regardless of the origin of lymphocytes, only *Dnase1l3-Rag1* DKO recipient mice developed auto antibodies directed against self-DNA and nucleosomes (**Fig. 6A-B**). These results proved that DNASE1L3 is produced by non-lymphoid cells and acts in a cell-extrinsic manner to enforce tolerance to DNA and established a system to test the role of individual genes specifically in lymphocytes in this model. By using splenocytes from *Myd88* KO, we observed that the anti-DNA response was abrogated upon their transfer into *Dnase1l3-Rag1* DKO recipients (**Fig. 6B**). Similar results were obtained when

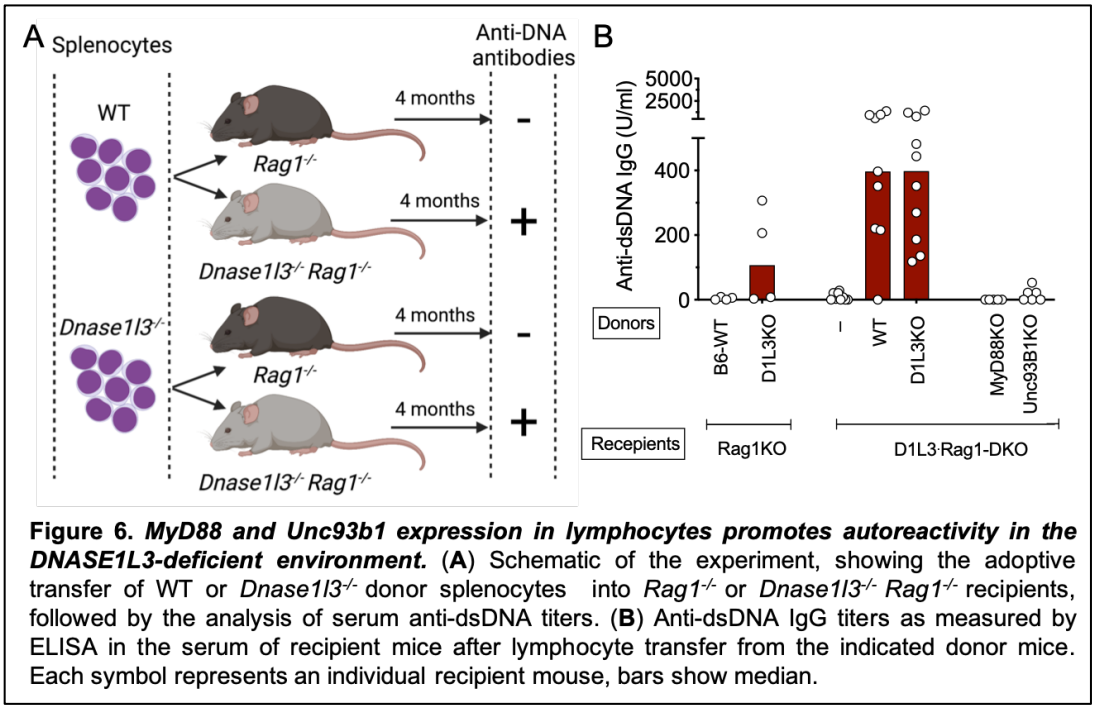

Figure 6. ***MyD88 and Unc93b1 expression in lymphocytes promotes autoreactivity in the DNASE1L3-deficient environment.*** (**A**) Schematic of the experiment, showing the adoptive transfer of WT or *Dnase1l3*$^{-/-}$ donor splenocytes into *Rag1*$^{-/-}$ or *Dnase1l3*$^{-/-}$ *Rag1*$^{-/-}$ recipients, followed by the analysis of serum anti-dsDNA titers. (**B**) Anti-dsDNA IgG titers as measured by ELISA in the serum of recipient mice after lymphocyte transfer from the indicated donor mice. Each symbol represents an individual recipient mouse, bars show median.

lymphocytes from Unc-93 homolog B1 (*Unc93b1)* KO mice were transferred in *Dnase1l3-Rag1* DKO (**Fig. 6B**). Consistent with the essential role of UNC93B1 in the endosomal TLR trafficking and

signaling *(Majer et al., 2019)*, these collective results have established B cell intrinsic roles for TLR7 and TLR9 in SLE pathogenesis mediated by DNASE1L3 deficiency.

The TLR7/9-MyD88 pathway also induces the production of multiple inflammatory cytokines including IFN-I *(Crowl et al., 2017)* mostly in a B cell-extrinsic manner. The vast majority of SLE patients display an IFN-I signature and this IFN-I signature is associated with disease severity *(Banchereau et al., 2017; Bennett et al., 2003)*. In addition, deletion of IFN-I receptor *(Ifnar)* in multiple experimental models of SLE ameliorated the disease *(Buechler et al., 2013; Santiago-Raber et al., 2003)*. To test IFN-I function in SLE induced by *Dnase1l3* deficiency, we established *Dnase1l3-Ifnar* DKO mice. These mice developed early autoreactivity to DNA and nucleosomes, but this autoreactivity was not amplified over time and did not cause kidney pathology at endpoint. These observations indicated that IFN-I is not required for the initiation of autoimmunity in *Dnase1l3* KO mice but rather to exacerbate the disease. We obtained similar results when we crossed *Dnase1l3* KO mice with *Tcf4* haplodeficient mice which lack the transcription factor E2-2 that is essential for the development of pDCs, suggesting that pDCs are likely the main source of IFN-I contributing to SLE in *Dnase1l3* KO mice. Accordingly, anti-Siglec H antibody mediated inhibition of pDCs production of IFN-I *in vivo* reduced the production of anti-DNA antibodies in *Dnase1l3* KO mice.

TLR7 was previously shown to be essential for the generation of the GC reaction and thus for the activation of T cell dependent B cell responses *(Soni et al., 2014)*. We have observed that while *Dnase1l3-Tlr7* DKO animals did not display GC in their spleens they still developed autoreactivity towards DNA. Therefore, autoreactive B cells in *Dnase1l3* KO mice were likely activated outside of the GC to produce autoantibodies. This was in line with our observation that plasmablasts ($CD138^+$ $CXCR3^+$, $MHC\text{-}II^+$ B cells) that accumulate in *Dnase1l3* KO mice were located in the extrafollicular space and did not display any somatic

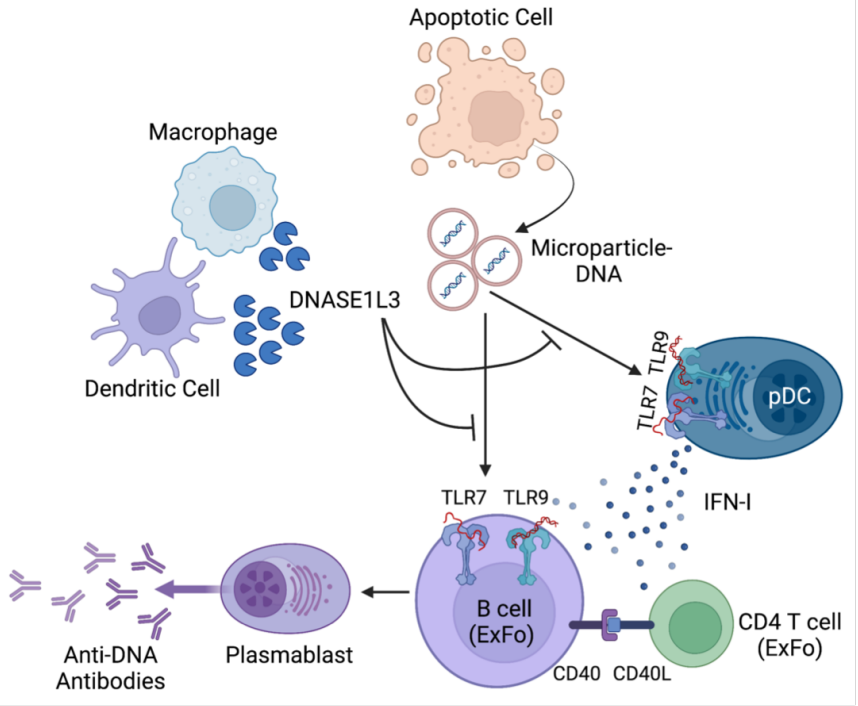

Figure 7. ***Mechanisms of action involved SLE mediated by Dnase1l3 deficiency.***
In the absence of DNASE1L3 produced by dendritic cells and macrophages, DNA associated to microparticles originating from dying cells accumulates and consequently stimulates plasmacytoid dendritic cells (pDCs) and B cells through toll like receptors (TLR) 7 and 9. The stimulation of pDCs induces the production of type I interferons (IFN-I) which together with the help provided by extrafollicular T cells (ExFo) further activate autoreactive B cells in the extrafollicular space and promote their differentiation into plasmablasts producing anti-DNA antibodies.

hypermutation, a hallmark of the GC reaction. Given the extrafollicular nature of autoreactive B cell responses in *Dnase1l3* KO mice we wondered whether they required T cell help. Therefore, we deleted *Cd40lg*, which is a molecule expressed by T cells that plays an essential role in B cell help *(Lesley et al., 2006),* in *Dnase1l3* KO mice. *Dnase1l3-Cd40lg* DKO mice did not show autoreactivity to DNA, reflecting the crucial nature of CD4 T cell help in this SLE model. In parallel, we observed an expansion of extrafollicular T cell ($CD4^+$, $CD62L^-$, $PSGL1^-$, $CD40L^{+++}$, $ICOS^{+++}$) which were located in close vicinity to extrafollicular plasmablasts in *Dnase1l3* mice. Finally, we showed that through their production of IFN-I, pDC play and important role in the extrafollicular development of autoreactive B cells. Indeed, pDC depletion and *Ifnar* deficiency in *Dnase1l3* KO mice significantly reduced the number of extrafollicular plasmablasts and T cells. In addition, pDCs were able to promote B cell differentiation into $CD138^+$ plasmablasts in an IFN-I dependent manner upon their *in vitro* activation. This work therefore deciphered the cellular and molecular mechanisms involved in SLE induced by *Dnase1l3* deficiency *(Soni et al., 2020)*. In particular, DNA that accumulates in MPs in *Dnase1l3* KO mice stimulate autoreactive B cells via both TLR7 and TLR9. This activation of autoreactive B cells occurs in the extrafollicular space, requires CD4 T cell help and IFN-I produced by pDCs, and ultimately leads to their differentiation into short-lived plasma cells producing anti-DNA antibodies (**Fig. 7**). This work was conducted together with Dr. Reizis and presented on multiple occasions at conferences as well as at national and international institutes.

c. *Dnase1l3 deficiency does not affect SSc pathogenesis in vivo*

Innate Immunity in Systemic Sclerosis Fibrosis: Recent Advances
Laurent P*, Sisirak V*, Lazaro E, Richez C, Duffau P, Blanco P, Truchetet ME, Contin-Bordes C, **Frontiers in Immunology**. 2018 Jul 23;9:1702. (*co-first authors)
Elevated Circulatory Levels of Microparticles Are Associated to Lung Fibrosis and Vasculopathy During Systemic Sclerosis.
Leleu D, Levionnois E, Laurent P, Lazaro E, Richez C, Duffau P, Blanco P, Sisirak V, Contin-Bordes C, Truchetet M-E, **Frontiers in Immunology**. 2020 Oct 23;11*:532177*
DNASE1L3 does not affect Systemic Sclerosis pathogenesis in two inducible models of the disease.
Garreau A, Dubois M, Santa P, Brisou D, Laurent P, Duluc D, Loizon S, Blanco P, Contin-Bordes C, Truchetet M-E and Sisirak V ***Manuscript in Preparation***

After joining Immunoconcept I also interacted with Dr. Contin-Bordes and Pr. Truchetet, members of the team of Pr. Blanco who are expert in the physiopathology of systemic sclerosis (SSc). SSc is a heterogeneous autoimmune disease characterized by three interconnected hallmarks (i) vasculopathy, (ii) aberrant immune activation (autoantibody production), and (iii) fibroblast dysfunction leading to extracellular matrix deposition and fibrosis, primarily in the skin and the lung *(Gabrielli et al., 2009)*. Such tissue fibrosis ultimately causes lethal organ failure making SSc one of the deadliest autoimmune disease *(Gabrielli et al., 2009)*. Interestingly, as we recently reviewed, innate immune cells play a major role in SSc pathogenesis including pDCs through their production

of IFN-I *(Laurent et al., 2018)*. The induction of IFN-I by pDCs in SSc was suggested to be mediated by self-DNA *(Ah Kioon et al., 2018; Lande et al., 2019)*. In addition, genetic studies have reported that a polymorphism in *DNASE1L3,* which causes the R206C mutation in the protein, was associated with SSc development *(Mayes et al., 2014; Zochling et al., 2014)*. The R206C mutation reduces DNASE1L3 function and secretion *(Coke et al., 2021)*, and SSc patients with such mutations were recently shown to display reduced circulatory DNASE1L3 activity and, consequently, impaired circulatory DNA fragmentation *(Skaug et al., 2023)*. **Hence, we studied whether *Dnase1l3* deficiency affects SSc pathogenesis *in vivo* and if so through which mechanisms.**

To explore the role of DNASE1L3 in SSc development we used two inducible model of SSc in *Dnase1l3* KO mice. The first model consists of daily subcutaneous injection of bleomycin, which is an antibiotic produced by *Streptomyces verticillus* and commonly used in the clinic for the treatment of cancer patients. Bleomycin causes tissues fibrosis at the site of the injection and, according to the dose that is administered, tissue fibrosis can also affect the lung *(Artlett, 2014)*. The second model is based on daily subcutaneous injections of hypochlorous acid (HOCl), which induces the generation of hydroxyl radicals leading to increased synthesis of collagen in the skin and lung, ultimately causing fibrosis *(Artlett, 2014)*. These two inducible models mostly instigate tissue fibrosis without triggering the development of autoantibodies and vascular defects that commonly affect SSc patients. Nevertheless, SSc induced in both models was reported to mediate innate immune activation that further fuels tissues fibrosis *(Laurent et al., 2018; Meng et al., 2019)*. We observed that bleomycin treatment induced skin thickening and lung fibrosis whereas HOCl treatment only induced skin thickening (**Fig. 8-9**). Tissue fibrosis was unaffected by *Dnase1l3* deficiency as

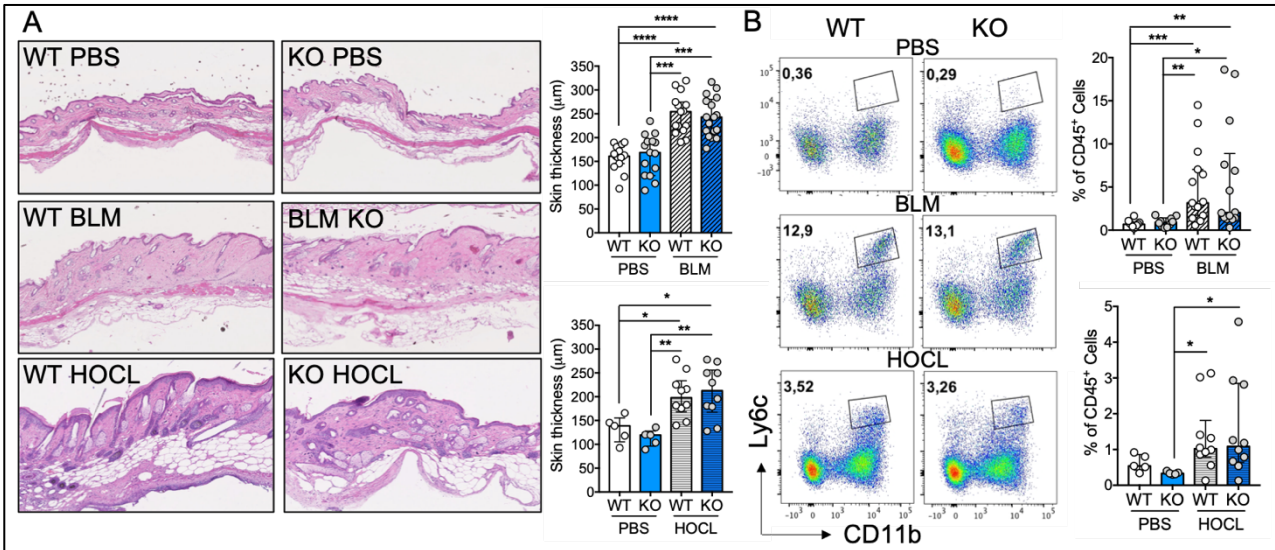

Figure 8. *Dnase1l3 deficiency does not affect skin fibrosis and inflammation induced by SSc development.*
WT and *Dnase1l3* KO mice were injected with PBS, bleomycin (BLM) or hypochlorous acid (HOCL) and their skins were harvested on day 30 for BLM and on day 40 for HOCL treatments. (**A**) Representative images of H&E stained skin sections of the indicated mice. Right panels indicate the measures of the skin thickness of individual indicated mice. (**B**) Representative flow cytometry plots of inflammatory monocytes infiltrating the skin identified as $CD45^+Ly6G^-Ly6C^+CD11b^+$ cells and quantification of their frequency among $CD45^+$ cells in the indicated animals. Data are presented as median with interquartile range and statistical significance was evaluated using nonparametric Kruskal Wallis test. *P<0.05, **P<0.01, ***P<0.001, ****P<0.0001.

reflected by the quantification of skin thickening and of lung collagen levels (Picro Sirius staining) (**Fig. 8A-9A**). The expression of profibrotic genes (*Col1a1, Col2a1* and *Tgfb1*) was increased by bleomycin treatment in the lung while HOCl only induced their expression in the skin. Nevertheless, the level of profibrotic gene expression was similar between WT and *Dnase1l3* KO mice (not shown). Induction of tissue fibrosis in both murine models of SSc was accompanied by immune changes in the affected tissues. In particular, in the skin we observed an increase in inflammatory monocytes ($CD11b^+$ $Ly6C^+$) (**Fig. 8B**) as well as granulocytes ($CD11b^+$ $Ly6G^+$), while in the lungs of bleomycin-treated animals, we observed an activation of T cells reflected by their increased expression of PD1 (**Fig. 9B**) and the accumulation of regulatory T cells ($CD4^+$ $FoxP3^+$). However, this tissue inflammation and immune activation that accompany skin and lung fibrosis was similar between control and *Dnase1l3* deficient mice (**Fig.8B-9B**).

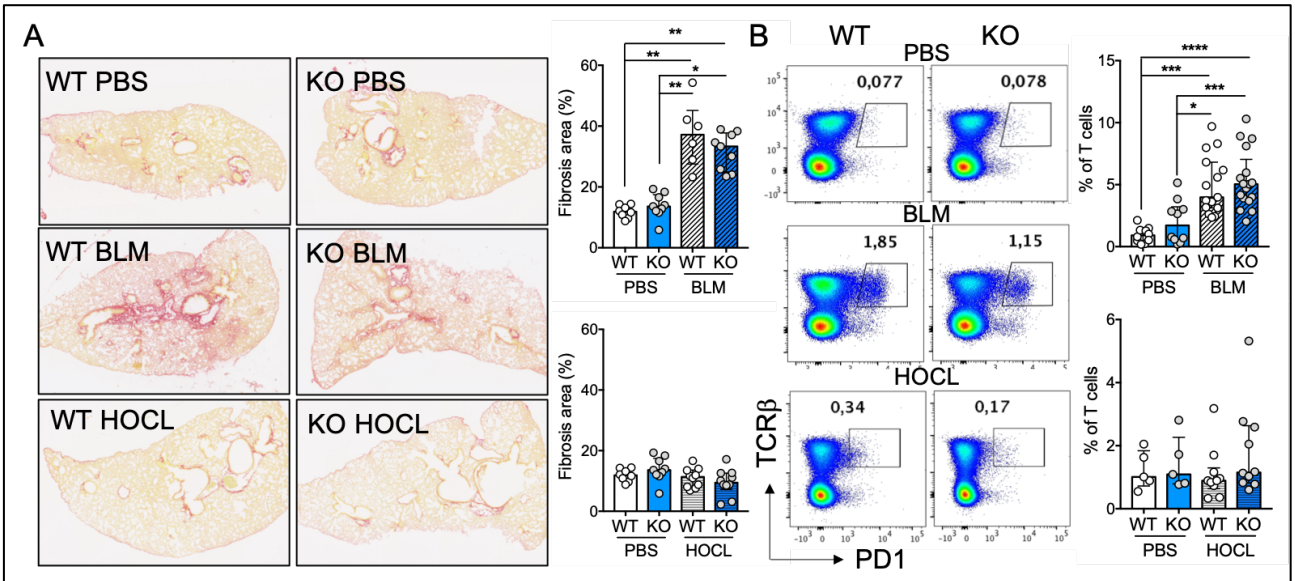

Figure 9. ***Dnase1l3* deficiency does not affect lung fibrosis and inflammation induced by SSc development.** WT and *Dnase1l3* KO mice were injected with PBS, bleomycin (BLM) or hypochlorous acid (HOCL) and their lungs were harvested on day 30 for BLM and on day 40 for HOCL treatments. (**A**) Representative images of Picro Sirus Red (collagen) stained lung sections of the indicated mice. Right panels indicate the percentage of red staining of individual indicated mice. (**B**) Representative flow cytometry plots of lung T cell's expression of PD1 and quantification of $PD1^+$ T cells frequency in the indicated animals. Data are presented as median with interquartile range and statistical significance was evaluated using nonparametric Kruskal Wallis test. *P<0.05, **P<0.01, ***P<0.001, ****P<0.0001.

Finally, we measured the level of total IgG, and we did not see any differences between control and *Dnase1l3* KO mice whether or not they were induced to develop SSc-like disease, indicating that these models do not recapitulate the autoreactive aspect of the disease (not shown). Given that *Dnase1l3* KO animals spontaneously develop anti-DNA autoreactivity we also assessed their levels upon bleomycin and HOCl treatment. While *Dnase1l3* KO mice displayed anti-DNA antibodies in their circulation, this amount was not affected by bleomycin nor HOCl treatment over the course of the experiment (not shown). Therefore, our results indicate that the deletion of *Dnase1l3* does not affect the development of SSc pathogenesis in two inducible models of the disease. Given that the models used in our study are mostly representative of tissue fibrosis, which is one of the three hallmarks of SSc in humans, we believe that it would be relevant to address the impact of *Dnase1l3*

deficiency in genetic models of SSc, for example *Fra2* transgenic mice. This model closely recapitulates the human pathology, in particular the autoimmune component of the disease *(Maurer et al., 2013)*. This work was done by a post-doctoral fellow Dr. Anne Garreau and a Master 2 student Maxime Dubois in Bordeaux who I directly supervised and in close collaboration with Dr. Contin-Bordes and Dr. Truchetet. The manuscript of these results is currently under preparation and will be submitted shortly.

With the group of Pr. Truchetet and Dr. Contin-Bordes, we also analyzed circulatory MPs of SSc patients. Multiple studies have reported that MPs accumulate in both SSc mouse models and patients and have a pathogenic role *(Kavian et al., 2015; Maugeri et al., 2018, 2012)*. Similarly, we observed that SSc patients display increased levels of circulatory MPs compared to heathy donors. These MPs originated from endothelial cells and platelets, and their total level was associated with disease severity, particularly interstitial lung disease and lung fibrosis. Contrary to those of control individuals, MPs from SSc patients stimulated the production of extracellular matrix by fibroblasts *in vitro*. These results that we recently published *(Leleu et al., 2020)* indicate that SSc patients accumulate MPs in their circulation and that these MPs have pathogenic functions through their ability to induce tissue fibrosis. There are ongoing studies to identify the molecules and the pathways that are involved in this profibrotic function of SSc patients' circulatory MPs.

d. Collaborative studies: Dnase1l3 function in sporadic SLE and in the regulation of circulatory DNA content and quality

Autoantibody-mediated impairment of DNASE1L3 activity in sporadic systemic lupus erythematosus
Hartl J, Serpas L, Wang Y, Rashidfarrokhi A, Perez OA, Sally B, Sisirak V, Soni C, Khodadadi-Jamayran A, Tsirigos A, Caiello I, Bracaglia C, Volpi S, Ghiggeri GM, Chida AS, Sanz I, Kim MY, Belmont HM, Silverman GJ, Clancy RM, Izmirly PM, Buyon JP, Reizis B, **Journal of Experimental Medicine**. 2021 May 3;218(5):e20201138.
Plasma DNA Profile Associated with DNASE1L3 Gene Mutations: Clinical Observations, Relationships to Nuclease Substrate Preference, and In Vivo Correction
Chan RWY, Serpas L, Ni M, Volpi S, Hiraki LT, Tam LS, Rashidfarrokhi A, Wong PCH, Tam LHP, Wang Y, Jiang P, Cheng ASH, Peng W, Han DSC, Tse PPP, Lau PK, Lee WS, Magnasco A, Buti E, Sisirak V, AlMutairi N, Chan KCA, Chiu RWK, Reizis B, Lo YMD, ***American Journal of Human Genetics***. 2020 Nov 5;107(5):882-894.
Dnase1l3 deletion causes aberrations in length and end-motif frequencies in plasma DNA
Serpas L, Chan RWY, Jiang P, Ni M, Sun K, Rashidfarrokhi A, Soni C, Sisirak V, Lee WS, Cheng SH, Peng W, Chan KCA, Chiu RWK, Reizis B, Lo YMD, **Proc Natl Acad Sci USA**. 2019 Jan 8;116(2):641-649.
Selectins impair regulatory T cell function and contribute to systemic lupus erythematosus pathogenesis
Scherlinger M, Guillotin V, Douchet I, Vacher P, Boizard A, Guegan J.P, Garreau A, Merillon N, Vermorel A, Ribeiro E, Machelart I, Lazaro E, Couzi L, Duffau P, Barnetche T, Pellegrin J.L, Viallard J.F, Saleh M, Schaeverbeke T, Truchetet M.E, Contin-Bordes C, Legembre P, Sisirak V, Richez C* and Blanco P*. **Science Translational Medicine**. 2021 Jun 30;13(600):eabi4994 (*co-corresponding authors)

We collaborated with Dr. Lo in Hong Kong who is an expert in the field of circulatory cell free DNA (cfDNA) to address the role of DNASE1L3 in the regulation of the quantity and the quality of circulatory cfDNA. We observed in both mice and humans that DNASE1L3 deficiency impacts the length and abundance of DNA in the circulation. The dominant cfDNA species of control individuals has a size of 166bp and corresponds to a single nucleosome. In DNASE1L3-deficient individuals this DNA species remains the dominant one, but there is a significant increase in larger DNA of polynucleosomal origin, indicating that DNASE1L3 plays an important role in cfDNA fragmentation. Accordingly, the cfDNA fragmentation index was 100 times inferior in DNASE1L3-deficient individuals compared to healthy donors. Furthermore, upon sequencing of cfDNA from DNASE1L3-deficient mice and humans, we observed a depletion of DNA fragments starting with CC nucleotides. We identified 8 end motifs of DNA starting with CC that were significantly reduced upon DNASE1L3 deficiency, indicating that DNASE1L3 fragments DNA at specific sites. Distribution of end motifs of cfDNA can be used as a readout of DNASE1L3 activity. Indeed, supplementation of *Dnase1l3* KO mice with an adenovirus encoding a human DNASE1L3 reconstituted cfDNA fragmentation profile and the distribution of end-motifs of cfDNA. Overall these results showed that DNASE1L3 controls the length and end-motifs of circulatory cfDNA *(Chan et al., 2020; Serpas et al., 2019)*.

We also continued our collaboration with Dr. Jill Buyon and Dr. Robert Clancy (Department of Rheumatology, New Your University Langone Medical Center) to understand the relevance of DNASE1L3 function in sporadic SLE patients. We reported that >50% of sporadic SLE patients with nephritis manifested reduced circulatory DNASE1L3 activity, which was associated with neutralizing autoantibodies to DNASE1L3. These patients had normal total plasma cfDNA levels but elevated levels of cfDNA in circulatory MPs. In addition, SLE patients displayed specific autoantibodies directed against MPs originating from dying cells. Pretreatment of MPs with DNASE1L3 prevented the binding of autoantibodies from a fraction of SLE patients. Interestingly, autoantibodies to DNASE1L3-sensitive antigens on MPs were prevalent in SLE patients who had nephritis and correlated with cfDNA levels in MPs and with disease severity. Therefore, our results revealed autoantibody-mediated impairment of DNASE1L3 activity as a common nongenetic mechanism facilitating anti-dsDNA autoreactivity in patients with severe sporadic SLE *(Hartl et al., 2021)*.

Finally, we collaborated with the group of Dr. Blanco at Immunoconcept, which observed that activated platelets from SLE patients express and release high levels of P-selectin. Circulatory levels of soluble or MP-associated P-selectin accumulated in SLE patients and correlated with SLE disease severity. P-selectin was shown *in vitro* to interact with its PSGL1 receptor on Treg cells and to inhibit their suppressive function. Consequently, this inhibition of the suppressive function of Tregs was proposed to exacerbate SLE pathogenesis. To test whether this novel pathogenic loop may play a

role in SLE *in vivo* we evaluated the therapeutic potential of targeting P-selectin in *Dnase1l3* KO mice. We observed that *Dnase1l3* KO mice show elevated levels of circulatory P-selectin particularly associated to MPs compared to control mice. We next treated *Dnase1l3* KO mice every 3 days during 10 weeks with an anti-P-selectin antibody or a control IgG. Anti-P-selectin treatment reduced the levels of anti-DNA autoantibodies and the extent of glomerulonephritis while control IgG did not affect SLE pathogenesis in *Dnase1l3* KO mice. Therefore, blocking P-selectin appears to be an attractive target to treat SLE patients and ameliorate their clinical outcomes *(Scherlinger et al., 2021)*.

e. Conclusions and significance

Overall, we have provided in-depth characterization of the molecular and cellular mechanisms of actions that regulate the development of SLE caused by the deficiency of DNASE1L3. In particular we have shown that sensing of endogenous nucleic acids *via* TLR7 and TLR9 by B cells and pDCs leads to the break of tolerance to DNA and subsequent initiation and maintenance of anti-DNA autoreactivity in *Dnase1l3* KO mice (**Fig. 7**). Furthermore, this autoreactive B cell response in *Dnase1l3* KO mice was shown to take place extrafollicularly and was dependent on CD4 T cell help. These observations are in accordance with data obtained in SLE patients showing that pathogenic B cell responses occur extrafollicularly *(Jenks et al., 2019, 2018)* and provide further rationale for therapies aimed at blocking endosomal TLR7-9 signaling as well as pDC function in SLE patients with *DNASE1L3* null mutations. Intriguingly, our results demonstrated a functional redundancy between TLR7 and TLR9 in the development of SLE in *Dnase1l3* KO mice. Previous studies have shown that TLR9 has a tolerogenic function in an animal model of SLE based on the hyperproliferation of autoreactive B cells (MRL.FAS^{lpr} mice), while TLR7 was reported to promote SLE *(Christensen et al., 2006; Leibler et al., 2022)*. In *Dnase1l3* KO mice both endosomal TLRs appear to be pathogenic, which is likely due to functional competition between the two receptors, whereby TLR9 deletion creates a hyperactive TLR7 *(Fukui et al., 2009)* and/or the ability of TLR7 to recognize both RNA and DNA degradation products such as guanosine and deoxyguanosine, respectively *(Shibata et al., 2016)*. Nevertheless, further studies are required to understand the overlapping functions of TLR7 and TLR9 in SLE development. In addition to the characterization of monogenic SLE induced by the deficiency of DNASE1L3, we have observed that more than 50% of sporadic SLE patients exhibit anti-DNASE1L3 antibodies preventing its function and consequently exacerbating the disease, particularly the development of nephritis. These results that were recently corroborated by the laboratory of Felipe Andrade *(Gomez-Bañuelos et al., 2023)* generalize the crucial role of DNASE1L3 in preventing DNA autoreactivity to sporadic SLE patients. While polymorphisms in DNASE1L3 were also associated to other autoimmune diseases including SSc, we were unable to establish the contribution of DNASE1L3 dysfunction to SSc pathogenesis *in vivo*. The SSc models that we used in this study are not fully representative of the human pathology, and

it will be important to study the impact of *Dnase1l3* deficiency in genetic models of SSc closely recapitulating the human disease. Finally, we also invalidated pDC function in IBD pathogenesis *in vivo,* indicating that contrary to SLE patients, IBD patients may not benefit from therapeutic strategies targeting pDCs.

IV. ONGOING & FUTURE RESEARCH PROJECTS

Thus far we have established that DNASE1L3 controls endogenous levels and likely the quality of extracellular DNA originating from dying cells. This DNASE1L3 function is key in preventing the development of systemic autoimmunity. Multiple studies have also reported that the control of intracellular levels of endogenous DNA by cell-intrinsic DNASEs also protect from the development of fatal auto-inflammatory disorders *(Santa et al., 2021)*. It thus appears that organisms have evolved crucial mechanisms that regulate the abundance and the immunostimulatory potential of endogenous DNA to avoid aberrant immune activation. The recognition of endogenous DNA by the immune system has recently been described to play an important role in pathological contexts beyond autoimmune and inflammatory disorders. Indeed, DNA originating from tumor cells was shown to activate anti-tumor immune responses as well as to boost the therapeutic efficacy of conventional cancer therapies (chemotherapy and radiotherapy) and immunotherapies *(Woo et al., 2015)*. In addition, endogenous DNA originating from adipocytes and hepatocytes of obese mice and humans was reported to stimulate chronic low grade inflammation that is responsible for the development of obesity-induced complications, including metabolic syndrome and type 2 diabetes (T2D) *(Ferriere et al., 2020)*. **While the function of endogenous DNA in cancer immunity and obesity-induced inflammation is clearly established, the function of DNASEs and how they regulate the immunostimulatory potential of endogenous DNA in these pathological contexts remain unknown**. Therefore, we developed two projects to characterize the involvement of DNASE1L3 and more generally of extracellular DNASEs in cancer and obesity and to further delineate their mechanisms of actions in these pathological contexts.

1. WHAT IS THE ROLE OF DNASE1L3 IN OBESITY-MEDIATED INFLAMMATION?

Self-nucleic acid sensing: a novel crucial pathway involved in obesity-mediated metaflammation and metabolic syndrome
Ferriere A, Santa P, Garreau A, Bandopadhyay P, Blanco P, Ganguly D and Sisirak V, **Frontiers in Immunology**. 2021 Jan 26;11:624256.
DNASE1L3 deficiency exacerbates obesity-mediated inflammation and metabolic syndrome
Ferriere A*, Roubertie A*, Bandopadhyay P, Santa P, Garreau A, Loizon S, Duluc D, Brisou D, Monchaux C, Rousseau B, Mora Charrot L, Gatta-Cherifi D, Cota D, Capuron L, Castanon N, Blanco P, Ganguly D and Sisirak V. (*co-fist authors **)To be submitted** (*See **Annex 6***)

a. *Rationale and driving hypothesis*

Obesity is a major global health issue, and its prevalence is constantly growing. It is estimated that more than 40% of the adult world population is overweight and 13% is obese. Obesity is associated with the development of metabolic syndrome, which constitute a main risk factor for the development of T2D, non-alcoholic fatty liver disease (NAFLD), atherosclerosis, and ischemic cardiovascular disease *(Saltiel and Olefsky, 2017*). These obesity-induced health complications have far-reaching consequences for life expectancy, quality of life and healthcare costs. The main tissue affected by obesity is the white adipose tissue (WAT), which becomes hypertrophied and heavily infiltrated by immune cells *(Saltiel and Olefsky, 2017*). A critical role for both the immune cell infiltration into the WAT and the ensuing WAT chronic low-grade inflammation called "metaflammation" was established in the development of obesity-associated metabolic syndrome *(McNelis and Olefsky, 2014)*. Specifically, anti-inflammatory M2-like macrophages (expressing CD301b) present in the lean WAT are polarized toward a proinflammatory M1-like phenotype (expressing $CD11c^{+}$) in the WAT of obese individuals and contribute to the development of insulin resistance (IR) through their production of inflammatory cytokines *(McNelis and Olefsky, 2014)*. However, the molecular mechanisms that contribute to WAT inflammation are not fully understood.

Aberrant accumulation of self-DNA and its recognition by innate immune cells was recently linked to obesity-induced WAT metaflammation as we have recently reviewed *(Ferriere et al., 2020)*. Indeed, obese individuals and mice exposed to a high-fat diet (HFD) show increased levels of circulatory cfDNA *(Garcia-Martinez et al., 2016; Nishimoto et al., 2016)*. The source and form of such cfDNA are multiple. Hepatocytes affected by NAFLD release MPs containing mtDNA *(Garcia-Martinez et al., 2016)*, while neutrophils release extracellular DNA traps (NETs) during obesity *(Revelo et al., 2016)*. Aberrant adipogenesis caused by obesity promotes adipocyte cell death, leading to the release of gDNA as well as mtDNA *(Nishimoto et al., 2016; Strissel et al., 2007)*. Notably, circulatory levels of cfDNA positively correlated with the severity of metabolic syndrome caused by obesity *(Garcia-Martinez et al., 2016; Nishimoto et al., 2016)*. The sensing of cfDNA via TLR-9 by macrophages *(Garcia-Martinez et al., 2016)* and pDCs *(Ghosh et al., 2016)* was shown to play an important role in WAT inflammation. Specifically, IFN-I produced by pDCs upon cfDNA detection promoted the switch from M2 to M1-like macrophages as well as the depletion of Tregs in the WAT of obese individuals *(Ghosh et al., 2016; Li et al., 2021)*. These observations are consistent with genetic studies showing that *Tlr9* deficiency ameliorated T2D and NAFLD development induced by obesity *(Garcia-Martinez et al., 2016; Nishimoto et al., 2016; Revelo et al., 2016)*. Moreover, pDC ablation and deficiencies in IFN-I responsiveness (*Ifnar*) and production (*Irf7*) were shown to ameliorate complications due to obesity *(Hannibal et al., 2017; Wang et al., 2013)*. Finally, mtDNA accumulation during obesity was suggested to promote WAT inflammation through activation of the cytosolic DNA sensors cGAS. Accordingly, loss of STING, which is essential for the transduction of

cGAS signaling, prevents metabolic syndrome induced by HFD *(Luo et al., 2018; Yu et al., 2019)*. Circulatory mtDNA isolated from obese patients was also reported to promote IL-1β production via AIM2 activation in macrophages *(Bae et al., 2019)*; however, the *in vivo* role of AIM2 in obesity remains controversial *(Gong et al., 2019)*. Thus, self-cfDNA clearly participates in obesity-induced inflammation, but how its abundance is regulated during obesity remains unknown.

While obesity represents a risk factor for multiple autoimmune diseases *(Matarese, 2023)*, including SLE *(Hanna Kazazian et al., 2019; Tedeschi et al., 2017)*, the function of DNASEs and their regulation during obesity remain poorly understood. Reports have shown that DNASE2 expression *(Saito et al., 2019)* and the overall circulatory DNASE activity *(Revelo et al., 2016)* may be reduced in mice upon HFD. However, DNASE1L3 function in obesity was never explored. Moreover, treatment of obese mice with recombinant DNASE1 did not affect the development of metabolic syndrome *(Revelo et al., 2016)*, likely due to the limited activity of DNASE1 in digesting "naked" DNA, which is not the main form of endogenous DNA accumulating during obesity. **Therefore, we proposed to dissect the role of DNASE1L3 in the development of metaflammation and the ensuing metabolic syndrome induced by obesity**.

To develop this project we initiated a collaboration with Dr. Ganguly at CSIR-Indian Institute of Chemical Biology in Kolkata, India, who has shown that DNA from the WAT of obese patients contribute to pDC production of IFN-I, which in turn favors the switch of macrophages toward a proinflammatory M1-like phenotype *(Ghosh et al., 2016)*. As coordinators we obtained the support of the Indo-French Centre for the Promotion of Advanced Research to conduct this project. I was also awarded a grant by Agence Nationale de la Recherche (ANR) young researcher program for this project. Amandine Ferriere, an MD-PhD student who graduated in December 2022, initiated this project, and another PhD student Anaïs Roubertie is currently pursuing this work under my supervision.

b. Currents results

Dnase1l3 deficiency increases weight gain in mice fed with HFD: In order to establish the impact of *Dnase1l3* deficiency on obesity-associated metaflammation and metabolic syndrome, we placed WT and *Dnase1l3* KO male mice on HFD containing 45% of fat or on normal diet (ND) as a control. All mice exposed to HFD gained more weight than mice on ND. However, *Dnase1l3* KO mice gained significantly more weight than their WT counterpart after being fed with a HFD (**Fig. 10A-B**). Conversely, *Dnase1l3* KO and WT mice fed with a ND showed no difference in body weight over time. After 12 weeks of HFD, the epididymal (visceral) AT mass was significantly increased in *Dnase1l3* KO mice compared to WT mice (**Fig. 10C**). Elevation in AT mass in *Dnase1l3* KO mice on

HFD was accompanied by an increase in the size of epididymal adipocytes (not shown). In addition, body composition, as evaluated by magnetic resonance imaging (MRI), also showed an increase in the total fat mass in *Dnase1l3* KO mice fed with a HFD when compared to WT mice on the same diet (**Fig. 10D**). In collaboration with Dr. Cota at the Neurocentre Magendie at the University of Bordeaux, we measured the food consumption, energy expenditure as well as feeding behavior of mice, by placing them in metabolic cages. The individual daily food intake and energy expenditure between WT and *Dnase1l3* KO mice was not significantly different (not shown). Yet, *Dnase1l3* KO mice showed an impaired feeding behavior, as manifested by their increased number of meals and increased food intake during diurnal phases, when mice are typically resting (not shown). The aforementioned results were validated with HFD containing 60% of fat as well as in female mice (not shown) and thus clearly indicate that *Dnase1l3* deficiency exacerbates weight gain and adiposity upon induction of obesity by HFD.

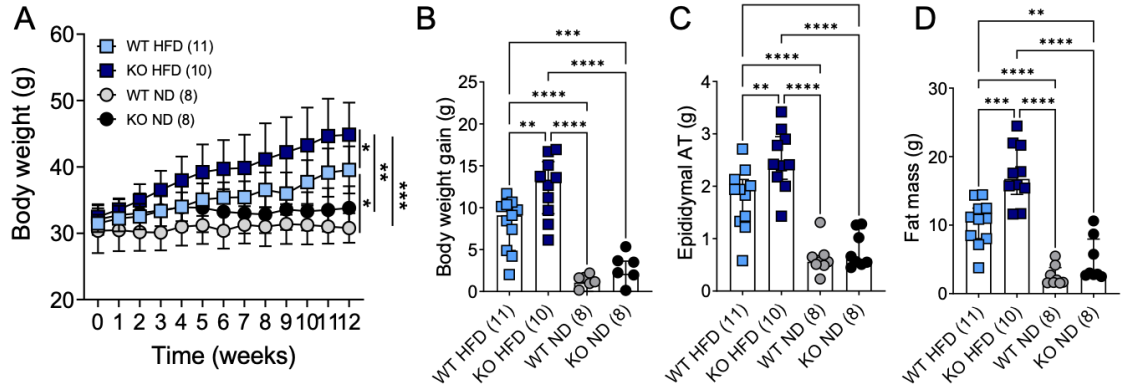

Figure 10. ***Dnase1l3 deficiency increases body weight gain upon high fat diet (HFD).***
WT and *Dnase1l3* KO male mice were exposed to normal (ND) or HFD for 12 weeks, starting at 12 weeks of age. (**A**) Weekly weight measurements of WT and KO mice fed with ND (circles) or HFD (squares). (**B**) Cumulative body weight gain after 12 weeks of diet in the indicated mice. (**C**) Individual weights of epididymal adipose tissue after 12 weeks of ND or HFD of the indicated mice. (**D**) Proportion of fat mass in the indicated mice as determined by magnetic resonance imaging (MRI) after 12 weeks of diet. Data are presented as median with interquartile range and statistical significance was evaluated using nonparametric Kruskal Wallis test. *P<0.05, **P<0.01, ***P<0.001, ****P<0.0001.

Dnase1l3 deficiency exacerbates the metabolic syndrome and NAFLD induced by HFD: We next assessed the impact of *Dnase1l3* deficiency on the development of metabolic complications associated with obesity. WT and *Dnase1l3* KO mice exposed to HFD containing 45% fat for 12 weeks showed an increased glucose intolerance and fasting glucose levels (**Fig. 11A-B**). In addition, fasting insulin levels were elevated in *Dnase1l3* KO mice that were fed with a HFD, and such elevated insulin levels contributed to the establishment of IR in *Dnase1l3* KO as measured by the HOMA-IR score (not shown). Similar results were obtained when mice were fed with a HFD containing 60% fat, with increased fasting glucose and insulin levels at 6 weeks post-initiation of the diet, indicating that *Dnase1l3* deficiency accelerates the occurrence of a metabolic syndrome in mice exposed to HFD (not shown). We next assessed the impact of *Dnase1l3* deficiency on the liver damage induced by obesity. We quantified alanine aminotransferase (ALAT) circulatory levels as a

marker of ongoing liver injury. After only 6 weeks of HFD there was an increase in circulatory ALAT levels specifically in *Dnase1l3* KO mice (not shown). The liver mass was not impacted at 12 weeks of HFD; however, hepatic steatosis was only increased in *Dnase1l3* KO mice (**Fig. 11C-D**), indicating that *Dnase1l3* deficiency also accelerate the onset of obesity-associated hepatic disorders.

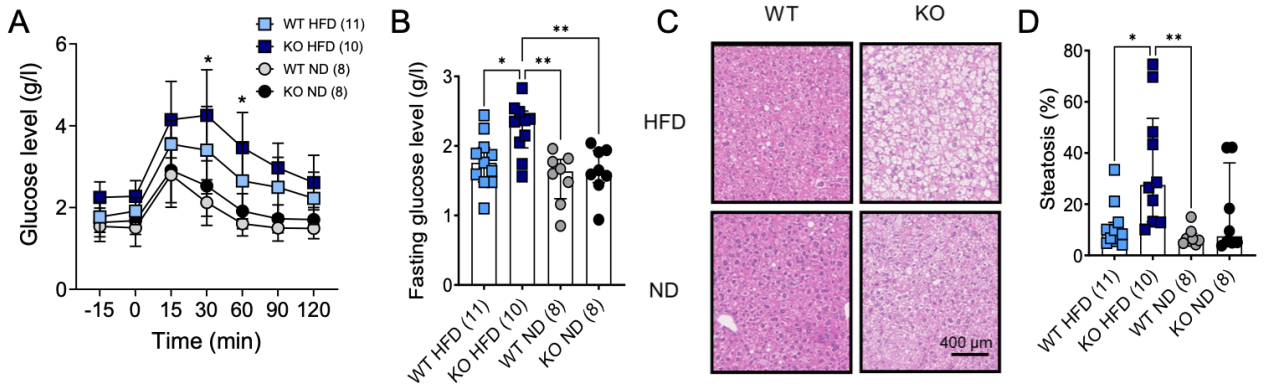

Figure 11. ***Dnase1l3* deficiency exacerbates glucose intolerance and liver steatosis induced by HFD.** WT and *Dnase1l3* KO male mice were exposed to normal (ND) or high fat diet (HFD) for 12 weeks, starting at 12 weeks of age. (**A**) Glucose tolerance tests were performed 12 weeks after diet initiation by the intraperitoneal injection of a glucose and the evaluation blood glucose levels at the indicated time points (**B**) Fasting blood glucose levels as measured 12 weeks after diet initiation. (**C**) Representative liver sections after H&E staining of each indicated group. (**D**) Semi-automated quantification of hepatic steatosis (%) by pathologist blinded to genotypes and experimental conditions. Data are presented as median with interquartile range and statistical significance was evaluated using nonparametric Kruskal Wallis test. *P<0.05, **P<0.01, ***P<0.001, ****P<0.0001.

***Dnase1l3* deficiency increases VAT immune infiltration and inflammation in obese mice**: To evaluate the impact of *Dnase1l3* deficiency on metaflammation induced by obesity, we used flow cytometry to analyze the immune compartment ($CD45^+$ cells) in the stromal vascular fraction (SVF) obtained from VAT of WT and *Dnase1l3* KO mice subjected or not to HFD. As expected, mice fed with a HFD containing 45% of fat during 12 weeks showed elevated absolute counts of total leucocytes and $CD11b^+$ and $CD64^+$ $F4/80^+$ macrophages. Importantly, $CD11c^+$ proinflammatory M1-like macrophage frequency, absolute counts and the ratio of M1 to M2 macrophages were significantly increased in the SVF of the VAT of *Dnase1l3* KO mice that were subjected to HFD compared to their WT counterparts (**Fig. 12**). In addition to macrophages, T cells, DCs, monocytes

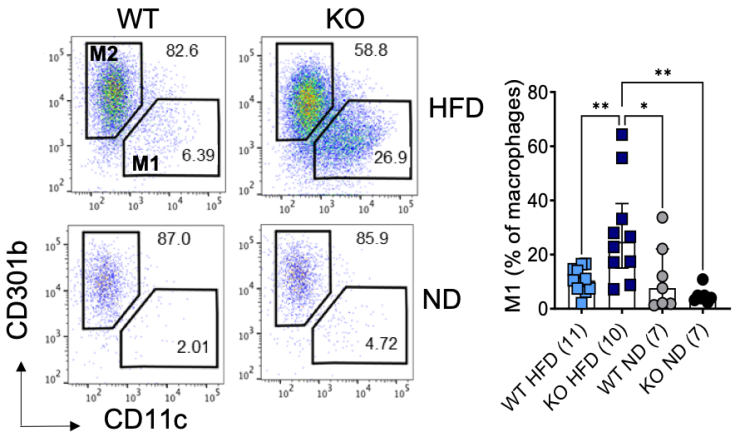

Figure 12. ***Dnase1l3* deficiency exacerbates adipose tissue inflammation induced by HFD.** WT and *Dnase1l3* KO male mice were exposed to normal (ND) or a high fat diet (HFD) and their visceral adipose tissue was harvested and analyzed by flow cytometry 12 weeks after the initiation of the diet. Representative plots of macrophages ($CD45^+$ $CD11b^+$ $CD64^+$ cells) showing an M1-like ($CD11c^+$) or an M2-like ($CD301b^+$) phenotype. Right panel shows the quantification of M1-like macrophages in the indicated mice. Data are presented as median with interquartile range and statistical significance was evaluated using nonparametric Kruskal Wallis test. *P<0.05, **P<0.01, ***P<0.001, ****P<0.0001.

and granulocytes in the SVF of the VAT were increased only in *Dnase1l3* KO mice upon HFD (not shown). Therefore, *Dnase1l3* deficiency increases the metaflammation in the VAT in response to HFD, which likely contributes to the earlier onset of metabolic complications observed in these mice.

Obese individual display elevated levels of cfDNA and reduced DNASE activity: In order to address the human relevance of our observations we initiated a collaboration with Dr. Gatta-Cherifi from the nutrition department of the Bordeaux Hospital and Dr. Capuron and Dr. Castanon from the NeutriNeuro research department at the University of Bordeaux. With their assistance we were able to obtain fresh blood samples of obese patients as well as frozen plasma from a large cohort of obese patients before and after they underwent therapeutic bariatric surgery. We first quantified the circulatory cfDNA in these individuals and observed that obese patients had significantly more cfDNA than age and sex-matched healthy controls (**Fig. 13A**). We observed that most of the cfDNA that accumulates in obese individuals originates from the soluble fraction of the plasma and not from the MP-enriched fraction (**Fig. 13B-C**). Contrary to what was previously reported, we have observed that obese individuals display significantly less MPs in their circulation (**Fig. 13D**). Therefore, we normalized the DNA quantity detected in the MP-enriched fraction to the number of MPs and observed that obese individual's MPs contained more DNA than healthy controls (**Fig. 13E**). The total levels of cfDNA were significantly correlated to pathological features of obese individuals including their body mass index (BMI), circulatory insulin levels and the IR score (not shown and **Fig. 13F**). In addition, in patients who underwent bariatric surgery, circulatory cfDNA levels returned to levels observed in healthy controls (**Fig. 13G**).

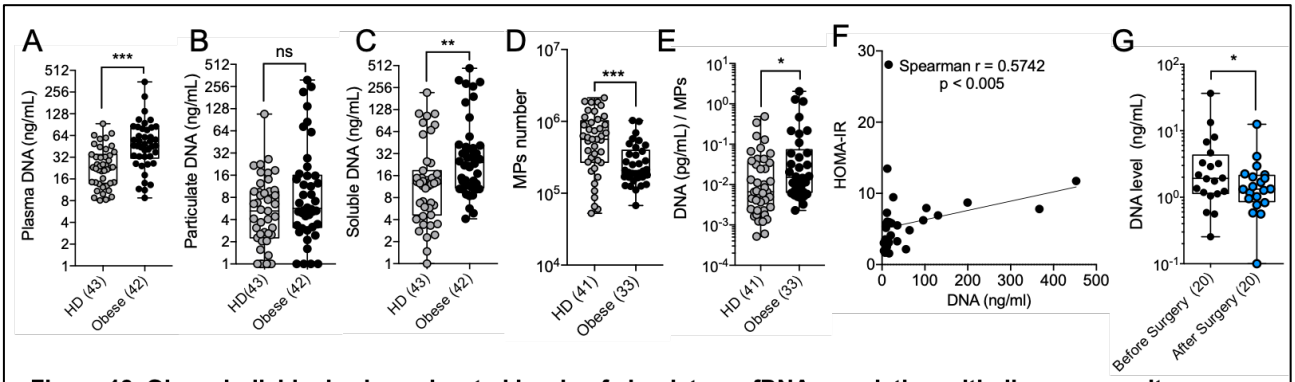

Figure 13. Obese individuals show elevated levels of circulatory cfDNA correlating with disease severity. Circulatory cfDNA levels of obese (OB) and healthy (HD) individuals (**A**) in the whole plasma, (**B**) in the MP-enriched fraction (**C**) in the MP-depleted fraction as measured by Q-PCR. (**D**) MP absolute counts in HD and OB as measured by flow cytometry. (**E**) Ratio of cfDNA quantified in the MP-enriched fraction on MPs counts in order to quantify DNA per MP. (**F**) Correlation between whole plasma cfDNA levels and the extent of insulin resistance (HOMA-IR) in OB individuals. (**G**) Circulatory cfDNA levels in in the whole plasma of OB individuals before and 3 to 12 months after bariatric surgery. Data are presented as the mean ± SD and statistical significance was evaluated using the Mann-Withney test and spearman rank correlation test. *p ≤ 0.05, **p ≤ 0.01, ***p ≤ 0.001.

The accumulation of cfDNA in obese individuals may be mediated by an impaired expression and/or activity of circulatory DNASEs. Therefore, we measured *DNASE1L3* expression level in peripheral blood mononuclear cells (PBMC) of obese individuals and healthy controls. We adopted a flow cytometry-based fluorescence *in situ* hybridization (Flow-FISH) strategy, which allows the detection of *DNASE1L3* mRNA simultaneously in all blood immune cells. This approached was selected as currently there are no specific antibodies for DNASE1L3 commercially available. The expression of *DNASE1L3* in PBMCs was detected only in pDCs. However, there were no significant differences in *DNASE1L3* expression in pDCs between heathy donors and obese patients (not shown). We next evaluated total circulatory DNASE activity by addressing the ability of the plasma to digest DNA *in vitro*. We observed that obese patients showed a significantly reduced DNASE activity compared to healthy controls (**Fig. 14A**). Such reduced DNASE activity was inversely correlated with the levels of circulatory cfDNA (**Fig. 14B**). These results suggest that obesity somehow impairs circulatory DNASE activity, which likely contributes to the accumulation of endogenous cfDNA that may ultimately fuel metaflammation.

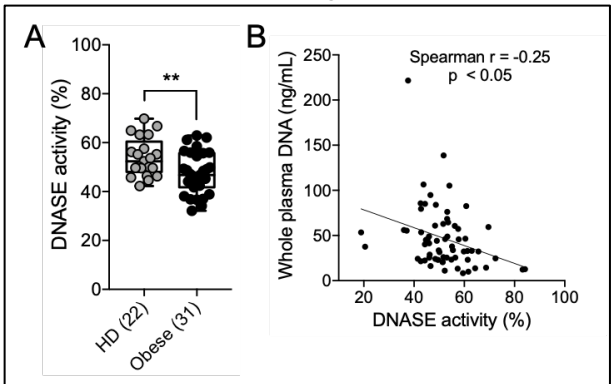

Figure 14. Obese individuals show a reduced DNASE activity. (**A**)Total DNASE activity in the plasma of healthy (HD) and obese (OB) individuals as measured by the Pico-Green assay. (**B**) Correlation between DNASE activity and whole plasma cfDNA levels in HD and OB individuals. Data are presented as the mean ± SD and statistical significance was evaluated using the Mann-Withney test and spearman rank correlation test. . **p ≤ 0.01

These results showing that DNASE1L3 regulates HFD-induced metaflammation and the ensuing metabolic syndrome were recently compiled in a paper that is presented in the **annex 6** and will be submitted shortly. Nevertheless, the mechanism of DNASE1L3 action in metaflammation and metabolic complications induced by obesity remains to be fully elucidated.

c. Future directions

Does DNASE1L3 regulate metaflammation induced by obesity? As we have shown previously the deficiency in DNASE1L3 induces the phenotypic switch of VAT macrophages toward a proinflammatory M1-like phenotype. This constitutes the main sign of AT inflammation and requires further investigation to ascertain the role of DNASE1L3 in the regulation of metabolic tissue inflammation. To do so we quantified the expression of genes encoding inflammatory cytokines involved in metaflammation (*Tnfα, Il-6, Il-1β and Ifnα)* in the liver and the VAT. We did not observe any differences in their expression between WT and *Dnase1l3* KO mice that were fed with a HFD. Consequently, we performed bulk RNA-sequencing on the liver and the VAT of WT and *Dnase1l3* KO mice fed either with a ND or a HFD. These results were obtained very recently, and their analysis

is not yet complete. Unexpectedly, our preliminary results do not show an inflammatory signature in the liver or the VAT of either WT or *Dnase1l3* KO mice upon their exposure to HFD. Nevertheless, we detect multiple differentially expressed genes, particularly in the liver, between WT and *Dnase1l3* KO mice fed HFD, and we are currently analyzing their potential contribution to the phenotype that we observed. The inability to detect metabolic tissue inflammation may be due to our approach to evaluate gene expression that was performed in the total tissue. Hence, we plan to repeat the transcriptomic analyses on purified macrophages and DCs from both the AT and liver of WT and *Dnase1l3* KO mice fed with a ND or a HFD. We are focusing on macrophages and DCs since they play a crucial role in metabolic tissue inflammation and express the highest levels of *Dnase1l3*. This analysis will also allow us to investigate how HFD affects the expression of *Dnase1l3* in macrophages and DCs located in metabolic tissues in WT mice. We have also observed that HFD caused an accumulation of multiple immune cells in the VAT of *Dnase1l3* KO mice, including T cells, NK cells and DCs. Nevertheless, using a basic immunophenotyping we did not observe an increased activation profile of immune cells in the VAT of *Dnase1l3* KO mice in comparison to WT mice that were fed HFD. Therefore, we propose to further characterize the ability of immune cells infiltrating AT to respond to *ex-vivo* stimulation by quantifying their production of inflammatory cytokines by intracellular cytokine staining (spectral flow cytometry). Specifically, the SVF of the VAT will be stimulated with PMA and ionomycin to asses T and NK cell ability to produce IFN-γ, TNF-α, IL-17 and IL-10. In addition, macrophages and DCs will be stimulated with various PRR ligands including DNA (CpG-A, *E. coli*-derived DNA, poly dA:dT, self-DNA…) and their production of TNF-α, IL-12, IL-10 and IFN-α will similarly be evaluated. Given that *Dnase1l3* deficiency exacerbated liver steatosis induced by HFD and that liver steatosis is commonly associated to liver inflammation, we will further characterize liver immune cells, their activation profile, and their ability to produce cytokines in response to stimulation as previously described. The development of liver steatosis is accompanied by the remodelling of liver macrophages. In particular, liver resident macrophages called Kupffer cells ($TIM4^+$ and $CLEC4C^+$) are depleted during the course of liver steatosis development and replaced by monocyte-derived macrophages that adopt a proinflammatory profile and further contribute to liver damage *(Remmerie et al., 2020; Tran et al., 2020)*. In addition, HFD-mediated liver steatosis was reported to cause the shedding of a scavenger receptor TREM2 on liver macrophages, preventing their ability to remove dying cells (efferocytosis), which in turn contribute to local inflammation and the development of NAFLD *(Wang et al., 2023)*. Therefore, an extensive analysis of liver Kupffer cells and monocyte-derived macrophages will be carried out to evaluate the impact of *Dnase1l3* deficiency on their dysfunction induced by HFD. Finally, this exhaustive analysis of metabolic tissue immune cells and their production of cytokines will be performed at 6 weeks and 12 weeks post HFD, to evaluate if the deficiency of *Dnase1l3* accelerates metaflammation that is induced by obesity.

What is the main source of DNASE1L3 during obesity? We have previously shown that *Dnase1l3* is highly expressed in cells of hematopoietic origin including macrophages and DCs. In addition, recent single-cell RNA-sequencing data has shown that liver endothelial cells express high levels of *DNASE1L3* as well. In order to assess whether hematopoietic-specific *Dnase1l3* deficiency contributes to the exacerbation of obesity-associated inflammation and metabolic syndrome, we generated BM chimeras. We transferred WT or *Dnase1l3* KO BM cells into both WT and *Dnase1l3* KO recipients that were conditioned with busulfan, which induces a general myeloablation. This allowed us to generate WT hosts reconstituted with *Dnase1l3* KO hematopoietic cells, *Dnase1l3* KO hosts reconstituted with WT hematopoietic cells, as well as the appropriate controls. Upon successful reconstitution of host mice with the donor hematopoietic cells we placed them on ND and HFD during 12 weeks. Unfortunately, these mice did not gain weight after being fed HFD. Busulfan conditioning induced an important weight loss and altered the animals' appetite, impacting the interpretation of our results. Thus, to further determine the specific source(s) of DNASE1L3 involved in metabolic syndrome induced by obesity, we will take advantage of conditionally targeted *Dnase1l3* (*Dnase1l3*$^{Flox/Flox}$) mice that we obtained in collaboration with Dr. Keyel (Texas Tech University, USA) and Dr. Reizis (New York University, USA). These mice will be crossed with (*Itgax*) CD11c-Cre and (*Lyz2*) LysM-Cre deleter strains (available as live stocks in the laboratory) to generate conditional *Dnase1l3* deficiency in DCs *(Caton et al., 2007)* and macrophages *(Clausen et al., 1999)* respectively. *Dnase1l3* conditional KO mice will be fed ND or HFD and the development of metabolic syndrome and tissue metaflammation will be monitored as previously described. Mice that are *Dnase1l3*$^{Flox/Flox}$ but negative for Cre-recombinase will be used as controls.

Does Dnase1l3 deficiency regulate endogenous DNA levels upon HFD in vivo? We have observed that in the absence of DNASE1L3, mice are more susceptible to metabolic syndrome and metaflammation induced by obesity. However, how DNASE1L3 regulates these processes and through which mechanisms remain open questions. In humans, obesity causes an accumulation of circulatory cfDNA, and we believe that this aberrant DNA accumulation consequently contributes to the activation of innate immune receptors involved in DNA sensing and ultimately causes metabolic tissue inflammation. As with our analysis in human samples, we initiated a quantification of circulatory cfDNA in WT and *Dnase1L3* KO mice that were placed either on ND or HFD. Our initial results show increased amounts of cfDNA in obese mice compared to lean mice. However, no differences in total cfDNA content were observed between WT and *Dnase1l3* KO mice. We will further pursue this analysis by quantifying the abundance of cfDNA by quantitative polymerase chain reaction (q-PCR) in the soluble fraction as well as in the MP-enriched fraction that is obtained upon high speed centrifugation of the plasma. Indeed, there is a possibility that obesity in *Dnase1l3* KO mice specifically enhances the accumulation of DNA within MPs derived from dying cells. In addition to quantifying the genomic cfDNA in the circulation using specific primers for murine repetitive B1

elements, we propose to measure the extent of circulatory mtDNA in each fraction of the plasma using specific primers for mitochondrial genes (*Polg* and *mt-C01*). This is particularly relevant since mtDNA was reported to accumulate in MPs of obese mice and humans *(Garcia-Martinez et al., 2016)* and was shown to exhibit more potent immunostimulatory potential than gDNA *(Caielli et al., 2016)*. In addition to the regulation of systemic cfDNA levels, DNASE1L3 may also have a tissue-restricted function and thus control tissue levels of endogenous cfDNA. To measure tissue content of cfDNA, we will place liver and AT explants in culture from 6 to 48h and measure the content of cfDNA from genomic and mitochondrial origin in the culture supernatants by q-PCR. Finally, a specific type of neutrophil cell death called NETosis was reported to contribute to obesity-mediated metaflammation *(Revelo et al., 2016)*. NETosis is characterized by the release of the nuclear DNA/chromatin in the extracellular space in the form of web-like structures called neutrophil extracellular traps (NETs), and such NET-derived DNA trough the activation of TLR9 was suggested to induce metabolic tissue inflammation *(Revelo et al., 2016)*. Given that DNASE1L3 is involved in the disposal of DNA originating from NETs *(Jiménez-Alcázar et al., 2017)*, we propose to study the abundance of NETs in the liver and AT of WT and *Dnase1l3* KO mice on ND versus HFD. NETs can be detected by florescent microscopy by the evaluation of the citrullinated histone H3 (H3Cit) abundance, which is specifically induced during the process of NETosis.

Does Dnase1l3 deficiency cause aberrant self-DNA sensing during obesity? DNA sensing by innate immune cells including macrophages and pDCs through TLR9 was shown to be involved in the development of metaflammation induced by obesity and consequently in the development of metabolic syndrome, T2D and NAFLD *(Garcia-Martinez et al., 2016; Nishimoto et al., 2016; Revelo et al., 2016)*. pDC-derived IFN-I production, which is activated downstream of TLR9 *(Ghosh et al., 2016)*, and its signalling through IFN-I receptor (*Ifnar*) *(Hannibal et al., 2017)* were also reported to contribute to obesity-mediated metaflammation and metabolic syndrome. The main function of DNASE1L3 is to control extracellular levels of endogenous DNA, which is involved in the activation of endosomal TLRs including TLR9 *(Soni et al., 2020)*. Hence, we propose to establish the involvement of TLR9 and IFN-I in the exacerbation of obesity-induced metaflammation. For this purpose, we recently obtained *Dnase1l3-Tlr9* and *Dnase1l3-Ifnar* DKO mice in collaboration with Dr. Reizis (New York University, USA). These mice, along with the appropriate single KO controls (*Ifnar*, *Tlr9* and *Dnase1l3)*, will be placed on ND or HFD. This will allow us to assess whether *Tlr9* and/or *Ifnar* deficiency prevents the exacerbation of the metaflammation induced by obesity caused by *Dnase1l3* KO, and thus to directly implicate aberrant endogenous DNA sensing in this process. This approach is based on current observations in the field and our own results on DNASE1L3 function. Nevertheless, in the event of negative results, our RNA-sequencing data generated from macrophages and DCs from WT and *Dnase1l3* KO mice fed a ND or HFD will allow us to identify

and test *in vivo* novel pathways involved in the exacerbation of metaflammation induced by *Dnase1l3* deficiency.

Does obesity in humans affects DNASE1L3 expression and function/activity? We have observed that, among PBMCs, *DNASE1L3* in human is mostly expressed by pDCs. *DNASE1L3* expression in blood pDCs is not affected by obesity. It is possible that obesity affects *DNASE1L3* expression in immune cells present in metabolic tissues rather than in the circulation. We have established a collaboration with Dr. Ganguly at the CSIR-Indian Institute of Chemical Biology in Kolkata, India, who has access to fresh AT from obese individual obtained after bariatric surgery. From this AT, we will extract macrophages, cDCs as well as pDCs and quantify their expression of *DNASE1L3* by q-PCR. As a control *DNASE1L3* expression will be measured in macrophages from lean individuals obtained from any abdominal surgeries. While we are sure to isolate macrophages from lean individuals' AT, the numbers of cDCs and pDCs in the AT of lean individuals are low and may likely be insufficient for the quantification of DNASE1L3 expression. We have also recently initiated a collaboration with Dr. Maya Saleh at Immunoconcept, Bordeaux who has performed single-cell RNA-sequencing approaches on liver immune cells from NAFLD affected liver and healthy livers. This approach will also allow us to evaluate how NAFLD mediated by obesity affects *DNASE1L3* expression in liver immune cells. While *DNASE1L3* expression was not affected in the PBMCs of obese patients, we have observed that their overall plasma DNASE activity was significantly reduced compared to healthy individuals. Circulatory DNASE activity was measured by the ability of plasma to digest "naked" DNA and therefore encompasses the activity of both DNASE1 and DNASE1L3. Hence, to further establish the human relevance of our results in mice we want to specifically quantify DNASE1L3 activity in the plasma of obese and lean individuals. We have observed that contrary to DNASE1, DNASE1L3 is capable of fragmenting DNA from purified nuclei. Furthermore, plasma of *DNASE1L3* null patients was unable to fragment nuclear DNA in comparison to the healthy donor plasma, indicating that DNASE1L3 specificity could be addressed by its ability to fragment nuclear DNA. Nuclear DNA fragmentation is detected by gel electrophoresis and is thus difficult to quantify particularly in obese individuals who, contrary to *DNASE1L3* null patients, exhibit the potential to induce nuclear DNA fragmentation. Therefore, we are currently establishing assays to quantitatively measure DNASE1L3 activity in the circulation of obese individuals. One assay showing promising results is based on the treatment of purified nuclei with patient's plasma, followed by the quantification of the remaining DNA by the DAPI nuclear integration. Finally, we will address how circulatory DNASE activity is impaired in obese individuals. We will spike the plasma of healthy and obese individuals with known quantities of recombinant DNASE1 or DNASE1L3 and test the ability of each nuclease to digest naked and nuclear DNA in order to determine whether there are soluble factors present in the circulation inhibiting their respective activity. If we detect impaired

digestion, we will establish experimental procedures to identify the main players involved in the inhibition of DNASEs.

What is the therapeutic potential of DNASE1L3 supplementation during obesity? We have generated an Adeno-associated virus (AAV) expressing human *DNASE1L3* and previously validated its ability to restore systemic DNASE1L3 activity *in vivo* in *Dnase1l3*-KO mice over an extended period of time (10 weeks) as measured by the DNASE1L3-specific capacity to digest nuclear DNA *(Sisirak et al., 2016)*. Therefore, WT and *Dnase1l3*-KO animals will be intravenously injected with DNASE1L3-AAVs prior to and after the induction of obesity by HFD in order to assess its prophylactic and therapeutic effects respectively. The impact of DNASE1L3 supplementation and reconstitution on the development of metabolic syndrome induced by obesity will be monitored by analysing disease features including weight gain, IR, glucose intolerance, AT metaflammation and NAFLD development. As a control, animals will be injected with the same AAV encoding an irrelevant protein (luciferase). Experiments conducted in *Dnase1l3*-KO animals will address cell-extrinsic properties of DNASE1L3 during obesity while experiments in WT mice will specifically explore the therapeutic potential of DNASE1L3 supplementation in the prevention or resolution of obesity-mediated metabolic syndrome.

d. Significance of the project

The goal of this project is to address the fundamental question of the form of self-cfDNA involved in the aberrant activation of inflammatory responses during obesity and regulation of its immunogenicity. Although multiple lines of evidence support a critical role for self-cfDNA recognition in the pathogenesis of obesity, the regulation of this process remains poorly understood. Confirmation of our hypothesis that DNASE1L3

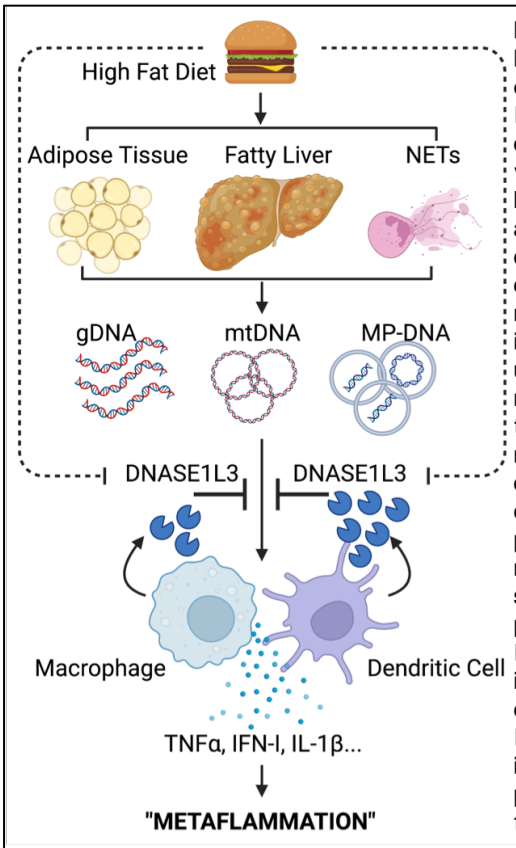

Figure 15. Model for DNASE1L3 function in obesity. High fat diet (HFD) induces obesity and the release of various forms of self-DNAs by the liver, adipose tissue and neutrophils (NETs). In excess, self-DNA activates dendritic cell (DC) and macrophage production of inflammatory cytokines that ultimately contribute to the metaflammation leading to the development of metabolic syndrome and obesity-associated complications. DNASE1L3 produced by DCs and macrophages disposes of self-DNAs and thus likely prevents the ability of self-DNA to activate innate immune cells and the ensuing metaflammation. HFD caused obesity likely inhibits DNASE1L3 function preventing its regulatory function.

constitutes a “safeguard” mechanism by digesting self-cfDNA and preventing its ability to cause obesity-induced inflammation and the ensuing metabolic syndrome will define an entirely novel pathogenic loop at play in this process (**Fig. 15**). Validation of the proposed project may also lead to the development of novel therapeutic strategies that reconstitute or enhance DNASE1L3 activity that could provide significant benefit for obese patients

2. ***WHAT IS THE FUNCTION OF DNASE1L3 IN ANTI-TUMOR IMMUNITY INDUCED BY THERAPY?***

a. *Rationale and driving hypothesis*

Cancer remains one of the leading causes of morbidity and mortality worldwide. The development of cancer is closely surveyed by the immune system, which is able to recognize tumor specific antigens and consequently mount anti-tumor immune responses that prevent the development of malignancy. The essential role of IFN-I in the induction of CTLs that ultimately kill tumor cells has long been established *(Diamond et al., 2011; Fuertes et al., 2011)*. The production of IFN-I within tumors was recently attributed to the recognition of tumor DNA by the cGAS/STING pathway in tumor-infiltrating DCs *(Andzinski et al., 2016; Woo et al., 2014)*. While spontaneous induction of this pathway is insufficient to fully prevent tumor growth *(Woo et al., 2014)*, it is potently stimulated in multiple therapeutic settings, including chemotherapy (CT) *(Kang et al., 2019; Wang et al., 2019)*, radiotherapy (RT) *(Deng et al., 2014; Vanpouille-Box et al., 2017)* and immunotherapy *(Pulido et al., 2021; Wang et al., 2017)*, and leads to T cell-mediated tumor regression. Such therapies were previously reported to induce cancer cell death that can activate anti-tumor immune responses, a phenomenon called immunogenic cell death (ICD) *(Galluzzi et al., 2017)*. ICD causes the release of multiple immunostimulatory DAMPs by the tumors, including tumor DNA that can be free *(Galluzzi et al., 2017)*, associated to proteins such as high mobility group box 1 (HMGB1) *(Galluzzi et al., 2017)*, originating from mitochondria *(Xu et al., 2017; Yamazaki et al., 2020)*, or packaged in MPs *(Diamond et al., 2018; Kitai et al., 2017)*. Besides the activation of cGAS, tumor DNA released in response to CT activates TLR9-mediated anti-tumor immunity *(Kang et al., 2019)*. Accordingly, therapeutic targeting of cGAS/STING *(Corrales et al., 2015)* or TLR9 *(Wang et al., 2016)* pathways as well as vaccination with tumor DNA-containing MPs *(Zhang et al., 2015)* have shown promising results in preclinical studies. In addition to DCs, CT and RT cause tumor cell-autonomous activation of cGAS, leading to the secretion of IFN-I and cyclic guanosine monophosphate–adenosine monophosphate (cGAMP), which contribute to the activation of bystander anti-tumor immune responses *(Marcus et al., 2018; Schadt et al., 2019)*. Conversely, AIM2 activation suppresses anti-tumor immunity *(Fukuda et al., 2021)*, likely by inhibiting the cGAS/STING pathway and causing DC death by pyroptosis *(Corrales et al., 2016)*. Thus, tumor-derived DNA is key in the activation of anti-tumor immune responses, particularly after CT, RT and immunotherapy. However, the precise

molecular properties of tumor-derived DNA and the mechanisms of both its release from tumors and transfer to DCs remain unknown. Furthermore, the regulation of the immunostimulatory properties of tumor-derived DNA is poorly understood.

The role of DNASEs in the regulation of anti-tumor immunity is only starting to be studied. Cell-intrinsic DNASE3 (TREX1) was shown to inhibit tumor cell-autonomous DNA-mediated IFN-I in response to high-dose RT *(Vanpouille-Box et al., 2017*), while *Trex1*-deficiency in mice stimulated T cell-mediated tumor control *(Hemphill et al., 2021)*. Nevertheless, cell-intrinsic DNASEs are essential in preventing fatal inflammatory/autoimmune syndromes *(Stetson et al., 2008; Yoshida et al., 2005)* rendering their study and therapeutic targeting difficult in cancer. On the other hand, the activity of extracellular DNASEs was shown to be reduced in the plasma of cancer patients *(Cherepanova et al., 2008; Jiang et al., 2020; Tamkovich et al., 2006)*. Such reduction of extracellular DNASE activity is often accompanied by an elevation of circulatory DNA levels in cancer patients, which mostly originates from tumor cells *(Han and Lo, 2021)*. These results suggest that tumors limit DNASE1 and DNASE1L3 expression and/or function. Accordingly, reduced *DNASE1L3* expression was reported in the vast majority of tumor tissues compared to normal adjacent tissues *(Chen et al., 2021; Deng et al., 2021)*. Such reduced *DNASE1L3* expression in breast cancer, lung cancer and hepatocellular carcinoma patients was even associated with poor survival *(Chen et al., 2021; Deng et al., 2021)*. While these observations indicate a role for extracellular DNASE1L3 in cancer, its function in this pathological context remains largely unknown. **Consequently, we proposed to dissect the role of DNASE1L3 in the regulation of cancer immunity, particularly in therapeutic contexts that induce immunogenic tumor cell death**.

To develop this project, a collaboration was initiated with Dr. Pouget and Dr. Constanzo (IRCM, Montpellier) who study the immunogenic properties of targeted radionuclide therapy (TRT). TRT is a novel RT approach based on extended/long-term delivery of low-dose radiation by the administration of radiolabeled cancer-binding molecules (i.e. antibodies) *(Pouget et al., 2022)*. TRT thus specifically irradiate tumor cells that overexpress unique targets, while minimizing exposure of healthy tissues *(Pouget et al., 2022)*. Their recent results indicate that TRT stimulates anti-tumor immunity driven by tumor cell-intrinsic and extrinsic activation of DNA-sensing PRRs. We recently obtained the support of the National Institute of Cancer (INCa PLBio 2022) to conduct this project. I am the coordinator of this project that was initiated by a post-doctoral fellow Dr. Anne Garreau in my laboratory and is currently being further developed by Pauline Santa, a PhD student working under my supervision.

b. Current results

Dnase1l3 deficiency inhibits the therapeutic efficacy of immunogenic CTs: To study the role of DNASE1L3 in cancer immunity, we have crossed *Dnase1l3*-KO mice with MMTV-PyMT mice. These mice expresses the middle T oncogene (PyMT) under the promoter of the mouse mammary tumor virus (MMTV), which induces the development of spontaneous mammary adenocarcinoma closely resembling human disease *(Guy et al., 1992)*. In addition, we established orthotopic mammary tumors in *Dnase1l3* KO mice by the injection of the mammary carcinoma cell line E0771 directly into the mammary gland. The deficiency of *Dnase1l3* did not impact the tumor growth in both tumor models (**Fig. 16**). We next treated the mice with the immunogenic CT doxorubicin, when tumors reached a volume of 50mm^3. Doxorubicin delayed the tumor growth in both models, however its efficacy was significantly reduced in *Dnase1l3* KO mice. Indeed, *Dnase1l3*-MMTV-PyMT mice survival was significantly shorter than those of MMTV-PyMT mice treated with doxorubicin (**Fig. 16A-B**). Similarly, E0771 tumors grew faster in *Dnase1l3* KO than in WT mice after the treatment with doxorubicin was terminated (**Fig. 16C**). Similar results were obtained with another CT called teniposide (not shown). These two CTs target topoisomerase II and were reported to activate anti-tumor immunity upon the detection of tumor DNA by cGAS *(Wang et al., 2019)* and TLR9 *(Kang et al., 2019)*. Thus, DNASE1L3 appears to be required for the therapeutic efficacy of CTs that induce an immunogenic tumor cell death.

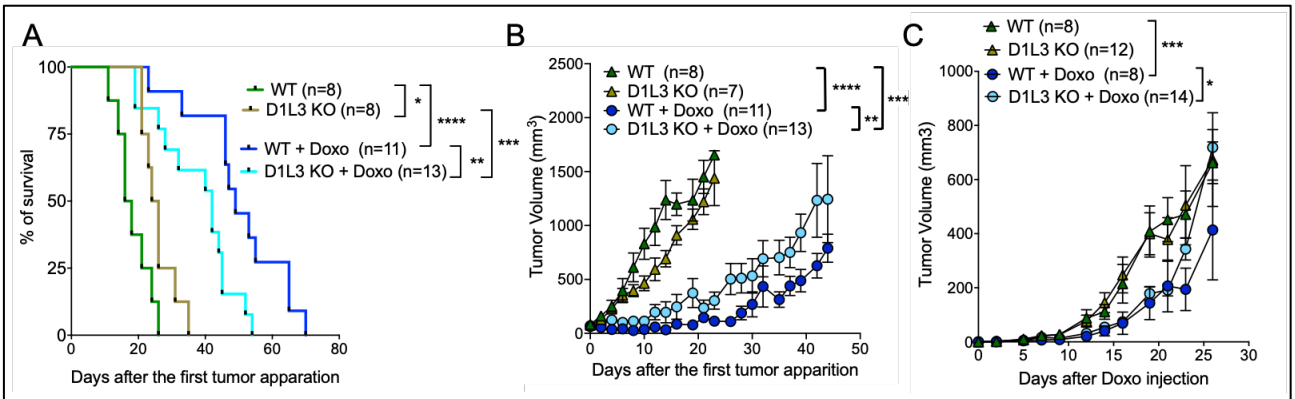

Figure 16. *Dnase1l3* deficiency reduces the therapeutic efficacy of Doxorubicin
(**A**) Kaplan-Meier survival curve of MMTV-PyMT-WT and MMTV-PyMT-*Dnase1l3* KO mice treated or not 5 consecutive times with Doxorubicin (4mg/kg) that was delivered every other day after the appearance of the first tumor. (**B**) Tumor volume of MMTV-PyMT-WT and MMTV-PyMT-*Dnase1l3* KO treated as described in A. (**C**) Tumor volume in WT and *Dnase1l3* KO injected with E0771 cell line followed by 5 consecutive treatments with Doxorubicin (4mg/kg). Mice injected with E0771 tumors were treated every other day when the tumor volume reached ~50mm^3. Data are presented as mean ± SD and *p ≤ 0.05 **p ≤ 0.01, ***p ≤ 0.001 were calculated using non parametric ANOVA tests.

DNASE1L3 specifically digests DNA released by CTs treated tumor cells: CTs targeting topoisomerase II function such as doxorubicin and teniposide were previously reported to induce tumor cell death without inducing DNA fragmentation *(Nakasone et al., 2012)*. So, we exposed E0771 mammary carcinoma cell line to both CTs and observed that the DNA released upon treatment is mostly large (>10Kb) (**Fig.17**). We next placed DNA originating from CT-treated cells in

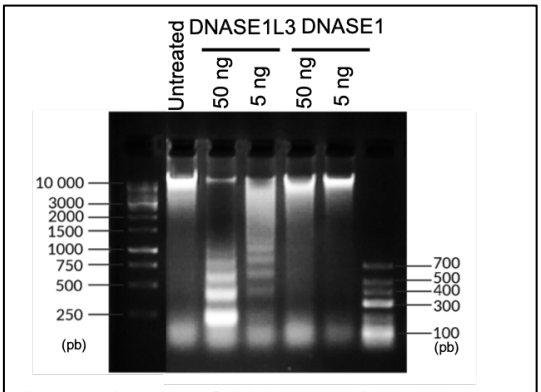

Figure 17. *DNASE1L3 specifically digests tumor DNA released upon CT*
E0771 tumor cells were treated *in vitro* with Teniposide (100μM) for 16h. Cell supernatants were left untreated or treated with recombinant DNASE1L3 and DNASE1 (1h at 37ºC) at indicated doses. DNA was next purified and its profile examined by gel electrophoresis.

the presence of increasing doses of recombinant DNASEs, and we observed that contrary to DNASE1, DNASE1L3 was capable of inducing the fragmentation of tumor cell DNA (**Fig. 17**). These results suggested that DNASE1L3 is likely involved in the processing of tumor DNA released upon ICD, which may in turn enhance its ability to stimulate anti-tumor immunity.

DC-intrinsic Dnase1l3 deficiency inhibits their ability to respond to TLR9 stimulation: We have previously observed that the expression of *Dnase1l3* is the highest in DCs and that its expression can be further enhanced by IFN-I treatment and activation with PRR agonists (not shown). Furthermore, supernatants of CT-treated cells increased the expression of *DNASE1L3* in DCs (not shown). These results indicated that *DNASE1L3* expression in DCs can be modulated by different inflammatory signals and suggested that it may play a DC-intrinsic function. Therefore, we stimulated DCs that were purified from the spleen of WT and *Dnase1l3* KO animals with various PRR ligands including CpG-A (TLR-9), poly U (TLR7) and poly dG:dC (cGAS). We observed that *Dnase1l3* KO DCs were severely impaired in their ability to produce inflammatory cytokines (IFN-α, TNF-α, IL-12) in response to CpG-A stimulation (**Fig. 18A**), whereas their ability to produce inflammatory cytokines in response to TLR7 and cGAS activation was unaffected (**Fig. 18B**). Hence, within DCs, DNASE1L3 likely play an important role in the regulation of inflammatory cytokine production, particularly in response to TLR9 stimulation. It remains critical to investigate whether TLR9-mediated DC activation within tumors upon CT is hampered by *Dnase1l3* deficiency.

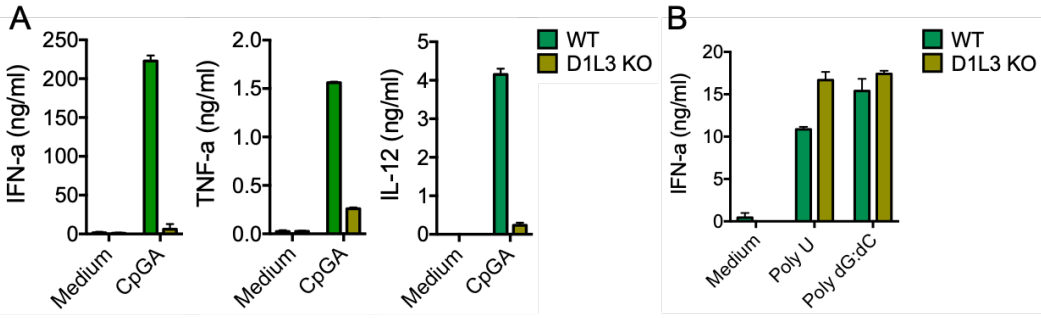

Figure 18. *Dnase1l3*-deficient DCs are selectively impaired in their ability to respond to DNA-mediated TLR9 stimulation. DCs from WT and *Dnase1l3* (D1L3) KO mice were sorted from the spleen and stimulated with (**A**) CpG-A (targeting TLR9), (**B**) Poly U (targeting TLR7) and Poly dG:dC (targeting cGAS). After 16h of stimulation the level of the indicated inflammatory cytokines in the cell culture supernatants was measured by ELISA. Data are presented as mean ± SD.

c. *Future directions*

What is the impact of Dnase1l3 deficiency on the efficacy of immunogenic cancer therapies: We have shown that loss of *Dnase1l3* affects the therapeutic potential of two CTs that are inhibitors of topoisomerase II, which may directly affect the quality of DNA that is released by dying tumor cells. Thus, we want to extend these observations to other immunogenic CTs with distinct mechanisms of action as well as to non-immunogenic CT. For this purpose, we will investigate the therapeutic potential of paclitaxel, a CT that is commonly used in breast cancer patients and induces ICD by targeting the cytoskeleton (tubulin) and thus does not directly affect tumor cell DNA *(Lau et al., 2020).* As a control, tumor-bearing mice will be treated with cisplatin, a CT that was previously reported to be poorly immunogenic *(Martins et al., 2011)*. To do so, WT and *Dnase1l3* KO mice harboring either spontaneous (MMTV-PyMT) or orthotopic (E0771 cell line) mammary tumors will be treated every other day 5 consecutive times with paclitaxel or cisplatin. The treatment will be initiated when tumors reach 50mm^3, and tumor growth will be monitored daily. Mouse survival will be quantified by using a tumor volume of 1500mm^3 as the endpoint. As MMTV-PyMT mice also spontaneously develop lung metastasis, we will also determine the impact of *Dnase1l3*-deficiency on lung metastasis development after the treatment of animals with CTs. The presence of lung metastasis will be followed *in vivo* by imaging using micro computed tomography and *ex vivo* after hematoxylin and eosin (H&E) staining of the lungs.

In addition to CT, RT induces tumor-derived DNA recognition by DCs and in a tumor cell-autonomous manner, ultimately leading to IFN-I mediated tumor rejection and abscopal effects (untreated tumor regression) *(Deng et al., 2014; Vanpouille-Box et al., 2017)*. Therefore, in collaboration with our partners (Dr. Pouget and Dr. Constanzo, IRCM, Montepellier), we will also address the impact of *Dnase1l3* deficiency on the therapeutic efficacy of RT. Given that both orthotopic and spontaneous mammary tumors express Her2 (*Erbb2* gene), it will be used as a specific target for TRT by giving mice that bear palpable tumors a single injection containing 5MBq of ^{177}Lu-anti-Her2 delivering low-dose radiation to tumors for a long period of time. In parallel, mammary tumors will be treated with conventional X ray-RT at a dose of 6 Gy, which will be delivered 3 times over 3 consecutive days. This fractionated approach is preferred as it was reported not to affect cell-intrinsic DNASE3 (TREX1) expression, which could have otherwise confounding effects in our experimental setting *(Vanpouille-Box et al., 2017*). Tumor growth, mouse survival and lung metastasis development (MMTV-PyMT mice) following RT approaches will be monitored as described above.

Vaccination with dead tumor cells is commonly used to evaluate the immunogenic potential of treatments inducing tumor cell death *(Galluzzi et al., 2017)*. The efficacy of such vaccination was recently shown to require endogenous tumor DNA sensing *(Fang et al., 2020; Zhang et al., 2015)*. Therefore, how loss of *Dnase1l3* affects the therapeutic potential of the vaccination by dying tumor

cells obtained after treatments with CT and RT will be evaluated. Hence, E0771 mammary cell lines will be treated *in vitro* with CT, RT and TRT and placed in culture for 18h. After thorough washing of cells to eliminate any residual treatment, WT and *Dnase1l3*-KO mice will be subcutaneously immunized with dying cells (1 x 10^6 cells) and then boosted 7 and 14 days after the first immunization. One week after the last boost, both WT and *Dnase1l3*-KO mice will be injected with live tumor cells (2,5 x 10^5 cells), and the tumor growth and mouse survival will be monitored as previously described. Given that DNASE1L3 specifically digests DNA in MPs released by dying cells *(Sisirak et al., 2016)*, similar vaccination protocols will be developed with purified tumor-cell derived MPs obtained upon ICD induction.

We have observed that *Dnase1l3* is selectively expressed in DCs and, to a lesser extent, in macrophages *(Sisirak et al., 2016)*. Given that both cells infiltrate tumors and play an important role in anti-tumor immune responses, we will determine the source of DNASE1L3 that is important in the regulation of the therapeutic potential of CT and RT *in vivo*. To do so, we will take advantage of CD11c-Cre and LysM-Cre *Dnase1l3*$^{Flox/Flox}$ mice that, as previously described, enable conditional deletion of *Dnase1l3* in DCs and macrophages, respectively. The *Dnase1l3* cKO mice will next be injected with E0771 cell line in order to establish orthotopic mammary tumors. When tumors reach a volume of 50mm^3, mice will be treated with therapies that showed an impaired therapeutic efficacy in mice with constitutive *Dnase1l3* deficiency. Upon treatment, tumor growth and mouse survival will be monitored as described above

What is the impact of Dnase1l3 deficiency on anti-tumor immunity induced by cancer therapies: The treatment of tumors with CT and RT causes tumor cell release of immunostimulatory constituents, including tumor-derived DNA, that activate inflammatory immune responses, in particular IFN-I production by tumor-infiltrating DCs *(Andzinski et al., 2016; Woo et al., 2014)*. IFN-I plays a crucial role in the activation of anti-tumor immune responses. We thus plan to determine how *Dnase1l3* deficiency affects the inflammatory immune responses induced by CTs and RTs. WT and *Dnase1l3* KO mice harboring orthotopic and spontaneous mammary carcinomas will be euthanized 1, 3, 5, and 10 days after the final treatment with CTs or RTs. Tumors will be harvested, and their RNA will be extracted. Using q-PCR we will initially quantify the expression of inflammatory genes (*Tnfα, Il-1β, Ifnα and Ifnβ, Ifnγ*) as well as the IFN signature (*Mx1, Cxcl10, Cxcr3, Isg15, Isg20, Oas1, Oas3, Ifi6*). This will allow us to identify the time point at which *Dnase1l3* deficiency has the greatest impact on inflammatory responses induced by CT and RT. Upon definition of this optimal time point, bulk RNA-sequencing will be performed from tumor-infiltrating immune cells ($CD45^+$ cells). We will specifically assess how *Dnase1l3* deficiency affects the inflammatory signature, the IFN signature and all the immune signatures (cytotoxic versus tolerogenic/exhausted). Such exhaustive analysis

will allow us to determine how DNASE1L3 negatively impacts anti-tumor immune responses induced by immunogenic therapies.

At the previously identified time points after CT or RT, we will harvest spontaneous and orthotopic mammary tumors and their draining lymph nodes from WT and *Dnase1l3* KO mice. In these organs we will characterize the immune infiltrate (DCs, macrophages, neutrophils, B, T and NK cells) and its extensive phenotype (activation versus exhaustion) by spectral flow cytometry. Briefly, the activation of DCs and macrophages will be addressed by the analysis of CD80, CD86 and CD40 surface expression. The production of inflammatory cytokines including IFN-α, IL-12, and TNF-α by DCs and macrophages will be addressed either directly after their isolation from tumors or upon *ex vivo* stimulation with PRR agonists, such as CpG oligonucleotides. CD4 or CD8 T cells will be analyzed for expression of activation markers CD44 ($CD45RB^-$) and granzyme B for CD8 T cells and their production of IFN-γ and TNF-α will be evaluated after *ex vivo* stimulation with PMA and ionomycin. Similarly, $NK1.1^+$ NK cell activation will be monitored by the expression of granzyme B and IFN-γ. In addition, expression of inhibitory molecules PD-L1 and PD-L2 will be analyzed on DCs and macrophages while the expression of their receptor PD1 will be assessed on both CD4 and CD8 T cells. Regulatory T cells will be identified as $Foxp3^+$ cells, and the ratio of effector T cells to Tregs will be quantified. Monocytic ($Ly6C^+$) and granulocytic ($Ly6G^+$) myeloid-derived suppressive cells ($CD11b^+$) that were shown to inhibit anti-tumor immune responses will also be quantified.

CT and RT ultimately lead to the activation of tumor antigen (Ag)-specific CD8 T cell responses that are essential for the elimination of the tumor. Therefore, we propose to determine the impact of *Dnase1l3* loss on the activation of tumor Ag-specific CD8 T cell responses induced by these therapies. To gain further insight into the function of DNASE1L3 in the establishment of specific anti-tumor immune responses, E0771 mammary carcinoma cells expressing the model antigen ovalbumin (Ova) were generated. We have already validated that these cells grow in mice with the same kinetics as unmodified E0771 cells when orthotopically injected in the mammary gland of mice. Furthermore, upon injection of E0771-Ova cells in control mice we could detect Ova-specific $CD8^+$ T cells in the tumor and its draining lymph nodes. We will next inject E0771-Ova cells in WT and *Dnase1l3* KO mice. When tumors reach a volume of $50mm^3$, mice will be treated as previously described with CT or RT, and 1, 3, 5 and 10 days after the last treatment, tumors and draining lymph nodes will be harvested and tumor-specific CD8 T cells, represented by Ova-specific CD8 T cells, will be quantified by flow cytometry using tetramer staining. In addition, CD8 T cells purified from tumors and the draining lymph nodes will be re-stimulated *in vitro* with exogenous Ova peptide, and their production of IFN-γ will be quantified by flow cytometry and ELISPOT.

What are the mechanisms of DNASE1L3 action in anti-tumor immunity induced by therapy: DCs were shown to capture DNA originating from tumors after their treatment with CT *(Kang et al., 2019)* or RT *(Deng et al., 2014)* and, upon DNA recognition by PRR, to produce IFN-I that is required for the activation of anti-tumor immune responses. In addition, tumors have been recently shown to accumulate DNA originating from NETs *(Ireland and Oliver, 2020; Teijeira et al., 2020)*. Such NETs were reported to protect tumor cells from the cytotoxic activity of NK and CD8 T cells by shielding them with their DNA *(Ireland and Oliver, 2020; Teijeira et al., 2020)*). Therefore, DNASE1L3 may modulate anti-tumor immune responses by regulating the uptake and recognition of DNA by DCs as well as intra-tumor NET-DNA accumulation. To address the first hypothesis that DNASE1L3 may regulate DC uptake of DNA, we will quantify the load of gDNA in the cytosol of DCs purified from mammary tumors 1 to 2 days after the last treatment with CT or RT. While, this approach will not allow us to discriminate tumor cell-derived DNA from that derived from stromal cells, it will reveal the impact of *Dnase1l3* deficiency on the load of DNA that is captured within the tumor environment. Additionally, DNA of E0771 tumor cells will be labelled prior to their use in vaccination experiments with cell-permeable DNA dye (Vibrant Green). 6h, 12h and 24h post-vaccination the amount of labelled DNA taken up by DCs in draining lymph nodes from control and *Dnase1l3*-deficient mice will be quantified by image stream technology (Amnis), which allows the imaging of cells at the same time as their flow cytometric analysis. The activation of DNA sensing pathways will also be defined in DCs isolated from tumors either treated or not with therapies. Specifically, the quantification of IRF-3 and IRF-7 phosphorylation by phospho-flow will be used to evaluate the activation of cGAS and TLR9, respectively. DCs isolated from mammary tumors that were grown in WT and *Dnase1l3* KO mice either treated or not with CT or RT will be stimulated *in vitro* with various PRR ligands, including nucleic acids, in order to assess whether the alteration of DC ability to respond to TLR9 ligands by *Dnase1l3* deficiency is maintained within tumors. Finally, NETs will be analyzed by fluorescent microscopy on tumor sections from WT and *Dnase1l3*-KO mice that were treated with RTs or CTs at the same time points as previously described. Neutrophils will be identified as $Ly6G^+$ cells, and the presence of NETs will be evaluated by the detection of H3Cit.

Our preliminary data indicate that the DNA released in culture supernatants upon the induction of E0771 cell death by doxorubicin and teniposide is unfragmented and can only be digested by DNASE1L3 and not DNASE1 (**Fig. 17**). These results suggest that DNASE1L3 may also function by processing and modifying the quality of DNA originating from tumors upon therapy and consequently enhance its ability to activate anti-tumor immune responses. Therefore, we will further evaluate the quality and quantity of DNA released by cells exposed to other CTs or RTs tested *in vivo* and test its sensitivity to recombinant extracellular DNASEs. We will also investigate the potential of DNASE-processed DNA to activate inflammatory responses. E0771 mammary cancer cells will be exposed to immunogenic (paclitaxel) and non-immunogenic (cisplatin) CTs as well as to conventional RT and

TRT and placed in culture for 18h. The cell culture supernatant will be placed in the presence or absence of recombinant DNASE1 and DNASE1L3 for 1h at 37ºC together. The DNA from culture supernatants will then be purified and its fragmentation profile determined upon migration on agarose gel and Agilent TapeStation. Purified g- and mtDNA will be quantified by q-PCR as described previously. Given that DNASE1L3 is involved in the digestion of DNA associated with MPs released by dying cells, MPs present in cell-culture supernatants will be purified and treated or not with extracellular DNASEs. After purification, the g- and mtDNA levels of MPs will be quantified, and their DNA fragmentation profile will be examined as previously described. We will also address, how the *in vivo* treatment of spontaneous and orthotopic mammary tumors affects circulatory cfDNA levels and fragmentation profile. For this purpose, the plasma of WT and *Dnase1l3* KO mice will be collected 24h after the last treatment of the mice, and the amount of g and mtDNA in the whole plasma, the soluble fraction of the plasma, and the MP-enriched fraction of the plasma will be quantified as previously described. Finally, mammary tumors will be resected from control and *Dnase1l3* KO animals 24h after the final treatments. Weight-matched fragment of tumor tissue will be minced and placed in culture medium and after 6h, 12h, 24h and 48h of culture, supernatants will be collected and total DNA amounts as well as its fragmentation profile will be determined. Similarly, MPs, their DNA load, and fragmentation will be assessed in these supernatants.

We will then determine how extracellular DNASE1 and DNASE1L3 regulate the immunostimulatory potential of dying cells obtained after CT and RT. E0771 cells will be treated with CTs, conventional X-ray RT and TRT. Cell culture supernatants will be harvested and then either left untreated or treated with DNASE1 or DNASE1L3 as previously described. The resulting supernatants will be added to the culture of mouse primary DCs. As a negative control DCs, will be treated with supernatants obtained from live cells, and as a positive control DCs will be activated with immunostimulatory CpG oligonucleotide. 12h and 24h after stimulation, DC activation will be monitored by their surface expression of maturation markers (CD80, CD86, CD40, MHC II, PD-L1 and PD-L2) by flow cytometry and their production of cytokines (IFN-I, TNFα, IL-12 IL-1β and IL-10) by ELISA. The production of cytokines by DCs will also be analyzed by flow cytometry in combination with specific markers differentiating the main DC subsets, including XCR1 (cDC1), CD11b (cDC2) and Siglec H (pDCs). This will allow us to determine the impact of DNASE treatment of supernatants derived from dying tumor cells on the activation of each individual DC subset. Similar experiments will be conducted with purified DNA complexed with liposomes (lipofectamine) and purified MPs from tumor cell supernatants that were treated or not with extracellular DNASEs. Results obtained in mice will be validated in humans by using breast cancer cell lines (MCF-7 and MDA-MB-231) treated with CT and RT in the presence or absence of recombinant DNASEs and primary DCs isolated from healthy donors' blood. In order to characterize the main DNA sensing pathway that may be activated by tumor cell-derived DNA specifically processed by DNASE1 or DNASE1L3 we will use DCs from

animals deficient for *Cgas* and *Tlr9* in these experimental settings, which are available in the laboratory (*Tlr9*) or will be obtained in collaboration with Dr. Faget (IRCM, Montpellier – *Cgas* KO). Finally, we will address cell-intrinsic and cell-extrinsic functions of DNASE1L3. Given that DNASE1L3 is selectively expressed in DCs, we will address the DC-intrinsic role of DNASE1L3 in response to tumor-derived DNA stimulation using DCs isolated from *Dnase1l3* KO hosts that will be stimulated as described above. In order to address how cell-extrinsic supplementation of extracellular DNASE1L3 may affect the therapeutic efficacy of CT and RT, we have already generated E0771 cells overexpressing human *DNASE1L3* and *DNASE1*. E0771 do not naturally express extracellular DNASEs, but upon viral transduction with vectors encoding either *DNASE1* or *DNASE1L3*, we were able to enforce their expression and secretion in E0771 culture supernatants. These cells will be injected in the mammary gland of WT and *Dnase1l3* KO mice, and tumors will be treated with CT or RT. Such an approach will allow us to determine *in vivo* whether supplementation of extracellular DNASEs by tumor cells may restore the therapeutic efficacy of immunogenic therapies upon loss of *Dnase1l3*, thus reflecting its cell-extrinsic properties.

d. Significance of the project

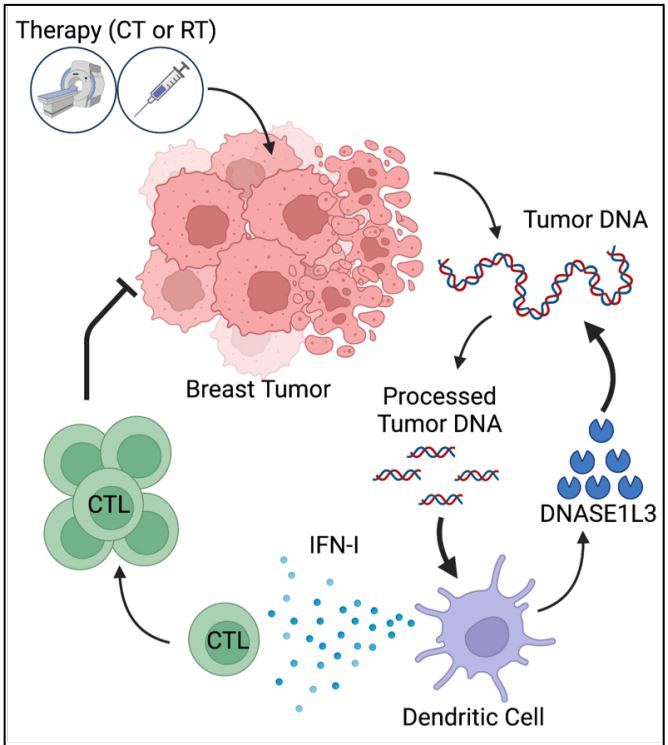

Figure 19. Model for DNASE1L3 function in therapy-induced cancer immunity.
Cancer therapies including radiotherapy (RT) and chemotherapy (CT) induce tumor cell death and their release of large DNA fragments. Processing of tumor DNA by DNASE1L3 produced by dendritic cells (DCs) into smaller DNA fragments may enhance tumor DNA ability to induce type I interferon (IFN-I) production by DCs. IFN-I in turn boosts cytotoxic T lymphocytes (CTL) activation and proliferation and ultimately their ability to kill tumor cells.

The proposed project will address novel questions about the role of extracellular DNASE1L3 in cancer immune surveillance and cell death immunogenicity. Overall, our preliminary results suggest that extracellular DNASE1L3 contributes to the activation of anti-tumor immunity. This defines a novel and unexpected function of extracellular DNASEs, which are thought to limit immune responses by disposing of endogenous DNA (**Fig. 19**). The ability of extracellular DNASE1L3 to promote the immunostimulatory capacity of DNA may be specific to the tumor context and mechanisms of tumor cell death induced upon therapeutic targeting. Such functional characterization of DNASE1L3 will generate novel insight that explains the clinical association of reduced DNASE1L3 expression in tumors with poor outcomes. It will also provide a mechanistic basis for developing therapeutic approaches based on

targeted delivery of extracellular DNASEs within primary tumors to boost anti-tumor immune responses. Finally, numerous patients affected by cancer have shown reduced *DNASE1L3* expression. If our results confirm that DNASE1L3 is required for the therapeutic efficacy of immunogenic therapies, quantifying *DNASE1L3* expression levels within tumors may be predictive of patients' responses to such treatments and suggest the use of alternative therapeutic approaches, which could have both patient and economic benefits by avoiding unnecessary treatment. Given that DNASE1L3 is secreted and detected in the circulation, establishing a novel method to specifically measure its activity could be used as a potential biomarker, leading to better management of patient care. Therefore, our project addresses the unexplored functions of extracellular DNASEs in cancer and is likely to open additional research perspectives including in cancer patients.

V. GENERAL CONCLUSIONS

It has been almost two decades ("DAMN!") since I initiated my research career aimed at defining the role of DCs in the pathologic contexts of cancer and autoimmunity. My doctoral work led to a better understanding of the mechanisms of action involved in the impairment of pDC function in breast cancer patients and their acquisition of "tolerogenic" properties, reflected by their ability to promote suppressive Treg amplification. During my postdoctoral experience, my studies characterized the pathogenic functions of pDCs in SLE development and provided solid rationale for their therapeutic targeting in this auto-immune syndrome. In addition, we identified a novel cell-extrinsic mechanism of tolerance to endogenous (self) DNA that is mediated by DNASE1L3, an endonuclease specifically secreted by DCs. The identification and functional characterization of DNASE1L3 allowed me to develop my own projects and to initiate my independent career. These projects now focus on the role of DNASE1L3 in regulating the immunostimulatory potential of endogenous DNA in the context of obesity and cancer immune surveillance. While in obesity DNASE1L3 seems to limit endogenous DNA potential to induce chronic low-grade inflammation, it appears that in cancer, DNASE1L3 is required for the therapeutic efficacy of current cytotoxic therapies, likely by "boosting" tumor DNA potential to stimulate anti-tumor immunity. If these observations are further validated, it will establish DNASE1L3 as a key enzyme balancing tolerance versus reactivity to endogenous DNA depending on the danger faced by the organism and/or depending on the modality of cell death that are utilized by the organism (apoptosis *versus* ICD). This new concept opens multiple novel research avenues that will be further explored as a long-term perspective by my independent research group.

VI. REFERENCES

Ablasser, A., Hemmerling, I., Schmid-Burgk, J.L., Behrendt, R., Roers, A., Hornung, V., 2014. TREX1 deficiency triggers cell-autonomous immunity in a cGAS-dependent manner. J. Immunol. 1950 192, 5993–5997.

Abraham, C., Cho, J.H., 2009. Inflammatory Bowel Disease. N. Engl. J. Med. 361, 2066–2078.

Ah Kioon, M.D., Tripodo, C., Fernandez, D., Kirou, K.A., Spiera, R.F., Crow, M.K., Gordon, J.K., Barrat, F.J., 2018. Plasmacytoid dendritic cells promote systemic sclerosis with a key role for TLR8. Sci. Transl. Med.

Ahn, J., Gutman, D., Saijo, S., Barber, G.N., 2012. STING manifests self DNA-dependent inflammatory disease. Proc. Natl. Acad. Sci. U. S. A. 109, 19386–19391.

Al-Mayouf, S.M., Sunker, A., Abdwani, R., Abrawi, S.A., Almurshedi, F., Alhashmi, N., Al Sonbul, A., Sewairi, W., Qari, A., Abdallah, E., Al-Owain, M., Al Motywee, S., Al-Rayes, H., Hashem, M., Khalak, H., Al-Jebali, L., Alkuraya, F.S., 2011. Loss-of-function variant in *DNASE1L3* causes a familial form of systemic lupus erythematosus. Nat. Genet. 43, 1186–1188.

Andzinski, L., Spanier, J., Kasnitz, N., Kröger, A., Jin, L., Brinkmann, M.M., Kalinke, U., Weiss, S., Jablonska, J., Lienenklaus, S., 2016. Growing tumors induce a local STING dependent Type I IFN response in dendritic cells. Int. J. Cancer 139, 1350–1357.

Arimura, K., Takagi, H., Uto, T., Fukaya, T., Nakamura, T., Choijookhuu, N., Hishikawa, Y., Yamashita, Y., Sato, K., 2017. Crucial role of plasmacytoid dendritic cells in the development of acute colitis through the regulation of intestinal inflammation. Mucosal Immunol. 10, 957–970.

Artlett, C.M., 2014. Animal models of systemic sclerosis: their utility and limitations. Open Access Rheumatol. Res. Rev. 6, 65–81.

Bae, J.H., Jo, S., Kim, S.J., Lee, J.M., Jeong, J.H., Kang, J.S., Cho, N.-J., Kim, S.S., Lee, E.Y., Moon, J.-S., 2019. Circulating Cell-Free mtDNA Contributes to AIM2 Inflammasome-Mediated Chronic Inflammation in Patients with Type 2 Diabetes. Cells 8.

Banchereau, R., Cepika, A.-M., Banchereau, J., Pascual, V., 2017. Understanding Human Autoimmunity and Autoinflammation Through Transcriptomics. Annu. Rev. Immunol. 35, 337–370.

Barbalat, R., Ewald, S.E., Mouchess, M.L., Barton, G.M., 2011. Nucleic acid recognition by the innate immune system. Annu. Rev. Immunol. 29, 185–214.

Bartok, E., Hartmann, G., 2020. Immune Sensing Mechanisms that Discriminate Self from Altered Self and Foreign Nucleic Acids. Immunity 53, 54–77.

Bauer, S., Kirschning, C.J., Häcker, H., Redecke, V., Hausmann, S., Akira, S., Wagner, H., Lipford, G.B., 2001. Human TLR9 confers responsiveness to bacterial DNA via species-specific CpG motif recognition. Proc. Natl. Acad. Sci. 98, 9237–9242.

Baumgart, D.C., Metzke, D., Schmitz, J., Scheffold, A., Sturm, A., Wiedenmann, B., Dignass, A.U., 2005. Patients with active inflammatory bowel disease lack immature peripheral blood plasmacytoid and myeloid dendritic cells. Gut 54, 228–236.

Bennett, L., Palucka, A.K., Arce, E., Cantrell, V., Borvak, J., Banchereau, J., Pascual, V., 2003. Interferon and granulopoiesis signatures in systemic lupus erythematosus blood. J. Exp. Med. 197, 711–723.

Bratke, K., Prieschenk, C., Garbe, K., Kuepper, M., Lommatzsch, M., Virchow, J.C., 2013. Plasmacytoid dendritic cells in allergic asthma and the role of inhaled corticosteroid treatment. Clin. Exp. Allergy 43, 312–321.

Buechler, M.B., Teal, T.H., Elkon, K.B., Hamerman, J.A., 2013. Cutting edge: Type I IFN drives emergency myelopoiesis and peripheral myeloid expansion during chronic TLR7 signaling. J. Immunol. Baltim. Md 1950 190, 886–891.

Bunin, A., Sisirak, V., Ghosh, H.S., Grajkowska, L.T., Hou, Z.E., Miron, M., Yang, C., Ceribelli, M., Uetani, N., Chaperot, L., Plumas, J., Hendriks, W., Tremblay, M.L., Häcker, H., Staudt, L.M., Green, P.H., Bhagat, G., Reizis, B., 2015. Protein Tyrosine Phosphatase PTPRS Is an Inhibitory Receptor on Human and Murine Plasmacytoid Dendritic Cells. Immunity 43, 277–288.

Caielli, S., Athale, S., Domic, B., Murat, E., Chandra, M., Banchereau, R., Baisch, J., Phelps, K., Clayton, S., Gong, M., Wright, T., Punaro, M., Palucka, K., Guiducci, C., Banchereau, J., Pascual, V., 2016. Oxidized mitochondrial nucleoids released by neutrophils drive type I interferon production in human lupus. J. Exp. Med. 213, 697–713.

Carbonella, A., Mancano, G., Gremese, E., Alkuraya, F.S., Patel, N., Gurrieri, F., Ferraccioli, G., 2017. An autosomal recessive DNASE1L3-related autoimmune disease with unusual clinical presentation mimicking systemic lupus erythematosus. Lupus 26, 768–772.

Caton, M.L., Smith-Raska, M.R., Reizis, B., 2007. Notch-RBP-J signaling controls the homeostasis of CD8- dendritic cells in the spleen. J. Exp. Med. 204, 1653–1664.

Chan, R.W.Y., Serpas, L., Ni, M., Volpi, S., Hiraki, L.T., Tam, L.-S., Rashidfarrokhi, A., Wong, P.C.H., Tam, L.H.P., Wang, Y., Jiang, P., Cheng, A.S.H., Peng, W., Han, D.S.C., Tse, P.P.P., Lau, P.K., Lee, W.-S., Magnasco, A., Buti, E., Sisirak, V., AlMutairi, N., Chan, K.C.A., Chiu, R.W.K., Reizis, B., Lo, Y.M.D., 2020. Plasma DNA Profile Associated with DNASE1L3 Gene Mutations: Clinical Observations, Relationships to Nuclease Substrate Preference, and In Vivo Correction. Am. J. Hum. Genet.

Chen, Jianlin, Ding, J., Huang, W., Sun, L., Chen, Jinping, Liu, Y., Zhan, Q., Gao, G., He, X., Qiu, G., Long, P., Wei, L., Lu, Z., Sun, Y., 2021. DNASE1L3 as a Novel Diagnostic and Prognostic Biomarker for Lung Adenocarcinoma Based on Data Mining. Front. Genet. 12.

Chen, Y.-L., Gomes, T., Hardman, C.S., Vieira Braga, F.A., Gutowska-Owsiak, D., Salimi, M., Gray, N., Duncan, D.A., Reynolds, G., Johnson, D., Salio, M., Cerundolo, V., Barlow, J.L., McKenzie, A.N.J., Teichmann, S.A., Haniffa, M., Ogg, G., 2019. Re-evaluation of human BDCA-2+ DC during acute sterile skin inflammation. J. Exp. Med. 217, e20190811.

Cherepanova, A.V., Tamkovich, S.N., Bryzgunova, O.E., Vlassov, V.V., Laktionov, P.P., 2008. Deoxyribonuclease Activity and Circulating DNA Concentration in Blood Plasma of Patients with Prostate Tumors. Ann. N. Y. Acad. Sci. 1137, 218–221. https://doi.org/10.1196/annals.1448.016

Christensen, S.R., Shupe, J., Nickerson, K., Kashgarian, M., Flavell, R.A., Shlomchik, M.J., 2006. Toll-like receptor 7 and TLR9 dictate autoantibody specificity and have opposing inflammatory and regulatory roles in a murine model of lupus. Immunity 25, 417–428.

Cisse, B., Caton, M.L., Lehner, M., Maeda, T., Scheu, S., Locksley, R., Holmberg, D., Zweier, C., den Hollander, N.S., Kant, S.G., Holter, W., Rauch, A., Zhuang, Y., Reizis, B., 2008. Transcription factor E2-2 is an essential and specific regulator of plasmacytoid dendritic cell development. Cell 135, 37–48.

Clausen, B.E., Burkhardt, C., Reith, W., Renkawitz, R., Förster, I., 1999. Conditional gene targeting in macrophages and granulocytes using LysMcre mice. Transgenic Res. 8, 265–277.

Coke, L.N., Wen, H., Comeau, M., Ghanem, M.H., Shih, A., Metz, C.N., Li, W., Langefeld, C.D., Gregersen, P.K., Simpfendorfer, K.R., 2021. Arg206Cys substitution in DNASE1L3 causes a defect in DNASE1L3 protein secretion that confers risk of systemic lupus erythematosus. Ann. Rheum. Dis. 80, 782–787.

Conrad, C., Gregorio, J., Wang, Y.-H., Ito, T., Meller, S., Hanabuchi, S., Anderson, S., Atkinson, N., Ramirez, P.T., Liu, Y.-J., Freedman, R., Gilliet, M., 2012. Plasmacytoid dendritic cells promote immunosuppression in ovarian cancer via ICOS costimulation of Foxp3(+) T-regulatory cells. Cancer Res. 72, 5240–5249.

Corrales, L., Glickman, L.H., McWhirter, S.M., Kanne, D.B., Sivick, K.E., Katibah, G.E., Woo, S.-R., Lemmens, E., Banda, T., Leong, J.J., Metchette, K., Dubensky, T.W., Gajewski, T.F., 2015. Direct Activation of STING in the Tumor Microenvironment Leads to Potent and Systemic Tumor Regression and Immunity. Cell Rep. 11, 1018–1030.

Corrales, L., Woo, S.-R., Williams, J.B., McWhirter, S.M., Dubensky, T.W., Gajewski, T.F., 2016. Antagonism of the STING Pathway via Activation of the AIM2 Inflammasome by Intracellular DNA. J. Immunol. 196(7):3191-8

Crow, Y.J., Hayward, B.E., Parmar, R., Robins, P., Leitch, A., Ali, M., Black, D.N., van Bokhoven, H., Brunner, H.G., Hamel, B.C., Corry, P.C., Cowan, F.M., Frints, S.G., Klepper, J., Livingston, J.H., Lynch, S.A., Massey, R.F., Meritet, J.F., Michaud, J.L., Ponsot, G., Voit, T., Lebon, P., Bonthron, D.T., Jackson, A.P., Barnes, D.E., Lindahl, T., 2006. Mutations in the gene encoding the 3'-5' DNA exonuclease TREX1 cause Aicardi-Goutières syndrome at the AGS1 locus. Nat. Genet. 38, 917–920.

Crowl, J.T., Gray, E.E., Pestal, K., Volkman, H.E., Stetson, D.B., 2017. Intracellular Nucleic Acid Detection in Autoimmunity. Annu. Rev. Immunol. 35, 313–336.

Deane, J.A., Pisitkun, P., Barrett, R.S., Feigenbaum, L., Town, T., Ward, J.M., Flavell, R.A., Bolland, S., 2007. Control of toll-like receptor 7 expression is essential to restrict autoimmunity and dendritic cell proliferation. Immunity 27, 801–810.

Deng, L., Liang, H., Xu, M., Yang, X., Burnette, B., Arina, A., Li, X.-D., Mauceri, H., Beckett, M., Darga, T., Huang, X., Gajewski, T.F., Chen, Z.J., Fu, Y.-X., Weichselbaum, R.R., 2014. STING-Dependent Cytosolic DNA Sensing Promotes Radiation-Induced Type I Interferon-Dependent Antitumor Immunity in Immunogenic Tumors. Immunity 41, 843–852.

Deng, Z., Xiao, M., Du, D., Luo, N., Liu, D., Liu, T., Lian, D., Peng, J., 2021. DNASE1L3 as a Prognostic Biomarker Associated with Immune Cell Infiltration in Cancer. OncoTargets Ther. 14, 2003–2017.

Dezutter-Dambuyant, C., Durand, I., Alberti, L., Bendriss-Vermare, N., Valladeau-Guilemond, J., Duc, A., Magron, A., Morel, A.-P., Sisirak, V., Rodriguez, C., Cox, D., Olive, D., Caux, C., 2016. A novel regulation of PD-1 ligands on mesenchymal stromal cells through MMP-mediated proteolytic cleavage. Oncoimmunology 5, e1091146.

Diamond, J.M., Vanpouille-Box, C., Spada, S., Rudqvist, N.-P., Chapman, J.R., Ueberheide, B.M., Pilones, K.A., Sarfraz, Y., Formenti, S.C., Demaria, S., 2018. Exosomes Shuttle TREX1-Sensitive IFN-Stimulatory dsDNA from Irradiated Cancer Cells to DCs. Cancer Immunol. Res. 6, 910–920.

Diamond, M.S., Kinder, M., Matsushita, H., Mashayekhi, M., Dunn, G.P., Archambault, J.M., Lee, H., Arthur, C.D., White, J.M., Kalinke, U., Murphy, K.M., Schreiber, R.D., 2011. Type I interferon is selectively required by dendritic cells for immune rejection of tumors. J. Exp. Med. 208, 1989–2003.

Diebold, S.S., Kaisho, T., Hemmi, H., Akira, S., Reis e Sousa, C., 2004. Innate antiviral responses by means of TLR7-mediated recognition of single-stranded RNA. Science 303, 1529–1531.

Dress, R.J., Dutertre, C.-A., Giladi, A., Schlitzer, A., Low, I., Shadan, N.B., Tay, A., Lum, J., Kairi, M.F.B.M., Hwang, Y.Y., Becht, E., Cheng, Y., Chevrier, M., Larbi, A., Newell, E.W., Amit, I., Chen, J., Ginhoux, F., 2019. Plasmacytoid dendritic cells develop from Ly6D+ lymphoid progenitors distinct from the myeloid lineage. Nat. Immunol. 20, 852–864.

Faget, J., Bendriss-Vermare, N., Gobert, M., Durand, I., Olive, D., Biota, C., Bachelot, T., Treilleux, I., Goddard-Leon, S., Lavergne, E., Chabaud, S., Blay, J.Y., Caux, C., Ménétrier-Caux, C., 2012. ICOS-ligand expression on plasmacytoid dendritic cells supports breast cancer progression by promoting the accumulation of immunosuppressive CD4+ T cells. Cancer Res. 72, 6130–6141.

Fang, C., Mo, F., Liu, L., Du, J., Luo, M., Men, K., Na, F., Wang, W., Yang, H., Wei, X., 2020. Oxidized mitochondrial DNA sensing by STING signaling promotes the antitumor effect of an irradiated immunogenic cancer cell vaccine. Cell. Mol. Immunol. 1–13.

Feng, J., Pucella, J.N., Jang, G., Alcántara-Hernández, M., Upadhaya, S., Adams, N.M., Khodadadi-Jamayran, A., Lau, C.M., Stoeckius, M., Hao, S., Smibert, P., Tsirigos, A., Idoyaga, J., Reizis, B., 2022. Clonal lineage tracing reveals shared origin of conventional and plasmacytoid dendritic cells. Immunity 55, 405-422.e11.

Ferriere, A., Santa, P., Garreau, A., Bandopadhyay, P., Blanco, P., Ganguly, D., Sisirak, V., 2020. Self-Nucleic Acid Sensing: A Novel Crucial Pathway Involved in Obesity-Mediated Metaflammation and Metabolic Syndrome. Front. Immunol. 11, 624256.

Flacher, V., Bouschbacher, M., Verronèse, E., Massacrier, C., Sisirak, V., Berthier-Vergnes, O., de Saint-Vis, B., Caux, C., Dezutter-Dambuyant, C., Lebecque, S., Valladeau, J., 2006. Human Langerhans cells express a specific TLR profile and differentially respond to viruses and Gram-positive bacteria. J. Immunol. Baltim. Md 1950 177, 7959–7967.

Fuertes, M.B., Kacha, A.K., Kline, J., Woo, S.-R., Kranz, D.M., Murphy, K.M., Gajewski, T.F., 2011. Host type I IFN signals are required for antitumor CD8+ T cell responses through CD8{alpha}+ dendritic cells. J. Exp. Med. 208, 2005–2016.

Fukuda, K., Okamura, K., Riding, R.L., Fan, X., Afshari, K., Haddadi, N.-S., McCauley, S.M., Guney, M.H., Luban, J., Funakoshi, T., Yaguchi, T., Kawakami, Y., Khvorova, A., Fitzgerald, K.A., Harris, J.E., 2021. AIM2 regulates anti-tumor immunity and is a viable therapeutic target for melanoma. J. Exp. Med. 218, e20200962.

Fukui, R., Saitoh, S., Matsumoto, F., Kozuka-Hata, H., Oyama, M., Tabeta, K., Beutler, B., Miyake, K., 2009. Unc93B1 biases Toll-like receptor responses to nucleic acid in dendritic cells toward DNA- but against RNA-sensing. J. Exp. Med. 206, 1339–1350.

Furie, R., Werth, V.P., Merola, J.F., Stevenson, L., Reynolds, T.L., Naik, H., Wang, W., Christmann, R., Gardet, A., Pellerin, A., Hamann, S., Auluck, P., Barbey, C., Gulati, P., Rabah, D., Franchimont, N., 2019. Monoclonal antibody targeting BDCA2 ameliorates skin lesions in systemic lupus erythematosus. J. Clin. Invest. 129, 1359–1371.

Gabrielli, A., Avvedimento, E.V., Krieg, T., 2009. Scleroderma. N. Engl. J. Med. 360, 1989–2003.

Galluzzi, L., Buqué, A., Kepp, O., Zitvogel, L., Kroemer, G., 2017. Immunogenic cell death in cancer and infectious disease. Nat. Rev. Immunol. 17, 97–111. https://doi.org/10.1038/nri.2016.107

Ganguly, D., 2022. Plasmacytoid Dendritic Cells and Cancer, in: Ganguly, D. (Ed.), Plasmacytoid Dendritic Cells. Springer Nature, Singapore, pp. 133–145.

Ganguly, D., Haak, S., Sisirak, V., Reizis, B., 2013. The role of dendritic cells in autoimmunity. Nat. Rev. Immunol. 13, 566–577.

Garcia-Martinez, I., Santoro, N., Chen, Y., Hoque, R., Ouyang, X., Caprio, S., Shlomchik, M.J., Coffman, R.L., Candia, A., Mehal, W.Z., 2016. Hepatocyte mitochondrial DNA drives nonalcoholic steatohepatitis by activation of TLR9. J. Clin. Invest. 126, 859–864.

Garcia-Romo, G.S., Caielli, S., Vega, B., Connolly, J., Allantaz, F., Xu, Z., Punaro, M., Baisch, J., Guiducci, C., Coffman, R.L., Barrat, F.J., Banchereau, J., Pascual, V., 2011. Netting neutrophils are major inducers of type I IFN production in pediatric systemic lupus erythematosus. Sci. Transl. Med. 3, 73ra20.

Ghosh, A.R., Bhattacharya, R., Bhattacharya, S., Nargis, T., Rahaman, O., Duttagupta, P., Raychaudhuri, D., Liu, C.S.C., Roy, S., Ghosh, P., Khanna, S., Chaudhuri, T., Tantia, O., Haak, S., Bandyopadhyay, S., Mukhopadhyay, S., Chakrabarti, P., Ganguly, D., 2016. Adipose Recruitment and Activation of Plasmacytoid Dendritic Cells Fuel Metaflammation. Diabetes 65, 3440–3452.

Ghosh, H.S., Cisse, B., Bunin, A., Lewis, K.L., Reizis, B., 2010. Continuous expression of the transcription factor e2-2 maintains the cell fate of mature plasmacytoid dendritic cells. Immunity 33, 905–916.

Gillibert-Duplantier, J., Duthey, B., Sisirak, V., Salaün, D., Gargi, T., Trédan, O., Finetti, P., Bertucci, F., Birnbaum, D., Bendriss-Vermare, N., Badache, A., 2012. Gene expression profiling identifies sST2 as an effector of ErbB2-driven breast carcinoma cell motility, associated with metastasis. Oncogene 31, 3516–3524.

Gomez-Bañuelos, E., Yu, Y., Li, J., Cashman, K.S., Paz, M., Trejo-Zambrano, M.I., Bugrovsky, R., Wang, Y., Chida, A.S., Sherman-Baust, C.A., Ferris, D.P., Goldman, D.W., Darrah, E., Petri, M., Sanz, I., Andrade, F., 2023. Affinity maturation generates pathogenic antibodies with dual reactivity to DNase1L3 and dsDNA in systemic lupus erythematosus. Nat. Commun. 14, 1388.

Gong, Z., Zhang, X., Su, K., Jiang, R., Sun, Z., Chen, W., Forno, E., Goetzman, E.S., Wang, J., Dong, H.H., Dutta, P., Muzumdar, R., 2019. Deficiency in AIM2 induces inflammation and adipogenesis in white adipose tissue leading to obesity and insulin resistance. Diabetologia 62, 2325–2339.

Guy, C.T., Cardiff, R.D., Muller, W.J., 1992. Induction of mammary tumors by expression of polyomavirus middle T oncogene: a transgenic mouse model for metastatic disease. Mol. Cell. Biol. 12, 954–961.

Han, D.S.C., Lo, Y.M.D., 2021. The Nexus of cfDNA and Nuclease Biology. Trends Genet. 37, 758–770.

Hanna Kazazian, N., Wang, Y., Roussel-Queval, A., Marcadet, L., Chasson, L., Laprie, C., Desnues, B., Charaix, J., Irla, M., Alexopoulou, L., 2019. Lupus Autoimmunity and Metabolic Parameters Are Exacerbated Upon High Fat Diet-Induced Obesity Due to TLR7 Signaling. Front. Immunol. 10.

Hannibal, T.D., Schmidt-Christensen, A., Nilsson, J., Fransén-Pettersson, N., Hansen, L., Holmberg, D., 2017. Deficiency in plasmacytoid dendritic cells and type I interferon signalling prevents diet-induced obesity and insulin resistance in mice. Diabetologia 60, 2033–2041.

Hartl, J., Serpas, L., Wang, Y., Rashidfarrokhi, A., Perez, O.A., Sally, B., Sisirak, V., Soni, C., Khodadadi-Jamayran, A., Tsirigos, A., Caiello, I., Bracaglia, C., Volpi, S., Ghiggeri, G.M., Chida, A.S., Sanz, I., Kim, M.Y., Belmont, H.M., Silverman, G.J., Clancy, R.M., Izmirly, P.M., Buyon, J.P., Reizis, B., 2021. Autoantibody-mediated impairment of DNASE1L3 activity in sporadic systemic lupus erythematosus. J. Exp. Med. 218, e20201138.

Hemmi, H., Takeuchi, O., Kawai, T., Kaisho, T., Sato, S., Sanjo, H., Matsumoto, M., Hoshino, K., Wagner, H., Takeda, K., Akira, S., 2000. A Toll-like receptor recognizes bacterial DNA. Nature 408, 740–745.

Hemphill, W.O., Simpson, S.R., Liu, M., Salsbury, F.R., Hollis, T., Grayson, J.M., Perrino, F.W., 2021. TREX1 as a Novel Immunotherapeutic Target. Front. Immunol. 12.

Homey, B., Alenius, H., Müller, A., Soto, H., Bowman, E.P., Yuan, W., McEvoy, L., Lauerma, A.I., Assmann, T., Bünemann, E., Lehto, M., Wolff, H., Yen, D., Marxhausen, H., To, W., Sedgwick, J., Ruzicka, T., Lehmann, P., Zlotnik, A., 2002. CCL27-CCR10 interactions regulate T cell-mediated skin inflammation. Nat. Med. 8, 157–165.

Ip, W.K.E., Hoshi, N., Shouval, D.S., Snapper, S., Medzhitov, R., 2017. Anti-inflammatory effect of IL-10 mediated by metabolic reprogramming of macrophages. Science 356, 513–519.

Ireland, A.S., Oliver, T.G., 2020. Neutrophils Create an ImpeNETrable Shield between Tumor and Cytotoxic Immune Cells. Immunity 52, 729–731.

Jenks, S.A., Cashman, K.S., Woodruff, M.C., Lee, F.E.-H., Sanz, I., 2019. Extrafollicular responses in humans and SLE. Immunol. Rev. 288, 136–148.

Jenks, S.A., Cashman, K.S., Zumaquero, E., Marigorta, U.M., Patel, A.V., Wang, X., Tomar, D., Woodruff, M.C., Simon, Z., Bugrovsky, R., Blalock, E.L., Scharer, C.D., Tipton, C.M., Wei, C., Lim, S.S., Petri, M., Niewold, T.B., Anolik, J.H., Gibson, G., Lee, F.E.-H., Boss, J.M., Lund, F.E., Sanz, I., 2018. Distinct Effector B Cells Induced by Unregulated Toll-like Receptor 7 Contribute to Pathogenic Responses in Systemic Lupus Erythematosus. Immunity 49, 725-739.e6.

Jiang, P., Sun, K., Peng, W., Cheng, S.H., Ni, M., Yeung, P.C., Heung, M.M.S., Xie, T., Shang, H., Zhou, Z., Chan, R.W.Y., Wong, J., Wong, V.W.S., Poon, L.C., Leung, T.Y., Lam, W.K.J., Chan, J.Y.K., Chan, H.L.Y., Chan, K.C.A., Chiu, R.W.K., Lo, Y.M.D., 2020. Plasma DNA End-Motif Profiling as a Fragmentomic Marker in Cancer, Pregnancy, and Transplantation. Cancer Discov. 10, 664–673.

Jiménez-Alcázar, M., Rangaswamy, C., Panda, R., Bitterling, J., Simsek, Y.J., Long, A.T., Bilyy, R., Krenn, V., Renné, C., Renné, T., Kluge, S., Panzer, U., Mizuta, R., Mannherz, H.G., Kitamura, D., Herrmann, M., Napirei, M., Fuchs, T.A., 2017. Host DNases prevent vascular occlusion by neutrophil extracellular traps. Science 358, 1202–1206.

Kang, T.H., Mao, C.-P., Kim, Y.S., Kim, T.W., Yang, A., Lam, B., Tseng, S.-H., Farmer, E., Park, Y.-M., Hung, C.-F., 2019. TLR9 acts as a sensor for tumor-released DNA to modulate anti-tumor immunity after chemotherapy. J. Immunother. Cancer 7.

Karnell, J.L., Wu, Y., Mittereder, N., Smith, M.A., Gunsior, M., Yan, L., Casey, K.A., Henault, J., Riggs, J.M., Nicholson, S.M., Sanjuan, M.A., Vousden, K.A., Werth, V.P., Drappa, J., Illei, G.G., Rees, W.A., Ratchford, J.N., VIB7734 Trial Investigators, 2021. Depleting plasmacytoid dendritic cells reduces local type I interferon responses and disease activity in patients with cutaneous lupus. Sci. Transl. Med. 13, eabf8442.

Kavian, N., Marut, W., Servettaz, A., Nicco, C., Chéreau, C., Lemaréchal, H., Guilpain, P., Chimini, G., Galland, F., Weill, B., Naquet, P., Batteux, F., 2015. Pantethine Prevents Murine Systemic Sclerosis Through the Inhibition of Microparticle Shedding. Arthritis Rheumatol. 67, 1881–1890.

Kawane, K., Ohtani, M., Miwa, K., Kizawa, T., Kanbara, Y., Yoshioka, Y., Yoshikawa, H., Nagata, S., 2006. Chronic polyarthritis caused by mammalian DNA that escapes from degradation in macrophages. Nature 443, 998–1002.

Keyel, P.A., 2017. Dnases in health and disease. Dev. Biol. 429, 1–11. https://doi.org/10.1016/j.ydbio.2017.06.028

Kiesler, P., Fuss, I.J., Strober, W., 2015. Experimental Models of Inflammatory Bowel Diseases. Cell. Mol. Gastroenterol. Hepatol. 1, 154–170.

Kießler, M., Plesca, I., Sommer, U., Wehner, R., Wilczkowski, F., Müller, L., Tunger, A., Lai, X., Rentsch, A., Peuker, K., Zeissig, S., Seifert, A.M., Seifert, L., Weitz, J., Bachmann, M., Bornhäuser, M., Aust, D., Baretton, G., Schmitz, M., 2021. Tumor-infiltrating plasmacytoid dendritic cells are associated with survival in human colon cancer. J. Immunother. Cancer 9, e001813.

Kisla Ekinci, R.M., Balci, S., Ozcan, D., Atmis, B., Bisgin, A., 2021. Monogenic lupus due to DNASE1L3 deficiency in a pediatric patient with urticarial rash, hypocomplementemia, pulmonary hemorrhage, and immune-complex glomerulonephritis. Eur. J. Med. Genet. 64, 104262.

Kitai, Y., Kawasaki, T., Sueyoshi, T., Kobiyama, K., Ishii, K.J., Zou, J., Akira, S., Matsuda, T., Kawai, T., 2017. DNA-Containing Exosomes Derived from Cancer Cells Treated with Topotecan Activate a STING-Dependent Pathway and Reinforce Antitumor Immunity. J. Immunol. 198, 1649–1659.

Kohrgruber, N., Gröger, M., Meraner, P., Kriehuber, E., Petzelbauer, P., Brandt, S., Stingl, G., Rot, A., Maurer, D., 2004. Plasmacytoid dendritic cell recruitment by immobilized CXCR3 ligands. J. Immunol. Baltim. Md 1950 173, 6592–6602.

Kühn, R., Löhler, J., Rennick, D., Rajewsky, K., Müller, W., 1993. Interleukin-10-deficient mice develop chronic enterocolitis. Cell 75, 263–274.

Labidi-Galy, S.I., Sisirak, V., Meeus, P., Gobert, M., Treilleux, I., Bajard, A., Combes, J.-D., Faget, J., Mithieux, F., Cassignol, A., Tredan, O., Durand, I., Ménétrier-Caux, C., Caux, C., Blay, J.-Y., Ray-Coquard, I., Bendriss-Vermare, N., 2011. Quantitative and functional alterations of plasmacytoid dendritic cells contribute to immune tolerance in ovarian cancer. Cancer Res. 71, 5423–5434.

Lande, R., Ganguly, D., Facchinetti, V., Frasca, L., Conrad, C., Gregorio, J., Meller, S., Chamilos, G., Sebasigari, R., Riccieri, V., Bassett, R., Amuro, H., Fukuhara, S., Ito, T., Liu, Y.-J., Gilliet, M., 2011.

Neutrophils activate plasmacytoid dendritic cells by releasing self-DNA-peptide complexes in systemic lupus erythematosus. Sci. Transl. Med. 3, 73ra19.

Lande, R., Lee, E.Y., Palazzo, R., Marinari, B., Pietraforte, I., Santos, G.S., Mattenberger, Y., Spadaro, F., Stefanantoni, K., Iannace, N., Dufour, A.M., Falchi, M., Bianco, M., Botti, E., Bianchi, L., Alvarez, M., Riccieri, V., Truchetet, M.-E., Wong, G.C.L., Chizzolini, C., Frasca, L., 2019. CXCL4 assembles DNA into liquid crystalline complexes to amplify TLR9-mediated interferon-α production in systemic sclerosis. Nat. Commun. 10, 1–14.

Lau, T.S., Chan, L.K.Y., Man, G.C.W., Wong, C.H., Lee, J.H.S., Yim, S.F., Cheung, T.H., McNeish, I.A., Kwong, J., 2020. Paclitaxel Induces Immunogenic Cell Death in Ovarian Cancer via TLR4/IKK2/SNARE-Dependent Exocytosis. Cancer Immunol. Res. 8, 1099–1111.

Laurent, P., Sisirak, V., Lazaro, E., Richez, C., Duffau, P., Blanco, P., Truchetet, M.-E., Contin-Bordes, C., 2018. Innate Immunity in Systemic Sclerosis Fibrosis: Recent Advances. Front. Immunol. 9.

Le Mercier, I., Poujol, D., Sanlaville, A., Sisirak, V., Gobert, M., Durand, I., Dubois, B., Treilleux, I., Marvel, J., Vlach, J., Blay, J.-Y., Bendriss-Vermare, N., Caux, C., Puisieux, I., Goutagny, N., 2013. Tumor promotion by intratumoral plasmacytoid dendritic cells is reversed by TLR7 ligand treatment. Cancer Res. 73, 4629–4640. https://doi.org/10.1158/0008-5472.CAN-12-3058

Leibler, C., John, S., Elsner, R.A., Thomas, K.B., Smita, S., Joachim, S., Levack, R.C., Callahan, D.J., Gordon, R.A., Bastacky, S., Fukui, R., Miyake, K., Gingras, S., Nickerson, K.M., Shlomchik, M.J., 2022. Genetic dissection of TLR9 reveals complex regulatory and cryptic proinflammatory roles in mouse lupus. Nat. Immunol. 23, 1457–1469.

Leleu, D., Levionnois, E., Laurent, P., Lazaro, E., Richez, C., Duffau, P., Blanco, P., Sisirak, V., Contin-Bordes, C., Truchetet, M.-E., 2020. Elevated Circulatory Levels of Microparticles Are Associated to Lung Fibrosis and Vasculopathy During Systemic Sclerosis. Front. Immunol. 11, 532177.

Lesley, R., Kelly, L.M., Xu, Y., Cyster, J.G., 2006. Naive CD4 T cells constitutively express CD40L and augment autoreactive B cell survival. Proc. Natl. Acad. Sci. U. S. A. 103, 10717–10722.

Li, C., Wang, G., Sivasami, P., Ramirez, R.N., Zhang, Y., Benoist, C., Mathis, D., 2021. Interferon-α-producing plasmacytoid dendritic cells drive the loss of adipose tissue regulatory T cells during obesity. Cell Metab. 33, 1610-1623.e5.

Liu, C.-H., Chou, C.-T., Chen, Chen-Hung, Chen, Chun-Hsiung, Yang, S.-Y., Ko, Y.-A., Wu, Y.-T., Wang, C.-C., Liu, F.-C., Yue, C.-T., Hung, S.-C., Tzeng, I.-S., Tsai, W.-C., Lin, K.-I., 2020. Aberrant distribution and function of plasmacytoid dendritic cells in patients with ankylosing spondylitis are associated with unfolded protein response. Kaohsiung J. Med. Sci. 36, 441–449.

Luo, X., Li, H., Ma, L., Zhou, J., Guo, X., Woo, S.-L., Pei, Y., Knight, L.R., Deveau, M., Chen, Y., Qian, X., Xiao, X., Li, Q., Chen, X., Huo, Y., McDaniel, K., Francis, H., Glaser, S., Meng, F., Alpini, G., Wu, C., 2018. Expression of STING Is Increased in Liver Tissues From Patients With NAFLD and Promotes Macrophage-Mediated Hepatic Inflammation and Fibrosis in Mice. Gastroenterology 155, 1971-1984.e4.

Majer, O., Liu, B., Woo, B.J., Kreuk, L.S.M., Van Dis, E., Barton, G.M., 2019. Release from UNC93B1 reinforces the compartmentalized activation of select TLRs. Nature 575, 371–374.

Marcus, A., Mao, A.J., Lensink-Vasan, M., Wang, L., Vance, R.E., Raulet, D.H., 2018. Tumor-Derived cGAMP Triggers a STING-Mediated Interferon Response in Non-tumor Cells to Activate the NK Cell Response 2018. Immunity 49, 754-763.e4.

Martins, I., Kepp, O., Schlemmer, F., Adjemian, S., Tailler, M., Shen, S., Michaud, M., Menger, L., Gdoura, A., Tajeddine, N., Tesniere, A., Zitvogel, L., Kroemer, G., 2011. Restoration of the immunogenicity of cisplatin-induced cancer cell death by endoplasmic reticulum stress. Oncogene 30, 1147–1158.

Matarese, G., 2023. The link between obesity and autoimmunity. Science 379, 1298–1300.

Maugeri, N., Capobianco, A., Rovere-Querini, P., Ramirez, G.A., Tombetti, E., Valle, P.D., Monno, A., D'Alberti, V., Gasparri, A.M., Franchini, S., D'Angelo, A., Bianchi, M.E., Manfredi, A.A., 2018. Platelet microparticles sustain autophagy-associated activation of neutrophils in systemic sclerosis. Sci. Transl. Med. 10, eaao3089.

Maugeri, N., Franchini, S., Campana, L., Baldini, M., Ramirez, G.A., Sabbadini, M.G., Rovere-Querini, P., Manfredi, A.A., 2012. Circulating platelets as a source of the damage-associated molecular pattern HMGB1 in patients with systemic sclerosis. Autoimmunity 45, 584–587.

Maurer, B., Distler, J.H.W., Distler, O., 2013. The Fra-2 transgenic mouse model of systemic sclerosis. Vascul. Pharmacol. 58, 194–201.

Mayes, M.D., Bossini-Castillo, L., Gorlova, O., Martin, J.E., Zhou, X., Chen, W.V., Assassi, S., Ying, J., Tan, F.K., Arnett, F.C., Reveille, J.D., Guerra, S., Teruel, M., Carmona, F.D., Gregersen, P.K., Lee, A.T., López-Isac, E., Ochoa, E., Carreira, P., Simeón, C.P., Castellví, I., González-Gay, M.Á., Ortego-Centeno, N., Ríos, R., Callejas, J.L., Navarrete, N., García Portales, R., Camps, M.T., Fernández-Nebro, A., González-Escribano, M.F., Sánchez-Román, J., García-Hernández, F.J., Castillo, M.J., Aguirre, M.Á., Gómez-Gracia, I., Fernández-Gutiérrez, B., Rodríguez-Rodríguez, L., Vicente, E., Andreu, J.L., Fernández de Castro, M., García de la Peña, P., López-Longo, F.J., Martínez, L., Fonollosa, V., Espinosa, G., Tolosa, C., Pros, A., Rodríguez Carballeira, M., Narváez, F.J., Rubio Rivas, M., Ortiz Santamaría, V., Díaz, B., Trapiella, L., Freire, M. del C., Sousa, A., Egurbide, M.V., Fanlo Mateo, P., Sáez-Comet, L., Díaz, F., Hernández, V., Beltrán, E., Román-Ivorra, J.A., Grau, E., Alegre Sancho, J.J., Blanco García, F.J., Oreiro, N., Fernández Sueiro, L., Zhernakova, A., Padyukov, L., Alarcón-Riquelme, M., Wijmenga, C., Brown, M., Beretta, L., Riemekasten, G., Witte, T., Hunzelmann, N., Kreuter, A., Distler, J.H.W., Voskuyl, A.E., Schuerwegh, A.J., Hesselstrand, R., Nordin, A., Airó, P., Lunardi, C., Shiels, P., van Laar, J.M., Herrick, A., Worthington, J., Denton, C., Wigley, F.M., Hummers, L.K., Varga, J., Hinchcliff, M.E., Baron, M., Hudson, M., Pope, J.E., Furst, D.E., Khanna, D., Phillips, K., Schiopu, E., Segal, B.M., Molitor, J.A., Silver, R.M., Steen, V.D., Simms, R.W., Lafyatis, R.A., Fessler, B.J., Frech, T.M., AlKassab, F., Docherty, P., Kaminska, E., Khalidi, N., Jones, H.N., Markland, J., Robinson, D., Broen, J., Radstake, T.R.D.J., Fonseca, C., Koeleman, B.P., Martin, J., 2014. Immunochip Analysis Identifies Multiple Susceptibility Loci for Systemic Sclerosis. Am. J. Hum. Genet. 94, 47–61.

McNelis, J.C., Olefsky, J.M., 2014. Macrophages, immunity, and metabolic disease. Immunity 41, 36–48.

Means, T.K., Latz, E., Hayashi, F., Murali, M.R., Golenbock, D.T., Luster, A.D., 2005. Human lupus autoantibody-DNA complexes activate DCs through cooperation of CD32 and TLR9. J. Clin. Invest. 115, 407–417.

Meng, M., Tan, J., Chen, W., Du, Q., Xie, B., Wang, N., Zhu, H., Wang, K., 2019. The Fibrosis and Immunological Features of Hypochlorous Acid Induced Mouse Model of Systemic Sclerosis. Front. Immunol. 10, 1861.

Michea, P., Vargas, P., Donnadieu, M.-H., Rosemblatt, M., Bono, M.R., Duménil, G., Soumelis, V., 2013. Epithelial control of the human pDC response to extracellular bacteria. Eur. J. Immunol. 43, 1264–1273.

Mombaerts, P., Iacomini, J., Johnson, R.S., Herrup, K., Tonegawa, S., Papaioannou, V.E., 1992. RAG-1-deficient mice have no mature B and T lymphocytes. Cell 68, 869–877.

Morel, L., Croker, B.P., Blenman, K.R., Mohan, C., Huang, G., Gilkeson, G., Wakeland, E.K., 2000. Genetic reconstitution of systemic lupus erythematosus immunopathology with polycongenic murine strains. Proc. Natl. Acad. Sci. U. S. A. 97, 6670–6675.

Moro-Sibilot, L., This, S., Blanc, P., Sanlaville, A., Sisirak, V., Bardel, E., Boschetti, G., Bendriss-Vermare, N., Defrance, T., Dubois, B., Kaiserlian, D., 2016. Plasmacytoid dendritic cells are dispensable for noninfectious intestinal IgA responses in vivo. Eur. J. Immunol. 46, 354–359.

Nakasone, E.S., Askautrud, H.A., Kees, T., Park, J.-H., Plaks, V., Ewald, A.J., Fein, M., Rasch, M.G., Tan, Y.-X., Qiu, J., Park, J., Sinha, P., Bissell, M.J., Frengen, E., Werb, Z., Egeblad, M., 2012. Imaging Tumor-Stroma Interactions during Chemotherapy Reveals Contributions of the Microenvironment to Resistance. Cancer Cell 21, 488–503.

Napirei, M., Karsunky, H., Zevnik, B., Stephan, H., Mannherz, H.G., Möröy, T., 2000. Features of systemic lupus erythematosus in Dnase1-deficient mice. Nat. Genet. 25, 177–181.

Napirei, M., Wulf, S., Eulitz, D., Mannherz, H.G., Kloeckl, T., 2005. Comparative characterization of rat deoxyribonuclease 1 (Dnase1) and murine deoxyribonuclease 1-like 3 (Dnase1l3). Biochem. J. 389, 355–364.

Nestle, F.O., Conrad, C., Tun-Kyi, A., Homey, B., Gombert, M., Boyman, O., Burg, G., Liu, Y.-J., Gilliet, M., 2005. Plasmacytoid predendritic cells initiate psoriasis through interferon-α production. J. Exp. Med. 202, 135–143.

Nishimoto, S., Fukuda, D., Higashikuni, Y., Tanaka, K., Hirata, Y., Murata, C., Kim-Kaneyama, J., Sato, F., Bando, M., Yagi, S., Soeki, T., Hayashi, T., Imoto, I., Sakaue, H., Shimabukuro, M., Sata, M., 2016. Obesity-induced DNA released from adipocytes stimulates chronic adipose tissue inflammation and insulin resistance. Sci. Adv. 2, e1501332.

Onuora, S., 2016. DNASE1L3 prevents anti-DNA responses. Nat. Rev. Rheumatol. 12, 437–437.

Onuora, S., 2014. Connective tissue diseases: depleting plasmacytoid dendritic cells: a new therapeutic approach in SLE? Nat. Rev. Rheumatol. 10, 573.

Ozçakar, Z.B., Foster, J., Diaz-Horta, O., Kasapcopur, O., Fan, Y.-S., Yalçınkaya, F., Tekin, M., 2013. DNASE1L3 mutations in hypocomplementemic urticarial vasculitis syndrome. Arthritis Rheum. 65, 2183–2189.

Paç Kisaarslan, A., Witzel, M., Unal, E., Rohlfs, M., Akyildiz, B., Dogan, M.E., Poyrazoglu, H., Klein, C., Patiroglu, T., 2020. Refractory and Fatal Presentation of Severe Autoimmune Hemolytic Anemia in a

Child With the DNASE1L3 Mutation Complicated With an Additional DOCK8 Variant. J. Pediatr. Hematol. Oncol.

Pellerin, A., Otero, K., Czerkowicz, J.M., Kerns, H.M., Shapiro, R.I., Ranger, A.M., Otipoby, K.L., Taylor, F.R., Cameron, T.O., Viney, J.L., Rabah, D., 2015. Anti-BDCA2 monoclonal antibody inhibits plasmacytoid dendritic cell activation through Fc-dependent and Fc-independent mechanisms. EMBO Mol. Med. 7, 464–476.

Pouget, J.-P., Santoro, L., Piron, B., Paillas, S., Ladjohounlou, R., Pichard, A., Poty, S., Deshayes, E., Constanzo, J., Bardiès, M., 2022. From the target cell theory to a more integrated view of radiobiology in Targeted radionuclide therapy: The Montpellier group's experience. Nucl. Med. Biol. 104–105, 53–64.

Prete, F., Catucci, M., Labrada, M., Gobessi, S., Castiello, M.C., Bonomi, E., Aiuti, A., Vermi, W., Cancrini, C., Metin, A., Hambleton, S., Bredius, R., Notarangelo, L.D., van der Burg, M., Kalinke, U., Villa, A., Benvenuti, F., 2013. Wiskott-Aldrich syndrome protein-mediated actin dynamics control type-I interferon production in plasmacytoid dendritic cells. J. Exp. Med. 210, 355–374.

Pulido, Á. de M., Hänggi, K., Celias, D.P., Gardner, A., Li, J., Batista-Bittencourt, B., Mohamed, E., Trillo-Tinoco, J., Osunmakinde, O., Peña, R., Onimus, A., Kaisho, T., Kaufmann, J., McEachern, K., Soliman, H., Luca, V.C., Rodriguez, P.C., Yu, X., Ruffell, B., 2021. The inhibitory receptor TIM-3 limits activation of the cGAS-STING pathway in intra-tumoral dendritic cells by suppressing extracellular DNA uptake. Immunity 54, 1154-1167.e7.

Reizis, B., 2019. Plasmacytoid Dendritic Cells: Development, Regulation, and Function. Immunity 50, 37–50.

Reizis, B., Bunin, A., Ghosh, H.S., Lewis, K.L., Sisirak, V., 2011. Plasmacytoid dendritic cells: recent progress and open questions. Annu. Rev. Immunol. 29, 163–183.

Remmerie, A., Martens, L., Thoné, T., Castoldi, A., Seurinck, R., Pavie, B., Roels, J., Vanneste, B., De Prijck, S., Vanhockerhout, M., Binte Abdul Latib, M., Devisscher, L., Hoorens, A., Bonnardel, J., Vandamme, N., Kremer, A., Borghgraef, P., Van Vlierberghe, H., Lippens, S., Pearce, E., Saeys, Y., Scott, C.L., 2020. Osteopontin Expression Identifies a Subset of Recruited Macrophages Distinct from Kupffer Cells in the Fatty Liver. Immunity 53, 641-657.e14.

Revelo, X.S., Ghazarian, M., Chng, M.H.Y., Luck, H., Kim, J.H., Zeng, K., Shi, S.Y., Tsai, S., Lei, H., Kenkel, J., Liu, C.L., Tangsombatvisit, S., Tsui, H., Sima, C., Xiao, C., Shen, L., Li, X., Jin, T., Lewis, G.F., Woo, M., Utz, P.J., Glogauer, M., Engleman, E., Winer, S., Winer, D.A., 2016. Nucleic Acid-Targeting Pathways Promote Inflammation in Obesity-Related Insulin Resistance. Cell Rep. 16, 717–730.

Rodero, M.P., Tesser, A., Bartok, E., Rice, G.I., Della Mina, E., Depp, M., Beitz, B., Bondet, V., Cagnard, N., Duffy, D., Dussiot, M., Frémond, M.-L., Gattorno, M., Guillem, F., Kitabayashi, N., Porcheray, F., Rieux-Laucat, F., Seabra, L., Uggenti, C., Volpi, S., Zeef, L.A.H., Alyanakian, M.-A., Beltrand, J., Bianco, A.M., Boddaert, N., Brouzes, C., Candon, S., Caorsi, R., Charbit, M., Fabre, M., Faletra, F., Girard, M., Harroche, A., Hartmann, E., Lasne, D., Marcuzzi, A., Neven, B., Nitschke, P., Pascreau, T., Pastore, S., Picard, C., Picco, P., Piscianz, E., Polak, M., Quartier, P., Rabant, M., Stocco, G., Taddio, A., Uettwiller, F., Valencic, E., Vozzi, D., Hartmann, G., Barchet, W., Hermine, O., Bader-Meunier, B., Tommasini, A., Crow, Y.J., 2017. Type I interferon-mediated autoinflammation due to DNase II deficiency. Nat. Commun. 8, 2176.

Rodrigues, P.F., Alberti-Servera, L., Eremin, A., Grajales-Reyes, G.E., Ivanek, R., Tussiwand, R., 2018. Distinct progenitor lineages contribute to the heterogeneity of plasmacytoid dendritic cells. Nat. Immunol. 19, 711–722.

Saito, Y., Hikita, H., Nozaki, Y., Kai, Y., Makino, Y., Nakabori, T., Tanaka, S., Yamada, R., Shigekawa, M., Kodama, T., Sakamori, R., Tatsumi, T., Takehara, T., 2019. DNase II activated by the mitochondrial apoptotic pathway regulates RIP1-dependent non-apoptotic hepatocyte death via the TLR9/IFN-β signaling pathway. Cell Death Differ. 26, 470–486.

Saltiel, A.R., Olefsky, J.M., 2017. Inflammatory mechanisms linking obesity and metabolic disease. J. Clin. Invest. 127, 1–4.

Santa, P., Garreau, A., Serpas, L., Ferriere, A., Blanco, P., Soni, C., Sisirak, V., 2021. The Role of Nucleases and Nucleic Acid Editing Enzymes in the Regulation of Self-Nucleic Acid Sensing. Front. Immunol. 12, 629922.

Santiago-Raber, M.-L., Baccala, R., Haraldsson, K.M., Choubey, D., Stewart, T.A., Kono, D.H., Theofilopoulos, A.N., 2003. Type-I interferon receptor deficiency reduces lupus-like disease in NZB mice. J. Exp. Med. 197, 777–788.

Sawai, C.M., Serpas, L., Neto, A.G., Jang, G., Rashidfarrokhi, A., Kolbeck, R., Sanjuan, M.A., Reizis, B., Sisirak, V., 2018. Plasmacytoid Dendritic Cells Are Largely Dispensable for the Pathogenesis of Experimental Inflammatory Bowel Disease. Front. Immunol. 9, 2475. 5

Sawai, C.M., Sisirak, V., Ghosh, H.S., Hou, E.Z., Ceribelli, M., Staudt, L.M., Reizis, B., 2013. Transcription factor Runx2 controls the development and migration of plasmacytoid dendritic cells. J. Exp. Med. 210, 2151–2159.

Schadt, L., Sparano, C., Schweiger, N.A., Silina, K., Cecconi, V., Lucchiari, G., Yagita, H., Guggisberg, E., Saba, S., Nascakova, Z., Barchet, W., Broek, M. van den, 2019. Cancer-Cell-Intrinsic cGAS Expression Mediates Tumor Immunogenicity 2019. Cell Rep. 29, 1236-1248.e7.

Scherlinger, M., Guillotin, V., Douchet, I., Vacher, P., Boizard-Moracchini, A., Guegan, J.-P., Garreau, A., Merillon, N., Vermorel, A., Ribeiro, E., Machelart, I., Lazaro, E., Couzi, L., Duffau, P., Barnetche, T., Pellegrin, J.-L., Viallard, J.-F., Saleh, M., Schaeverbeke, T., Legembre, P., Truchetet, M.-E., Dumortier, H., Contin-Bordes, C., Sisirak, V., Richez, C., Blanco, P., 2021. Selectins impair regulatory T cell function and contribute to systemic lupus erythematosus pathogenesis. Sci. Transl. Med. 13, eabi4994.

Scherlinger, M., Guillotin, V., Truchetet, M.-E., Contin-Bordes, C., Sisirak, V., Duffau, P., Lazaro, E., Richez, C., Blanco, P., 2018. Systemic lupus erythematosus and systemic sclerosis: All roads lead to platelets. Autoimmun. Rev. 17, 625–635. https://doi.org/10.1016/j.autrev.2018.01.012

Scherlinger, M., Sisirak, V., Richez, C., Lazaro, E., Duffau, P., Blanco, P., 2017. New Insights on Platelets and Platelet-Derived Microparticles in Systemic Lupus Erythematosus. Curr. Rheumatol. Rep. 19, 48.

Serpas, L., Chan, R.W.Y., Jiang, P., Ni, M., Sun, K., Rashidfarrokhi, A., Soni, C., Sisirak, V., Lee, W.-S., Cheng, S.H., Peng, W., Chan, K.C.A., Chiu, R.W.K., Reizis, B., Lo, Y.M.D., 2019. Dnase1l3 deletion causes aberrations in length and end-motif frequencies in plasma DNA. Proc. Natl. Acad. Sci. U. S. A. 116, 641–649.

Seth, S., Oberdörfer, L., Hyde, R., Hoff, K., Thies, V., Worbs, T., Schmitz, S., Förster, R., 2011. CCR7 essentially contributes to the homing of plasmacytoid dendritic cells to lymph nodes under steady-state as well as inflammatory conditions. J. Immunol. Baltim. Md 1950 186, 3364–3372.

Shibata, T., Ohto, U., Nomura, S., Kibata, K., Motoi, Y., Zhang, Y., Murakami, Y., Fukui, R., Ishimoto, T., Sano, S., Ito, T., Shimizu, T., Miyake, K., 2016. Guanosine and its modified derivatives are endogenous ligands for TLR7. Int. Immunol. 28, 211–222. https://doi.org/10.1093/intimm/dxv062

Sisirak, V., Faget, J., Gobert, M., Goutagny, N., Vey, N., Treilleux, I., Renaudineau, S., Poyet, G., Labidi-Galy, S.I., Goddard-Leon, S., Durand, I., Le Mercier, I., Bajard, A., Bachelot, T., Puisieux, A., Puisieux, I., Blay, J.-Y., Ménétrier-Caux, C., Caux, C., Bendriss-Vermare, N., 2012. Impaired IFN-α production by plasmacytoid dendritic cells favors regulatory T-cell expansion that may contribute to breast cancer progression. Cancer Res. 72, 5188–5197.

Sisirak, V., Ganguly, D., Lewis, K.L., Couillault, C., Tanaka, L., Bolland, S., D'Agati, V., Elkon, K.B., Reizis, B., 2014. Genetic evidence for the role of plasmacytoid dendritic cells in systemic lupus erythematosus. J. Exp. Med. 211, 1969–1976.

Sisirak, V., Sally, B., D'Agati, V., Martinez-Ortiz, W., Özçakar, Z.B., David, J., Rashidfarrokhi, A., Yeste, A., Panea, C., Chida, A.S., Bogunovic, M., Ivanov, I.I., Quintana, F.J., Sanz, I., Elkon, K.B., Tekin, M., Yalçınkaya, F., Cardozo, T.J., Clancy, R.M., Buyon, J.P., Reizis, B., 2016. Digestion of Chromatin in Apoptotic Cell Microparticles Prevents Autoimmunity. Cell 166, 88–101.

Sisirak, V., Vey, N., Goutagny, N., Renaudineau, S., Malfroy, M., Thys, S., Treilleux, I., Labidi-Galy, S.I., Bachelot, T., Dezutter-Dambuyant, C., Ménétrier-Caux, C., Blay, J.-Y., Caux, C., Bendriss-Vermare, N., 2013. Breast cancer-derived transforming growth factor-β and tumor necrosis factor-α compromise interferon-α production by tumor-associated plasmacytoid dendritic cells. Int. J. Cancer 133, 771–778.

Sisirak, V., Vey, N., Vanbervliet, B., Duhen, T., Puisieux, I., Homey, B., Bowman, E.P., Trinchieri, G., Dubois, B., Kaiserlian, D., Lira, S.A., Puisieux, A., Blay, J.-Y., Caux, C., Bendriss-Vermare, N., 2011. CCR6/CCR10-mediated plasmacytoid dendritic cell recruitment to inflamed epithelia after instruction in lymphoid tissues. Blood 118, 5130–5140.

Skaug, B., Guo, X., Li, Y.J., Charles, J., Pham, K.T., Couturier, J., Lewis, D.E., Bracaglia, C., Caiello, I., Mayes, M.D., Assassi, S., 2023. Reduced digestion of circulating genomic DNA in systemic sclerosis patients with the DNASE1L3 R206C variant. Rheumatol. Oxf. Engl. kead050.

Soni, C., Perez, O.A., Voss, W.N., Pucella, J.N., Serpas, L., Mehl, J., Ching, K.L., Goike, J., Georgiou, G., Ippolito, G.C., Sisirak, V., Reizis, B., 2020. Plasmacytoid Dendritic Cells and Type I Interferon Promote Extrafollicular B Cell Responses to Extracellular Self-DNA. Immunity 52, 1022-1038.e7.

Soni, C., Wong, E.B., Domeier, P.P., Khan, T.N., Satoh, T., Akira, S., Rahman, Z.S.M., 2014. B cell-intrinsic TLR7 signaling is essential for the development of spontaneous germinal centers. J. Immunol. Baltim. Md 1950 193, 4400–4414.

Stetson, D.B., Ko, J.S., Heidmann, T., Medzhitov, R., 2008. Trex1 prevents cell-intrinsic initiation of autoimmunity. Cell 134, 587–598.

Strissel, K.J., Stancheva, Z., Miyoshi, H., Perfield, J.W., DeFuria, J., Jick, Z., Greenberg, A.S., Obin, M.S., 2007. Adipocyte Death, Adipose Tissue Remodeling, and Obesity Complications. Diabetes 56, 2910–2918.

Swiecki, M., Wang, Y., Riboldi, E., Kim, A.H.J., Dzutsev, A., Gilfillan, S., Vermi, W., Ruedl, C., Trinchieri, G., Colonna, M., 2014. Cell depletion in mice that express diphtheria toxin receptor under the control of SiglecH encompasses more than plasmacytoid dendritic cells. J. Immunol. Baltim. Md 1950 192, 4409–4416.

Tamkovich, S.N., Cherepanova, A.V., Kolesnikova, E.V., Rykova, E.Y., Pyshnyi, D.V., Vlassov, V.V., Laktionov, P.P., 2006. Circulating DNA and DNase Activity in Human Blood. Ann. N. Y. Acad. Sci. 1075, 191–196.

Tedeschi, S.K., Barbhaiya, M., Malspeis, S., Lu, B., Sparks, J.A., Karlson, E.W., Willett, W., Costenbader, K.H., 2017. Obesity and the risk of systemic lupus erythematosus among women in the Nurses' Health Studies. Semin. Arthritis Rheum. 47, 376–383.

Teijeira, Á., Garasa, S., Gato, M., Alfaro, C., Migueliz, I., Cirella, A., de Andrea, C., Ochoa, M.C., Otano, I., Etxeberria, I., Andueza, M.P., Nieto, C.P., Resano, L., Azpilikueta, A., Allegretti, M., de Pizzol, M., Ponz-Sarvisé, M., Rouzaut, A., Sanmamed, M.F., Schalper, K., Carleton, M., Mellado, M., Rodriguez-Ruiz, M.E., Berraondo, P., Perez-Gracia, J.L., Melero, I., 2020. CXCR1 and CXCR2 Chemokine Receptor Agonists Produced by Tumors Induce Neutrophil Extracellular Traps that Interfere with Immune Cytotoxicity. Immunity 52, 856-871.e8.

Tran, S., Baba, I., Poupel, L., Dussaud, S., Moreau, M., Gélineau, A., Marcelin, G., Magréau-Davy, E., Ouhachi, M., Lesnik, P., Boissonnas, A., Le Goff, W., Clausen, B.E., Yvan-Charvet, L., Sennlaub, F., Huby, T., Gautier, E.L., 2020. Impaired Kupffer Cell Self-Renewal Alters the Liver Response to Lipid Overload during Non-alcoholic Steatohepatitis. Immunity 53, 627-640.e5.

Treilleux, I., Blay, J.-Y., Bendriss-Vermare, N., Ray-Coquard, I., Bachelot, T., Guastalla, J.-P., Bremond, A., Goddard, S., Pin, J.-J., Barthelemy-Dubois, C., Lebecque, S., 2004. Dendritic cell infiltration and prognosis of early stage breast cancer. Clin. Cancer Res. Off. J. Am. Assoc. Cancer Res. 10, 7466–7474.

Tsokos, G.C., Lo, M.S., Costa Reis, P., Sullivan, K.E., 2016. New insights into the immunopathogenesis of systemic lupus erythematosus. Nat. Rev. Rheumatol. 12, 716–730.

Tusseau, M., Lovšin, E., Samaille, C., Pescarmona, R., Mathieu, A.-L., Maggio, M.-C., Selmanović, V., Debeljak, M., Dachy, A., Novljan, G., Janin, A., Januel, L., Gibier, J.-B., Chopin, E., Rouvet, I., Goncalves, D., Fabien, N., Rice, G.I., Lesca, G., Labalme, A., Romagnani, P., Walzer, T., Viel, S., Perret, M., Crow, Y.J., Avčin, T., Cimaz, R., Belot, A., 2022. DNASE1L3 deficiency, new phenotypes, and evidence for a transient type I IFN signaling. J. Clin. Immunol. 42, 1310–1320.

Van der Fits, L., Mourits, S., Voerman, J.S.A., Kant, M., Boon, L., Laman, J.D., Cornelissen, F., Mus, A.-M., Florencia, E., Prens, E.P., Lubberts, E., 2009. Imiquimod-induced psoriasis-like skin inflammation in mice is mediated via the IL-23/IL-17 axis. J. Immunol. Baltim. Md 1950 182, 5836–5845. https://doi.org/10.4049/jimmunol.0802999

Vanbervliet, B., Homey, B., Durand, I., Massacrier, C., Aït-Yahia, S., de Bouteiller, O., Vicari, A., Caux, C., 2002. Sequential involvement of CCR2 and CCR6 ligands for immature dendritic cell recruitment: possible role at inflamed epithelial surfaces. Eur. J. Immunol. 32, 231–242.

Vanpouille-Box, C., Alard, A., Aryankalayil, M.J., Sarfraz, Y., Diamond, J.M., Schneider, R.J., Inghirami, G., Coleman, C.N., Formenti, S.C., Demaria, S., 2017. DNA exonuclease Trex1 regulates radiotherapy-induced tumour immunogenicity. Nat. Commun. 8.

Vermi, W., Soncini, M., Melocchi, L., Sozzani, S., Facchetti, F., 2011. Plasmacytoid dendritic cells and cancer. J. Leukoc. Biol. 90, 681–690.

Victora, G.D., Nussenzweig, M.C., 2022. Germinal Centers. Annu. Rev. Immunol. 40, 413–442.

Wang, H., Hu, S., Chen, X., Shi, H., Chen, C., Sun, L., Chen, Z.J., 2017. cGAS is essential for the antitumor effect of immune checkpoint blockade. Proc. Natl. Acad. Sci. 114, 1637–1642.

Wang, S., Campos, J., Gallotta, M., Gong, M., Crain, C., Naik, E., Coffman, R.L., Guiducci, C., 2016. Intratumoral injection of a CpG oligonucleotide reverts resistance to PD-1 blockade by expanding multifunctional CD8 $^{+}$ T cells. Proc. Natl. Acad. Sci. 113, E7240–E7249.

Wang, X., He, Q., Zhou, C., Xu, Y., Liu, D., Fujiwara, N., Kubota, N., Click, A., Henderson, P., Vancil, J., Marquez, C.A., Gunasekaran, G., Schwartz, M.E., Tabrizian, P., Sarpel, U., Fiel, M.I., Diao, Y., Sun, B., Hoshida, Y., Liang, S., Zhong, Z., 2023. Prolonged hypernutrition impairs TREM2-dependent efferocytosis to license chronic liver inflammation and NASH development. Immunity 56, 58-77.e11.

Wang, X.-A., Zhang, R., Zhang, S., Deng, S., Jiang, D., Zhong, J., Yang, L., Wang, T., Hong, S., Guo, S., She, Z.-G., Zhang, X.-D., Li, H., 2013. Interferon regulatory factor 7 deficiency prevents diet-induced obesity and insulin resistance. Am. J. Physiol.-Endocrinol. Metab. 305, E485–E495.

Wang, Z., Chen, J., Hu, J., Zhang, H., Xu, F., He, W., Wang, X., Li, M., Lu, W., Zeng, G., Zhou, P., Huang, P., Chen, S., Li, W., Xia, L., Xia, X., 2019. cGAS/STING axis mediates a topoisomerase II inhibitor-induced tumor immunogenicity. J. Clin. Invest.

Weisenburger, T., von Neubeck, B., Schneider, A., Ebert, N., Schreyer, D., Acs, A., Winkler, T.H., 2018. Epistatic Interactions Between Mutations of Deoxyribonuclease 1-Like 3 and the Inhibitory Fc Gamma Receptor IIB Result in Very Early and Massive Autoantibodies Against Double-Stranded DNA. Front. Immunol. 9.

Werth, V.P., Furie, R.A., Romero-Diaz, J., Navarra, S., Kalunian, K., van Vollenhoven, R.F., Nyberg, F., Kaffenberger, B.H., Sheikh, S.Z., Radunovic, G., Huang, X., Clark, G., Carroll, H., Naik, H., Gaudreault, F., Meyers, A., Barbey, C., Musselli, C., Franchimont, N., LILAC Trial Investigators, 2022. Trial of Anti-BDCA2 Antibody Litifilimab for Cutaneous Lupus Erythematosus. N. Engl. J. Med. 387, 321–331.

Wilber, A., Lu, M., Schneider, M.C., 2002. Deoxyribonuclease I-like III is an inducible macrophage barrier to liposomal transfection. Mol. Ther. J. Am. Soc. Gene Ther. 6, 35–42.

Woo, S.-R., Corrales, L., Gajewski, T.F., 2015. Innate Immune Recognition of Cancer. Annu. Rev. Immunol. 33, 445–474.

Woo, S.-R., Fuertes, M.B., Corrales, L., Spranger, S., Furdyna, M.J., Leung, M.Y.K., Duggan, R., Wang, Y., Barber, G.N., Fitzgerald, K.A., Alegre, M.-L., Gajewski, T.F., 2014. STING-Dependent Cytosolic DNA Sensing Mediates Innate Immune Recognition of Immunogenic Tumors. Immunity 41, 830–842.

Xu, M.M., Pu, Y., Han, D., Shi, Y., Cao, X., Liang, H., Chen, X., Li, X.-D., Deng, L., Chen, Z.J., Weichselbaum, R.R., Fu, Y.-X., 2017. Dendritic Cells but Not Macrophages Sense Tumor Mitochondrial DNA for Cross-priming through Signal Regulatory Protein α Signaling. Immunity 47, 363-373.e5.

Yamazaki, T., Kirchmair, A., Sato, A., Buqué, A., Rybstein, M., Petroni, G., Bloy, N., Finotello, F., Stafford, L., Navarro Manzano, E., Ayala de la Peña, F., García-Martínez, E., Formenti, S.C., Trajanoski, Z., Galluzzi, L., 2020. Mitochondrial DNA drives abscopal responses to radiation that are inhibited by autophagy. Nat. Immunol. 21, 1160–1171.

Yang, J.-Y., Kim, M.-S., Kim, E., Cheon, J.H., Lee, Y.-S., Kim, Y., Lee, S.-H., Seo, S.-U., Shin, S.-H., Choi, S.S., Kim, B., Chang, S.-Y., Ko, H.-J., Bae, J.-W., Kweon, M.-N., 2016. Enteric Viruses Ameliorate Gut Inflammation via Toll-like Receptor 3 and Toll-like Receptor 7-Mediated Interferon-β Production. Immunity 44, 889–900.

Yoshida, H., Okabe, Y., Kawane, K., Fukuyama, H., Nagata, S., 2005. Lethal anemia caused by interferon-beta produced in mouse embryos carrying undigested DNA. Nat. Immunol. 6, 49–56.

Yu, Y., Liu, Y., An, W., Song, J., Zhang, Y., Zhao, X., 2019. STING-mediated inflammation in Kupffer cells contributes to progression of nonalcoholic steatohepatitis. J. Clin. Invest. 129, 546–555.

Zhang, H., Tang, K., Zhang, Y., Ma, R., Ma, J., Li, Y., Luo, S., Liang, X., Ji, T., Gu, Z., Lu, J., He, W., Cao, X., Wan, Y., Huang, B., 2015. Cell-free Tumor Microparticle Vaccines Stimulate Dendritic Cells via cGAS/STING Signaling. Cancer Immunol. Res. 3, 196–205.

Zigmond, E., Bernshtein, B., Friedlander, G., Walker, C.R., Yona, S., Kim, K.-W., Brenner, O., Krauthgamer, R., Varol, C., Müller, W., Jung, S., 2014. Macrophage-Restricted Interleukin-10 Receptor Deficiency, but Not IL-10 Deficiency, Causes Severe Spontaneous Colitis. Immunity 40, 720–733.

Zitvogel, L., Galluzzi, L., Kepp, O., Smyth, M.J., Kroemer, G., 2015. Type I interferons in anticancer immunity. Nat. Rev. Immunol. 15, 405–414.

Zochling, J., Newell, F., Charlesworth, J.C., Leo, P., Stankovich, J., Cortes, A., Zhou, Y., Stevens, W., Sahhar, J., Roddy, J., Nash, P., Tymms, K., Rischmueller, M., Lester, S., Proudman, S., Brown, M.A., 2014. An Immunochip-based interrogation of scleroderma susceptibility variants identifies a novel association at DNASE1L3. Arthritis Res. Ther. 16.

VII. SELECTED PUBLICATIONS (ANNEXES)

ANNEX 1, Sisirak et al, Cancer Research, 2012

Impaired IFN-α production by plasmacytoid dendritic cells favors regulatory T-cell expansion that may contribute to breast cancer progression

ANNEX 2, Sisirak et al, Journal of Experimental Medicine. 2014

Genetic evidence for the role of plasmacytoid dendritic cells in systemic lupus erythematosus.

ANNEX 3, Sisirak et al, Cell. 2016

Digestion of Chromatin in Apoptotic Cell Microparticles Prevents Autoimmunity.

ANNEX 4, Sawai et al, Frontiers in Immunology. 2018

Plasmacytoid dendritic cells are dispensable for inflammatory bowel disease pathogenesis.

ANNEX 5, Soni et al, Immunity. 2020

Plasmacytoid dendritic cells promote extrafollicular anti-DNA responses in lupus through type I interferon

ANNEX 6, Ferriere et al, In preparation

DNASE1L3 deficiency exacerbates obesity-mediated inflammation and metabolic syndrome

Impaired IFN-α Production by Plasmacytoid Dendritic Cells Favors Regulatory T-cell Expansion That May Contribute to Breast Cancer Progression

Vanja Sisirak[1,2,3,4,5], Julien Faget[1,2,3,4,5], Michael Gobert[1,2,3,4,5], Nadège Goutagny[1,2,3,4,5], Nelly Vey[1,2,3,4,5], Isabelle Treilleux[6], Sarah Renaudineau[1,2,3,4,5], Gaelle Poyet[1,2,3,4,5], Sana Intidhar Labidi-Galy[1,2,3,4,5,6], Sophie Goddard-Leon[6], Isabelle Durand[1,2,3,4,5,6], Isabelle Le Mercier[1,2,3,4,5], Agathe Bajard[6], Thomas Bachelot[1,2,3,4,5,6], Alain Puisieux[1,2,3,4,5,6,7], Isabelle Puisieux[1,2,3,4,5,6], Jean-Yves Blay[1,2,3,4,5,6], Christine Ménétrier-Caux[1,2,3,4,5,6], Christophe Caux[1,2,3,4,5,6], and Nathalie Bendriss-Vermare[1,2,3,4,5]

Abstract

Infiltration and dysfunction of immune cells have been documented in many types of cancers. We previously reported that plasmacytoid dendritic cells (pDC) within primary breast tumors correlate with an unfavorable prognosis for patients. The role of pDC in cancer remains unclear but they have been shown to mediate immune tolerance in other pathophysiologic contexts. We postulated that pDC may interfere with antitumor immune response and favor tolerance in breast cancer. The present study was designed to decipher the mechanistic basis for the deleterious impact of pDC on the clinical outcome. Using fresh human breast tumor biopsies ($N = 60$ patients), we observed through multiparametric flow cytometry increased tumor-associated (TA) pDC (TApDC) rates in aggressive breast tumors, i.e., those with high mitotic index and the so-called triple-negative breast tumors (TNBT). Furthermore, TApDC expressed a partially activated phenotype and produced very low amounts of IFN-α following toll-like receptor activation *in vitro* compared with patients' blood pDC. Within breast tumors, TApDC colocalized and strongly correlated with TA regulatory T cells (TATreg), especially in TNBT. Of most importance, the selective suppression of IFN-α production endowed TApDC with the unique capacity to sustain FoxP3$^+$ Treg expansion, a capacity that was reverted by the addition of exogenous IFN-α. These findings indicate that IFN-α–deficient TApDC accumulating in aggressive tumors are involved in the expansion of TATreg *in vivo*, contributing to tumor immune tolerance and poor clinical outcome. Thus, targeting pDC to restore their IFN-α production may represent an attractive therapeutic strategy to overcome immune tolerance in breast cancer. *Cancer Res; 72(20); 5188–97. ©2012 AACR.*

Introduction

Functional alteration of tumor-associated dendritic cells (TADC) that play a critical role in antitumor immunity, as well as mobilization of immunosuppressive regulatory T cells (Treg) that shut down immune responses, have been associated with tumor tolerance (1). Most cancers, including breast tumors, are highly infiltrated by immune cells. Tumor-resident DC are conditioned by the tumor microenvironment to favor tolerogenic responses that could contribute to disease progression (2). Indeed, we previously showed that plasmacytoid DC (pDC) and Treg infiltrating breast tumors correlate with an adverse clinical outcome (3, 4), suggesting that both pDC and Treg are involved in breast cancer progression.

pDC are well known for their role in antiviral immunosurveillance through their massive production of type I IFN-α/β/ω in response to DNA or RNA viruses, recognized by toll-like receptors (TLR) 9 and 7, respectively (see ref. 5 for review). Beside their direct antiviral properties, type I IFNs produced by pDC activate natural killer (NK) cells, macrophages, and CD11c$^+$ myeloid DC (mDC) to elicit antimicrobial/viral/tumor immune responses (5). Moreover, differentiated mature pDC are capable of efficient antigen (cross)-presentation (6, 7) directing T-cell responses with considerable flexibility (5). Of importance, recent works have also established a critical role of pDC in noninfectious autoimmune/inflammatory pathologies (lupus, psoriasis) because of uncontrolled production of IFN-α following their chronic activation by self-nucleic acids (8, 9).

Authors' Affiliations: [1]Université de Lyon; [2]Université Lyon 1, ISPB; [3]INSERM U1052, Centre de Recherche en Cancérologie de Lyon; [4]CNRS UMR5286, Centre de Recherche en Cancérologie de Lyon; [5]LabEx DEVweCAN; [6]Centre Léon Bérard, Lyon, France; and [7]Institut Universitaire de France, Paris, France

Note: Supplementary data for this article are available at Cancer Research Online (http://cancerres.aacrjournals.org/).

V. Sisirak and J. Faget contributed equally to this work.

Corresponding Author: Nathalie Bendriss-Vermare, Centre de Recherche en Cancérologie de Lyon, INSERM U1052 CNRS 5286, Centre Léon Bérard, 28 rue Laennec, 69373 Lyon cedex 08, France. Phone: 33-4-7878-2750; Fax: 33-4-7878-2720; E-mail: nathalie.bendriss-vermare@lyon.unicancer.fr

doi: 10.1158/0008-5472.CAN-11-3468

In addition to immune activation, increasing evidence suggests that pDC also play regulatory functions. Under certain circumstances, the tolerogenic role of pDC as inducers of Treg in the periphery has been clearly illustrated *in vivo* (see ref. 10 for review) as well as their capacity to induce the differentiation (11–13) and expansion (14, 15) of Treg *in vitro*.

pDC are also involved in antitumor immunity, as underlined by their recent identification in several human and murine solid cancers (4, 16–19). Only sparse information are available on TApDC functions showing (i) poor stimulation of CD4 and CD8 T cells (18, 19), (ii) induction of anergic and/or suppressive CD4 and CD8 T cells (19, 20), (iii) promotion of multiple myeloma cell growth, survival, and drug resistance (21), but also (iv) involvement in therapeutic response to TLR7 ligands (22, 23). In breast cancer, we previously reported an accumulation of suppressive and activated Treg that proliferate *in situ* and that are associated with a poor prognosis (3), indicating that TATreg can expand in the tumor microenvironment.

To understand the negative impact of TApDC on breast tumor patients' outcome and its possible link with TATreg, we investigated herein, their functional competence within breast tumors. We show that TApDC are impaired for their IFN-α production and consequently promote immune tolerance through TATreg expansion and differentiation of interleukin 10 (IL-10)-secreting T cells, leading to tumor progression and poor clinical outcome in breast cancer. Thus, restoring the production of IFN-α by pDC within breast tumors emerges as an appealing therapeutic strategy to trigger antitumor immunity.

Materials and Methods

Patients, human tissue samples, and blood

Fresh tumor and blood samples (collected on CTAD anticoagulant) from 60 patients diagnosed with primary breast carcinoma were obtained before any treatment from the Centre Léon Bérard (CLB) tissue bank after patient informed consent. The study was reviewed and approved by the Institutional Review Board of CLB. Discarded human tonsil material was obtained anonymously according to the institutional regulations in compliance with French law. Healthy human blood was obtained anonymously from the Etablissement Français du Sang (Lyon, France). Written informed consent was obtained from all study participants in accordance with the Declaration of Helsinki. The breast cancer patients' characteristics are detailed in Supplementary Table S1. All clinical and biologic data related to breast cancer patients were collected prospectively and included in a regularly updated institutional database at CLB.

Isolation of pDC, naïve and memory $CD4^+$ T cells, and *in vitro* generation of monocyte-derived DC

Breast tumor samples, tonsils, and blood were processed as previously described (3). pDC and naïve or memory $CD4^+$ T cells were obtained from tissues after magnetic enrichment or fluorescence-activated cell sorting (FACS)-sorting. Monocyte-derived DC (MoDC) were obtained from blood-purified monocytes. Detailed methods are provided in Supplementary Methods.

Stimulation of pDC

TApDC were cultured at 5×10^5 cells/mL in 96-well flat-bottomed plates in complete medium for 24 hours in the presence of IL-3 (20 ng/mL), inactivated flu virus (100 HAU/mL), CpG-A (5 μg/mL), CpG-B (5 μg/mL), and R848 (1 μg/mL). Healthy pDC were cultured in presence of IL-3 with or without breast TUMSN (25%) for 16 hours before TLR activation. Cells and supernatants were harvested after 24 hours and 40 hours for TApDC and healthy pDC culture, respectively, to analyze cell surface expression of activation markers and cell viability (by propidium iodide exclusion) by flow cytometry and cytokine/chemokine production by ELISA.

DC T-cell cocultures

Allogeneic naïve $CD4^+$ T cells, Treg, and conventional memory $CD4^+$ T cells were cultured in complete medium with or without (i) IL-2 (100 IU/mL) and (ii) purified TApDC, healthy pDC, mDC, and MoDC pretreated for 24 hours with IL-3, granulocyte macrophage colony-stimulating factor (GM-CSF; 10 ng/mL), CpG-B, R848, or flu or purified healthy pDC that were preincubated for 40 hours in IL-3 with (TUMSN-pDC) or without breast tumor supernatants, and TLR-L. T lymphocytes were added on preactivated DC subsets (ratio 1:5) and cocultured for 4 days in triplicate in 96-well round-bottomed plates. Proliferation was assessed by carboxyfluorescein succinimidyl ester (CFSE; Invitrogen) dilution in experiments analyzing FoxP3 expression after gating on $CD3^+$ cells or by DNA synthesis analyzed by ^{3}H-TdR uptake (Betaplate scintillation counter, Perkin Elmer). Viable cells were selected by 4′, 6-diamidino-2-phenylindole exclusion or Live/Dead reagent (Invitrogen) in case of cell permeabilization. Cytokines secretion was measured by ELISA in the supernatants. At day 4, for naïve T cells and TUMSN-pDC coculture, T cells were harvested, washed, and restimulated at 10^5 cells/well in triplicate for 16 hours with phorbol 12-myristate 13-acetate (50 ng/mL) and ionomycin (2 μg/mL; Sigma-Aldrich), while for other T/pDC cocultures, supernatants of coculture were harvested and frozen without any further stimulation of T cells.

Immunohistochemical analysis on tumor tissue

Stainings using CD3 (4) and FoxP3 (3) antibodies were carried out on tissue microarray paraffin sections from 151 patients with invasive nonmetastatic breast cancer using a BenchMark Series automated slide stainer (Ventana) as previously described. After heat-induced Ag retrieval in tris-based buffer pH 8, BDCA2 staining was carried out using mouse anti-BDCA2 (clone 104C12, Dendritics) at 5 μg/mL incubated at 37°C for 30 minutes, revealed with biotinylated secondary antibody bound to streptavidin peroxidase conjugate (UltraView kit and Amplification kit, Ventana), and revealed with 3,3′-diaminobenzidine (Dako) as substrate. Sections were counterstained with hematoxylin. The density of $BDCA2^+$ cells was assessed semiquantitatively allowing the stratification of the tumors as positive or negative for BDCA2. $FOXP3^+$ cells were enumerated using the ARIOL system (Applied Imaging). To compare the role of high number of $FOXP3^+$ cells, we chose as cutoff the highest quartile ($\geq$26.7 in non-TNBT and $\geq$61.8 in TNBT).

Statistical analyses

Comparison of independent samples was done by the student *t* test or nonparametric Wilcoxon tests when appropriate. Comparison of percentages was done by χ^2 test. Correlation analysis of the data was conducted using the Fischer exact test, Spearman test, or the Pearson test when appropriate. Data for cytokine production and T-cell proliferation are expressed as mean ± SD. Percentages of inhibition of IFN-α production by pDC were compared using a nonparametric Friedman test for paired samples. Differences were considered significant for P values less than 0.05 and are indicated as * for $P < 0.05$, ** for $P < 0.01$, and *** for $P < 0.001$.

Results

High TApDC infiltration is associated with aggressive breast tumors

We previously reported that infiltration of primary breast tumors by pDC identified as $CD123^+$ cells by immunohistochemistry (IHC) correlates with poor prognosis, with a median follow-up of 5 years (4). We updated our clinical database with a median follow-up of 12 years and we observed that the presence of $CD123^+$ pDC still represents a major independent adverse prognostic factor for both overall survival (OS; $P = 0.002$) and relapse-free survival (RFS; $P < 10^{-3}$; Supplementary Fig. S1). In a prospective study including 79 newly diagnosed breast tumors patients and using flow cytometry, pDC and mDC were identified in primary breast tumor specimens as lineage $^-CD4^+CD11c^-CD123^+BDCA2^+$ and lineage $^-CD4^+CD11c^+BDCA1^+$ cells, respectively (Supplementary Fig. S2A). Comparative analyses showed that the mean percentage of DC among total cells in primary tumors was 0.15 ± 0.18% for pDC versus 0.04 ± 0.05% for mDC ($P < 10^{-3}$; Fig. 1A, left panel). We also observed significant lower pDC and to a lesser extent mDC frequencies in patients' blood (mean pDC: 0.25 ± 0.22%, $n = 48$), when compared with healthy donors' blood (mean pDC: 0.37 ± 0.19%, $n = 48$; $P = 0.006$; Fig. 1A, right panel). These observations suggest preferential pDC recruitment within the tumor mass. Because the median follow-up of our prospective cohort was 43 months, there were not enough events to analyze RFS and OS. However, we observed significant increased TApDC in aggressive tumors with high mitotic index (MI) that mirrors the rate at which tumor cells divide (0.22 ± 0.22 compared with 0.10 ± 0.11, $P = 0.03$) and triple negative breast tumors (TNBT; hormone-receptors and HER2-neu negative) (0.29 ± 0.28 compared with 0.12 ± 0.12, $P = 0.05$) compared with low MI and non-TN tumors, respectively (Fig. 1B). The presence of high numbers of TApDC was correlated only with those parameters that are characteristic of tumor aggressiveness (Supplementary Table S1 and Fig. 1C). These observations were confirmed by IHC analysis as we observed that TApDC infiltration was massive in 50% of TNBT ($n = 25$ tumors), compared with only 19% other tumors ($n = 162$ tumors; $P = 0.05$). Importantly, such correlations were not observed for TAmDC (Supplementary Table S1). Thus, using 2 different methods (flow cytometry and IHC) to identify pDC in 2 independent cohorts, we showed that high numbers of TApDC correlated with tumor aggressiveness, strengthening our previous report on the deleterious impact of TApDC on breast tumors patients outcome (4).

Breast TApDC display a partially activated phenotype and are impaired for IFN-α production in response to TLR ligands

In contrast to tonsil pDC or paired blood pDC, TApDC (gated on $CD4^+CD123^+$ cells; Supplementary Fig. S2B) specifically exhibit a partially activated phenotype with moderate but significantly higher levels of activation markers such as CD40, CD83, CD86, and HLA-DR and reduced BDCA2 expression (Fig. 2A and B), a characteristic resting pDC marker. Thus, the breast tumors environment favors TApDC activation.

pDC are the most potent type I IFNs producing cells in response to TLR7 or 9 ligands (5). IFN-α production by purified TApDC (>98%) was strongly reduced in response to both TLR7 (flu; 76.3% of inhibition, $P < 0.01$) and TLR9 (CpG-A) ligands (89% of inhibition) compared with healthy tonsil used as a control tissue (Fig. 3A, left panel). In contrast, patients' blood pDC produced similar levels of IFN-α than pDC from healthy donor blood in response to TLR activation (Fig. 3B). These results indicate that the capacity of pDC to produce IFN-α is selectively altered at the tumor site. Moreover, this inhibition was specific for IFN-α, because the production of other immune mediators such as IP-10/CXCL10 remained unaffected after TApDC activation (Fig. 3A, right panel). The weak IFN-α response of TApDC suggested that breast tumor cells or other cells present in tumor tissue actively suppress the ability of pDC to produce IFN-α. To study this effect in more detail, healthy pDC were exposed to supernatants derived from cell cultures of single-cell suspensions of primary breast tumors (TUMSN) and 6 different breast cancer cell lines (BCCSN) before TLR stimulation. Most TUMSN ($n = 25/33$; Fig. 3C left panel, $n = 10$ TUMSN shown), but not the BCCSN (Supplementary Fig. S3A), significantly inhibited pDC IFN-α production in response to flu (TLR7-L) and CpG-A (TLR9-L; mean% of inhibition: 60.6 ± 14%, $P < 0.05$ and 75 ± 18.6%, $P < 0.05$, respectively), in a dose-dependent manner (Supplementary Fig. S3B). Importantly, IP-10/CXCL10 production remained unaffected (Fig. 3C, right panel). Altogether our observations show that pDC are exposed to soluble factors in breast tumors environment that inhibits their IFN-α production.

Breast tumors' environment conditions pDC to induce selective Treg expansion

$BDCA2^+$ TApDC mainly colocalized with $CD3^+$ lymphoid aggregates in breast tumors (Fig. 4 and Supplementary Fig. S4A) compared with epithelial $cytokeratin^+$ areas (42% vs. 14% of tumors analyzed, $n = 20$; Supplementary Fig. S4B) leading us to investigate TApDC capacity to activate T cells *in vitro*. First, we showed that CD40, CD80, and CD86 expression increased following TLR stimulation in TApDC at levels comparable to tonsil pDC (Fig. 4B and Supplementary Fig. S5). Consistent with the acquisition of a mature phenotype, TLR-stimulated TApDC trigger potent naïve $CD4^+$ T-cell proliferation (Fig. 4C) and differentiation into Tr1-like cells producing high levels of IL-10 and IFN-γ (Fig. 4D), as observed for tonsil pDC (Fig. 4C and D). Furthermore, we observed that similarly to TApDC,

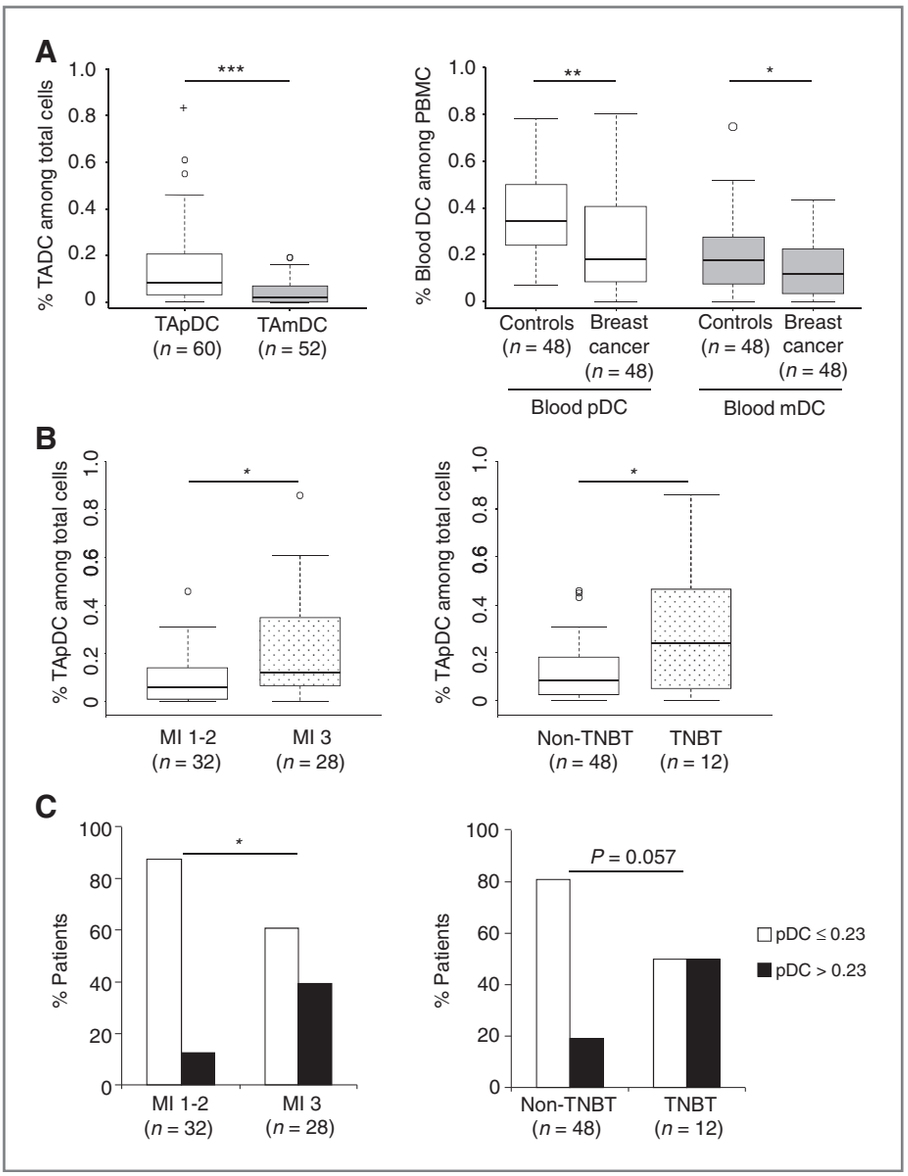

Figure 1. pDC infiltrate highly aggressive tumors. A, box plot set of the frequencies of lineage-negative $CD4^+$ $CD11c^-$ pDC and $CD4^+$ $CD11c^+$ mDC (see Supplementary Fig. S2A for DC identification) among total cells of primary tumors ($n = 60$ or $n = 52$) are indicated (left). The frequencies of pDC and mDC within peripheral blood mononuclear cell (PBMC) of breast cancer patients ($n = 48$) and healthy donors ($n = 48$) are indicated (right). ***, $P < 0.001$; **, $P < 0.01$; *, $P < 0.05$; paired Student t test. Box plot set of pDC levels (B) determined as in A, and percentages of breast cancer patients with low- or high-pDC numbers (C; the highest quartile >0.23% was used as cutoff value) among patients with breast tumors with a MI 1–2 versus 3 and with TNBT versus non-TNBT. MI was established by counting mitoses in 10 high-power (×400) fields (HPF) per tumor section and then averaging the number by HPF (1.96 mm^2). Mitotic cell counts between 1 and 9, between 10 and 19, and more than 20 were defined as MI 1, MI 2, and MI 3, respectively. *, $P < 0.05$; nonparametric Wilcoxon test in B and Fisher exact test in C.

higher numbers of $FoxP3^+$ TATreg infiltrate TNBT than non-TNBT (3rd quartile = 61.8 compared with 26.6 $FoxP3^+$ cells, respectively). Importantly, we observed a significant positive correlation between TApDC and TATreg frequencies in TNBT ($r^2 = 0.749$, $P = 0.002$, $n = 14$), and to a lower extent in non-TNBT ($r^2 = 0.413$, $P = 0.004$, $n = 48$; Fig. 5A). Such correlations (i) were not as significant for TAmDC ($r^2 = 0.672$, $P = 0.05$ in TNBT and $r^2 = 0.291$, $P = 0.08$ in non-TNBT; not shown) and (ii) were confirmed by IHC analysis as we observed that 50% of TNBT and 42% of non-TNBT containing TApDC also contained high numbers of $FoxP3^+$ TATreg in lymphoid areas ($P = 0.02$) although tumors lacking pDC were poorly or not infiltrated by TATreg (17.7% and 0% for non-TNBT and TNBT, respectively; Fig. 5B). Thus, because (i) TApDC infiltrates are associated with TATreg infiltrates, (ii) TApDC and TATreg are in close contact within lymphoid infiltrates (Fig. 4A and Faget, manuscript in preparation), and (iii) both cell subsets are associated with poor prognosis in breast tumors (3, 4), we consequently investigated whether TApDC showing reduced capacity to secrete type I IFN may favor TATreg accumulation. Importantly, we observed that in absence of exogenous IL-2, R848-activated pDC have the highest capacity to promote the proliferation of purified allogeneic Treg while all DC subsets (pDC, mDC, and MoDC) induced similar proliferation of purified memory conventional T cells (Fig. 5C). Interestingly, TUMSN-pretreated pDC, in IL-3 alone or in TLR-7L (flu or R848), potently increased by 2.8- to 4.6-fold the percentage of $FoxP3^{high}$ T cells (9.3 ± 1.1%, 8.6 ± 0.5%, and 7.3 ± 0.5%, respectively) among $CD4^+CD45RO^+$ T cells compared with absence of TUMSN (2% for IL-3 and 2.6 ± 0.5% for both TLR-L; Fig. 5D). Furthermore, IL-3-treated TApDC and TUMSN-conditioned healthy donor pDC were more potent than IL-3-treated healthy donor pDC to favor Treg expansion among $CD4^+CD45RO^+$ T cells (9% vs. 1.5% of $CD3^+$ T

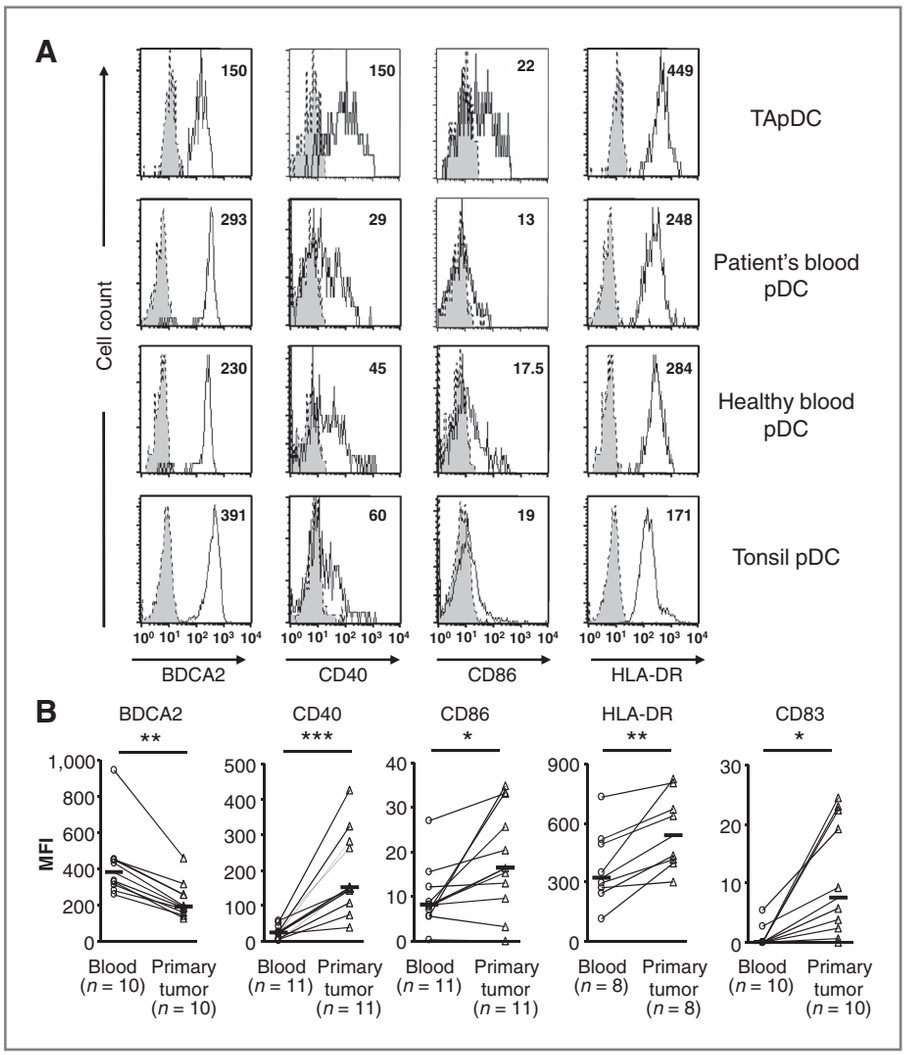

Figure 2. TApDC isolated from human primary breast tumors display a partially activated phenotype. A, pDC from primary breast tumors, patient or healthy blood, and tonsils were compared for BDCA2, CD40, CD83, and CD86 expression after gating on $CD4^+$ $CD123^+$ cells [corresponding to >98% $BDCA2^+$ pDCs (Supplementary Fig. S2B)] without any purification steps. Dotted line represents specific isotype controls. Mean fluorescence intensity (MFI) values of total cells are indicated in each histogram. Results are representative of 5 independent experiments. B, phenotype of pDC from primary tumor and paired blood was compared for different breast cancer patients. Each symbol represents a single sample ($n > 8$ patients) and mean values are represented by horizontal lines in each series. *, $P < 0.05$; **, $P < 0.01$; ***, $P < 0.001$; nonparametric Wilcoxon test.

cells; Fig. 6A). However, TUMSN-conditioned healthy pDC did not induce the differentiation of $FoxP3^+$ Treg from naïve $CD4^+$ T cells (Supplementary Fig. S6). Thus, TApDC mainly favored Treg expansion rather than differentiation. Collectively, these observations show that breast tumors environment amplified pDC unique capacity to stimulate Treg expansion.

Exogenous IFN-α reverts immunosuppressive T-cell responses induced by TApDC and breast tumor environment

We hypothesized that the defect in IFN-α production by TApDC could favor Treg amplification. Addition of 1,000 IU/mL exogenous IFN-α (Fig. 6A) strongly reduced by 78% Treg amplification from $CD4^+CD45RO^+$ T cells induced by IL-3-treated TApDC. Similar results were obtained using healthy pDC cultured in IL-3 or IL-3 + TUMSN with respectively 1.5% and 7.7% of $FoxP3^{high}$ T cells without IFN-α versus 0.9% and 4.8% in the presence of IFN-α (Fig. 6A). Furthermore, IFN-α inhibited IL-10 and enhanced IFN-γ secretion by total $CD4^+$ T cells induced by IL-3-treated TApDC suggesting a switch in T-cell response toward Th1 polarization (Fig. 6B). Collectively, these data indicate that TApDC capacity to promote immunosuppressive T-cell responses through $FoxP3^{high}$ Treg expansion and IL-10-secreting T cells is strongly amplified in tumors as a result of their impaired IFN-α production.

Discussion

The negative prognostic value of pDC and Treg infiltration in human breast tumors (3, 4) prompted us to examine the contribution of pDC and their interaction with Treg in breast cancer immune evasion mechanisms. We show herein that TApDC are preferentially infiltrating aggressive breast tumors. Moreover, TApDC are highly repressed for their IFN-α production after TLR stimulation. Such IFN-α-deficient TApDC strongly correlate with TATreg infiltrate in TNBT, promote TATreg expansion, and prime IL-10-secreting $CD4^+$ T cells. Finally, these tolerogenic properties of TApDC are reverted by exogenous IFN-α. Altogether, our observations show that TApDC altered for their IFN-α production contributes to establish immune tolerance through Treg expansion leading to tumor progression and poor clinical outcome in breast cancer.

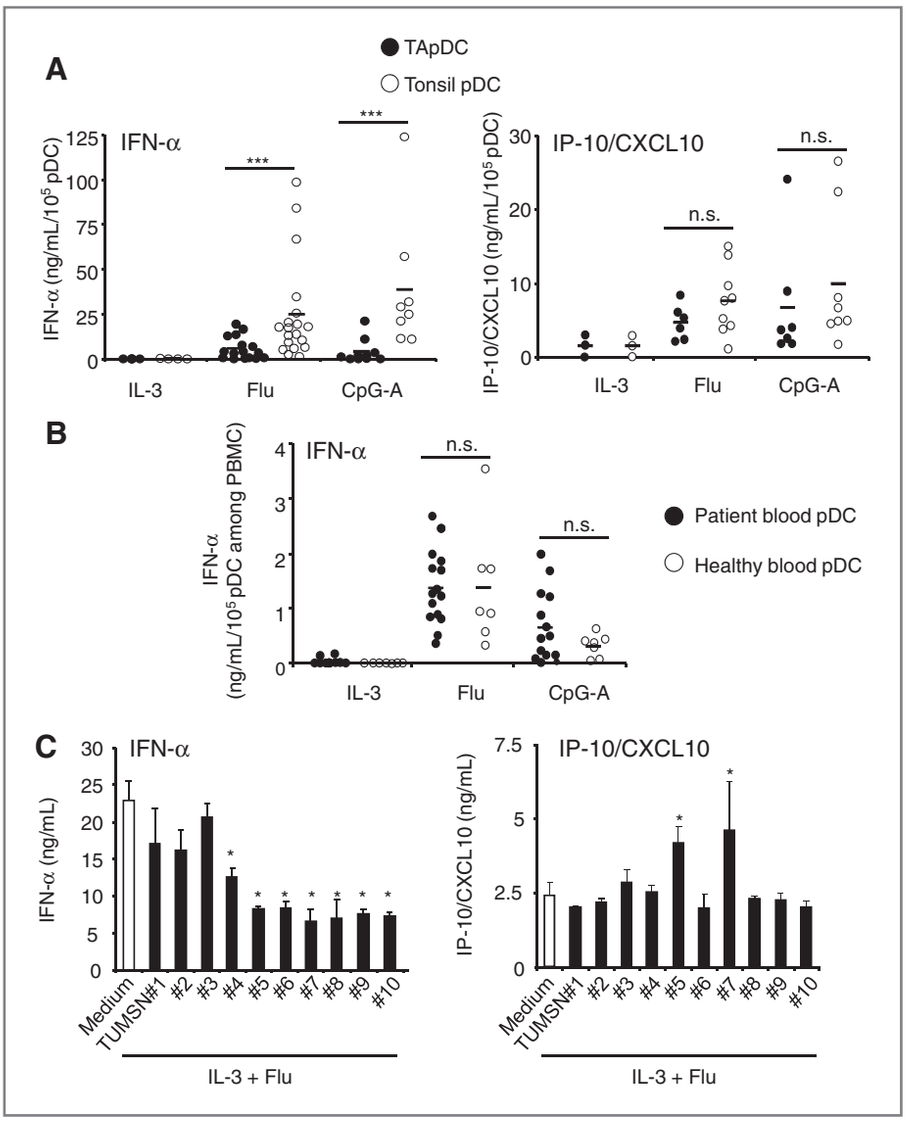

Figure 3. Specific inhibition of IFN-α production by TApDC in response to TLR activation is mediated by soluble factors from breast tumor environment. Purified pDC from breast tumors and healthy tonsil (A) and peripheral blood mononuclear cell (PBMC) from breast cancer patients and healthy donors (B) were cultured with IL-3, flu, and CpG-A for 24 hours. IFN-α and IP-10/CXCL10 production was quantified by ELISA. Results were standardized to ng/mL for 1×10^5 pDC for each sample. Each symbol represents a single sample and mean values are represented by horizontal lines. ***, $P < 0.001$; nonparametric Wilcoxon test. C, healthy pDC were pretreated with IL-3 ± TUMSN (25%) derived from 10 patients for 16 hours before flu activation for another 24 hours. IFN-α and IP-10/CXCL10 production was measured by ELISA. Data are expressed as mean ± SD by subtracting the quantity of each cytokine detected in TUMSN alone with no pDC. Data are representative of more than 4 independent experiments, representing more than 30 TUMSN from individual patients. *, $P < 0.05$; nonparametric Wilcoxon test. n.s., not significant.

pDC are well recognized for their role in antiviral immunosurveillance driven by type I IFNs production (5). In addition, excessive production of IFN-α by pDC that are chronically activated by [LL37/self-nucleic acids] complexes participated to the development/maintenance of noninfectious autoimmune/inflammatory pathologies (8, 9). In contrast, in breast tumors we observe that TApDC are strongly inhibited for their IFN-α production upon stimulation with exogenous TLR-L *in vitro*, in agreement with a previous study in head and neck cancer (16) and our recent work in ovarian carcinoma (24). As (i) tumors have been shown to express LL37 (25) and (ii) endogenous danger signals such as self-nucleic acids (26) are released from dying tumor cells, it is tempting to speculate that, upon (LL37/self-nucleic acids) complexes recognition TApDC might contribute to tumor immunosurveillance through type I IFNs production. This is consistent with the partially activated phenotype of breast TApDC. Thus, the tumor has evolved mechanisms to inhibit type I IFNs secretion by TApDC to prevent an effective antitumor response and favor tumor progression. This hypothesis is currently under investigation but it is supported by recent works showing that (i) type I IFN is selectively required by DC for immune rejection of tumors (27, 28) and (ii) the type I IFN signature is predictive of responses to anthracyclines in breast cancer patients (29).

Consistent with TApDC defect in IFN-α production, we show that soluble factors derived from breast tumors environment block type I IFNs production by healthy activated pDC *in vitro*. We recently showed in ovarian cancer that TGF-β and TNF-α from breast tumors environment cooperate to inhibit IFN-α secretion by TApDC (24). Our ongoing study is pointing to similar mechanisms in breast tumors (Sisirak, submitted) but also to cell-associated molecules such as BST-2 that (i) is expressed by BCC lines and (ii) inhibits TLR-triggered IFN-α secretion by healthy pDC (30). It is likely that the main source of inhibitory factors in the breast tumors environment are the immune cells and/or stromal cells

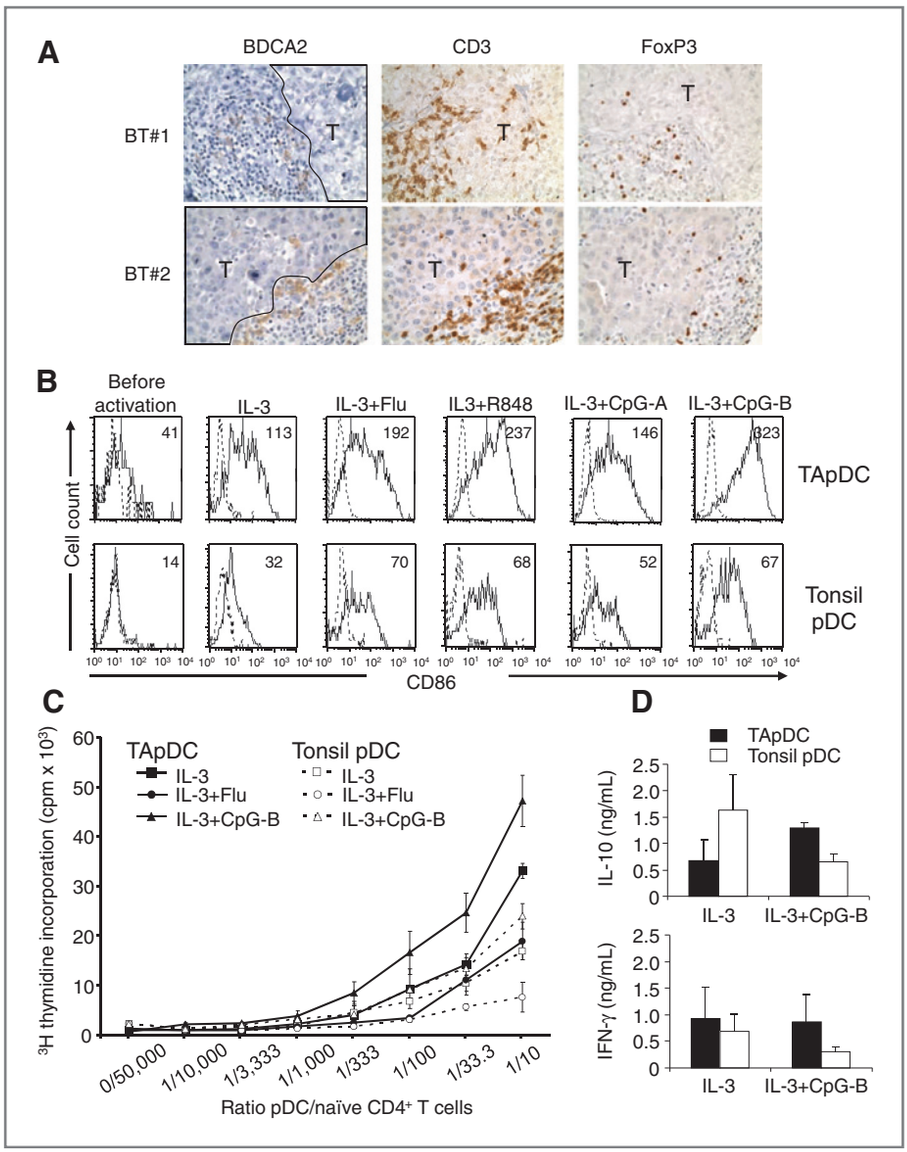

Figure 4. TLR-activated TApDC acquire a fully mature phenotype and induce naïve CD4$^+$ T-cell proliferation and differentiation of IL-10–secreting T cells. A, IHC analysis on paraffin-embedded breast tumor sections was conducted using anti-BDCA2, anti-CD3, or anti-FoxP3 (brown; ×40). T, tumor mass. B, activation phenotype of 40-hour differentially stimulated TApDC and tonsil pDC was monitored by analyzing CD86 expression by flow cytometry. Data are representative of 5 independent experiments and MFI values of total cells are indicated in each histogram. C, purified tonsil pDC and TApDC were cultured with IL-3, flu, or CpG-B for 24 hours and then incubated at graded doses with allogeneic naïve CD4$^+$ T cells for 5 days as specified in Supplementary Materials and Methods. T-cell proliferation was determined by ^{3}H thymidine incorporation. Data are expressed as mean ± SD and are representative of 3 independent experiments. D, purified tonsil pDC and TApDC were cultured with IL-3 or CpG-B for 24 hours and then incubated with allogeneic naïve CD4$^+$ T cells for 5 days as specified in Supplementary Materials and Methods. T-cell cytokine production was determined in coculture supernatant by ELISA. Data are expressed as mean ± SD and representative of 2 independent experiments.

(fibroblasts and mesenchymal stem cells) because BCC lines supernatants did not block pDCs' innate functions.

The absence of inhibition of pDC maturation and production of IP-10/CXCL10 formally excludes a general downregulation of TLR expression by the breast tumors environment in contrast to what has been observed in head and neck cancer (16). Our ongoing studies are identifying the molecular mechanisms involved in TApDC dysfunction (Sisirak, submitted).

Although TApDCs' innate functions are strongly impaired by breast tumors, they exhibit similarly to ovarian cancers (24) exacerbated ability to induce allogeneic naïve CD4$^+$ T-cell proliferation and differentiation into IL-10-producing cells, that were shown to be suppressive cells *in vitro* (11). Taken together with the study showing that pDC induce IL-10-producing CD8$^+$ Treg in ovarian cancer (20), these findings suggest that pDC will favor an immunosuppressive IL-10-rich environment. Our FACS and IHC analysis show strong correlation between TATreg and TApDC infiltrate as well as their *in situ* colocalization in breast tissues. In line with these observations, we observe that breast TApDC are specialized in promoting the expansion of preexisting natural Foxp3$^+$ Treg *in vitro*, in agreement with other studies showing that pDC induce Treg proliferation (14, 15, 31–34). We also report herein, that soluble factors from the breast tumors environment condition pDC to become tolerogenic through their ability to promote Treg expansion. A tolerogenic role for pDC was also recently reported *in vivo* in different mouse models (see ref. 10 for review), by either promoting Treg or Tr1 cells or directly suppressing effector T-cell responses. Although in other contexts, pDC-driven Treg generation from naïve T cells has been reported both *in vitro* (12, 13, 35–38) and *in vivo* (39, 40), breast tumors environment-conditioned pDC do not induce FoxP3$^+$ Treg differentiation from naïve CD4$^+$ T cells (Supplementary

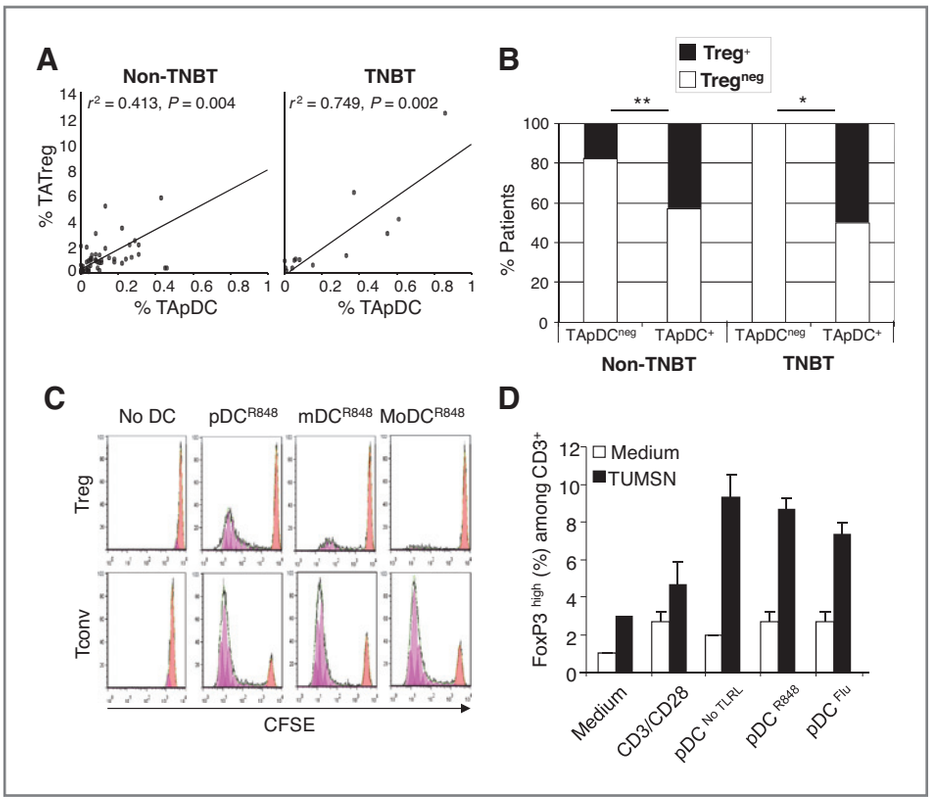

Figure 5. IFN-α–deficient TApDC increase Treg expansion. A, Spearman rank correlations between the proportions of $CD4^+BDCA2^+CD123^+$ pDC and $CD4^+CD45RO^+CD25^{high}$ Treg as determined by flow cytometry in non-TNBT ($n = 48$) and TNBT ($n = 12$). B, percentages of breast cancer patients with low or high numbers of TATreg [the highest quartile ≥26.7 and 61.8 $FoxP3^+$ cells for non-TNBT and TNBT, respectively, was used as cutoff value as defined in a retrospective study by IHC (3)] among patients with or without TApDC in non-TNBT ($n = 133$) versus TNBT ($n = 18$). *, $P < 0.05$; **, $P < 0.01$; Fischer exact test. C, pDC, mDC, and MoDC were preactivated for 24 hours with IL-3 or GM-CSF and R848, washed, and cocultured for 5 days with CFSE-labeled conventional memory $CD4^+CD25^{Low/Neg}CD127^{+/-}$ T cells (Tconv) or $CD4^+CD25^{high}CD127^-$ Treg in the absence of IL-2. At day 5, CFSE dilution was analyzed on $CD3^+$ T cells. Percentages of CFSE-diluted cells are indicated. D, healthy pDC were pretreated for 16 hours with IL-3 with or without 25% TUMSN before activation or not with R848 or flu for 24 hours. Memory $CD4^+$ T cells were then added with IL-2 (100 IU/mL) at 25% v/v for 5 days. Anti-CD3/anti-CD28 expandbeads were used as control. FoxP3 expression was analyzed on $CD3^+$ viable cells.

Fig. S6). These results provide evidence that TApDC may contribute to tumor progression through Treg expansion. This unique capacity of TApDC is because of ICOS/ICOS-L interaction between TApDC and TATreg, respectively (Faget; submitted for publication).

Of most importance, the inhibition of type I IFNs production by TApDC is required for this tolerogenic TApDC function because exogenous IFN-α (i) blocks TApDC-mediated Treg expansion and (ii) potentiates IFN-γ and inhibits IL-10 production by memory $CD4^+$ T cells highlighting a shift toward Th1 phenotype instead of tolerogenic memory $CD4^+$ T-cell activation. Our findings are supported by recent publications showing that through a direct effect on Ag-presenting cells and by affecting Treg proliferation and differentiation, IFN-α sustains and drives $CD4^+$ effector functions (41, 42). Thus, *in vivo* local interactions between IFN-α-deficient TApDC and TAT cell (ref. 3 and Faget; submitted for publication) lead to TATreg and Tr1 expansion, favoring an immunosuppressive environment that may contribute to tumor immune escape and progression.

Overall, our data provide direct evidence that TApDC have an important immunopathologic role through Treg expansion in human breast cancer that likely explain their deleterious impact on the clinical outcome. The positive correlation between TApDC and TATreg content and tumor aggressiveness as observed in TNBT strengthens our previous observations showing that infiltration of primary breast tumors by pDC correlates with poor prognosis (4). It also corroborates our recent findings in ovarian cancer and from others in melanoma showing that TApDC accumulation correlates with early relapse (24, 43). TNBT represent about 15% of all breast cancers but they have the severest prognosis. It represents an important clinical challenge and little is known about their biology (44). Mechanisms beyond this predominant TApDC infiltration in TNBT is an important question that is currently under investigation. Of note, because of the low incidence of TNBT, we could not analyze the impact of TN status on the functional alteration of *ex vivo* purified TApDC nor the impact of pDC on the clinical outcome of TNBT.

In conclusion, we identify in human breast cancer a TApDC defect in IFN-α production leading to TATreg expansion and contributing to breast tumor progression. These findings uncover the mechanisms that mediate the deleterious impact of pDC infiltration in breast tumors and would provide new

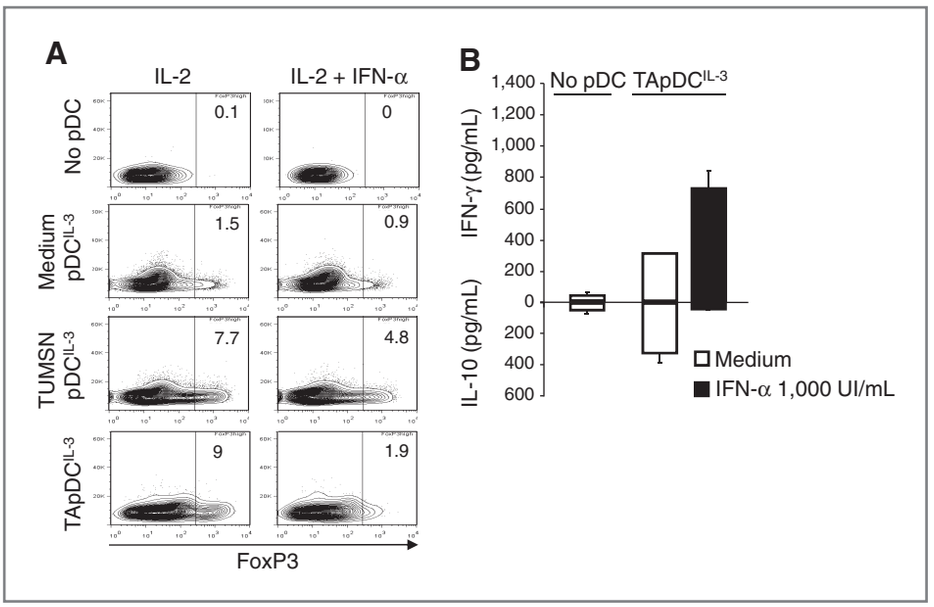

Figure 6. Exogenous IFN-α reverts tolerogenic properties of TApDC. A, healthy pDC or TApDC were pretreated with IL-3 ± 25% TUMSN for 24 hours and then cocultured with memory $CD4^+$ T cells in the presence of IL-2 (100 IU/mL) ± IFN-α (1,000 IU/mL) for 5 days. FoxP3 expression was analyzed on $CD3^+$ viable cells. B, 24-hour IL-3– or IL-3+R848–activated TApDC were cocultured with healthy $CD4^+$ T cells during 5 days in presence of IL-2 (100 IU/mL) ± IFN-α (1,000 IU/mL). IL-10 and IFN-γ secretion was measured by ELISA. Data are representative of 3 independent experiments.

therapeutic approaches targeting pDC, as in skin cancers (22, 23, 45, 46). We recently obtained evidences in a mouse mammary tumors model that reactivation of TApDC leads to tumor regression and antitumor immune responses (Le Mercier and colleagues, manuscript in preparation). Thus, restoring TApDC innate function might represent an attractive therapeutic strategy for localized breast tumors.

Disclosure of Potential Conflicts of Interest

No potential conflicts of interest were disclosed.

Authors' Contributions

Conception and design: V. Sisirak, J. Faget, J.-Y. Blay, C. Menetrier-Caux, C. Caux, N. Bendriss-Vermare
Development of methodology: V. Sisirak
Acquisition of data (provided animals, acquired and managed patients, provided facilities, etc.): V. Sisirak, J. Faget, M. Gobert, N. Goutagny, N. Vey, I. Treilleux, G. Poyet, S.I. Labidi-Galy, S. Goddard-Leon, T. Bachelot, I. Puisieux
Analysis and interpretation of data (e.g., statistical analysis, biostatistics, computational analysis): V. Sisirak, J. Faget, N. Goutagny, S.I. Labidi-Galy, A. Bajard, J.-Y. Blay, C. Caux, N. Bendriss-Vermare
Writing, review, and/or revision of the manuscript: V. Sisirak, T. Bachelot, J.-Y. Blay, C. Caux, N. Bendriss-Vermare
Administrative, technical, or material support (i.e., reporting or organizing data, constructing databases): V. Sisirak, S. Renaudineau, A. Puisieux, J.-Y. Blay, N. Bendriss-Vermare
Study supervision: J.-Y. Blay, C. Caux, N. Bendriss-Vermare
Performing technical experiments: M. Gobert
Contributed new reagents or analytic tools: I. Durand
Provided helpful discussions: I. Le Mercier

Acknowledgments

The authors are grateful to the breast cancer patients who consented to participate in this study and to the medical staff and the Centre de Ressources Biologiques from the CLB who provided us with breast tumor specimens. We thank doctors and colleagues from clinics and hospitals who provide us with blood and tonsils samples. We thank X.-N. N'Guyen and C. Rigal for early technical contribution and A. Besse for help with statistical analyses.

Grant Support

This work was funded by institutional grants from Breast Cancer Research Fundation, Association pour la Recherche sur le Cancer (ARC), Comité départemental de Saône-et-Loire et du Rhône de la Ligue nationale contre le cancer, Lyon Biopole DEMINAP and PLATINE projects, and Institut National du Cancer grant ACI-63-04, ACI 2007-2009, and Met-escape 2007. V. Sisirak is a recipient of a grant from the Région Rhône-Alpes and from ARC. J. Faget and M. Gobert are recipients of a grant from the Ligue Nationale contre le cancer.

The funders had no role in study design, data collection and analysis, decision to publish, or preparation of the manuscript.

The costs of publication of this article were defrayed in part by the payment of page charges. This article must therefore be hereby marked *advertisement* in accordance with 18 U.S.C. Section 1734 solely to indicate this fact.

Received October 21, 2011; revised June 20, 2012; accepted July 12, 2012; published OnlineFirst July 25, 2012.

References

1. Zitvogel L, Tesniere A, Kroemer G. Cancer despite immunosurveillance: immunoselection and immunosubversion. Nat Rev Immunol 2006;6:715–27.
2. Joyce JA, Pollard JW. Microenvironmental regulation of metastasis. Nat Rev Cancer 2009;9:239–52.
3. Gobert M, Treilleux I, Bendriss-Vermare N, Bachelot T, Goddard-Leon S, Arfi V, et al. Regulatory T cells recruited through CCL22/CCR4 are selectively activated in lymphoid infiltrates surrounding primary breast tumors and lead to an adverse clinical outcome. Cancer Res 2009; 69:2000–9.
4. Treilleux I, Blay JY, Bendriss-Vermare N, Ray-Coquard I, Bachelot T, Guastalla JP, et al. Dendritic cell infiltration and prognosis of early stage breast cancer. Clin Cancer Res 2004;10: 7466–74.
5. Reizis B, Bunin A, Ghosh HS, Lewis KL, Sisirak V. Plasmacytoid dendritic cells: recent progress and open questions. Annu Rev Immunol 2011;29:163–83.
6. Villadangos JA, Young L. Antigen-presentation properties of plasmacytoid dendritic cells. Immunity 2008;29:352–61.
7. Hoeffel G, Ripoche AC, Matheoud D, Nascimbeni M, Escriou N, Lebon P, et al. Antigen crosspresentation by human plasmacytoid dendritic cells. Immunity 2007;27:481–92.
8. Ganguly D, Chamilos G, Lande R, Gregorio J, Meller S, Facchinetti V, et al. Self-RNA-antimicrobial peptide complexes activate human

dendritic cells through TLR7 and TLR8. J Exp Med 2009;206: 1983–94.
9. Lande R, Gregorio J, Facchinetti V, Chatterjee B, Wang YH, Homey B, et al. Plasmacytoid dendritic cells sense self-DNA coupled with antimicrobial peptide. Nature 2007;449:564–9.
10. Matta BM, Castellaneta A, Thomson AW. Tolerogenic plasmacytoid DC. Eur J Immunol 2010;40:2667–76.
11. Ito T, Yang M, Wang YH, Lande R, Gregorio J, Perng OA, et al. Plasmacytoid dendritic cells prime IL-10-producing T regulatory cells by inducible costimulator ligand. J Exp Med 2007;204: 105–15.
12. Martin-Gayo E, Sierra-Filardi E, Corbi AL, Toribio ML. Plasmacytoid dendritic cells resident in human thymus drive natural Treg cell development. Blood 2010;115:5366–75.
13. Moseman EA, Liang X, Dawson AJ, Panoskaltsis-Mortari A, Krieg AM, Liu YJ, et al. Human plasmacytoid dendritic cells activated by CpG oligodeoxynucleotides induce the generation of $CD4^+CD25^+$ regulatory T cells. J Immunol 2004;173:4433–42.
14. Ito T, Hanabuchi S, Wang YH, Park WR, Arima K, Bover L, et al. Two functional subsets of FOXP3(+) regulatory T cells in human thymus and periphery. Immunity 2008;28:870–80.
15. Ouabed A, Hubert FX, Chabannes D, Gautreau L, Heslan M, Josien R. Differential control of T regulatory cell proliferation and suppressive activity by mature plasmacytoid versus conventional spleen dendritic cells. J Immunol 2008;180:5862–70.
16. Hartmann E, Wollenberg B, Rothenfusser S, Wagner M, Wellisch D, Mack B, et al. Identification and functional analysis of tumor-infiltrating plasmacytoid dendritic cells in head and neck cancer. Cancer Res 2003;63:6478–87.
17. Zou W, Machelon V, Coulomb-L'Hermin A, Borvak J, Nome F, Isaeva T, et al. Stromal-derived factor-1 in human tumors recruits and alters the function of plasmacytoid precursor dendritic cells. Nat Med 2001;7: 1339–46.
18. Perrot I, Blanchard D, Freymond N, Isaac S, Guibert B, Pacheco Y, et al. Dendritic cells infiltrating human non-small cell lung cancer are blocked at immature stage. J Immunol 2007;178: 2763–9.
19. Watkins SK, Zhu Z, Riboldi E, Shafer-Weaver KA, Stagliano KE, Sklavos MM, et al. FOXO3 programs tumor-associated DCs to become tolerogenic in human and murine prostate cancer. J Clin Invest 2011;121:1361–72.
20. Wei S, Kryczek I, Zou L, Daniel B, Cheng P, Mottram P, et al. Plasmacytoid dendritic cells induce $CD8^+$ regulatory T cells in human ovarian carcinoma. Cancer Res 2005;65:5020–6.
21. Chauhan D, Singh AV, Brahmandam M, Carrasco R, Bandi M, Hideshima T, et al. Functional interaction of plasmacytoid dendritic cells with multiple myeloma cells: a therapeutic target. Cancer Cell 2009; 16:309–23.
22. Stary G, Bangert C, Tauber M, Strohal R, Kopp T, Stingl G. Tumoricidal activity of TLR7/8-activated inflammatory dendritic cells. J Exp Med 2007;204:1441–51.
23. Urosevic M, Dummer R, Conrad C, Beyeler M, Laine E, Burg G, et al. Disease-independent skin recruitment and activation of plasmacytoid predendritic cells following imiquimod treatment. J Natl Cancer Inst 2005;97:1143–53.
24. Labidi-Galy SI, Sisirak V, Meeus P, Gobert M, Treilleux I, Bajard A, et al. Quantitative and functional alterations of plasmacytoid dendritic cells contribute to immune tolerance in ovarian cancer. Cancer Res 2011; 71:5423–34.
25. Heilborn JD, Nilsson MF, Jimenez CI, Sandstedt B, Borregaard N, Tham E, et al. Antimicrobial protein hCAP18/LL-37 is highly expressed in breast cancer and is a putative growth factor for epithelial cells. Int J Cancer 2005;114:713–9.
26. Shi Y, Evans JE, Rock KL. Molecular identification of a danger signal that alerts the immune system to dying cells. Nature 2003;425: 516–21.
27. Fuertes MB, Kacha AK, Kline J, Woo SR, Kranz DM, Murphy KM, et al. Host type I IFN signals are required for antitumor $CD8^+$ T cell responses through CD8{alpha}$^+$ dendritic cells. J Exp Med 2011; 208:2005–16.
28. Diamond MS, Kinder M, Matsushita H, Mashayekhi M, Dunn GP, Archambault JM, et al. Type I interferon is selectively required by dendritic cells for immune rejection of tumors. J Exp Med 2011;208: 1989–2003.
29. Quidville V, Conforti R, Zoubir M, André F, Mathieu MC, Delaloge S, et al. Lymphocyte infiltration and interferon response to predict efficacy of anthracyclines. Annals Oncol 2009;20:56.
30. Cao W, Bover L, Cho M, Wen X, Hanabuchi S, Bao M, et al. Regulation of TLR7/9 responses in plasmacytoid dendritic cells by BST2 and ILT7 receptor interaction. J Exp Med 2009;206:1603–14.
31. Irla M, Kupfer N, Suter T, Lissilaa R, Benkhoucha M, Skupsky J, et al. MHC class II-restricted antigen presentation by plasmacytoid dendritic cells inhibits T cell-mediated autoimmunity. J Exp Med 2010;207:1891–905.
32. Janke M, Witsch EJ, Mages HW, Hutloff A, Kroczek RA. Eminent role of ICOS costimulation for T cells interacting with plasmacytoid dendritic cells. Immunology 2006;118:353–60.
33. Kang HK, Liu M, Datta SK. Low-dose peptide tolerance therapy of lupus generates plasmacytoid dendritic cells that cause expansion of autoantigen-specific regulatory T cells and contraction of inflammatory Th17 cells. J Immunol 2007;178:7849–58.
34. Sharma MD, Baban B, Chandler P, Hou DY, Singh N, Yagita H, et al. Plasmacytoid dendritic cells from mouse tumor-draining lymph nodes directly activate mature Tregs via indoleamine 2,3-dioxygenase. J Clin Invest 2007;117:2570–82.
35. Chen W, Liang X, Peterson AJ, Munn DH, Blazar BR. The indoleamine 2,3-dioxygenase pathway is essential for human plasmacytoid dendritic cell-induced adaptive T regulatory cell generation. J Immunol 2008;181:5396–404.
36. Hanabuchi S, Ito T, Park WR, Watanabe N, Shaw JL, Roman E, et al. Thymic stromal lymphopoietin-activated plasmacytoid dendritic cells induce the generation of $FOXP3^+$ regulatory T cells in human thymus. J Immunol 2010;184:2999–3007.
37. Manches O, Munn D, Fallahi A, Lifson J, Chaperot L, Plumas J, et al. HIV-activated human plasmacytoid DCs induce Tregs through an indoleamine 2,3-dioxygenase-dependent mechanism. J Clin Invest 2008;118:3431–9.
38. Martin P, Del Hoyo GM, Anjuere F, Arias CF, Vargas HH, Fernandez L, et al. Characterization of a new subpopulation of mouse $CD8\alpha^+$ $B220^+$ dendritic cells endowed with type 1 interferon production capacity and tolerogenic potential. Blood 2002;100:383–90.
39. Hadeiba H, Sato T, Habtezion A, Oderup C, Pan J, Butcher EC. CCR9 expression defines tolerogenic plasmacytoid dendritic cells able to suppress acute graft-versus-host disease. Nat Immunol 2008;9: 1253–60.
40. Ochando JC, Homma C, Yang Y, Hidalgo A, Garin A, Tacke F, et al. Alloantigen-presenting plasmacytoid dendritic cells mediate tolerance to vascularized grafts. Nat Immunol 2006;7:652–62.
41. Pace L, Vitale S, Dettori B, Palombi C, La Sorsa V, Belardelli F, et al. APC activation by IFN-alpha decreases regulatory T cell and enhances Th cell functions. J Immunol 2010;184:5969–79.
42. Golding A, Rosen A, Petri M, Akhter E, Andrade F. Interferon-alpha regulates the dynamic balance between human activated regulatory and effector T cells: implications for antiviral and autoimmune responses. Immunology 2010;131:107–17.
43. Jensen TO, Schmidt H, Moller HJ, Donskov F, Hoyer M, Sjoegren P, et al. Intratumoral neutrophils and plasmacytoid dendritic cells indicate poor prognosis and are associated with pSTAT3 expression in AJCC stage I/II melanoma. Cancer 2012;118:2476–85.
44. Hudis CA, Gianni L. Triple-negative breast cancer: an unmet medical need. Oncologist 2011;16(Suppl 1):1–11.
45. Liu C, Lou Y, Lizee G, Qin H, Liu S, Rabinovich B, et al. Plasmacytoid dendritic cells induce NK cell-dependent, tumor antigen-specific T cell cross-priming and tumor regression in mice. J Clin Invest 2008;118: 1165–75.
46. Nierkens S, Van den Brok MH, Garcia Z, Togher S, Wagenaars J, Wassink M, et al. Immune adjuvant efficacy of CpG oligonucleotide in cancer treatment is founded specifically upon TLR9 function in plasmacytoid dendritic cells. Cancer Res 2011;71:6428–37.

Published September 1, 2014

Genetic evidence for the role of plasmacytoid dendritic cells in systemic lupus erythematosus

Vanja Sisirak,[1] Dipyaman Ganguly,[1] Kanako L. Lewis,[1] Coline Couillault,[1] Lena Tanaka,[3] Silvia Bolland,[4] Vivette D'Agati,[2] Keith B. Elkon,[3] and Boris Reizis[1]

[1]Department of Microbiology and Immunology and [2]Department of Pathology, Columbia University Medical Center, New York, NY 10032
[3]Department of Medicine, University of Washington, Seattle, WA 98195
[4]Laboratory of Immunogenetics, National Institute of Allergy and Infectious Diseases, Rockville, MD 20852

Systemic lupus erythematosus (SLE) is an autoimmune disorder characterized by the production of antibodies to self-nucleic acids, immune complex deposition, and tissue inflammation such as glomerulonephritis. Innate recognition of self-DNA and -RNA and the ensuing production of cytokines such as type I interferons (IFNs) contribute to SLE development. Plasmacytoid dendritic cells (pDCs) have been proposed as a source of pathogenic IFN in SLE; however, their net contribution to the disease remains unclear. We addressed this question by reducing gene dosage of the pDC-specific transcription factor E2-2 (Tcf4), which causes a specific impairment of pDC function in otherwise normal animals. We report that global or DC-specific *Tcf4* haplodeficiency ameliorated SLE-like disease caused by the overexpression of the endosomal RNA sensor Tlr7. Furthermore, *Tcf4* haplodeficiency in the B6.*Sle1*.*Sle3* multigenic model of SLE nearly abolished key disease manifestations including anti-DNA antibody production and glomerulonephritis. *Tcf4*-haplodeficient SLE-prone animals showed a reduction of the spontaneous germinal center reaction and its associated gene expression signature. These results provide genetic evidence that pDCs are critically involved in SLE pathogenesis and autoantibody production, confirming their potential utility as therapeutic targets in the disease.

CORRESPONDENCE
B. Reizis:
bvr2101@columbia.edu

Abbreviations used: cDC, classical DC; CKO, conditional KO; dsDNA, double-stranded DNA; GC, germinal center; IFNAR, IFN-α receptor; PCA, principal component analysis; pDC, plasmacytoid DC; SLE, systemic lupus erythematosus.

Systemic lupus erythematosus (SLE) is an autoimmune disorder in which the production of autoantibodies leads to the formation and deposition of immune complexes, resulting in tissue damage. The hallmark of SLE is the presence of pathogenic autoantibodies specific for nuclear antigens such as double-stranded DNA (dsDNA), chromatin, and RNA-containing antigens (Fairhurst et al., 2006). Aberrant recognition of self-nucleic acids through innate immunoreceptors, including endosomal Toll-like receptors TLR7 and TLR9 (specific for single-stranded RNA and unmethylated CpG DNA, respectively), is thought to be at the crux of autoantibody production and SLE pathogenesis (Marshak-Rothstein and Rifkin, 2007; Shlomchik, 2009). For example, a duplication of mouse *Tlr7* gene (the spontaneous *Yaa* mutation) accelerates SLE development, whereas multiple copies of *Tlr7* (as a transgene) are sufficient to cause SLE-like disease (Pisitkun et al., 2006; Deane et al., 2007; Fairhurst et al., 2008).

One of the main consequences of innate recognition of DNA/RNA is the secretion of type I IFN (IFN-α/β), a key antiviral cytokine typically produced during viral infections. Notably, leukocytes from many SLE patients manifest an IFN signature, i.e., the expression of IFN-induced genes (Baechler et al., 2003; Bennett et al., 2003). Because of the powerful adjuvant activity of IFN, increased IFN levels are thought to promote immune hyperactivation and tissue damage in the disease (Elkon and Wiedeman, 2012). Genetic ablation of

V. Sisirak and D. Ganguly contributed equally to this paper.

D. Ganguly's present address is Division of Cancer Biology and Inflammatory Disorders, CSIR-Indian Institute of Chemical Biology, Kolkata, West Bengal 700032, India.

K. L. Lewis' present address is Division of Biological Sciences, University of California, San Diego, La Jolla, CA 92093.

The Rockefeller University Press $30.00
J. Exp. Med. 2014 Vol. 211 No. 10 1969-1976
www.jem.org/cgi/doi/10.1084/jem.20132522

Published September 1, 2014

IFN-α receptor (IFNAR) ameliorates experimental SLE in the Tlr7-overexpressing model (Buechler et al., 2013) as well as in NZB/NZW-derived strains (Santiago-Raber et al., 2003; Agrawal et al., 2009). Conversely, IFN overexpression strongly exacerbates experimental SLE (Liu and Davidson, 2013). Hence, the blockade of IFN signaling (for example, using antibodies to IFN or IFNAR) represents a potential therapeutic approach to SLE (Bronson et al., 2012).

Plasmacytoid DCs (pDCs) are a distinct lineage of DCs specialized in IFN production in response to viral nucleic acids sensed through TLR7 and TLR9 (Gilliet et al., 2008; Reizis et al., 2011). In addition to virus-derived DNA and RNA, pDCs can be activated by self-nucleic acids complexed with antibodies (Båve et al., 2003) or DNA/RNA-binding proteins such as HMGB1 (Tian et al., 2007). In particular, DNA complexes released from activated neutrophils induce pDCs to secrete IFN, which fuels the "vicious circle" of myeloid cell activation in SLE patients (Garcia-Romo et al., 2011; Lande et al., 2011). TLR-activated pDCs become resistant to glucocorticoids, underlying the limited efficacy of these drugs in SLE (Guiducci et al., 2010a). Therefore, pDCs have been proposed as a key source of aberrant IFN production and a major driver of SLE progression (Rönnblom and Alm, 2001). In experimental SLE, minor signs of pDC activation have been described in the *Tlr7* transgenic model (Buechler et al., 2013), and antibody-mediated pDC ablation prevented trauma-induced skin inflammation in the (NZBxNZW)F1 model (Guiducci et al., 2010b). However, the precise role and significance of pDC function in SLE remains moot, largely because models for specific, long-term pDC ablation have not been available.

We have previously identified the transcription factor E2-2 (official symbol Tcf4) as a specific regulator of pDC development in mice and in humans (Cisse et al., 2008). Tcf4 is expressed in pDCs but not in classical DCs (cDCs), and its deletion abolishes the development of pDCs but not of cDCs or other immune cell types. Importantly, even monoallelic loss of *Tcf4* causes specific impairment of pDC function in mice and human patients. For example, $Tcf4^{+/-}$ mice fail to produce IFN in response to the TLR9 ligand CpG but show normal IFN induction by the TLR3/RIG-I ligand poly-I:C and normal T cell–dependent antibody responses (Cisse et al., 2008). Thus, *Tcf4* haplodeficiency represents a specific tool for constitutive functional blockade of pDCs. In this study, we applied this tool to determine the role of pDCs in two distinct genetic models of SLE.

RESULTS AND DISCUSSION

Tcf4 haplodeficiency ameliorates SLE caused by Tlr7 overexpression

To validate *Tcf4* haplodeficiency as a pDC-specific tool, we first used a model of SLE induced by the administration of saturated hydrocarbon tetramethylpentadecane (pristane). This model is characterized by autoreactivity to small ribonucleoproteins (anti-Smith antigen, anti-Sm), which is dependent on TLR7-induced IFN production by inflammatory monocytes rather than by pDCs (Lee et al., 2008). We found that the expression of IFN-inducible genes and anti-Sm antibody production were similar in pristane-treated WT and $Tcf4^{+/-}$ animals (unpublished data). Thus, *Tcf4* haplodeficiency does not generally affect autoantibody production that is not dependent on pDCs.

Next, we used a monogenic SLE model based on multiple transgenic copies of the *Tlr7* locus. These *Tlr7*.Tg animals develop an SLE-like disease characterized by anti-RNA antibody production, expansion of monocyte-like myeloid cells in the blood, massive immune activation, and glomerulonephritis (Deane et al., 2007). We have used a line of *Tlr7*.Tg animals with moderate Tlr7 mRNA overexpression (4–8-fold) and the transgene integrated on the Y-chromosome. On the hybrid B6129F1 background, nearly all *Tlr7*.Tg males became

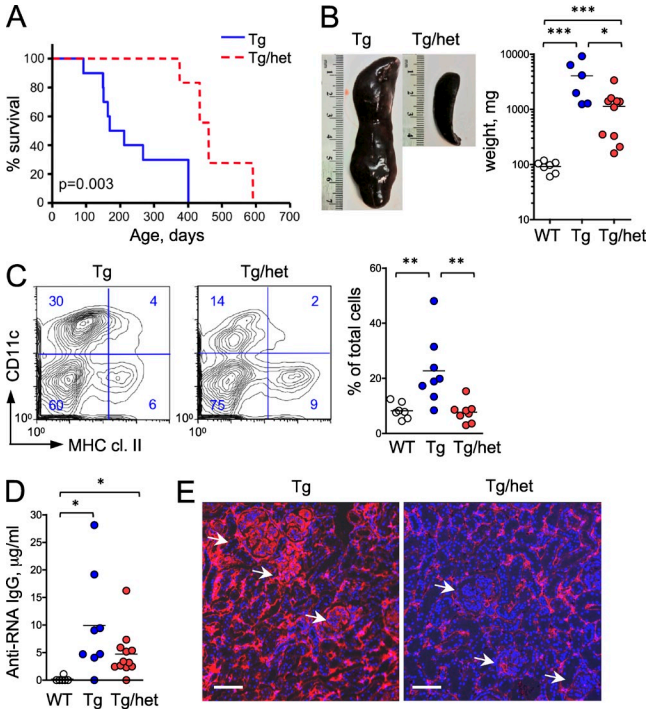

Figure 1. *Tcf4* haplodeficiency ameliorates SLE-like disease in Tlr7 transgenic mice. *Tlr7*.Tg males, haplodeficient for *Tcf4* (Tg/het) or their *Tcf4*-sufficient littermates (Tg), were analyzed. (A) Kaplan-Meier survival plot (n = 7–10). Significance was determined by log-rank test. (B) Splenic size (left) and splenic weights were determined for individual 50-wk-old transgenic animals and WT controls (right). (C) Peripheral blood cells from the indicated mice were analyzed by flow cytometry (left); thresholds of positive staining and percentages of cells within the resulting quadrants are indicated. The frequencies of the $CD11c^+$ MHC cl. II^- population (top left quadrant) in individual 30-wk-old animals were determined (right). Data were pooled from 3 independent experiments. (D) Anti-RNA IgG levels in the sera of 30–40-wk-old animals were determined by ELISA. Data were pooled from 3 independent experiments. (E) Kidney cryosections of 50–60-wk-old animals were stained for IgG (red) and DNA (blue) and analyzed by fluorescence microscopy (bars, 100 µm). Arrows show kidney glomeruli. Shown is a representative of 5 animals in each group from 2 independent experiments. Horizontal bars indicate mean. *, $P \le 0.05$; **, $P \le 0.01$; ***, $P \le 0.001$.

Published September 1, 2014

moribund and succumbed to the disease within 1 yr (Fig. 1 A). The presence of a single null allele of *Tcf4* did not reduce the level of *Tlr7* overexpression in pDCs and B cells from *Tcf4*$^{+/-}$ *Tlr7*.Tg animals (unpublished data). Nevertheless, all *Tcf4*$^{+/-}$ *Tlr7*.Tg males survived beyond 1 yr (Fig. 1 A) and showed a significantly lower (albeit still elevated) spleen weight at 50 wk (Fig. 1 B). Moreover, the increased population of CD11c^{+} MHC cl. II^{-} myeloid cells in the peripheral blood at 30 wk of age was reduced to normal levels (Fig. 1 C). No consistent changes in other blood cell types were detected in *Tlr7*.Tg animals (unpublished data). A trend toward lower levels of anti-RNA antibodies was observed in older *Tcf4*$^{+/-}$ animals at the same age, although the difference was not significant due to high variability (Fig. 1 D). No anti-DNA antibodies were detected in the majority of control or *Tcf4*$^{+/-}$ animals (unpublished data). The kidneys of *Tlr7*.Tg males at 50–60 wk showed abundant IgG deposition in both glomeruli and tubular interstitium, with the latter suggesting interstitial nephritis. In contrast, *Tcf4*$^{+/-}$ *Tlr7*.Tg males showed reduced IgG deposition in the kidneys (Fig. 1 E). Thus, global haplodeficiency of *Tcf4* improved survival and reduced immune activation in the *Tlr7*.Tg model of SLE.

Tcf4 haplodeficiency in DCs ameliorates Tlr7-induced SLE

Although Tcf4 deficiency primarily affects pDCs, Tcf4 is also expressed at low levels in B cells, as well as in nonimmune tissues including the brain. To confirm that the effect of *Tcf4* haplodeficiency in *Tlr7*.Tg mice originates in pDCs, we combined a single conditional (floxed) allele of *Tcf4* with the *Itgax*-Cre deleter strain. This strain (also known as *CD11c*-Cre) mediates Cre recombination specifically in the DC lineage including cDCs and pDCs (Caton et al., 2007). However, Tcf4 is not expressed in cDCs; therefore, any consequences of *Itgax*-Cre–mediated deletion of Tcf4 would reflect its function in pDCs only. We therefore analyzed conditional KO (CKO) *Tlr7*.Tg *Tcf4*$^{+/flox}$ *Itgax*-Cre^{+} males and their *Tlr7*.Tg *Tcf4*$^{+/flox}$ *Itgax*-Cre^{-} littermate controls for SLE manifestations.

Because *Tlr7*.Tg animals on pure B6 background survive for >1 yr, differential survival could not be assessed in this experiment. Nevertheless, similar to the germline *Tcf4* haplodeficiency, DC-specific *Tcf4* haplodeficiency significantly reduced splenomegaly (Fig. 2 A) and completely abolished myeloid cell expansion (Fig. 2 B). It also significantly reduced the fraction of activated T cells, although the latter was still increased relative to WT (Fig. 2 C). Control *Tlr7*. Tg animals at 30–40 wk showed increased levels of total serum IgG and IgM (Fig. 2 D), the presence of anti-RNA IgG (Fig. 2 E), and the associated autoreactivity to cytoplasmic antigens (Fig. 2 F). In contrast, *Tlr7*.Tg CKO animals had normal Ig levels and no significant anti-RNA autoreactivity (Fig. 2, D–F). This was accompanied by reduced IgG deposition in the kidneys of CKO mice (Fig. 2 G). Thus, *Tcf4* haplodeficiency in the DC lineage reduces autoreactivity and immune activation in *Tlr7*. Tg animals, similar to the germline *Tcf4* haplodeficiency. These data confirm that the effect is intrinsic to Tcf4-expressing cells within the DC lineage, which correspond to pDCs.

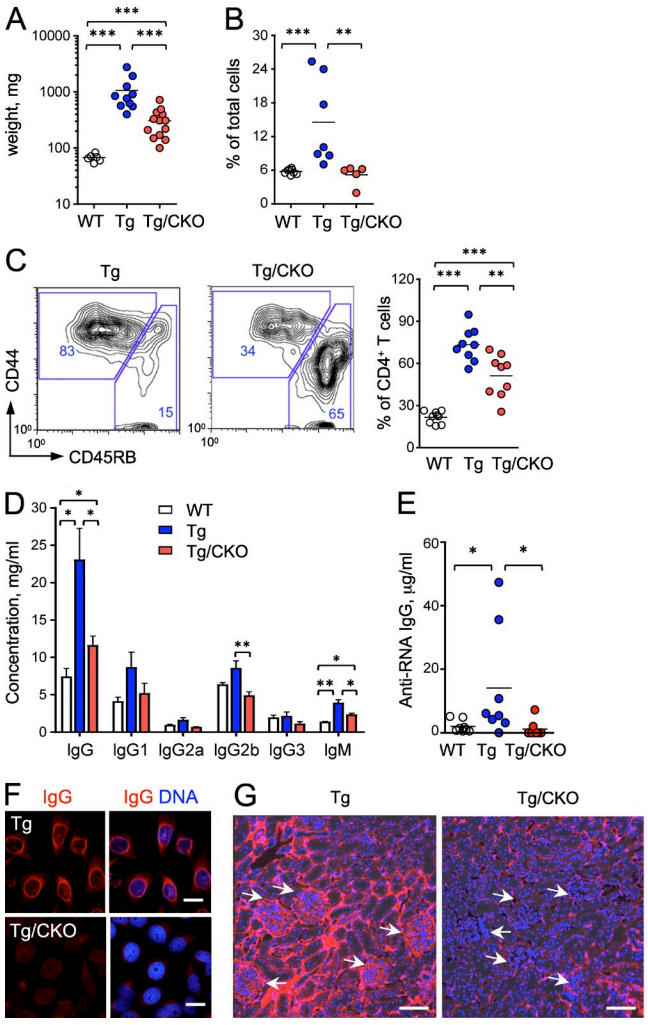

Figure 2. DC-specific *Tcf4* haplodeficiency ameliorates disease in Tlr7 transgenic mice. *Tlr7*.Tg *Tcf4*$^{flox/+}$ *Itgax*-Cre^{-} males (Tg) or their *Itgax*-Cre^{+} littermates with DC-specific *Tcf4* CKO (Tg/CKO) were analyzed along with WT controls. (A) Splenic weights were determined in individual 60-wk-old animals. (B) Frequencies of CD11c^{+} MHC cl. II^{-} myeloid cells in the peripheral blood of 30–40-wk-old animals were determined by flow cytometry. Data were pooled from 3 independent experiments. (C) Peripheral blood cells from the indicated 30–40-wk-old mice were analyzed by flow cytometry, gated on CD4^{+} T cells, and the frequencies of activated CD44^{+} CD45RB^{-} cells among CD4^{+} T cells were determined. Data were pooled from 4 independent experiments. (D) Levels of total IgM, IgG, and IgG subclasses in the sera of 30–40-wk-old animals were determined by ELISA (mean ± SD of 5 animals per group pooled from 2 independent experiments). (E) Anti-RNA IgG levels in the sera of 30–40-wk-old animals were determined by ELISA. Data were pooled from 3 independent experiments. (F) Fixed HEp-2 cells were incubated with sera from Tg mice, stained for IgG (red) alone or with DNA (blue), and analyzed by fluorescence microscopy (bars, 20 µm). Images are representative of 2 independent staining experiments. (G) Kidney cryosections of 60-wk-old animals were stained for IgG (red) and DNA (blue) and analyzed by fluorescence microscopy (bars, 100 µm). Arrows show kidney glomeruli. Images are representative of 6 animals in each group from 2 independent experiments. Horizontal bars indicate mean. *, $P \le 0.05$; **, $P \le 0.01$; ***, $P \le 0.001$.

Published September 1, 2014

Tcf4 haplodeficiency ameliorates SLE in B6.Sle1.Sle3 animals

Although *Tlr7*.Tg animals develop robust SLE-like disease, this monogenic model contrasts with the complex polygenic nature of human SLE. Furthermore, Tlr7-driven SLE does not recapitulate several important features of the human disease, including the production of antibodies against dsDNA (anti-dsDNA) and prominent glomerulonephritis. We therefore turned to a polygenic model that harbors large genomic intervals from the NZW strain (*Sle1*, *Sle2*, and *Sle3*) on B6 background (Morel et al., 2000). Notably, the homozygosity for only two intervals, *Sle1* and *Sle3*, is sufficient to cause full-blown SLE with nearly complete penetrance (Morel et al., 2000). We therefore analyzed animals on B6 background that were homozygous for *Sle1* and *Sle3*, heterozygous for *Sle2*, and either haplosufficient or haplodeficient for *Tcf4*.

The spleens of B6.*Sle1.Sle3* $Tcf4^{+/-}$ animals at 30 wk were significantly smaller than in $Tcf4^{+/+}$ littermates, although still enlarged relative to WT (Fig. 3 A). Peripheral blood leukocytes of B6.*Sle1.Sle3* mice showed no myeloid cell expansion or other major changes except for a slight decrease of B cell fraction (unpublished data). In contrast, the observed increase in the fraction of activated T cells was abolished in $Tcf4^{+/-}$ animals (Fig. 4 B). Peripheral blood leukocytes in B6.*Sle1.Sle3* animals showed increased expression of Sca-1, an IFN-inducible gene whose induction on B and T cells is associated with persistent IFN signaling (Lee et al., 2008). In $Tcf4^{+/-}$ animals, the levels of Sca-1 on B and T cells were significantly reduced to normal or near-normal levels, respectively (Fig. 3 C). Similar changes in T cell activation and Sca-1 expression were observed in the spleens of experimental animals (unpublished data).

B6.*Sle1.Sle3* mice showed increased levels of total serum IgG (particularly IgG1) and IgM, which were reduced to normal levels by *Tcf4* haplodeficiency (Fig. 3 D). The majority (9 out of 11) of control B6.*Sle1.Sle3* mice showed high titers of anti-dsDNA IgG and 5 out of 9 showed anti-RNA IgG (Fig. 3 E). Both the frequency and titers of these autoantibodies were significantly reduced in $Tcf4^{+/-}$ animals (Fig. 3 E), accompanied by the loss of anti-nuclear IgG reactivity (Fig. 3 F) and reduced IgG deposition in the kidneys (Fig. 3 G). We conclude that *Tcf4* haplodeficiency greatly reduced autoantibody production and immune activation in the B6.*Sle1.Sle3* model of SLE.

Tcf4 haplodeficiency ameliorates kidney inflammation in SLE models

Because glomerulonephritis is a key inflammatory manifestation and morbidity cause in SLE, we analyzed the effect of *Tcf4* haplodeficiency on kidney pathology in both experimental models. Control *Tlr7*.Tg animals at 50 wk manifested a relatively mild kidney inflammation with minimal glomerular deposits (Fig. 4 A and not depicted). Nevertheless, *Tlr7*.Tg CKO animals showed significant reductions in mean glomerular size (Fig. 4 B), extent of endocapillary proliferation and leukocyte infiltration, and median cumulative score of the disease (Fig. 4 C). Control B6.*Sle1.Sle3* animals at 30 wk manifested prominent glomerulonephritis with interstitial inflammation, leukocyte infiltration, and glomerular deposits. In contrast, $Tcf4^{+/-}$ B6.*Sle1.Sle3* littermates

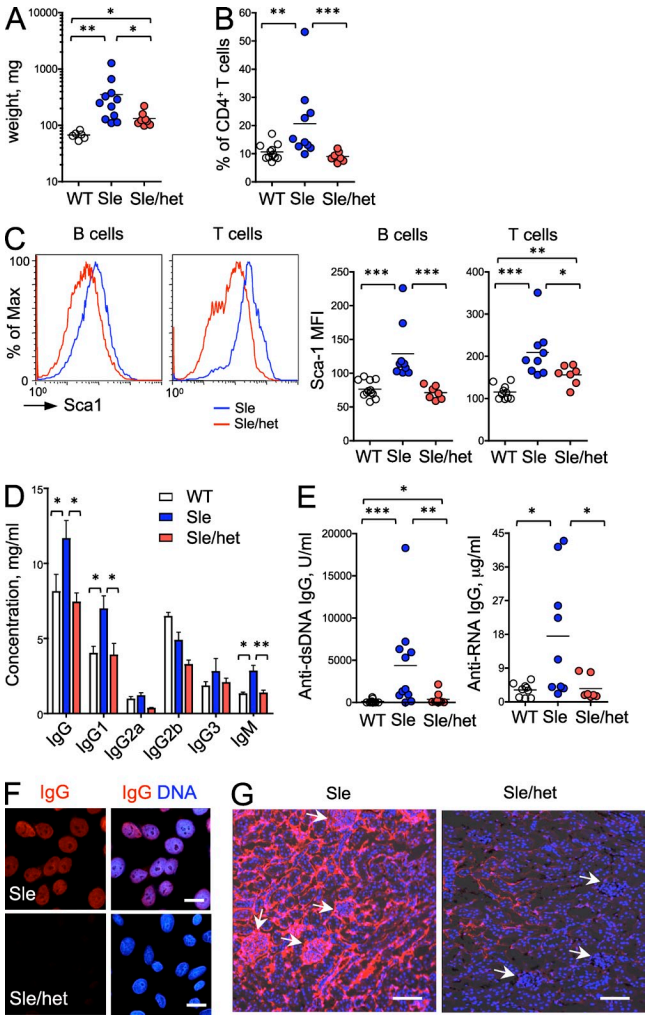

Figure 3. *Tcf4* haplodeficiency ameliorates immune activation in B6.*Sle1.Sle3* mice. 30-wk-old B6.*Sle1.Sle3* mice (Sle) or their *Tcf4* haplodeficient littermates (Sle/het) were analyzed along with WT controls. (A) Splenic weights were determined in individual indicated animals. (B) Peripheral blood cells from the indicated mice were analyzed by flow cytometry, gated on $CD4^+$ T cells, and the frequencies of activated $CD44^+$ $CD45RB^-$ cells among $CD4^+$ T cells were determined. Data were pooled from 3 independent experiments. (C) Sca-1 expression on gated B and T cells (left) and mean fluorescent intensities (MFIs) of Sca-1 on these cells from individual mice was determined by flow cytometry. Data were pooled from 3 independent experiments (right). (D and E) Levels of total IgM, IgG, and IgG subclasses (mean ± SD; D), anti-dsDNA, and anti-RNA IgG (E) in the sera of indicated experimental groups were measured by ELISA. Data were pooled from 2 independent experiments. (F) Fixed Hep2 cells were incubated with sera from Sle mice, stained for IgG (red) alone or with DNA (blue), and analyzed by fluorescence microscopy (bars, 20 µm). Images are representative of 2 independent staining experiments. (G) Kidney cryosections were stained for IgG (red) and DNA (blue) and analyzed by florescence microscopy (bars, 100 µm). Arrows show kidney glomeruli. Images are representative of 9 animals in each group from 3 independent experiments. Horizontal bars indicate mean. *, $P \leq 0.05$; **, $P \leq 0.01$; ***, $P \leq 0.001$.

Published September 1, 2014

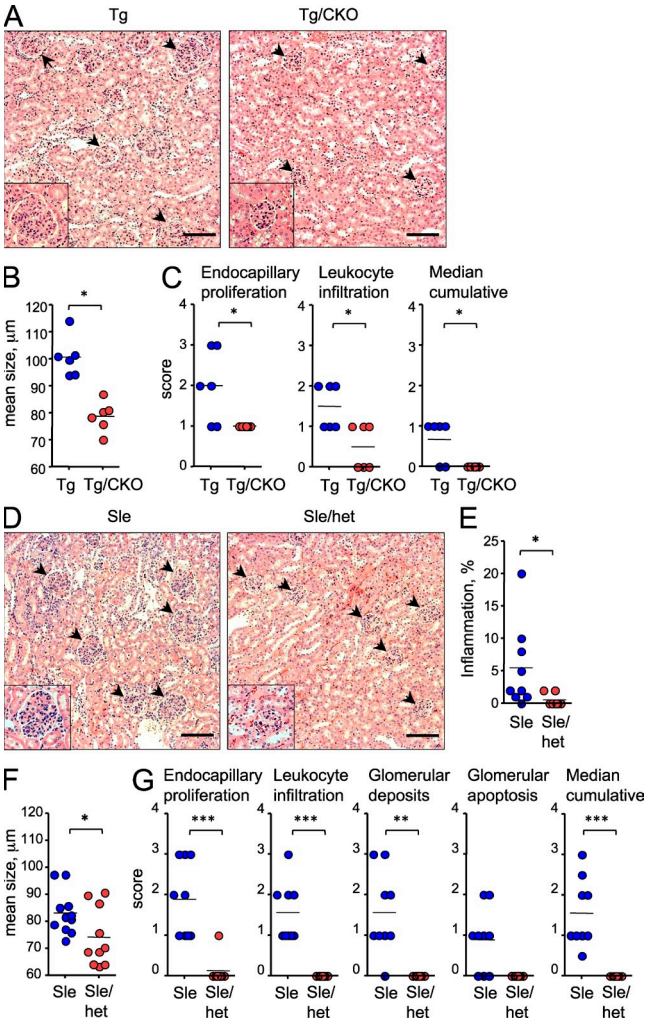

Figure 4. *Tcf4* haplodeficiency ameliorates kidney disease in SLE-prone mice. (A) Kidney paraffin sections from *Tlr7*.Tg animals with or without DC-specific *Tcf4* CKO (Tg/CKO) were stained with H&E and analyzed by microscopy (bars, 100 µm). Arrows show kidney glomeruli, with a representative glomerulus on the inset. Images are representative of 6 animals in each group from 2 independent experiments. (B) Mean diameter of kidney glomeruli was determined in individual 60-wk-old *Tlr7*.Tg animals. (C) Histopathological score of indicated disease parameters in the kidneys from individual *Tlr7*.Tg animals were determined using microscopy. (D) Kidney paraffin sections from B6.*Sle1.Sle3* mice with (Sle/het) or without (Sle) *Tcf4* haplodeficiency were stained with H&E and analyzed by microscopy (bars, 100 µm). Arrows show kidney glomeruli, with a representative glomerulus on the inset. Images are representative of 9 animals in each group from 2 independent experiments. (E–G) Percentage of parenchyma with interstitial inflammation in the kidneys (E), mean diameter of kidney glomeruli (F), and histopathological scores of indicated disease parameters (G) were determined in individual B6.*Sle1.Sle3* animals. Horizontal bars indicate mean. *, $P \leq 0.05$; **, $P \leq 0.01$; ***, $P \leq 0.001$.

showed a lower degree of interstitial inflammation, smaller glomeruli, and a nearly complete absence of glomerulonephritis (Fig. 4, D–G). We conclude that *Tcf4* haplodeficiency ameliorates autoreactivity-driven kidney inflammation in both *Tlr7*.Tg and B6.*Sle1.Sle3* models of SLE.

Tcf4 haplodeficiency reduces the germinal center (GC) signature of SLE

To explore the molecular correlates of SLE amelioration by *Tcf4* haplodeficiency, we performed microarray expression analysis of total splenocytes from WT, B6.*Sle1.Sle3* (Sle), and B6.*Sle1.Sle3 Tcf4*$^{+/-}$ (Sle/het) animals. Hierarchical clustering showed that Sle and Sle/het samples were highly similar yet distinct from the WT (Fig. 5 A). Indeed, principal component analysis (PCA) identified two major clusters of genes that were coordinately up- or down-regulated in both Sle samples compared with WT (Fig. 5 B and Dataset S1). Genes that were up-regulated in both Sle and Sle/het splenocytes (Fig. 5 B, cluster 1b) included proliferation-associated genes and granulocyte-specific genes, as well as genes associated with immune activation such as high mobility group proteins and defensins (Dataset S1). Consistent with previous observations in the B6.*Sle1.Sle2.Sle3* mice (Sriram et al., 2012), IFN-inducible genes were not significantly up-regulated in either Sle sample. Notably, PCA identified a distinct cluster of 49 genes that were up-regulated in Sle but not in Sle/het splenocytes (Fig. 5 B, cluster 2a). This cluster included several genes that are highly specific for GC B cells, including the *Aicda* gene encoding activation-induced cytidine deaminase (AID) (Dataset S1). Also present were several genes expressed in plasma cells (e.g., *Xbp1*) and in follicular helper T cells (*Il21* and *Pdcd1*). The reduction of *Aicda* overexpression in splenocytes from *Tcf4*-haplodeficient animals was confirmed by qRT-PCR for both B6.*Sle1.Sle3* and Tlr7.Tg models (Fig. 5 C). Furthermore, immunofluorescent staining revealed massive GC reaction in the spleens of B6.*Sle1.Sle3* mice that was virtually abolished in *Tcf4*-haplodeficient littermates (Fig. 5 D). We conclude that *Tcf4* haplodeficiency does not generally affect the SLE-associated gene expression profile, but specifically reduces the GC reaction and the associated expression signature.

A recent work used germline deletion of the transcription factor Irf8 or proton-coupled oligopeptide transporter Slc15a4 to test the role of pDCs in NZB and B6.*Fas*^{lpr} models of SLE, respectively (Baccala et al., 2013). However, Irf8 deletion affects the development and/or function of multiple immune cell types (Wang and Morse, 2009), whereas Slc15a4 regulates cytokine responses to Tlr9 and NOD-like receptor ligands in both pDCs and cDCs (Sasawatari et al., 2011). Here, we used haplodeficiency for Tcf4, a specific regulator of pDC development, to target pDC function in experimental SLE. In the case of the *Tlr7*.Tg model, we confirmed that the effect was intrinsic to the DC lineage, in which only pDCs express Tcf4. Although a minor subset of noncanonical CD8$^+$ cDCs is depleted by full Tcf4 deficiency (Bar-On et al., 2010), it is unaffected by reduced gene dosage of Tcf4 (our unpublished data). Furthermore, *Tcf4* haplodeficiency did not affect autoreactivity in the pDC-independent model of pristane-induced SLE. Therefore, our approach specifically interrogates the net contribution of the pDC lineage to experimental SLE.

We found that *Tcf4* haplodeficiency significantly ameliorated SLE manifestations in both *Tlr7*.Tg transgenic model

Published September 1, 2014

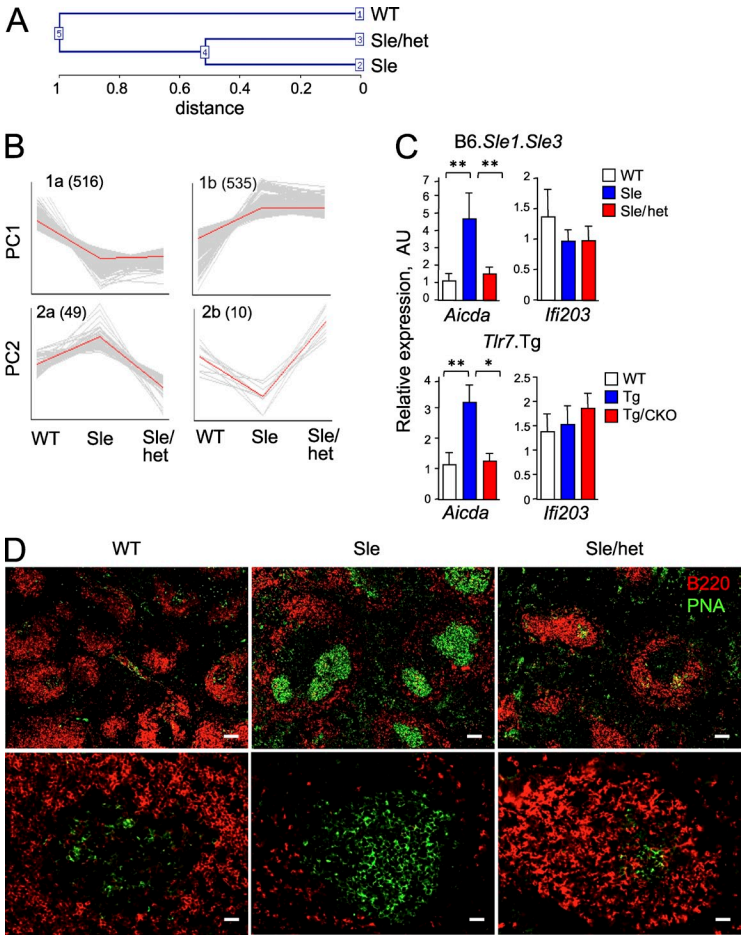

Figure 5. *Tcf4* haplodeficiency reduces GC signature in SLE-prone mice. (A and B) Total splenocytes from individual 30-wk-old WT ($n = 2$), B6.*Sle1.Sle3* (Sle, $n = 3$), or B6.*Sle1.Sle3 Tcf4*$^{+/-}$ (Sle/het, $n = 3$) mice were analyzed by expression microarrays. (A) Unsupervised hierarchical clustering of the total expression profiles of each sample group. (B) Unsupervised PCA-based clustering of genes whose expression was significantly changed between groups. Shown are clusters of genes with common pattern of differential expression according to the two principal components (PC1 and PC2). No additional clusters or principal components were identified in the PCA. Data represent expression trajectories of individual genes (gray) and a mean trajectory (red) across sample groups; the number of genes in each cluster is indicated. (C) The expression of *Aicda* was analyzed in total splenocytes from B6.*Sle1.Sle3* mice without (Sle) or with (Sle/het) *Tcf4* haplodeficiency (top), or from *Tlr7*.Tg animals without (Tg) or with (Tg/CKO) DC-specific *Tcf4* CKO (bottom). The expression of the IFN-inducible gene *Ifi203* is shown as a control. Data represent relative expression in each sample group as determined by qRT-PCR (mean ± SD of 5 and 3 animals per group for Sle and Tg samples, respectively). *, $P \le 0.05$; **, $P \le 0.01$. (D) Spleen sections from WT, B6.*Sle1.Sle3* (Sle), or B6.*Sle1.Sle3 Tcf4*$^{+/-}$ (Sle/het) mice were stained for total B cells (B220, red) and GC B cells (PNA, green). Shown is overall splenic architecture (top row: bars 100 µm) and representative GCs (bottom row: bars 20 µm). Representative of 3 spleens per genotype.

and B6.*Sle1.Sle3* multigenic model. Unlike human SLE patients, these and other mouse SLE models do not manifest a prominent IFN signature (Perry et al., 2011); hence, we could not detect a consistent reduction of IFN-inducible genes. It is therefore likely that the role of pDCs in experimental SLE and possibly in human SLE patients goes beyond IFN production. Indeed, a recent study in human systemic sclerosis revealed an important role for chemokine production by pDCs (van Bon et al., 2014). In that respect, it is notable that *Tcf4* haplodeficiency profoundly decreased autoantibody production, GC reaction, and the ensuing glomerulonephritis in both SLE models. These data suggest a particular importance of pDCs in autoreactive B cell activation and plasma cell differentiation in SLE. This function of pDCs may be mediated through direct interaction with B cells (Jego et al., 2003; Shaw et al., 2010) and/or indirectly by supporting helper T cell differentiation (Cervantes-Barragan et al., 2012).

Our results suggest that TCF4-driven pDC expression program may be relevant in human SLE. Although *TCF4* polymorphism has not been implicated in SLE by genome-wide association studies, it is likely to be constrained by critical functions of TCF4 in brain development. In contrast, major SLE-associated genes, including transcriptional (*IRF7*, *IKZF1*, *PRDM1*, and *JAZF1*) and signaling (*TNFAIP3* and *BLK*) regulators (Deng and Tsao, 2010) represent direct targets of TCF4 in pDCs (Ghosh et al., 2010). Thus, these genes might contribute to SLE predisposition in part through their activity in the pDC lineage. In addition, our results highlight the beneficial effect of functional pDC impairment on SLE pathogenesis, providing the rationale for pDC-targeted therapeutic approaches. Indeed, pDC ablation or functional impairment would be less immunosuppressive than a global blockade of IFN signaling, and would target multiple pDC functions such as secretion of chemokines. Collectively, our data suggest the targeting of the pDC lineage (e.g., by depleting antibodies) as a viable therapeutic strategy to ameliorate SLE.

MATERIALS AND METHODS

Animals. All experiments were performed according to the investigator's protocol approved by the Institutional Animal Care and Use Committee of Columbia University. *Tcf4*$^{+/-}$ animals (Zhuang et al., 1996) were on pure 129SvEvTac background (>N12); all other animals were on pure C57BL/6 (B6) background (>N12). Pristane was administered i.p. into *Tcf4*$^{+/-}$ animals or *Tcf4*$^{+/-}$ littermates as previously described (Lee et al., 2008). *Tlr7*.Tg males (Y-linked transgenic line 7.6; Deane et al., 2007) were crossed with *Tcf4*$^{+/-}$ females to generate B6129F1 *Tcf4*$^{+/-}$ *Tlr7*.Tg males or *Tcf4*$^{+/+}$ *Tlr7*.Tg littermates. Age-matched B6129F1 males bred in the same colony were used as WT controls. For conditional targeting of Tcf4, *Tlr7*.Tg males carrying the *Itgax*-Cre transgene (Caton et al., 2007) were crossed with *Tcf4*$^{flox/flox}$

females (Bergqvist et al., 2000) to generate *Tcf4*$^{flox/+}$ *Tlr7*.Tg males with or without the Cre transgene. Age-matched B6 males bred in the same colony were used as WT controls.

For the cross with B6.*Sle1.Sle3* strain, a new null allele of *Tcf4* was derived by recombining the *Tcf4*^{flox} allele in the female germline using the *Tek*-Cre transgenic strain (The Jackson Laboratory). After crossing out the Cre transgene, *Tcf4*$^{+/-}$ animals were crossed to BcN.LmoJ animals homozygous for *Sle1*, *Sle2*, and *Sle3* loci (Morel et al., 2000; The Jackson Laboratory). The resulting *Tcf4*$^{+/-}$ animals heterozygous for *Sle1*, *Sle2*, and *Sle3* were backcrossed to BcN.LmoJ to achieve homozygosity for *Sle1* and *Sle3*. The integrity of *Sle* loci was confirmed by PCR genotyping for microsatellite markers spanning each locus. No differences in any SLE manifestations have been observed between male and female B6.*Sle1.Sle3* animals; thus, both male and female mice were included in the analysis along with age-matched B6 WT controls.

Flow cytometry. Suspensions of peripheral blood leukocytes or splenocytes were subjected to red blood cell lysis, washed, and stained with directly conjugated fluorescent antibodies to the indicated surface markers (eBioscience). The samples were acquired on the LSR II flow cytometer (BD) and analyzed using FlowJo software (Tree Star).

Autoantibody measurement. Immunoglobulin levels in the serum were determined by ELISA using alkaline phosphatase–conjugated antibodies to IgM, IgG, and IgG isotypes (SouthernBiotech). Anti-RNA and anti-dsDNA IgG concentrations were determined by ELISA as previously described (Blanco et al., 1991) using yeast RNA or calf thymus DNA as antigens.

Histopathology. 2-µm sections of formalin-fixed kidneys were stained with H&E and evaluated by a pathologist (V. D'Agati) who was blinded to sample identity. Mesangial and endocapillary proliferation, leukocyte infiltration, glomerular deposits, and apoptosis were scored separately on a scale from 0 (none) to 4 (highest) and added to yield a cumulative score. The percentage of cortical parenchyma with interstitial inflammation was also determined. To measure immune complex deposition, kidneys were fixed in 4% paraformaldehyde, dehydrated in 30% sucrose, and frozen in OCT (TissueTek). Frozen sections (5 µm) were stained with DAPI and PE-labeled goat anti–mouse IgG antibody (eBioscience). For the analysis of GC reaction, frozen spleen sections (5 µm) were stained with PE-labeled anti–mouse B220 (eBioscience) and biotin-conjugated peanut agglutinin (PNA; Vector Laboratories), followed by FITC-conjugated Streptavidin (eBioscience). Anti-nuclear antibodies were detected by staining fixed HEp-2 cells (MBL Bion) with mouse serum (1:100 dilution), followed by PE-labeled goat anti–mouse IgG and DAPI. Images were captured on a confocal fluorescent microscope (LSM 710 NLO) and processed by Zen software (Carl Zeiss).

Gene expression analysis. Total splenocytes from individual WT B6 ($n = 2$), B6.*Sle1.Sle3* ($n = 3$), or B6.*Sle1.Sle3 Tcf4*$^{+/-}$ ($n = 3$) animals at 30 wk were used for microarray analysis. Total RNA was isolated, reverse transcribed, amplified, labeled, and hybridized to Mouse Genome 1.0 ST arrays (Affymetrix). The results were gcRMA-normalized by the manufacturer's software and analyzed using the NIA Array software (Sharov et al., 2005). The qRT-PCR analysis of total splenocytes from individual mice was performed as previously described (Cisse et al., 2008; Ghosh et al., 2010).

Statistics. Unless noted otherwise, significance was estimated by nonparametric Mann-Whitney test.

Accession nos. Microarray data have been deposited in the Gene Expression Omnibus (GEO) database under the accession no. GSE57324.

Online supplemental material. Dataset S1 shows genome-wide expression analysis of splenocytes from B6.*Sle1.Sle3* mice with or without *Tcf4* haplodeficiency. Online supplemental material is available at http://www.jem.org/cgi/content/full/jem.20132522/DC1.

We thank Dr. Nicole Heise for reagents and advice.

This research was supported by the National Institutes of Health grant AI072571 and the Lupus Research Institute (B. Reizis), the S.L.E. Lupus Research Foundation (D. Ganguly), and the Cancer Research Institute (V. Sisirak).

The authors declare no competing financial interests.

Submitted: 5 December 2013
Accepted: 10 July 2014

REFERENCES

Agrawal, H., N. Jacob, E. Carreras, S. Bajana, C. Putterman, S. Turner, B. Neas, A. Mathian, M.N. Koss, W. Stohl, et al. 2009. Deficiency of type I IFN receptor in lupus-prone New Zealand mixed 2328 mice decreases dendritic cell numbers and activation and protects from disease. *J. Immunol.* 183:6021–6029. http://dx.doi.org/10.4049/jimmunol.0803872

Baccala, R., R. Gonzalez-Quintial, A.L. Blasius, I. Rimann, K. Ozato, D.H. Kono, B. Beutler, and A.N. Theofilopoulos. 2013. Essential requirement for IRF8 and SLC15A4 implicates plasmacytoid dendritic cells in the pathogenesis of lupus. *Proc. Natl. Acad. Sci. USA.* 110:2940–2945. http://dx.doi.org/10.1073/pnas.1222798110

Baechler, E.C., F.M. Batliwalla, G. Karypis, P.M. Gaffney, W.A. Ortmann, K.J. Espe, K.B. Shark, W.J. Grande, K.M. Hughes, V. Kapur, et al. 2003. Interferon-inducible gene expression signature in peripheral blood cells of patients with severe lupus. *Proc. Natl. Acad. Sci. USA.* 100:2610–2615. http://dx.doi.org/10.1073/pnas.0337679100

Bar-On, L., T. Birnberg, K.L. Lewis, B.T. Edelson, D. Bruder, K. Hildner, J. Buer, K.M. Murphy, B. Reizis, and S. Jung. 2010. CX3CR1^{+} CD8α^{+} dendritic cells are a steady-state population related to plasmacytoid dendritic cells. *Proc. Natl. Acad. Sci. USA.* 107:14745–14750. http://dx.doi.org/10.1073/pnas.1001562107

Båve, U., M. Magnusson, M.L. Eloranta, A. Perers, G.V. Alm, and L. Rönnblom. 2003. FcγRIIa is expressed on natural IFN-α-producing cells (plasmacytoid dendritic cells) and is required for the IFN-α production induced by apoptotic cells combined with lupus IgG. *J. Immunol.* 171:3296–3302. http://dx.doi.org/10.4049/jimmunol.171.6.3296

Bennett, L., A.K. Palucka, E. Arce, V. Cantrell, J. Borvak, J. Banchereau, and V. Pascual. 2003. Interferon and granulopoiesis signatures in systemic lupus erythematosus blood. *J. Exp. Med.* 197:711–723. http://dx.doi.org/10.1084/jem.20021553

Bergqvist, I., M. Eriksson, J. Saarikettu, B. Eriksson, B. Corneliussen, T. Grundström, and D. Holmberg. 2000. The basic helix-loop-helix transcription factor E2-2 is involved in T lymphocyte development. *Eur. J. Immunol.* 30:2857–2863.http://dx.doi.org/10.1002/1521-4141(200010)30:10<2857::AID-IMMU2857>3.0.CO;2-G

Blanco, F., J. Kalsi, and D.A. Isenberg. 1991. Analysis of antibodies to RNA in patients with systemic lupus erythematosus and other autoimmune rheumatic diseases. *Clin. Exp. Immunol.* 86:66–70. http://dx.doi.org/10.1111/j.1365-2249.1991.tb05775.x

Bronson, P.G., C. Chaivorapol, W. Ortmann, T.W. Behrens, and R.R. Graham. 2012. The genetics of type I interferon in systemic lupus erythematosus. *Curr. Opin. Immunol.* 24:530–537. http://dx.doi.org/10.1016/j.coi.2012.07.008

Buechler, M.B., T.H. Teal, K.B. Elkon, and J.A. Hamerman. 2013. Cutting edge: Type I IFN drives emergency myelopoiesis and peripheral myeloid expansion during chronic TLR7 signaling. *J. Immunol.* 190:886–891. http://dx.doi.org/10.4049/jimmunol.1202739

Caton, M.L., M.R. Smith-Raska, and B. Reizis. 2007. Notch-RBP-J signaling controls the homeostasis of CD8^{-} dendritic cells in the spleen. *J. Exp. Med.* 204:1653–1664.

Cervantes-Barragan, L., K.L. Lewis, S. Firner, V. Thiel, S. Hugues, W. Reith, B. Ludewig, and B. Reizis. 2012. Plasmacytoid dendritic cells control T-cell response to chronic viral infection. *Proc. Natl. Acad. Sci. USA.* 109:3012–3017. http://dx.doi.org/10.1073/pnas.1117359109

Cisse, B., M.L. Caton, M. Lehner, T. Maeda, S. Scheu, R. Locksley, D. Holmberg, C. Zweier, N.S. den Hollander, S.G. Kant, et al. 2008. Transcription factor E2-2 is an essential and specific regulator of plasmacytoid dendritic cell development. *Cell.* 135:37–48. http://dx.doi.org/10.1016/j.cell.2008.09.016

Deane, J.A., P. Pisitkun, R.S. Barrett, L. Feigenbaum, T. Town, J.M. Ward, R.A. Flavell, and S. Bolland. 2007. Control of toll-like receptor 7 expression is essential to restrict autoimmunity and dendritic cell proliferation. *Immunity*. 27:801–810. http://dx.doi.org/10.1016/j.immuni.2007.09.009

Deng, Y., and B.P. Tsao. 2010. Genetic susceptibility to systemic lupus erythematosus in the genomic era. *Nat Rev Rheumatol*. 6:683–692. http://dx.doi.org/10.1038/nrrheum.2010.176

Elkon, K.B., and A. Wiedeman. 2012. Type I IFN system in the development and manifestations of SLE. *Curr. Opin. Rheumatol.* 24:499–505. http://dx.doi.org/10.1097/BOR.0b013e3283562c3e

Fairhurst, A.M., A.E. Wandstrat, and E.K. Wakeland. 2006. Systemic lupus erythematosus: multiple immunological phenotypes in a complex genetic disease. *Adv. Immunol.* 92:1–69. http://dx.doi.org/10.1016/S0065-2776(06)92001-X

Fairhurst, A.M., S.H. Hwang, A. Wang, X.H. Tian, C. Boudreaux, X.J. Zhou, J. Casco, Q.Z. Li, J.E. Connolly, and E.K. Wakeland. 2008. Yaa autoimmune phenotypes are conferred by overexpression of TLR7. *Eur. J. Immunol.* 38:1971–1978. http://dx.doi.org/10.1002/eji.200838138

Garcia-Romo, G.S., S. Caielli, B. Vega, J. Connolly, F. Allantaz, Z. Xu, M. Punaro, J. Baisch, C. Guiducci, R.L. Coffman, et al. 2011. Netting neutrophils are major inducers of type I IFN production in pediatric systemic lupus erythematosus. *Sci. Transl. Med.* 3:73ra20. http://dx.doi.org/10.1126/scitranslmed.3001201

Ghosh, H.S., B. Cisse, A. Bunin, K.L. Lewis, and B. Reizis. 2010. Continuous expression of the transcription factor e2-2 maintains the cell fate of mature plasmacytoid dendritic cells. *Immunity*. 33:905–916. http://dx.doi.org/10.1016/j.immuni.2010.11.023

Gilliet, M., W. Cao, and Y.J. Liu. 2008. Plasmacytoid dendritic cells: sensing nucleic acids in viral infection and autoimmune diseases. *Nat. Rev. Immunol.* 8:594–606.

Guiducci, C., M. Gong, Z. Xu, M. Gill, D. Chaussabel, T. Meeker, J.H. Chan, T. Wright, M. Punaro, S. Bolland, et al. 2010a. TLR recognition of self nucleic acids hampers glucocorticoid activity in lupus. *Nature*. 465:937–941. http://dx.doi.org/10.1038/nature09102

Guiducci, C., C. Tripodo, M. Gong, S. Sangaletti, M.P. Colombo, R.L. Coffman, and F.J. Barrat. 2010b. Autoimmune skin inflammation is dependent on plasmacytoid dendritic cell activation by nucleic acids via TLR7 and TLR9. *J. Exp. Med.* 207:2931–2942. http://dx.doi.org/10.1084/jem.20101048

Jego, G., A.K. Palucka, J.P. Blanck, C. Chalouni, V. Pascual, and J. Banchereau. 2003. Plasmacytoid dendritic cells induce plasma cell differentiation through type I interferon and interleukin 6. *Immunity*. 19:225–234. http://dx.doi.org/10.1016/S1074-7613(03)00208-5

Lande, R., D. Ganguly, V. Facchinetti, L. Frasca, C. Conrad, J. Gregorio, S. Meller, G. Chamilos, R. Sebasigari, V. Riccieri, et al. 2011. Neutrophils activate plasmacytoid dendritic cells by releasing self-DNA-peptide complexes in systemic lupus erythematosus. *Sci. Tiansl. Med.* 3:73ra19. http://dx.doi.org/10.1126/scitranslmed.3001180

Lee, P.Y., Y. Kumagai, Y. Li, O. Takeuchi, H. Yoshida, J. Weinstein, E.S. Kellner, D. Nacionales, T. Barker, K. Kelly-Scumpia, et al. 2008. TLR7-dependent and FcγR-independent production of type I interferon in experimental mouse lupus. *J. Exp. Med.* 205:2995–3006. http://dx.doi.org/10.1084/jem.20080462

Liu, Z., and A. Davidson. 2013. IFNα Inducible Models of Murine SLE. *Front. Immunol.* 4:306. http://dx.doi.org/10.3389/fimmu.2013.00306

Marshak-Rothstein, A., and I.R. Rifkin. 2007. Immunologically active autoantigens: the role of toll-like receptors in the development of chronic inflammatory disease. *Annu. Rev. Immunol.* 25:419–441. http://dx.doi.org/10.1146/annurev.immunol.22.012703.104514

Morel, L., B.P. Croker, K.R. Blenman, C. Mohan, G. Huang, G. Gilkeson, and E.K. Wakeland. 2000. Genetic reconstitution of systemic lupus erythematosus immunopathology with polycongenic murine strains. *Proc. Natl. Acad. Sci. USA*. 97:6670–6675. http://dx.doi.org/10.1073/pnas.97.12.6670

Perry, D., A. Sang, Y. Yin, Y.Y. Zheng, and L. Morel. 2011. Murine models of systemic lupus erythematosus. *J. Biomed. Biotechnol.* 2011:271694. http://dx.doi.org/10.1155/2011/271694

Pisitkun, P., J.A. Deane, M.J. Difilippantonio, T. Tarasenko, A.B. Satterthwaite, and S. Bolland. 2006. Autoreactive B cell responses to RNA-related antigens due to TLR7 gene duplication. *Science*. 312:1669–1672. http://dx.doi.org/10.1126/science.1124978

Reizis, B., A. Bunin, H.S. Ghosh, K.L. Lewis, and V. Sisirak. 2011. Plasmacytoid dendritic cells: recent progress and open questions. *Annu. Rev. Immunol.* 29:163–183. http://dx.doi.org/10.1146/annurev-immunol-031210-101345

Rönnblom, L., and G.V. Alm. 2001. A pivotal role for the natural interferon alpha-producing cells (plasmacytoid dendritic cells) in the pathogenesis of lupus. *J. Exp. Med.* 194:F59–F63. http://dx.doi.org/10.1084/jem.194.12.f59

Santiago-Raber, M.L., R. Baccala, K.M. Haraldsson, D. Choubey, T.A. Stewart, D.H. Kono, and A.N. Theofilopoulos. 2003. Type-I interferon receptor deficiency reduces lupus-like disease in NZB mice. *J. Exp. Med.* 197:777–788. http://dx.doi.org/10.1084/jem.20021996

Sasawatari, S., T. Okamura, E. Kasumi, K. Tanaka-Furuyama, R. Yanobu-Takanashi, S. Shirasawa, N. Kato, and N. Toyama-Sorimachi. 2011. The solute carrier family 15A4 regulates TLR9 and NOD1 functions in the innate immune system and promotes colitis in mice. *Gastroenterology*. 140:1513–1525. http://dx.doi.org/10.1053/j.gastro.2011.01.041

Sharov, A.A., D.B. Dudekula, and M.S. Ko. 2005. A web-based tool for principal component and significance analysis of microarray data. *Bioinformatics*. 21:2548–2549. http://dx.doi.org/10.1093/bioinformatics/bti343

Shaw, J., Y.H. Wang, T. Ito, K. Arima, and Y.J. Liu. 2010. Plasmacytoid dendritic cells regulate B-cell growth and differentiation via CD70. *Blood*. 115:3051–3057. http://dx.doi.org/10.1182/blood-2009-08-239145

Shlomchik, M.J. 2009. Activating systemic autoimmunity: B's, T's, and tolls. *Curr. Opin. Immunol.* 21:626–633. http://dx.doi.org/10.1016/j.coi.2009.08.005

Sriram, U., L. Varghese, H.L. Bennett, N.R. Jog, D.K. Shivers, Y. Ning, E.M. Behrens, R. Caricchio, and S. Gallucci. 2012. Myeloid dendritic cells from B6.NZM Sle1/Sle2/Sle3 lupus-prone mice express an IFN signature that precedes disease onset. *J. Immunol.* 189:80–91. http://dx.doi.org/10.4049/jimmunol.1101686

Tian, J., A.M. Avalos, S.Y. Mao, B. Chen, K. Senthil, H. Wu, P. Parroche, S. Drabic, D. Golenbock, C. Sirois, et al. 2007. Toll-like receptor 9-dependent activation by DNA-containing immune complexes is mediated by HMGB1 and RAGE. *Nat. Immunol.* 8:487–496. http://dx.doi.org/10.1038/ni1457

van Bon, L., A.J. Affandi, J. Broen, R.B. Christmann, R.J. Marijnissen, L. Stawski, G.A. Farina, G. Stifano, A.L. Mathes, M. Cossu, et al. 2014. Proteome-wide analysis and CXCL4 as a biomarker in systemic sclerosis. *N. Engl. J. Med.* 370:433–443. http://dx.doi.org/10.1056/NEJMoa1114576

Wang, H., and H.C. Morse III. 2009. IRF8 regulates myeloid and B lymphoid lineage diversification. *Immunol. Res.* 43:109–117. http://dx.doi.org/10.1007/s12026-008-8055-8

Zhuang, Y., P. Cheng, and H. Weintraub. 1996. B-lymphocyte development is regulated by the combined dosage of three basic helix-loop-helix genes, E2A, E2-2, and HEB. *Mol. Cell. Biol.* 16:2898–2905.

SUPPLEMENTAL MATERIAL

Sisirak et al., http://www.jem.org/cgi/content/full/jem.20132522/DC1

Dataset S1. Genome-wide expression analysis of splenocytes from B6.*Sle1.Sle3* mice with or without *Tcf4* haplodeficiency. Probes used in the analysis included those used by the Immgen consortium that have definitive RefSeq annotations. Array results lists hybridization signals for all samples (each sample derived from a separate animal) and Log_{10}-transformed mean signals generated by the NIA Array software. PCA lists genes within each PCA-generated cluster (Fig. 5 B) with Log_{10}-transformed fold change between samples and correlation with the respective principal component. Indicated for cluster 1b are genes associated with the granulocyte signature and proliferation signature (modules 41 and 11 of the Immgen dataset, respectively). Indicated for cluster 2a are genes showing preferential expression in GC B cells in the Immgen dataset, and genes showing preferential expression in GC and/or plasma cells within the B cell lineage, as determined by the analysis of GEO dataset GDS1695. Dataset 1 is provided as an Excel file.

Article

Cell

Digestion of Chromatin in Apoptotic Cell Microparticles Prevents Autoimmunity

Graphical Abstract

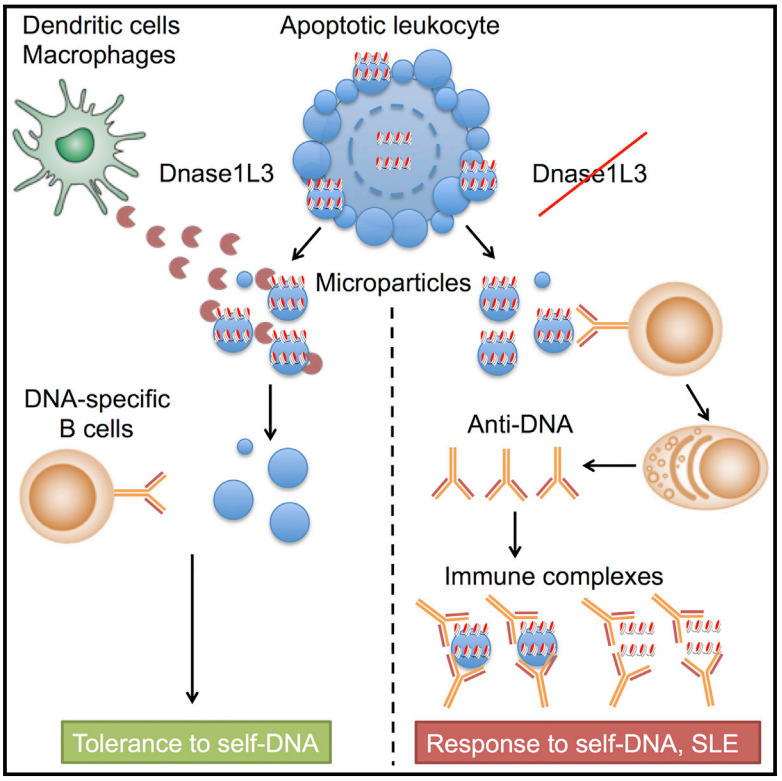

Authors

Vanja Sisirak, Benjamin Sally, Vivette D'Agati, ..., Robert M. Clancy, Jill P. Buyon, Boris Reizis

Correspondence

boris.reizis@nyumc.org

In Brief

Extracellular microparticle-associated chromatin is a potential self-antigen normally digested by circulating DNASE1L3. The loss of this tolerance mechanism in mice and humans contributes to lupus, and the restoration of this mechanism may represent a therapeutic opportunity in the disease.

Highlights

- Rapid anti-DNA antibody response, followed by SLE in *Dnase1l3*-deficient mice
- Autoreactivity is repressed by circulating DNASE1L3 and is independent of STING
- DNASE1L3 digests genomic DNA in microparticles released from apoptotic cells
- DNASE1L3 prevents autoantibody binding to chromatin on microparticle surface

Sisirak et al., 2016, Cell *166*, 88–101
June 30, 2016
http://dx.doi.org/10.1016/j.cell.2016.05.034

CellPress

Cell

Article

Digestion of Chromatin in Apoptotic Cell Microparticles Prevents Autoimmunity

Vanja Sisirak,[1,12] Benjamin Sally,[1,2,12] Vivette D'Agati,[3] Wilnelly Martinez-Ortiz,[4] Z. Birsin Özçakar,[5] Joseph David,[1] Ali Rashidfarrokhi,[1] Ada Yeste,[6] Casandra Panea,[2] Asiya Seema Chida,[7] Milena Bogunovic,[8] Ivaylo I. Ivanov,[2] Francisco J. Quintana,[6] Inaki Sanz,[7] Keith B. Elkon,[9] Mustafa Tekin,[10] Fatoş Yalçınkaya,[5] Timothy J. Cardozo,[4] Robert M. Clancy,[11] Jill P. Buyon,[11] and Boris Reizis[1,2,11,*]

[1]Department of Pathology, New York University School of Medicine, New York, NY 10016, USA
[2]Department of Microbiology and Immunology, Columbia University Medical Center, New York, NY 10032, USA
[3]Department of Pathology, Columbia University Medical Center, New York, NY 10032, USA
[4]Department of Biochemistry and Molecular Pharmacology, New York University School of Medicine, New York, NY 10016, USA
[5]Division of Pediatric Nephrology, Department of Pediatrics, School of Medicine, Ankara University, Ankara, 06100, Turkey
[6]Ann Romney Center for Neurologic Diseases, Brigham and Women's Hospital, Harvard Medical School, Boston, MA 02115, USA
[7]Division of Rheumatology, Department of Medicine, Emory University, Atlanta, GA 30322, USA
[8]Department of Microbiology and Immunology, Milton S. Hershey Medical Center, Pennsylvania State University, Hershey, PA 17033, USA
[9]Department of Medicine, University of Washington, Seattle, WA 98195, USA
[10]Department of Human Genetics, Miller School of Medicine, University of Miami, Miami, FL 33136, USA
[11]Department of Medicine, New York University School of Medicine, New York, NY 10016, USA
[12]Co-first author
*Correspondence: boris.reizis@nyumc.org
http://dx.doi.org/10.1016/j.cell.2016.05.034

SUMMARY

Antibodies to DNA and chromatin drive autoimmunity in systemic lupus erythematosus (SLE). Null mutations and hypomorphic variants of the secreted deoxyribonuclease DNASE1L3 are linked to familial and sporadic SLE, respectively. We report that DNASE1L3-deficient mice rapidly develop autoantibodies to DNA and chromatin, followed by an SLE-like disease. Circulating DNASE1L3 is produced by dendritic cells and macrophages, and its levels inversely correlate with anti-DNA antibody response. DNASE1L3 is uniquely capable of digesting chromatin in microparticles released from apoptotic cells. Accordingly, DNASE1L3-deficient mice and human patients have elevated DNA levels in plasma, particularly in circulating microparticles. Murine and human autoantibody clones and serum antibodies from human SLE patients bind to DNASE1L3-sensitive chromatin on the surface of microparticles. Thus, extracellular microparticle-associated chromatin is a potential self-antigen normally digested by circulating DNASE1L3. The loss of this tolerance mechanism can contribute to SLE, and its restoration may represent a therapeutic opportunity in the disease.

INTRODUCTION

The hallmark of systemic lupus erythematosus (SLE) is the production of antibodies (Abs) to nuclear antigens, such as ribonucleoproteins and DNA. Auto-Ab production by self-reactive B cells triggers and is further amplified by the activation of the innate immune system, including myeloid cell activation and secretion of type I interferon (interferon α/β; IFN) (Choi et al., 2012). Ultimately, auto-Abs forming immune complexes with nucleic acids are deposited in tissues, where they cause chronic inflammation, such as vasculitis and glomerulonephritis. High-affinity immunoglobulin G (IgG) Abs to double-stranded DNA (dsDNA) are particularly pathogenic and associated with the severity of clinical disease in SLE (Pisetsky, 2016). Furthermore, Abs to chromatin, including nucleosomes, are common in SLE and may serve as especially sensitive biomarkers of the disease (Rekvig et al., 2014). Thus, the loss of B cell tolerance to DNA and/or chromatin represents a major mechanism of SLE pathogenesis.

DNA-reactive antigen receptors are present in the normal B cell repertoire (Wardemann and Nussenzweig, 2007). Therefore, a major question of SLE pathogenesis concerns the physical form(s) of DNA that can be recognized by autoreactive B cells and the mechanisms that normally prevent such recognition. DNA from apoptotic cells is degraded by the intracellular enzyme DNASE2, whose deletion in mice causes IFN-driven autoinflammation (Nagata and Kawane, 2011). Similarly, DNA of reverse-transcribed retroelements is degraded by an intracellular exonuclease TREX1, and the loss of TREX1 causes IFN-driven inflammatory disease in human patients (Aicardi-Goutieres syndrome) and in mice (Crow, 2015; Volkman and Stetson, 2014). Importantly, these inflammatory conditions are driven by innate DNA sensing that requires the cytoplasmic protein STING (Ahn et al., 2012; Gall et al., 2012). Other potentially immunogenic forms of DNA are neutrophil extracellular traps (NETs) and oxidized mitochondrial DNA released by activated granulocytes (Caielli et al., 2016; Lood et al., 2016). These stimuli may engage endosomal Toll-like receptor (TLR) TLR9 or STING

to induce IFN production, yet their role as B cell antigens remains unclear. Finally, genomic DNA of apoptotic cells is incorporated into membrane-coated microparticles (Pisetsky et al., 2011), which are normally present in the plasma of healthy subjects and SLE patients (Dieker et al., 2016; Nielsen et al., 2011, 2012). These microparticles (MP) were shown to expose chromatin on their surface (Ullal et al., 2011, 2014) and therefore may represent antigens for DNA-reactive B cells. However, the relationship of MP DNA to total DNA in human plasma (Snyder et al., 2016; Sun et al., 2015), the regulation of MP DNA, and potential role for MP DNA in SLE remain obscure.

A recent study (Al-Mayouf et al., 2011) identified several families with a high incidence of aggressive SLE with anti-dsDNA reactivity in children. The phenotype segregated with homozygosity for the same frameshift mutation in the *DNASE1L3* gene. A subsequent study (Ozçakar et al., 2013) identified independent *DNASE1L3* mutations in two families with autosomal-recessive hypocomplementemic urticarial vasculitis syndrome (HUVS). HUVS is often associated with SLE, and indeed 3 out of 4 surviving *DNASE1L3*-deficient children developed severe SLE with anti-dsDNA Abs. Furthermore, previously described associations of *PXK* gene with sporadic SLE and a related systemic autoimmune disease scleroderma (Martin et al., 2013) have been reassigned to the adjacent *DNASE1L3* gene (Mayes et al., 2014; Zochling et al., 2014). The disease-associated *DNASE1L3* polymorphism (*rs35677470*) creates an amino acid substitution (R206C) that reduces DNase activity (Ueki et al., 2009). Collectively, these data establish DNASE1L3 as a genetic determinant of SLE susceptibility and an essential factor protecting humans from the disease.

DNASE1L3 is homologous to DNASE1, a secreted DNase that digests DNA in the gastrointestinal tract (Baron et al., 1998). DNASE1 and DNASE1L3 together are responsible for the DNase activity in serum (Napirei et al., 2009). However, unlike DNASE1 or its other homologs, DNASE1L3 contains a short, positively charged C-terminal peptide that allows it to digest DNA encapsulated into liposomes (Wilber et al., 2002). In addition, DNASE1L3 is more efficient than DNASE1 in the internucleosomal cleavage of genomic DNA in isolated cell nuclei (Napirei et al., 2005), suggesting that it might digest chromatin within apoptotic or necrotic cells (Mizuta et al., 2013). However, neither the natural form of DNA targeted by DNASE1L3 nor the mechanism whereby DNASE1L3 protects from SLE has been elucidated.

Here, we show that the loss of DNASE1L3 in mice caused a rapid Ab response to dsDNA and chromatin. We also found that DNASE1L3 is capable of digesting chromatin in apoptotic cell-derived MP, and its absence caused the accumulation of and Ab response to MP-associated DNA. These results suggest that chromatin in apoptotic MP represents an important antigenic form of DNA in SLE and identifies DNASE1L3 as a regulator of this antigenic chromatin's ability in the steady state.

RESULTS

Dnase1l3-Deficient Mice Rapidly Develop Anti-DNA Auto-Abs

We analyzed mice in which essential coding exons of the *Dnase1l3* gene have been replaced with a *LacZ* reporter cassette (Figure S1A). The *Dnase1l3*^{LacZ} allele was crossed onto two common inbred backgrounds, C57BL/6 (B6) and 129SvEv (129). Homozygous *Dnase1l3*$^{LacZ/LacZ}$ knockout (KO) mice were born at Mendelian ratios and were grossly normal and fertile. All KO mice on both B6 and 129 backgrounds developed anti-nuclear Abs (ANA) with perinuclear staining (Figure 1A), which is characteristic of severe human SLE. Anti-dsDNA IgG in the sera of KO mice were elevated at 5 weeks and progressively increased with age (Figure 1B). Both male and female KO mice developed anti-dsDNA with the same kinetics (data not shown). Anti-dsDNA primarily comprised IgG2a and IgG2b isotypes pathogenic in other SLE models (Ehlers et al., 2006) (Figure 1C). ELISPOT analysis showed that anti-dsDNA IgG Ab-secreting cells (ASC) were abundant in KO spleens and detectable as early as 4–6 weeks of age (Figures 1D and 1E). In contrast, neither total IgG nor anti-RNA IgG were elevated, even in old mice (Figures S1B and S1C). The analysis of KO sera by autoantigen microarray and ELISA revealed increased reactivity to several protein and ribonucleoprotein autoantigens at 40 weeks, but not earlier (Figures S1D–S1F).

To test Ab response to chromatin, we tested IgG reactive with native purified polynucleosomes. KO mice rapidly developed high titers of anti-chromatin IgG on both 129 and B6 backgrounds (Figure 1F; data not shown). No reactivity to purified histones was observed (data not shown). The analysis of a synchronized cohort of KO mice showed that anti-chromatin IgG developed even more rapidly than anti-dsDNA IgG at 5 weeks (Figures 1G and 1H). Thus, *Dnase1l3*-deficient mice manifest rapid and specific responses to dsDNA and chromatin, suggesting that the endogenous genomic DNA represents the primary autoantigen in this model.

Dnase1l3-Deficient Mice Develop Features of SLE

Peripheral blood of KO mice harbored a progressively increasing fraction of CD11c^{+} MHC class II^{-} CD11b^{+} Ly-6C^{-} monocytes (Figures 2A and 2B), which correspond to Gr1^{-} monocytes expanded in other SLE models (Santiago-Raber et al., 2009). By 50 weeks of age, KO mice manifested splenomegaly (Figures 2C and 2D) with reduced marginal zone B (MZB) cell population and increased fractions of monocytes and activated T cells (Figures S2A–S2C). The enlarged spleens showed spontaneous germinal center (GC) formation and an increased fraction of GC B cells (significant on the 129 background; Figures 2E and 2F). All 50-week-old KO mice on both backgrounds showed IgG deposition in the kidney glomeruli (Figure 2G). Finally, KO mice on the 129 background developed glomerulonephritis, including enlargement of glomeruli, mesangial and endocapillary proliferation, glomerular deposits, and interstitial inflammation of the kidney cortex (Figures 2H and 2I). KO mice on the B6 background showed glomerular enlargement, but no overt glomerulonephritis. Thus, anti-DNA response in *Dnase1l3*-deficient mice is followed by immune activation, IgG deposition, and a background-dependent glomerulonephritis.

Despite the early onset of the anti-DNA response, the observed immune activation was largely absent from KO mice up to 27 weeks of age (Figures 2D, 2E, and S2A–S2C). The development of experimental SLE can be accelerated by a surge in IFN production, e.g., after the adenoviral delivery of IFN (Mathian et al., 2005). We injected young KO or control mice with the

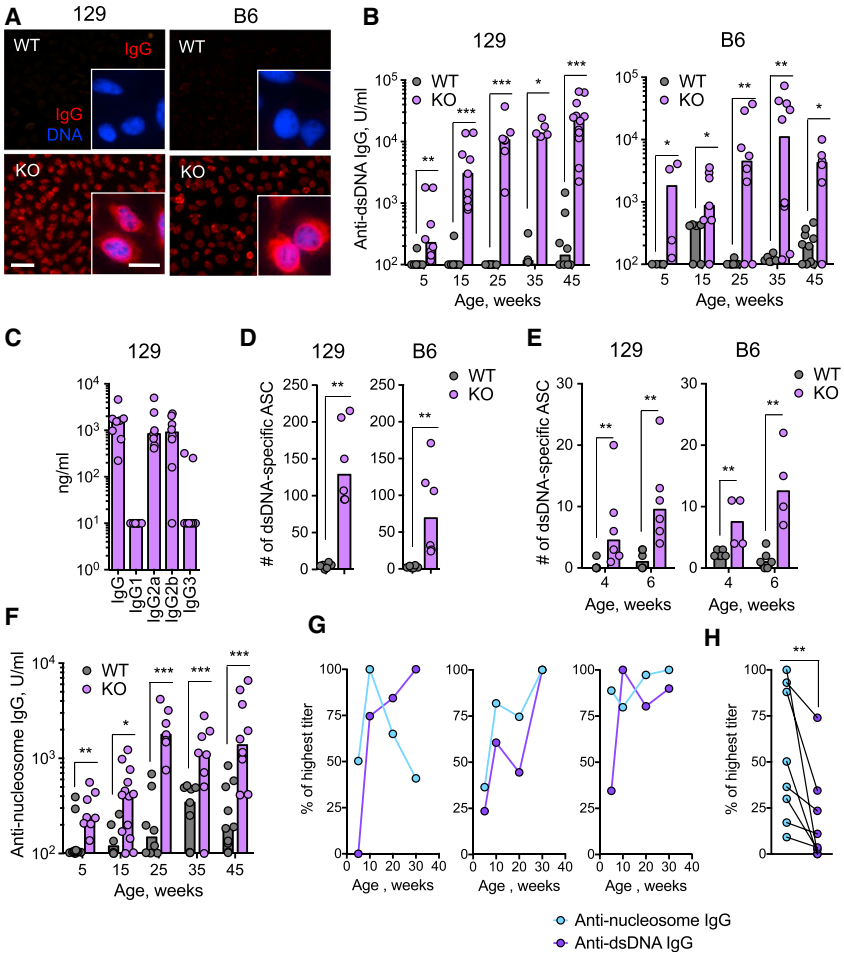

Figure 1. *Dnase1l3*-Deficient Mice Develop Abs to dsDNA and Chromatin

(A) ANA in the sera of *Dnase1l3* knockout (KO) and control wild-type (WT) mice. Fixed Hep2 cells incubated with sera from 50-week-old mice on 129 or B6 backgrounds, followed by staining for IgG (red) and DNA (blue), are shown. Representative of six animals per group (scale bars, 50 μm and in the inset 20 μm).

(B) Serum titers of anti-dsDNA IgG in WT or KO mice on the indicated backgrounds over time as determined by ELISA (individual animals and median).

(C) Serum titers of anti-dsDNA IgG subclasses in 40-week-old KO mice on the 129 background as measured by ELISA (individual animals and median).

(D and E) Anti-dsDNA IgG Ab-secreting cells (ASC) in WT and KO mice as determined by ELISPOT. ASC numbers per 5×10^5 splenocytes in 50-week-old (D) and 4- to 6-week-old (E) mice (individual animals and median) are shown.

(F) Serum titers of anti-nucleosome IgG in WT or KO mice on the 129 background as determined by ELISA (individual animals and median).

(G and H) Relative titers of anti-dsDNA and anti-nucleosome IgG in a synchronous cohort of KO mice analyzed over time. Titers are presented as a percent of the maximal value reached at any time point in each animal. The kinetics in three representative individual mice (G) and values in individual mice at 5 weeks (H) are shown. Significance is estimated by a paired Wilcoxon test.

Statistical significance: *$p \leq 0.05$; **$p \leq 0.01$; ***$p \leq 0.001$.

See also Figure S1.

adenoviral vector encoding IFN-α5, resulting in elevated serum IFN and elevated expression of IFN-inducible protein Sca-1 for at least 5 weeks post-injection (Figures S2D and S2E). IFN-treated KO mice showed rapid accrual of anti-dsDNA IgG (Figure S2F), as well as the appearance of anti-RNA IgG (Figure S2G). Furthermore, IFN-treated KO mice showed monocyte expansion and T cell activation as early as 1 week post-injection (Figures S2H and S2I), and two-thirds of these mice died after 35 weeks (Figure S2J). Therefore, immune activation in KO mice can be accelerated by IFN expression, recapitulating severe SLE in *DNASE1L3*-deficient human patients.

Circulating Dnase1l3 Protects from Autoreactivity

If DNASE1L3 acts similarly to DNASE2 or TREX1 as proposed (Ghodke-Puranik and Niewold, 2015; Picard et al., 2015), autoreactivity in KO mice should involve intracellular DNA accumulation and sensing through STING. However, the deletion of STING did not diminish ANA, anti-dsDNA IgG and ASC, IgG deposition (Figures 3A–3D), or splenomegaly (Figure S3A) in KO mice. The median anti-dsDNA titers were increased in DNASE1L3/STING double-deficient KO mice, although not significantly (Figure 3B). In contrast, all these manifestations were completely abolished by the deletion of MyD88, the transducer of TLR and IL-1 receptor signals (Figures 3A–3D and S3A). These data suggest that DNASE1L3 does not target DNA within cells, consistent with the secreted nature of this DNase.

We detected circulating DNASE1L3 in mouse serum using the digestion of liposome-coated plasmid DNA as a readout (Figure 3E). We then set up reciprocal bone marrow (BM) transfers between wild-type (WT) and KO mice and measured serum DNASE1L3 activity over time. The KO → WT and WT → KO chimeras showed progressive loss and gain of serum DNASE1L3, respectively (Figure S3B), suggesting that circulating DNASE1L3 is produced by hematopoietic cells. Importantly, the loss of circulating DNASE1L3 in KO → WT chimeras led to the development of anti-dsDNA ASC (Figure S3C). In a cohort of KO → WT chimeras in which DNASE1L3 activity disappeared by 40 weeks post-transfer (Figure 3F), anti-dsDNA IgG appeared at the same time point (Figure 3G), eventually leading to ANA, IgG deposition, glomerular enlargement, and mild glomerulonephritis (Figures S3D–S3G). Thus, autoreactivity in *Dnase1l3*-deficient mice inversely correlates with circulating DNASE1L3 produced by hematopoietic cells.

To directly test the effect of circulating DNASE1L3 on autoreactivity, we injected young KO mice with an adenoviral vector-encoding human DNASE1L3 (Ad-DNASE1L3). Adenoviral vectors in vivo transduce hepatocytes and maintain ectopic

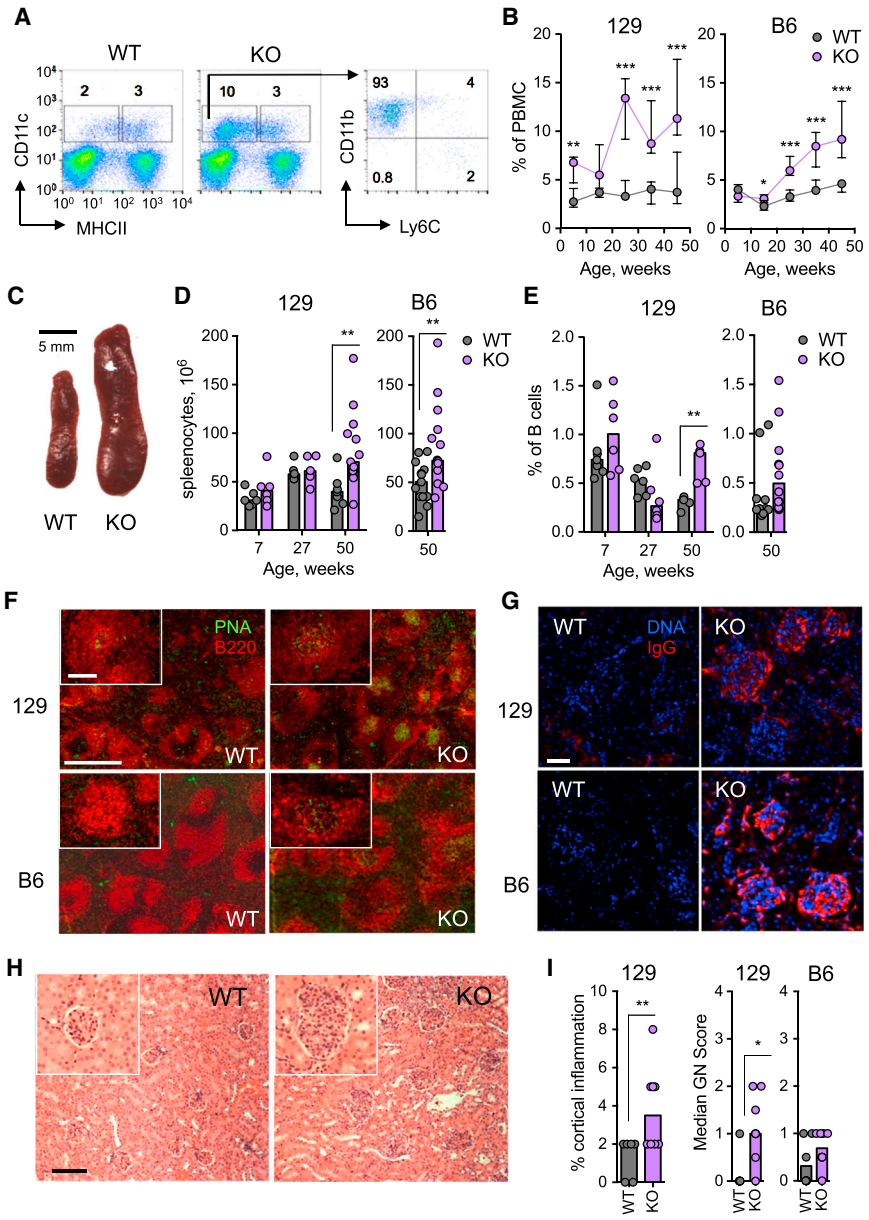

Figure 2. *Dnase1l3*-Deficient Mice Develop Late-Onset Immune Activation and Kidney Inflammation

(A and B) Monocyte population in the peripheral blood of *Dnase1l3* knockout (KO) and control wild-type (WT) mice. (A) Representative staining of peripheral blood mononuclear cells (PBMC) from WT and KO mice, with the fraction and phenotype of CD11c$^+$ MHC cl. II$^-$ monocytes indicated. (B) Fractions of CD11c$^+$ MHC cl. II$^-$ monocytes among PBMC at the indicated time points (median ± interquartile range of nine animals per group).

(C) Representative spleens from WT and KO mice on a 129 background at 50 weeks of age.

(D) Absolute number of splenocytes in WT or KO mice at the indicated time points (individual animals and median).

(E) The GC B cell population in the spleens of WT or KO mice at the indicated time points. The fractions of GC B cells (B220$^+$ PNA$^+$ CD95$^+$) among total B220$^+$ B cells (individual animals and median) are shown.

(F) The GC reaction in the spleens of WT or KO mice at 50 weeks of age. Splenic sections stained for total B cells (B220, red) and GC B cells (PNA, green; scale bar, 200 μm) with the individual GC in the inset (scale bar, 20 μm) are shown. Representative of six mice per genotype.

(G) IgG deposition in the kidneys of WT or KO mice at 50 weeks of age. Kidney sections stained for IgG (red) and DNA (blue) are shown. Representative of ten animals per group (scale bar, 50 μm).

(H) Kidney architecture in WT or KO mice on a 129 background at 50 weeks of age. Kidney sections stained with hematoxylin/eosin (scale bars, 50 μm) with a representative glomerulus in the inset are shown. Representative of eight animals per group.

(I) Histopathological score of glomerulonephritis in WT or KO mice at 50 weeks of age. The percentage of kidney cortex affected by inflammation and the median cumulative score of glomerulonephritis in mice on the indicated backgrounds are shown.

Statistical significance: *p ≤ 0.05; **p ≤ 0.01; ***p ≤ 0.001.

See also Figure S2.

protein production in them for several weeks. Accordingly, DNASE1L3 activity in the sera of Ad-DNASE1L3-treated KO mice was restored at 4 weeks, but largely disappeared at 12 weeks post-injection (Figure 3H). Importantly, the development of anti-dsDNA IgG titers was transiently but significantly delayed in KO animals treated with Ad-DNASE1L3 compared to the control Ad-GFP (Figure 3I). Collectively, these results show that circulating DNASE1L3 restricts anti-DNA autoreactivity, likely targeting an extracellular DNA substrate.

Circulating DNASE1L3 Is Produced by Mononuclear Phagocytes

We explored the hematopoietic cell type responsible for the production of circulating DNASE1L3. Microarray expression datasets suggested a restricted expression of *DNASE1L3* in dendritic cells (DC) in both humans and mice (Figures S4A and S4B), as confirmed by qRT-PCR (Figure S4C). In addition, the expression of *Dnase1l3* was apparent in macrophages (MΦ) in select tissues, including the spleen, liver, and intestine (Figure S4B). We used the fluorescent detection of LacZ in the targeted *Dnase1l3* allele to confirm the highest expression of *Dnase1l3* in conventional DC (cDC) and in a small fraction of splenic MΦ (Figure 4A). Consistent with microarray and qRT-PCR data (Figures S4B and S4C), low levels of expression were also detected in plasmacytoid DC (pDC), MZB, and B-1a cells (Figure 4A).

Lymphocyte-deficient *Rag1*$^{-/-}$ mice had normal levels of serum DNASE1L3, ruling out the contribution of B cells (Figure 4B). In contrast, a transient depletion of CD11c^{hi} cells (which

include all cDC and intestinal MΦ) reduced serum DNASE1L3 by >75% (Figure 4C). Treatment of WT mice with clodronate liposomes (which deplete tissue MΦ as well as reduce cDC numbers; Figure S4D) reduced serum DNASE1L3 by ~50% (Figure 4D). Finally, a single treatment with anti-Csf1r Ab (which primarily depletes intestinal MΦ) reduced serum DNASE1L3 by ~15% (Figure 4E). Because tissue MΦ are replaced slowly after BM transfer (Lavin et al., 2015), the production of DNASE1L3 by MΦ may explain the relatively slow decline of DNASE1L3 levels in KO → WT chimeras (Figure 3F). We conclude that circulating DNASE1L3 is predominantly produced by mononuclear phagocytes, including cDC and certain tissue MΦ.

DNASE1L3 Digests Chromatin in Apoptotic Cell-Derived Microparticles

To identify the putative extracellular DNA substrate of DNASE1L3, we examined the ability of recombinant human DNASE1L3 to digest different forms of DNA. As reported previously (Wilber et al., 2002) and confirmed by the analysis of KO mice (Figure 3E), DNASE1L3, but not DNASE1, could digest liposome-coated plasmid DNA (Figures 5A and 5B). In addition, DNASE1L3 was more efficient than DNASE1 in digesting genomic DNA within native polynucleosomes (Figure 5C). The polymorphic R206C variant of DNASE1L3 showed a reduced enzymatic activity on all DNA substrates (Figures 5B and 5C). In contrast, both specific activities of DNASE1L3, but not the digestion of "naked" DNA, were abolished by the deletion of its C-terminal peptide (Figures 5B and 5C). Molecular modeling of DNASE1L3 by homology to DNASE1 suggested that the C-terminal peptide comprises a stable α-helix protruding at a fixed angle from the conserved DNase domain (Figures S5A–S5E). Its stable helical conformation and the positive charge likely facilitate both the membrane binding/penetration and the displacement of DNA from bound histones.

Microparticles (MP) released from apoptotic cells are akin to liposomes and contain nucleosomal DNA (Pisetsky et al., 2011). Indeed, DNASE1L3, but not DNASE1, digested genomic DNA in MP generated from apoptotic Jurkat T cells (Figure 5D) and primary splenocytes (data not shown). MP showed low propidium iodide staining unless permeabilized (data not shown), suggesting that DNASE1L3 can penetrate intact MP membranes. Similar to the digestion of liposome-coated and polynucleosomal DNA, the digestion of MP DNA was slightly reduced by the R206C polymorphism, but completely abolished by the C-terminal deletion. As previously reported (Ullal et al., 2011), a fraction of MP can be stained with anti-DNA/histone 2a/2b monoclonal Ab (mAb) PR1-3 (Figure 5E). The staining was enhanced by fixation/permeabilization (data not shown), confirming that MP contain chromatin both internally and at the surface. The PR1-3 staining was abolished by pre-treatment with DNASE1L3, but not by the C-terminal deletion mutant of DNASE1L3 or by DNASE1 (Figure 5E).

We examined DNASE1L3 variants with a hexahistidine (His) tag near the C-terminal peptide (Figure 5A). The tag at the C terminus (His-CT) abolished the digestion of both liposome-coated and nucleosomal DNA, whereas the tag preceding the C-terminal peptide (His-preCT) abolished only the digestion of nucleosomal DNA (Figure 5F). The His-preCT tag is predicted to change the conformation of the C-terminal α-helical peptide relative to the DNase domain (Figure S5E). Importantly, this tag prevented the digestion of DNA within MP (Figure 5F) and on their surface (Figure 5G), suggesting that the ability to digest nucleosomal DNA is essential for this activity.

Consistent with in vitro results, serum from KO animals was unable to digest liposome-coated DNA even after prolonged incubation (Figure 5H). It was also unable to digest polynucleosomes during a short (15-min) incubation (Figure 5I), although longer incubation resulted in complete digestion (Figure S5F). Importantly, the serum from KO animals was completely unable to digest MP DNA (Figure 5J). Thus, DNASE1L3 has two unique and separable activities, i.e., the digestion of liposome-coated DNA and of nucleosomal DNA. These activities enable DNASE1L3 to digest chromatin within and on the surface of apoptotic MP, suggesting this DNA forms as a natural substrate of DNASE1L3.

DNASE1L3 Restricts the Amount of DNA in Circulating Microparticles

We tested the relationship between DNASE1L3 and the DNA content of MP in vivo. Following intravenous (i.v.) injection of Jurkat cell MP, their DNA was rapidly cleared from WT mice, but persisted in the serum, spleen, and liver of KO mice (Figure S6A). We then analyzed endogenous MP from murine plasma, characterized by their small size, the absence of platelet and erythrocyte markers, and positivity for apoptotic cell marker Annexin V (Figure S6B). Although the number of MP in the plasma of KO mice was unchanged (Figure S6C), their genomic DNA content was increased >100-fold (Figure 6A). Accordingly, the amount of DNA in total plasma from KO mice was increased >10-fold (Figure 6B). Furthermore, a fraction of plasma MP from young KO animals exposed chromatin on their surface, as revealed by positive staining with PR1-3 (Figure 6C).

To test whether DNASE1L3 similarly digests circulating MP DNA in humans, we analyzed two DNASE1L3 null patients with HUVS (Özçakar et al., 2013). Neither patient 1 (HUVS+SLE in remission) nor patient 2 (HUVS only) had active SLE, ruling out any secondary effects of the disease. Using the digestion of liposome-coated plasmid DNA, we confirmed that the patients had no DNASE1L3 activity in plasma, whereas their haplodeficient parents showed ~50% activity (Figure 6D). We also analyzed three additional subjects who were heterozygous for the R206C variant of DNASE1L3. These subjects manifested ~60% of control DNASE1L3 activity in plasma (Figure 6D), suggesting that the R206C variant is ~5-fold less active than the common variant.

Plasma of DNASE1L3 null patients failed to digest nucleosomal DNA (Figure 6E), as well as MP DNA (Figure 6F), and even the plasma of haplodeficient parents showed detectable impairments in these assays. We then isolated endogenous plasma MP from the human plasma and confirmed that Annexin V^+ MP express markers of leukocytes and include a granulocyte marker-positive fraction (Figure S6D) (Nielsen et al., 2011). MP from DNASE1L3 null patients contained >1,000-fold more DNA than those from healthy controls, and MP from haplodeficient parents or R206C carriers also showed an increased DNA

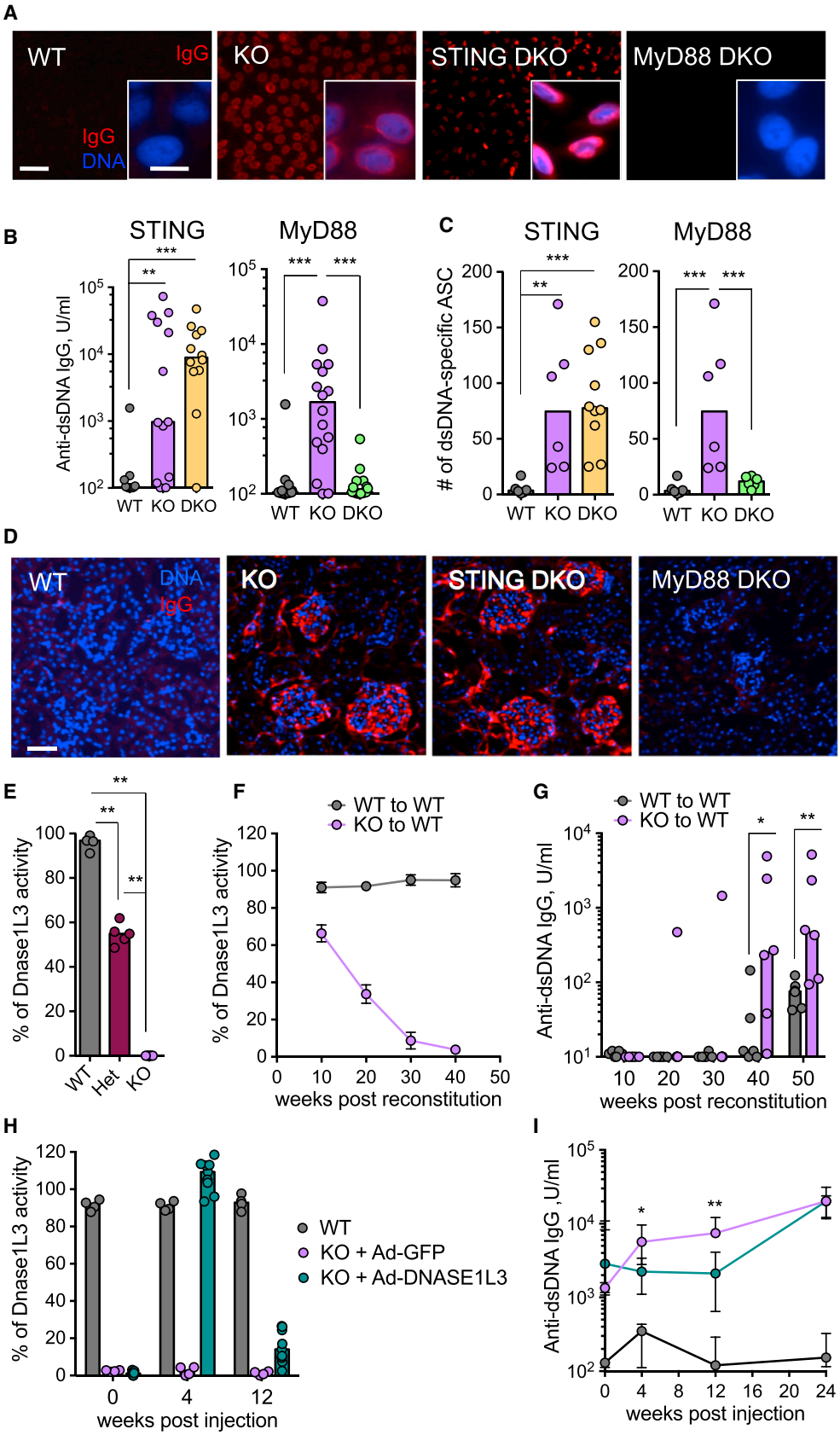

(legend on next page)

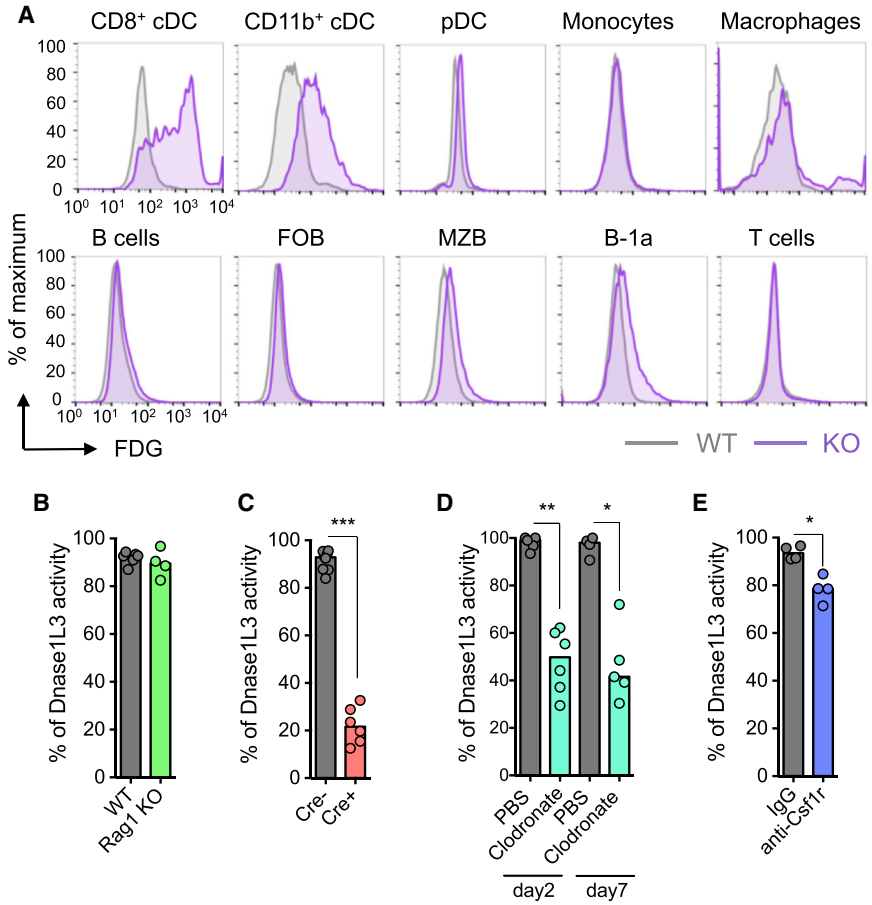

Figure 4. Circulating DNASE1L3 Is Produced Primarily by Dendritic Cells and Macrophages

(A) Single-cell analysis of Dnase1L3 expression in immune cells. Splenocytes from *Dnase1l3*$^{LacZ/LacZ}$ KO or WT control mice were stained for LacZ activity using the fluorescent substrate fluorescein di(β-D-galactopyranoside) (FDG). Histograms of FDG staining in the indicated gated cell populations (representative of three independent experiments) are shown. Similar results were obtained with heterozygous *Dnase1l3*$^{LacZ/+}$ mice (data not shown).

(B) Dnase1L3 activity in the sera of Rag1-deficient animals (individual animals and median).

(C) Dnase1L3 activity in the sera of DC-depleted animals. Animals with Cre-inducible diphtheria toxin receptor (DTR) with or without the DC-specific Cre deleter (CD11c-Cre) were administered diphtheria toxin (DTX) for 2 weeks, and their sera was analyzed for DNASE1L3 activity (individual animals and median).

(D) Dnase1L3 activity in the sera of wild-type animals treated with PBS- or clodronate-containing liposomes to deplete macrophages on the indicated days after treatment (individual animals and median).

(E) Dnase1L3 activity in the sera of wild-type animals 12 days after injection of control IgG or anti-Csf1r blocking Ab (individual animals and median).

Statistical significance: *p ≤ 0.05; **p ≤ 0.01; ***p ≤ 0.001.

See also Figure S4.

content (Figure 6G). The analysis of human plasma samples showed that nearly all detectable genomic DNA is contained within the MP fraction (Figure S6E). Accordingly, total unfractionated plasma of DNASE1L3 null patients also harbored increased amounts of circulating DNA (Figure 6H). Collectively, genetic evidence in animals and humans demonstrates that DNASE1L3 digests genomic DNA circulating in plasma, specifically within apoptotic cell-derived MP.

DNASE1L3 Prevents the Recognition of Microparticle DNA by Auto-Abs

We tested whether the DNASE1L3-sensitive chromatin on the surface of microparticles is targeted by auto-Abs in experimental SLE. The serum of KO mice from a young age contained IgG binding to Jurkat MP (Figures 7A and 7B). The binding was abolished by pre-treatment of MP with DNASE1L3 (Figure 7C), confirming that it is directed toward DNASE1L3-sensitive chromatin

Figure 3. Autoreactivity in *Dnase1l3*-Deficient Mice Does Not Require STING and Is Restricted by Circulating DNASE1L3

(A–D) *Dnase1l3* knockout (KO) mice were crossed with STING-deficient or MyD88-deficient mice to generate double-KO (dKO) mice and analyzed along with the respective wild-type (WT) controls. (A) Serum ANA at 45 weeks of age. Results are shown as in Figure 1A; representative of six animals per group. (B) Serum titers of anti-dsDNA IgG at 35 weeks of age as determined by ELISA (individual animals and median). The difference between KO and STING dKO mice in the left panel is not statistically significant. (C) Anti-dsDNA IgG Ab-secreting cells (ASC) at 50 weeks of age as determined by ELISPOT. The numbers of ASC per 5 × 10^5 splenocytes (individual animals and median) are shown. (D) IgG deposition in the kidneys at 50 weeks of age. Results are shown as in Figure 2G; representative of five animals per group (scale bar, 50 μm).

(E) The relative activity of circulating DNASE1L3 in WT, KO, or heterozygous (Het) animals, as measured by the ability of serum to digest liposome-bound plasmid DNA (individual animals and median).

(F and G) WT recipients were lethally irradiated and reconstituted with WT or KO BM (KO-to-WT and control WT-to-WT chimeras, respectively). (F) Serum DNASE1L3 activity in chimeras at the indicated time points after reconstitution (mean ± SD of six animals per group). (G) Serum anti-dsDNA IgG titers at the indicated time points as measured by ELISA (individual animals and median).

(H and I) Autoreactivity in KO mice reconstituted with circulating DNASE1L3. Young 4-week-old KO mice were injected with adenoviruses encoding DNASE1L3 (Ad-DNASE1L3) or GFP (Ad-GFP). (H) Serum Dnase1L3 activity in KO mice administered Ad-DNASE1L3 or Ad-GFP at the indicated time points, along with age-matched wild-type controls (individual animals and median). (I) Serum anti-dsDNA IgG titers in the same mice as measured by ELISA. Data represent median ± a range of four (KO + Ad-GP) and nine (WT or KO + Ad-DNASE1L3) animals per group.

Statistical significance: *p ≤ 0.05; **p ≤ 0.01; ***p ≤ 0.001.

See also Figure S3.

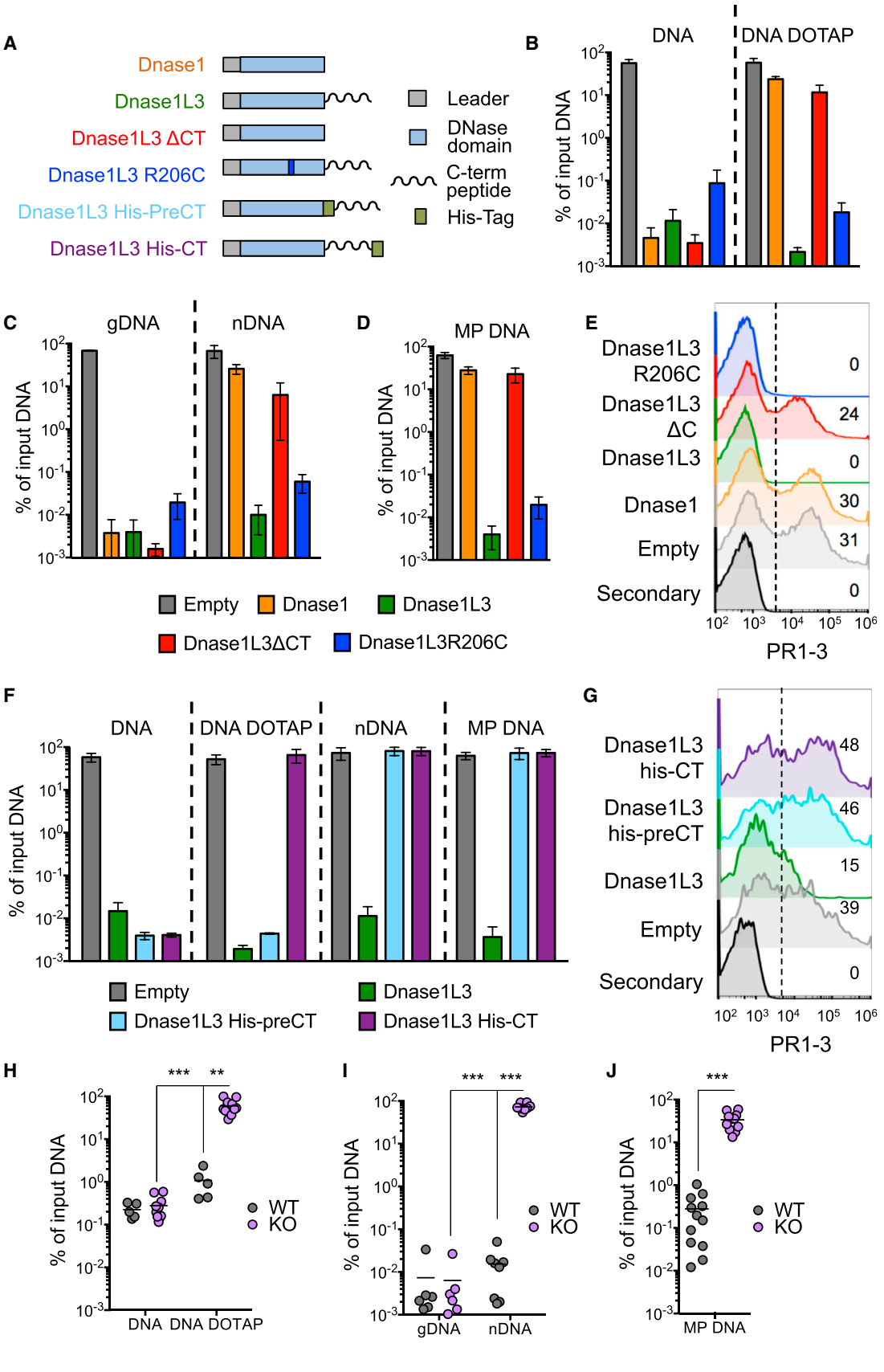

(legend on next page)

on their surface. Similar DNASE1L3-sensitive binding was also displayed by several anti-DNA/anti-nucleosome mAbs from mouse SLE models (Figure S7A), including the prototypic mAb 3H9 (Shlomchik et al., 1987). To directly test whether MP can elicit anti-DNA responses, we injected wild-type animals with MP generated from syngeneic apoptotic splenocytes. MP injections in animals treated with the IFN adenovirus, but not in naive animals, induced high titers of anti-nucleosome IgG (Figure 7D). Thus, in the context of elevated IFN, MP can represent antigens that elicit chromatin-specific B cell responses.

We asked whether DNASE1L3-sensitive chromatin in MP is recognized by auto-Abs in human SLE. The *DNASE1L3*-deficient patient 1 (HUVS+SLE in remission), but not patient 2 (HUVS without SLE), or their healthy parents harbored serum IgG binding to MP in a DNASE1L3-sensitive manner (Figure 7E). Human IgG carrying the 9G4 idiotope are prominent among SLE-associated auto-Abs and bind multiple antigens, including DNA, cell nuclei, and apoptotic cell membranes (Jenks et al., 2013; Richardson et al., 2013). Two $9G4^{+}$ mAb clones from SLE patients (75G15 and 74C2) that show strong binding to apoptotic cell membranes (Richardson et al., 2013) showed DNASE1L3-sensitive binding to MP (Figure S7B). Finally, we tested whether DNASE1L3-sensitive chromatin on MP represents an antigen in patients with sporadic SLE. None of healthy control subjects (n = 10) and 64% of SLE patients (n = 53) harbored IgG binding to MP (Figures 7F, 7G, and S7C). The binding to MP showed a weak but significant correlation with anti-dsDNA titers (data not shown), as observed for IgG binding to endogenous MP in SLE (Ullal et al., 2011). Importantly, the binding was sensitive to DNASE1L3 pre-treatment in ~36% of patients (Figures 7F, 7G, and S7C suggesting that it is directed against chromatin components on the surface of MP. Collectively, our data in mice and humans suggest that chromatin on circulating apoptotic MP is an antigen for DNA-reactive B cells and Abs produced by them. This chromatin is a physiological substrate for circulating DNASE1L3, which limits its availability and may thereby protect from anti-DNA reactivity and SLE.

DISCUSSION

SLE in *DNASE1L3*-deficient human patients is characterized by early onset, absence of a sex bias, and the presence of anti-dsDNA IgG (Al-Mayouf et al., 2011; Ozçakar et al., 2013). These features were recapitulated in *Dnase1l3*-deficient mice, all of which develop anti-dsDNA reactivity on two distinct genetic backgrounds. Hereditary SLE has been difficult to model in mice: for instance, null mutations in the complement component *C1Q* cause SLE in human patients (Ghodke-Puranik and Niewold, 2015; Picard et al., 2015), but no overt pathology in inbred mice (Heidari et al., 2006). Thus, our results establish a mouse model of familial SLE and confirm DNASE1L3 as an evolutionarily conserved mediator of tolerance to DNA.

Dnase1l3-deficient mice rapidly developed IgG to dsDNA and particularly to chromatin, whereas the reactivity to other self-antigens was either absent or developed later. Similarly, major signs of immune activation (splenomegaly, GC reaction, and T cell activation) appeared only in old animals. This delay likely reflects the lack of additional disease-promoting mutations common in SLE models, such as those causing lymphoproliferation (e.g., Fas^{lpr}) or heightened RNA sensing (e.g., *Yaa*). Another important aspect is the paucity of immune stimulation in specific pathogen-free mice as opposed to human patients. Indeed, the treatment with IFN induced anti-RNA response, accelerated immune activation, and caused significant mortality. These data suggest that the reactivity to nucleosomal DNA within chromatin causes all subsequent pathological features and can yield a severe SLE-like disease following an inflammatory stimulus.

Ablation of STING-dependent cytoplasmic DNA sensing abolishes inflammatory disease caused by DNASE2 or TREX1 deficiency (Ahn et al., 2012; Gall et al., 2012), but exacerbates autoimmunity in polygenic or chemically induced models (Sharma et al., 2015). In contrast, the deletion of STING had a minimal effect on anti-DNA responses or the ensuing disease in *Dnase1l3*-deficient mice. The observed essential role of MyD88 may reflect its activity downstream of TLRs or IL-1 receptor; the specific signal(s) involved remain to be identified but are likely to be cell extrinsic. Notably, no signs of activation or developmental abnormalities could be detected in DCs or B cells from young *Dnase1l3* null mice. Therefore, the primary anti-DNA Ab response may result from direct antigen receptor-mediated expansion and plasmablast differentiation of DNA-reactive B cells, likely via extrafollicular activation and class switching. These antigen-specific primary signals may be further amplified

Figure 5. DNASE1L3 Can Digest Intact Chromatin and Genomic DNA in Apoptotic Microparticles

(A) Schematic of the different DNase constructs used.

(B–D) Digestion of different DNA substrates by recombinant DNases. DNA substrates were incubated with a control supernatant (empty, gray) or supernatants containing DNASE1, DNASE1L3, DNASE1L3's C-terminal truncation (DNASE1L3 ΔCT), or DNASE1L3's R206C substitution variant. The amount of remaining DNA was measured by qPCR and expressed as a percent of input DNA (mean ± SD of three independent experiments). (B) The digestion of plasmid DNA alone (DNA) or in complex with liposomal reagent (DNA DOTAP). (C) The digestion of purified human genomic DNA (gDNA) or purified human nucleosomes (nDNA). (D) The digestion of DNA within microparticles (MP) from apoptotic human cells (MP DNA).

(E) The digestion of chromatin on the surface of MP by recombinant DNases. MP from apoptotic human cells were incubated with recombinant DNases and stained with anti-nucleosome mAb PR1-3. Histograms of PR1-3 fluorescence and the percent of positive MP are shown; representative of three experiments.

(F) Digestion of DNA substrates by DNASE1L3 mutants with a hexahistidine tag at the C terminus (His-CT) or preceding it (His-preCT). DNA substrates and data presentation are as in (B)–(D).

(G) The digestion of chromatin on the surface of MP by hexahistidine-containing DNASE1L3 mutants. Data are presented as in (E).

(H–J) Digestion of different DNA substrates by sera from *Dnase1l3*-deficient knockout (KO) or control wild-type (WT) animals. The digestion of plasmid DNA with or without DOTAP (H), human purified or nucleosomal genomic DNA (I), or DNA within MP from apoptotic human cells (J) was measured as in (B)–(D). The results from sera of individual animals (circles) and median (lines) are shown.

Statistical significance: $^{**}p \leq 0.01$; $^{***}p \leq 0.001$.

See also Figure S5.

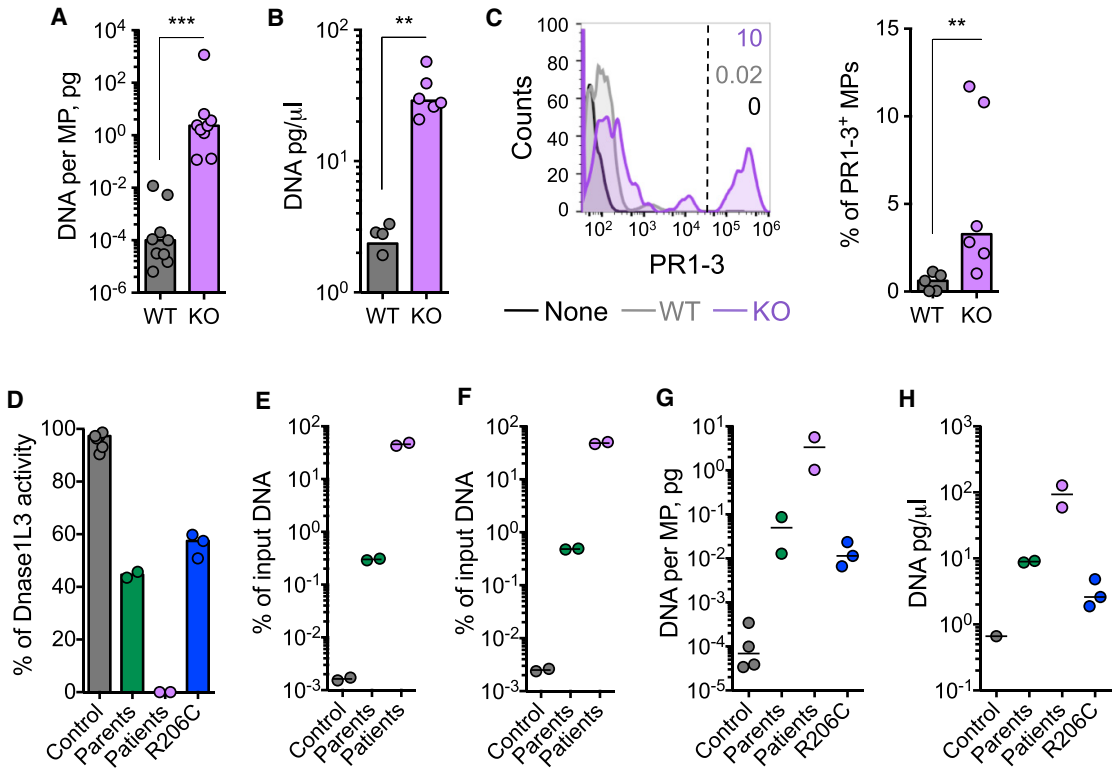

Figure 6. DNASE1L3 Deficiency in Mice and Human Patients Causes the Accumulation of DNA in Circulating Microparticles

(A) The genomic DNA cargo of circulating microparticles (MP) from *Dnase1l3* knockout (KO) or control wild-type (WT) animals. MP were isolated from the plasma of 10-week-old mice and analyzed by qPCR for mouse genomic DNA. Results show the amount of DNA per MP in individual mice (circles) and group median (bar).

(B) The amount of genomic DNA per volume of unfractionated plasma from WT and KO animals (individual animals and median).

(C) The binding of anti-nucleosome mAb PR1-3 to circulating MP isolated from the plasma of young KO or WT mice. Representative histograms of PR1-3 fluorescence and the frequency of positive MP (individual animals and median) are shown.

(D–H) Plasma from human *DNASE1L3*-deficient patients (n = 2), their haplodeficient parents (n = 2), individuals with the DNASE1L3 R206C polymorphism (n = 3), and normal control subjects (n = 2–5) were analyzed. Data represent individual human subjects and the median (bar or line). (D) DNASE1L3 activity in the soluble fraction of patients' plasma, measured using the digestion of DOTAP-coated plasmid DNA and expressed as a percent of the activity in a reference control plasma. (E) The digestion of human nucleosomes by the soluble fraction of patients' plasma. (F) The digestion of DNA in MP from apoptotic human cells by the soluble fraction of patients' plasma. (G) The amount of genomic DNA in circulating MP isolated from the plasma. Results show the amount of DNA per MP as determined by qPCR for human genomic DNA. (H) The amount of genomic DNA per volume of unfractionated plasma as determined by qPCR.

Statistical significance: $^{**}p \leq 0.01$; $^{***}p \leq 0.001$.

See also Figure S6.

by MyD88-dependent signals in B cells and/or other cell types. Collectively, the mechanism of anti-DNA reactivity in *Dnase1l3*-deficient mice likely reflects the primary loss of antigen-specific B cell tolerance to DNA.

The development of anti-dsDNA Abs inversely correlated with the levels of circulating DNASE1L3, suggesting that DNASE1L3 acts in a cell-extrinsic manner to shield autoreactive B cells from antigenic self-DNA. Notably, we found that *Dnase1l3* is expressed in DCs and select tissue macrophages, which produce the bulk of secreted DNASE1L3. These observations support the role of DCs and macrophages in self-tolerance and restriction of autoimmunity (Ganguly et al., 2013; Lavin et al., 2015). This tolerogenic function has been primarily associated with engulfment of apoptotic cells, induction of T cell tolerance, and expression of anti-inflammatory cytokines and surface molecules by the phagocytes. Our work describes a different mechanism of tolerogenic activity by these cells, whereby their secretion of a DNA-processing enzyme enforces global B cell tolerance to DNA.

Our data show that DNASE1L3 (1) is available systemically and acts in a cell-extrinsic manner, (2) has a unique capacity to digest membrane-encapsulated DNA, and (3) has a preferential capacity to digest DNA within nucleosomes. These properties point to the chromatin within circulating MP as the physiological substrate of DNASE1L3. DNA-containing MP are normally present in the human plasma (Dieker et al., 2016; Nielsen et al., 2011, 2012) and are derived from cells that die within the vessel lumen, such as rapidly turning over myeloid cells. Notably, the majority of genomic DNA detectable in human plasma was contained within the MP fraction. Indeed, total human plasma DNA was shown to be primarily derived from leukocytes and to comprise nucleosomal fragments of chromatin (Holdenrieder et al., 2005; Snyder et al., 2016; Sun et al., 2015). Accordingly, DNASE1L3 deficiency increased both the DNA cargo of circulating MP and

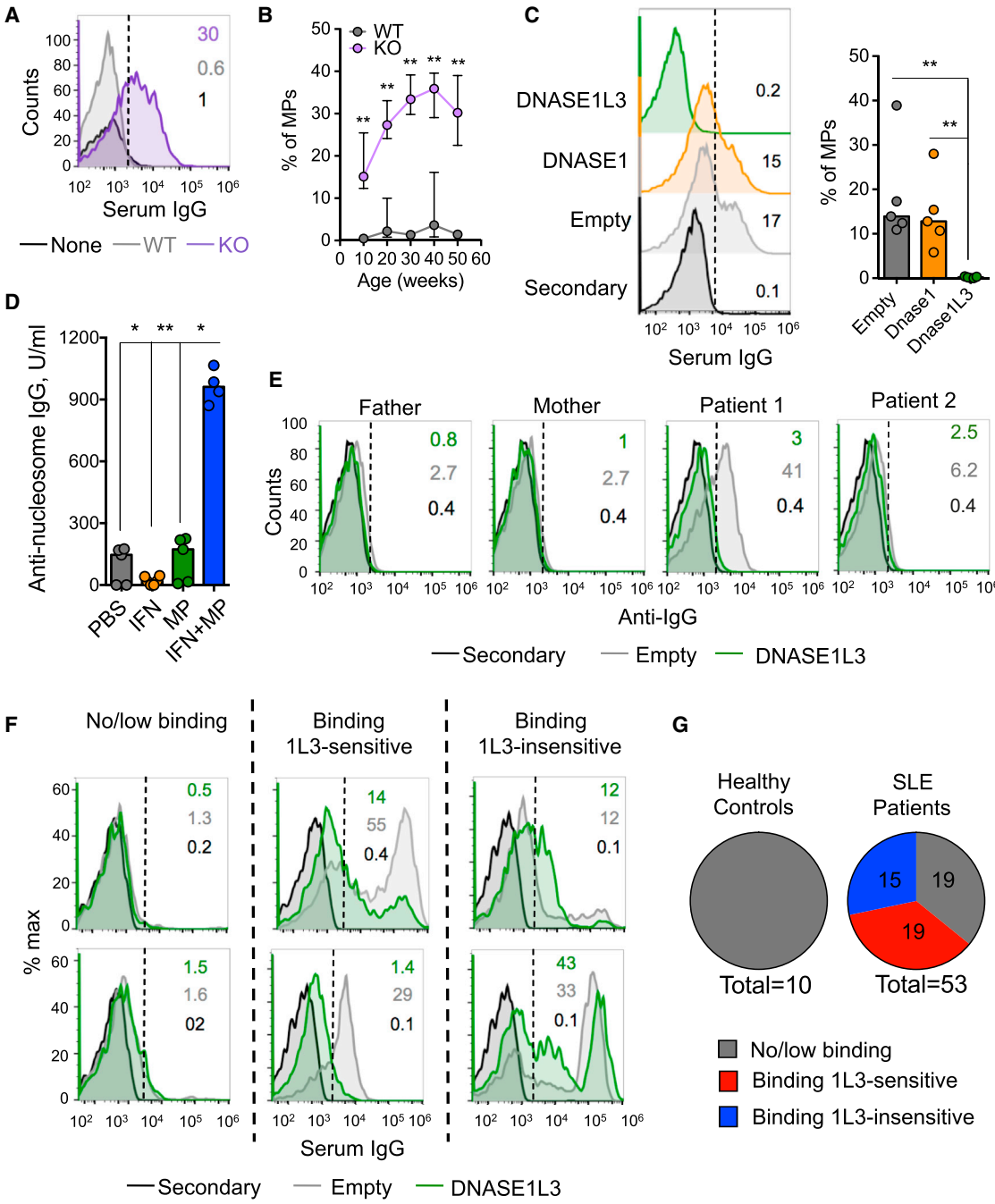

Figure 7. DNASE1L3-Sensitive Chromatin on Apoptotic Microparticles Is Antigenic in Mice and Human Patients

(A–C) Binding of mouse serum IgG to the surface of microparticles (MP). Human apoptotic MP were incubated with sera from *Dnase1l3* knockout (KO) or control wild-type (WT) animals, followed by secondary anti-mouse IgG Ab. (A) Representative histograms of IgG fluorescence and the percent of positive MP. (B) Fractions of IgG-positive MP stained with sera from WT or KO mice of the indicated ages (median ± range of five animals per group). (C) MP were incubated with supernatants containing human DNASE1, DNASE1L3, or an empty control prior to staining with KO serum. Representative histograms of IgG fluorescence and the frequency of positive MP stained by sera from individual KO mice (bars represent the median) are shown.Statistical significance: *$p \leq 0.05$; **$p \leq 0.01$; ***$p \leq 0.001$.

(D) Anti-nucleosome response in the animals immunized with MP. Wild-type mice were administered IFN-α adenovirus (IFN), MP from syngeneic apoptotic splenocytes (MP), or both, and serum IgG to nucleosomes were measured by ELISA 1 week after the last MP immunization. Titers from individual animals (circles) and median titers (bars) are shown.

(E–G) DNASE1L3-sensitive binding of IgG from human patients to the surface of MP. Human apoptotic MP were treated with DNASE1L3-containing supernatant (DNASE1L3) or a control supernatant (empty), incubated with plasma from human subjects, followed by secondary anti-human IgG Ab. Representative

(legend continued on next page)

the total amount of DNA in the plasma of *DNASE1L3*-deficient animals and human subjects. Although other potential DNA substrates of DNASE1L3 cannot be ruled out, these data implicate MP-associated DNA as the relevant endogenous target of DNASE1L3.

Chromatin in apoptotic blebs and circulating MP becomes exposed at the membrane surface and accessible to auto-Abs (Casciola-Rosen et al., 1994; Radic et al., 2004; Ullal et al., 2011). This chromatin would be accessible to DNA-reactive B cells, comprising a potentially antigenic form of DNA. We found that exposed chromatin on MP is digested by DNASE1L3 and becomes a target of auto-Abs in *Dnase1l3*-deficient animals and in the *DNASE1L3*-deficient human patient with SLE history. Importantly, DNASE1L3-sensitive chromatin on the surface of MP appears to be targeted by prototypic autoreactive clones from murine and human SLE, as well as by serum IgG from at least one-third of patients with sporadic SLE. The latter is consistent with the binding of IgG and complement to plasma MP in human SLE patients (Nielsen et al., 2012; Ullal et al., 2011). Therefore, MP-associated chromatin appears to represent a common antigenic form of self-DNA in SLE.

In conclusion, we identify chromatin in microparticles as a latent self-antigen for autoreactive B cells, and circulating DNASE1L3 as an essential factor that restricts chromatin antigenicity and prevents anti-DNA responses. These results provide a mechanistic explanation for the association of null and hypomorphic DNASE1L3 mutations with familial and sporadic SLE, respectively. They also uncover a cell-extrinsic mechanism of tolerance to DNA that involves a secreted enzyme and therefore can be developed for therapeutic purposes. In particular, the observed delay of anti-DNA reactivity by DNASE1L3 re-expression warrants the exploration of DNASE1L3 protein delivery as a therapeutic tool in SLE and other systemic autoimmune diseases.

EXPERIMENTAL PROCEDURES

Animals

All experiments were performed according to the investigator's protocol approved by the Institutional Animal Care and Use Committees of Columbia University and New York University. Mice with a targeted germline replacement of *Dnase1l3* (*Dnase1l3*^{LacZ}) were purchased from Taconic Knockout Repository (model TF2732), backcrossed onto 129SvEvTac or C57BL/6 backgrounds for >10 generations, and intercrossed to obtain *Dnase1l3*$^{LacZ/LacZ}$ knockout animals. Age-matched wild-type mice of the respective backgrounds were bred in the same animal colony and used as controls. Genetic deletion of STING and MyD88, hematopoietic reconstitution, and cell-depletion experiments are described in the Supplemental Experimental Procedures.

Human Subjects

DNASE1L3-deficient HUVS patients 1 and 2 correspond to patients IV-4 and IV-5 from family 1 described in (Ozçakar et al., 2013). Their study was approved by the Ethics Committees of Ankara University (Turkey) and the IRB at the University of Miami, and informed consents were obtained from the parents. Blood from patients with sporadic SLE and healthy controls was obtained from the NYU IRB-approved Rheumatology SAMPLE (Specimen and Matched Phenotype Linked Evaluation) Biorepository. All patients signed an IRB-approved informed consent. Additional information is provided in the Supplemental Experimental Procedures.

Adenoviruses

Adenoviral vector encoding IFN-α5 has been previously described (Mathian et al., 2005). Adenoviral vector-encoding human DNASE1L3 was constructed by Welgen. Adenoviral particles were produced and purified at Welgen and were injected into the indicated mice i.v. at 0.5 to 1 × 10^{10} particles per mouse.

Analysis of Autoreactivity

Flow cytometry, immunochemistry, ANA, ELISA, ELISPOT, antigen arrays, and the analysis of kidney IgG deposition and histopathology are described in the Supplemental Experimental Procedures.

Recombinant DNases

Cloned open reading frame (ORF) of human DNASE1 and DNASE1L3 (NCBI: NP_004935.1) were subcloned into pMCSV-IRES-GFP (pMIG) retroviral expression vector. The constructs for DNASE1L3 variants were generated using the Q5 site-directed mutagenesis kit (NEB) and included the R206 → C substitution, the C-terminal truncation (amino acids [aa] 282–305), and the insertions of hexahistidine between aa 282–283 (His-preCT) or between aa 305 and the stop codon (His-CT). The resultant constructs or the empty pMIG were used as plasmids for the transient transfection of HEK293 cells, with equal efficiency of transfection confirmed by GFP expression. To avoid contamination with DNases in bovine serum, transfection was performed in medium with 15% KnockOUT serum supplement (Thermo Fisher). Transfected cells were cultured for 48 hr, and the supernatants were collected, filtered, supplemented with 4 mM $CaCl_2$ and 4 mM $MgCl_2$, and frozen in aliquots.

Analysis of DNASE1L3 Activity

To measure the digestion of liposome-coated DNA, pMIG plasmid DNA was pre-incubated with DOTAP (Roche) in HBSS. Native or DOTAP-coated plasmid (1 ng/reaction) was incubated with an equal volume of DNase-containing supernatants or sera for 60 min at 37°C in a total volume of 2 μl. The amount of remaining DNA was measured by qPCR with GFP-specific primers and expressed as a percent of input DNA using a calibration curve with serial plasmid dilutions. For the measurement of relative DNASE1L3 activity in vivo, the digestion was performed for 10 min using 1 μl of mouse serum or human serum or plasma in a final volume of 5 μl. After qPCR, the amount of remaining DNA was converted to a percent of DNASE1L3 activity using a calibration curve with serial dilutions of control wild-type serum or plasma.

Purified human polynucleosomes from HeLa cells (Epicypher) or purified Jurkat cell DNA (2 ng/reaction) were incubated with an equal volume of DNase-containing supernatants for 15 min at 37°C in a total volume of 2 μl. The amount of remaining DNA was measured by qPCR with primers specific for human genomic *Alu* repeats and expressed as a percent of input DNA using a calibration curve with serial DNA dilutions.

Generation and Analysis of Microparticles

MP from Jurkat cells were generated as previously described (Ullal et al., 2011). Briefly, the cells were cultured in the presence of 1 mM staurosporine (Sigma-Aldrich) overnight, harvested, and collected by centrifugation for

histograms of IgG fluorescence and the percent of positive MP are shown. (E) DNASE1L3-sensitive binding of IgG from *DNASE1L3*-deficient patients or their haplodeficient parents. Representative histograms of IgG fluorescence and the percent of positive MP are shown. (F) DNASE1L3-sensitive binding of IgG from patients with sporadic SLE. Two representative histograms of IgG fluorescence for each reactivity pattern are shown. (G) The fraction of SLE patients with the reactivity patterns are shown in (F).
See also Figure S7.

5 min at 1,500 rpm. The supernatants were collected and centrifuged at 22,000 × *g* for 30 min to pellet the MP, which were analyzed on the Accuri C6 flow cytometer (BD Biosciences) to determine absolute numbers and ensure >95% enrichment. Where indicated, MP (10^5/μl in PBS) were incubated with an equal volume of DNase-containing transfection supernatants for 1 hr at 37°C. The generation and administration of MP from mouse splenocytes is described in the Supplemental Experimental Procedures.

To isolate MP from human plasma, blood was collected in tubes containing EDTA, and blood cells were removed by centrifugation at 2,000 × *g* for 10 min at 4°C. In some experiments, a second centrifugation step (3,000 × *g* for 10 min) was used to remove platelets as previously described (Nielsen et al., 2011). The resultant plasma (either fresh or stored at −80°C) was centrifuged at 22,000 × *g* for 30–60 min to pellet the MP, and the supernatant was used to measure DNASE1L3 activity and Ab binding specificities. To isolate MP from murine plasma, animals were euthanized and immediately exsanguinated by cardiac puncture into heparin-containing tubes. Plasma was isolated by centrifugation at 2,000 × *g* for 10 min 4°C and centrifuged at 22,000 × *g* for 30 min to pellet the MP. Plasma MP were resuspended and counted by flow cytometry after staining for CD42b and CD235a (human) or CD41 and Ter119 (mouse) to exclude platelets and erythrocytes.

To test the ability of mouse serum or human plasma to digest MP DNA, Jurkat MP (5 × 10^5/μl in PBS) were incubated with an equal volume of serum/plasma for 1 hr at 37°C in a final reaction volume of 10 μl. The DNA content of Jurkat cell-derived MP, human plasma MP, and total plasma was measured by qPCR for human genomic *Alu* repeats. The DNA content of murine plasma MP and total plasma was measured by qPCR for mouse genomic *B1* repeats. Data were converted into the amount of genomic DNA using calibration curves with the respective genomic DNA and expressed as the percent of input DNA or as amount of DNA per MP.

For surface staining, 2.5 × 10^5 native or DNase-treated Jurkat cell MP were stained with either purified anti-DNA/histone 2a/2b mAb PR1-3 (10 μg/ml) or mouse sera (1:10 dilution) for 30 min at 4°C. Stained MP were washed by centrifugation at 22,000 × *g* for 30 min, incubated with PE-labeled goat anti–mouse IgG secondary Ab (eBioscience) at a 1:200 dilution for 30 min at 4°C, and analyzed by flow cytometry without further washing. Staining with human sera or plasma was done as above at 1:20 dilution, using PE-labeled goat anti-human IgG secondary Ab (eBioscience).

Statistics

Statistical significance was estimated by nonparametric Mann-Whitney test.

SUPPLEMENTAL INFORMATION

Supplemental Information includes Supplemental Experimental Procedures and seven figures and can be found with this article online at http://dx.doi.org/10.1016/j.cell.2016.05.034.

AUTHOR CONTRIBUTIONS

V.S., B.S., V.D., W. M.-O., J.D., A.R., and A.Y. performed and interpreted the experiments. F.J.Q., T.J.C., R.M.C, J.P.B., and B.R. supervised and interpreted the experiments. Z.B.O., C.P., A.S.C., M.B., I.I.I., I.S., M.T., F.Y., K.B.E., R.M.C., and J.P.B. provided samples and reagents. K.B.E., R.M.C., and J.P.B. provided advice and feedback. B.R. conceived and supervised the project. V.S. and B.R. wrote the manuscript.

ACKNOWLEDGMENTS

We thank G. Silverman for help and discussions, M. Shlomchik and A. Davidson for reagents, and S. Rasmussen for technical assistance. This work was supported by NIH grants (AR064460 and AI072571 to B.R.; DK098378 to I.I.I.), the Lupus Research Institute (to B.R.), the Judith and Stewart Colton Center for Autoimmunity (to B.R. and J.P.B.), and the Irvington Institute Fellowship of the Cancer Research Institute (to V.S.). K.B.E. is a co-founder and consultant of Resolve Therapeutics, which develops soluble nucleases for therapeutic purposes.

Received: October 7, 2015
Revised: March 22, 2016
Accepted: May 6, 2016
Published: June 9, 2016

REFERENCES

Ahn, J., Gutman, D., Saijo, S., and Barber, G.N. (2012). STING manifests self DNA-dependent inflammatory disease. Proc. Natl. Acad. Sci. USA *109*, 19386–19391.

Al-Mayouf, S.M., Sunker, A., Abdwani, R., Abrawi, S.A., Almurshedi, F., Alhashmi, N., Al Sonbul, A., Sewairi, W., Qari, A., Abdallah, E., et al. (2011). Loss-of-function variant in DNASE1L3 causes a familial form of systemic lupus erythematosus. Nat. Genet. *43*, 1186–1188.

Baron, W.F., Pan, C.Q., Spencer, S.A., Ryan, A.M., Lazarus, R.A., and Baker, K.P. (1998). Cloning and characterization of an actin-resistant DNase I-like endonuclease secreted by macrophages. Gene *215*, 291–301.

Caielli, S., Athale, S., Domic, B., Murat, E., Chandra, M., Banchereau, R., Baisch, J., Phelps, K., Clayton, S., Gong, M., et al. (2016). Oxidized mitochondrial nucleoids released by neutrophils drive type I interferon production in human lupus. J. Exp. Med. *213*, 697–713.

Casciola-Rosen, L.A., Anhalt, G., and Rosen, A. (1994). Autoantigens targeted in systemic lupus erythematosus are clustered in two populations of surface structures on apoptotic keratinocytes. J. Exp. Med. *179*, 1317–1330.

Choi, J., Kim, S.T., and Craft, J. (2012). The pathogenesis of systemic lupus erythematosus-an update. Curr. Opin. Immunol. *24*, 651–657.

Crow, Y.J. (2015). Type I interferonopathies: mendelian type I interferon upregulation. Curr. Opin. Immunol. *32*, 7–12.

Dieker, J., Tel, J., Pieterse, E., Thielen, A., Rother, N., Bakker, M., Fransen, J., Dijkman, H.B., Berden, J.H., de Vries, J.M., et al. (2016). Circulating apoptotic microparticles in systemic lupus erythematosus patients drive the activation of dendritic cell subsets and prime neutrophils for NETosis. Arthritis Rheumatol. *68*, 462–472.

Ehlers, M., Fukuyama, H., McGaha, T.L., Aderem, A., and Ravetch, J.V. (2006). TLR9/MyD88 signaling is required for class switching to pathogenic IgG2a and 2b autoantibodies in SLE. J. Exp. Med. *203*, 553–561.

Gall, A., Treuting, P., Elkon, K.B., Loo, Y.M., Gale, M., Jr., Barber, G.N., and Stetson, D.B. (2012). Autoimmunity initiates in nonhematopoietic cells and progresses via lymphocytes in an interferon-dependent autoimmune disease. Immunity *36*, 120–131.

Ganguly, D., Haak, S., Sisirak, V., and Reizis, B. (2013). The role of dendritic cells in autoimmunity. Nat. Rev. Immunol. *13*, 566–577.

Ghodke-Puranik, Y., and Niewold, T.B. (2015). Immunogenetics of systemic lupus erythematosus: A comprehensive review. J. Autoimmun. *64*, 125–136.

Heidari, Y., Bygrave, A.E., Rigby, R.J., Rose, K.L., Walport, M.J., Cook, H.T., Vyse, T.J., and Botto, M. (2006). Identification of chromosome intervals from 129 and C57BL/6 mouse strains linked to the development of systemic lupus erythematosus. Genes Immun. *7*, 592–599.

Holdenrieder, S., Stieber, P., Chan, L.Y., Geiger, S., Kremer, A., Nagel, D., and Lo, Y.M. (2005). Cell-free DNA in serum and plasma: comparison of ELISA and quantitative PCR. Clin. Chem. *51*, 1544–1546.

Jenks, S.A., Palmer, E.M., Marin, E.Y., Hartson, L., Chida, A.S., Richardson, C., and Sanz, I. (2013). 9G4+ autoantibodies are an important source of apoptotic cell reactivity associated with high levels of disease activity in systemic lupus erythematosus. Arthritis Rheum. *65*, 3165–3175.

Lavin, Y., Mortha, A., Rahman, A., and Merad, M. (2015). Regulation of macrophage development and function in peripheral tissues. Nat. Rev. Immunol. *15*, 731–744.

Lood, C., Blanco, L.P., Purmalek, M.M., Carmona-Rivera, C., De Ravin, S.S., Smith, C.K., Malech, H.L., Ledbetter, J.A., Elkon, K.B., and Kaplan, M.J. (2016). Neutrophil extracellular traps enriched in oxidized mitochondrial DNA are interferogenic and contribute to lupus-like disease. Nat. Med. *22*, 146–153.

Martin, J.E., Assassi, S., Diaz-Gallo, L.M., Broen, J.C., Simeon, C.P., Castellvi, I., Vicente-Rabaneda, E., Fonollosa, V., Ortego-Centeno, N., González-Gay, M.A., et al.; Spanish Scleroderma Group; SLEGEN consortium; U.S. Scleroderma GWAS group; BIOLUPUS (2013). A systemic sclerosis and systemic lupus erythematosus pan-meta-GWAS reveals new shared susceptibility loci. Hum. Mol. Genet. *22*, 4021–4029.

Mathian, A., Weinberg, A., Gallegos, M., Banchereau, J., and Koutouzov, S. (2005). IFN-alpha induces early lethal lupus in preautoimmune (New Zealand Black x New Zealand White) F1 but not in BALB/c mice. J. Immunol. *174*, 2499–2506.

Mayes, M.D., Bossini-Castillo, L., Gorlova, O., Martin, J.E., Zhou, X., Chen, W.V., Assassi, S., Ying, J., Tan, F.K., Arnett, F.C., et al.; Spanish Scleroderma Group (2014). Immunochip analysis identifies multiple susceptibility loci for systemic sclerosis. Am. J. Hum. Genet. *94*, 47–61.

Mizuta, R., Araki, S., Furukawa, M., Furukawa, Y., Ebara, S., Shiokawa, D., Hayashi, K., Tanuma, S., and Kitamura, D. (2013). DNase γ is the effector endonuclease for internucleosomal DNA fragmentation in necrosis. PLoS ONE *8*, e80223.

Nagata, S., and Kawane, K. (2011). Autoinflammation by endogenous DNA. Adv. Immunol. *110*, 139–161.

Napirei, M., Wulf, S., Eulitz, D., Mannherz, H.G., and Kloeckl, T. (2005). Comparative characterization of rat deoxyribonuclease 1 (Dnase1) and murine deoxyribonuclease 1-like 3 (Dnase1l3). Biochem. J. *389*, 355–364.

Napirei, M., Ludwig, S., Mezrhab, J., Klöckl, T., and Mannherz, H.G. (2009). Murine serum nucleases–contrasting effects of plasmin and heparin on the activities of DNase1 and DNase1-like 3 (DNase1l3). FEBS J. *276*, 1059–1073.

Nielsen, C.T., Østergaard, O., Johnsen, C., Jacobsen, S., and Heegaard, N.H. (2011). Distinct features of circulating microparticles and their relationship to clinical manifestations in systemic lupus erythematosus. Arthritis Rheum. *63*, 3067–3077.

Nielsen, C.T., Østergaard, O., Stener, L., Iversen, L.V., Truedsson, L., Gullstrand, B., Jacobsen, S., and Heegaard, N.H. (2012). Increased IgG on cell-derived plasma microparticles in systemic lupus erythematosus is associated with autoantibodies and complement activation. Arthritis Rheum. *64*, 1227–1236.

Ozçakar, Z.B., Foster, J., 2nd, Diaz-Horta, O., Kasapcopur, O., Fan, Y.S., Yalçınkaya, F., and Tekin, M. (2013). DNASE1L3 mutations in hypocomplementemic urticarial vasculitis syndrome. Arthritis Rheum. *65*, 2183–2189.

Picard, C., Mathieu, A.L., Hasan, U., Henry, T., Jamilloux, Y., Walzer, T., and Belot, A. (2015). Inherited anomalies of innate immune receptors in pediatric-onset inflammatory diseases. Autoimmun. Rev. *14*, 1147–1153.

Pisetsky, D.S. (2016). Anti-DNA antibodies - quintessential biomarkers of SLE. Nat. Rev. Rheumatol. *12*, 102–110.

Pisetsky, D.S., Gauley, J., and Ullal, A.J. (2011). Microparticles as a source of extracellular DNA. Immunol. Res. *49*, 227–234.

Radic, M., Marion, T., and Monestier, M. (2004). Nucleosomes are exposed at the cell surface in apoptosis. J. Immunol. *172*, 6692–6700.

Rekvig, O.P., van der Vlag, J., and Seredkina, N. (2014). Review: antinucleosome antibodies: a critical reflection on their specificities and diagnostic impact. Arthritis Rheumatol. *66*, 1061–1069.

Richardson, C., Chida, A.S., Adlowitz, D., Silver, L., Fox, E., Jenks, S.A., Palmer, E., Wang, Y., Heimburg-Molinaro, J., Li, Q.Z., et al. (2013). Molecular basis of 9G4 B cell autoreactivity in human systemic lupus erythematosus. J. Immunol. *191*, 4926–4939.

Santiago-Raber, M.L., Amano, H., Amano, E., Baudino, L., Otani, M., Lin, Q., Nimmerjahn, F., Verbeek, J.S., Ravetch, J.V., Takasaki, Y., et al. (2009). Fcgamma receptor-dependent expansion of a hyperactive monocyte subset in lupus-prone mice. Arthritis Rheum. *60*, 2408–2417.

Sharma, S., Campbell, A.M., Chan, J., Schattgen, S.A., Orlowski, G.M., Nayar, R., Huyler, A.H., Nündel, K., Mohan, C., Berg, L.J., et al. (2015). Suppression of systemic autoimmunity by the innate immune adaptor STING. Proc. Natl. Acad. Sci. USA *112*, E710–E717.

Shlomchik, M.J., Aucoin, A.H., Pisetsky, D.S., and Weigert, M.G. (1987). Structure and function of anti-DNA autoantibodies derived from a single autoimmune mouse. Proc. Natl. Acad. Sci. USA *84*, 9150–9154.

Snyder, M.W., Kircher, M., Hill, A.J., Daza, R.M., and Shendure, J. (2016). Cell-free DNA comprises an in vivo nucleosome footprint that informs its tissues-of-origin. Cell *164*, 57–68.

Sun, K., Jiang, P., Chan, K.C., Wong, J., Cheng, Y.K., Liang, R.H., Chan, W.K., Ma, E.S., Chan, S.L., Cheng, S.H., et al. (2015). Plasma DNA tissue mapping by genome-wide methylation sequencing for noninvasive prenatal, cancer, and transplantation assessments. Proc. Natl. Acad. Sci. USA *112*, E5503–E5512.

Ueki, M., Takeshita, H., Fujihara, J., Iida, R., Yuasa, I., Kato, H., Panduro, A., Nakajima, T., Kominato, Y., and Yasuda, T. (2009). Caucasian-specific allele in non-synonymous single nucleotide polymorphisms of the gene encoding deoxyribonuclease I-like 3, potentially relevant to autoimmunity, produces an inactive enzyme. Clin. Chim. Acta *407*, 20–24.

Ullal, A.J., Reich, C.F., 3rd, Clowse, M., Criscione-Schreiber, L.G., Tochacek, M., Monestier, M., and Pisetsky, D.S. (2011). Microparticles as antigenic targets of antibodies to DNA and nucleosomes in systemic lupus erythematosus. J. Autoimmun. *36*, 173–180.

Ullal, A.J., Marion, T.N., and Pisetsky, D.S. (2014). The role of antigen specificity in the binding of murine monoclonal anti-DNA antibodies to microparticles from apoptotic cells. Clin. Immunol. *154*, 178–187.

Volkman, H.E., and Stetson, D.B. (2014). The enemy within: endogenous retroelements and autoimmune disease. Nat. Immunol. *15*, 415–422.

Wardemann, H., and Nussenzweig, M.C. (2007). B-cell self-tolerance in humans. Adv. Immunol. *95*, 83–110.

Wilber, A., Lu, M., and Schneider, M.C. (2002). Deoxyribonuclease I-like III is an inducible macrophage barrier to liposomal transfection. Mol. Ther. *6*, 35–42.

Zochling, J., Newell, F., Charlesworth, J.C., Leo, P., Stankovich, J., Cortes, A., Zhou, Y., Stevens, W., Sahhar, J., Roddy, J., et al. (2014). An Immunochip-based interrogation of scleroderma susceptibility variants identifies a novel association at DNASE1L3. Arthritis Res. Ther. *16*, 438.

frontiers in Immunology

ORIGINAL RESEARCH
published: 25 October 2018
doi: 10.3389/fimmu.2018.02475

Plasmacytoid Dendritic Cells Are Largely Dispensable for the Pathogenesis of Experimental Inflammatory Bowel Disease

Catherine M. Sawai[1,2], *Lee Serpas*[1], *Antonio Galvao Neto*[1], *Geunhyo Jang*[1], *Ali Rashidfarrokhi*[1], *Roland Kolbeck*[3], *Miguel A. Sanjuan*[3], *Boris Reizis*[1,4]* and *Vanja Sisirak*[1,5]*

[1] Department of Pathology, New York University School of Medicine, New York, NY, United States, [2] INSERM, ACTION Laboratory, University of Bordeaux, Bordeaux, France, [3] Department of Respiratory, Inflammation and Autoimmunity, MedImmune LLC, Gaithersburg, MD, United States, [4] Department of Medicine, New York University School of Medicine, New York, NY, United States, [5] CNRS-UMR, Immunoconcept, Université de Bordeaux, Bordeaux, France

OPEN ACCESS

Edited by:
Keith Elkon,
University of Washington,
United States

Reviewed by:
Luisa Cervantes-Barragan,
Washington University School of Medicine in St. Louis, United States
Kristi Kuhn,
University of Colorado Denver,
United States

***Correspondence:**
Boris Reizis
boris.reizis@nyumc.org;
Vanja Sisirak
vsisirak@immuconcept.org

Specialty section:
This article was submitted to Autoimmune and Autoinflammatory Disorders, a section of the journal Frontiers in Immunology

Received: 20 July 2018
Accepted: 08 October 2018
Published: 25 October 2018

Citation:
Sawai CM, Serpas L, Neto AG, Jang G, Rashidfarrokhi A, Kolbeck R, Sanjuan MA, Reizis B and Sisirak V (2018) Plasmacytoid Dendritic Cells Are Largely Dispensable for the Pathogenesis of Experimental Inflammatory Bowel Disease. Front. Immunol. 9:2475. doi: 10.3389/fimmu.2018.02475

Inflammatory bowel disease (IBD) is a chronic inflammatory condition caused by an aberrant immune response to microbial components of the gastrointestinal tract. Plasmacytoid dendritic cells (pDCs) are innate immune cells specialized in the production of type I interferons and were recently implicated in the pathogenesis of autoimmune disorders such as lupus and scleroderma. While pDCs were shown to infiltrate intestinal mucosa of IBD patients and proposed to participate in intestinal inflammation, their net contribution to the disease remains unclear. We addressed this question by targeting the pDC-specific transcription factor TCF4 (E2-2) in experimental IBD caused by deficiency of Wiskott-Aldrich syndrome protein (WASP) or of interleukin-10 (IL-10). Monoallelic *Tcf4* deletion, which was previously shown to abrogate experimental lupus, did not affect autoimmunity manifestations or colitis in WASP-deficient animals. Furthermore, conditional biallelic *Tcf4* targeting resulted in a near-complete pDC ablation, yet had no effect on the development of colitis in IL-10-deficient mice. Our results suggest that, in contrast to other inflammatory and autoimmune diseases, pDCs do not play a major role in the pathogenesis of intestinal inflammation during IBD.

Keywords: Plasmacytoid dendritic cell (PDC), Interferon Type I, colitis, Inflammatory bowel disease (IBD), autoimmune disease

INTRODUCTION

Dendritic cells (DCs) are major antigen-presenting cells that are essential for the initiation and regulation of immune responses. DCs are commonly subdivided into classical or conventional DCs (cDCs) and plasmacytoid DCs (pDCs). The pDCs are a distinct lineage whose function, phenotype, and core gene expression program are conserved across mammalian species (1, 2). They express a specific set of pathogen recognition receptors (PRR) including endosomal Toll-like receptor (TLR)-7 and TLR9 that recognize the nucleic acid ligands single stranded (ss)-RNA and unmethylated CpG-containing DNA, respectively (1, 2). In response to such stimuli pDCs rapidly produce copious amounts of type I interferon (IFNα/β, IFN-I), up to 1,000 times more than any other cell type (1, 2). IFN-I produced by pDCs is essential for inducing the expression

of multiples genes with anti-viral properties and activates a broad range of immune cells subsequently providing anti-viral immunity (1, 2). In addition to their role in anti-viral immune responses, pDCs were shown to produce high amounts of IFN-I in response to self-nucleic acids and thus contribute to the development of inflammatory and autoimmune disorders (3–9). For instance, systemic lupus erythematous (SLE) patients (10, 11) have an accumulation of IFN-I-producing pDCs in the affected tissues, which likely contributes to the increased expression in IFN-I-inducible genes and overall "IFN-I signature" characteristic of SLE. In addition, recent studies using murine disease models that specifically lack pDCs have further confirmed their contribution to the pathogenesis of SLE (12, 13), systemic sclerosis (14), type I diabetes (15), and type II diabetes (16). These studies have provided a rationale for targeting pDCs as a therapeutic approach for such diseases, and antibodies that deplete pDCs in humans are currently being developed (17).

Within the small and large intestine pDCs are found primarily in the lamina propria (LP) and gut-associated lymphoid tissues (18). A distinct population of pDCs with reduced ability to produce IFN-I is also thought to populate Peyer's patches (19, 20). pDCs were previously proposed to contribute to B cell production of intestinal immunoglobulin A (IgA) (21). However, these results were recently challenged by the observation that pDC ablation had no major impact on intestinal IgA production *in vivo* (22). Through the production of IFN-I, intestinal pDCs were shown to participate in the clearance of enteropathogenic viruses such as rotavirus (23). Conversely, intestinal pDCs were described to mediate the tolerogenic effects of polysaccharide A (PSA), an immunomodulatory molecule of the gut commensal *Bacteroides fragilis* (24), and liver pDCs were implicated in the establishment of tolerance in response to ingested/oral antigens (25, 26). Thus, pDCs are clearly present in the gastrointestinal tract and appear to have context-dependent functions. Given the abundance of immunostimulatory microbial DNA/RNA in the intestine, pDCs may also contribute to the development of autoimmune and inflammatory conditions in the gastrointestinal tract.

Inflammatory bowel disease (IBD) comprises two major syndromes, Crohn's disease (CD) and ulcerative colitis (UC), which are progressive inflammatory conditions that affect the entire gastrointestinal tract and the colonic mucosa, respectively. IBD development is caused by dysregulated immune responses in genetically predisposed individuals to microbial components of the gastrointestinal tract (27). A role for pDCs in IBD has been suggested by the increase in their frequency and number in the inflamed intestinal mucosa of flaring IBD patients compared to healthy controls (28). In addition, pDCs from the peripheral blood (PB) of IBD patients generally display an activated phenotype defined by the increased expression of co-stimulatory molecules and the ability to spontaneously produce inflammatory cytokines such as tumor necrosis factor (TNF)-α and interleukin (IL)-6, but they also show impaired production of IFN-I in response to TLR7 and 9 stimulation (28). Another study documented increases in both activation of pDCs and IFN-I levels in Wiskott-Aldrich syndrome (WAS) patients who manifest a pleiotropic autoimmunity that includes colitis (29). Wiskott-Aldrich syndrome protein (WASP, gene symbol: *Was*)-deficient animals display a similar phenotype, including pDC hyperactivation and heightened IFN-I production. Furthermore, this study showed that the overall pathology including colitis in *Was*-deficient animals was ameliorated by IFN-I receptor (*Ifnar*) deficiency (29). While IFN-I clearly plays an important role in the development of colitis in *Was*-deficient animals, whether such IFN-I originates from pDCs and whether pDCs contribute at all to the overall pathology in this model was not tested. Finally, a recent study used genetic ablation of pDCs in an experimental model of colitis induced by dextran sodium sulfate (DSS) treatment and concluded that pDCs play a pathogenic role in IBD (30). However, in this model pDC ablation was achieved by diphtheria toxin (DT) treatment of Siglec H-DTR mice, which also depletes subsets of macrophages and DC progenitors, calling into question its specificity (31). Thus, the role of pDCs in the pathogenesis of IBD, if any, remains unclear and requires further study.

We have previously identified the E-protein transcription factor encoded by the gene *Tcf4* (E2-2) as a master regulator of pDC development in humans and mice (32). TCF4 is preferentially expressed in pDCs, and its deletion abolishes the development of pDCs but not of other immune cells including cDCs. Importantly, even monoallelic loss of *Tcf4* causes a specific defect in pDC function in mice and human patients. Indeed, $Tcf4^{+/-}$ mice show aberrant pDC phenotype and impaired pDC-driven IFN-I response to the TLR9 agonist CpG-oligodeoxynucleotide (CpG-ODN) (32). Using *Tcf4* haplodeficiency for specific functional impairment of pDCs, we have demonstrated a crucial role for pDCs in two genetic models of experimental SLE (13). Furthermore, monoallelic or complete deletion of *Tcf4* in the DC lineage confirmed the deleterious function of pDCs in SLE (13) and showed a pathogenic role in autoimmune diabetes in NOD mice (15), respectively. Using a similar approach, here we explored the role of pDCs in two distinct models of IBD. We established *Tcf4* haplodeficiency in *Was*-deficient animals that are prone to systemic autoimmunity and that develop severe colitis with 100% penetrance. Additionally, we conditionally deleted *Tcf4* in DCs, which results in a specific deficiency in pDCs, in IBD-prone *Il10*-deficient mice (33). Although targeting of *Tcf4* in *Was*- or *Il10*-deficient mice altered and selectively depleted pDCs, respectively, we did not observe any further impact on the development of IBD in either model. Thus, our study using two distinct genetic models of the disease suggests that pDCs do not play a major role in genetically-induced IBD pathogenesis.

MATERIALS AND METHODS

Mice

All experiments were performed according to the investigator's protocol approved by the Institutional Animal Care and Use Committee of New York University Langone Medical Center. $Tcf4^{+/-}$ (E2-$2^{+/-}$) animals (34) were on pure 129SvEvTac (129Sv) background (>N12); all other animals were on pure C57BL/6J (B6) background (>N12). *Was*-deficient females (Strain 019458, The Jackson Laboratory) were crossed with

Tcf4$^{+/-}$ males to generate B6.129F1 *Was*$^{-/y}$ *Tcf4*$^{+/-}$ males or *Was*$^{-/y}$ *Tcf4*$^{+/+}$ littermates. Age-matched B6.129F1 males bred in the same colony were used as WT controls. For the conditional targeting of *Tcf4, Il10*-deficient animals (Strain 002251, The Jackson Laboratory) were crossed with the *Itgax* (CD11c)-Cre transgenic mice (35) floxed for *Tcf4* alleles (36) to generate *Il10*$^{-/-}$ *Tcf4*$^{Fl/Fl}$ mice with or without the *Itgax*-Cre transgene. Age-matched B6 males bred in the same colony were used as WT controls. No phenotypic differences have been observed between male and female *Il10*-deficient animals; thus, both male and female mice were included in the analysis.

Macroscopic Colitis Assessment

Was-deficient *Tcf4*$^{+/+}$ or *Tcf4*$^{+/-}$ mice as well as their respective WT controls were euthanized at the age of 6 months. *Il10*$^{-/-}$ *Tcf4*$^{Fl/Fl}$ either positive or negative for the *Itgax*-Cre transgene together with their respective WT control were euthanized at 3 months. The colons were extracted, emptied of their content, photographed and measured for length. Samples from the colon were harvested and stored in TRIzol (Thermo Fisher) for RNA extraction. Animals were also followed prior to their euthanasia, and the occurrence of rectal prolapse was monitored on a weekly basis.

Flow Cytometry

Single cell suspensions were prepared from the spleen, lymph nodes and mesenteric lymph nodes by tissue digestion in the presence of collagenase D (1 mg/ml, Sigma Aldrich) and DNase1 (20 μg/ml, Sigma Aldrich) at 37°C for 30 min and filtration through a cell strainer 70 μm (Thermo Fisher). Cell suspensions were subjected to red blood cell lysis, washed, and stained with unconjugated and conjugated fluorescent antibodies listed in **Table S1**. Intracellular staining for Foxp3 and BCL6 were performed using the transcription factor staining buffer set (Thermo Fisher) according to the manufacturer's instructions. For optimal resolution of CXCR5 across CD4$^+$ T cell subsets, staining with CXCR5 biotinylated antibody to identify CD4$^+$ T follicular helper (Tfh) cells was performed for 1 h at room temperature, prior to conventional staining with other relevant markers. Samples were acquired on an Attune flow cytometer (Thermo Fisher) and analyzed using FlowJo software (Tree Star).

Autoantibody Measurement

Anti-dsDNA IgG concentration in the sera of animals was determined by ELISA as previously described (37) using calf thymus DNA as antigen. Anti-nuclear antibodies were detected by staining fixed HEp-2 cells (MBL Bion) with mouse serum (1:100 dilution), followed by PE-labeled goat anti–mouse IgG (Thermo-Fisher). Images were captured on a confocal fluorescent microscope (LSM 710 NLO) and processed by ZEN software (Carl Zeiss). For the profiling of IgG and IgM autoantibodies in the sera of mice we used a 98-plex autoantigen array provided by the UT Southwestern Genomics and Microarray Core facility. Briefly, samples were treated with DNase1, diluted 1/50 and incubated with the autoantigen array. Autoantibodies binding to antigens on the array were detected with Cy3 labeled anti-IgG and Cy5 labeled anti-IgM antibodies, and the arrays were scanned with a GenePix® 4400A Microarray Scanner. Images were analyzed using GenePix 7.0 software, and the averaged net fluorescent intensity (NFI) of each autoantigen was normalized to the internal control (IgG or IgM) that collectively were presented as heat maps of signal intensity.

Histopathology

For histological analysis, intestines were cut longitudinally, rolled by the "Swiss roll" method (38), fixed in formalin, embedded in paraffin, sectioned through the central part of the roll and stained with hematoxylin and eosin. The stained slides were scanned with a Leica SCN400 F whole-slide scanner, and the images were analyzed using the SlidePath Digital Image Hub. Histological sections were then scored on a 0–4 scale with 0.5 increments according to the following criteria: 0, intact crypt architecture, normal epithelium with goblet cells, no neutrophil infiltration; 1, patchy neutrophil infiltration, occasional epithelial dysplasia; 2, foci of neutrophils, occasional cryptitis, epithelial damage; 3, diffuse leukocyte infiltration, crypt abscesses (debris and neutrophils inside of lumen), transmural infiltration to visceral peritoneum, crypt dropout; 4, severe loss of tissue architecture, widespread crypt damage.

Gene Expression Analysis

For gene expression analysis of colon tissue, fragments of large intestine measuring 1 × 1 mm (30–35 mg) were homogenized in TRIzol (Thermo Fisher) using Lysing Matrix D beads (MP Biomedical) and a Fast-Prep-24 Instrument tissue homogenizer (MP Biomedical). Spleen single cell suspensions were also lysed in the presence of TRIzol, and the RNA was isolated after precipitation with chloroform and washing with 100% ethanol. After reverse transcription with SuperScript III (ThermoFisher), quantitative PCR of cDNA was performed using SYBR green (Roche) on a Bio-Rad CFX96 Touch™ instrument.

Statistics

Data are represented as median with the distribution of all individual animals depicted. The data are pooled from at least 3 independent experiments. Unless noted otherwise, sample distribution was analyzed by the nonparametric Kruskal-Wallis test, and in cases when significance was reached with Kruskal-Wallis test, each group was individually compared using the *post-hoc* Dunn's multiple comparison test. The significance is defined as follows $^*P \leq 0.05$, $^{**}P \leq 0.01$, $^{***}P \leq 0.001$.

RESULTS

Tcf4 Haplodeficiency Does not Prevent Aberrant Immune Activation Caused by *Was* Deficiency

In order to evaluate pDC function in autoimmunity mediated by *Was* deficiency, we crossed *Tcf4*$^{+/-}$ haplodeficient males (129Sv background) with *Was*$^{-/-}$ females (C57BL/6J background). As *Was* is located on the X chromosome, the F_1 generation males obtained on the hybrid (B6/129Sv)F_1 background are deficient for WASP (*Was*$^{-/y}$) and either proficient or haplodeficient for *Tcf4*. We observed a similar frequency of pDCs, defined by the

expression of CD11c and Siglec H (**Figure 1A**), in the spleen of *Was*$^{-/y}$ *Tcf4*$^{+/-}$ animals compared to *Was*$^{-/y}$ and wild type (WT) animals on the same hybrid background (**Figure 1B**) However, the absolute number of pDCs within the spleen of *Was*$^{-/y}$ *Tcf4*$^{+/-}$ mice was significantly reduced compared to *Was*$^{-/y}$ mice (**Figure 1B**). Within lymph nodes (LN), pooling axillary, inguinal and cervical LN, both the frequency and number of pDCs were significantly increased in *Was*$^{-/y}$ mice compared to WT control but remained unchanged in *Was*$^{-/y}$ *Tcf4*$^{+/-}$ mice (**Figure 1B**). In the mesenteric LN (MLN) the frequency and numbers of pDCs in *Was*$^{-/y}$ and *Was*$^{-/y}$ *Tcf4*$^{+/-}$ mice were increased compared to control animals with a trend toward a lower number of pDCs in *Was*$^{-/y}$ *Tcf4*$^{+/-}$ mice (**Figures S1A,B**). Haplodeficiency of *Tcf4* was previously shown to alter the phenotype of pDCs, which was associated with an inability to produce IFN-I (32, 39). In agreement with these reports we observed that pDCs from *Was*$^{-/y}$ *Tcf4*$^{+/-}$ mice in the spleen and LN express higher levels of cDC specific markers such as CD11c and CD8α (**Figure 1C**). The increased expression of CD11c and CD8α was consistently observed among all *Was*$^{-/y}$ *Tcf4*$^{+/-}$ mice and was significantly higher than in *Was*$^{-/y}$ and WT animals (**Figure 1D**). Similarly, pDCs from the MLNs of *Was*$^{-/y}$ *Tcf4*$^{+/-}$ mice upregulated CD11c and CD8α on their surface (**Figures S1C,D**). The impact of *Tcf4* haplodeficiency was specific to pDCs and did not affect the overall distribution of cDCs in the spleen, LN, and MLN of *Was*-deficient animals (**Figure S1E**). Thus, our results indicate that *Tcf4* haplodeficiency reduces pDC numbers in *Was*-deficient mice and strongly impairs their phenotype, further validating *Tcf4* haplodeficiency as a pDC-specific tool.

We explored the impact of pDC impairment due to *Tcf4* haplodeficiency on the phenotype of *Was*-deficient animals. The splenomegaly in *Was*$^{-/y}$ mice showed a trend toward reduction in *Was*$^{-/y}$ *Tcf4*$^{+/-}$ mice, which reached significance for total splenocyte numbers (**Figure 2A**). We then analyzed the activation status of CD4^{+} T cells by the expression of CD45RB (naïve T cells) and CD44 (activated T cells) markers. We observed that *Was*$^{-/y}$ and *Was*$^{-/y}$ *Tcf4*$^{+/-}$ mice exhibited higher frequency of activated CD4^{+} T cells in comparison to control WT animals (**Figure 2B**). Similar results were observed in LNs and MLNs, indicating a systemic activation of CD4^{+} T cells in *Was*$^{-/y}$ animals regardless of *Tcf4* status (**Figure 2B**). However, no defect in CD8^{+} T cell number and activation profile was detected (not shown). In addition to CD4^{+} T cell activation, an increased frequency and number of regulatory CD4^{+} T cells expressing the transcription factor forkhead box P3 (Foxp3) was observed in *Was*$^{-/y}$ and *Was*$^{-/y}$ *Tcf4*$^{+/-}$ mice, most likely in response to the aberrant immune activation in these mice (**Figure S2A**). *Was*-deficient mice were previously described to display an abnormal distribution of peripheral B cells including loss of a marginal zone B (MZB) cell population (40). Consistent with this report, *Was*$^{-/y}$ mice showed strongly reduced frequency and numbers of CD21/35^{+} CD23^{-} of MZB cells with no change in the population of CD23^{+} CD21/35^{-} follicular B cells (FOB) (**Figure 2C, Figure S2B**). The loss of MZB cells was not rescued by specific pDC ablation in *Was*$^{-/y}$ *Tcf4*$^{+/-}$ mice (**Figure 2C, S2B**). Another feature of multiple autoimmune strains is the accumulation of an unusual population of age-associated B cells (ABCs), negative for both FOB (CD23) and MZB (CD21/35) markers (41, 42). The frequency of ABCs in both *Was*$^{-/y}$ and *Was*$^{-/y}$ *Tcf4*$^{+/-}$ mice was significantly increased compared to WT controls (**Figure 2C**). However, the absolute numbers in *Was*$^{-/y}$ *Tcf4*$^{+/-}$ remained comparable to WT mice (**Figure S2B**). In addition to the altered frequency of different B cell subsets, we observed that FOB and ABC cells from *Was*$^{-/y}$ and *Was*$^{-/y}$ *Tcf4*$^{+/-}$ mice displayed an activated phenotype as reflected by increased expression of CD40 (**Figure S2C**). Finally, *Was*$^{-/y}$ mice had an increased frequency of germinal center B cells (GCB) characterized by the expression of CD95 (Fas) and peanut agglutinin (PNA) (**Figure 2D**). The increase in GC frequency was associated with an increase in CD4^{+} Tfh expressing the chemokine receptor CXCR5 and the transcription factor BCL6 (**Figure 2E**, **Figure S2E**). Although *Tcf4* haplodeficiency was associated with a reduction in the absolute number of GCB in the spleen compared to *Was*$^{-/y}$ (**Figure S2D**) the frequency of GCB was still increased compared to WT controls (**Figure 2D**). As observed in *Was*$^{-/y}$ animals, the frequency and absolute numbers of CD4^{+} Tfh cells were significantly increased in *Was*$^{-/y}$ *Tcf4*$^{+/-}$ animals compared to control (**Figure 2E, Figure S2E**). Overall, apart from decreased splenomegaly, Tcf4 haplodeficiency had no impact on the general immune activation caused by *Was*-deficiency.

Tcf4 Haplodeficiency Does not Prevent Autoantibody Production in *Was*-Deficient Mice

Multiple features of autoimmunity have been observed in *Was*-deficient mice, including increased levels of autoreactive antibodies such as anti-dsDNA antibodies (40). We have previously observed that *Tcf4* haplodeficiency was able to reduce the autoreactive anti-RNA and anti-dsDNA antibodies secretion in two experimental models of SLE (13). Therefore, we sought to investigate if such *Tcf4* targeting may also impact the production of autoreactive antibodies in *Was*-deficient mice. We observed that compared to controls, *Was*$^{-/y}$ animals showed significantly higher titers of auto-antibodies directed against double-stranded DNA (dsDNA) (**Figure 3A**). Specific targeting of pDCs in *Was*$^{-/y}$ *Tcf4*$^{+/-}$ mice did not affect the production of such autoantibodies (**Figure 3A**). The overall prevalence of antinuclear antibodies (ANA) was also increased in *Was*-deficient mice regardless of *Tcf4* status (**Figure 3B**). While the occurrence of ANA remained consistent between both groups, ANA staining from *Was*$^{-/y}$ sera showed a perinuclear distribution while that of *Was*$^{-/y}$ *Tcf4*$^{+/-}$ sera was primarily nuclear (**Figure 3B**). This differential ANA profile prompted us to analyze the overall autoreactivity in those mice using an autoantigen microarray. While WT and *Tcf4*$^{+/-}$ mice displayed very little autoreactive IgG with the exception of one outlier (mouse WT2), 3 out of 4 mice in the *Was*$^{-/y}$ and *Was*$^{-/y}$ *Tcf4*$^{+/-}$ groups showed a broad range of autoreactive IgG specific to nucleic acids, multiple protein, and ribonucleoproteins (**Figure 3C**). In addition, these autoreactive IgG profiles detected across *Was*$^{-/y}$ animals were

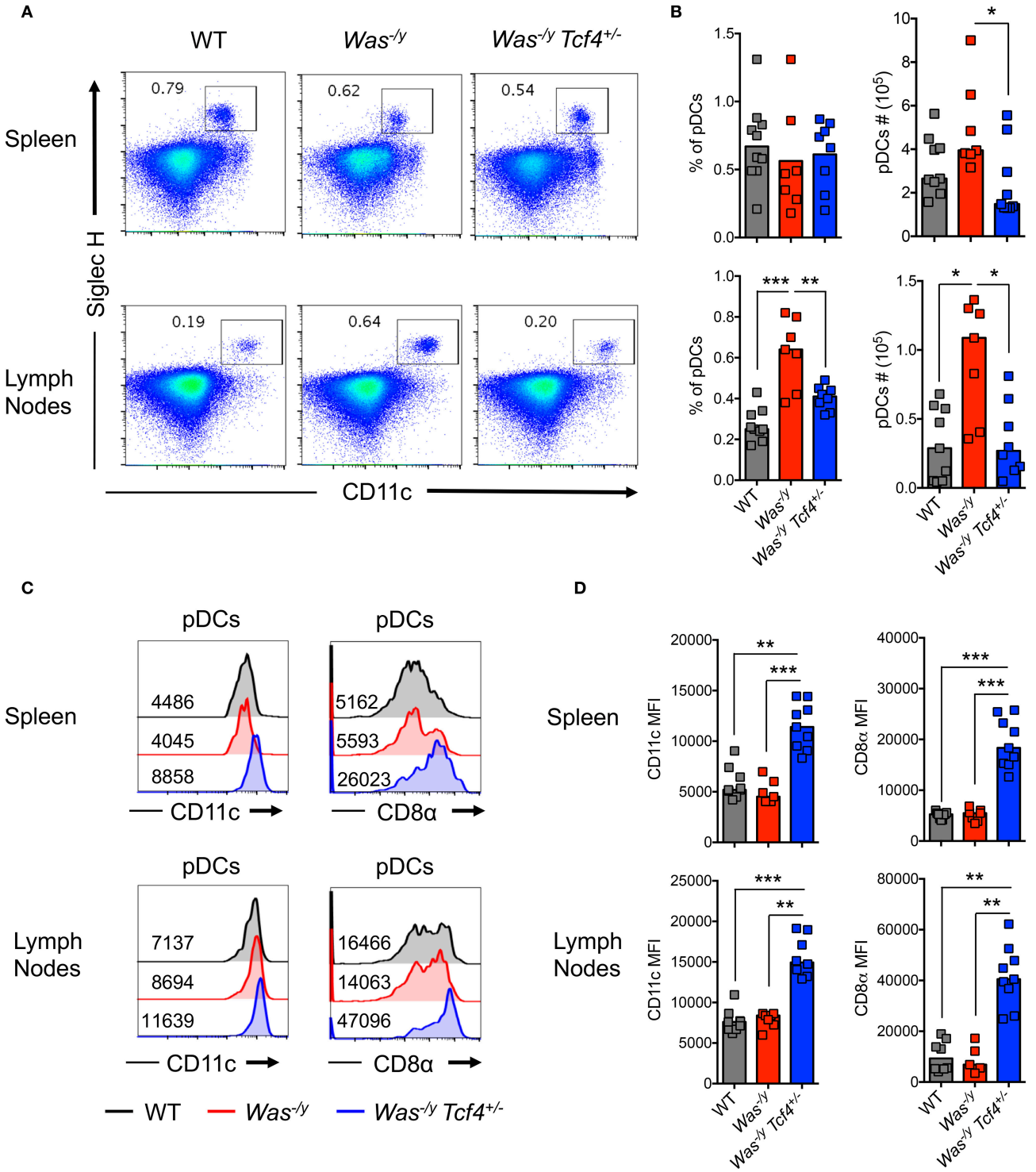

FIGURE 1 | Reduced numbers and altered phenotype of pDCs upon *Tcf4* haplodeficiency in *Was*-deficient mice.WT, *Was*$^{-/y}$ or *Was*$^{-/y}$ *Tcf4*$^{+/-}$ mice were analyzed at 30 weeks of age. **(A)** pDCs were identified by flow cytometry analysis of CD11c and Siglec H expression from CD11b^{-} live cells in the spleen and LNs. The frequency of pDCs is indicated in each plot. **(B)** Frequency and absolute numbers of pDCs (CD11b^{-} CD11c^{+} Siglec H^{+} pDCs among total live cells) in the spleen and LN of individual mice are shown. Horizontal bars indicate median value. Data were pooled from 4 independent experiments. **(C)** CD11c and CD8α expression with the mean fluorescent intensity (MFI) indicated on pDCs (CD11b^{-} CD11c^{+} Siglec H^{+}) from the spleen and LN as analyzed by flow cytometry. **(D)** MFI of CD11c and CD8α on pDCs from the spleen and LN of each individual mice as pooled from 4 independent experiments. Horizontal bars indicate the median. Statistical significance estimated by Kruskal-Wallis test followed by a *post-hoc* Dunn's multiple comparison test is indicated as follows $^{*}P \leq 0.05$, $^{**}P \leq 0.01$, $^{***}P \leq 0.001$.

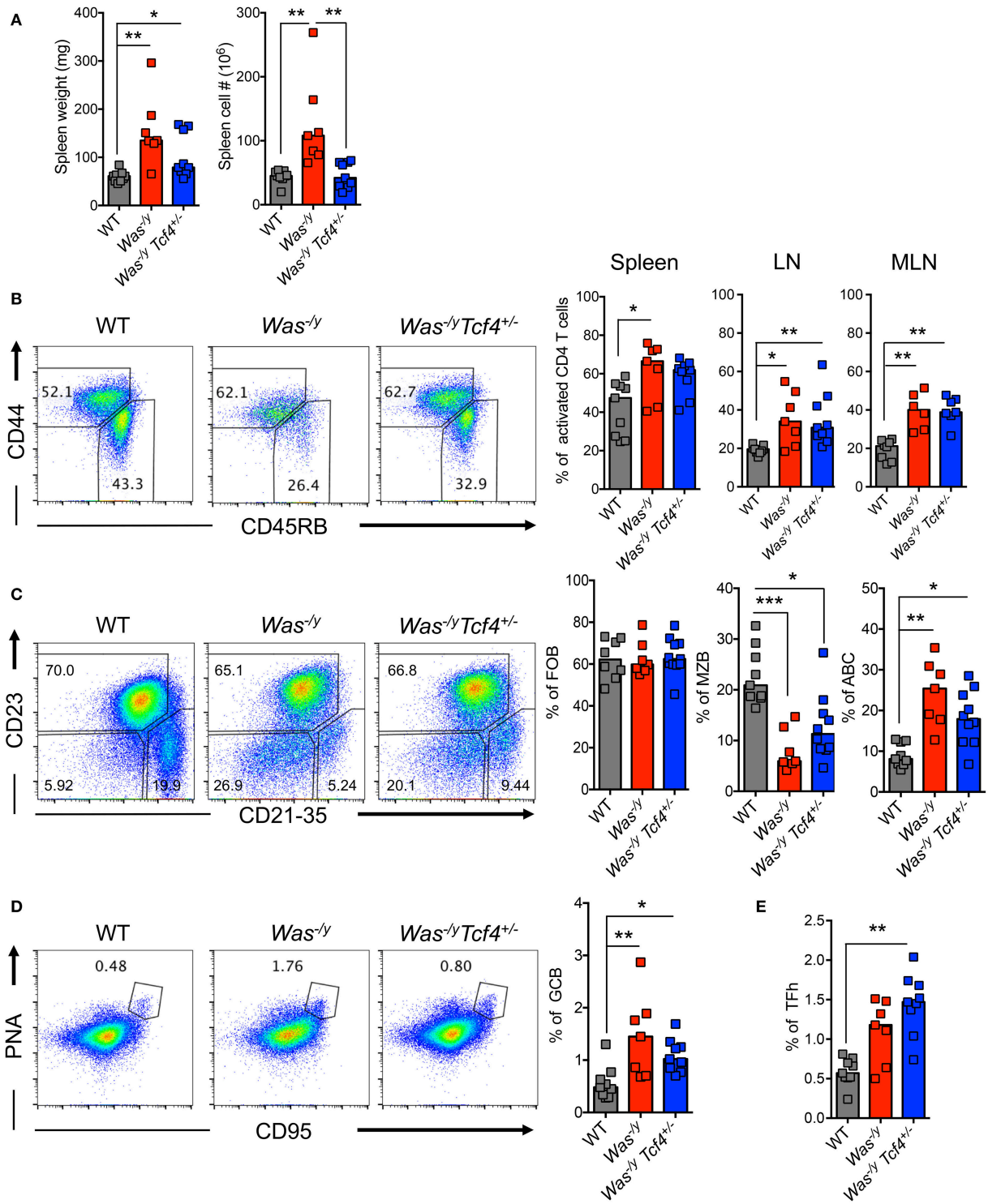

FIGURE 2 | No change in overall immune activation upon *Tcf4* haplodeficiency in *Was*-deficient mice. Analysis of WT, *Was*$^{-/y}$ or *Was*$^{-/y}$ *Tcf4*$^{+/-}$ mice at 30 weeks of age. **(A)** Spleen weight and cellularity were measured from individual mice. **(B–E)** T and B lymphocyte populations within the spleen were analyzed by flow cytometry. **(B)** The frequency of both naïve (CD44^{-}, CD45RB^{+}) and activated (CD44^{+}, CD45RB^{-}) cells among live CD4^{+} T cells was determined in the spleen, LN and MLN of the indicated animals. **(C)** The frequency of follicular B cells (FOB, CD23^{+}, CD21^{-}), marginal zone B cells (MZB, CD23^{-}, CD21^{+}) and age associated B cells (ABC, CD23^{-}, CD21^{-}) among mature B220^{+} CD93^{-} B cells was measured. **(D)** Analysis of germinal center B cells (GCB, PNA^{+} and CD95^{+} among total B220^{+} B cells) and **(E)** T follicular helper cell (TFh, CXCR5^{+}, PD1^{+}, and BCL6^{+} among CD4^{+} T cells) frequencies. Values from individual animals are shown and horizontal bars represent median. Data were pooled from 4 independent experiments and statistical significance estimated by Kruskal-Wallis test followed by a *post-hoc* Dunn's multiple comparison test is indicated as follows $^{*}P \leq 0.05$, $^{**}P \leq 0.01$, $^{***}P \leq 0.001$.

largely unaffected by *Tcf4* haplodeficiency (**Figure 3C**). Similar results were observed from the quantification of autoreactive IgM (**Figure S3**). Importantly, *Tcf4* haplodeficiency in *Sle1.Sle3* lupus prone mice strongly reduced the levels of most autoreactive IgGs (**Figure 3C**), consistent with our previous observation (13). Collectively these results demonstrate that pDC impairment due to *Tcf4* haplodeficiency does not impact the production of autoantibodies in *Was*-deficient animals.

Tcf4 Haplodeficiency Does not Affect Colitis Development in *Was*-Deficient Mice

In addition to systemic autoimmunity, WASP-deficient individuals (10%) and mice (100%) develop spontaneous colitis (43). Colitis development in animals lacking WASP is mediated by $CD4^+$ T cells (44) and facilitated by innate immune cells (45). Therefore, we studied whether pDC impairment affects colitis development in *Was*-deficient mice. Mice were analyzed at 6 months of age, and at that time they did not show rectal prolapse, rectal bleeding or major weight loss (not shown). However, the colon length of $Was^{-/y}$ mice was significantly shorter than that of WT control animals (**Figures 4A,B**). The reduction in colon length, which is a sign of colonic inflammation, was similar in $Was^{-/y}$ $Tcf4^{+/-}$ mice (**Figures 4A,B**). Histological analysis of the large intestine of $Was^{-/y}$ and $Was^{-/y}$ $Tcf4^{+/-}$ mice showed severe colitis (**Figure 4C**). Irrespectively of *Tfc4*-haplodeficiency, colons of *Was*-deficient animals exhibited diffuse leukocyte infiltration, epithelial dysplasia and crypt dropout (**Figure 4D**). While $CD4^+$ T cells were previously described as the main constituents of this leukocyte infiltration [43], we also noted an accumulation of plasma cells (black arrows) and Russell bodies (plasma cells accumulating Ig, white arrows) in the colon of $Was^{-/y}$ and $Was^{-/y}$ $Tcf4^{+/-}$ mice (**Figure 4D**). Similar levels of colonic inflammation were observed in mice that were analyzed at 10 months of age (not shown). These results indicate that *Tcf4* haplodeficiency, which specifically impairs pDC numbers and function, does not prevent the development of colitis in *Was*-deficient mice. The expression of IFN-inducible marker Sca-1 on lymphocytes is a faithful marker of aberrant IFN signaling (46) and was specifically reduced by *Tcf4* haplodeficiency in SLE-prone mice (13). In contrast, we did not observe any increase in Sca1 expression on T and B cells from $Was^{-/y}$ mice compared to WT controls (**Figure S4A**). In addition, the expression profile of IFN-I inducible genes in the spleen (**Figure S4B**) and the colon (**Figure S4C**) were similar in WT control mice and $Was^{-/y}$ mice regardless of their *Tcf4* status. Overall, genetic impairment of pDCs did not affect autoimmunity or IBD caused by *Was* deficiency suggesting that these cells are largely dispensable in this model.

Conditional Deletion of *Tcf4* Depletes pDCs in *Il10*-Deficient Mice

Because *Tcf4* haplodeficiency results in only a partial impairment of pDCs, we sought to examine the effect of a more profound pDC depletion on colitis. To this end, we used mice in which conditional (floxed) alleles of *Tcf4* are combined with a DC-specific *Itgax* (CD11c)-Cre deleter strain (35). As *Tcf4* is not expressed by cDCs, *Itgax*-Cre mediated deletion of *Tcf4* affects only pDCs and causes their profound constitutive depletion (15). We crossed the DC-specific *Tcf4* conditional knockout (CKO) strain with *Il10*-deficient mice ($Il10^{-/-}$) that develop colitis resembling human IBD (33). Although colitis in *IL10*-deficient humans develops early in childhood, in *Il10*-deficient mice on pure C57BL/6J background, colitis only occurs in adult animals and in a milder form of disease than observed in other genetic backgrounds [47]. We next analyzed $Il10^{-/-}$ *Itgax*-Cre^- $Tcf4^{flox/flox}$ ($Il10^{-/-}$ $Tcf4^{Fl/Fl}$), $Il10^{-/-}$ *Itgax*-Cre^+ $Tcf4^{flox/flox}$ ($Il10^{-/-}$ $Tcf4^{CKO}$), and $Il10^{+/+}$ $Tcf4^{Fl/Fl}$ (WT) control mice at 3 months of age to evaluate the impact of such targeting on pDC distribution. The frequency of pDCs was consistently reduced in the spleen and MLNs of $Il10^{-/-}$ $Tcf4^{CKO}$ mice compared to both WT and $Il10^{-/-}$ $Tcf4^{Fl/Fl}$ controls (**Figures 5A,B**). This reduced frequency was associated with significantly lower absolute numbers of pDCs in the spleen and MLNs of $Il10^{-/-}$ $Tcf4^{CKO}$ mice compared to controls (**Figure 5B**). Although conditional loss of *Tcf4* had a slight effect on the frequency of overall cDCs in the spleen compared to WT controls, there was no impact on the absolute numbers or other detectable change in the subsets of cDCs (**Figures S5A,B**). An increased number of cDCs as well as variation in the frequency and numbers of cDC subsets were observed in the MLN upon *Il10* deficiency and were independent of the conditional loss of *Tcf4* (**Figure S5B**). Thus, conditional deletion of *Tcf4* in mice that are deficient for *Il10* causes specific and constitutive pDC ablation.

pDC Depletion Does not Affect the Aberrant Immune Activation in *Il10*-Deficient Mice

In contrast to *Was*-deficient mice, $Il10^{-/-}$ mice do not show major signs of systemic autoimmunity. Indeed, T and B cells develop normally and no aberrant production of autoantibodies is detected in mice that lack IL-10 [33]. Although $Il10^{-/-}$ $Tcf4^{Fl/Fl}$ and $Il10^{-/-}$ $Tcf4^{CKO}$ animals had a minor splenomegaly compared to WT controls, there was no difference in spleen cellularity (**Figure 6A**). However, $Il10^{-/-}$ $Tcf4^{Fl/Fl}$ mice consistently showed an increase in MLN cell numbers that is associated with intestinal inflammation and was also detected in $Il10^{-/-}$ $Tcf4^{CKO}$ animals (**Figure 6B**). The increased MLN cellularity was primarily associated with significantly increased numbers of T and B cells (**Figure 6B**). In addition, we observed a modest increase in $CD4^+$ T cell activation in the MLN, but not the spleen, of $Il10^{-/-}$ $Tcf4^{CKO}$ mice (**Figure S6A**). Although alterations in the frequency of B cell subsets in the spleen were detected in *Il10*-deficient animals regardless of *Tcf4* status compared to WT control, the absolute numbers for each B cell subset show no major differences across all the analyzed mice (**Figure S6B**). Despite the trend of reduced frequency, the number of GCBs was significantly increased in the MLN in $Il10^{-/-}$ $Tcf4^{CKO}$ animals due to the increased MLN cellularity (**Figure S6B**). T and B cells both in the spleen and MLN of $Il10^{-/-}$ $Tcf4^{Fl/Fl}$ mice showed increased expression

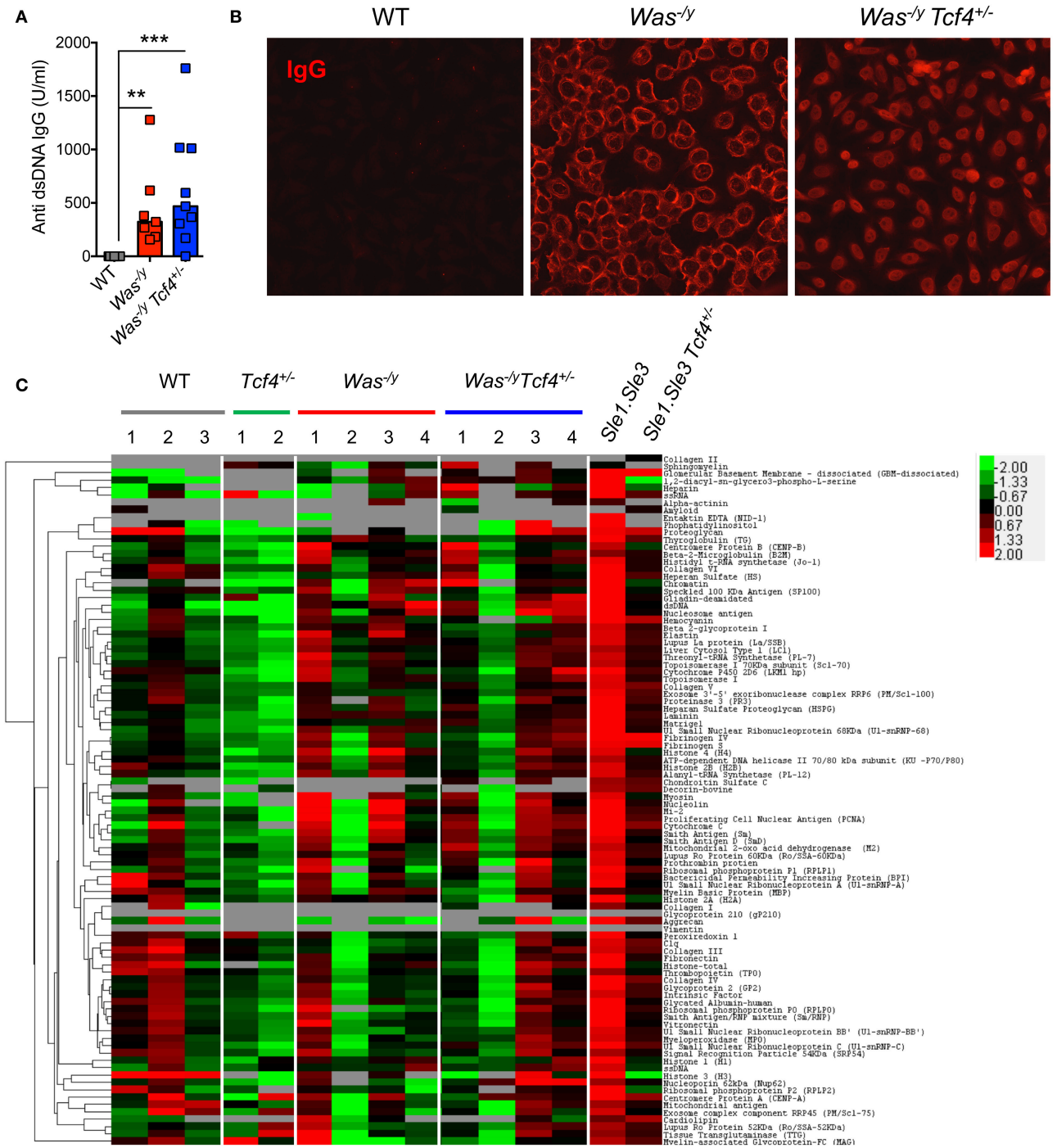

FIGURE 3 | *Tcf4* haplodeficiency does not affect autoreactive antibody production in *Was*-deficient mice. Sera from WT, *Was*$^{-/y}$, or *Was*$^{-/y}$ *Tcf4*$^{+/-}$ mice were obtained at 30 weeks of age and analyzed for autoreactive antibody production. **(A)** Anti-dsDNA IgG levels in the sera of indicated mice were determined by ELISA. Data were pooled from 4 independent experiments and bars represent the median. **(B)** ANA staining of IgG (red) using fixed Hep-2 cells following incubation with the sera of mice with the indicated genotype as analyzed by fluorescent microscopy. Images are representative of 2 independent staining experiments that include 6 animals for each genotype. **(C)** IgG autoreactivity in the indicated mice at 30 weeks of age as measured by an antigen array. Shown are heat maps of the relative IgG seroreactivity to the indicated antigens. Statistical significance estimated by Kruskal-Wallis test followed by a *post-hoc* Dunn's multiple comparison test is indicated as follows $^{**}P \leq 0.01$, $^{***}P \leq 0.001$.

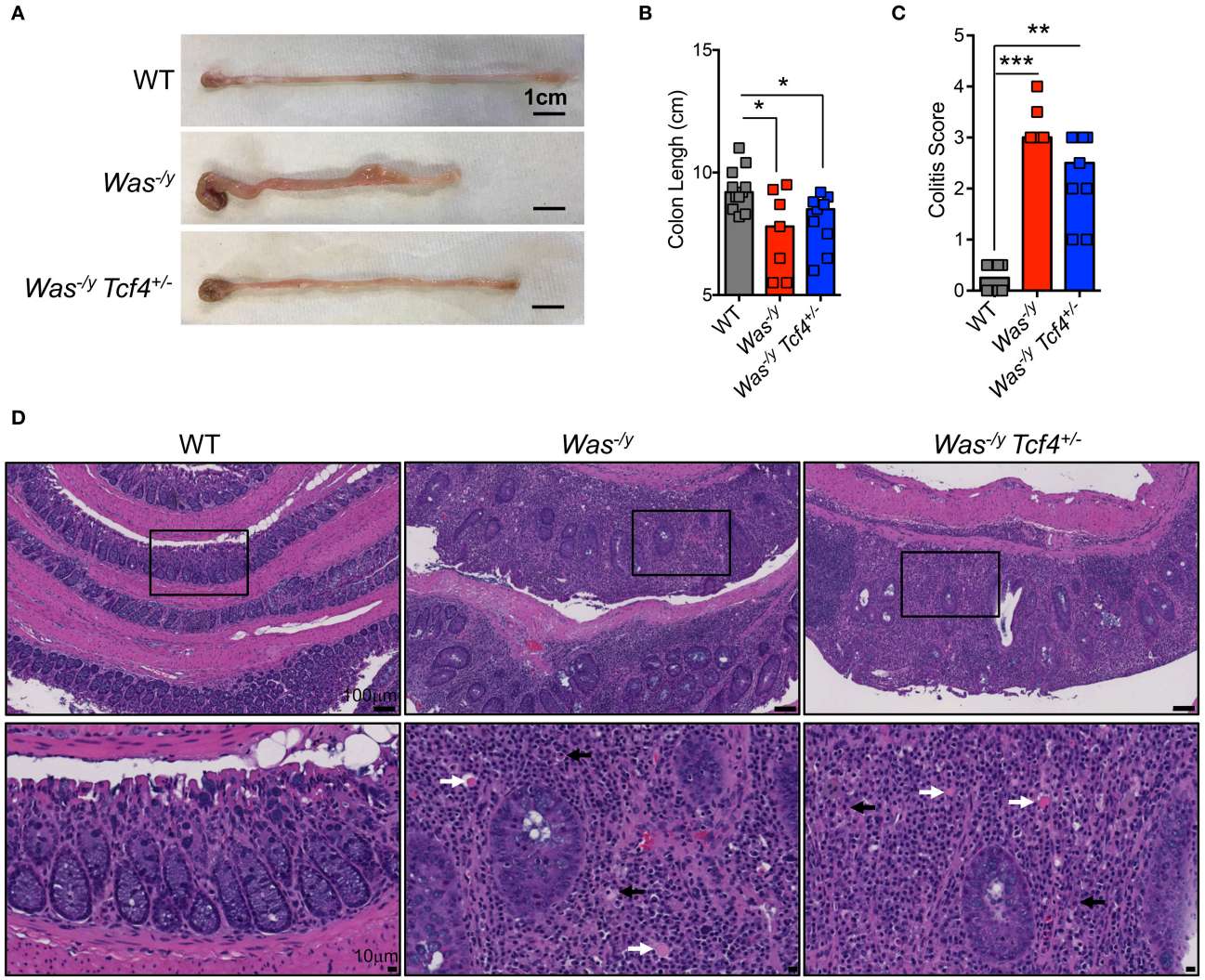

FIGURE 4 | No significant impact of *Tcf4* haplodeficiency on colitis development in *Was*-deficient mice. WT, *Was*$^{-/y}$ or *Was*$^{-/y}$ *Tcf4*$^{+/-}$ mice were analyzed at 30 weeks of age. **(A)** Representative pictures of colon (scale bars, 1 cm) and **(B)** colon lengths from individual mice of the indicated genotype are shown. Bars represent median value. Data were pooled from 4 independent experiments. **(C)** Histopathological scores of the colon pathology were determined from individual indicated animals. Bars represent the median, and data were pooled from 3 independent experiments. **(D)** Colon paraffin sections of the indicated mice were stained by hematoxylin and eosin (H&E) and analyzed by microscopy. Upper panels taken at 10X magnification (scale bar, 100 µm) and lower panels show a 40X magnification (scale bar, 10 µm) of the indicated area (square). In the magnified panels, black arrows indicate plasma cells and white arrows Russell bodies. Images are representative of at least 5 animals in each group from 3 independent experiments. Statistical significance estimated by Kruskal-Wallis test followed by a *post-hoc* Dunn's multiple comparison test is indicated as follows $^{*}P \leq 0.05$, $^{**}P \leq 0.01$, $^{***}P \leq 0.001$.

of Sca1, and such increased Sca1 expression was also found in *Il10*$^{-/-}$ *Tcf4*^{CKO} mice (**Figures 6C,D**). Sca1 was previously described to be a reliable marker of elevated IFN signaling (46), and we have recently confirmed that Sca1 expression is abolished in *Ifnar*-deficient T and B cells (our unpublished data). Therefore, the induction of Sca1 in *Il10*$^{-/-}$ mice independently of *Tcf4* ablation suggests that pDCs are not the major source of the aberrant IFN-I signaling induced by *Il10* deficiency. These results demonstrate that profound pDC depletion does not affect the immune activation observed in *Il10*-deficient mice.

pDC Depletion Does not Prevent the Development of Colitis in *Il10*-Deficient Mice

As expected, *Il10* deficiency was associated with the development of rectal prolapse. Indeed, 2 out of 8 *Il10*$^{-/-}$ *Tcf4*$^{Fl/Fl}$ mice and 3 out 8 *Il10*$^{-/-}$ *Tcf4*^{CKO} mice showed rectal prolapse, while none of the 7 WT control mice did (**Figure 7A**). Rectal prolapse only occurred in adult animals when they were older than 2.5 months (**Figure 7B**). In addition, *Il10*$^{-/-}$ *Tcf4*$^{Fl/Fl}$ mice displayed a significant shortening of their colon, indicating the presence of colonic inflammation (**Figure 7C**). Although

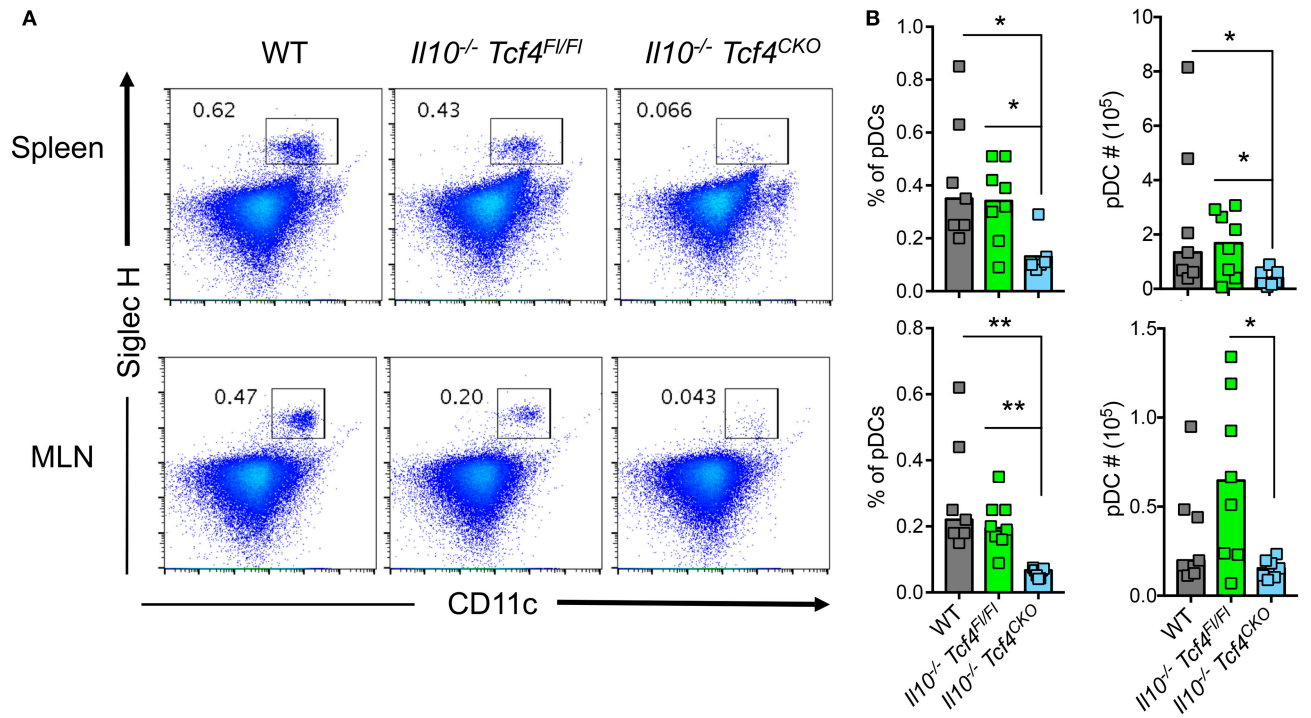

FIGURE 5 | DC-specific deletion of *Tcf4* significantly depletes pDCs in *Il10*-deficient mice. *Il10*$^{-/-}$ *Itgax*-Cre^{-} *Tcf4*$^{flox/flox}$ (*Il10*$^{-/-}$ *Tcf4*$^{Fl/Fl}$) or *Il10*$^{-/-}$ *Itgax*-Cre^{+} *Tcf4*$^{flox/flox}$ (*Il10*$^{-/-}$*Tcf4*^{CKO}) littermates with DC-specific *Tcf4* CKO were analyzed along WT controls at 15 weeks of age. **(A,B)** pDCs were analyzed by flow cytometry of cells from the spleen and MLN. The frequency of CD11b^{-} CD11c^{+} Siglec H^{+} pDCs is indicated in each plot. **(B)** Frequency and absolute numbers of CD11b^{-} CD11c^{+} Siglec H^{+} pDCs among total live cells in the spleen and MLN of individual animals are shown, and horizontal bars indicate the median. Data represent 3 independent experiments. Statistical significance estimated by Kruskal-Wallis test followed by a *post-hoc* Dunn's multiple comparison test is indicated as follows *$P \leq 0.05$, **$P \leq 0.01$.

more variability among animals was observed, a trend for reduced colon length was also observed in *Il10*$^{-/-}$ *Tcf4*^{CKO} mice (**Figure 7C**). We next performed histological analysis of the colon sections and observed a significantly increased pathological scores in both *Il10*$^{-/-}$ *Tcf4*$^{Fl/Fl}$ and *Il10*$^{-/-}$ *Tcf4*^{CKO} animals compared to WT ones (**Figure 7D**). Colon pathology in *Il10*$^{-/-}$ *Tcf4*$^{Fl/Fl}$ and *Il10*$^{-/-}$ *Tcf4*^{CKO} mice included massive leukocyte infiltration, neutrophils within the epithelium and lumen, crypt abscesses, epithelial dysplasia, and crypt damage (**Figure 7E**). Collectively, these histological features are characteristic of the substantial colonic inflammation caused by loss of IL-10, and their development was unaffected by specific pDC depletion.

DISCUSSION

We have explored the function of pDCs in IBD pathogenesis in mice that lack WASP or IL-10 and consequently spontaneously develop colitis. We observed that specific abrogation of pDCs does not impact the development of IBD *in vivo* in either model. The specific deletion of pDCs was achieved through targeting of the transcription factor TCF4, which is the master regulator of pDC fate and maintenance (32, 39). Indeed, we established a global monoallelic deletion of *Tcf4* in *Was*-deficient mice that causes a constitutive reduction in pDC numbers and a DC-specific loss of *Tcf4* in *Il10-deficient* mice inducing a complete and constitutive pDC abrogation. Such targeting of pDCs has been extensively analyzed previously. Indeed, we have shown that *Tfc4* haplodeficiency strongly impairs pDC ability to produce IFN-I in response to CpG-ODN A (32) and pushes them toward a "cDC-like" phenotype (32, 39). In addition, conditional ablation of *Tcf4* was also reported to reduce pDCs numbers and ablate pDCs-driven IFN-I response upon viral infections (48). The great majority of these studies revealed that cDCs are not affected by *Tcf4* haplodeficiency nor its complete conditional ablation, demonstrating the specificity of this system for targeting pDCs. *Tcf4* haplodeficiency and conditional targeting were also shown to ameliorate the development of SLE (13) and type 1 diabetes (15) *in vivo*, confirming key roles for pDCs in such pathologies. Finally, an identical *Tcf4* targeting was also used to rule out the involvement of pDCs in an experimental model of psoriasis (49), and we now extend these observations to genetic models of IBD.

WASP regulates leukocyte actin dynamics, controlling migration and a variety of effector functions (50). Deficiency in WASP causes the X-linked Wiskott-Aldrich syndrome that is associated with aberrant systemic immune activation and colitis in 10% of individuals. The aberrant systemic autoimmunity is recapitulated in mice that lack WASP, which unlike humans

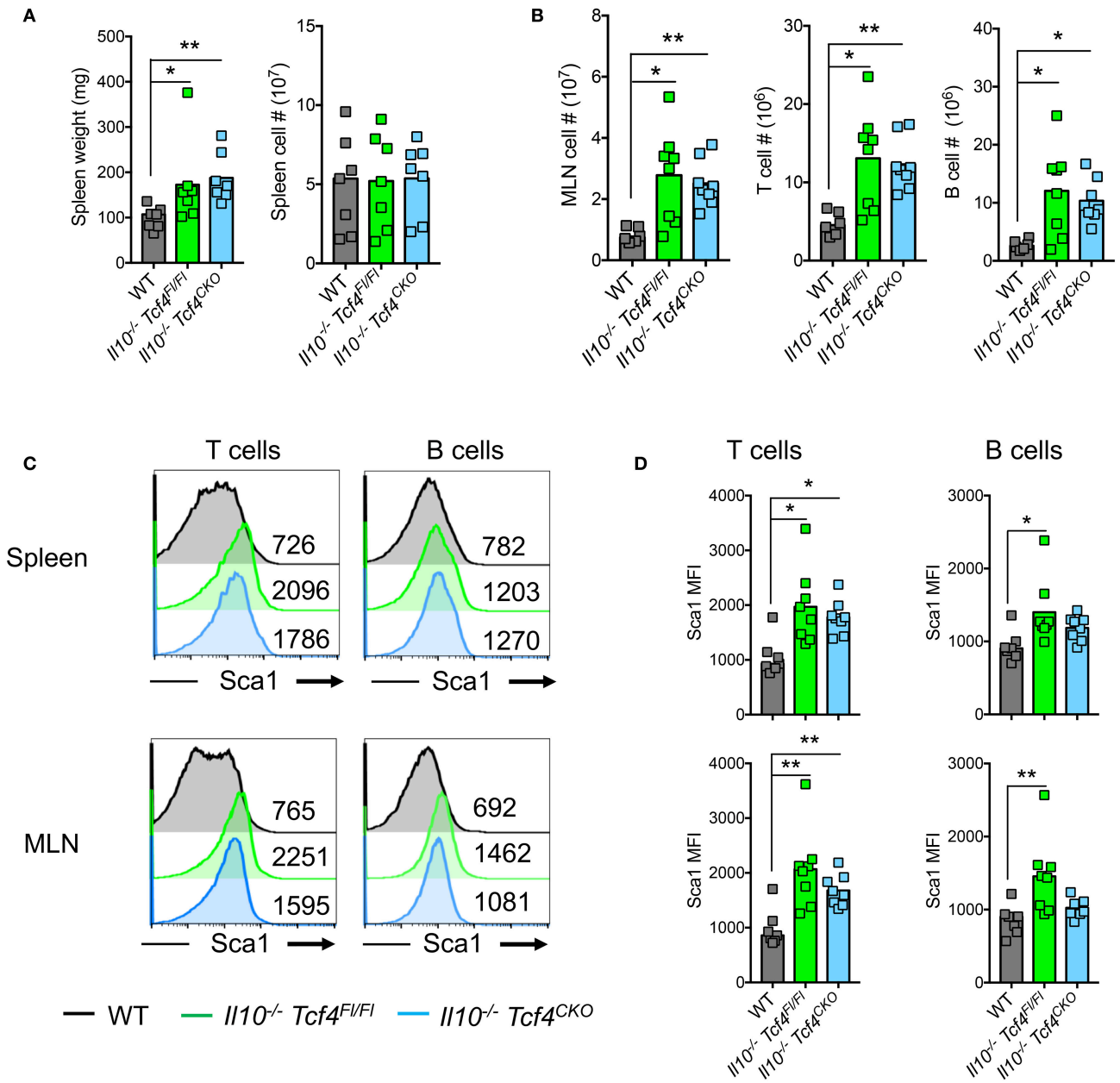

FIGURE 6 | DC-specific deletion of *Tcf4* does not impact the overall immune activation in *Il10*-deficient mice. $Il10^{-/-}$ *Itgax*-Cre^{-} $Tcf4^{flox/flox}$ ($Il10^{-/-}$ $Tcf4^{Fl/Fl}$) or $Il10^{-/-}$ *Itgax*-Cre^{+} $Tcf4^{flox/flox}$ ($Il10^{-/-}Tcf4^{CKO}$) littermates with DC-specific *Tcf4* CKO were analyzed along WT controls at 15 weeks of age. **(A)** Spleen weight and cellularity of individual animals were measured. **(B)** MLN cellularity and the absolute numbers of ($TCR\beta^{+}$) T cells and ($B220^{+}$) B cells were determined by flow cytometry from individual mice. **(C,D)** Sca1 expression on ($TCR\beta^{+}$) T cells and ($B220^{+}$) B cells from the spleen and MLNs was assessed by flow cytometry. **(C)** Histograms show representative analysis of Sca1 expression and the MFI of Sca1 is indicated in each plot and **(D)** plots show Sca1 MFI of individual animals. In all plots, horizontal bars represent the median. Data for all panels pooled from 3 independent experiments. Statistical significance estimated by Kruskal-Wallis test followed by a *post-hoc* Dunn's multiple comparison test is indicated as follows $^{*}P \leq 0.05$, $^{**}P \leq 0.01$.

develop colitis with 100% penetrance, thus representing a relevant experimental model of IDB. While *Tcf4* haplodeficiency in *Was*-deficient mice specifically reduced pDC numbers it did not affect the heightened activation of immune responses or the development of colitis. These results differ from observations obtained in animal models of SLE in which pDC targeting ameliorated the overall pathology (12, 13). The observed difference in the effect of pDC ablation between these two diseases models is likely due to T and B cell-intrinsic functions of WASP. Indeed, conditional *Was*-deficiency in B cells is sufficient for the induction of B cell hyperactivation, loss of MZB and aberrant production of autoantibodies directed against a

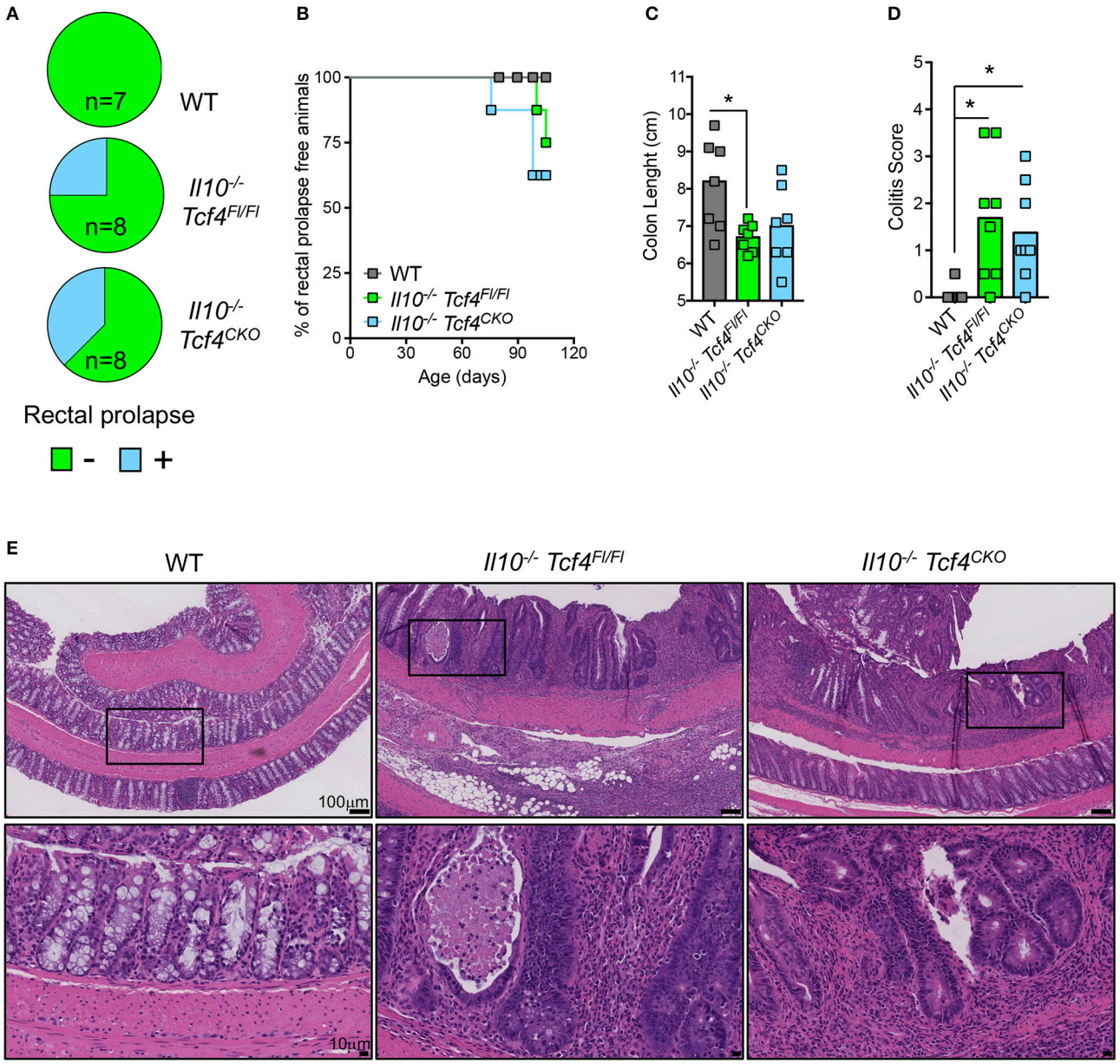

FIGURE 7 | DC-specific deletion of *Tcf4* does not prevent colitis development in *Il10*-deficient mice. *Il10*$^{-/-}$ *Itgax*-Cre^{-} *Tcf4*$^{flox/flox}$ (*Il10*$^{-/-}$ *Tcf4*$^{Fl/Fl}$) or *Il10*$^{-/-}$ *Itgax*-Cre^{+} *Tcf4*$^{flox/flox}$ (*Il10*$^{-/-}$*Tcf4*^{CKO}) littermates with DC-specific *Tcf4* CKO were analyzed along WT controls at 15 weeks of age. **(A)** Rectal prolapse in animals of the indicated genotype. Data are represented as pie charts indicating the frequency of animals with (blue) and without (green) rectal prolapse. **(B)** Kaplan-Meier plot indicating the percentage of rectal prolapse free mice over time in the indicated genotype (n = 8/genotype). **(C)** Colon lengths from individual mice of the indicated genotype. Data were pooled from 3 independent experiments and horizontal bars represent the median. **(D)** Histopathological scores of the colon pathology were determined from individual indicated animals. Bars represent the median and data were pooled from 3 independent experiments. **(E)** Colon paraffin sections of the indicated mice were stained by H&E and analyzed by microscopy (scale bars, 100 µm). Upper panels represent a 10X magnification (scale bar, 100 µm) and lower panels show a 40X magnification (scale bar, 10 µm) of the indicated area (square). Images are representative of 6 animals in each group from 3 independent experiments. Statistical significance estimated by Kruskal-Wallis test followed by a *post-hoc* Dunn's multiple comparison test is indicated as follows $^{*}P \leq 0.05$.

variety of self-molecules including DNA (40). Although, TCF4 is also expressed at low levels in B cells we did not observe significant differences in B cell phenotype and function between *Was*$^{-/y}$ *and Was*$^{-/y}$ *Tcf4*$^{+/-}$ mice ruling out B cell-intrinsic effect of *Tcf4* haplodeficiency. This conclusion is also supported by our previous observation and two recently published reports showing respectively that *Tcf4* haplodeficiency (32) and conditional deletion specifically in B cells (51, 52) did not affect their overall development, phenotype or function. The absence of a B cell intrinsic TCF4 function is thought to be due to its redundancy with the homologous E protein E2a (encoded by *Tcf3*) (51, 52). In addition, WASP also regulates the function of

T cells (43), particularly the suppressive potential of Tregs (53). Accordingly, transfer of *Was*-deficient $CD4^+$ T cells into *Rag2*-deficient mice is sufficient to induce colitis (44). *Was*-deficient innate immune cells were also suggested to exacerbate colitis after the observation that the transfer of WT naïve CD4 T cells in *Was/Rag1* double-deficient mice induced a more severe colitis compared to their transfer into *Rag1*-deficient mice (45). It was recently shown that conditional *Was*-deficiency in macrophages but not in DCs (including pDCs) in the *Rag1*-deficient recipients led to the aggravation of such intestinal inflammation upon transfer of WT naïve $CD4^+$ T cells (54). These results thus indicate that the IBD pathogenesis upon naïve $CD4^+$ T cell transfer into *Was/Rag1* double-deficient mice is mainly driven by macrophages. However, the specific contributions of both macrophages and DCs to spontaneous colitis development in *Was*-deficient mice remains to be established. Finally, WAS patients were reported to display elevated serum levels of IFN-I as well as an IFN-I signature, reflected by the increased expression of IFN-I stimulated genes in PB leukocytes (29). IFN-I causing this signature was proposed to originate from pDCs after identifying that pDCs from WAS patients or *Was*-deficient mice were more responsive to TLR9 stimulation and as a result produced elevated levels of IFN-I (29). We were unable to detect an IFN-I signature as measured by the expression of IFN-I stimulated genes in *Was*-deficient animals and thus could not establish a link between pDCs and the aberrant IFN-I signature observed in WAS patients. These observations are consistent with previous reports showing that contrary to human SLE patients, murine models of SLE do not manifest a prominent IFN-I signature (13, 55) despite considerable evidence for IFN-I signaling in the pathogenesis of SLE *in vivo* (56, 57). Therefore, the lack of an observable IFN-I signature does not rule out the role of IFN-I and pDCs in murine models of autoimmunity. It is possible that a detectable IFN-I signature may have preceded the onset of disease (58) but was not present at late stages of the diseases (6 months) when we measured it in *Was*-deficient mice.

We also studied the role of pDCs during IBD pathogenesis in *Il10*-deficient mice. These mice are unable to produce the anti-inflammatory cytokine IL-10, which is essential for the control of immune responses and thus prevents colitis development. We specifically depleted pDCs using conditional targeting of both alleles of *Tcf4* mediated by *Itgax*-Cre in $Il10^{-/-}$ mice. Although this strategy profoundly diminished the pool of pDCs in $Il10^{-/-}$ mice, we did not detect any major impact on the development of colitis. The $Il10^{-/-}$ mice are considered the gold standard colitis model that closely recapitulates human IBD. Mutations in *IL10* or the genes encoding its receptors *IL10RA/IL10RB* in humans were shown to cause autosomal recessive disease with CD-like colitis (59) and GWAS studies have identified associations between these three genes and sporadic IBD (60). While *IL10* and *IL10R* deficiency in humans induces a severe IBD that occurs early in childhood, the severity of IBD in *Il10*-deficent mice is strongly dependent on the genetic background as well as the husbandry conditions (47). In our study *Il10*-deficient mice were kept on a pure C57BL/6J background and housed in Specific Pathogen Free (SPF) conditions, both of which are factors associated with an attenuated IBD phenotype that is initiated only in adult animals. Therefore, our results provide strong genetic evidence in an experimental model of adult IBD with clear relevance to the human pathology that pDCs are dispensable in colitis pathogenesis. These results are in accordance with the observation that specific loss of *Il10ra* in macrophages is sufficient to phenocopy the global *Il10* deficiency (61). Indeed, IL-10 appears to act primarily on macrophages to prevent the development of colitis. This protective role of IL-10 was recently attributed to its ability to induce the metabolic reprogramming of macrophages subsequently preventing their aberrant production of IL-1β (62).

In contrast to our observations, pDCs were previously proposed to play an important role in colitis, exacerbating the overall IBD pathogenesis (29, 30). Using Siglec-H DTR knock in mice to inducibly deplete pDCs following DT treatment, Arimura *et al*. concluded that pDC depletion ameliorates DSS-induced colitis (30). In these settings pDCs were proposed to play an important role in the recruitment of pro-inflammatory monocytes and macrophages into the inflamed intestinal epithelium, consequently exacerbating the disease (30). Such discrepancies with our observations may be due to the use of different models of colitis and systems for pDC ablation. We used genetic IBD models that are T cell-dependent while Arimura et al. used T cell-independent DSS-induced colitis that arises from disruption of the intestinal barrier, which allows the entry of luminal microbes into the intestinal mucosa and consequently activates innate immune responses (63). Furthermore, Siglec H is not restricted to pDCs and was shown to be expressed on a subset of intestinal macrophages (31). Therefore, treatment of Siglec-H-DTR mice with DT should not only deplete pDCs but also a population of intestinal macrophages that may participate in the disease induced by DSS. In addition, pDCs were also suggested to contribute to development of IBD in *Was*-deficient mice (29). Prete et al. found that pDCs lacking *Was* produce heightened levels of IFN-I and that *Ifnar*-deletion in *Was*-deficient mice reduced the overall pathology including colitis (29). Although these results indicate an important role of IFN-I signaling in colitis development in *Was*-deficient mice, whether pDCs are the major source of this pathogenic IFN-I was not established. Our results demonstrating no impact of *Tcf4* specific targeting on the occurrence and the severity of colitis in *Was*-deficient animals argue against an important role of pDCs in this process.

Overall pDCs appear to be dispensable for disease development in common monogenic models of IBD. They may have a minor role in IBD that arises upon destruction of the intestinal barrier by environmental factors such as DSS. In this model pDCs do not appear to be the main effectors of IBD development, but rather exacerbate the disease [30]. Nevertheless, pDCs may contribute to the development of colitis when aberrantly activated. Accordingly, specific ablation of the inhibitory protein tyrosine phosphatase receptor type S (PTPRS) on pDCs was associated with the development of mild intestinal inflammation in mice (64). Lack of PTPRS on pDCs resulted in spontaneous IFN-I production by pDCs, which may be involved in establishing this inflammation. pDCs were also suggested to promote tolerance and ameliorate IBD upon stimulation

by enteric viruses (65). While enteric viruses activate pDC production of IFN-I *ex-vivo* (65), direct *in vivo* evidence for pDC functions in the prevention of colitis development after infection with enteric viruses has not been demonstrated. Similarly, it was shown that IFN-I production resulting from CpG-ODN A stimulation protects mice from the development of experimental and spontaneous models of IBD induced by DSS treatment and *Il10*-deficiency, respectively (66, 67). The preventive impact of CpG-ODN A treatment on the overall IBD pathogenesis was shown to depend on IFNAR and TLR9 signaling (66, 67). However, whether pDCs play an important role in this process was not addressed. Therefore, it appears that IFN-I plays a controversial role in IBD, either contributing to the disease when aberrantly produced in a chronic manner or ameliorating the disease when acutely stimulated. The function of IFN-I in IBD thus needs further clarification as well as the role of pDCs as a source of such IFN-I. On the other hand, independently of IFN-I, pDCs were shown to mediate the protective role of PSA in IBD pathogenesis induced by intra-rectal administration of the haptenating agent 2,4,6-trinitrobenzene sulfonic acid (TNBS) (24). Indeed, selective depletion of pDCs following DT treatment of BDCA-2-DTR transgenic mice (68) abrogated the beneficial effect of PSA on IBD pathogenesis (24). This protective function of pDCs was only observed after PSA treatment whereas pDC depletion alone did not ameliorate colitis. These data indicate that pDCs are not essential in IBD pathogenesis, but their targeting by PSA may prevent colitis development, most likely through their ability to stimulate $CD4^+$ T cell production of IL-10 (24).

Characterization of the deleterious role of pDCs in multiple autoimmune disorders such as SLE (12, 13), systemic sclerosis (14), and type I diabetes (15) has led to the development of novel therapeutic strategies aimed at specifically depleting pDCs (17). Our results indicate that such therapies may not benefit IBD patients. On the other hand, the observation that pDC-specific deletion does not impact IBD pathogenesis suggests that therapeutic pDC depletion will not be associated with off-target effects within the gastrointestinal tract of treated individuals.

AUTHOR CONTRIBUTIONS

BR, MS, and RK initiated and supervised the project. CS, VS, MS, and BR designed experiments, analyzed, and interpreted results. CS and VS performed experiments with the help of LS, GJ, and AR. AN performed the histological analysis. The manuscript was written by CS, VS, and BR with the input from all authors.

ACKNOWLEDGMENTS

Supported by research grant from Medimmune, LLC; NIH grant AI072571 and the Colton Center for Autoimmunity (BR); and the Cancer Research Institute Postdoctoral Fellowship (VS).

SUPPLEMENTARY MATERIAL

The Supplementary Material for this article can be found online at: https://www.frontiersin.org/articles/10.3389/fimmu.2018.02475/full#supplementary-material

REFERENCES

1. Reizis B, Bunin A, Ghosh HS, Lewis KL, Sisirak V. Plasmacytoid dendritic cells: recent progress and open questions. *Annu Rev Immunol.* (2011) 29:163–83. doi: 10.1146/annurev-immunol-031210-101345
2. Swiecki M, Colonna M. The multifaceted biology of plasmacytoid dendritic cells. *Nat Rev Immunol.* (2015) 15:471–85. doi: 10.1038/nri3865
3. Ganguly D, Chamilos G, Lande R, Gregorio J, Meller S, Facchinetti V, et al. Self-RNA-antimicrobial peptide complexes activate human dendritic cells through TLR7 and TLR8. *J Exp Med.* (2009) 206:1983–94. doi: 10.1084/jem.20090480
4. Garcia-Romo GS, Caielli S, Vega B, Connolly J, Allantaz F, Xu Z, et al. Netting neutrophils are major inducers of type I IFN production in pediatric systemic lupus erythematosus. *Sci Transl Med.* (2011) 3:73ra20. doi: 10.1126/scitranslmed.3001201
5. Ghosh AR, Bhattacharya R, Bhattacharya S, Nargis T, Rahaman O, Duttagupta P, et al. Adipose recruitment and activation of plasmacytoid dendritic cells fuel metaflammation. *Diabetes.* 2016:3440–52. doi: 10.2337/db16-0331
6. Lande R, Ganguly D, Facchinetti V, Frasca L, Conrad C, Gregorio J, et al. Neutrophils activate plasmacytoid dendritic cells by releasing self-DNA-peptide complexes in systemic lupus erythematosus. *Sci Transl Med.* (2011) 3:73ra19. doi: 10.1126/scitranslmed.3001180
7. Lande R, Gregorio J, Facchinetti V, Chatterjee B, Wang YH, Homey B, et al. Plasmacytoid dendritic cells sense self-DNA coupled with antimicrobial peptide. *Nature* (2007) 449:564–9. doi: 10.1038/nature06116
8. Means TK, Latz E, Hayashi F, Murali MR, Golenbock DT, Luster AD. Human lupus autoantibody-DNA complexes activate DCs through cooperation of CD32 and TLR9. *J Clin Invest.* (2005) 115:407–17. doi: 10.1172/JCI23025
9. Bave U, Magnusson M, Eloranta ML, Perers A, Alm GV, Ronnblom L. Fc gamma RIIa is expressed on natural IFN-alpha-producing cells (plasmacytoid dendritic cells) and is required for the IFN-alpha production induced by apoptotic cells combined with lupus IgG. *J Immunol.* (2003) 171:3296–302. doi: 10.4049/jimmunol.171.6.3296
10. Baechler EC, Batliwalla FM, Karypis G, Gaffney PM, Ortmann WA, Espe KJ, et al. Interferon-inducible gene expression signature in peripheral blood cells of patients with severe lupus. *Proc Natl Acad Sci USA.* (2003) 100:2610–5. doi: 10.1073/pnas.0337679100
11. Bennett L, Palucka AK, Arce E, Cantrell V, Borvak J, Banchereau J, et al. Interferon and granulopoiesis signatures in systemic lupus erythematosus blood. *J Exp Med.* (2003) 197:711–23. doi: 10.1084/jem.20021553
12. Rowland SL, Riggs JM, Gilfillan S, Bugatti M, Vermi W, Kolbeck R, et al. Early, transient depletion of plasmacytoid dendritic cells ameliorates autoimmunity in a lupus model. *J Exp Med.* (2014) 211:1977–91. doi: 10.1084/jem.20132620
13. Sisirak V, Ganguly D, Lewis KL, Couillault C, Tanaka L, Bolland S, et al. Genetic evidence for the role of plasmacytoid dendritic cells in systemic lupus erythematosus. *J Exp Med.* (2014) 211:1969–76. doi: 10.1084/jem.20132522
14. Ah Kioon MD, Tripodo C, Fernandez D, Kirou KA, Spiera RF, Crow MK, et al. Plasmacytoid dendritic cells promote systemic sclerosis with a key role for TLR8. *Sci Transl Med.* (2018) 10. doi: 10.1126/scitranslmed.aam8458
15. Hansen L, Schmidt-Christensen A, Gupta S, Fransen-Pettersson N, Hannibal TD, Reizis B, et al. E2-2 dependent plasmacytoid dendritic cells control autoimmune diabetes. *PLoS ONE* (2015) 10:e0144090. doi: 10.1371/journal.pone.0144090
16. Hannibal TD, Schmidt-Christensen A, Nilsson J, Fransen-Pettersson N, Hansen L, Holmberg D. Deficiency in plasmacytoid dendritic cells and type I interferon signalling prevents diet-induced obesity and insulin resistance in mice. *Diabetologia* (2017) 60:2033–41. doi: 10.1007/s00125-017-4341-0
17. Pellerin A, Otero K, Czerkowicz JM, Kerns HM, Shapiro RI, Ranger AM, et al. Anti-BDCA2 monoclonal antibody inhibits plasmacytoid dendritic cell

activation through Fc-dependent and Fc-independent mechanisms. *EMBO Mol Med.* (2015) 7:464–76. doi: 10.15252/emmm.201404719
18. Wendland M, Czeloth N, Mach N, Malissen B, Kremmer E, Pabst O, et al. CCR9 is a homing receptor for plasmacytoid dendritic cells to the small intestine. *Proc Natl Acad Sci USA*. (2007) 104:6347–52. doi: 10.1073/pnas.0609180104
19. Contractor N, Louten J, Kim L, Biron CA, Kelsall BL. Cutting edge: Peyer's patch plasmacytoid dendritic cells (pDCs) produce low levels of type I interferons: possible role for IL-10, TGFbeta, and prostaglandin E2 in conditioning a unique mucosal pDC phenotype. *J Immunol.* (2007) 179:2690–4. doi: 10.4049/jimmunol.179.5.2690
20. Li HS, Gelbard A, Martinez GJ, Esashi E, Zhang H, Nguyen-Jackson H, et al. Cell-intrinsic role for IFN-alpha-STAT1 signals in regulating murine Peyer patch plasmacytoid dendritic cells and conditioning an inflammatory response. *Blood* (2011) 118:3879–89. doi: 10.1182/blood-2011-04-349761
21. Tezuka H, Abe Y, Asano J, Sato T, Liu J, Iwata M, et al. Prominent role for plasmacytoid dendritic cells in mucosal T cell-independent IgA induction. *Immunity* (2011) 34:247–57. doi: 10.1016/j.immuni.2011.02.002
22. Moro-Sibilot L, This S, Blanc P, Sanlaville A, Sisirak V, Bardel E, et al. Plasmacytoid dendritic cells are dispensable for noninfectious intestinal IgA responses *in vivo*. *Eur J Immunol.* (2016) 46:354–9. doi: 10.1002/eji.201545977
23. Deal EM, Jaimes MC, Crawford SE, Estes MK, Greenberg HB. Rotavirus structural proteins and dsRNA are required for the human primary plasmacytoid dendritic cell IFNalpha response. *PLoS Pathog.* (2010) 6:e1000931. doi: 10.1371/journal.ppat.1000931
24. Dasgupta S, Erturk-Hasdemir D, Ochoa-Reparaz J, Reinecker HC, Kasper DL. Plasmacytoid dendritic cells mediate anti-inflammatory responses to a gut commensal molecule via both innate and adaptive mechanisms. *Cell Host Microbe* (2014) 15:413–23. doi: 10.1016/j.chom.2014.03.006
25. Dubois B, Joubert G, Gomez de Aguero M, Gouanvic M, Goubier A, Kaiserlian D. Sequential role of plasmacytoid dendritic cells and regulatory T cells in oral tolerance. *Gastroenterology* (2009) 137:1019–28. doi: 10.1053/j.gastro.2009.03.055
26. Goubier A, Dubois B, Gheit H, Joubert G, Villard-Truc F, Asselin-Paturel C, et al. Plasmacytoid dendritic cells mediate oral tolerance. *Immunity* (2008) 29:464–75. doi: 10.1016/j.immuni.2008.06.017
27. Kaser A, Zeissig S, Blumberg RS. Inflammatory bowel disease. *Annu Rev Immunol.* (2010) 28:573–621. doi: 10.1146/annurev-immunol-030409-101225
28. Baumgart DC, Metzke D, Guckelberger O, Pascher A, Grotzinger C, Przesdzing I, et al. Aberrant plasmacytoid dendritic cell distribution and function in patients with Crohn's disease and ulcerative colitis. *Clin Exp Immunol.* (2011) 166:46–54. doi: 10.1111/j.1365-2249.2011.04439.x
29. Prete F, Catucci M, Labrada M, Gobessi S, Castiello MC, Bonomi E, et al. Wiskott-Aldrich syndrome protein-mediated actin dynamics control type-I interferon production in plasmacytoid dendritic cells. *J Exp Med.* (2013) 210:355–74. doi: 10.1084/jem.20120363
30. Arimura K, Takagi H, Uto T, Fukaya T, Nakamura T, Choijookhuu N, et al. Crucial role of plasmacytoid dendritic cells in the development of acute colitis through the regulation of intestinal inflammation. *Mucosal Immunol.* (2017) 10:957–70. doi: 10.1038/mi.2016.96
31. Swiecki M, Wang Y, Riboldi E, Kim AH, Dzutsev A, Gilfillan S, et al. Cell depletion in mice that express diphtheria toxin receptor under the control of SiglecH encompasses more than plasmacytoid dendritic cells. *J Immunol.* (2014) 192:4409–16. doi: 10.4049/jimmunol.1303135
32. Cisse B, Caton ML, Lehner M, Maeda T, Scheu S, Locksley R, et al. Transcription factor E2-2 is an essential and specific regulator of plasmacytoid dendritic cell development. *Cell* (2008) 135:37–48. doi: 10.1016/j.cell.2008.09.016
33. Kuhn R, Lohler J, Rennick D, Rajewsky K, Muller W. Interleukin-10-deficient mice develop chronic enterocolitis. *Cell* (1993) 75:263–74. doi: 10.1016/0092-8674(93)80068-P
34. Zhuang Y, Cheng P, Weintraub H. B-lymphocyte development is regulated by the combined dosage of three basic helix-loop-helix genes, E2A, E2-2, and HEB. *Mol Cell Biol.* (1996) 16:2898–905. doi: 10.1128/MCB.16.6.2898
35. Caton ML, Smith-Raska MR, Reizis B. Notch-RBP-J signaling controls the homeostasis of CD8- dendritic cells in the spleen. *J Exp Med.* (2007) 204:1653–64. doi: 10.1084/jem.20062648
36. Bergqvist I, Eriksson M, Saarikettu J, Eriksson B, Corneliussen B, Grundstrom T, et al. The basic helix-loop-helix transcription factor E2-2 is involved in T lymphocyte development. *Eur J Immunol.* (2000) 30:2857–63. doi: 10.1002/1521-4141(200010)30:10<2857::AID-IMMU2857>3.0.CO;2-G
37. Blanco F, Kalsi J, Isenberg DA. Analysis of antibodies to RNA in patients with systemic lupus erythematosus and other autoimmune rheumatic diseases. *Clin Exp Immunol.* (1991) 86:66–70. doi: 10.1111/j.1365-2249.1991.tb05775.x
38. Moolenbeek C, Ruitenberg EJ. The "Swiss roll": a simple technique for histological studies of the rodent intestine. *Lab Anim.* (1981) 15:57–9. doi: 10.1258/002367781780958577
39. Ghosh HS, Cisse B, Bunin A, Lewis KL, Reizis B. Continuous expression of the transcription factor e2-2 maintains the cell fate of mature plasmacytoid dendritic cells. *Immunity* (2010) 33:905–16. doi: 10.1016/j.immuni.2010.11.023
40. Recher M, Burns SO, de la Fuente MA, Volpi S, Dahlberg C, Walter JE, et al. B cell-intrinsic deficiency of the Wiskott-Aldrich syndrome protein (WASp) causes severe abnormalities of the peripheral B-cell compartment in mice. *Blood* (2012) 119:2819–28. doi: 10.1182/blood-2011-09-379412
41. Hao Y, O'Neill P, Naradikian MS, Scholz JL, Cancro MP. A B-cell subset uniquely responsive to innate stimuli accumulates in aged mice. *Blood* (2011) 118:1294–304. doi: 10.1182/blood-2011-01-330530
42. Rubtsov AV, Rubtsova K, Fischer A, Meehan RT, Gillis JZ, Kappler JW, et al. Toll-like receptor 7 (TLR7)-driven accumulation of a novel CD11c(+) B-cell population is important for the development of autoimmunity. *Blood* (2011) 118:1305–15. doi: 10.1182/blood-2011-01-331462
43. Snapper SB, Rosen FS, Mizoguchi E, Cohen P, Khan W, Liu CH, et al. Wiskott-Aldrich syndrome protein-deficient mice reveal a role for WASP in T but not B cell activation. *Immunity* (1998) 9:81–91. doi: 10.1016/S1074-7613(00)80590-7
44. Nguyen DD, Maillard MH, Cotta-de-Almeida V, Mizoguchi E, Klein C, Fuss I, et al. Lymphocyte-dependent and Th2 cytokine-associated colitis in mice deficient in Wiskott-Aldrich syndrome protein. *Gastroenterology* (2007) 133:1188–97. doi: 10.1053/j.gastro.2007.07.010
45. Nguyen DD, Wurbel MA, Goettel JA, Eston MA, Ahmed OS, Marin R, et al. Wiskott-Aldrich syndrome protein deficiency in innate immune cells leads to mucosal immune dysregulation and colitis in mice. *Gastroenterology* (2012) 143:719–29.e2. doi: 10.1053/j.gastro.2012.06.008
46. Lee PY, Kumagai Y, Li Y, Takeuchi O, Yoshida H, Weinstein J, et al. TLR7-dependent and FcgammaR-independent production of type I interferon in experimental mouse lupus. *J Exp Med.* (2008) 205:2995–3006. doi: 10.1084/jem.20080462
47. Keubler LM, Buettner M, Hager C, Bleich A. A multihit model: colitis lessons from the interleukin-10-deficient mouse. *Inflamm Bowel Dis.* (2015) 21:1967–75. doi: 10.1097/MIB.0000000000000468
48. Cervantes-Barragan L, Lewis KL, Firner S, Thiel V, Hugues S, Reith W, et al. Plasmacytoid dendritic cells control T-cell response to chronic viral infection. *Proc Natl Acad Sci USA*. (2012) 109:3012–7. doi: 10.1073/pnas.1117359109
49. Wohn C, Ober-Blobaum JL, Haak S, Pantelyushin S, Cheong C, Zahner SP, et al. Langerin(neg) conventional dendritic cells produce IL-23 to drive psoriatic plaque formation in mice. *Proc Natl Acad Sci USA*. (2013) 110:10723–8. doi: 10.1073/pnas.1307569110
50. Thrasher AJ, Burns SO. WASP: a key immunological multitasker. *Nat Rev Immunol.* (2010) 10:182–92. doi: 10.1038/nri2724
51. Gloury R, Zotos D, Zuidscherwoude M, Masson F, Liao Y, Hasbold J, et al. Dynamic changes in Id3 and E-protein activity orchestrate germinal center and plasma cell development. *J Exp Med.* (2016) 213:1095–111. doi: 10.1084/jem.20152003
52. Wohner M, Tagoh H, Bilic I, Jaritz M, Poliakova DK, Fischer M, et al. Molecular functions of the transcription factors E2A and E2-2 in controlling germinal center B cell and plasma cell development. *J Exp Med.* (2016) 213:1201–21. doi: 10.1084/jem.20152002
53. Maillard MH, Cotta-de-Almeida V, Takeshima F, Nguyen DD, Michetti P, Nagler C, et al. The Wiskott-Aldrich syndrome protein is required for the function of CD4(+)CD25(+)Foxp3(+) regulatory T cells. *J Exp Med.* (2007) 204:381–91. doi: 10.1084/jem.20061338

54. Biswas A, Shouval DS, Griffith A, Goettel JA, Field M, Kang YH, et al. WASP-mediated regulation of anti-inflammatory macrophages is IL-10 dependent and is critical for intestinal homeostasis. *Nat Commun.* (2018) 9:1779–93. doi: 10.1038/s41467-018-03670-6
55. Perry D, Sang A, Yin Y, Zheng YY, Morel L. Murine models of systemic lupus erythematosus. *J Biomed Biotechnol.* (2011) 2011:271694. doi: 10.1155/2011/271694
56. Elkon KB, Wiedeman A. Type I IFN system in the development and manifestations of SLE. *Curr Opin Rheumatol.* (2012) 24:499–505. doi: 10.1097/BOR.0b013e3283562c3e
57. Santiago-Raber ML, Baccala R, Haraldsson KM, Choubey D, Stewart TA, Kono DH, et al. Type-I interferon receptor deficiency reduces lupus-like disease in NZB mice. *J Exp Med.* (2003) 197:777–88. doi: 10.1084/jem.20021996
58. Sriram U, Varghese L, Bennett HL, Jog NR, Shivers DK, Ning Y, et al. Myeloid dendritic cells from B6.NZM Sle1/Sle2/Sle3 lupus-prone mice express an IFN signature that precedes disease onset. *J Immunol.* (2012) 189:80–91. doi: 10.4049/jimmunol.1101686
59. Uhlig HH. Monogenic diseases associated with intestinal inflammation: implications for the understanding of inflammatory bowel disease. *Gut* (2013) 62:1795–805. doi: 10.1136/gutjnl-2012-303956
60. Cho JH. The genetics and immunopathogenesis of inflammatory bowel disease. *Nat Rev Immunol.* (2008) 8:458–66. doi: 10.1038/nri2340
61. Zigmond E, Bernshtein B, Friedlander G, Walker CR, Yona S, Kim KW, et al. Macrophage-restricted interleukin-10 receptor deficiency, but not IL-10 deficiency, causes severe spontaneous colitis. *Immunity* (2014) 40:720–33. doi: 10.1016/j.immuni.2014.03.012
62. Ip WKE, Hoshi N, Shouval DS, Snapper S, Medzhitov R. Anti-inflammatory effect of IL-10 mediated by metabolic reprogramming of macrophages. *Science* (2017) 356:513–9. doi: 10.1126/science.aal3535
63. Kiesler P, Fuss IJ, Strober W. Experimental models of inflammatory bowel diseases. *Cell Mol Gastroenterol Hepatol.* (2015) 1:154–70. doi: 10.1016/j.jcmgh.2015.01.006
64. Bunin A, Sisirak V, Ghosh HS, Grajkowska LT, Hou ZE, Miron M, et al. Protein tyrosine phosphatase PTPRS is an inhibitory receptor on human and murine plasmacytoid dendritic cells. *Immunity* (2015) 43:277–88. doi: 10.1016/j.immuni.2015.07.009
65. Yang JY, Kim MS, Kim E, Cheon JH, Lee YS, Kim Y, et al. Enteric viruses ameliorate gut inflammation via toll-like receptor 3 and toll-like receptor 7-mediated interferon-beta production. *Immunity* (2016) 44:889–900. doi: 10.1016/j.immuni.2016.03.009
66. Katakura K, Lee J, Rachmilewitz D, Li G, Eckmann L, Raz E. Toll-like receptor 9-induced type I IFN protects mice from experimental colitis. *J Clin Invest.* (2005) 115:695–702. doi: 10.1172/JCI22996
67. Rachmilewitz D, Karmeli F, Takabayashi K, Hayashi T, Leider-Trejo L, Lee J, et al. Immunostimulatory DNA ameliorates experimental and spontaneous murine colitis. *Gastroenterology* (2002) 122:1428–41. doi: 10.1053/gast.2002.32994
68. Swiecki M, Gilfillan S, Vermi W, Wang Y, Colonna M. Plasmacytoid dendritic cell ablation impacts early interferon responses and antiviral NK and CD8(+) T cell accrual. *Immunity* (2010) 33:955–66. doi: 10.1016/j.immuni.2010.11.020

Conflict of Interest Statement: MS and RK were employees of Medimmune, LLC.

The remaining authors declare that the research was conducted in the absence of any commercial or financial relationships that could be construed as a potential conflict of interest.

Article

Immunity

Plasmacytoid Dendritic Cells and Type I Interferon Promote Extrafollicular B Cell Responses to Extracellular Self-DNA

Graphical Abstract

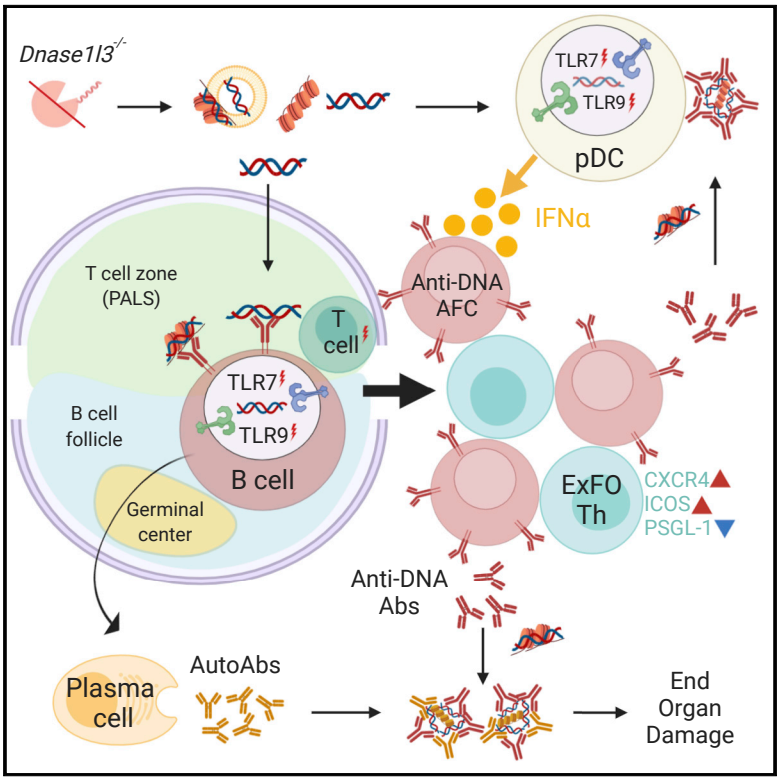

Highlights

- Anti-DNA antibody response is driven by T-dependent extrafollicular plasmablasts
- IFN-I signaling propagates anti-DNA responses and SLE-like disease
- IFN-I produced by pDCs promotes plasmablast proliferation and differentiation
- TLR9 drives anti-DNA responses and autoimmunity redundantly with TLR7

Authors

Chetna Soni, Oriana A. Perez, William N. Voss, ..., Gregory C. Ippolito, Vanja Sisirak, Boris Reizis

Correspondence

vsisirak@immuconcept.org (V.S.), boris.reizis@nyulangone.org (B.R.)

In Brief

Autoantibodies to self-DNA are a defining feature of systemic lupus erythematosus (SLE), yet the mechanisms of their development remain poorly understood. Soni et al. show that anti-DNA autoreactivity is driven by extrafollicular B cell differentiation into short-lived plasmablasts, which is facilitated by plasmacytoid dendritic cells, type I interferon, and endosomal Toll-like receptors 7 and 9.

Soni et al., 2020, Immunity *53*, 1022–1038
June 16, 2020
https://doi.org/10.1016/j.immuni.2020.04.015

CellPress

CellPress

Immunity

Article

Plasmacytoid Dendritic Cells and Type I Interferon Promote Extrafollicular B Cell Responses to Extracellular Self-DNA

Chetna Soni,[1] Oriana A. Perez,[1] William N. Voss,[2] Joseph N. Pucella,[1] Lee Serpas,[1] Justin Mehl,[1] Krystal L. Ching,[1] Jule Goike,[3] George Georgiou,[2,3] Gregory C. Ippolito,[2,4] Vanja Sisirak,[5,*] and Boris Reizis[1,6,7,*]

[1]Department of Pathology, New York University Grossman School of Medicine, New York, NY 10016, USA
[2]Department of Molecular Biosciences, University of Texas at Austin, Austin, TX 78712, USA
[3]Department of Chemical Engineering, University of Texas at Austin, Austin, TX 78712, USA
[4]Department of Oncology, Dell Medical School, University of Texas at Austin, Austin, TX 78712, USA
[5]CNRS-UMR 5164, ImmunoConcEpt, Université de Bordeaux, 33076 Bordeaux, France
[6]Department of Medicine, New York University Grossman School of Medicine, New York, NY 10016, USA
[7]Lead Contact
*Correspondence: vsisirak@immuconcept.org (V.S.), boris.reizis@nyulangone.org (B.R.)
https://doi.org/10.1016/j.immuni.2020.04.015

SUMMARY

Class-switched antibodies to double-stranded DNA (dsDNA) are prevalent and pathogenic in systemic lupus erythematosus (SLE), yet mechanisms of their development remain poorly understood. Humans and mice lacking secreted DNase DNASE1L3 develop rapid anti-dsDNA antibody responses and SLE-like disease. We report that anti-DNA responses in *Dnase1l3*$^{-/-}$ mice require CD40L-mediated T cell help, but proceed independently of germinal center formation via short-lived antibody-forming cells (AFCs) localized to extrafollicular regions. Type I interferon (IFN-I) signaling and IFN-I-producing plasmacytoid dendritic cells (pDCs) facilitate the differentiation of DNA-reactive AFCs *in vivo* and *in vitro* and are required for downstream manifestations of autoimmunity. Moreover, the endosomal DNA sensor TLR9 promotes anti-dsDNA responses and SLE-like disease in *Dnase1l3*$^{-/-}$ mice redundantly with another nucleic acid-sensing receptor, TLR7. These results establish extrafollicular B cell differentiation into short-lived AFCs as a key mechanism of anti-DNA autoreactivity and reveal a major contribution of pDCs, endosomal Toll-like receptors (TLRs), and IFN-I to this pathway.

INTRODUCTION

Systemic lupus erythematosus (SLE) is a systemic autoimmune disease defined by class-switched antibodies (Abs) to nuclear antigens. More than half of SLE patients develop high titers of immunoglobulin G (IgG) to double-stranded DNA (dsDNA), which correlate with disease activity, severity, and lupus nephritis (Pisetsky, 2016; Yung and Chan, 2015). B cells that produce these Abs represent major targets of emerging therapies in SLE (Hale et al., 2018). Autoreactive B cell responses can be driven by the germinal center (GC) reaction (Vinuesa et al., 2009), which is supported by CD4$^+$ follicular helper T (GC-Tfh) cells (Lesley et al., 2006; Seo et al., 2002; Vinuesa et al., 2016). Apart from the GC, autoreactive B cell differentiation can occur in the extrafollicular (ExFO) regions (Jenks et al., 2018, 2019; William et al., 2002). The ExFO pathway in a lymphoproliferation-driven SLE model MRL.*lpr* is promoted by extrafollicularly localized CD4$^+$ T-helper (ExFO-Th) cells expressing CXCR4, CD40L, and inducible T cell costimulator (ICOS) (Odegard et al., 2008). An ExFO T cell population in patients with lupus nephritis has been recently defined (Caielli et al., 2019). However, the relative contribution of the ExFO pathway and its dedicated helper T cells to the initiation and propagation of anti-dsDNA responses remains to be explored.

A high concentration of circulating type I interferons (IFN-I) and the expression of IFN-stimulated gene signature in SLE patients correlate with high anti-DNA Ab titers and disease severity (Bennett et al., 2003; Kirou et al., 2005; Weckerle et al., 2011). The overall pathogenic effect of IFN-I signaling in murine SLE has been demonstrated (Agrawal et al., 2009; Santiago-Raber et al., 2003), although in some cases, it appears independent of auto-Ab production (Buechler et al., 2013). Furthermore, both the target cells of IFN-I signaling and the IFN-I-producing cell types in auto-Ab responses are poorly understood. Plasmacytoid dendritic cells (pDCs) are efficient producers of IFN-I that promote SLE pathogenesis (Rowland et al., 2014; Sisirak et al., 2014). However, other cell types such as stromal follicular dendritic cells (Das et al., 2017) or B cells themselves (Hamilton et al., 2017) have been proposed as IFN-I producers in SLE. Given the emerging therapeutic strategies to block IFN-I in SLE

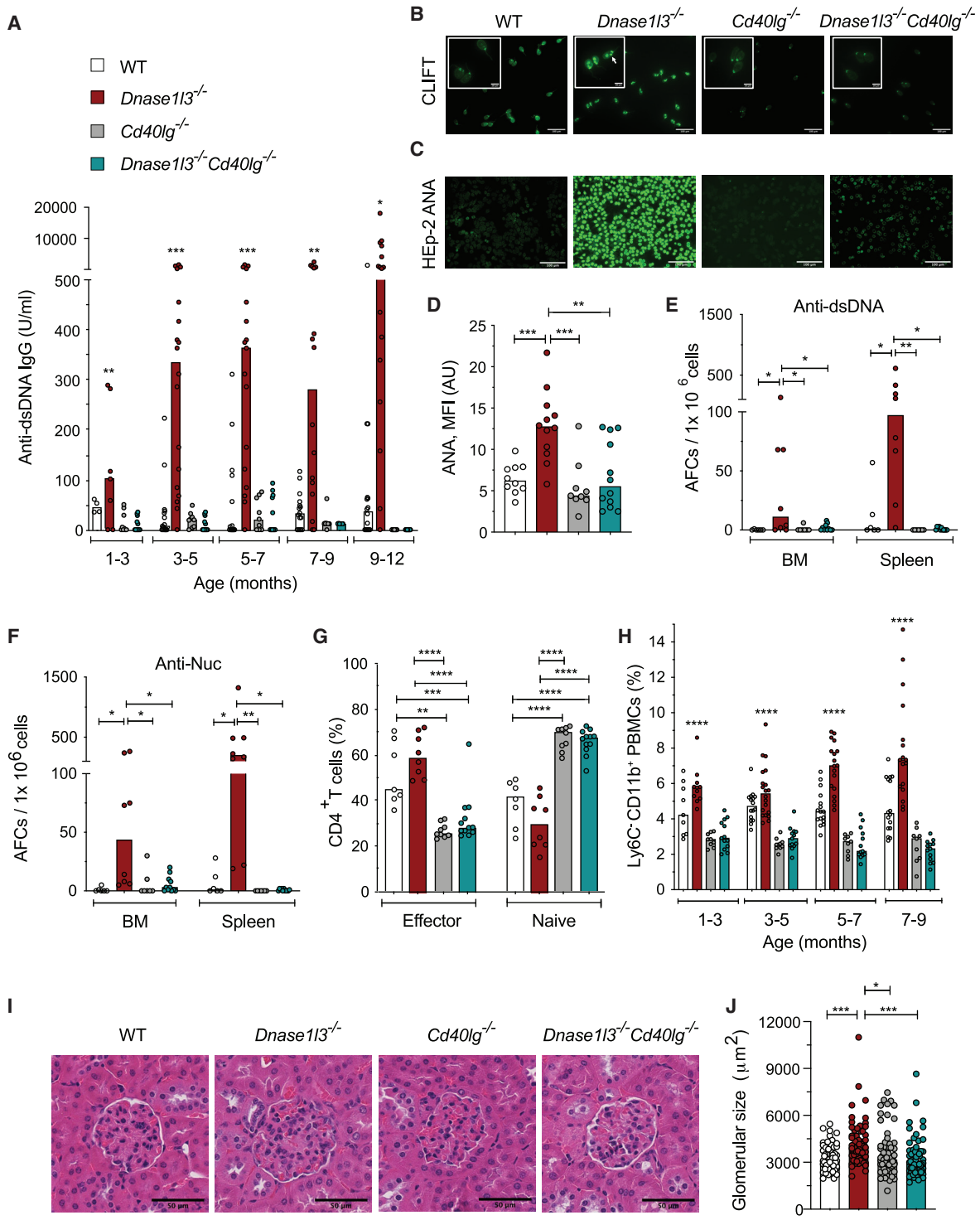

Figure 1. CD40L Deficiency in *Dnase1l3*$^{-/-}$ Mice Abolishes Autoimmunity

Wild-type (WT), *Dnase1l3*$^{-/-}$, *Cd40lg*$^{-/-}$, and *Dnase1l3*$^{-/-}$*Cd40lg*$^{-/-}$ mice were examined for Abs at the indicated ages or at the 12-month endpoint.

(A) Serum anti-dsDNA IgG titers measured by ELISA.

(B) CLIFT assay for anti-dsDNA IgG (representative of ≥ 4 mice per strain). Arrow indicates positive staining of the kinetoplast. Scale bar, 100 μm (insets, 20 μm).

(C and D) ANA assay, showing images representative of ≥8 mice per strain (C), and quantitation of fluorescence intensity (D). Scale bars, 100 μm.

(E and F) Frequency of anti-dsDNA (E) and anti-nucleosome (anti-Nuc) (F) AFCs in the bone marrow (BM) or spleen as determined by ELISpot.

(G) Fractions of effector and naive T cells among splenic CD4^{+} T cells at the endpoint.

(legend continued on next page)

(Muskardin and Niewold, 2018), the precise cellular sources and mechanisms of IFN-I activity in anti-dsDNA responses warrant clarification.

Aberrant immune activation via innate pathways of nucleic acid (NA) sensing plays a fundamental role in SLE. The key extracellular NA-sensing pathway involves MyD88-dependent endosomal Toll-like receptors (TLRs) TLR7 and TLR9 that recognize single-stranded RNA and unmethylated DNA, respectively. Both receptors are expressed in B cells and pDCs and facilitate auto-Ab production and IFN-I secretion by these respective cell types in response to endogenous NAs (Barrat et al., 2005; Leadbetter et al., 2002). TLR7 is necessary for autoreactivity in all tested models, and its aberrant expression facilitates SLE in mice and humans (Celhar et al., 2012). The loss of TLR9 reduces anti-nucleosome (anti-Nuc) Abs yet exacerbates the disease in some SLE models, suggesting a net tolerogenic effect of this receptor (Christensen and Shlomchik, 2007; Sharma et al., 2015). These results remain to be reconciled with the activation of IFN-I production in human pDCs by extracellular DNA via TLR9 (Barrat and Su, 2019) and pose a fundamental question about the innate mechanisms driving anti-DNA responses in SLE.

DNASE1L3 is a secreted DNase that is a critical gatekeeper of tolerance to DNA. Homozygous null mutations in *DNASE1L3* cause rare familial forms of SLE with anti-dsDNA Ab responses (Al-Mayouf et al., 2011; Ozçakar et al., 2013). Furthermore, a coding polymorphism that reduces DNASE1L3 activity is associated with SLE, scleroderma, and arthritis (Westra et al., 2018; Zochling et al., 2014). Finally, *Dnase1l3*$^{-/-}$ mice develop rapid and specific anti-dsDNA responses, followed by generalized immune activation and SLE-like disease (Sisirak et al., 2016; Weisenburger et al., 2018). DNASE1L3 acts extracellularly to reduce the availability of antigenic cell-free DNA, e.g., by restricting DNA length (Serpas et al., 2019) and reducing its exposure on apoptotic cell microparticles (Sisirak et al., 2016). Thus, *Dnase1l3*$^{-/-}$ mice represent a clinically relevant model of anti-dsDNA responses driven by extracellular DNA, in which these responses can be studied independently of other auto-Abs, lymphoproliferation, or systemic inflammation.

Here, we took advantage of the specificity and defined kinetics of this model to address the cellular and molecular basis of dsDNA-specific Ab responses. We identified a central role of CD40 ligand (CD40L)-dependent ExFO differentiation in anti-DNA reactivity and established pDC-derived IFN-I as an important signal for its maintenance. We also found that TLR9 promoted anti-DNA responses and the resulting pathology, and this effect was partially redundant with TLR7. Thus, extracellular self-DNA drives TLR-dependent IFN-I production and continuous ExFO differentiation of Ab-forming cells (AFCs) that drive anti-DNA autoreactivity and pathology in SLE.

RESULTS

Anti-DNA Reactivity and Autoimmunity in Dnase1l3-Deficient Mice Require CD40L

To test whether rapid anti-Nuc and anti-dsDNA responses in *Dnase1l3*$^{-/-}$ mice (Sisirak et al., 2016) depend on T cell help via CD40L-CD40 signaling (Lesley et al., 2006), we deleted *Cd40lg* in *Dnase1l3*$^{-/-}$ mice. While *Dnase1l3*$^{-/-}$ mice developed high titers of anti-dsDNA IgG, *Dnase1l3*$^{-/-}$*Cd40lg*$^{-/-}$ mice did not develop any anti-dsDNA Abs detectable by ELISA or *Crithidia luciliae* immunofluorescence test (CLIFT) (Figures 1A and 1B). They also did not show reactivity to nuclear antigens in the anti-nuclear Ab (ANA) assay (Figures 1C and 1D). Accordingly, dsDNA- and Nuc-reactive AFCs in the bone marrow (BM) and spleen were undetectable by ELISpot in *Dnase1l3*$^{-/-}$*Cd40lg*$^{-/-}$ mice (Figures 1E and 1F). Whereas the numbers of mature follicular (FO) B cells were unaffected (Figure S1A), *Dnase1l3*$^{-/-}$*Cd40lg*$^{-/-}$ mice harbored a reduced fraction of IgG^{+} AFC (Figures S1B and S1C) and lower total IgG titers compared to *Dnase1l3*$^{-/-}$ mice, although they were similar to those in wild-type (WT) mice (Figure S1D). However, unlike total IgG responses, anti-dsDNA AFCs and Abs were completely abrogated (Figures 1A, 1B, 1E, and S1B).

Consistent with disrupted CD40L signaling, the fractions of CD62L^{-}CD44^{hi} effector CD4^{+} T cells were significantly lower while those of naive CD62L^{+}CD44^{-}CD4^{+} T cells were higher in *Dnase1l3*$^{-/-}$*Cd40lg*$^{-/-}$ compared to WT and *Dnase1l3*$^{-/-}$ mice (Figure 1G). In parallel, the frequency of CD4^{+}CD25^{hi}Foxp3^{+} regulatory T (Treg) cells was significantly reduced in *Dnase1l3*$^{-/-}$*Cd40lg*$^{-/-}$ mice (Figure S1E). As expected, GC B cells were completely absent in *Dnase1l3*$^{-/-}$*Cd40lg*$^{-/-}$ mice (Figures S1F and S1G), and GC-Tfh cells were also reduced (Figure S1H). Notably, *Dnase1l3*$^{-/-}$*Cd40lg*$^{-/-}$ mice lost manifestations of generalized immune activation such as progressive expansion of Ly6C^{-} monocytes in the blood (Figure 1H) and splenomegaly (Figure S1I). *Dnase1l3*$^{-/-}$ mice on the C57BL/6 (B6) background do not develop overt glomerulonephritis but have enlarged glomeruli at 1 year of age (Sisirak et al., 2016). We observed a complete restoration to normal glomerular size in *Dnase1l3*$^{-/-}$*Cd40lg*$^{-/-}$ mice (Figures 1I and 1J). Thus, anti-dsDNA responses and all disease manifestations in *Dnase1l3*$^{-/-}$ mice require CD40-CD40L signaling, suggesting a strict T cell dependence and revealing the primary role of auto-Abs in this model of SLE-like disease.

Germinal Center Formation Is Dispensable for Autoreactivity

Spontaneous formation of GC in the absence of infection or immunization requires TLR7, whose deletion abolishes GC formation and autoreactivity in several models of autoimmunity (Jackson et al., 2014; Soni et al., 2014). To test whether the T-cell-dependent anti-dsDNA response requires GC formation,

(H) Fractions of CD11b^{+}Ly6C^{-} population among total peripheral blood mononuclear cells (PBMCs) at indicated time points.
(I) Glomeruli from H&E-stained kidney sections (representative of three or more mice per group). Scale bars, 50 μm.
(J) Size of ≥20 glomeruli per kidney section from ≥3 mice per group.
In (A) and (H), significant differences between *Dnase1l3*$^{-/-}$ versus *Dnase1l3*$^{-/-}$*Cd40lg*$^{-/-}$ mice are shown. Symbols represent individual mice, except in (J), where they represent individual glomeruli. All bars indicate median. *p ≤ 0.05, **p ≤ 0.01, ***p ≤ 0.001, and ****p ≤ 0.0001.
See also Figure S1.

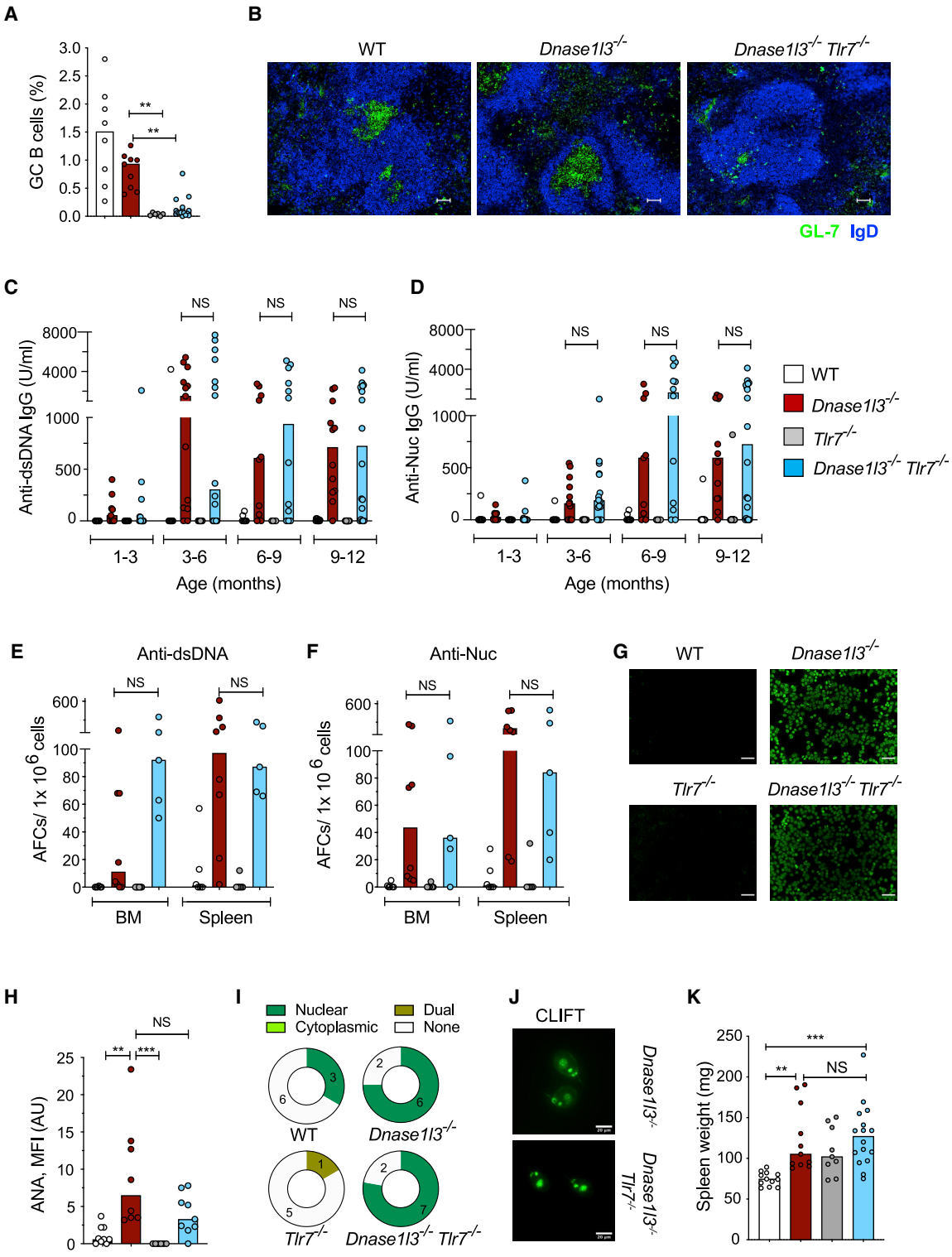

Figure 2. TLR7-Deficient *Dnase1l3*$^{-/-}$ Mice Do Not Develop GCs but Retain Anti-DNA Reactivity

WT, *Dnase1l3*$^{-/-}$, *Tlr7*$^{-/-}$, and *Dnase1l3*$^{-/-}$*Tlr7*$^{-/-}$ mice were examined for Abs at the indicated ages or at the 12-month endpoint.

(A) Fraction of CD38^{-} GL-7^{+} GC B cells among splenic B cells at the endpoint.

(B) Spleen sections stained for GC B cells (green) and follicular B cells (blue). Representative of ≥3 mice per group. Scale bars, 30 μm.

(C and D) Serum anti-dsDNA (C) and anti-Nuc (D) IgG titers measured by ELISA.

(E and F) Frequency of anti-dsDNA (E) and anti-Nuc (F) AFCs in the BM or spleen as determined by ELISpot.

(legend continued on next page)

we generated *Dnase1l3*$^{-/-}$*Tlr7*$^{-/-}$ mice. The absence of TLR7 in both WT and *Dnase1l3*$^{-/-}$ mice significantly reduced the fraction of GC B cells and GC formation in the spleen (Figures 2A and 2B). Despite the loss of GCs, *Dnase1l3*$^{-/-}$*Tlr7*$^{-/-}$ mice accumulated anti-dsDNA and anti-Nuc Abs (Figures 2C and 2D) and AFC (Figures 2E and 2F) comparably to GC-sufficient *Dnase1l3*$^{-/-}$ mice. *Dnase1l3*$^{-/-}$*Tlr7*$^{-/-}$ mice also showed positive ANA with a characteristic perinuclear and homogeneous staining pattern (Figures 2G–2I) and characteristic kinetoplast staining specific for dsDNA by CLIFT (Figure 2J). Accordingly, TLR7 deficiency did not rescue splenomegaly in old *Dnase1l3*$^{-/-}$ mice (Figure 2K).

We tested whether anti-dsDNA Abs in *Dnase1l3*$^{-/-}$*Tlr7*$^{-/-}$ mice might be produced by GC B cells residing in the lymph nodes (LNs). Unlike spleens, LNs of *Dnase1l3*$^{-/-}$*Tlr7*$^{-/-}$ mice harbored a substantial number of GC B cells (Figure S2A), as well as total class-switched IgG^{+} B cells (Figure S2B). However, dsDNA and Nuc-reactive AFCs were virtually absent from the LN of both *Dnase1l3*$^{-/-}$ or *Dnase1l3*$^{-/-}$*Tlr7*$^{-/-}$ mice (Figures S2C and S2D), suggesting that the bulk of autoreactive AFCs were generated in the spleen. Thus, the ablation of TLR7-dependent GC formation does not affect anti-dsDNA responses in *Dnase1l3*$^{-/-}$ mice, arguing against a major role of the GC pathway in this process.

Autoreactivity Is Driven by ExFO B Cell Differentiation

Given that DNA-specific AFCs were abundant in the spleens of *Dnase1l3*$^{-/-}$ mice, we stained spleen sections for markers of GCs (GL7), plasmablasts (PBs) and plasma cells (CD138), and macrophages bordering the follicular areas (CD169). In WT spleens, small clusters of CD138^{+} cells were localized near the bridging channels between the follicular and MZs (Figures 3A). In contrast, *Dnase1l3*$^{-/-}$ mice showed an expansion of CD138^{+} cells outside of the follicular areas (Figures 3A and S3A). By flow cytometry, we noted a 2-fold increase in the fraction of CXCR3^{+}MHCII^{hi} AFCs (Shi et al., 2015) among CD138^{+} B cells in *Dnase1l3*$^{-/-}$ splenocytes; these cells were almost undetectable in the absence of CD40L (Figures S3B and 3B). To target the proliferative PBs rather than long-lived plasma cells, we treated *Dnase1l3*$^{-/-}$ mice with cyclophosphamide or PBS for 3 days. 4 days later, mice were injected with thymidine analog 5-ethynyl-2′-deoxyuridine (EdU) to label proliferating cells and examined 12 h later. Cyclophosphamide treatment significantly reduced the fractions of total EdU^{+}, CD138^{+} PB, and GL7^{+-} CD38^{-} GC B cells among total B cells (Figure S3C). Notably, cyclophosphamide caused a major reduction in splenic dsDNA- and Nuc-specific AFCs (Figure 3C) and a similarly significant reduction in anti-dsDNA and anti-Nuc Ab titers (Figure 3D) and ANA staining (Figure S3D). We also treated *Dnase1l3*$^{-/-}$ mice with a B-cell-depleting Ab (anti-CD20), which rapidly reduced FO B cells but spared CD138^{+} PB and GC B cells (Figures S3E and S3F). Depletion of naive B cells significantly reduced anti-dsDNA and anti-Nuc Abs only by 4 weeks post-treatment (Figure 3E), consistent with the depletion of B cells as a source of PB. Finally, ELISpot analysis of sorted B cell populations showed that dsDNA- and Nuc-specific AFCs were present only among CD138^{+} PBs (Figure 3F), suggesting these short-lived cells as the primary source of autoreactivity.

To gain insight into the receptor repertoire of B cell fractions in *Dnase1l3*$^{-/-}$ mice, we sorted FO, GC, PB, and total IgG^{+} B cells individually from two *Dnase1l3*$^{-/-}$ mice (Figures S3G and S3H) and one age- and sex-matched WT mouse and sequenced in bulk immunoglobulin heavy chain variable regions (V_H). Complementarity-determining regions (CDRs) of DNA-reactive hybridomas are enriched for positively charged amino acids arginine (Arg) and lysine (Lys), reflecting the binding to negatively charged DNA (Radic and Weigert, 1994). Indeed, the overall V_H repertoire from PB, GC and IgG^{+} fractions from both *Dnase1l3*$^{-/-}$ mice had a 2- to 3-fold higher frequency of Arg and Lys in the CDRH3 region (Figure 3G). Among V_H families, B cells from *Dnase1l3*$^{-/-}$ mice showed increased utilization of V_H1–5 (Figure 3H), V_H5–17 (Figure 3I) and V_H1-81 (data not shown). The recurrent usage of V_H5–17 was previously noted in anti-dsDNA hybridomas from a different *Dnase1l3*$^{-/-}$ strain (Weisenburger et al., 2018), warranting its further analysis. V_H5–17 clonotypes contained more Arg and Lys residues in the CDRH3 region specifically in the PB of both *Dnase1l3*$^{-/-}$ mice (Figure S3I). Furthermore, in all fractions, the mean CDRH3 isoelectric point and mean CDRH3 hydrophobicity (Kyte-Doolittle index) were higher for the V_H5–17 clonotypes in *Dnase1l3*$^{-/-}$ mice (Figures 3J and S3J). Somatic hypermutations (SHMs) in the V_H regions were not notably higher in any of the B cell fractions from *Dnase1l3*$^{-/-}$ mice, and no dominant clones were observed (Figure S3K; data not shown). Similar to V_H5–17, CDRH3 of V_H1–5 clonotypes from PB and GC fractions of *Dnase1l3*$^{-/-}$, but not WT, mice contained more positively charged amino acids (Figure S3L), supporting the involvement of V_H5–17 and V_H1–5 clones in DNA binding. Collectively, the observed selection for positive charges across all CDRH3 and within particular V_H families suggests a polyclonal expansion of DNA-reactive B cells in *Dnase1l3*$^{-/-}$ mice. The expansion was observed in PB as well as in GC and did not involve extensive SHM typically associated with GC reaction, further supporting short-lived PBs as a source of anti-dsDNA reactivity in *Dnase1l3*$^{-/-}$ mice.

Given the T-cell-dependent anti-dsDNA B cell response in *Dnase1l3*$^{-/-}$ mice, we analyzed ExFO-Th cells (CD62L^{-} PSGL-1^{lo} CXCR4^{hi} ICOS^{hi}) (Figure S3M) and found that this population expanded with age in *Dnase1l3*$^{-/-}$ mice (Figure 3K) in a CD40L-dependent manner (Figures 3L and 3M). ExFO Th cells showed the highest expression of CXCR4, CD40L, and ICOS compared to total T cells or CD62L^{-} PSGL-1^{hi} T cells (Figures S3N and S3O). In addition to their higher frequency (Figure S3P), ExFO Th cells from *Dnase1l3*$^{-/-}$ mice also had significantly higher expression of all three proteins compared to WT (Figures S3N

(G and H) ANA assay, showing images representative of ≥6 mice per strain (G), and quantitation of fluorescence intensity (H). Scale bars, 100 μm.
(I) Distribution of ANA reactivity patterns in mice from each group.
(J) CLIFT assay for anti-dsDNA IgG (representative of ≥ 4 mice per strain). Scale bar, 20 μm.
(K) Spleen weights at the endpoint.
Symbols represent individual mice; bars indicate median. NS, not significant; **p ≤ 0.01, and ***p ≤ 0.001.
See also Figure S2.

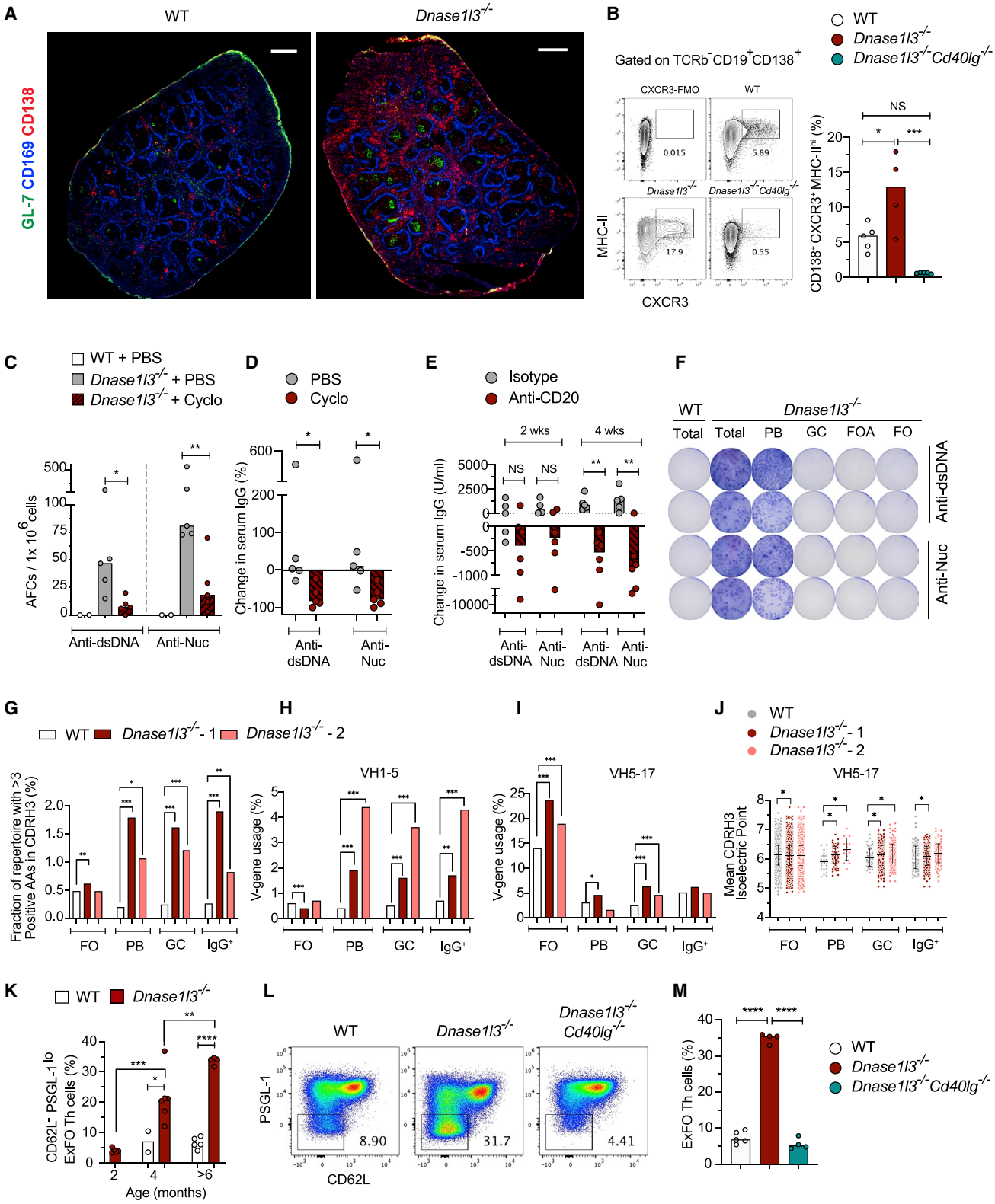

Figure 3. DNA-Reactive B Cells in *Dnase1l3*$^{-/-}$ Mice Develop Primarily through ExFO Differentiation into Plasmablasts

(A) Spleen sections representative of three to five WT or *Dnase1l3*$^{-/-}$ mice stained for CD138 (red), CD169 (blue), and GL-7 (green). Scale bar, 1,000 μm.

(B) Shown are representative flow plots and quantitation of the fraction of CXCR3^{+}MHC-II^{hi} (ExFO) B cells, pre-gated on splenic TCRβ^{-}B220^{+}CD19^{+}CD138^{+} cells from WT (open symbols), *Dnase1l3*$^{-/-}$ (red), and *Dnase1l3*$^{-/-}$*Cd40lg*$^{-/-}$ (green) mice. CXCR3-FMO (fluorescence minus one) was used for gate allocation.

(legend continued on next page)

and S3O). Thus, the expansion of DNA-reactive ExFO AFC in *Dnase1l3*$^{-/-}$ mice is associated with and supported by the expansion of ExFO Th cells. Overall, DNA-specific B cell response appears to proceed through short-lived auto-Ab-secreting cells with help from T cells in the ExFO regions.

IFN-I Signaling Facilitates ExFO Anti-dsDNA Responses

Given the importance of IFN-I signaling in SLE pathogenesis, we tested its role in ExFO-driven anti-DNA responses by generating *Dnase1l3*$^{-/-}$*Ifnar1*$^{-/-}$ mice deficient in DNASE1L3 and the IFN-I receptor IFNAR1. The induction of IFN-I-inducible marker Sca-1 on T and B cells (Sisirak et al., 2016) was completely rescued in *Dnase1l3*$^{-/-}$*Ifnar1*$^{-/-}$ mice, confirming a functional blockade of IFN-I signaling (Figures S4A and S4B). Although *Dnase1l3*$^{-/-}$*Ifnar1*$^{-/-}$ mice showed the initial emergence of anti-dsDNA and anti-Nuc IgG at 1–3 months, the titers were reduced in the majority of animals by 3–6 months and reaching significance at 9–12 months (Figures 4A and 4B). Accordingly, the numbers of anti-dsDNA and anti-Nuc AFCs at the endpoint were variable but reduced in *Dnase1l3*$^{-/-}$*Ifnar1*$^{-/-}$ mice, reaching significance for anti-dsDNA (Figures 4C and 4D). The reduction in anti-dsDNA reactivity was also observed by CLIFT (Figure S4C). Moreover, the frequency of total class-switched IgD^{-} IgM^{-} IgG2a.2b^{+} B cells, but not GC B cells, was significantly reduced in *Dnase1l3*$^{-/-}$*Ifnar1*$^{-/-}$ spleens (Figures S4D and S4E). Overall ANA reactivity was also significantly reduced in *Dnase1l3*$^{-/-}$*Ifnar1*$^{-/-}$ mice, with more samples showing reactivity to cytoplasmic antigens (Figures 4E and 4F). Accordingly, all features of immune activation and pathology were abolished in *Dnase1l3*$^{-/-}$*Ifnar1*$^{-/-}$ mice, including splenomegaly (Figure S4F), T cell activation (Figure S4G), expansion of Ly6C^{-} monocytes (Figure S4H), the deposition of IgG and complement (C3) in the kidney glomeruli, and the increase in glomerular size (Figures 4G–4K). Thus, IFN-I signaling appears dispensable for the initial breach of tolerance to DNA but facilitates the amplification of anti-DNA responses and their downstream pathogenic sequelae.

Consistent with reduced anti-DNA responses, spleens of *Dnase1l3*$^{-/-}$*Ifnar1*$^{-/-}$ mice showed an overall decrease of CD138^{+} PBs in the ExFO regions (Figures 5A and 5B), with a significant reduction of CXCR3^{+} MHC-II^{hi} CD138^{+} PBs (Figures 5C and 5D). Accordingly, the frequency of ExFO Th cells was significantly reduced in *Dnase1l3*$^{-/-}$*Ifnar1*$^{-/-}$ mice (Figures 5E and 5F), and the elevated expression of ICOS and CD40L on these cells was completely rescued (Figures 5G,H). *Dnase1l3*$^{-/-}$ mouse spleens harbored multiple CD4^{+} T cells in close proximity with CD138^{+} PB clusters in the red pulp and bridging channels (Figure S5A) and a higher fraction of Ki67^{+} proliferating cells in the GC and T cell zones, with an elevated ratio of proliferating cells to CD4^{+} T cells (Figures 5I–5K and S5B). Notably, this ratio was significantly reduced in *Dnase1l3*$^{-/-}$*Ifnar1*$^{-/-}$ spleens (Figure 5K). Thus, IFN-I is necessary for the maintenance of ExFO B and T cell responses that drive autoreactivity in *Dnase1l3*$^{-/-}$ mice.

Next, we investigated the effect of IFN-I on B cell differentiation into PBs *in vitro*. Splenic B cells were activated with anti-IgM and anti-CD40 in the presence of interleukin-4 (IL-4) and increasing doses of IFN-α, which induced a dose-dependent expression of Sca-1 and CD69 on the resulting CD138^{+} PBs (Figures S5C and S5D). A similar pattern of activation and responsiveness to IFN-α was observed between B cells from WT and *Dnase1l3*$^{-/-}$ mice, which were used interchangeably. Purified carboxyflurescein succinimidyl ester (CFSE)-labeled B cells from *Ifnar1*$^{+/+}$ or *Ifnar1*$^{-/-}$ mice were left unactivated (UA) or activated (A) with anti-IgM, anti-CD40, and IL-4 with or without IFN-α for 3 days. The proliferation and differentiation of CFSE-labeled B cells into CD138^{+} PB were comparable between *Ifnar1*$^{+/+}$ and *Ifnar1*$^{-/-}$ mice in the absence of IFN-α but were increased by IFN-α in IFNAR-proficient B cells (Figures 5L–5O and S5E). The enhancing effect of IFN-α was not observed when B cells were stimulated by lipopolysaccharide (LPS) in the presence of IL-4 (Figures S5F and S5G). Consistent with previous reports (Le Bon et al., 2001; Le Bon et al., 2006), these data suggest that IFN-I may directly facilitate antigen-receptor-driven B cell differentiation into PBs, supporting the observed role of IFN-I in the ExFO-driven differentiation of autoreactive B cells.

pDCs Facilitate ExFO Anti-dsDNA Responses through IFN-I

Having established the role of IFN-I in anti-DNA reactivity in *Dnase1l3*$^{-/-}$ mice, we tested the role of IFN-I-producing pDCs by reducing the dosage of the pDC-specific transcription factor TCF4 (Cisse et al., 2008; Sisirak et al., 2014). *Dnase1l3*$^{-/-}$*Tcf4*$^{+/-}$ mice on pure 129 background had reduced percentages of

(C and D) Frequency of anti-dsDNA and anti-Nuc Ab-forming cells (AFCs) determined by ELISpot (C) and percent change in serum anti-dsDNA or anti-Nuc IgG titers determined by ELISA (D) in 6-month-old WT mice (open) or *Dnase1l3*$^{-/-}$ mice treated with PBS (gray) or cyclophosphamide (cyclo; red).
(E) Change in serum titers of anti-dsDNA or anti-Nuc IgG in 6-month-old *Dnase1l3*$^{-/-}$ mice after one dose (100 μg/mouse; intraperitoneally [i.p.]) of treatment with IgG2a isotype control (gray) or anti-CD20 Ab (red) at 2 weeks and upon a second dose of a similar treatment at 4 weeks.
(F) Image of ELISpot plate representative of two experiments with two mice per experiment. Shown are two serial dilutions of anti-dsDNA and anti-Nuc AFCs from total splenocytes of >6-month-old WT and *Dnase1l3*$^{-/-}$ mice OR from flow-sorted plasmablasts (PBs), GC B cells (GC), follicular activated B cells (FOA), and naive follicular B cells (FO) from >6-month-old *Dnase1l3*$^{-/-}$ mice. Sorted GC, FOA, and FO cells were activated for 2 h with 5 μg/mL anti-CD40 + 1 μg/mL LPS and plated onto DNA or Nuc-coated ELISpot plates.
(G) Percentage of clonotypes in each repertoire that contain >3 positively charged amino acids (AA) within the CDR-H3 region in FO, PB, GC, and IgG^{+} B cells from WT (open), *Dnase1l3*$^{-/-}$-1 (red), and *Dnase1l3*$^{-/-}$-2 (salmon).
(H and I) Percentage of clonotypes that use the V-gene IGHV1–5 (H), and V-gene IGH5–17 (I) in the indicated B cell subsets and mice.
(J) Mean isoelectric point of the CDR-H3 region among the clonotypes that use the V-gene IGH5-17. Each point represents one clonotype. Error bars represent the mean and SD of all clonotypes in each group.
(K) Flow analysis of the fraction of CD62L^{-}PSGL-1^{lo}ExFO Th cells among splenic B220^{-}TCRβ^{+}CD4^{+} T cells of WT and *Dnase1l3*$^{-/-}$ mice at the indicated ages.
(L and M) Representative flow plots of pre-gated splenic B220^{-}TCRβ^{+}CD4^{+} cells with low ExFO Th cells shown within the gate (L); quantitation of the fraction of ExFO Th cells (M) from >6-month-old WT, *Dnase1l3*$^{-/-}$, and *Dnase1l3*$^{-/-}$*Cd40lg*$^{-/-}$ mice.
For (B)–(E), (K), and (M), symbols represent individual mice, and bars indicate median. *p ≤ 0.05, **p ≤ 0.01, ***p ≤ 0.001, and ****p ≤ 0.0001.
See also Figure S3.

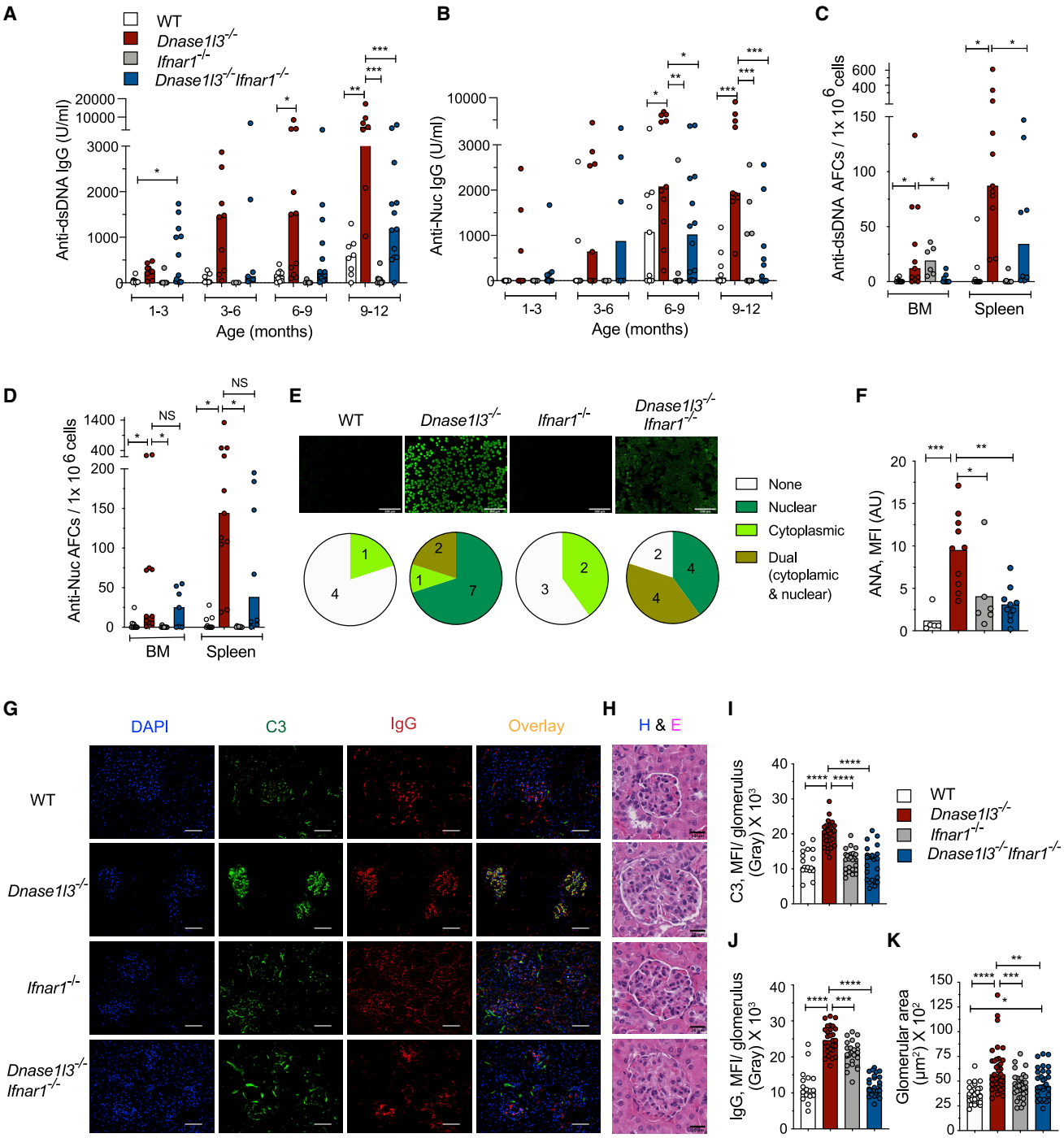

Figure 4. Autoreactivity and Autoimmune Manifestations in *Dnase1l3*$^{-/-}$ Mice Are Facilitated by IFN-I Signaling

WT, *Dnase1l3*$^{-/-}$, *Ifnar1*$^{-/-}$, and *Dnase1l3*$^{-/-}$ *Ifnar1*$^{-/-}$ mice were examined for Abs at the indicated ages or at the 12-month endpoint.

(A and B) Serum anti-dsDNA (A) and anti-Nuc (B) IgG titers determined by ELISA.

(C and D) ELISpot analysis of the number of anti-dsDNA (C) and anti-Nuc (D) AFCs in BM or spleen cells.

(E) Images of HEp-2 cells stained with sera to detect ANAs (representative of n ≥ 5 per strain). Scale bars, 100 μm. Pie charts with numbers indicate distribution of ANA reactivity patterns in mice from each group.

(F) Quantitation of ANA fluorescence intensity.

(legend continued on next page)

pDCs compared to *Tcf4*$^{+/+}$ *Dnase1l3*$^{-/-}$ littermates (Figure S6A), which was also shown to be accompanied by profoundly impaired IFN-I production (Cisse et al., 2008). As expected, B cell subsets, including naive CD23^{hi} CD21^{lo} FO B cells and CD23^{lo} CD21^{hi} IgM^{hi} marginal zone (MZ) B cells, were comparable to WT (Figures S6B and S6C). The induction of Sca-1 expression on B and T cells was rescued in *Dnase1l3*$^{-/-}$ *Tcf4*$^{+/-}$ mice (Figures S6D and 6E), suggesting a global decrease of IFN-I production. Similar to IFNAR1 deficiency, pDC impairment in *Dnase1l3*$^{-/-}$ mice caused a significant reduction of anti-dsDNA and anti-Nuc IgG titers starting at 5–6 months of age (Figures 6A and 6B). Accordingly, splenic anti-DNA AFCs were also significantly reduced in 1-year-old *Dnase1l3*$^{-/-}$*Tcf4*$^{+/-}$ mice (Figure 6C), concomitant with reduced expansion of CD138^{+} PBs in ExFO regions (Figures 6D and 6H) but normal GC B cell numbers (Figure S6F). *Dnase1l3*$^{-/-}$*Tcf4*$^{+/-}$ mice also showed a tendency toward reduced ANA; although the effect was variable, the ANA pattern showed a higher propensity for dual nuclear and cytoplasmic staining (Figures 6E, 6I, and 6J). The reduction in anti-dsDNA titers was further confirmed by CLIFT, wherein only two out of seven sera from *Dnase1l3*$^{-/-}$*Tcf4*$^{+/-}$ mice were positive compared to five out of seven samples from *Dnase1l3*$^{-/-}$ mice at a 1:25 dilution (Figure 6F). A similar reduction of anti-dsDNA titers and a shift toward cytoplasmic ANA staining was observed after the treatment of *Dnase1l3*$^{-/-}$ mice with anti-SiglecH monoclonal Ab (mAb), which inhibits IFN-I production by pDCs (data not shown). All other manifestations of autoimmunity were abolished in *Dnase1l3*$^{-/-}$*Tcf4*$^{+/-}$ mice, including splenomegaly (Figure 6K), T cell activation (Figure S6G), glomerular deposition of C3 and IgG (Figure S6H), and increased size of kidney glomeruli (Figures 6G and 6L). Overall, pDC impairment by *Tcf4* haplodeficiency phenocopied the loss of IFN-I signaling in *Dnase1l3*$^{-/-}$ mice, suggesting pDCs as the primary source of pathogenic IFN-I.

Immunofluorescence staining of *Dnase1l3*$^{-/-}$ spleens revealed the accumulation of B220^{lo} SiglecH^{+} pDCs near the clusters of CD138^{+} PBs at the border of T cell zones, with frequent juxtaposition of the two cell types (Figure S6I). Although short of a formal proof, these data suggest that some pDCs are located in the ExFO region and may directly interact with proliferating PBs. Finally, we activated primary pDCs to produce IFN-α with the TLR9 ligand CpG-A (Figures S6J and S6K) and tested their effect on B cell differentiation. CFSE-labeled B cells from *Dnase1l3*$^{-/-}$ or *Dnase1l3*$^{-/-}$*Ifnar1*$^{-/-}$ mice were stimulated for 3 days with anti-IgM, anti-CD40, and IL-4 in the absence or presence of CpG-A-stimulated pDCs. CpG-A-stimulated pDCs significantly increased the proliferation and differentiation of activated B cells into CD138^{+} SSC^{hi} PBs, and this effect was abolished by IFNAR1 deficiency (Figures 6M, 6N, S6L, and S6M). We confirmed that IFNAR1 was expressed on activated B cells (Figure S6N), IFN-α was detectable in the co-culture supernatant only when pDCs were activated with CpG (Figure S6O), and CD69 was not upregulated on IFNAR1-deficient B cells (Figure S6P). Collectively, these data suggest that pDCs, via the production of IFN-I, directly facilitate anti-DNA responses driven by ExFO B cell differentiation.

Endosomal TLR Signaling Drives Anti-DNA Reactivity and SLE-like Disease

The observed contribution of pDCs, along with the essential requirement for MyD88-dependent signaling (Sisirak et al., 2016), suggested the role of endosomal TLRs in anti-DNA reactivity. Having excluded the sole contribution of TLR7, we generated *Dnase1l3*$^{-/-}$*Tlr9*$^{-/-}$ mice deficient in DNASE1L3 and the endosomal DNA sensor TLR9. Compared to *Dnase1l3*$^{-/-}$ mice, these mice showed only a modest reduction of anti-Nuc Abs but similar titers of anti-dsDNA Abs (Figures 7A and 7B) and similar numbers of anti-dsDNA and anti-Nuc AFCs (Figure 7C). Furthermore, CXCR3^{+} MHC-II^{hi} CD138^{+} ExFO PB and ExFO Th cells were not reduced in *Dnase1l3*$^{-/-}$*Tlr9*$^{-/-}$ mice (Figures S7A and S7B), although a significant reduction of GC B cells was observed (Figure S7C). Total ANA titers in *Dnase1l3*$^{-/-}$*Tlr9*$^{-/-}$ mice were not reduced (Figures 7D); however, the pattern of ANA reactivity shifted toward cytoplasmic or dual nuclear/cytoplasmic staining (Figure 7E). We also observed a significant decrease in immune activation, including splenomegaly (Figure S7D) and expansion of Ly6c^{-} CD11b^{+} myeloid cells (Figures S7E and S7F). Thus, TLR9 alone is largely dispensable for autoreactivity but contributes to downstream consequences of DNASE1L3 deficiency.

To test whether the contribution of TLR9 might be partially compensated by TLR7, we generated *Dnase1l3*$^{-/-}$ mice deficient in both TLR7 and TLR9 (*Dnase1l3*$^{-/-}$*Tlr7*$^{-/-}$*Tlr9*$^{-/-}$). Unlike *Dnase1l3*$^{-/-}$*Tlr9*$^{-/-}$ mice, *Dnase1l3*$^{-/-}$*Tlr7*$^{-/-}$*Tlr9*$^{-/-}$ mice completely lost the reactivity to pure dsDNA in the CLIFT assay (Figure 7F), all anti-dsDNA and anti-Nuc reactivity by ELISA (Figures 7G and 7H), and anti-dsDNA and anti-Nuc AFCs (Figure 7I). This was accompanied by a near-complete loss of ExFO Th cells and of CD138^{+} PB cells expressing CXCR3 (Figures 7J and 7K), in addition to the expected loss of GC B cells (Figure S7G). Similarly, ANA reactivity was completely abolished (Figures 7L and 7M), as was splenomegaly (Figure S7H) and the expansion of CD11b^{+}Ly6c^{-} myeloid cells (data not shown). Finally, increased glomerular size (Figures 7N and 7O) and the glomerular deposition of IgG and C3 (Figure S7I) were fully rescued in *Dnase1l3*$^{-/-}$*Tlr7*$^{-/-}$*Tlr9*$^{-/-}$ mice at the endpoint. Notably, these kidney manifestations were partially reduced in *Dnase1l3*$^{-/-}$*Tlr9*$^{-/-}$ and particularly in *Dnase1l3*$^{-/-}$*Tlr7*$^{-/-}$ mice (Figures 7N, 7O, and S7I), suggesting independent contributions by both TLR9 and TLR7. Altogether, these results reveal essential but partially redundant

(G–K) Images of kidney sections representative of ≥3 mice per group stained for IgG, (red) and C3 (green), and DAPI (blue). Scale bars, 40 μm (G). Images of glomeruli from H&E-stained kidney sections, representative of ≥3 mice per group. Scale bars, 20 μm (H). Quantitation of mean fluorescence intensity of C3 (I) and IgG deposits (J) and size of ≥20 glomeruli per kidney section (K) from three or four mice per strain.

In (A)–(D) and (F), symbols represent individual mice. In (I)–(K), each symbol represents an individual glomerulus. All bars indicate median. NS, not significant; *p ≤ 0.05, **p ≤ 0.01, ***p ≤ 0.001, and ****p ≤ 0.0001.

See also Figure S4.

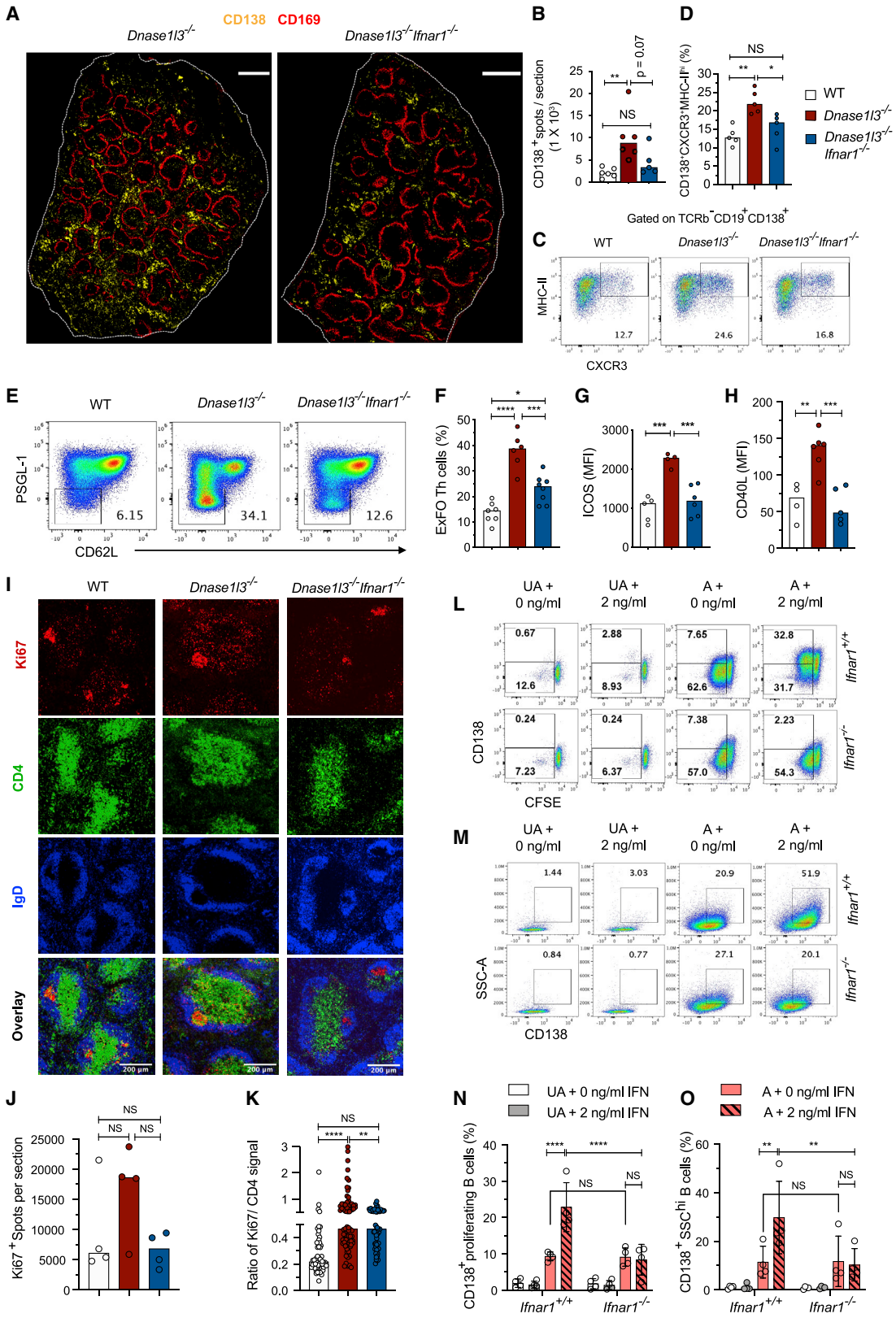

(legend on next page)

contributions of TLR9 and TLR7 to autoimmunity driven by extracellular DNA.

DISCUSSION

Dnase1l3$^{-/-}$ mice model the human genetic DNASE1L3 deficiency that results in SLE and may be relevant for severe sporadic SLE that is frequently associated with reduced extracellular DNase activity (Bruschi et al., 2019). In addition to its clinical relevance, the *Dnase1l3*$^{-/-}$ model manifests prominent anti-dsDNA responses in the absence of additional pathogenetic features such as lymphoproliferation, systemic inflammation, or defects of antigen receptor signaling. Importantly, immunopathology in *Dnase1l3*$^{-/-}$ mice comprises three distinct phases: (1) initial breach of tolerance to DNA (1–3 months); (2) amplification of anti-DNA Ab responses without reactivity to other self-antigens (3–9 months); and (3) spreading of autoreactivity, immune activation and immune complex deposition (9–12 months). This separation of anti-DNA Ab responses from their consequences or other confounding factors make *Dnase1l3*$^{-/-}$ mice an attractive reductionist model of DNA-specific reactivity in SLE.

We found that the ExFO pathway represented the predominant route of autoreactive B cell differentiation in *Dnase1l3*$^{-/-}$ mice, generating short-lived AFCs that produced anti-Nuc and anti-dsDNA Abs. ExFO B cell responses are generally associated with infections, rapidly generating Abs to protect against pathogens (Cunningham et al., 2007; Finke et al., 2001). Although the ExFO-generated PBs have been implicated in a lymphoproliferation-driven model of autoreactivity (William et al., 2002), long-lived plasma cells and the GC pathway leading to them are thought to predominate in other models (Degn et al., 2017; Hoyer et al., 2004). Our results do not rule out the role of GC, which may be prominent at late stages of the disease accompanied by broad autoreactivity (Sisirak et al., 2016) and contribute to the generation of pathogenic Abs that synergize with anti-dsDNA Abs to induce renal disease. Furthermore, anti-dsDNA response in *Dnase1l3*$^{-/-}$ mice can be greatly enhanced by additional genetic lesions that cause the expansion of GCs (Weisenburger et al., 2018). Collectively, our analysis suggests the ExFO pathway as the primary route of differentiation of DNA-reactive B cells, which continuously generates anti-DNA and can be amplified by additional factors that elicit GC-derived plasma cells.

We found that autoreactivity and inflammation in *Dnase1l3*$^{-/-}$ mice required CD40L signaling and were associated with the expansion of CXCR4^{hi}ICOS^{hi} ExFO-Th cells (Odegard et al., 2008), which was also CD40L dependent. This is consistent with the role of T cells in general and ExFO-Th cells in particular in other models of ExFO-driven autoreactive responses (Deng et al., 2017; Sweet et al., 2011). Notably, a population of T cells supporting ExFO B cell expansion in human SLE patients has been described recently (Caielli et al., 2019). Together with this and other descriptions of ExFO B cell differentiation in human SLE (Jenks et al., 2018; Tipton et al., 2015), our data emphasize the predominant role of the ExFO pathway in autoimmunity, including in polyclonal B cell responses driven by DNA. This is consistent with the dynamic nature of anti-dsDNA responses and may also explain the low efficiency of B-cell-focused therapies, as these are often inefficient against PBs (Hale et al., 2018). Indeed, a short 3-day treatment with the anti-proliferative drug cyclophosphamide effectively reduced anti-dsDNA titers, while a month-long treatment with B-cell-depleting anti-CD20 Ab was required for a similar reduction. Therefore, targeting actively proliferating short-lived PBs in lupus patients with high anti-dsDNA titers represents an important therapeutic goal (Soni and Reizis, 2018).

Given the critical role of IFN-I signaling in SLE pathogenesis and specifically in GC-driven B cell autoreactivity (Domeier et al., 2018), we tested the potential role of this pathway in ExFO-driven anti-dsDNA responses. Our analysis in *Dnase1l3*$^{-/-}$ mice revealed that IFN-I was dispensable for the initial emergence of anti-dsDNA Abs but facilitated their subsequent maintenance and amplification. Notably, IFN-I was required for the optimal expansion of ExFO CD138^{+} B cells and ICOS^{hi}ExFO-Th cells. These data agree with enhanced generation of short-lived PBs after overexpression

Figure 5. IFN-I Signaling Promotes ExFO B Cell Proliferation and Differentiation into AFCs

(A and B) Confocal images of half spleens representative of >4, 8- to 9-month-old WT, *Dnase1l3*$^{-/-}$, and *Dnase1l3*$^{-/-}$*Ifnar1*$^{-/-}$ mice, stained for CD169 (red) and CD138^{+} (yellow). Scale bar, 1,000 μm (A).

(B) Total number of CD138^{+} spots per half spleen represented in (A). Each symbol represents half a spleen section

(C and D) Staining profiles of gated splenic CD19^{+}CD138^{+} cells (CXCR3^{+}MHC-II^{hi} ExFO B cells highlighted) (C) and frequencies of ExFO B cells (D) in >10-month-old WT, *Dnase1l3*$^{-/-}$, and *Dnase1l3*$^{-/-}$*Ifnar1*$^{-/-}$ mice.

(E–H) Flow cytometric staining profiles of gated splenic CD4^{+} T cells (PSGL-1^{lo}CD62L^{lo}ExFO Th cells highlighted) (E). Fraction of ExFO Th cells among splenic CD4^{+} T cells (F), mean fluorescence intensity of ICOS (G), and CD40L (H) expressed in ExFO Th cells of 6- to 8-month-old WT, *Dnase1l3*$^{-/-}$, and *Dnase1l3*$^{-/-}$*Ifnar1*$^{-/-}$ mice.

In (C)–(H), wherever applicable, symbols represent individual mice, and bars indicate median.

(I–K) Confocal images of spleen sections representative of three >8-month-old WT, *Dnase1l3*$^{-/-}$, and *Dnase1l3*$^{-/-}$*Ifnar1*$^{-/-}$ mice stained for Ki67^{+} proliferating cells (red), CD4^{+} T cells (green), and IgD^{+} B cells (blue). Scale bars, 200 μm (I). Quantitation of total number of Ki67^{+} spots per half spleen represented in Figure S5B. Each symbol represents half a spleen section (J). Ratio of mean fluorescence intensity of Ki67 versus CD4 within a region of interest (ROI) marking CD4^{+} T cell zones, excluding GC areas, from spleen sections represented in Figure S5B. Each symbol represents a single ROI (K).

(L–O) Flow cytometric analysis of proliferation and differentiation of B cells upon *in vitro* activation with anti-IgM and anti-CD40 in the presence or absence of IFN-α. Shown are representative flow plots from four independent experiments of purified CFSE-labeled unactivated (UA) or activated (A) B cells from *Ifnar1*$^{+/+}$ or *Ifnar1*$^{-/-}$ mice cultured for 72 h in the absence (0 ng/mL) or presence of 2 ng/mL of IFN-α. The cells in the gates indicate CFSE^{lo} proliferating B cells, with (upper gate) or without (lower gate) CD138 expression (L) or CD138^{+}SSC^{hi} B cells (M), under the indicated conditions. Fraction of CD138^{+} proliferating (N) and CD138^{+}SSC^{hi} blasting (O) B cells. Each symbol represents an independent experiment.

Error bars show mean ± SD. Two-way ANOVA followed by Tukey's multiple comparison test was used to compare different treatments within a genotype, or two-way ANOVA followed by Sidak's multiple comparison test was used to compare different treatments between the two genotypes. NS, not significant; *$p \leq 0.05$, **$p \leq 0.01$, ***$p \leq 0.001$, and ****$p \leq 0.0001$. See also Figure S5.

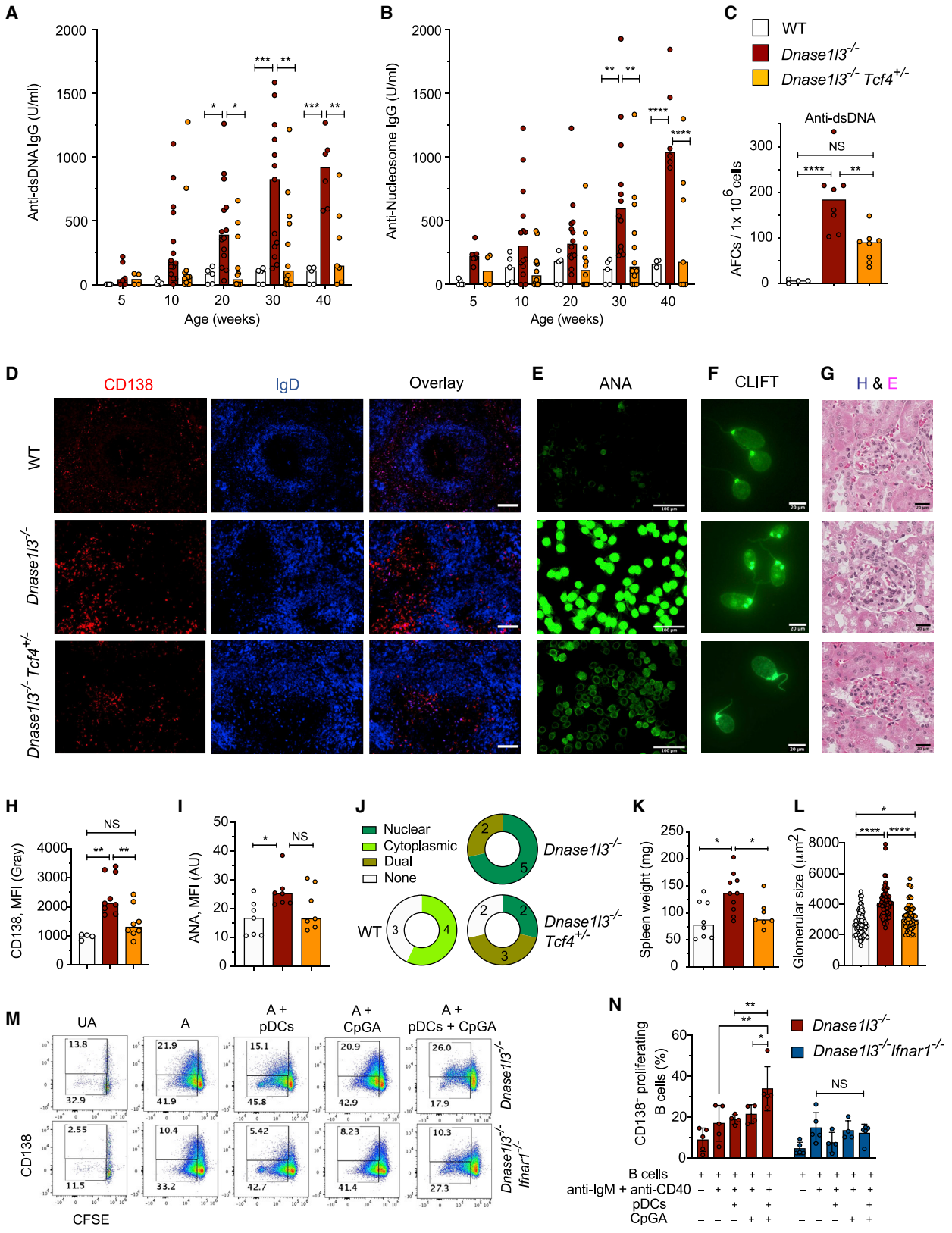

(legend on next page)

of IFN-I in lupus-prone mice (Mathian et al., 2011) and establish the role of endogenous IFN-I in the ExFO pathway. *In vitro*, IFN-I enhanced B cell differentiation into CD138$^+$ PBs that was driven by BCR and CD40 signaling, but not by LPS, which presumably mimics B cell responses driven by bacterial pathogens. Thus, continuous activation of self-reactive B cells by antigenic self-DNA, alongside costimulatory signals from T cells, makes B cells responsive to IFN-I-mediated differentiation into AFCs and therefore may be particularly important for auto-Ab responses in SLE.

Although the responsiveness of human pDCs to self-DNA (Barrat et al., 2005; Caielli et al., 2016) and the important role of murine pDCs in several SLE models (Rowland et al., 2014; Sisirak et al., 2014) are well established, the mechanism of pDC activity in SLE remains unclear. Furthermore, pDCs appear dispensable in certain models of SLE-like autoreactivity such as Wiskott-Aldrich syndrome deficiency (Sawai et al., 2018). We found that the functional impairment of pDCs phenocopied IFN-I blockade, including the impairment of ExFO-driven anti-DNA responses prior to the abrogation of all downstream pathology. The production of IFN-I by pDCs *in vivo* has been difficult to detect in this or any other SLE model, likely because of its low and/or transient nature. Nevertheless, in addition to genetic evidence, we were able to show that activated pDCs facilitated CD40-driven PB differentiation *in vitro*, and this effect was IFN-I dependent. Together with similar observations for human pDCs *in vitro* (Jego et al., 2003), these results underscore the emerging role of pDCs as essential IFN-I producers in SLE. They further support Ab-mediated depletion or functional impairment of pDCs as a viable and potentially specific therapeutic strategy in SLE (Barrat and Su, 2019).

Autoreactivity in *Dnase1l3*$^{-/-}$ mice is independent of STING-dependent cytosolic DNA sensing and is completely dependent on MyD88 (Sisirak et al., 2016). We found that the loss of the sole known endosomal DNA receptor, TLR9, had no major effect on anti-dsDNA response as noticed in another Dnase1l3-deficient mouse strain (Weisenburger et al., 2018) and caused a minor albeit significant reduction of immune activation. However, the loss of TLR9 in the absence of TLR7 completely abrogated autoreactivity and pathology, suggesting that TLR9 promoted anti-DNA response yet its pathogenic function was partially compensated by TLR7. The mechanism of such compensation may include a functional competition between the two receptors, whereby TLR9 deletion creates a hyperactive TLR7 (Fukui et al., 2009). This scenario is consistent with the observed shift in auto-Ab reactivity by ANA staining pattern as also observed in other SLE models (Christensen et al., 2006; Nickerson et al., 2010). Another possible mechanism includes the ability of TLR7 to recognize both RNA and DNA degradation products such as guanosine and deoxyguanosine, respectively (Shibata et al., 2016). Indeed, the self-antigen in DNASE1L3 deficiency and presumably other SLE forms comprises chromatin in apoptotic microparticles (Nielsen et al., 2011; Pisetsky et al., 2011; Sisirak et al., 2016), which are likely to contain DNA and RNA and their degradation products. Irrespective of the mechanism, the synergistic yet partially redundant role of TLR9 and TLR7 in anti-DNA autoreactivity is consistent with (1) the redundancy between the two receptors in an Ab-independent kidney inflammation driven by monocytes (Kuriakose et al., 2019) and (2) the requirement for endosomal TLR sensing, but not TLR9 alone, in DNA-driven autoimmunity in Dnase2-deficient mice (Pawaria et al., 2015). Our results help reconcile the neutral or even pathogenic effects of deleting TLR9 alone in several SLE models (Celhar et al., 2012; Christensen and Shlomchik, 2007; Sharma et al., 2015) with the emerging pathogenic role of TLR9 in human SLE (Barrat et al., 2005; Caielli et al., 2016). Collectively, our analysis of autoreactivity driven by extracellular DNA supports a prominent role for ExFO B cell differentiation into AFCs that requires endosomal TLR signaling and is facilitated by pDCs and IFN-I.

STAR★METHODS

Detailed methods are provided in the online version of this paper and include the following:

- KEY RESOURCES TABLE
- RESOURCE AVAILABILITY
  - Lead Contact
  - Materials Availability

Figure 6. Functional Impairment of pDCs in *Dnase1l3*$^{-/-}$ Mice Ameliorates Autoreactivity and Disease

WT, *Dnase1l3*$^{-/-}$, and *Dnase1l3*$^{-/-}$ mice with monoallelic deficiency of *Tcf4* (*Dnase1l3*$^{-/-}$*Tcf4*$^{+/-}$) were examined for Abs at the indicated ages or at the 12-month endpoint.

(A and B) Serum anti-dsDNA IgG (A) and anti-Nuc (B) IgG titers by ELISA.

(C) Frequency of anti-dsDNA AFCs in the spleen by ELISpot.

(D) Spleen sections stained for CD138$^+$ cells (red) and follicular B cells (blue). Representative of three or more mice per group. Scale bars, 40 μm.

(E) ANA assay images (representative of seven mice per group). Scale bar, 100 μm.

(F) CLIFT assay for anti-dsDNA IgG (representative of five mice per group). Scale bar, 20 μm.

(G) Glomeruli from H&E-stained kidney sections (representative of three mice per group). Scale bars, 20 μm.

(H) Intensity of CD138 fluorescence in ≥4 images of spleen sections from the indicated mice.

(I and J) Quantitation of ANA fluorescence intensity (I) and distribution of ANA reactivity patterns (J) in seven mice per indicated group.

(K) Spleen weights of indicated mice at the endpoint.

(L) Quantitation of the size of ≥20 glomeruli per kidney section from three mice per group. Each symbol represents an individual glomerulus; bars indicate median.

(M and N) Purified CFSE-labeled B cells from *Dnase1l3*$^{-/-}$ or *Dnase1l3*$^{-/-}$*Ifnar1*$^{-/-}$ mice were left unactivated (UA), activated with anti-IgM + anti-CD40 (A), or activated with anti-IgM + anti-CD40 in the presence of unstimulated pDCs (A+ pDCs), 1 μM CpG-A (A+ CpG-A), or pDCs stimulated with 1 μM CpG-A (A+ pDCs+ CpG-A) for 72 h, after which the B cells were analyzed for proliferation and differentiation using flow cytometry. Gating strategy (M) and quantitation (N) of CFSE^{lo}CD138$^+$ proliferating B cells.

Error bars show mean ± SD from four independent experiments (symbols). NS, not significant; *p ≤ 0.05, **p ≤ 0.01, ***p ≤ 0.001, and ****p ≤ 0.0001.

See also Figure S6.

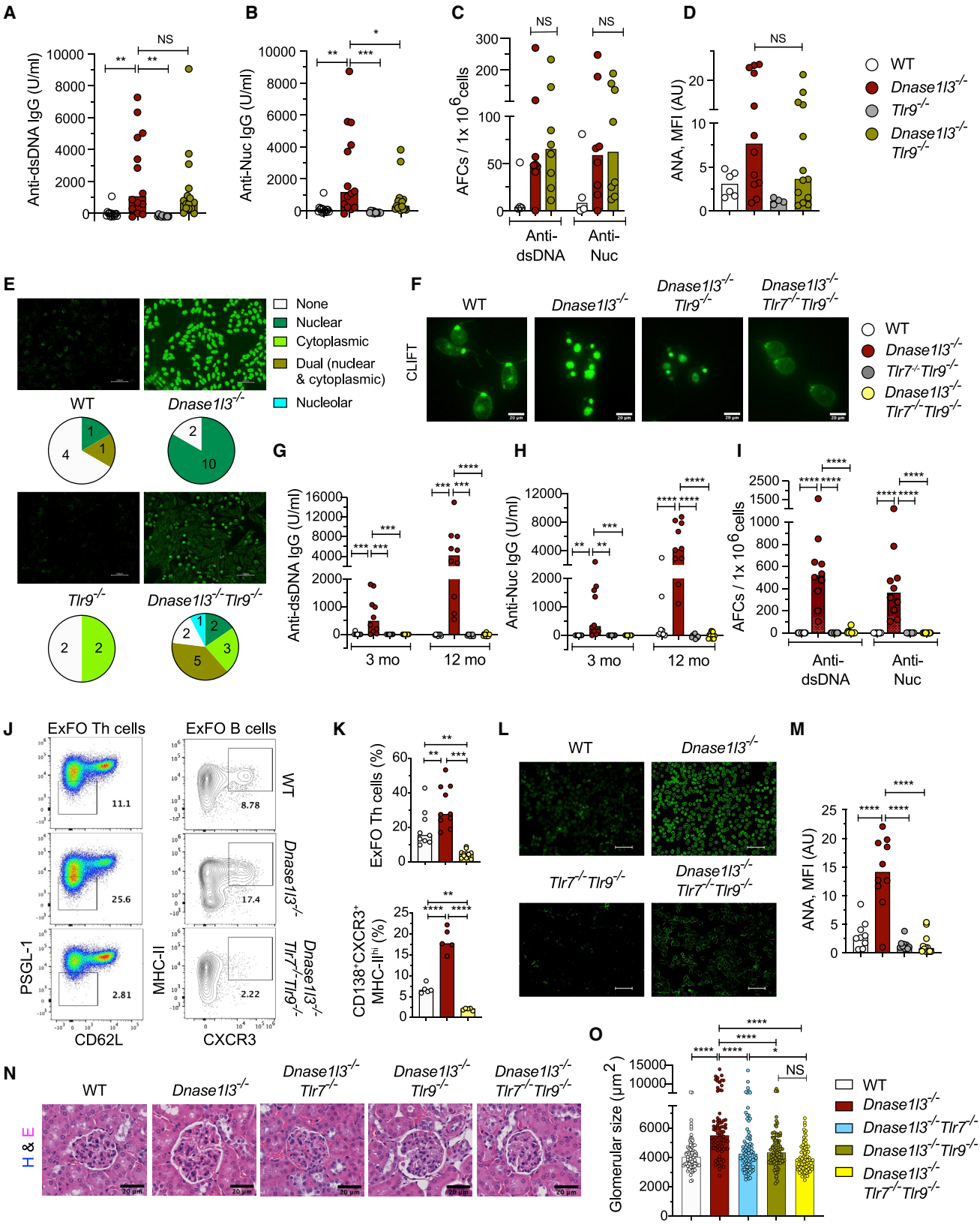

(legend on next page)

SUPPLEMENTAL INFORMATION

Supplemental Information can be found online at https://doi.org/10.1016/j.immuni.2020.04.015.

ACKNOWLEDGMENTS

This work was supported by NIH grants AI072571 (B.R.), AR071703 (B.R. and G.C.I.), AR070591 (B.R.), CA232666 (O.A.P.), AI100853 (O.A.P. and L.S.), AR069515 (L.S.), HL145997 (J.N.P), CA009161 (J.N.P.), CA110624 (G.C.I.), and AR071703 (G.C.I.); and by the Lupus Research Alliance (B.R.), the Colton Center for Autoimmunity (B.R.), the Idex Junior Chair program from Bordeaux University (V.S.), and a Cancer Research Institute CLIP grant (V.S.).

AUTHOR CONTRIBUTIONS

V.S. initiated, performed, and analyzed experiments. C.S., O.A.P., L.S., J.N.P., K.L.C., J.M., W.N.V., and J.G. performed and analyzed experiments. G.G. and G.C.I. supervised the analysis of B cell repertoire. B.R. analyzed the results and supervised the project. C.S. and B.R. wrote the manuscript with input from all coauthors.

DECLARATION OF INTERESTS

The authors declare no competing interests.

Received: September 11, 2019
Revised: March 13, 2020
Accepted: April 23, 2020
Published: May 25, 2020

REFERENCES

Agrawal, H., Jacob, N., Carreras, E., Bajana, S., Putterman, C., Turner, S., Neas, B., Mathian, A., Koss, M.N., Stohl, W., et al. (2009). Deficiency of type I IFN receptor in lupus-prone New Zealand mixed 2328 mice decreases dendritic cell numbers and activation and protects from disease. J. Immunol. *183*, 6021–6029.

Al-Mayouf, S.M., Sunker, A., Abdwani, R., Abrawi, S.A., Almurshedi, F., Alhashmi, N., Al Sonbul, A., Sewairi, W., Qari, A., Abdallah, E., et al. (2011). Loss-of-function variant in DNASE1L3 causes a familial form of systemic lupus erythematosus. Nat. Genet. *43*, 1186–1188.

Barrat, F.J., and Su, L. (2019). A pathogenic role of plasmacytoid dendritic cells in autoimmunity and chronic viral infection. J. Exp. Med. *216*, 1974–1985.

Barrat, F.J., Meeker, T., Gregorio, J., Chan, J.H., Uematsu, S., Akira, S., Chang, B., Duramad, O., and Coffman, R.L. (2005). Nucleic acids of mammalian origin can act as endogenous ligands for Toll-like receptors and may promote systemic lupus erythematosus. J. Exp. Med. *202*, 1131–1139.

Bennett, L., Palucka, A.K., Arce, E., Cantrell, V., Borvak, J., Banchereau, J., and Pascual, V. (2003). Interferon and granulopoiesis signatures in systemic lupus erythematosus blood. J. Exp. Med. *197*, 711–723.

Bolger, A.M., Lohse, M., and Usadel, B. (2014). Trimmomatic: a flexible trimmer for Illumina sequence data. Bioinformatics *30*, 2114–2120.

Bolotin, D.A., Poslavsky, S., Mitrophanov, I., Shugay, M., Mamedov, I.Z., Putintseva, E.V., and Chudakov, D.M. (2015). MiXCR: software for comprehensive adaptive immunity profiling. Nat. Methods *12*, 380–381.

Bruschi, M., Bonanni, A., Petretto, A., Vaglio, A., Pratesi, F., Santucci, L., Migliorini, P., Bertelli, R., Galetti, M., Belletti, S., et al. (2019). Neutrophil extracellular traps (NETs) profiles in patients with incident SLE and lupus nephritis. J. Rheumatol.

Buechler, M.B., Teal, T.H., Elkon, K.B., and Hamerman, J.A. (2013). Cutting edge: Type I IFN drives emergency myelopoiesis and peripheral myeloid expansion during chronic TLR7 signaling. J. Immunol. *190*, 886–891.

Caielli, S., Athale, S., Domic, B., Murat, E., Chandra, M., Banchereau, R., Baisch, J., Phelps, K., Clayton, S., Gong, M., et al. (2016). Oxidized mitochondrial nucleoids released by neutrophils drive type I interferon production in human lupus. J. Exp. Med. *213*, 697–713.

Figure 7. TLR9 and TLR7 Are Redundantly Required for Autoreactivity and Autoimmunity

WT, *Dnase1l3*$^{-/-}$, *Tlr9*$^{-/-}$, or *Tlr7*$^{-/-}$ mice or crosses thereof were examined for Abs at the indicated ages or at the 12-month endpoint.
(A and B) Serum anti-dsDNA IgG (A) and anti-Nuc (B) IgG titers by ELISA.
(C) Frequency of anti-dsDNA and anti-Nuc AFCs in the spleen by ELISpot.
(D and E) ANA assay, showing quantitation of fluorescence intensity (D), and representative images and the distribution of reactivity patterns in mice from each group (E).
(F) CLIFT assay for anti-dsDNA IgG (representative of $\geq$ 4 mice per strain). Scale bar, 20 μm.
(G and H) Serum anti-dsDNA IgG (A) and anti-Nuc (B) IgG titers by ELISA.
(I) Frequency of anti-dsDNA and anti-Nuc AFCs in the spleen as determined by ELISpot.
(J) Staining profiles of gated splenic CD4$^+$ T cells (PSGL-1^{lo}CD62L$^-$ ExFO Th cells highlighted) and CD19$^+$ CD138$^+$ cells (CXCR3$^+$ MHC-II^{hi} ExFO B cells highlighted).
(K) Frequencies of populations highlighted in (J) at the endpoint.
(L and M) ANA assay showing images representative of $\geq$8 mice per strain (L), and quantitation of fluorescence intensity (M). Scale bars, 100 μm.
(N) Glomeruli from H&E-stained kidney sections (representative of four mice per group). Scale bars, 20 μm.
(O) Size of $\geq$20 glomeruli per kidney section from four mice per group.
Symbols represent individual mice, except in (O), where they represent individual glomeruli. All bars indicate median. NS, not significant; *p $\leq$ 0.05, **p $\leq$ 0.01, ***p $\leq$ 0.001, and ****p $\leq$ 0.0001.
See also Figure S7.

Caielli, S., Veiga, D.T., Balasubramanian, P., Athale, S., Domic, B., Murat, E., Banchereau, R., Xu, Z., Chandra, M., Chung, C.H., et al. (2019). A $CD4^+$ T cell population expanded in lupus blood provides B cell help through interleukin-10 and succinate. Nat. Med. *25*, 75–81.

Celhar, T., Magalhães, R., and Fairhurst, A.M. (2012). TLR7 and TLR9 in SLE: when sensing self goes wrong. Immunol. Res. *53*, 58–77.

Christensen, S.R., and Shlomchik, M.J. (2007). Regulation of lupus-related autoantibody production and clinical disease by Toll-like receptors. Semin. Immunol. *19*, 11–23.

Christensen, S.R., Shupe, J., Nickerson, K., Kashgarian, M., Flavell, R.A., and Shlomchik, M.J. (2006). Toll-like receptor 7 and TLR9 dictate autoantibody specificity and have opposing inflammatory and regulatory roles in a murine model of lupus. Immunity *25*, 417–428.

Cisse, B., Caton, M.L., Lehner, M., Maeda, T., Scheu, S., Locksley, R., Holmberg, D., Zweier, C., den Hollander, N.S., Kant, S.G., et al. (2008). Transcription factor E2-2 is an essential and specific regulator of plasmacytoid dendritic cell development. Cell *135*, 37–48.

Cunningham, A.F., Gaspal, F., Serre, K., Mohr, E., Henderson, I.R., Scott-Tucker, A., Kenny, S.M., Khan, M., Toellner, K.M., Lane, P.J., and MacLennan, I.C. (2007). Salmonella induces a switched antibody response without germinal centers that impedes the extracellular spread of infection. J. Immunol. *178*, 6200–6207.

Das, A., Heesters, B.A., Bialas, A., O'Flynn, J., Rifkin, I.R., Ochando, J., Mittereder, N., Carlesso, G., Herbst, R., and Carroll, M.C. (2017). Follicular dendritic cell activation by TLR ligands promotes autoreactive B cell responses. Immunity *46*, 106–119.

Degn, S.E., van der Poel, C.E., Firl, D.J., Ayoglu, B., Al Qureshah, F.A., Bajic, G., Mesin, L., Reynaud, C.A., Weill, J.C., Utz, P.J., et al. (2017). Clonal evolution of autoreactive germinal centers. Cell *170*, 913–926.e919.

Deng, R., Hurtz, C., Song, Q., Yue, C., Xiao, G., Yu, H., Wu, X., Muschen, M., Forman, S., Martin, P.J., and Zeng, D. (2017). Extrafollicular $CD4^+$ T-B interactions are sufficient for inducing autoimmune-like chronic graft-versus-host disease. Nat. Commun. *8*, 978.

Domeier, P.P., Chodisetti, S.B., Schell, S.L., Kawasawa, Y.I., Fasnacht, M.J., Soni, C., and Rahman, Z.S.M. (2018). B-cell-intrinsic type 1 interferon signaling is crucial for loss of tolerance and the development of autoreactive B cells. Cell Rep. *24*, 406–418.

Edgar, R.C. (2010). Search and clustering orders of magnitude faster than BLAST. Bioinformatics *26*, 2460–2461.

Finke, D., Baribaud, F., Diggelmann, H., and Acha-Orbea, H. (2001). Extrafollicular plasmablast B cells play a key role in carrying retroviral infection to peripheral organs. J. Immunol. *166*, 6266–6275.

Fukui, R., Saitoh, S., Matsumoto, F., Kozuka-Hata, H., Oyama, M., Tabeta, K., Beutler, B., and Miyake, K. (2009). Unc93B1 biases Toll-like receptor responses to nucleic acid in dendritic cells toward DNA- but against RNA-sensing. J. Exp. Med. *206*, 1339–1350.

Hale, M., Rawlings, D.J., and Jackson, S.W. (2018). The long and the short of it: insights into the cellular source of autoantibodies as revealed by B cell depletion therapy. Curr. Opin. Immunol. *55*, 81–88.

Hamilton, J.A., Wu, Q., Yang, P., Luo, B., Liu, S., Hong, H., Li, J., Walter, M.R., Fish, E.N., Hsu, H.C., and Mountz, J.D. (2017). Cutting Edge: Endogenous IFN-β Regulates Survival and Development of Transitional B Cells. J. Immunol. *199*, 2618–2623.

Hoyer, B.F., Moser, K., Hauser, A.E., Peddinghaus, A., Voigt, C., Eilat, D., Radbruch, A., Hiepe, F., and Manz, R.A. (2004). Short-lived plasmablasts and long-lived plasma cells contribute to chronic humoral autoimmunity in NZB/W mice. J. Exp. Med. *199*, 1577–1584.

Jackson, S.W., Scharping, N.E., Kolhatkar, N.S., Khim, S., Schwartz, M.A., Li, Q.Z., Hudkins, K.L., Alpers, C.E., Liggitt, D., and Rawlings, D.J. (2014). Opposing impact of B cell-intrinsic TLR7 and TLR9 signals on autoantibody repertoire and systemic inflammation. J. Immunol. *192*, 4525–4532.

Jego, G., Palucka, A.K., Blanck, J.P., Chalouni, C., Pascual, V., and Banchereau, J. (2003). Plasmacytoid dendritic cells induce plasma cell differentiation through type I interferon and interleukin 6. Immunity *19*, 225–234.

Jenks, S.A., Cashman, K.S., Zumaquero, E., Marigorta, U.M., Patel, A.V., Wang, X., Tomar, D., Woodruff, M.C., Simon, Z., Bugrovsky, R., et al. (2018). Distinct effector B cells induced by unregulated Toll-like receptor 7 contribute to pathogenic responses in systemic lupus erythematosus. Immunity *49*, 725–739.e726.

Jenks, S.A., Cashman, K.S., Woodruff, M.C., Lee, F.E., and Sanz, I. (2019). Extrafollicular responses in humans and SLE. Immunol. Rev. *288*, 136–148.

Kirou, K.A., Lee, C., George, S., Louca, K., Peterson, M.G., and Crow, M.K. (2005). Activation of the interferon-alpha pathway identifies a subgroup of systemic lupus erythematosus patients with distinct serologic features and active disease. Arthritis Rheum. *52*, 1491–1503.

Kuriakose, J., Redecke, V., Guy, C., Zhou, J., Wu, R., Ippagunta, S.K., Tillman, H., Walker, P.D., Vogel, P., and Häcker, H. (2019). Patrolling monocytes promote the pathogenesis of early lupus-like glomerulonephritis. J. Clin. Invest. *129*, 2251–2265.

Le Bon, A., Schiavoni, G., D'Agostino, G., Gresser, I., Belardelli, F., and Tough, D.F. (2001). Type i interferons potently enhance humoral immunity and can promote isotype switching by stimulating dendritic cells in vivo. Immunity *14*, 461–470.

Le Bon, A., Thompson, C., Kamphuis, E., Durand, V., Rossmann, C., Kalinke, U., and Tough, D.F. (2006). Cutting edge: enhancement of antibody responses through direct stimulation of B and T cells by type I IFN. J. Immunol. *176*, 2074–2078.

Leadbetter, E.A., Rifkin, I.R., Hohlbaum, A.M., Beaudette, B.C., Shlomchik, M.J., and Marshak-Rothstein, A. (2002). Chromatin-IgG complexes activate B cells by dual engagement of IgM and Toll-like receptors. Nature *416*, 603–607.

Lesley, R., Kelly, L.M., Xu, Y., and Cyster, J.G. (2006). Naive CD4 T cells constitutively express CD40L and augment autoreactive B cell survival. Proc. Natl. Acad. Sci. USA *103*, 10717–10722.

Mathian, A., Gallegos, M., Pascual, V., Banchereau, J., and Koutouzov, S. (2011). Interferon-α induces unabated production of short-lived plasma cells in pre-autoimmune lupus-prone (NZB×NZW)F1 mice but not in BALB/c mice. Eur. J. Immunol. *41*, 863–872.

Muskardin, T.L.W., and Niewold, T.B. (2018). Type I interferon in rheumatic diseases. Nat. Rev. Rheumatol. *14*, 214–228.

Nickerson, K.M., Christensen, S.R., Shupe, J., Kashgarian, M., Kim, D., Elkon, K., and Shlomchik, M.J. (2010). TLR9 regulates TLR7- and MyD88-dependent autoantibody production and disease in a murine model of lupus. J. Immunol. *184*, 1840–1848.

Nielsen, C.T., Østergaard, O., Johnsen, C., Jacobsen, S., and Heegaard, N.H. (2011). Distinct features of circulating microparticles and their relationship to clinical manifestations in systemic lupus erythematosus. Arthritis Rheum. *63*, 3067–3077.

Odegard, J.M., Marks, B.R., DiPlacido, L.D., Poholek, A.C., Kono, D.H., Dong, C., Flavell, R.A., and Craft, J. (2008). ICOS-dependent extrafollicular helper T cells elicit IgG production via IL-21 in systemic autoimmunity. J. Exp. Med. *205*, 2873–2886.

Ozçakar, Z.B., Foster, J., 2nd, Diaz-Horta, O., Kasapcopur, O., Fan, Y.S., Yalçınkaya, F., and Tekin, M. (2013). DNASE1L3 mutations in hypocomplementemic urticarial vasculitis syndrome. Arthritis Rheum. *65*, 2183–2189.

Pawaria, S., Moody, K.L., Busto, P., Nündel, K., Baum, R., Sharma, S., Gravallese, E.M., Fitzgerald, K.A., and Marshak-Rothstein, A. (2015). An unexpected role for RNA-sensing toll-like receptors in a murine model of DNA accrual. Clin. Exp. Rheumatol. *33* (4, Suppl 92), S70–S73.

Pisetsky, D.S. (2016). Anti-DNA antibodies–quintessential biomarkers of SLE. Nat. Rev. Rheumatol. *12*, 102–110.

Pisetsky, D.S., Gauley, J., and Ullal, A.J. (2011). Microparticles as a source of extracellular DNA. Immunol. Res. *49*, 227–234.

Radic, M.Z., and Weigert, M. (1994). Genetic and structural evidence for antigen selection of anti-DNA antibodies. Annu. Rev. Immunol. *12*, 487–520.

Rowland, S.L., Riggs, J.M., Gilfillan, S., Bugatti, M., Vermi, W., Kolbeck, R., Unanue, E.R., Sanjuan, M.A., and Colonna, M. (2014). Early, transient

depletion of plasmacytoid dendritic cells ameliorates autoimmunity in a lupus model. J. Exp. Med. *211*, 1977–1991.

Santiago-Raber, M.L., Baccala, R., Haraldsson, K.M., Choubey, D., Stewart, T.A., Kono, D.H., and Theofilopoulos, A.N. (2003). Type-I interferon receptor deficiency reduces lupus-like disease in NZB mice. J. Exp. Med. *197*, 777–788.

Sawai, C.M., Serpas, L., Neto, A.G., Jang, G., Rashidfarrokhi, A., Kolbeck, R., Sanjuan, M.A., Reizis, B., and Sisirak, V. (2018). Plasmacytoid dendritic cells are largely dispensable for the pathogenesis of experimental inflammatory bowel disease. Front. Immunol. *9*, 2475.

Seo, S.J., Fields, M.L., Buckler, J.L., Reed, A.J., Mandik-Nayak, L., Nish, S.A., Noelle, R.J., Turka, L.A., Finkelman, F.D., Caton, A.J., and Erikson, J. (2002). The impact of T helper and T regulatory cells on the regulation of anti-double-stranded DNA B cells. Immunity *16*, 535–546.

Serpas, L., Chan, R.W.Y., Jiang, P., Ni, M., Sun, K., Rashidfarrokhi, A., Soni, C., Sisirak, V., Lee, W.S., Cheng, S.H., et al. (2019). *Dnase1l3* deletion causes aberrations in length and end-motif frequencies in plasma DNA. Proc. Natl. Acad. Sci. USA *116*, 641–649.

Sharma, S., Fitzgerald, K.A., Cancro, M.P., and Marshak-Rothstein, A. (2015). Nucleic acid-sensing receptors: rheostats of autoimmunity and autoinflammation. J. Immunol. *195*, 3507–3512.

Shi, W., Liao, Y., Willis, S.N., Taubenheim, N., Inouye, M., Tarlinton, D.M., Smyth, G.K., Hodgkin, P.D., Nutt, S.L., and Corcoran, L.M. (2015). Transcriptional profiling of mouse B cell terminal differentiation defines a signature for antibody-secreting plasma cells. Nat. Immunol. *16*, 663–673.

Shibata, T., Ohto, U., Nomura, S., Kibata, K., Motoi, Y., Zhang, Y., Murakami, Y., Fukui, R., Ishimoto, T., Sano, S., et al. (2016). Guanosine and its modified derivatives are endogenous ligands for TLR7. Int. Immunol. *28*, 211–222.

Sisirak, V., Ganguly, D., Lewis, K.L., Couillault, C., Tanaka, L., Bolland, S., D'Agati, V., Elkon, K.B., and Reizis, B. (2014). Genetic evidence for the role of plasmacytoid dendritic cells in systemic lupus erythematosus. J. Exp. Med. *211*, 1969–1976.

Sisirak, V., Sally, B., D'Agati, V., Martinez-Ortiz, W., Özçakar, Z.B., David, J., Rashidfarrokhi, A., Yeste, A., Panea, C., Chida, A.S., et al. (2016). Digestion of chromatin in apoptotic cell microparticles prevents autoimmunity. Cell *166*, 88–101.

Soni, C., and Reizis, B. (2018). DNA as a self-antigen: nature and regulation. Curr. Opin. Immunol. *55*, 31–37.

Soni, C., Wong, E.B., Domeier, P.P., Khan, T.N., Satoh, T., Akira, S., and Rahman, Z.S. (2014). B cell-intrinsic TLR7 signaling is essential for the development of spontaneous germinal centers. J. Immunol. *193*, 4400–4414.

Sweet, R.A., Ols, M.L., Cullen, J.L., Milam, A.V., Yagita, H., and Shlomchik, M.J. (2011). Facultative role for T cells in extrafollicular Toll-like receptor-dependent autoreactive B-cell responses in vivo. Proc. Natl. Acad. Sci. USA *108*, 7932–7937.

Tipton, C.M., Fucile, C.F., Darce, J., Chida, A., Ichikawa, T., Gregoretti, I., Schieferl, S., Hom, J., Jenks, S., Feldman, R.J., et al. (2015). Diversity, cellular origin and autoreactivity of antibody-secreting cell population expansions in acute systemic lupus erythematosus. Nat. Immunol. *16*, 755–765.

Vinuesa, C.G., Sanz, I., and Cook, M.C. (2009). Dysregulation of germinal centres in autoimmune disease. Nat. Rev. Immunol. *9*, 845–857.

Vinuesa, C.G., Linterman, M.A., Yu, D., and MacLennan, I.C. (2016). Follicular helper T cells. Annu. Rev. Immunol. *34*, 335–368.

Weckerle, C.E., Franek, B.S., Kelly, J.A., Kumabe, M., Mikolaitis, R.A., Green, S.L., Utset, T.O., Jolly, M., James, J.A., Harley, J.B., and Niewold, T.B. (2011). Network analysis of associations between serum interferon-α activity, autoantibodies, and clinical features in systemic lupus erythematosus. Arthritis Rheum. *63*, 1044–1053.

Weisenburger, T., von Neubeck, B., Schneider, A., Ebert, N., Schreyer, D., Acs, A., and Winkler, T.H. (2018). Epistatic interactions between mutations of deoxyribonuclease 1-like 3 and the inhibitory Fc gamma receptor IIB result in very early and massive autoantibodies against double-stranded DNA. Front. Immunol. *9*, 1551.

Westra, H.J., Martínez-Bonet, M., Onengut-Gumuscu, S., Lee, A., Luo, Y., Teslovich, N., Worthington, J., Martin, J., Huizinga, T., Klareskog, L., et al. (2018). Fine-mapping and functional studies highlight potential causal variants for rheumatoid arthritis and type 1 diabetes. Nat. Genet. *50*, 1366–1374.

William, J., Euler, C., Christensen, S., and Shlomchik, M.J. (2002). Evolution of autoantibody responses via somatic hypermutation outside of germinal centers. Science *297*, 2066–2070.

Yung, S., and Chan, T.M. (2015). Mechanisms of kidney injury in lupus nephritis: the role of anti-dsDNA antibodies. Front. Immunol. *6*, 475.

Zhuang, Y., Cheng, P., and Weintraub, H. (1996). B-lymphocyte development is regulated by the combined dosage of three basic helix-loop-helix genes, E2A, E2-2, and HEB. Mol. Cell. Biol. *16*, 2898–2905.

Zochling, J., Newell, F., Charlesworth, J.C., Leo, P., Stankovich, J., Cortes, A., Zhou, Y., Stevens, W., Sahhar, J., Roddy, J., et al. (2014). An Immunochip-based interrogation of scleroderma susceptibility variants identifies a novel association at DNASE1L3. Arthritis Res. Ther. *16*, 438.

STAR★METHODS

KEY RESOURCES TABLE

REAGENT or RESOURCE	SOURCE	IDENTIFIER
Antibodies		
V450- anti-mouse CD19 (1D3)	BD Biosciences	Cat # 560375; RRID:AB_1645269
PE/Cy7 anti-mouse CD4 (RM4-5)	eBioscience	Cat # 25-0042-82; RRID:AB_469578
APC-anti-mouse CD4 (GK1.5)	eBioscience	Cat # 17-0041-81; RRID:AB_469319
BV711-anti-mouse CD4 (RM4-5)	BioLegend	Cat # 100549; RRID:AB_11219396
PE anti-mouse CD11b (M1/70)	eBioscience	Cat # 12-0112-81; RRID:AB_465546
FITC anti-mouse CD11c (N418)	eBioscience	Cat # 11-0114-82; RRID:AB_464940
AF700 anti-mouse CD44 (IM7)	BD PharMingen	Cat # 560567; RRID:AB_1727480
APC anti-mouse CD44 (IM7)	eBioscience	Cat # 17-0441-83; RRID:AB_469391
PeCy7 anti-mouse CD69 (H1.2F3)	eBioscience	Cat # 25-0691-81; RRID:AB_469636
PE anti mouse PD-1 (29F.IA12)	BioLegend	Cat # 135205; RRID:AB_1877232
BV605 anti-mouse ICOS (C398.4A)	BioLegend	Cat # 313537; RRID:AB_2687078
PE anti-mouse CD162 (PSGL-1) (2PH1)	BD PharMingen	Cat # 555306; RRID:AB_395719
BV711 anti-mouse CD40L (MR1)	BD Bioscience	Cat # 740685; RRID:AB_2740371
PE anti-mouse CD138 (281-2)	BD PharMingen	Cat # 561070; RRID:AB_2033998
PEy7 anti-mouse CD138 (281-2)	BioLegend	Cat # 142514; RRID:AB_2562198
FITC anti-mouse CD62L (MEL-14)	eBioscience	Cat # 11-0621-82; RRID:AB_465109
PerCP/Cy5.5 anti-mouse CD25 (PC61)	BioLegend	Cat # 102029; RRID:AB_893291
Pacific Blue anti-mouse B220 (RA3-6B2)	BioLegend	Cat # 103227; RRID:AB_492876
BV605 anti-mouse B220 (RA3-6B2)	BioLegend	Cat # 103243; RRID:AB_11203907
Alexa Fluor 488 anti-mouse FOXP3 (FJK-16S)	eBioscience	Cat # 53-5773-82; RRID:AB_763537
FITC Rat and mouse T and B cell activation antigen (GL-7)	BD PharMingen	Cat # 562080; RRID:AB_10894953
APC anti-mouse IgD (11-26c.2a)	BioLegend	Cat # 405714; RRID:AB_10643423
FITC anti-mouse IgM (II/41)	eBioscience	Cat # 11-5790-81; RRID:AB_465244
PerCP/Cy5.5 anti-mouse Sca-I (D7)	eBioscience	Cat # 45-5981-82; RRID:AB_914372
PE/Cy7 anti-mouse Sca-I (D7)	eBioscience	Cat # 25-5981-81; RRID:AB_469668
AF700 anti-mouse MHC-II (M5/114.15.2)	eBioscience	Cat # 56-5321-82; RRID:AB_494009
PE/Cy7 anti-mouse Ly6G (1A8)	BioLegend	Cat # 127617; RRID:AB_1877262
APC anti-mouse Ly6C (HK1.4)	eBioscience	Cat # 17-5932-82; RRID:AB_1724153
PE anti-mouse Ki67 (16A8)	BioLegend	Cat # 652403; RRID:AB_2561524
PE anti-mouse IFNAR (AR1-5A3)	BioLegend	Cat # 127312; RRID:AB_2248800
PerCP-eFluor 710 anti-mouse CXCR4 (2B11)	eBioscience	Cat # 46-9991-80; RRID:AB_10670192
BV711 anti-mouse Siglec-H (440c)	BD Bioscience	Cat # 747671; RRID:AB_2744232
FITC goat anti-mouse C3	Immunology Consultants Laboratory Inc	Cat # GC3-90F-Z
FITC rat anti-mouse kappa (187.1)	SouthernBiotech	Cat # 1170-02; RRID:AB_2794663
PE goat anti-mouse IgG F(ab)' Polyclonal	eBioscience	Cat # 12-4010-82; RRID:AB_11063706
Biotin anti-mouse IgG polyclonal	eBioscience	Cat # 13-4013-85; RRID:AB_466650
Biotin anti-mouse IgM (II/41)	eBioscience	Cat # 13-5790-81; RRID:AB_466674
Biotin anti-mouse IgD (11-26c (11-26)	eBioscience	Cat # 13-5993-81; RRID:AB_466859
Biotin anti-mouse CD19 (1D3)	eBioscience	Cat # 13-0193-82; RRID:AB_657656
Biotin anti-mouse CD93 (AA4.1)	eBioscience	Cat # 13-5892-81; RRID:AB_466766
Biotin anti-mouse CD5 (53-7.3)	eBioscience	Cat # 13-0051-81; RRID:AB_466338
Biotin anti-mouse Ly6G (1A8)	BioLegend	Cat # 127603; RRID:AB_1186105
Biotin anti-mouse Ter-119 (TER-119)	eBioscience	Cat # 13-5921-81; RRID:AB_466796

(*Continued on next page*)

Continued

REAGENT or RESOURCE	SOURCE	IDENTIFIER
Biotin anti-mouse CD41 (MWReg30)	BioLegend	Cat # 133930; RRID:AB_2572133
Biotin anti-mouse NK1.1 (PK136)	eBioscience	Cat # 13-5941-81; RRID:AB_466803
Biotin anti-mouse TCRβ (H57-597)	eBioscience	Cat # 13-5961-81; RRID:AB_466818
Biotin anti-mouse CD3ε (145-2C11)	BioLegend	Cat # 100303; RRID:AB_350220
Biotin anti-mouse CD11b (M1/70)	eBioscience	Cat # 13-0112-81; RRID:AB_466358
Biotin anti-mouse CD24 (M1/69)	eBioscience	Cat # 13-0242-81; RRID:AB_466396
Biotin anti-mouse F4/80 (BM8)	eBioscience	Cat # 13-4801-81; RRID:AB_466656
Biotin anti-mouse CXCR5 (2G8)	BD Biosciences	Cat # 551960; RRID:AB_394301
Biotin anti-mouse IgG2a/2b (R2-40)	BD Biosciences	Cat # 553398; RRID:AB_394836
Biotin anti-mouse CD43 (eBioR2/60)	eBioscience	Cat # 13-0431-82; RRID:AB_466439
Alkaline phosphatase conjugated goat anti-mouse IgG	Jackson Immunoresearch	Cat # 115-055-071; RRID:AB_2338535
Mouse IgG-UNLB (Unconjugated) normal mouse serum	SouthernBiotech	Cat # 0107-01; RRID:AB_2732898
Goat Anti-Mouse IgG-UNLB	SouthernBiotech	Cat # 1010-01; RRID:AB_2794121
TruStain FcX anti-mouse CD16/32 (93)	BioLegend	Cat # 101319; RRID:AB_1574973
BV421 anti-mouse CD183 (CXCR3-173)	BioLegend	Cat # 126529; RRID:AB_2563100
*InVivo*mAb mouse IgG2a isotype control (C1.18.4)	Bio X Cell	Cat # BE0085; RRID:AB_1107771
Purified mouse-anti-CD20 (5D2)	Genentech, Inc.	NA
F(ab)'2 fragment goat anti-mouse IgM, μ chain specific	Jackson ImmunoResearch	Cat # 115-006-075;AB_2338474
LEAF purified anti-mouse CD40	BioLegend	Cat # 102810; RRID:AB_312943
Chemicals, Peptides, and Recombinant Proteins		
Nucleosome antigen, calf thymus	Arotec Diagnostics	Cat # ATN02
Deoxyribonucleic acid, calf thymus	Calbiochem	Cat # 2618
Poly-L-lysine solution	Sigma Aldrich	Cat # P8920-100ML
Non-Fat Dry Milk	LabScientific	Cat # M-0841
Pierce Diethanolamine Substrate Buffer (5X)	Thermo Scientific	Cat # 34064
Phosphatase substrate	Sigma Aldrich	Cat # S0942-200TAB
ANA substrate slides	Antibodies Incorporated	Cat # 15-123
Crithidia luciliae sensitive (anti-dsDNA) indirect immunofluorescence test	Euroimmun	Cat # FA 1572-1010-1
ELISPot plates	Millipore	Cat # MSIPS4W10
Fetal Bovine Serum	Sigma Aldrich	Cat # F0926-500
VECTOR Blue alkaline phosphatase (Blue AP) substrate kit	Vector Laboratories	Cat # SK-5300
EDTA	Fisher	Cat # BP24821
Neutral Buffered Formalin (10%)	Thermo Scientific	Cat # 22-050-104 (5701)
Ethanol, Absolute	Fisher Scientific	Cat # BP2818-500
Tissue Plus O.C.T. Compound	Thermo Fisher Scientific	Cat # 23-730-571
Acetone	Fisher Scientific	Cat # A18-1
DAPI (4',6 Diamidino 2 Phenylindole, Dilactate)	Thermo Fisher Scientific	Cat # D3571
Paraformaldehyde 4% in PBS	Thermo Fisher Scientific (Alfa Aesar)	Cat # J19943-K2
Cyclophosphamide monohydrate (CYTOPAC)	Sigma Aldrich	Cat # C7397-1G
2′-deoxy-ethyryluridine (EdU)	Carbosynth	Cat # NE08701
Recombinant mouse IFNα1 (carrier free)	BioLegend	Cat # 751804
ODN2216 (CpGA)	Invivogen	Cat # Tlrl-2216-1
Recombinant mouse IL-4 protein	R&D systems	Cat # 404-ML-010
RPMI medium 1640 with L-glutamine	GIBCO	Cat # 11875-119

(*Continued on next page*)

Continued

REAGENT or RESOURCE	SOURCE	IDENTIFIER
L-glutamine 200mM	Thermo Fisher Scientific	Cat # 25030-164
Beta-mercaptoethanol	Sigma Aldrich	Cat # 444203-250ML
Penicillin-Streptomycin 10,000U/ml	GIBCO	Cat # 15140122
RBC lysis buffer	BioLegend	Cat # 420301
Live/Dead fixable aqua dead cell stain	Thermo Fisher Scientific	Cat # L34965
Bovine serum albumin	Sigma Aldrich	Cat # A9647-100G
Sucrose	Sigma Aldrich	Cat # S0389-1KG
LPS-EK Ultrapure	Invivogen	Cat # Tlrl-peklps
Trizol LS reagent	Ambion	Cat # 10296028
Streptavidin PerCP/Cy5.5	Thermo Fisher Scientific	Cat # 45-4317-82; AB_10311495
Streptavidin PE/Cy7	Thermo Fisher Scientific	Cat # 25-4317-82; AB_10116480
Prolong Diamond antifade	Thermo Fisher Scientific	Cat # P36961
CellTrace CFSE cell proliferation kit	Thermo Fisher Scientific	Cat # C34554
Critical Commercial Assays		
Click-iT EdU Alexa Fluor 647 Flow Cytometry Assay Kit	Thermo Scientific	Cat # C10419
RNeasy Mini Kit	QIAGEN	Cat # 74104
SuperScript IV First strand synthesis system	Thermo Fisher Scientific	Cat # 18091050
FastStart high fidelity PCR system	Roche Applied Science	N/A
Lumikine mIFNα bioluminescence ELISA kit	Invivogen	Cat # lumi-mifna
Streptavidin microbeads	Miltenyi Biotec	Cat # 130-048-101
FOXP3/transcription factor staining buffer set	eBioscience	Cat # 00-5523
Deposited Data		
VH repertoir sequencing data	N/A	SRA PRJNA630283; https://www.ncbi.nlm.nih.gov/sra/PRJNA630283
Experimental Models: Organisms/Strains		
Mouse: WT: C57BL/6J	The Jackson Laboratory	Stock # 000664; RRID:IMSR_JAX:000664
Mouse: WT: 129SvEvTac	Taconic Farms	Model # 129SVE-F or 129SVE-M; RRID:IMSR_TAC:129sve
Mouse: *Dnase1l3*$^{-/-}$ [B6NCrl.Cg-*Dnase1l3*$^{tm1c(KOMP)Wtsi}$/TwinMmucd]	Taconic animal repository	Model TF2732; RRID:MMRRC_065348-UCD
Mouse: *Cd40lg*$^{-/-}$ [B6.129S2-*Cd40lg*^{tm1Imx}/J]	The Jackson Laboratory	Stock # 002770; RRID:IMSR_JAX:002770
Mouse: *Tlr7*$^{-/-}$ [B6.129S1-*Tlr7*^{tm1Flv}/J]	The Jackson Laboratory	Stock # 008380; RRID:IMSR_JAX:008380
Mouse: *Ifnar1*$^{-/-}$ [B6.129S2-*Ifnar1*^{tm1Agt}/Mmjax]	The Jackson Laboratory	Stock # 032045-JAX; RRID:MMRRC_032045-JAX
Mouse: *Tcf4*$^{+/-}$[B6;129-*Tcf4*^{tm1Zhu}/J]	The Jackson Laboratory	Stock No: 013598; RRID:MGI:3040597
Mouse: C57BL/6J-*Tlr9*^{M7Btlr}/ Mmjax	The Jackson Laboratory	MMRRC Stock No. 34329-JAX/CpG11; RRID:MMRRC_034329-JAX
Oligonucleotides		
VH Forward Primers Primer (5′ - > 3′)		
mVH-Fwd1 GAKGTRMAGCTTCAGGAGTC	Sigma Aldrich	N/A
mVH-Fwd2 GAGGTBCAGCTBCAGCAGTC	Sigma Aldrich	N/A
mVH-Fwd3 CAGGTGCAGCTGAAGSASTC	Sigma Aldrich	N/A
mVH-Fwd4 GAGGTCCARCTGCAACARTC	Sigma Aldrich	N/A
mVH-Fwd5 CAGGTYCAGCTBCAGCARTC	Sigma Aldrich	N/A
mVH-Fwd6 CAGGTYCARCTGCAGCAGTC	Sigma Aldrich	N/A
mVH-Fwd7 CAGGTCCACGTGAAGCAGTC	Sigma Aldrich	N/A

(*Continued on next page*)

Continued

REAGENT or RESOURCE	SOURCE	IDENTIFIER
mVH-Fwd8 GAGGTGAASSTGGTGGAATC	Sigma Aldrich	N/A
mVH-Fwd9 GAVGTGAWGYTGGTGGAGTC	Sigma Aldrich	N/A
mVH-Fwd10 GAGGTGCAGSKGGTGGAGTC	Sigma Aldrich	N/A
mVH-Fwd11 GAKGTGCAMCTGGTGGAGTC	Sigma Aldrich	N/A
mVH-Fwd12 GAGGTGAAGCTGATGGARTC	Sigma Aldrich	N/A
mVH-Fwd13 GAGGTGCARCTTGTTGAGTC	Sigma Aldrich	N/A
mVH-Fwd14 GARGTRAAGCTTCTCGAGTC	Sigma Aldrich	N/A
mVH-Fwd15 GAAGTGAARSTTGAGGAGTC	Sigma Aldrich	N/A
mVH-Fwd16 CAGGTTACTCTRAAAGWGTSTG	Sigma Aldrich	N/A
mVH-Fwd17 CAGGTCCAACTVCA GCARCC	Sigma Aldrich	N/A
mVH-Fwd18 GATGTGAACTTGGAAGTGTC	Sigma Aldrich	N/A
mVH-Fwd19 GAGGTGAAGGTCATCGAGTC	Sigma Aldrich	N/A
VH Reverse Primers (5′ - > 3′)		
mVH-Rev-IgG CCARKGGATAGACHGATGGGG	Sigma Aldrich	N/A
mVH-Rev-IgA TGGTGGGATTTCTCGCAGAC	Sigma Aldrich	N/A
mVH-Rev-IgM GCAGGAGACGAGGGGGAAGA	Sigma Aldrich	N/A
Software and Algorithms		
ImageJ	https://imagej.nih.gov/ij/	RRID: SCR_001935
CTL Immunospot analyzer	http://www.immunospot.com/ImmunoSpot-analyzers-software	RRID: SCR_011082
Adobe Photoshop CC2018	https://www.adobe.com/products/photoshop.html	RRID: SCR_014199
Adobe Illustrator CC2018	https://www.adobe.com/products/illustrator.html	RRID: SCR_010279
FLowjo v10	Treestar Inc	RRID: SCR_008520
GraphPad Prism 7	Graphpad Inc	RRID: SCR_002798
Imaris	https://imaris.oxinst.com/packages	RRID: SCR_007370
Keyence BZ Analyzer software	https://www.keyence.co.jp/products/microscope/fluorescence-microscope/bz-8100/models/bz-h1a/	RRID: SCR_017205
Slidepath Gateway digital pathology	Leica Microsystems	RRID: SCR_005597

RESOURCE AVAILABILITY

Lead Contact

Further information and requests for resources and reagents should be directed to and will be fulfilled by the Lead Contact, Boris Reizis (boris.reizis@nyulangone.org).

Materials Availability

All animal strains are available from repositories described above. No new animal strains or reagents were generated.

Data and Code Availability

VH repertoire sequencing data have been deposited in the NCBI SRA database accession codePRJNA630283.

EXPERIMENTAL MODEL AND SUBJECT DETAILS

Mouse strains

All experiments were performed in accordance with the animal protocol approved by the Institutional Animal Care and use committee of Columbia University and New York University. All the mouse strains were on a C57BL/6 background and C57BL/6J (Stock 000664) mice were used as WT controls unless otherwise mentioned. As described previously (Sisirak et al., 2016), mice with a targeted germline disruption of *Dnase1l3* with *Dnase1L3*^{LacZ} (*Dnase1l3*$^{-/-}$) were purchased from Taconic Animal repository (Model TF2732) and backcrossed onto C57BL/6 or 129SvEvTac for > 10 generations and the colonies were maintained in house.

Breeding pairs of wild-type (WT), *Cd40lg*$^{-/-}$ [002770 - B6.129S2-*Cd40lg*^{tm1Imx}/J], *Tlr7*$^{-/-}$ [008380 – B6.129S1-*Tlr7*^{tm1Flv}/J], *Tlr9*$^{-/-}$ [034329-JAX C57BL/6J-Tlr9^{M7Btlr}/Mmjax] and *Ifnar1*$^{-/-}$ [032045-JAX B6.129S2-*Ifnar1*^{tm1Agt}/Mmjax] mice were purchased from Jackson Laboratories (Bar Harbor, ME) and bred and maintained in house. *Dnase1l3*$^{-/-}$ mice on a pure B6 background were crossed with *Cd40lg*$^{-/-}$, *Tlr7*$^{-/-}$, *Tlr9*$^{-/-}$or *Ifnar1*$^{-/-}$ to generate *Dnase1l3*$^{-/-}$*Cd40lg*$^{-/-}$, *Dnase1l3*$^{-/-}$*Tlr7*$^{-/-}$, *Dnase1l3*$^{-/-}$*Tlr9*$^{-/-}$and *Dnase1l3*$^{-/-}$*Ifnar1*$^{-/-}$ mice respectively. *Dnase1l3*$^{-/-}$*Tlr7*$^{-/-}$ *and Dnase1l3*$^{-/-}$*Tlr9*$^{-/-}$mice were bred to generate *Dnase1l3*$^{-/-}$*Tlr7*$^{-/-}$*Tlr9*$^{-/-}$ triple deficient strain. All the double and triple deficient mice were bred and maintained in house. *Dnase1l3*$^{-/-}$ mice on a pure 129Sv background were crossed with *Tcf4*$^{+/-}$ animals (Zhuang et al., 1996) on pure 129SvEvTac (129Sv) background to generate *Dnase1l3*$^{-/-}$*Tcf4*$^{+/-}$ mice and bred and maintained in house. 129SvEvTac mice (Taconic farms) were used as WT controls for this cohort.

METHOD DETAILS

Serology: Ig and autoantibody titers

Relative titers of anti-dsDNA, anti-Nucleosome in sera were measured by ELISA. Briefly, Nunc-Immuno maxisorp 96 well flat bottom plates were coated with 50 μl/ well of 0.01% poly-L lysine (Sigma Aldrich) for one hour at RT, washed with PBS and coated with 50 μl/ well of 10 μg/ml calf-thymus DNA (Calbiochem) or 1 μg/ml calf-thymus nucleosomes (Arotec diagnostics) in PBS, overnight at 4°C. Excess antigen was washed off using 2-3 washes with PBS. Antigen-coated plates were blocked with 250 μl/ well of PBS with 4% non-fat dry milk (NFDM) for 3h at RT. Blocked plates were washed once with PBS and coated with diluted serum in PBS and incubated overnight at 4°C. Unbound serum antibodies were washed off with 3 washes of PBS + 1% NFDM. The bound IgG was detected using a 1:1000 dilution of goat anti-mouse IgG-AP-conjugate (Jackson Immunoresearch) diluted in PBS + 1% NFDM. Unbound secondary antibody was washed with PBS+ 1% NFDM and developed using diethanolamine substrate buffer (Thermo Fisher Scientific, 34064) and PNPP phosphatase substrate tablets (Sigma Aldrich, SIGMAS0942). For relative quantitation of antigen-specific IgG titers, serum from an anti-DNA or anti-Nuc positive animal was used as a standard using serial double dilutions. O.D. at the lowest serum dilution was arbitrarily assigned a value of 100 U/ml. Standard curve was plotted as O.D. at 405nm versus antigen concentration (U/ml). Relative IgG titers of samples were calculated using the straight-line equation and multiplied with the dilution factor. In all ELISA assays, in each plate, controls and test samples were run together and analyzed using the same standard curve.

Total serum IgG titers were determined by coating the ELISA plates with 5 μg/ml mouse IgG (Southern Biotech) and probing the bound serum antibody with anti-mouse IgG-AP (Jackson Immunoresearch).

ANA analysis

For detection of ANA and assessment of ANA staining patterns, HEp-2 human tissue culture substrate slides (Antibodies Incorporated, Davis, CA) were coated with sera at a 1:50 dilution in PBS for 1h at RT in a hydrated chamber and probed with rat anti-mouse κ- FITC conjugate (Southern Biotechnologies Associates, Birmingham, AL) at a 1:200 dilution. Immunofluorescence images were captured using a Keyence BZ-X710 fluorescence microscope at 20X magnification. The color intensity of images was enhanced slightly using Adobe Photoshop CC (Adobe Systems, San Jose, CA) or ImageJ. This was necessary for better visualization and was carried out consistently between all images while maintaining the integrity of the data. Immunofluorescence intensity was quantitated using ImageJ 1.51 s image processing and analysis software (NIH, USA).

Crithidia luciliae Immunofluorescence test – CLIFT

Crithidia luciliae is a protozoan routinely used in the clinic as a substrate to specifically detect antibodies to pure dsDNA (without proteins). A positive test shows staining of the kinetoplast of the protozoan, while staining for basal body or nucleus or both without it, is considered a negative test. The substrate was purchased from Euroimmun (Lubeck, Germany). Serum samples from 12-month-old mice were tested at 1:25 dilution. Anti-dsDNA binding was detected using rat anti-mouse Igκ-FITC conjugate (Southern Biotechnologies Associates, Birmingham, AL). Fluorescence images were acquired using a Zeiss Ax10 fluorescence microscope at 63X magnification and processed using ImageJ software.

ELISpot

ELISpot plates (Millipore, Ref# MSIPS4W10; Multiscreen HTS) were coated with 0.01% poly-L lysine for 1h at RT, followed by coating with 100 μg/ ml calf thymus DNA (Sigma Aldrich) or 10 μg/ ml calf thymus nucleosomes (Arotec diagnostics) overnight at 4°C. Blocked with PBS + 5% FCS for 2-3h at RT. Freshly isolated splenocytes or BM cells were resuspended in freshly prepared warm 15% RPMI 1640 media + antibiotics + 1mM L-glutamine at 20 × 10^6 cells/ ml. 1x10^6 total cells were plated on the top wells and serially double diluted (1:2). ELISpot plates were then incubated for 18h at 37°C with 5% CO_2. Washed with PBS + 1% FCS to remove the cells and probed with a 1:500 dilution of goat anti-mouse IgG AP (Jackson Immunoresearch) for 3-4h at 4°C. After washing, plates were developed using the Vector Blue AP Substrate Kit III (Vector Labs). Spots were captured and counted using ImmunoSpot S6 Analyzer (Cellular Technology Limited, Shaker Heights, OH). For analysis of total IgG-secreting AFCs, ELISPot plates were coated with goat anti-mouse IgG (SouthernBiotech) at 5 μg/ml and blocked with PBS + 5% BSA. Plates were washed with PBS + 1% BSA and probed with a 1:500 dilution of goat anti-mouse IgG AP (Jackson Immunoresearch).

Flow cytometry

Cell suspensions of peripheral blood, mesenteric and inguinal lymph nodes or splenocytes were subjected to red blood cell lysis, washed and resuspended in staining buffer (1% FCS + 2% BSA + 1mM EDTA in PBS). Cells were stained with indicated cell surface markers. For intracellular staining, cells were surface stained and subsequently fixed and permeabilized using FOXP3 intracellular staining kit (eBioscience) and stained with anti-FOXP3-FITC conjugate. EdU positive cells were stained with Click-iT EdU Alexa Fluor 647 Flow cytometry assay kit (Thermo Fisher Scientific # C10424), as per instructions. Samples were acquired using Attune NxT (Thermo Fisher) flow cytometer and analyzed using FLowJo software version 9 or 10 (Tree Star).

Kidney histopathology

For imaging of kidneys, we use at least 4-5 mice per genotype that are closest to the average values of anti-DNA titers and spleen weight for that genotype. One half from each kidney was fixed with 10% neutral formalin for 24h at RT, and stored in 75% ethanol and subsequently embedded in paraffin. 5 μm thick sections were stained with Hematoxylin and Eosin and captured using the PerkinElmer Vectra multispectral imaging system at 40X magnification and glomerular size was analyzed using Slidepath software (Leica Biosystems digital image hub).

Immunofluorescence analysis of kidney and spleen sections

For imaging of the spleens and kidneys we use at least 4-5 mice per genotype that are closest to the average values of anti-DNA titers and spleen weight for that genotype. One half from both kidneys were frozen in OCT (Tissue Tek). 5-10 μm thick kidney sections were fixed using chilled acetone for 10 min. Sections were stained with DAPI, goat anti-mouse IgG-PE conjugate (eBioscience) and goat anti-mouse C3-FITC conjugate (Immunology consultant's Laboratory Inc., Oregon). Images were captured using Keyence BZ-X710 fluorescence microscope at 40X magnification. Immunofluorescence intensity was quantitated using ImageJ 1.51 s image processing and analysis software (NIH, USA). The color intensity of images was enhanced slightly using Adobe Photoshop CC (Adobe Systems, San Jose, CA). This was necessary for better visualization and was carried out consistently on whole images of control and test sections.

Spleen were either frozen in OCT and then sectioned and fixed using chilled acetone or were fixed in 4% PFA overnight followed by 8-10 hours of dehydration in 30% sucrose, after which they were frozen in OCT for cryosectioning. 5-10 μm thick spleen sections were stained with indicated anti mouse Ab-conjugates: GL-7-FITC, IgD-APC, CD138-PE, CD169-APC, Ki67-PE, CD4-FITC/ APC, SiglecH-APC and B220-FITC. Images were captured using Keyence BZ-X710 fluorescence microscope at 4X or 20X magnification or using the Zeiss 880 confocal microscope, maintained by NYU Langone Health's Microscopy Laboratory. Scanning of whole sections was achieved using ZEN imaging software– tile and stitch functions. All images were acquired with similar functions. Image analysis was done using Bitplane's Imaris version 9.2.0. Quantification of *in situ* mean fluorescence intensity sum of CD138 staining was determined using isosurfacing function with subtraction of background staining of spleen capsule. Quantitative analysis of total number of $CD138^+$ or $Ki67^+$ spots per half spleen represented, were calculated by rendering $CD138^+$ or $Ki67^+$ cells with spots using Imaris image analysis software.

Cyclophosphamide treatment

Ten 6-mo-old *Dnase1l3*$^{-/-}$ mice were bled on day 0 to get pretreatment serum titers of anti-dsDNA and anti-Nucleosome antibodies. 5 mice each were subsequently injected intraperitonially with equal volume of either PBS or 500 μg cyclophosphamide monohydrate (CYTOPAC, Sigma Aldrich) reconstituted in PBS per mouse for three consecutive days. Mice were rested for 4 days. Subsequently mice were treated with 1 mg EdU (Carbosynth) intravenously for 12 h after which they were euthanized.

Anti-CD20 treatment

Serum was collected from five-month-old *Dnase1l3*$^{-/-}$ female mice (pretreatment). Subsequently they were injected (i.p) with 100 μg of anti-mouse CD20 (clone 5D2), a kind gift from Genentech, or an IgG2a isotype control antibody (C1.18.4, Bio X cell, cat # BE0085), ~every 15 days for a month. Serum was collected after two weeks of each treatment. Mice were euthanized at six-months of age and spleen was analyzed for AFCs and cellular populations.

Sorting of B cell subsets

Plasmablasts (PB): $CD19^+$ $B220^{+/-}$ $SiglecH^-$ $TCRb^-$ $CD138^{hi}$; Germinal center B cells (GC): $CD19^+$ $B220^+$ $SiglecH^-$ $TCRb^-$ $CD138^-$ $CD38^-$ $GL\text{-}7^{hi}$; Naive Follicular B cells (FO): $CD19^+$ $B220^+$ $SiglecH^-$ $TCRb^-$ $CD138^-$ $CD38^+$ $GL\text{-}7^-$ $CD44^-$ $Sca1^-$; Follicular activated B cells (FOA): $CD19^+$ $B220^+$ $SiglecH^-$ $TCRb^-$ $CD138^-$ $CD38^+$ $GL\text{-}7^-$ $CD44^{hi}$ $Sca1^{hi}$ and class-switched B cells (IgG^+): $CD19^+$ $B220^+$ $SiglecH^-$ $TCRb^-$ IgD^- IgM^- $IgG2a/2b^+$ were sorted from total splenocytes of > 6 mo old WT or *Dnase1l3*$^{-/-}$ mice using the BD FACSAria III Sorter. Sorted cells were used for ELISPot analysis or BCR repertoire analysis.

BCR sequencing and analysis

VH Sequencing

Sorted B cell subsets FO, PB, GC and IgG^+ were lysed in TRIzol® Reagent (Invitrogen) and total RNA was extracted and purified using the RNeasy Mini Kit (QIAGEN). cDNA was synthesized from 500 ng total RNA using the SuperScript IV First-Strand Synthesis System (Invitrogen). Variable heavy (VH) transcript was amplified with a multiplex primer set (primer details in Key Resources Table) using

FastStart High Fidelity PCR System (Roche) under the following conditions: 2 min at 95C; 4 cycles of 92C for 30 s, 50C for 30 s, 72C for 1 min; 4 cycles of 92C for 30 s, 55C for 30 s, 72C for 1 min; 22 cycles of 92C for 30 s, 63C for 30 s, 72C for 1 min; 72C for 7 min; hold at 4C, and sequenced by 2x300 paired-end Illumina MiSeq.

Bioinformatic Analysis

Raw 2x300 reads were trimmed depending on sequence quality using Trimmomatic (Bolger et al., 2014) and annotated using MiXCR (Bolotin et al., 2015). Sequences with $\geq$ 2 reads were grouped into clonotypes by clustering those with $\geq$ 95% CDR-H3 amino acid identity (Edgar, 2010). CDR-H3 characteristics were analyzed using custom Python scripts.

Statistics

p values for the analysis of positively charged amino acids within the CDR-H3 and V-gene usage were determined using Fisher's Exact test. p values for the analysis of the mean CDR-H3 isoelectric point and hydrophobicity were determined using Student's t test or Mann-Whitney *U* test.

In vitro B cell proliferation/ differentiation assay

Naive B cells were MACS-purified by negative selection from splenocytes of WT, *Dnase1l3*$^{-/-}$, *Ifnar1*$^{-/-}$ or *Dnase1l3*$^{-/-}$*Ifnar1*$^{-/-}$ mice using CD43 microbeads. Purified B cells were labeled with 3 μM Cell trace CFSE (Invitrogen), in PBS+ 2% BSA for 10 mins at RT. CFSE labeled cells were washed twice with PBS and subsequently suspended in RPMI + 10% FBS + 2mM L-glutamine + 10 μM β-Mercaptoethanol and plated in round bottom 96 well plates at a concentration of 0.5x10^6 cells/ well in 200 μL media. Cells were either left unactivated or activated with: (1) 5 μg/ml anti-IgM (Jackson Immunoresearch) + anti-CD40 (LEAF-purified, BioLegend) and 5 ng/ml recombinant mouse IL-4 (R&D systems) OR (2) 1 μg/ml LPS (LPS-EK Ultrapure, InvivoGen) + 5 ng/ml recombinant mouse IL-4. Unactivated (UA) and activated (A) B cells were supplemented or not with recombinant mouse IFNα1 (BioLegend) at indicated concentrations. B cells were analyzed for activation, proliferation and differentiation after 3 days of culture.

pDC purification

RBC lysed splenocytes or bone marrow cells of *Dnase1l3*$^{-/-}$ mice were resuspended in RPMI + 10% FCS and were allowed to adhere to sterile tissue culture treated 100 mm petriplates for 1h at 37°C after which adherent cells were discarded. Floating cells were resuspended at 10 x10^6 cells in 90 μL of wash buffer and labeled with the following cocktail of biotinylated antibodies: Anti-IgG, anti-IgM, anti-IgD, anti-CD19, anti-CD93, anti-CD5, anti Ly6G, anti-Ter119, anti-CD41, anti NK1.1, anti-TCRb, anti CD3, anti CD11b, anti-CD24 and anti-F4/80 each at 1: 200 dilution for 20 mins at 4°C. Labeled cells were washed and stained with Streptavidin microbeads for 20 mins at 4°C. Unlabeled cells were collected by negative selection. Up-to 45%–50% pure pDCs (B220^{lo} SiglecH$^+$ CD11c^{lo}) could be routinely identified by flow cytometry.

pDC, B cell co-culture assay

pDCs were purified from *Dnase1l3*$^{-/-}$ BM cells using MACS negative selection (described above) and B cells were purified from *Dnase1l3*$^{-/}$ or *Dnase1l3*$^{-/-}$*Ifnar1*$^{-/-}$ mice by negative selection using CD43 microbeads and were labeled with cell trace CFSE. 0.5 × 10^6 purified B cells per well were left unactivated (UA) or activated (A) with 5 μg/ml anti-IgM (Jackson Immunoresearch) + anti-CD40 (BioLegend) and 5 ng/ml recombinant mouse IL-4 (R&D systems). Activated B cells were cultured in the presence of ~2x10^4 purified unactivated pDCs (A + pDCs) OR treated with 1 μg/ml CpGA (ODN 2216, InvioGen) (A + CpG) OR co-cultured with ~2x10^4 purified pDCs activated with 1 μg/ml CpGA (A + pDCs + CpGA). Cells were co-cultured for three days after which B cells were analyzed for activation, proliferation and differentiation by flow cytometry and supernatant was analyzed for IFNα production by ELISA.

IFNα ELISA

Purified BM or splenic pDCs at various concentrations were left unstimulated or stimulated with 1 μg/ml CpGA (ODN 2216, InvioGen) for 18h and supernatant was collected. Supernatants were collected from pDC + B cells cocultures as described above. Secreted IFNα in culture supernatants was measured using mouse IFN-alpha bioluminescence ELISA kit (InvivoGen) following manufacturer's instructions.

QUANTIFICATION AND STATISTICAL ANALYSIS

Comparisons between multiple groups were performed by one-way ANOVA followed by multiple comparisons analysis, Tukey's test, unless otherwise mentioned. Comparisons between two groups were performed by non-parametric Student's t test with Mann-Whitney analysis. P values less than or equal to 0.05 were considered significant and significance was assigned according to the following breakdown: *p < 0.05, ** p < 0.01, *** p < 0.001 and **** p < 0.0001. Graph Pad Prism software versus 7 or 8 was used for all statistical analysis.

DNASE1L3 DEFICIENCY EXACERBATES OBESITY-MEDIATED INFLAMMATION AND METABOLIC SYNDROME

A. Ferriere[1], A. Roubertie[1], P. Bandopadhyay[2], P. Santa[1], A. Garreau[1], S. Loizon[1], D. Duluc[1], D. Brisou[1], B. Gatta-Cherifi[4], D. Cota[5], L. Capuron[3], N. Castanon[3], C. Monchaux[3], B. Rousseau[6], L. Mora Charrot[6], P. Blanco[1], D. Ganguly[2] and V.Sisirak[1]

[1]CNRS UMR 5164, Immuno-ConcEpT Team, Université de Bordeaux, France,

[2]IICB-Translational Research Unit of Excellence (IICB-TRUE), Division of Cancer Biology & Inflammatory Disorders, Kolkata, India,

[3]Nutrition and Integrative Neurobiology (NutrINeurO), INRA, Université de Bordeaux, France

[4]CHU de Bordeaux, Hôpital Haut-Lévèque, Pessac, France

[5]INSERM U1215, Neurocentre Magendie, Université de Bordeaux, France

[6]Université de Bordeaux, France

Key Words: Metaflammation, DNASE1L3, DNASEs, DNA sensing, Obesity.

*Correspondance to Vanja Sisirak, UMR CNRS 5164, Immunoconcept, Université de Bordeaux, Bât 1B, RdC, 146, rue Léo Saignat, 33076 Bordeaux. E-mail: vanja.sisirak@u-bordeaux.fr

ABSTRACT

Obesity is a global health issue affecting 13% of the world population. The development of metabolic syndrome and complications associated with obesity are attributed to the chronic low-grade inflammation that occurs in metabolic tissues such as the visceral adipose tissue (VAT). Recently, cell-free self-DNA (cfDNA), which accumulates systemically in obese individuals, was shown to contribute to VAT inflammation and consequently to development of metabolic syndrome. While deoxyribonucleases (DNASEs) regulate endogenous levels of cfDNAs, no study has evaluated their functions in obesity-mediated inflammation.

Objective. We aimed to define DNASE1L3 role in the regulation of cfDNA immunostimulatory potential during obesity and whether its dysregulation plays a role in VAT inflammation in obese subjects.

Methods. *Dnase1l3* deficient and wild type control mice were fed with a normal and high fat diet during 13 weeks and their body weight gain, metabolic parameters and hepatic function were evaluated at regular intervals. At endpoint, VAT inflammation was determined by flow cytometry and the extent of VAT expansion and liver steatosis were quantified by histology. Plasma level of cfDNA was measured by quantitative PCR, while *DNASE1L3* expression in peripheral blood mononuclear cells (PBMCs) was assessed by flow cytometry-based fluorescence *in situ* hybridization (Flow-FISH), in healthy and obese individuals. Finally, the total DNASEs activity of our cohort of patients was evaluated by single radial enzyme-diffusion (SRED) and a new DNASEs activity assay based on the PicoGreen dye.

Results. Using a mouse model of diet induced obesity, we showed that *Dnase1l3* deficiency exacerbated i) weight gain, ii) metabolic syndrome, iii) hepatic steatosis, and iv) VAT inflammation. Plasma cfDNA levels were higher in obese individual and positively correlated with severity of obesity. While the expression of *DNASE1L3* was not modulated in obese patients, plasma DNASEs activity was decreased compared to healthy controls.

Conclusion. Therefore, DNASE1L3 plays an important role in the regulation of obesity-associated inflammation and metabolic syndrome *in vivo*. In addition, DNASE function is impaired in obese individuals likely contributing to the alteration of systemic cfDNA levels. Validation of these results could lead to the development of new therapeutic tool, long-awaited in obesity, based on strategies that reconstitute of enhance DNASE1L3 activity.

INTRODUCTION

Obesity is a major public health issue affecting 13% of the world's population, or more than 650 million people (*Tremmel et al., 2017*). Its prevalence has tripled between 1975 and 2016 and affects both developed and emerging countries. Obesity is commonly associated to the development of metabolic syndrome, which is a cluster of conditions including increased blood pressure, high blood sugar, excess body fat around the waist, and abnormal cholesterol or triglyceride levels. Obesity-associated metabolic syndrome represents a major risk factor for developing multiple chronic diseases such as type 2 diabetes (T2D), cardiovascular diseases, non-alcoholic steatohepatitis (NASH), neuropsychiatric diseases, severe coronavirus disease 2019 (COVID-19) and cancers (*Yanovski and Yanovski, 2002*), which together account for more than 5 million deaths worldwide each year *(Yanovski and Yanovski, 2002*). Since the COVID-19 pandemic these numbers are probably underestimated (*K Y et al., 2021*). Therefore, obesity has far-reaching consequences for life expectancy, quality of life as well as healthcare costs.

A critical role for both the immune cell infiltration into the VAT and the ensuing VAT chronic low-grade inflammation called metabolic inflammation or “metaflammation” was established in the development of obesity-associated metabolic syndrome (*McNelis and Olefsky, 2014*). Mainly, anti-inflammatory M2-like macrophages present in the lean VAT switch toward a proinflammatory M1-like phenotype in the VAT of obese individuals and contribute to obesity pathogenesis through their production of pro-inflammatory cytokines, such as tumor necrosis factor (TNF)-α and interleukin 1 (IL-1)-β (*McNelis and Olefsky, 2014*). These cytokines directly inhibit insulin signalling and lead to cardiovascular and metabolic complications related to obesity. However, targeting either TNF-α (*Bernstein et al., 2006*) or IL-1β (*van Asseldonk et al., 2011*) showed only a marginal impact on obese patients’ clinical outcomes. Furthermore, recent single-cell Ribonucleic Acid sequencing (scRNAseq) studies have revealed a higher complexity of macrophages beyond the classic M1/M2 distinction in the VAT of obese individuals and mice (*Jaitin et al., 2019*). Thus, understanding the mechanisms involved in this metaflammation has become a crucial issue in obesity research.

Excess nutrient intake causes an accumulation of free fatty acids, cholesterol crystals (*Shi et al., 2006*), and impair intestinal permeability resulting in increased circulating levels of Lipopolysaccharide (LPS) originating from Gram-positive intestinal bacterial species (*Amar et al., 2011*). These lipids and bacterial molecules act as endogenous damage associated molecular patterns (DAMPs) and pathogen associated molecular patterns (PAMPs) respectively and stimulate pathogen recognition receptors (PRRs) including Toll-like Receptor (TLR)-4 and the NLR family pyrin domain containing 3 (NLRP3) inflammasome (*Shi et al., 2006; Vandanmagsar et al., 2011; Wen et al., 2011*). Their stimulation leads

to the production of inflammatory cytokines responsible for the VAT inflammation ultimately causing obesity-mediated complications (*Holland et al., 2011; Vandanmagsar et al., 2011*).

Recently, multiple studies have shown that endogenous self-DNA, accumulate systemically in response to obesity, acts as a DAMP by activating PRRs involved in DNA sensing (such as TLR-9, cyclic GMP-AMP synthase (cGAS) and absent in melanoma (AIM)-2), and consequently exacerbates obesity-mediated inflammation and metabolic syndrome (*Ganguly et al., 2018*). Indeed, circulatory levels of endogenous cell-free (cf)DNA rise in obese individuals and mice exposed to high-fat diet (HFD) (*Strissel et al., 2007; Garcia-Martinez et al., 2016; Nishimoto et al., 2016; Revelo et al., 2016*). Forms and sources of such endogenous cfDNA are diverse and include i) microparticles (MPs) containing mitochondrial DNA (mtDNA) released by NASH affected hepatocytes (*Garcia-Martinez et al., 2016*), ii) neutrophils extracellular traps (NETs) which are fibres composed of DNA and antimicrobial peptides released by NETotic neutrophils (*Revelo et al., 2016*) and iii) genomic DNA (gDNA) and mtDNA released by apoptotic adipocytes (*Nishimoto et al., 2016*). The observation that circulatory cfDNA levels were positively correlated with the extent of VAT size, insulin resistance and liver damage in obese individuals (*Garcia-Martinez et al., 2016; Nishimoto et al., 2016*) further indicated that they contribute to the severity of obesity-induced metabolic syndrome. Hence, studies in mice and human have shown that the recognition of endogenous cfDNAs by macrophages and plasmacytoid dendritic cells (pDCs) *via* TLR-9 causes inflammatory responses contributing to the development of metabolic syndrome induced by obesity (*Ghosh et al., 2016; Nishimoto et al., 2016; Revelo et al., 2016*). Particularly, Ghosh *et al.* have shown that DNA released by VAT explant cultures isolated from obese patients was associated with high mobility group box 1 (HMGB1), and that this HMGB1-DNA complex activated TLR-9 mediated type I interferon (IFN-I) production by pDCs (*Ghosh et al., 2016*). IFN-I consequently caused the switch of M2-like into M1-like macrophages (*Ghosh et al., 2016*) and participated in the depletion of regulatory T cells (Tregs) in the VAT (*Li et al., 2021*), which are both involved in VAT metaflammation. The later results are also consistent with studies indicating that genetic deficiencies of *Tlr-9*, *Ifnar* (IFN-I receptor), *Irf7* (Interferon regulatory factor 7) as well as specific pDCs ablation ameliorate the extent of metabolic syndrome in a mouse model of diet-induced obesity (*Wang et al., 2013; Garcia-Martinez et al., 2016; Nishimoto et al., 2016; Revelo et al., 2016; Hannibal et al., 2017*). In addition, obesity causes bacterial CpG DNA leakage from the gastrointestinal tract to the liver by modulating intestinal permeability which was shown to accelerate NASH pathogenesis in a TLR-9 dependent manner (*Henao-Mejia et al., 2012*). The mtDNA released by hepatocytes and adipocytes during obesity also activates intracellular DNA sensors cGAS (*Luo et al., 2018; Yu et al., 2018; Bai and Liu, 2019*) and the AIM2 inflammasome in macrophages (*Bae et al., 2019*), leading to the production of inflammatory cytokines and IL-1β respectively. The role of cGAS in obesity-mediated inflammation is further supported by

studies indicating that specific macrophage deficiency of STING (stimulator of interferon genes) which is essential for the transduction of cGAS-mediated signalling prevented NASH induced by HFD (*Bai and Liu, 2019*), while the *in vivo* role of AIM2 in obesity remains controversial (*Gong et al., 2019*). Therefore, endogenous DNA that accumulates during obesity plays a key role in the inflammation of metabolic tissues. Yet, how its abundance and immunostimulatory potential are regulated during obesity remains poorly understood.

Multiple safeguard mechanisms are involved in the disposal of endogenous DNA to prevent aberrant immune activation and consequently the development of inflammatory and autoimmune syndromes. These protective mechanisms include circulatory (or extracellular) deoxyribonucleases (DNASEs) such as DNASE1 and DNASE1L3 which are respectively produced by exocrine and myeloid cells (dendritic cells (DCs) and macrophages) (*Santa et al., 2021*). Together both DNASEs account for all circulatory DNASEs activity (*Napirei et al., 2009*), but they display different specificities. DNASE1 preferentially digest "naked" DNA (*Napirei et al., 2005*) while DNASE1L3 digests membrane-encapsulated DNA (*Wilber et al., 2002*) either in its naked or nucleosome-bound form (*Napirei et al., 2005*). Nevertheless, *Dnase1* deficiency in mice did not affect neither the levels of circulatory cfDNA nor its fragmentation profile (*Cheng et al., 2018*), while *Dnase1l3* deficiency caused an abnormal accumulation of DNA-associated to MPs and of larger DNA fragments (*Serpas et al., 2019*). Accordingly, the deficiency of DNASE1L3 in mice and humans led to the development of systemic lupus erythematosus (SLE) (*Al-Mayouf et al., 2011; Sisirak et al., 2016*), which an autoimmune syndrome characterized by an aberrant production of DNA specific auto-antibodies, while DNASE1 involvement in SLE pathogenesis remains still debated (*Kenny et al., 2019*). Interestingly obesity was reported to represent a risk factor for SLE development (*Tedeschi et al., 2017*) and conversely SLE prone mice have shown an exacerbated obesity-mediated metabolic syndrome induced by HFD (*Hanna Kazazian et al., 2019*). Furthermore, studies in mice have revealed that HFD reduces circulatory DNASEs activity (*Revelo et al., 2016*). These results are in accordance with recent observations indicating that hypercholesterolemia impairs DNASE1 and DNASE1L3 activity both in mice and humans (*Dhawan et al., 2021*). However, treatment of obese mice with recombinant DNASE1 did not affect the development of metabolic syndrome (*Revelo et al., 2016*). This lack of DNASE1 therapeutic potential in obesity may be due to soluble mediators present in obese mice that block DNASE1 function and/or to its limited ability to only digest naked DNA. Given that DNASE1L3 is expressed in myeloid cells (*Sisirak et al., 2016; Soni and Reizis, 2018*) present in metabolic tissues, has a unique function in disposing of multiple forms of DNA that accumulates during obesity (*Sisirak et al., 2016; Jiménez-Alcázar et al., 2017*), and is functionally impaired by excessive cholesterol levels (*Dhawan et al., 2021*), we postulated that it likely regulates endogenous DNA levels and its immunostimulatory potential during obesity.

We observed that *Dnase1l3*-deficiency increased the weight gain as well as exacerbated the metabolic syndrome induced by HFD-mediated obesity in mice. In the VAT of obese mice, we also found an increase in pro-inflammatory M1-like macrophages in absence of DNASE1L3, indicating that *Dnase1l3* deficiency aggravate metabolic tissues inflammation induced by obesity. Finally, we have shown that obese patients display elevated levels of circulatory cfDNA which were correlated with disease severity. In addition to the accumulation of circulatory cfDNA, obese patients also exhibited reduced circulatory DNASE activity. Thus, our study underlines an important role of DNASE1L3 in the regulation of endogenous DNA ability to contribute to obesity-mediated metaflammation and metabolic syndrome.

METHODS

Key Resources

All the key resources, their origin, their specification as well as their concentration of usage are indicated in the ***Supplementary table 1***.

Animals

Animal care and animal experimental procedures were done in accordance with the EU Directive 2010/63/EU for animal care, and all the animal protocols (#20125 and #33484) were approved by the local ethics committee and the French ministry of research. The *Dnase1l3*-KO mice on C57BL/6J background (*Dnase1l3*$^{LacZ/LacZ}$) were described previously (*Sisirak et al., 2016*). Age-matched wild-type (WT) control mice of the same backgrounds were used as controls and all mice (WT and *Dnase1l3*-KO) were co-housed during 15 days before the initiation of experiments. Twelve to 15 weeks-old mice were housed in groups of 5 animals in standard cages and maintained in a temperature- and humidity-controlled facility under a 12:12 LD cycle (8:00 on), with *ad libitum* consumption of water and either standard rodent chow (standard Diet A03 or AIN93G AMF butter, SAFE, Augy, France) or HFD (60% of fat [260HF] or 45% of fat [246HF], SAFE, Augy, France) for 13 weeks. The number and the sex of mice used for the different experiments is further detailed in the figures' panels and in the figures' legends.

Murine body weight, food intake and feeding efficiency measurements

Mouse body weight and food intake per cage (expressed as g of food eaten daily) were recorded weekly during all the experiments. Twelve weeks after the initiation of HFD, mice were isolated in single cage to measure individual food intake during a period of 8 days. Feeding efficiency was

calculated as the ratio between cumulative body weight gain and cumulative caloric intake over the same period of time.

Glucose tolerance test (GTT) and insulin tolerance test (ITT)

At baseline, 6 and 12 weeks after the initiation of special diet, all mice were subjected to a GTT (intraperitoneal (i.p) injection of 10% D-(+)-Glucose at 1 g/kg) and mice fed with a 60% HFD were also subjected to an ITT (i.p injection of insulin at 0.75 U/kg). The animals were fasted for 6 h before the tests. Blood samples were taken from the tail vein at 0, 15, 30, 60, 90 and 120 min after the i.p injections of glucose or insulin.

Body composition analysis

Mouse body composition analysis was performed with the Echo Magnetic Resonance Imagery (MRI) (EchoMedical Systems, Houston, TX, USA) at 12 weeks as previously described (*Binder et al., 2013*).

Murine plasma collection and analysis

Mouse cheek blood samples (~100µl) were collected 3 days after each GTT at baseline, 6 and 12 weeks after special diet initiation. Mice were fasted for 6 h and anaesthetised with isoflurane prior blood sampling. Blood glucose level was measured using a Accucheck performa glucometer (Roche diabetes care France). Total cholesterol (CT), low density lipoprotein-cholesterol (LDL), Triglyceride (Tg) and Alanine Aminotransferase (ALAT) were measured by Pentra C400 automated clinical chemistry analyzer (Horiba, France). Insulin concentration was measured using an ultrasensitive Enzyme Linked Immuno Sorbent Assay or ELISA (Crystal Chem Inc 90080). Insulin sensitivity was estimated by calculating the Homeostasis Model Assessment of Insulin Resistance (HOMA-IR: fasting insulin (mg/mL) x fasting glycemia (g/L)) / 405).

Mouse tissue harvesting and isolation of immune cells

At the endpoint, all mice were anaesthetised with isoflurane, euthanized by cervical dislocation and subjected to transcardial perfusion with 10 ml PBS. Subcutaneous adipose tissue (SAT), VAT (epididymal), and the liver were harvested, weighted and placed in cold media. AT samples were mechanically minced and digested (collagenase I-a 4 mg/mL) during 20 min at 37°C to obtain AT single cell suspension. This single cell suspension was further filtered through a 70 µm cell strainer and spun at 450 *g* for 5 min at room temperature (RT). The cell pellet containing the stromal vascular fraction (SVF) was then subjected to red blood cell lysis and washed in PBS and resuspended in flow cytometry staining buffer (4% BSA, 2 mM EDTA). Absolute cell numbers in the AT SVF were determined by the BD-Accuri C6 flow cytometer (BD-Biosciences)

Flow cytometry

Prior to surface staining of the SVF of AT, FC receptors were blocked using an anti-CD16/32 antibody for 10 min at 4°C. Then specific surface antigens were stained with fluorescent labelled primary antibodies for 20 min at 4°C. The following antibodies were used: anti-CD8 APC, anti-CD11b APC-Cy7, anti-CD11c APC-Cy7, anti-TCR-β APC-eFluor 780, anti-CD64 BV605, anti-CD137 BV711, anti-Ly6G BV711, anti-F4/80 FITC, anti-CD4 FITC, anti-MHCII Pacific Blue, anti-Ly6C Pacific Blue, anti-CD11c PE, anti-B220 PE CF584, anti-CD301b PE-Cy7, anti CD45 PerCP-Cy5.5 and Zombie AmCyan for viability (***Supplementary table 1***). Upon staining cells were fixed using the Foxp3 Staining Buffer Set according to manufacturers' instructions. Intra-cellular labelling with the anti-FoxP3 PE antibody was performed during 45 min at RT after fixation/permeabilization using the same kit. After washing the cells, samples were acquired on the Fortessa flow cytometer (BD Bioscience) and analyzed using FLowJo software version 10 (BD Bioscience).

Histopathology

Murine VAT, SAT and livers were fixed with 10% neutral formalin for 24h at RT (Sigma HT501128-4L), and stored in 70% ethanol and subsequently embedded in paraffin. Sections were stained with Hematoxylin and Eosin and captured at 40X magnification (Histology facility, Necker Hospital, Paris). Adipocytes perimeters and surfaces were quantified using software NDP View2Plus (Hamamatsu Photonics, France). Steatosis was quantified blindly to genotype by a single pathologist using QuPath bioimage analysis software (*Bankhead et al., 2017*) and a SLIC segmentation (*sequence- and ligation-independent cloning* - (*Achanta et al., 2012*)), tool included in QuPath.

Healthy donors (HD) and obese patients (OB) samples

The data were collected under conditions of regular clinical care. The study was approved by the local Committee for the Protection of Persons (Bordeaux, France). All patients provided written informed consent after reading a complete description of the study. Included patients were aged between 18 and 65 years and followed in the Nutrition Department of the Bordeaux University Hospital. They had severe obesity meeting the eligibility criteria for bariatric surgery (according to the guidelines of the French Health Authority: Body mass index or BMI >40 kg/m^2 or >35 kg/m^2 in the presence of complications susceptible to be improved by bariatric surgery). Anthropometric and biological data were collected (**Supplementary table 2 and 3**). Blood from sex- and age-matched healthy donors (BMI <30 kg/m^2) were obtained from the local Blood Transfusion Center (Etablissement Français du Sang).

Pre-Analytical human blood sample processing

Blood, collected in 7 ml EDTA tubes, was rapidly spun at 3500 *g* for 15 min (without brakes). Platelet-poor plasma was gently collected and spun again at 3500 *g* for 15 min (without brakes) to obtain platelet-free plasma (PFP). PFP were stored at -80°C. Peripheral blood mononuclear cells (PBMCs) were isolated from the remaining blood by Ficoll gradient and used directly for flow cytometry. Briefly, the blood was diluted in PBS 1:2 and gently layered on top of the density gradient medium. After a centrifugation at 800 *g* for 20 min at RT without brakes the immune cells were recovered at the interface. Absolute PBMC numbers were determined by the BD-Accuri C6 flow cytometer (BD-Biosciences)

Circulatory cfDNA quantification

As described in *Zhang et al., 2009*, we used 200µl of PFP for the quantification of cfDNA. Twenty microliters of PFP were used to directly quantify cfDNA in the whole plasma fraction (WPF). The rest of the PFP was spun at 22,000 *g* for 30–60 min at RT to pellet the MPs. 150 µL of the supernatant was collected to constitute the soluble fraction (without MPs or MP- fraction) while the pellet was resuspended in 10 µL and constituted the MPs-associated fraction (MP+ fraction). One µL of the MP-associated fraction was collected to quantify absolute MP counts. For that purpose, red blood cells and platelets specific surface antigens were stained with anti-human CD235a APC and CD41 APC respectively for 20 min at 4°C. The double negative population (MPs not originating from platelets or red blood cells) was quantified by flow cytometry after setting a threshold on forward scatter (FSC) at 2500 to only limit the number of very small events corresponding to the electronic noise of the machine. The number of events obtained was corrected by the dilution factor. MPs were acquired on a BD Accuri™ C6 Plus Flow Cytometer (BD Biosciences). Then, the DNA was purified from these three fractions using a QIAamp DNA Blood Mini Kit (Qiagen). DNA concentration was quantified by quantitative Polymerase Chain Reaction (qPCR) using a CFX384 thermocycler (Bio-Rad TM). The specific primers used targeted ALU repetitive elements that are abundant in the genome and amplified a fragment of 200bp (ALU Fwd: AAAATTAGCCGGGCGTG and ALU Rev AGACGGAGTCTCGCTCTGTC). The cycling conditions were 95°C for 12 min, followed by 45 cycles at 95°C for 20 sec and 65°C for 50 sec 56°C to anneal for 1 min, and 1 min of extension at 72°C as in (*Zhang et al., 2009*). The data were analyzed using Bio-Rad TM CFX Manager software (Bio-Rad TM). DNA levels were calculated according to a standard in each fraction.

PrimeFlow RNA Assay (Flow-Fish)

Fresh PBMCs of obese patients and HD were used to perform the PrimeFlow RNA assay according to the manufacturer's instructions (Thermo Fischer Scientific). The probe specifically targeting the DNASE1L3 was designed by Thermo Fisher Scientific, and procedures used for the design and generation of the probes as well as the probe sequences are considered proprietary by the company (Thermo Fischer Scientific). A control probe targeting the mRNA of RPL13A which is ubiquitously expressed was also used to verify hybridization. The probes were conjugated to an APC fluorescent dye to allow detection by flow cytometry. Extracellular staining was also performed using the following antibodies: Anti-Human CD19 Pacific Blue, anti-CD4 SuperBright 600, anti-CD3 SuperBright 645, anti-CD304 BV711, anti-HAL-DR BV785, anti-CD123 FITC, anti-CD16 PE-EF610, anti-CD11c PE, anti-CD141 (BDCA3) PE-Cy7, anti-CD14 AF700, anti-CD1c (BDCA1) APC-Cy7, Zombie Amcyan for viability (***Supplementary table 1***). Data acquisition was performed using Fortessa flow cytometer (BD Bioscience LRSFortessa) and analyzed using FLowJo software version 9 or 10 (BD Biosciences).

DNASEs activity measurement

Plasma DNASEs activity was measured by Single Radial Enzyme Diffusion (SRED). Calf thymus DNA (1 mg/mL) was dissolved in a solution containing 20 mM Tris HCL pH7.8, 10 mM $MnCl_2$, 2 mM $CaCl_2$ and ClearSight DNA stain. The solution was heated 10 min at 50°C and mixed with a solution containing 2% ultrapure agarose. The final solution was poured into a plate and left to solidify at RT for 1 h. After solidification, wells were made by using biopsy punches of 1,5 mm diameter and were spaced 2 cm apart. 10 µL of plasma samples were deposited in wells and the gel was incubated at 37°C during 16 h. After UV exposure, the total enzymatic activity, reflected by the size of the dark circle, was measured using MacBiophotonics ImageJ sofware. To quantify more precisely DNASEs activity in a high throughput manner we optimized the QuantiT-PicoGreen™ dsDNA assay (Thermo Fisher) which quantifies the amount of degraded DNA and converts it into absolute units of DNASEs activity based on standards of known concentration. For that purpose, 50 ng of calf thymus input DNA under 100 µl was incubated in presence of 25 µl of human plasma or known concentration of DNASE1 prepared in HBBSS buffer containing 5mM MgCl2. The assay was performed for 2h at 37°C and the enzymatic DNASEs activity was stopped by the addition of PBS containing 25mM EDTA. The amount of the remaining DNA was quantified by the QuantiT-PicoGreen™ dsDNA assay kit using the plate reader Varioskan™ LUX (Thermo Scientific) following the manufacturer protocol. The concentration of the DNA contained in the human plasma used for the DNASEs assay was also independently quantified by the QuantiT-PicoGreen™ dsDNA assay and subtracted from the digestion assay.

Statistical analyses

Statistical analyses were performed using GraphPad Prism 9 software. First, sample normal distribution was assessed using the D'Agostino & Pearson omnibus normality test. Parametric statistics were used when distribution was normal using one-way ANOVA or t-test. For non-normal distribution, statistical validity was assessed with non-parametric test (Mann-Whitney or Kruskal–Wallis H test followed by multiple comparison of ranks when appropriate). Spearman rank correlation was used in data analysis. The statistical significance was set at $p \leq 0.05$. All data are presented as means ± SD.

RESULTS

Dnase1l3 deficiency increases weight gain in mice fed with HFD

To test the role of DNASE1L3 in the development of obesity, we compared the weight gain and adiposity of *Dnase1l3*-KO mice and control WT mice upon their exposure to HFD. For that purpose, 12 weeks old male mice of each genotype were given *ad libitum* either a HFD containing 45% or 60% of fat during 12 weeks. WT and *Dnase1l3*-KO mice were also exposed to a chow (normal) diet (ND) containing 20% of fat as a control. First, we observed that mice exposed to both HFDs gained significantly more weight than mice on ND (**Fig. 1A,D**). Importantly, *Dnase1l3*-KO mice showed a significant weight gain compared to WT mice when exposed to both HFDs (45% or 60% HFD) (**Fig. 1A, D**). The weight gain of *Dnase1l3*-KO mice was starting to be significantly higher 6 weeks following the initiation of HFD ($p<0.05$) (**Fig. 1B,E**) and remained significantly more elevated than in WT mice over time (**Fig. 1C,F**). Indeed, after 12 weeks of HFD, *Dnase1l3*-KO mice gained 15% more weight than their WT counterpart (+12.4 ± 3.6 g *vs* +8.1 ± 3.1 g in *Dnase1l3*-KO and WT mice fed with 45% HFD and +19.4 ± 4.5 g *vs* +13.8 ± 1.2 g in *Dnase1l3*-KO and WT mice fed with 60% HFD, $p<0.001$) (**Fig. 1C,F**). Conversely, *Dnase1l3*-KO and WT mice fed with a ND showed no difference in body weight over time (**Fig. 1A-C, 1D-F**). After 12 weeks of HFD and ND, individual epididymal (visceral) and inguinal (subcutaneous) AT were collected and weighed. Their mass was significantly increased in *Dnase1l3*-KO mice compared to WT mice fed with 45% HFD ($p<0.001$) while in mice fed a 60% HFD this difference was not significant (**Fig. 1G and Fig. S1A-C**). Elevation in AT mass in *Dnase1l3*-KO mice that were fed a HFD was accompanied with an increase in epididymal adipocytes perimeter and surface (**Fig. 1H-J and Fig. S1D,E**). Body composition, as evaluated by MRI, also showed an increase in the total fat mass (39.1 ± 6.3% *vs* 26.1 ± 7.1%, $p<0.001$) and a decrease in total lean mass (43.7 ± 6.6% *vs* 56.7 ± 8.2%, $p<0.001$) in *Dnase1l3*-KO mice fed with 45% HFD when compared to WT mice on a same diet (**Fig. 1K,L**). Finally, to evaluate the mechanisms that may be responsible for the susceptibility of *Dnase1l3*-KO mice to gain more weight in response to HFD, we measured the cumulative food intake by cage until the end of the

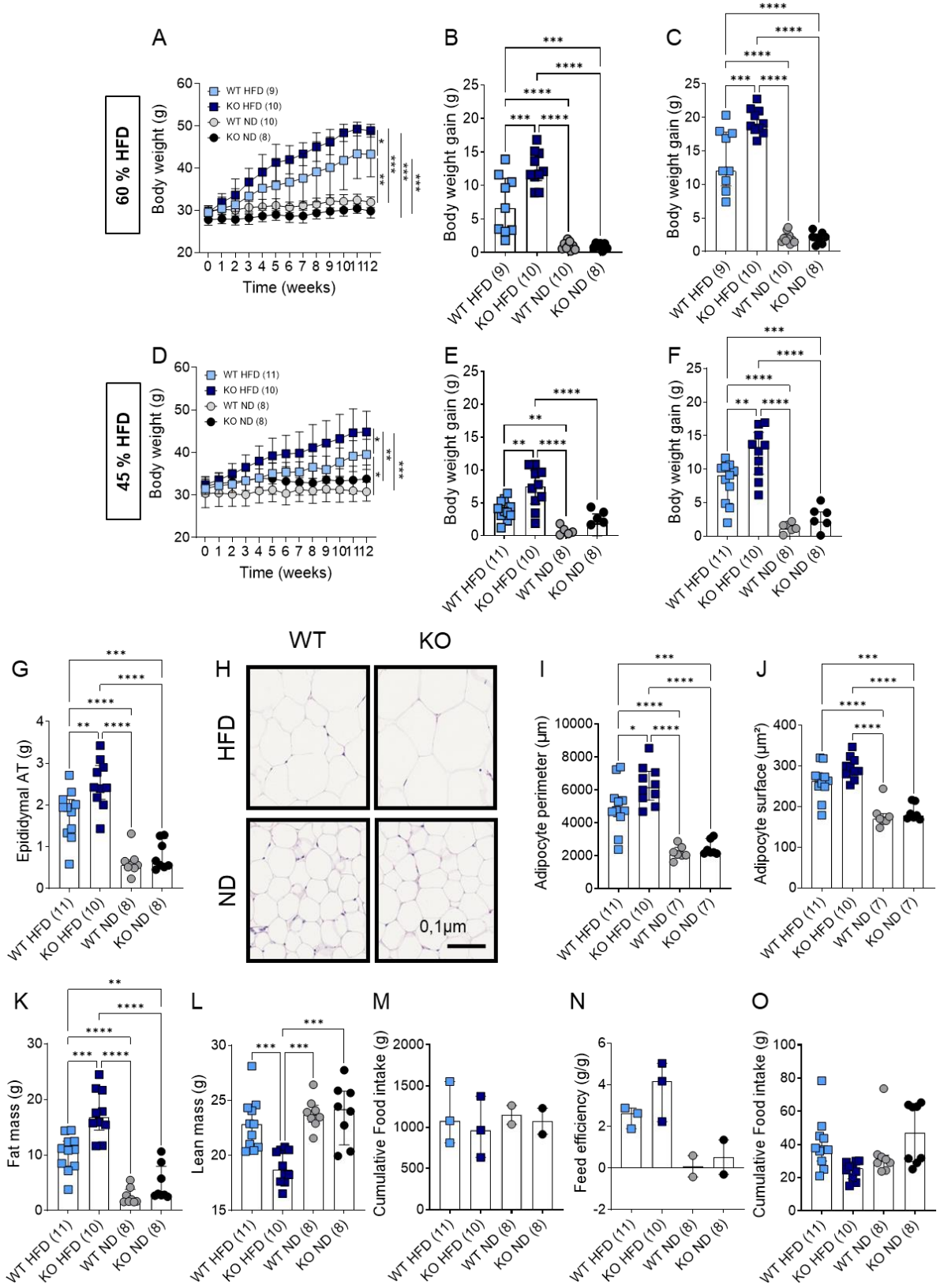

Figure 1: *Dnase1l3* deficiency increases weight gain in mice fed HFD

Wild-type (WT) and *Dnase1l3*$^{-/-}$ (KO) male mice were exposed to normal (ND) or high fat diet (HFD) for 12 weeks, starting at 12 weeks of age. HFD contained either 60% (A-C) or 45% of fat (D-O). (A, D) Weekly weight measurements of WT and KO mice fed an ND (circles) or HFD (squares). Cumulative body weight gain after 6 (B, E) and 12 (C, F) weeks of diet in the indicated mice. (G) Individual weights of epididymal adipose tissue (VAT) after 12 weeks of ND or HFD in the indicated mice. (H) Representative Hematoxylin and Eosin (H&E) staining of the VAT harvested after 12 weeks of ND or HFD of the indicated mice. Mean perimeter (I) and surface (J) of 30 adipocytes per mouse from the VAT as measure by immunohistochemistry upon H&E staining. Proportion of fat (K) and lean (L) mass in WT and KO mice as determined by magnetic resonance imaging (MRI) after 12 weeks of diet. Cumulative food intake (M) and feed efficiency (N) measured per cage after 12 weeks of diet. The feed efficiency was calculated by the ratio of food intake to body weight gain. (O) Individual cumulative food intake after 8 days of isolation of individual mice in individual cages. Data were combined from two independent experiments with the indicated mouse numbers and presented as mean ± SD. Statistical significance was calculated by two-way ANOVA and indicated as follows: *$p \leq 0.05$, **$p \leq 0.01$, ***$p \leq 0.001$.

experiment and we observed no difference between all the experimental groups (**Fig. 1M**). The ratio of food intake to body weight gain, which correspond to the feed efficiency remained similar between WT and *Dnase1l3*-KO mice either fed a HFD or a ND (**Fig. 1N**). Furthermore, 1 week before endpoint, all the mice were isolated in individual cages to measure their individual food intake. In accordance with previous observations, individual food intake of *Dnase1l3*-KO and WT mice was similar independently of the diet (**Fig. 1O**).

The vast majority of studies on the impact of HFD on obesity and the ensuing metaflammation are conducted in male mice because they are less exposed to hormonal and cyclical variations in estrogen and are more likely to rapidly develop complications of obesity (*Marriott and Huet-Hudson, 2006; Singer et al., 2015*). However, there are profound sex differences in adiposity and obesity-associated diseases in humans (*Link and Reue, 2017*), with women being more affected than man. Therefore, we also analyzed the impact of *Dnase1l3* deficiency on diet-induced obesity using female mice. As shown in **Fig. S1F-K**, *Dnase1l3*-KO female mice, exposed for 12 weeks to 45% HFD, showed an increased weight gain and adiposity compared to HFD-fed WT mice. As with male mice, cumulative food intake of *Dnase1l3*-KO and WT mice was similar independently of the diet (**Fig. S1L-M**). Together, our results indicate that *Dnase1l3* deficiency exacerbate weight gain and adiposity upon induction of obesity by HFD, independently of the sex of the mice and without impacting their feeding habits.

Dnase1l3 deficiency exacerbates the development of metabolic syndrome induced by HFD

We next assessed the impact of *Dnase1l3* deficiency on the development of metabolic complications associated with obesity. First, we confirmed that WT and *Dnase1l3*-KO mice had similar fasting glucose levels and glucose tolerance right before initiating their special diets (**Fig. S2**). In line with the weight gain observed previously, WT and *Dnase1l3*-KO mice exposed 6 weeks to 60% HFD were more glucose intolerant than mice of both genotypes on ND (**Fig. 2A-B**). In mice exposed to 60% HFD, *Dnase1l3*-KO mice were showing a significantly higher glucose intolerance compared to their WT counterpart (**Fig. 2A-B**). Furthermore, fasting blood glucose levels of *Dnase1l3*-KO mice were significantly higher than in WT mice fed with a 60% HFD (2.3 ± 0.4 *vs* 1.8 ± 0.4 mmol/L, $p<0.05$) (**Fig. 2C**). Insulin levels and the HOMA-ratio, corresponding to the extent of insulin resistance, followed the same trend (**Fig. 2D-E**). We also observed that *Dnase1l3*-KO mice were more insulin resistant than WT mice upon 60% HFD, since their circulating glucose levels was significantly less reduced in response to insulin injection (**Fig. 2F**). Finally, 60% HFD also induced a hyperlipidaemia, particularly in *Dnase1l3*-KO mice as manifested by an elevation in circulatory total and LDL-cholesterol levels (**Fig. 2G-H**). We also evaluated these metabolic parameters in WT and *Dnase1l3*-KO mice 12 weeks after exposure to 60% HFD and ND

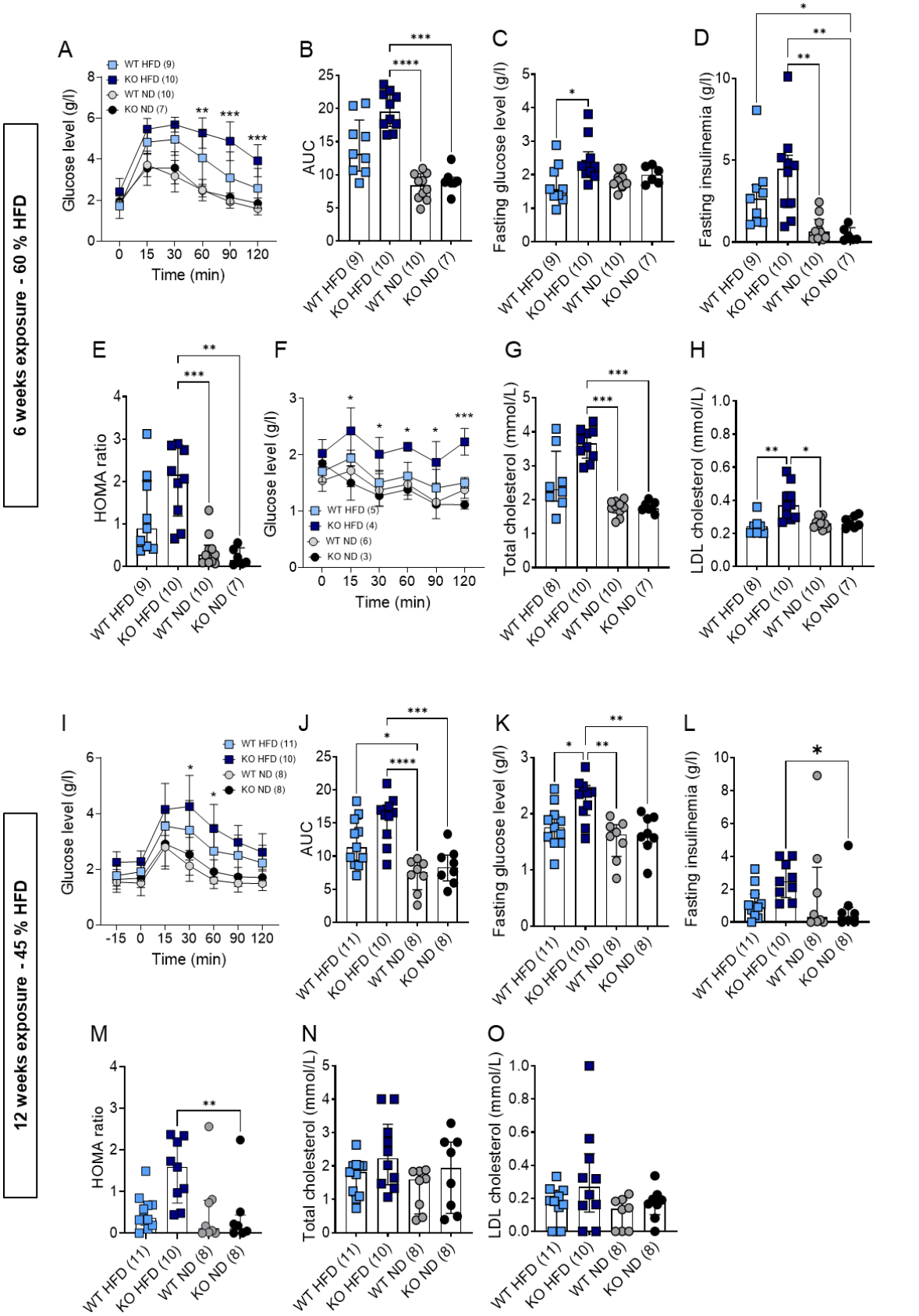

Figure 2: Dnase1l3 deficiency accelerates the development of metabolic syndrome induced by HFD

Metabolic profile of *Dnase1l3*-KO and WT mice exposed during 6 weeks to a 60% HFD (A-H) and 12 weeks to a 45% HFD (I-O) and a chow diet as control. (A, I) Glucose tolerance tests (GTT) were performed by the intraperitoneal injection (IP) of a glucose solution (1 g/kg) and the evaluation blood glucose at the indicated time points by a glucometer. (B, J) Area under the curve of the GTT. (C, K) Fasting blood glucose levels as measured by a glucometer (D, L) Fasting insulin levels as evaluated by ELISA. (E, M) HOMA-ratio was calculated according to the formula: fasting glucose (mg/dL) X fasting insulin (µU/mL) / 405. (F) Insulin Tolerance Test (ITT) was performed upon IP insulin injection (0.75U/kg) and the measurement of blood glucose at different time points. (G, N) Circulatory total cholesterol levels and (H, O) LDL-cholesterol levels as measured by spectrophotometry. Data were combined from two independent experiments with the indicated mouse numbers and presented as mean ± SD. Statistical significance was calculated by two-way ANOVA and indicated as follows: *p ≤ 0.05, **p ≤ 0.01, ***p ≤ 0.001.

(**Fig.S3 A-G**). At this later time point, 60% HFD induced the same degree of glucose intolerance (**Fig. S3A-C**) and insulin resistance (**Fig. S3D-E**) in WT and *Dnase1l3*-KO mice, but the hyperlipidaemia remained slightly more elevated in *Dnase1l3*-KO mice (**Fig. S3 F-G**). Therefore, our results indicate that the absence of DNASE1L3 accelerates the development of metabolic syndrome induced by obesity.

To further address whether *Dnase1l3* deficiency accelerates metabolic disorders induced by obesity, we exposed *Dnase1l3*-KO and WT mice to a 45% fat containing HFD. This diet closely mimics the western diet and was reported to induce development of metabolic syndrome with a slower kinetics than the 60% HFD (*Takahashi et al., 1999*). In accordance with these previous observations, six weeks of exposure to a 45% HFD were not sufficient to lead to metabolic complications (**Fig. S3H-N**). Yet 12 weeks of exposure to a 45% HFD significantly worsen glucose intolerance (**Fig. 2I-J**) and insulin resistance (**Fig. 2K-N**) of *Dnase1l3*-KO mice only, without effectively affecting the levels of circulatory lipids (**Fig. 2M-N**). Together these results confirm that *Dnase1l3* deficiency accelerates the occurrence of a metabolic syndrome in mice exposed to a HFD.

Not all obese individuals are at equal risk for obesity-induced metabolic diseases. Although obesity is more common in women, they seem to be relatively protected from its metabolic impact (*Meyer et al., 2006; Barrett-Connor, 2009*). Therefore, we wondered if *Dnase1l3* deficiency could have a different impact on glucose tolerance and insulin resistance in female mice. Even though female mice exposed to a 45% HFD gain more weight than mice on ND, they were protected from metabolic syndrome since they did not develop any glucose intolerance nor insulin resistance, unlike males (**Fig. S4**). Therefore, *Dnase1l3* deficiency exacerbates the weight gain of female mice upon exposure to HFD, but female mice as women appear to be resistant to metabolic syndrome irrelevant of DNASE1L3 presence or absence.

Dnase1l3 deficiency exacerbates the development of HFD-induced liver steatosis

Obesity often causes a spectrum of liver abnormalities, known as non-alcoholic fatty liver disease (NAFLD), characterized by an increase in intrahepatic triglyceride content (*i.e.* steatosis) with or without inflammation and fibrosis (*i.e.* steatohepatitis). We next assessed the impact of *Dnase1l3* deficiency on the liver damage associated with obesity. We used ALAT as a marker of ongoing liver malfunction. After only 6 weeks of HFD (either 45% or 60% HFD) there is an increase in circulatory ALAT levels specifically in *Dnase1l3*-KO mice (**Fig. 3A,D**). WT mice fed with both HFDs and mice on ND showed similar ALAT values to those measured at baseline (**Fig. 3A,D and Fig. S2G**). The liver mass appeared to be increased in WT and *Dnase1l3*-KO mice fed a 60% HFD compared to mice fed a ND, while it was not impacted by a 45% HFD diet (**Fig. 3B,E**). Finally, with the software-assisted analysis of

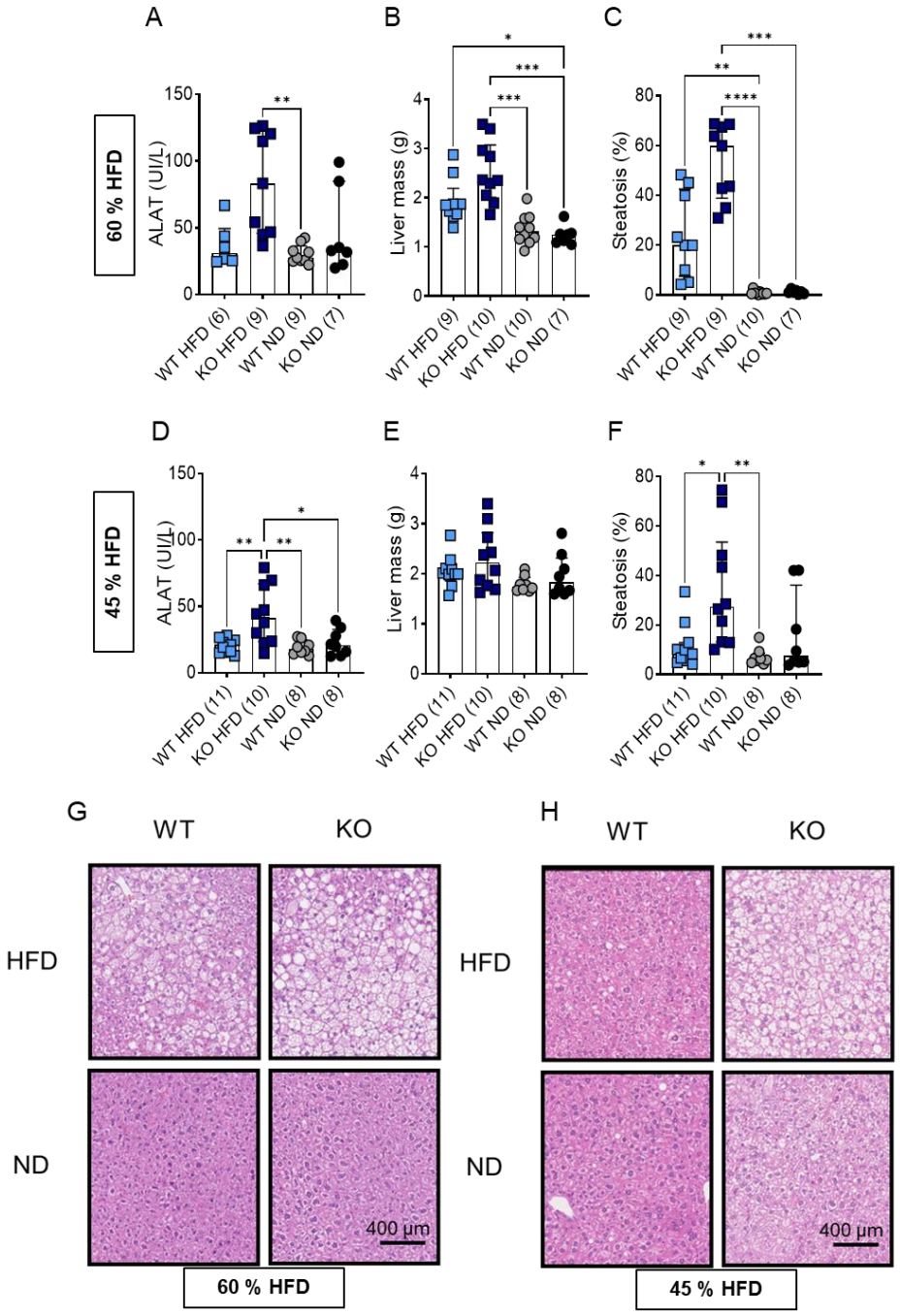

Figure 3: Dnase1l3 deficiency exacerbates the development of HFD-induced steatosis

Liver pathology of Dnase1l3-KO and WT mice exposed 6 to 12 weeks to 60% HFD (A-C, G) and 45% HFD (D-F, H) and a chow diet as control was evaluated. (A, C) ALAT levels after 6 weeks of diet exposure as measured by spectrophotometry. (B, E) Individuals weights of livers measurer after 12 weeks of diet exposure. (C, F) Semi-automated quantification of hepatic steatosis (%) by pathologist blinded to genotypes and experimental conditions. (G, H) Representative liver section after Hematoxylin and Eosin staining of each group. Data were combined from two independent experiments with the indicated mouse numbers and presented as mean ± SD. Statistical significance was calculated by two-way ANOVA and indicated as follows: *p ≤ 0.05, **p ≤ 0.01, ***p ≤ 0.001.

histological sections of liver we were able to quantify hepatic steatosis. These analyses were performed by a single pathologist blinded to genotype and numerically assisted with quPath software to obtain a better uniformity and comparability of samples between experiments. A 60% HFD induced a hepatic steatosis in obese mice that is more severe in Dnase1l3-KO mice compared to WT mice (Fig. 3C,G). Interestingly, in mice fed with 45% HFD, hepatic steatosis was only increased in Dnase1l3-KO mice (Fig. 3F,H). These results suggest that Dnase1l3 deficiency accelerate the onset of obesity-associated hepatic disorders.

Dnase1l3 deficiency increases VAT immune infiltration and inflammation in obese mice

During obesity, the VAT is highly infiltrated by immune cells that acquire a pro-inflammatory phenotype. Particularly, anti-inflammatory M2-like macrophages that are abundant in the lean WAT switch to pro-inflammatory M1-like macrophages in the obese WAT. Such M1-like macrophages were shown to contribute to "metaflammation" induced by obesity. This inflammatory state is directly linked to insulin resistance and complications associated to obesity (*Lumeng et al., 2007*). To evaluate the impact of *Dnase1l3* deficiency on this metaflammation induced by obesity, we analyzed by flow cytometry the immune compartment ($CD45^+$ cells) in the SVF obtained from VAT of WT and *Dnase1l3* KO mice subjected or not to HFD (**Fig. S5**). As expected, mice fed during 12 weeks with a 60% HFD showed elevated absolute counts of leucocytes (**Fig. 4A**) and $CD11b^+$ and $CD64^+$ macrophages (**Fig. 4C**). We next analysed either the anti-inflammatory M2-like profile ($CD301b^+$ cells) or pro-inflammatory M1-like profile ($CD11c^+$ cells) of the macrophages present in the SVF of VAT (**Fig. 4B**). $CD11c^+$ M1 like macrophage frequency (**Fig. 4D**), counts (**Fig. 4E**) and the ratio of M1 to M2 macrophages (**Fig. 4F**) were significantly enriched in the SVF of VAT of mice that were subjected to 60% HFD. In addition to macrophages, T cells, B cells, DCs, monocytes and granulocytes (**Fig.S5**) in the SVF of VAT, were increased upon 60% HFD (**Fig. S6 A-G**). We did not observe any significant difference in the overall immune cell infiltration neither in the activation and/or inflammatory profile of all the analysed immune cells between WT and *Dnase1l3*-KO mice fed for 12 weeks with a 60% HFD (**Fig. 4A-F and Fig. S6A-N)**. Therefore, after 12 weeks of 60% HFD the VAT immune infiltrate as well as its inflammatory profile is not significantly affected by the absence of DNASE1L3. This observation is in accordance with our previous results showing that *Dnase1l3* deficiency exacerbated metabolic disorders induced by the 60% HFD only 6 weeks after the initiation of the diet but not at 12 weeks after the diet initiation. These data suggest that the obesity induced by 12 weeks of 60% HFD is too excessive to see any impact of *Dnase1l3* deficiency on the overall metabolic and inflammatory profile. Therefore, we performed the same experiment using an HFD containing 45% of fat, which is inducing a milder weight gain and

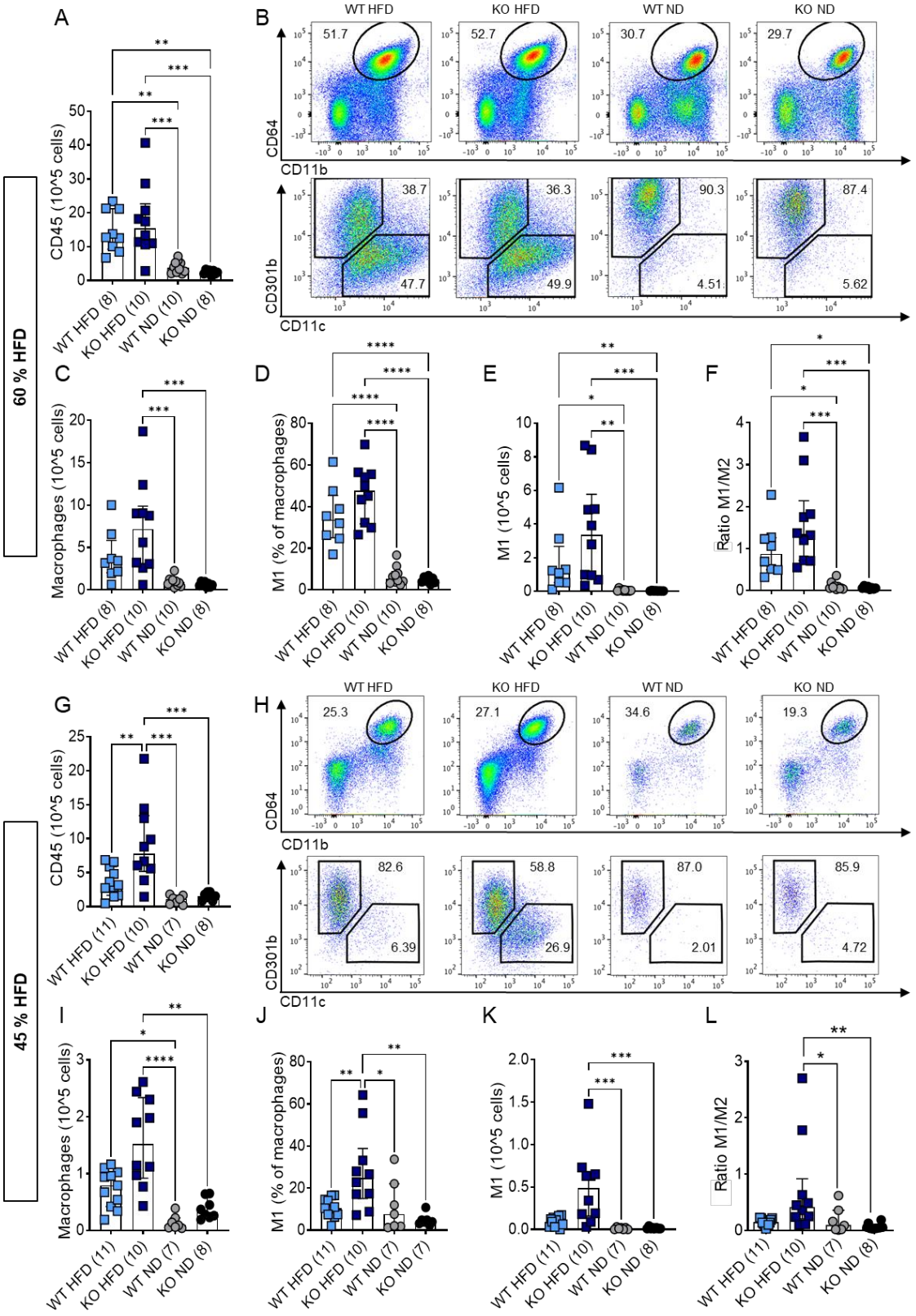

Figure 4: *Dnase1l3* deficiency increases macrophages infiltration and their switch toward and M1 pro-inflammatory profile in the white adipose tissue of obese mice

Mice were fed with 60% HFD (A-F), 45% HFD (G-L) or standard diet as controls. After 12 weeks mice were euthanized and leucocytes from the stromal vascular fraction (SVF) of the VAT of obese (square) and lean (circle) WT and *Dnase1l3*-KO mice were analysed by flow cytometry. (A, G) Absolute numbers of viable $CD45^+$. (B, H) Representative plots and frequency of macrophages ($CD45^+$ $CD11b^+$ $CD64^+$ cells) showing either the proinflammatory M1-like ($CD11c^+$ cells) or the anti-inflammatory M2 like ($CD301b^+$ cells) phenotype. (C, I) Absolute number of viable total macrophages identified as $CD45^+$ $CD64^+$ and $CD11b^+$ cells. (D, J) Percentage of M1-like macrophages identified as $CD45^+$ $CD64^+$ $CD11b^+$ and $CD11c^+$ cells out of total macrophages. (E, K) Absolute numbers of M1-like macrophages. (F, L) Ratio of the percentage of M1 to M2-like macrophages. Data were combined from two independent experiments with the indicated mouse numbers and presented as mean ± SD. Statistical significance was calculated by two-way ANOVA and indicated as follows: $*p \leq 0.05$, $**p \leq 0.01$, $***p \leq 0.001$.

metabolic syndrome and it is doing so with a slower kinetics. We observed that after 12 weeks of feeding with a 45% HFD, only *Dnase1l3*-KO mice showed a significant increase in the number of $CD45^+$ in the SVF of the VAT (**Fig. 4G**). As $CD45^+$ cells were elevated, most immune cells (**Fig. S6J-P**) including macrophages (**Fig. 4I**) were also significantly increased in the SVF of the VAT of *Dnase1l3*-KO mice subjected to a 45% HFD. We further analysed macrophages (**Fig. 4H**) and observed that in comparison to WT mice, *Dnase1l3*-KO mice accumulated more proinflammatory M1-like macrophages (**Fig. 4J-L**). As in male mice, weight gain in HFD-fed *Dnase1l3*-KO female mice is accompanied by an increase in pro-inflammatory M1 macrophages and a decrease in anti-inflammatory M2 macrophages in the VAT (**Fig. S7A-F**) which could potentially accelerate the onset of complications in these mice. Together, our results indicate that *Dnase1l3* deficiency accelerates the onset of metaflammation in the VAT in response to HFD which could explain the earlier onset of metabolic complications observed in these mice.

Obese patients show an accumulation of circulatory cfDNA

Recent studies have reported an increase in circulatory cfDNA in obese patients (*Garcia-Martinez et al., 2016; Nishimoto et al., 2016*). However, the form (free *vs* associated to MPs) of such circulatory cfDNA that accumulate in obese individuals remains poorly characterized. Furthermore, circulatory cfDNA levels are controlled by extracellular DNASEs, including DNASE1 and DNASE1L3. Particularly DNASE1L3 was shown to play an important role in the regulation of DNA levels associated to MPs (*Sisirak et al., 2016*) and its fragmentation profile (*Serpas et al., 2019*). We therefore evaluated plasma cfDNA quantity and form in a cohort of obese individuals (n=26) and age- and sex-matched HD (n=27) detailed in **Supplementary table 2**. We used a quantitative PCR approach previously described (*Zhang et al., 2009*) to quantify the amount of circulatory gDNA, based on the amplification of *ALU* repetitive elements. We observed that obese patients show significantly more circulatory genomic cfDNA than HD (68.69 ± 22.39 *vs* 29.64 ± 10.7 ng/mL, p=0.024) (**Fig. 5A**). Importantly, circulatory genomic cfDNA levels positively correlated with BMI, insulinemia and HOMA-IR of obese patients and HD (**Fig. 5B-D**). On the other hand, we did not observe a significant correlation between cfDNA levels and patient fasting glycemia, ALAT and LDL-cholesterol levels (**Fig. S8**). We also measured circulatory genomic cfDNA levels in a longitudinal cohort (n=20) of obese patients before and 3 to 12 months after bariatric surgery (**Supplementary table 3**). We observed that weight loss after bariatric surgery is associated with reduced circulatory genomic cfDNA levels in obese individuals (4.7 ± 8.1 *vs* 2.0 ± 2.6 ng/mL, p =0.009) to quantities found in HD (1.5 ± 1.6 ng/mL) (**Fig. 5E**). We further studied

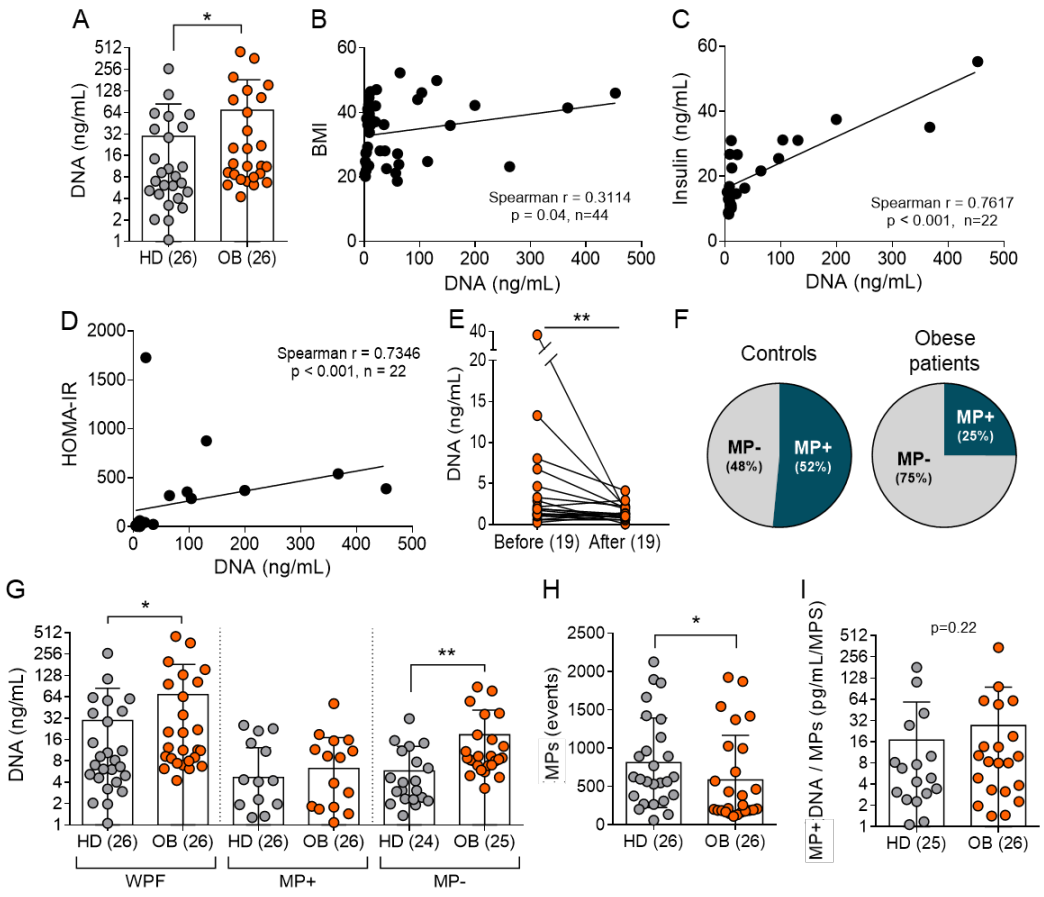

Figure 5: Obese patients show an accumulation of circulatory cell-free (cf)DNA

(A) cfDNA levels in peripheral blood mononuclear cell (PBMC) of obese patients (OB) and healthy donors (HD) quantified by qPCR (*Zhang et al., 2009*). Correlation between cfDNA and BMI (B), cfDNA and Insulin level (C) and cfDNA and HOMA-IR (D) in HD and OB. HOMA-IR (Homeostasis Model Assessment of Insulin Resistance) was calculated by the formula: fasting glucose (mg/dL) X fasting insulin (µU/mL) / 405. (E) Circulating cfDNA levels in PBMC of OB before and 3 to 12 months after bariatric surgery. (F) percentage of soluble (MP-) and MP-associated fraction (MP+) of cfDNA in whole plasma fraction (WPF). (G) cfDNA levels in WPF, MP+ and MP- of OB and HD. (H) MPs levels in plasma of HD and OB. (I) Ratio of MP+DNA on MPs levels (MP+/MPs). Number of patients used (n) is indicated for each analysis. Data are presented as the mean ± SD. *$p \leq 0.05$, **$p \leq 0.01$, ***$p \leq 0.001$ using Mann-Withney test and spearman rank correlation test.

circulatory gDNA levels that are either free or associated to MPs. For that purpose, we spun the plasma at high speed (22.10^3 *g*) and quantified gDNA in the soluble fraction (free) and in the pellet (MP-associated). In obese patients, most (75%) of the circulatory gDNA was detected in the soluble fraction of the plasma while only a small proportion (25%) was found in the fraction enriched in MPs (**Fig. 5F**). Conversely, in HD circulatory genomic DNA was detected in the same proportion in the soluble and the MP-associated-fraction (52 and 48%). The increase of total cfDNA that we previously observed in mostly due to an accumulation of cfDNA in a soluble fraction (**Fig. 5G**). While the amount of genomic DNA in the MP enriched fraction remained similar between obese patients and HD (**Fig. 5G**), we consistently observed a significant reduction of MPs numbers in the plasma of obese patients (**Fig. 5H**). Therefore, we normalized the genomic DNA quantities detected in this fraction to the number of MPs. Despite this, the ratio DNA per MPs was similar between obese patients and HD (p=0.22) (**Fig. 5I**). Thus, obese patients show increased levels of circulatory cfDNA. This increase occurs mostly at the level of soluble DNA and appears to be associated to obesity severity.

Obese patients show an impairment of circulatory DNASEs activity

As mentioned previously, the levels of circulatory cfDNA are regulated by extracellular DNASEs, particularly DNASE1L3 (*Sisirak et al., 2016*). Consequently, the accumulation of plasmatic cfDNA in obese individuals reflects an impaired regulation of extracellular DNASEs expression and/or activity. Given that *DNASE1L3* was previously reported to be highly expressed by haematopoietic cells such as dendritic cells and macrophages (*Wilber et al., 2002; Sisirak et al., 2016*), we measured its expression simultaneously in PBMC, from obese and healthy individuals by flow cytometry-based fluorescence *in situ* hybridization (Flow-FISH). This approach, based on an fluorescently-labelled (APC) oligonucleotide probe specific to the *DNASE1L3* mRNA, was preferred due to the lack of antibodies targeting specifically DNASE1L3. In combination with classical flow cytometry antibodies we could identify the immune populations of interest (**Fig. S9**) and within those cells evaluate the mean florescent intensity (MFI) of the *DNASE1L3* probe as a surrogate of its expression level. We first observed that among PBMC, *DNASE1L3* mRNA is mainly expressed in plasmacytoid dendritic cells (pDCs) and nearly absent in other myeloid and lymphoid lineages (**Fig. 6A**). We next analyzed DNASE1L3 expression at the global level in PBMCs and observed that its expression is similar between obese patients and HD (**Fig. 6C**). Similarly, DNASE1L3 expression levels in different immune subsets are similar between obese individuals and HD (**Fig. 6B**). In addition to DNASE1L3 expression analysis, we measured DNASEs activity in the plasma of obese patients and HD using a single radial enzyme-diffusion (SRED) assay. For this

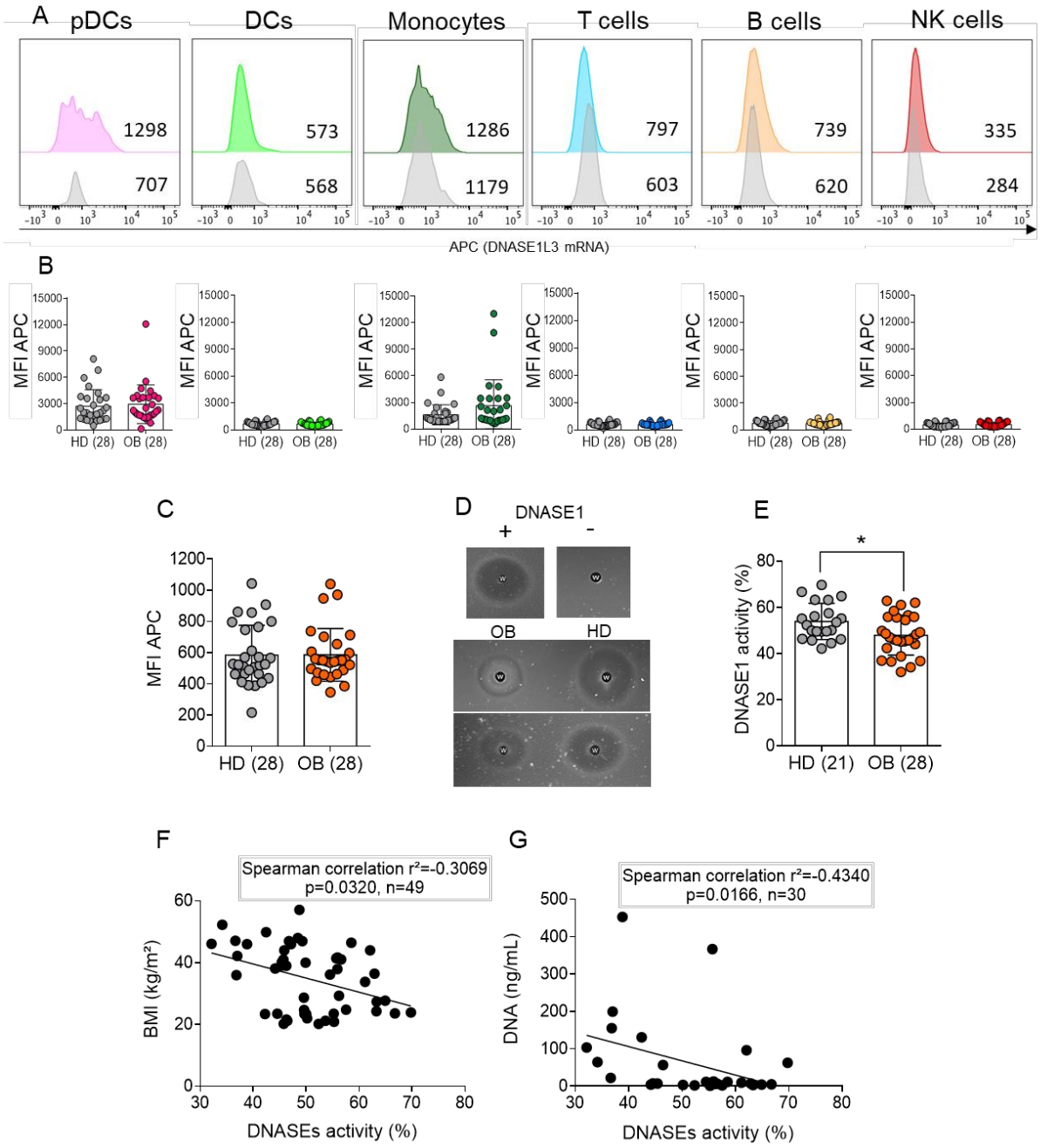

Figure 6: Obese patients show an impairment of circulatory DNASEs activity

DNASE1L3 expression was measured simultaneously in most of the peripheral blood mononuclear cells (PBMCs), from obese patients (OB) and healthy individuals (HD), by flow cytometry-based fluorescence *in situ* hybridization (Flow-FISH). The MFI (Mean Florescent Intensity) of APC fluorochrome reflects the amount of *DNASE1L3* mRNA. (A) The MFI of APC signal is plotted for each immune cell subpopulation of a HD and a OB representative of their respective groups. (B) MFI of APC signal (*DNASE1L3* mRNA) in pDCs, DCs, monocytes, B cells, T cells and NK cells. (C) Global MFI of APC signal. (D) Quantification of total DNASEs activity by single radial enzyme-diffusion (SRED). Plasma from OB and HD is dispensed into a circular well in an agarose gel layer in which DNA is uniformly distributed. The diameter of the dark circle of hydrolyzed DNA correlates linearly with the activity of DNASEs. (E) Percentage of DNASE1 activity in the plasma of OB and HD measured by a new DNASEs activity assay based on the PicoGreen dye. A known quantity of dsDNA is incubated with increasing amounts of DNASE1 as standard and with the plasma of HD and OB. The amount of remaining dsDNA was measured by the PicoGreen assay and normalized to DNASE1 activity. Correlation between DNASEs activity and BMI (F) and circulatory DNA level (G) in HD and OB. Data are presented as the mean ± SD. *$p \leq 0.05$, **$p \leq 0.01$, ***$p \leq 0.001$ using t-test or Mann Whitney test according to the normal or non-normal sample distribution and spearman rank correlation test.

assay, the plasma was dispensed into a circular well in an agarose gel in which DNA was uniformly distributed. As plasmatic DNASE degrades DNA embedded in the gel, dark circles form around the well and the diameter of these dark circles are directly correlated to total DNASEs activity. In the small number of analyzed individuals we observed a reduction of the overall DNASEs activity in obese individuals (**Fig. 6D**). Given that this method is difficult to extend to numerous patients and to quantify precisely we generated a new DNASEs activity assay based on the QuantiT-PicoGreen™ dsDNA assay aimed at measuring dsDNA levels. We placed dsDNA in presence of increasing amounts of DNASE1 as standard as well as in presence of the plasma of HD and obese individuals for 2h. Next, the amount of remaining dsDNA was quantified and normalized to DNASE1 activity. We observed that obese patients showed a significant reduction of global DNASEs activity in comparison to HD (**Fig.6E**). Furthermore, plasmatic DNASEs activity was inversely correlated to the BMI of the patients and their DNA levels (**Fig 6F, G**). Thus, obesity affects DNASEs activity likely contributing to aberrant cfDNA accumulation.

DISCUSSION

Endogenous DNAs and their recognition by the innate immune system play an important role in the pathogenesis of obesity, but the mechanisms involved in their regulation during obesity remain poorly understood. We explored herein the function of an extracellular DNASE, called DNASE1L3, in the development of metaflammation and metabolic syndrome induced by obesity. Our results indicate that DNASE1L3 protects from obesity mediated-inflammation and metabolic complications likely by controlling endogenous DNA levels and their capacity to activate inflammatory responses.

We first characterized the impact of *Dnase1l3* deficiency on mice weight gain after their exposure to HFD. Our results showed that *Dnase1l3* deficiency exacerbated HFD-induced weight gain and adiposity of the visceral and subcutaneous AT. Weight gain in *Dnase1l3*-KO mice occurred very rapidly after the introduction of the HFD (4-5 weeks) without affecting mice food intake. As weight gain is linked to an imbalance between calories intake (feeding) and energy expenditure (*Grobe, 2017*), we can extrapolate our results by concluding that the exacerbated weight gain of *Dnase1l3*-KO mice is probably secondary to a decrease in their energy expenditure. Nevertheless, it would be necessary to confirm this postulate by evaluating oxygen consumption (VO_2), carbon dioxide production (VCO_2), respiratory quotient (RER) (VCO_2/VO_2), and the physical activity of *Dnase1l3*-KO mice in comparison to WT mice fed both with a ND and HFD.

In addition to exacerbating weight gain, we observed that the deficiency of *Dnase1l3* accelerated the onset of glucose intolerance and insulin resistance in mice fed with a HFD. The development of these metabolic complications of obesity was previously linked to the metaflammation that occurs in the AT (*McLaughlin et al., 2017*). Indeed, an elevated production of inflammatory cytokines such as TNF-α and IFN-I was reported, through the activation of canonical kinases (JNK, IKKβ) and transcription factors (AP1 and NF-κB), to interfere with insulin receptor signalling and to prevent insulin action on the regulation of extracellular glucose levels (*Schenk et al., 2008*). This is in accordance with our results showing an that *Dnase1l3* deficiency also amplify AT inflammation in response to diet-induced obesity as manifested by an elevation in the representation of pro-inflammatory M1-like macrophages in the AT.

DNASE1L3 was previously shown to control extracellular levels of DNA associated to MPs and its fragmentation profile (Serpas et al., 2019; Chan et al., 2020b). Aberrant accumulation of endogenous DNA in *Dnase1l3*-KO mice caused the development of systemic lupus erythematosus (SLE) (*Sisirak et al., 2016*). Particularly *via* TLR7/9 stimulation, endogenous DNA induced the production of IFN-I by pDCs contributing to SLE pathogenesis mediated by the absence of DNASE1L3 (*Soni et al., 2020*). Such immunostimulatory pathways involved in SLE development in *Dnase1l3*-KO mice were also recently reported to contribute to obesity-mediated metaflammation and the ensuing metabolic syndrome (*Ferriere et al., 2020*). Indeed, multiple studies have shown that endogenous DNA originating from adipocytes and NETs accumulate during obesity and through TLR9 simulation, induce AT tissue inflammation (*Nishimoto et al., 2016; Revelo et al., 2016*). In addition, *Ifnar* deficiency and pDCs deletion was shown to protect mice from AT metaflammation induced by obesity (*Hannibal et al., 2017; Chan et al., 2020a*). In humans, adipose tissues explants were shown to release self-DNA associated with the nuclear protein HMGB1, which in turn stimulated pDC production of IFN-I in a TLR9-dependent manner (*Ghosh et al., 2016*). IFN-I derived from pDCs play and important role in polarizing macrophages toward a pro-inflammatory M1-like phenotype (*Ghosh et al., 2016*), and depleting AT Tregs (*Li et al., 2021*), which both contribute to AT inflammation. Therefore, the absence of DNASE1L3 during obesity most likely enhance endogenous DNA availability and ultimately its ability to exacerbate inflammatory responses

in a TLR9- and IFN-I-dependent manner. To conclusively confirm this hypothesis, it will be important to block TLR9 and/or IFN-I in *Dnase1L3*-KO mice fed with a HFD.

The development of NASH in mice fed a HFD was also shown to at least partially depend on TLR9 activation. Indeed, hepatocytes from NASH livers were described to release MPs harbouring mtDNA that activated liver macrophage production of inflammatory cytokines through TLR9 (*Garcia-Martinez et al., 2016*). DNA originating from NETs also accumulate in the liver of mice and humans affected by NASH (*van der Windt et al., 2018*). Inhibition of NETs formation as well as digestion of NETs-DNA by DNASE1, ameliorated NASH development *in vivo* and prevented NASH evolution into hepatocellular carcinoma (*van der Windt et al., 2018; Zhao et al., 2020*). Given that NETs trigger inflammatory responses *via* TLR9 activation (*Garcia-Romo et al., 2011*), it is likely that their role in NASH pathogenesis depends on TLR9 activation as well. In addition to TLR9, mtDNA derived from hepatocytes was shown to activate cGAS/STING pathway in liver macrophages and consequently to participate in NASH development during obesity (*Luo et al., 2018; Yu et al., 2018*). We have observed that *Dnase1l3* deficiency aggravate NASH in response to HFD. While WT mice did not show any signs of liver steatosis upon 12 weeks of HFD containing 45% of fat, *Dnase1l3*-KO mice displayed increased circulatory levels of ALAT and of liver steatosis, indicating that DNASE1L3 is key in controlling liver homeostasis in response to HFD. Since DNASE1L3 regulate the levels of DNA associated to MPs (*Sisirak et al., 2016*) and NETs (*Jiménez-Alcázar et al., 2017*) which are both forms of DNA found to contribute to NASH, its deletion may delay their disposal and thus enhance their capacity to stimulate liver inflammation which is key in NASH pathogenesis (*Huby and Gautier, 2022*).

As we previously discussed, the absence of DNASE1L3 in mice and humans causes the development of SLE which is manifested by an aberrant production of anti-DNA auto-antibodies (*Al-Mayouf et al., 2011; Sisirak et al., 2016*). Auto-immunity in response to *Dnase1l3* deficiency affect both female and male individuals. Nevertheless, in male mice anti-DNA antibodies autoreactivity is significantly lower than in female mice and ultimately causes a milder SLE with a longer kinetics, particularly in mice on a C576Bl/6 background (*Sisirak et al., 2016; Soni et al., 2020*). The impact of *Dnase1l3* deficiency on metaflammation and the metabolic syndrome induced by obesity was done mostly in male mice, thus reducing any confounding impact of auto-immunity on our observations. In addition, when we quantified

anti-DNA autoantibodies, we did not observe a clinically significant elevation in their titers in males *Dnase1l3*-KO mice compared to their WT counterpart (**SD Fig.10A-E**). In females, only two *Dnase1l3*-KO mice had elevated levels of anti-DNA antibodies before the initiation of the HFD. However, all mice gained weight on this diet. Thus, antibodies do not appear to influence weight gain in these mice. After 12 weeks of HFD both male and female *Dnase1l3*-KO mice did not show a significant increase in anti-DNA anti-bodies in comparison to *Dnase1l3*-KO that were fed with ND (**SD Fig.10A-E**). While obesity induced by HFD was reported to exacerbate SLE pathogenesis in SLE-prone *Tlr8* KO (*Hanna Kazazian et al., 2019*) and FcγRIIb KO (*Udompornpitak et al., 2022*) mice, it did not affect anti-DNA autoreactivity in *Dnase1l3*-KO mice. However, the impact of obesity on SLE features in *Dnase1l3*-KO should be further studied, particularly using mice that initially show similar extend of auto-reactivity towards DNA prior to the initiation of the HFD.

For historical and economic reasons, mouse models of diet-induced obesity (DIO) most often use an HFD diet containing 60% fat. In experimental setting using this diet, we observed that *Dnase1l3*-deficiency increased glucose intolerance and insulin resistance after 6 weeks of diet while at endpoint (12 weeks after the initiation of HFD) these differences waned. Accordingly, at endpoint we did not find significant differences in AT tissue inflammation reflected by the accumulation of proinflammatory M1-like macrophages between WT mice and *Dnase1l3*-KO mice fed with a HFD. This is likely due to the fact that the massive fat intake using the 60% HFD causes a rapid onset obesity-mediated complications (*Casimiro et al., 2021*) and at late time points the impact of such diet on metabolic parameters and AT inflammation is too strong to observe any effects of *Dnase1l3* deficiency. Conversely, when mice were place on a HFD containing 45% of fat, glucose intolerance, insulin resistance and AT tissue inflammation were significantly exacerbated in *Dnase1l3*-KO mice only after 12 weeks HFD initiation. This HFD containing 45% fat is related Western diet that are responsible for the current obesity pandemic (*Speakman, 2019*), and cause obesity-associated complication with a slower kinetics (*Takahashi et al., 1999*). Therefore, these results indicate that the absence of DNASE1L3, rather than exacerbating, accelerates the onset of metabolic disorders.

Studies evaluating the impact of HFD on obesity are mostly performed with male mice because they are more likely to rapidly develop complications of obesity such as metabolic syndrome (*Marriott and Huet-Hudson, 2006; Shi et al., 2006; Singer et al., 2015*). However, patients who

undergo bariatric surgery are overwhelmingly female (*Pratt et al., 2009*). We therefore studied the impact of *Dnase1L3* deficiency on obesity mediated metabolic syndrome and metaflammation upon their exposure to 45% HFD in female mice. As for male, female *Dnase1L3*-KO mice showed a significantly increased weight gain compared to WT mice. But, after 12 weeks of HFD they did not develop glucose intolerance nor insulin resistance. This is an accordance with the literature showing that females mice are less susceptible to HFD mediated metabolic disorders (*Meyer et al., 2006; Barrett-Connor, 2009*). AT inflammation and liver steatosis appeared to be more elevated in female *Dnase1l3*-KO mice compared to WT mice upon 12 weeks of HFD although not significantly. It was described previously that AT and liver inflammation in female mice takes a longer exposure to a HFD (~15 weeks) (*Varghese et al., 2021*) and thus in female mice *Dnase1l3* deficiency may lower the threshold for the induction of metabolic tissue inflammation induced by HFD as well. These sex differences are largely related to the effects of estrogen (*Palmer and Clegg, 2015*). However, replacement therapy is not sufficient to prevent the risk of obesity-associated diseases, suggesting that other inherent differences between males and females are at work (*Barrett-Connor, 2009; Riant et al., 2009*), such an increase in AT Treg cells in female mice (*Pettersson et al., 2012*).

We finally investigated the human relevance of our finding in *Dnase1l3* deficient mice. We quantified circulating self-DNA levels in the plasma of obese patients and healthy donors. As previously described (*Garcia-Martinez et al., 2016; Ghosh et al., 2016; Nishimoto et al., 2016*), we showed that endogenous cfDNA levels were significantly increased in obese patients compared with healthy donors. Importantly, we observed that the levels of cfDNA were positively correlated with patient BMI and insulin resistance. In addition, bariatric surgery, which causes an important weight loss in obese patients, induced a significant reduction of circulatory cfDNA, to levels observed in healthy individuals. These observations support the hypothesis that in obese patients an aberrant accumulation of cfDNA contribute to obesity and its associated complications. Garcia *et al.* showed that patients with NAFLD induced by obesity display elevated levels of MP harbouring DNA which exhibited potent a proinflammatory potential through the stimulation of TLR9 (*Garcia-Martinez et al., 2016*). We therefore quantified circulating DNA in the MP fraction of obese patients' plasma. We observed that cfDNA accumulating in our cohort of obese individuals was mostly contained in a soluble fraction which was depleted of MPs. While the MP fraction of the plasma contained

similar amounts of DNA between obese patients and healthy donors, the number of MP detected in the circulation obese individuals was significantly reduced.

We have previously described that the main sources of DNASE1L3 in mice are myeloid cell including DCs and macrophages (*Sisirak et al., 2016*) while DNASE1 is mostly produces by exocrine cells (*Napirei et al., 2004*). In humans, transcriptomic data and recent studies have shown that DNASE1L3 is specifically expressed in pDCs, monocytes and monocyte-derived DCs (*Inokuchi et al., 2020*). Due to the current lack of antibodies specifically recognizing human DNASE1L3, we analyzed its expression in the PBMCs of obese patients and healthy controls by *in situ* hybridization based flow cytometry. We observed that DNASE1L3 expression is restricted to pDCs among PBMCs, however obesity did not affect its expression profile. These results suggest DNASE1L3 expression might be specifically regulated in immune cells within metabolic tissues affected by obesity and/or its activity may be negatively regulated by soluble factors induced by obesity. In accordance with these hypothesis, a recent study has shown that hypercholesterolemia negatively regulates DNASE1 and DNASE1L3 expression with the AT and the liver (*Dhawan et al., 2021*). Our results also indicate that the ability of the plasma from obese patients to digest target DNA was significantly reduced compared to healthy controls, and that the extent of this DNASEs activity reduction was correlated to the severity of obesity. These results suggest that circulatory DNASEs activity is impaired during obesity and such impairment contribute to obesity pathogenesis. Further studies are required to specifically address the impact of obesity on individual circulatory DNASEs including DNASE1 and DNASE1L3. In patients with SLE, antibodies targeting either DNASE1 (*Yeh et al., 2003*) and DNASE1L3 (*Hartl et al., 2021*) activity were shown to inhibit their activity and contribute to disease severity. Given that obesity was also associated to an increase in autoantibodies toward self-DNA (*Revelo et al., 2016; Dhawan et al., 2022*), it is possible that obese individuals may develop anti-DNASEs autoreactivity as well. Moreover, Dhawan *et al.* showed recently that endoplasmic reticulum stress could be a causal factor leading to the alteration of the NET-induced DNASEs response during atherogenic dyslipidemia (*Dhawan et al., 2021*). ER stress has been widely implicated in the pathogenesis of obesity and therefore could as well contribute in the impairment of DNASEs functions.

Although multiple lines of evidence have established that self-DNA recognition contribute to obesity-mediated pathogenesis, our study for the first show an important role for the

extracellular DNASE1L3 in regulation of self-DNA pathogenic potential in this context. DNASE1L3 appears to constitutes a “safeguard” mechanism by digesting self-DNA and preventing its ability to cause obesity-induced inflammation and the ensuing metabolic syndrome. These results define an entirely novel pathogenic loop at play in obesity and may also lead to the development of novel therapeutic tools that are critical for obese patients. Indeed, restoring or boosting DNASE1L3 activity may be of therapeutic benefit for obese individuals, by reducing the pro-inflammatory potential of self-DNA that accumulate during obesity.

REFERENCES

Achanta, R., Shaji, A., Smith, K., Lucchi, A., Fua, P., and Süsstrunk, S. (2012). SLIC superpixels compared to state-of-the-art superpixel methods. *IEEE Trans Pattern Anal Mach Intell* 34, 2274–2282. doi: 10.1109/TPAMI.2012.120.

Al-Mayouf, S. M., Sunker, A., Abdwani, R., Abrawi, S. A., Almurshedi, F., Alhashmi, N., et al. (2011). Loss-of-function variant in DNASE1L3 causes a familial form of systemic lupus erythematosus. *Nat Genet* 43, 1186–1188. doi: 10.1038/ng.975.

Amar, J., Chabo, C., Waget, A., Klopp, P., Vachoux, C., Bermúdez-Humarán, L. G., et al. (2011). Intestinal mucosal adherence and translocation of commensal bacteria at the early onset of type 2 diabetes: molecular mechanisms and probiotic treatment. *EMBO Mol Med* 3, 559–572. doi: 10.1002/emmm.201100159.

Bae, J. H., Jo, S. I., Kim, S. J., Lee, J. M., Jeong, J. H., Kang, J. S., et al. (2019). Circulating Cell-Free mtDNA Contributes to AIM2 Inflammasome-Mediated Chronic Inflammation in Patients with Type 2 Diabetes. *Cells* 8, 328. doi: 10.3390/cells8040328.

Bai, J., and Liu, F. (2019). The cGAS-cGAMP-STING Pathway: A Molecular Link Between Immunity and Metabolism. *Diabetes* 68, 1099–1108. doi: 10.2337/dbi18-0052.

Bankhead, P., Loughrey, M. B., Fernández, J. A., Dombrowski, Y., McArt, D. G., Dunne, P. D., et al. (2017). QuPath: Open source software for digital pathology image analysis. *Sci Rep* 7, 16878. doi: 10.1038/s41598-017-17204-5.

Barrett-Connor, E. (2009). Women and heart disease: neglected directions for future research. *J Cardiovasc Transl Res* 2, 256–257. doi: 10.1007/s12265-009-9110-0.

Bernstein, L. E., Berry, J., Kim, S., Canavan, B., and Grinspoon, S. K. (2006). Effects of etanercept in patients with the metabolic syndrome. *Arch Intern Med* 166, 902–908. doi: 10.1001/archinte.166.8.902.

Binder, E., Bermúdez-Silva, F. J., André, C., Elie, M., Romero-Zerbo, S. Y., Leste-Lasserre, T., et al. (2013). Leucine supplementation protects from insulin resistance by regulating adiposity levels. *PLoS One* 8, e74705. doi: 10.1371/journal.pone.0074705.

Casimiro, I., Stull, N. D., Tersey, S. A., and Mirmira, R. G. (2021). Phenotypic sexual dimorphism in response to dietary fat manipulation in C57BL/6J mice. *J Diabetes Complications* 35, 107795. doi: 10.1016/j.jdiacomp.2020.107795.

Chan, C. C., Damen, M. S. M. A., Moreno-Fernandez, M. E., Stankiewicz, T. E., Cappelletti, M., Alarcon, P. C., et al. (2020a). Type I interferon sensing unlocks dormant adipocyte inflammatory potential. *Nat Commun* 11, 2745. doi: 10.1038/s41467-020-16571-4.

Chan, R. W. Y., Serpas, L., Ni, M., Volpi, S., Hiraki, L. T., Tam, L.-S., et al. (2020b). Plasma DNA Profile Associated with DNASE1L3 Gene Mutations: Clinical Observations, Relationships to Nuclease Substrate Preference, and In Vivo Correction. *Am J Hum Genet* 107, 882–894. doi: 10.1016/j.ajhg.2020.09.006.

Cheng, T. H. T., Lui, K. O., Peng, X. L., Cheng, S. H., Jiang, P., Chan, K. C. A., et al. (2018). DNase1 Does Not Appear to Play a Major Role in the Fragmentation of Plasma DNA in a Knockout Mouse Model. *Clinical Chemistry* 64, 406–408. doi: 10.1373/clinchem.2017.280446.

Dhawan, U. K., Bhattacharya, P., Narayanan, S., Manickam, V., Aggarwal, A., and Subramanian, M. (2021). Hypercholesterolemia Impairs Clearance of Neutrophil Extracellular Traps and Promotes Inflammation and Atherosclerotic Plaque Progression. *Arterioscler Thromb Vasc Biol* 41, 2598–2615. doi: 10.1161/ATVBAHA.120.316389.

Dhawan, U. K., Margraf, A., Lech, M., and Subramanian, M. (2022). Hypercholesterolemia promotes autoantibody production and a lupus-like pathology via decreased DNase-mediated clearance of DNA. *J Cell Mol Med*. doi: 10.1111/jcmm.17556.

Ferriere, A., Santa, P., Garreau, A., Bandopadhyay, P., Blanco, P., Ganguly, D., et al. (2020). Self-Nucleic Acid Sensing: A Novel Crucial Pathway Involved in Obesity-Mediated Metaflammation and Metabolic Syndrome. *Front Immunol* 11, 624256. doi: 10.3389/fimmu.2020.624256.

Ganguly, D. (2018). Do Type I Interferons Link Systemic Autoimmunities and Metabolic Syndrome in a Pathogenetic Continuum? *Trends in Immunology* 39, 28–43. doi: 10.1016/j.it.2017.07.001.

Garcia-Martinez, I., Santoro, N., Chen, Y., Hoque, R., Ouyang, X., Caprio, S., et al. (2016). Hepatocyte mitochondrial DNA drives nonalcoholic steatohepatitis by activation of TLR9. *J Clin Invest* 126, 859–864. doi: 10.1172/JCI83885.

Garcia-Romo, G. S., Caielli, S., Vega, B., Connolly, J., Allantaz, F., Xu, Z., et al. (2011). Netting neutrophils are major inducers of type I IFN production in pediatric systemic lupus erythematosus. *Sci Transl Med* 3, 73ra20. doi: 10.1126/scitranslmed.3001201.

Ghosh, A. R., Bhattacharya, R., Bhattacharya, S., Nargis, T., Rahaman, O., Duttagupta, P., et al. (2016). Adipose Recruitment and Activation of Plasmacytoid Dendritic Cells Fuel Metaflammation. *Diabetes* 65, 3440–3452. doi: 10.2337/db16-0331.

Gong, Z., Zhang, X., Su, K., Jiang, R., Sun, Z., Chen, W., et al. (2019). Deficiency in AIM2 induces inflammation and adipogenesis in white adipose tissue leading to obesity and insulin resistance. *Diabetologia* 62, 2325–2339. doi: 10.1007/s00125-019-04983-x.

Grobe, J. L. (2017). Comprehensive Assessments of Energy Balance in Mice. *Methods Mol Biol* 1614, 123–146. doi: 10.1007/978-1-4939-7030-8_10.

Hanna Kazazian, N., Wang, Y., Roussel-Queval, A., Marcadet, L., Chasson, L., Laprie, C., et al. (2019). Lupus Autoimmunity and Metabolic Parameters Are Exacerbated Upon High Fat Diet-Induced Obesity Due to TLR7 Signaling. *Front. Immunol.* 10, 2015. doi: 10.3389/fimmu.2019.02015.

Hannibal, T. D., Schmidt-Christensen, A., Nilsson, J., Fransén-Pettersson, N., Hansen, L., and Holmberg, D. (2017). Deficiency in plasmacytoid dendritic cells and type I interferon

signalling prevents diet-induced obesity and insulin resistance in mice. *Diabetologia* 60, 2033–2041. doi: 10.1007/s00125-017-4341-0.

Hartl, J., Serpas, L., Wang, Y., Rashidfarrokhi, A., Perez, O. A., Sally, B., et al. (2021). Autoantibody-mediated impairment of DNASE1L3 activity in sporadic systemic lupus erythematosus. *J Exp Med* 218, e20201138. doi: 10.1084/jem.20201138.

Henao-Mejia, J., Elinav, E., Jin, C., Hao, L., Mehal, W. Z., Strowig, T., et al. (2012). Inflammasome-mediated dysbiosis regulates progression of NAFLD and obesity. *Nature* 482, 179–185. doi: 10.1038/nature10809.

Holland, W. L., Bikman, B. T., Wang, L.-P., Yuguang, G., Sargent, K. M., Bulchand, S., et al. (2011). Lipid-induced insulin resistance mediated by the proinflammatory receptor TLR4 requires saturated fatty acid–induced ceramide biosynthesis in mice. *J. Clin. Invest.* 121, 1858–1870. doi: 10.1172/JCI43378.

Huby, T., and Gautier, E. L. (2022). Immune cell-mediated features of non-alcoholic steatohepatitis. *Nat Rev Immunol* 22, 429–443. doi: 10.1038/s41577-021-00639-3.

Inokuchi, S., Mitoma, H., Kawano, S., Nakano, S., Ayano, M., Kimoto, Y., et al. (2020). Homeostatic Milieu Induces Production of Deoxyribonuclease 1-like 3 from Myeloid Cells. *J Immunol* 204, 2088–2097. doi: 10.4049/jimmunol.1901304.

Jaitin, D. A., Adlung, L., Thaiss, C. A., Weiner, A., Li, B., Descamps, H., et al. (2019). Lipid-Associated Macrophages Control Metabolic Homeostasis in a Trem2-Dependent Manner. *Cell* 178, 686-698.e14. doi: 10.1016/j.cell.2019.05.054.

Jiménez-Alcázar, M., Rangaswamy, C., Panda, R., Bitterling, J., Simsek, Y. J., Long, A. T., et al. (2017). Host DNases prevent vascular occlusion by neutrophil extracellular traps. *Science* 358, 1202–1206. doi: 10.1126/science.aam8897.

K Y, S. K., R Bhat, P. K., and Sorake, C. J. (2021). Double trouble: a pandemic of obesity and COVID-19. *Lancet Gastroenterol Hepatol* 6, 608. doi: 10.1016/S2468-1253(21)00190-4.

Kenny, E. F., Raupach, B., Abu Abed, U., Brinkmann, V., and Zychlinsky, A. (2019). *Dnase1* -deficient mice spontaneously develop a systemic lupus erythematosus-like disease. *Eur. J. Immunol.* 49, 590–599. doi: 10.1002/eji.201847875.

Li, C., Wang, G., Sivasami, P., Ramirez, R. N., Zhang, Y., Benoist, C., et al. (2021). Interferon-α-producing plasmacytoid dendritic cells drive the loss of adipose tissue regulatory T cells during obesity. *Cell Metab* 33, 1610-1623.e5. doi: 10.1016/j.cmet.2021.06.007.

Link, J. C., and Reue, K. (2017). Genetic Basis for Sex Differences in Obesity and Lipid Metabolism. *Annu Rev Nutr* 37, 225–245. doi: 10.1146/annurev-nutr-071816-064827.

Lumeng, C. N., Bodzin, J. L., and Saltiel, A. R. (2007). Obesity induces a phenotypic switch in adipose tissue macrophage polarization. *J Clin Invest* 117, 175–184. doi: 10.1172/JCI29881.

Luo, X., Li, H., Ma, L., Zhou, J., Guo, X., Woo, S.-L., et al. (2018). Expression of STING Is Increased in Liver Tissues From Patients With NAFLD and Promotes Macrophage-Mediated Hepatic Inflammation and Fibrosis in Mice. *Gastroenterology* 155, 1971-1984.e4. doi: 10.1053/j.gastro.2018.09.010.

Marriott, I., and Huet-Hudson, Y. M. (2006). Sexual dimorphism in innate immune responses to infectious organisms. *Immunol Res* 34, 177–192. doi: 10.1385/IR:34:3:177.

McLaughlin, T., Ackerman, S. E., Shen, L., and Engleman, E. (2017). Role of innate and adaptive immunity in obesity-associated metabolic disease. *J Clin Invest* 127, 5–13. doi: 10.1172/JCI88876.

McNelis, J. C., and Olefsky, J. M. (2014). Macrophages, Immunity, and Metabolic Disease. *Immunity* 41, 36–48. doi: 10.1016/j.immuni.2014.05.010.

Meyer, M. R., Haas, E., and Barton, M. (2006). Gender differences of cardiovascular disease: new perspectives for estrogen receptor signaling. *Hypertension* 47, 1019–1026. doi: 10.1161/01.HYP.0000223064.62762.0b.

Napirei, M., Ludwig, S., Mezrhab, J., Klöckl, T., and Mannherz, H. G. (2009). Murine serum nucleases - contrasting effects of plasmin and heparin on the activities of DNase1 and DNase1-like 3 (DNase1l3): Murine serum nucleases. *FEBS Journal* 276, 1059–1073. doi: 10.1111/j.1742-4658.2008.06849.x.

Napirei, M., Ricken, A., Eulitz, D., Knoop, H., and Mannherz, H. G. (2004). Expression pattern of the deoxyribonuclease 1 gene: lessons from the Dnase1 knockout mouse. *Biochem J* 380, 929–937. doi: 10.1042/BJ20040046.

Napirei, M., Wulf, S., Eulitz, D., Mannherz, H. G., and Kloeckl, T. (2005). Comparative characterization of rat deoxyribonuclease 1 (Dnase1) and murine deoxyribonuclease 1-like 3 (Dnase1l3). *Biochem J* 389, 355–364. doi: 10.1042/BJ20042124.

Nishimoto, S., Fukuda, D., Higashikuni, Y., Tanaka, K., Hirata, Y., Murata, C., et al. (2016). Obesity-induced DNA released from adipocytes stimulates chronic adipose tissue inflammation and insulin resistance. *Sci Adv* 2, e1501332. doi: 10.1126/sciadv.1501332.

Palmer, B. F., and Clegg, D. J. (2015). The sexual dimorphism of obesity. *Mol Cell Endocrinol* 402, 113–119. doi: 10.1016/j.mce.2014.11.029.

Pettersson, U. S., Waldén, T. B., Carlsson, P.-O., Jansson, L., and Phillipson, M. (2012). Female mice are protected against high-fat diet induced metabolic syndrome and increase the regulatory T cell population in adipose tissue. *PLoS One* 7, e46057. doi: 10.1371/journal.pone.0046057.

Pratt, G. M., Learn, C. A., Hughes, G. D., Clark, B. L., Warthen, M., and Pories, W. (2009). Demographics and outcomes at American Society for Metabolic and Bariatric Surgery Centers of Excellence. *Surg Endosc* 23, 795–799. doi: 10.1007/s00464-008-0077-8.

Revelo, X. S., Ghazarian, M., Chng, M. H. Y., Luck, H., Kim, J. H., Zeng, K., et al. (2016). Nucleic Acid-Targeting Pathways Promote Inflammation in Obesity-Related Insulin Resistance. *Cell Rep* 16, 717–730. doi: 10.1016/j.celrep.2016.06.024.

Riant, E., Waget, A., Cogo, H., Arnal, J.-F., Burcelin, R., and Gourdy, P. (2009). Estrogens protect against high-fat diet-induced insulin resistance and glucose intolerance in mice. *Endocrinology* 150, 2109–2117. doi: 10.1210/en.2008-0971.

Santa, P., Garreau, A., Serpas, L., Ferriere, A., Blanco, P., Soni, C., et al. (2021). The Role of Nucleases and Nucleic Acid Editing Enzymes in the Regulation of Self-Nucleic Acid Sensing. *Front. Immunol.* 12, 629922. doi: 10.3389/fimmu.2021.629922.

Schenk, S., Saberi, M., and Olefsky, J. M. (2008). Insulin sensitivity: modulation by nutrients and inflammation. *J Clin Invest* 118, 2992–3002. doi: 10.1172/JCI34260.

Serpas, L., Chan, R. W. Y., Jiang, P., Ni, M., Sun, K., Rashidfarrokhi, A., et al. (2019). *Dnase1l3* deletion causes aberrations in length and end-motif frequencies in plasma DNA. *Proc. Natl. Acad. Sci. U.S.A.* 116, 641–649. doi: 10.1073/pnas.1815031116.

Shi, H., Kokoeva, M. V., Inouye, K., Tzameli, I., Yin, H., and Flier, J. S. (2006). TLR4 links innate immunity and fatty acid-induced insulin resistance. *J Clin Invest* 116, 3015–3025. doi: 10.1172/JCI28898.

Singer, K., Maley, N., Mergian, T., DelProposto, J., Cho, K. W., Zamarron, B. F., et al. (2015). Differences in Hematopoietic Stem Cells Contribute to Sexually Dimorphic Inflammatory Responses to High Fat Diet-induced Obesity. *J Biol Chem* 290, 13250–13262. doi: 10.1074/jbc.M114.634568.

Sisirak, V., Sally, B., D'Agati, V., Martinez-Ortiz, W., Özçakar, Z. B., David, J., et al. (2016). Digestion of Chromatin in Apoptotic Cell Microparticles Prevents Autoimmunity. *Cell* 166, 88–101. doi: 10.1016/j.cell.2016.05.034.

Soni, C., Perez, O. A., Voss, W. N., Pucella, J. N., Serpas, L., Mehl, J., et al. (2020). Plasmacytoid Dendritic Cells and Type I Interferon Promote Extrafollicular B Cell Responses to Extracellular Self-DNA. *Immunity* 52, 1022-1038.e7. doi: 10.1016/j.immuni.2020.04.015.

Soni, C., and Reizis, B. (2018). DNA as a self-antigen: nature and regulation. *Current Opinion in Immunology* 55, 31–37. doi: 10.1016/j.coi.2018.09.009.

Speakman, J. R. (2019). Use of high-fat diets to study rodent obesity as a model of human obesity. *Int J Obes (Lond)* 43, 1491–1492. doi: 10.1038/s41366-019-0363-7.

Strissel, K. J., Stancheva, Z., Miyoshi, H., Perfield, J. W., DeFuria, J., Jick, Z., et al. (2007). Adipocyte Death, Adipose Tissue Remodeling, and Obesity Complications. *Diabetes* 56, 2910–2918. doi: 10.2337/db07-0767.

Takahashi, M., Ikemoto, S., and Ezaki, O. (1999). Effect of the fat/carbohydrate ratio in the diet on obesity and oral glucose tolerance in C57BL/6J mice. *J Nutr Sci Vitaminol (Tokyo)* 45, 583–593. doi: 10.3177/jnsv.45.583.

Tedeschi, S. K., Barbhaiya, M., Malspeis, S., Lu, B., Sparks, J. A., Karlson, E. W., et al. (2017). Obesity and the risk of systemic lupus erythematosus among women in the Nurses' Health Studies. *Seminars in Arthritis and Rheumatism* 47, 376–383. doi: 10.1016/j.semarthrit.2017.05.011.

Tremmel, M., Gerdtham, U.-G., Nilsson, P., and Saha, S. (2017). Economic Burden of Obesity: A Systematic Literature Review. *IJERPH* 14, 435. doi: 10.3390/ijerph14040435.

Udompornpitak, K., Charoensappakit, A., Sae-Khow, K., Bhunyakarnjanarat, T., Dang, C. P., Saisorn, W., et al. (2022). Obesity Exacerbates Lupus Activity in Fc Gamma Receptor IIb Deficient Lupus Mice Partly through Saturated Fatty Acid-Induced Gut Barrier Defect and Systemic Inflammation. *J Innate Immun*, 1–22. doi: 10.1159/000526206.

van Asseldonk, E. J. P., Stienstra, R., Koenen, T. B., Joosten, L. A. B., Netea, M. G., and Tack, C. J. (2011). Treatment with Anakinra improves disposition index but not insulin sensitivity in nondiabetic subjects with the metabolic syndrome: a randomized, double-blind, placebo-controlled study. *J Clin Endocrinol Metab* 96, 2119–2126. doi: 10.1210/jc.2010-2992.

van der Windt, D. J., Sud, V., Zhang, H., Varley, P. R., Goswami, J., Yazdani, H. O., et al. (2018). Neutrophil extracellular traps promote inflammation and development of hepatocellular carcinoma in nonalcoholic steatohepatitis. *Hepatology* 68, 1347–1360. doi: 10.1002/hep.29914.

Vandanmagsar, B., Youm, Y.-H., Ravussin, A., Galgani, J. E., Stadler, K., Mynatt, R. L., et al. (2011). The NLRP3 inflammasome instigates obesity-induced inflammation and insulin resistance. *Nat Med* 17, 179–188. doi: 10.1038/nm.2279.

Varghese, M., Griffin, C., Abrishami, S., Eter, L., Lanzetta, N., Hak, L., et al. (2021). Sex hormones regulate metainflammation in diet-induced obesity in mice. *J Biol Chem* 297, 101229. doi: 10.1016/j.jbc.2021.101229.

Wang, X.-A., Zhang, R., Zhang, S., Deng, S., Jiang, D., Zhong, J., et al. (2013). Interferon regulatory factor 7 deficiency prevents diet-induced obesity and insulin resistance. *American Journal of Physiology-Endocrinology and Metabolism* 305, E485–E495. doi: 10.1152/ajpendo.00505.2012.

Wen, H., Gris, D., Lei, Y., Jha, S., Zhang, L., Huang, M. T.-H., et al. (2011). Fatty acid-induced NLRP3-ASC inflammasome activation interferes with insulin signaling. *Nat Immunol* 12, 408–415. doi: 10.1038/ni.2022.

Wilber, A., Lu, M., and Schneider, M. C. (2002). Deoxyribonuclease I-like III Is an Inducible Macrophage Barrier to Liposomal Transfection. *Molecular Therapy* 6, 35–42. doi: 10.1006/mthe.2002.0625.

Yanovski, S. Z., and Yanovski, J. A. (2002). Obesity. *N Engl J Med* 346, 591–602. doi: 10.1056/NEJMra012586.

Yeh, T.-M., Chang, H.-C., Liang, C.-C., Wu, J.-J., and Liu, M.-F. (2003). Deoxyribonuclease-inhibitory antibodies in systemic lupus erythematosus. *J Biomed Sci* 10, 544–551. doi: 10.1159/000072382.

Yu, Y., Liu, Y., An, W., Song, J., Zhang, Y., and Zhao, X. (2018). STING-mediated inflammation in Kupffer cells contributes to progression of nonalcoholic steatohepatitis. *Journal of Clinical Investigation* 129, 546–555. doi: 10.1172/JCI121842.

Zhang, H., Zhang, S. B., Sun, W., Yang, S., Zhang, M., Wang, W., et al. (2009). B1 sequence-based real-time quantitative PCR: a sensitive method for direct measurement of mouse plasma DNA levels after gamma irradiation. *Int J Radiat Oncol Biol Phys* 74, 1592–1599. doi: 10.1016/j.ijrobp.2009.03.009.

Zhao, X., Yang, L., Chang, N., Hou, L., Zhou, X., Yang, L., et al. (2020). Neutrophils undergo switch of apoptosis to NETosis during murine fatty liver injury via S1P receptor 2 signaling. *Cell Death Dis* 11, 379. doi: 10.1038/s41419-020-2582-1.

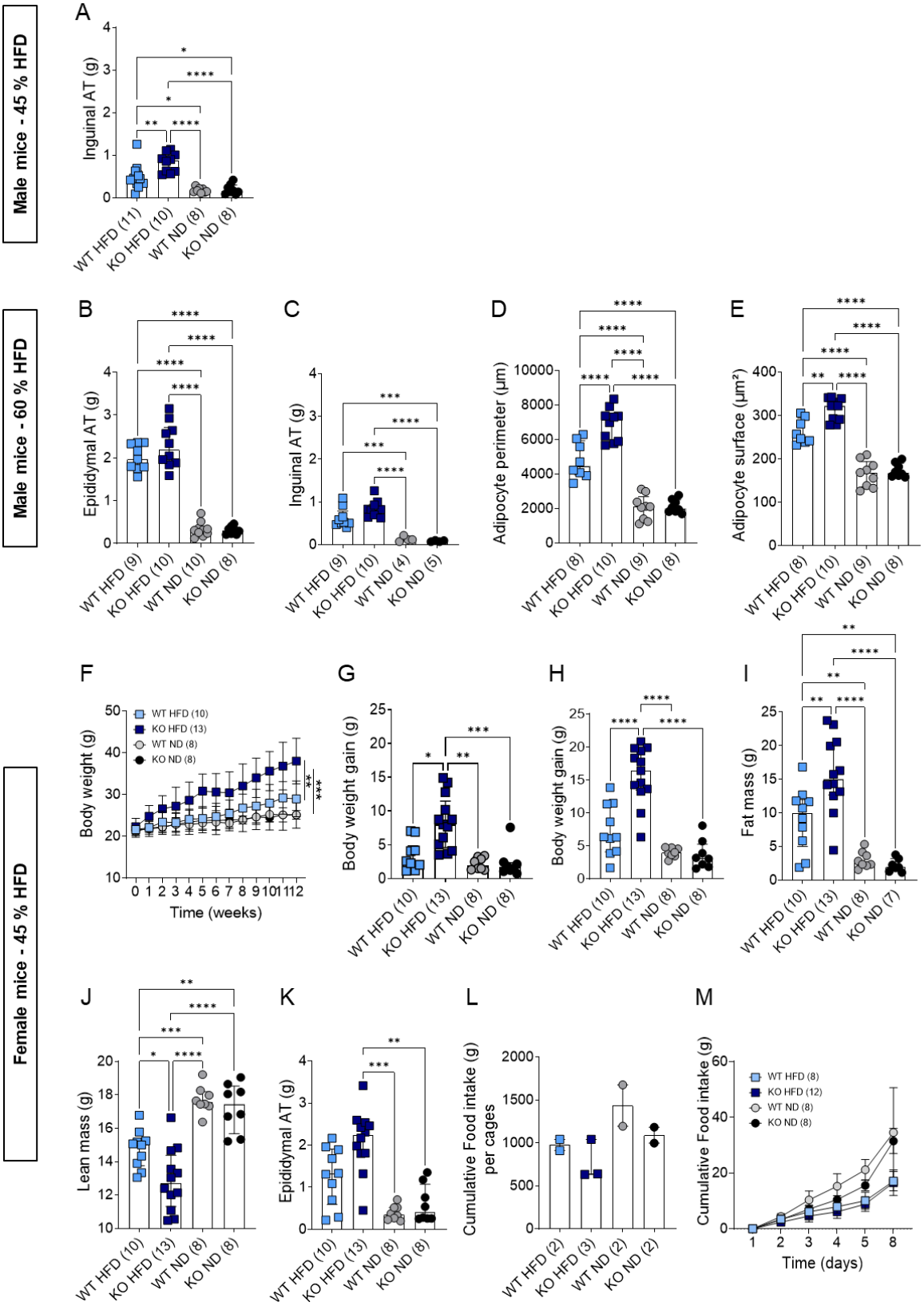

Supplementary Figure 1: *Dnase1l3* deficiency increases weight gain in mice fed HFD

Individual weights of inguinal adipose tissue (VAT) collected from wild-type (WT) and *Dnase1l3*$^{-/-}$ (KO) male mice fed with 45% HFD (A). Individual weights of epididymal (B) and inguinal (C) AT collected from WT and KO male mice fed with 60% HFD. Mean perimeter (D) and surface (E) of 30 adipocytes per mouse from the VAT as measure by immunohistochemistry upon H&E staining from WT and KO male mice fed with 60% HFD. Female WT and *Dnase1L3*-KO mice at were fed a ND or a 45% HFD for 12 weeks, starting at 12 weeks of age. (F) Weekly weight measurements of mice of the indicated genotypes fed an ND (circles) or HFD (squares). Cumulative body weight gain after 6 (G) and 12 (H) weeks of diet. Proportion of fat (I) and lean (J) mass in the indicated mice as determined by magnetic resonance imaging (MRI). (K) Individual weights of VAT. (L) Cumulative food intake per cage after 12 weeks of diet and (M) individual food intake after 8 days of isolation in individual cages. Data were combined from two independent experiments in each cases with the indicated mouse numbers and presented as mean ± SD. Statistical significance was calculated by two-way ANOVA and indicated as follows: *p ≤ 0.05, **p ≤ 0.01, ***p ≤ 0.001.

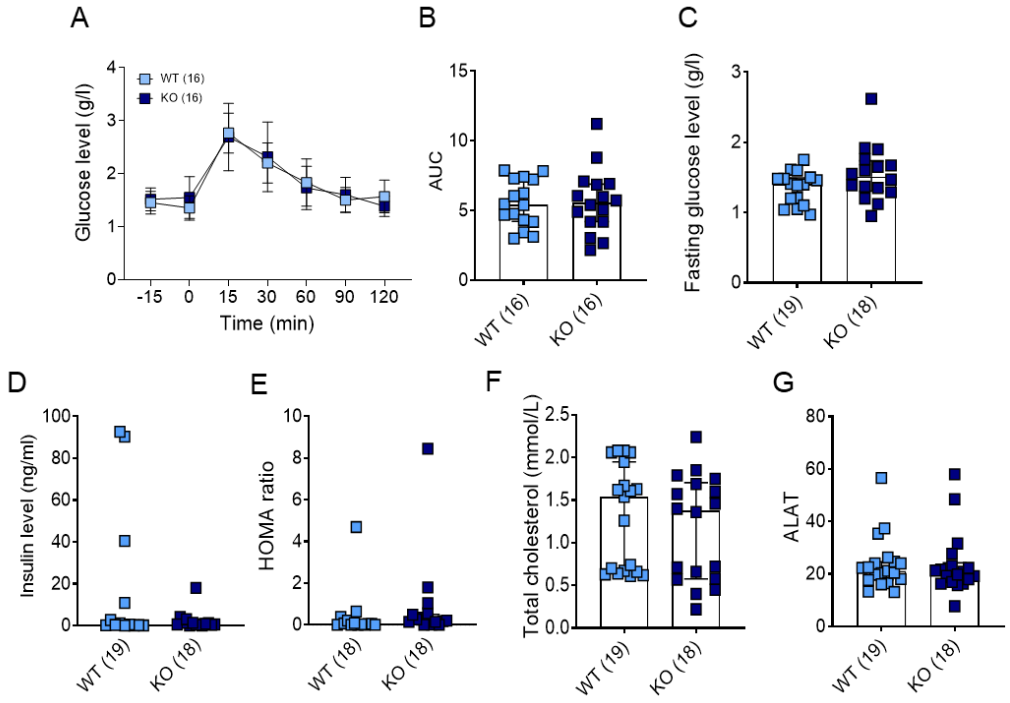

Supplementary Figure 2: Basal weight and metabolic profile of WT and *Dnase1l3*-KO male mice
(A) Glucose tolerance test (GTT) were performed by an intraperitoneal (IP) injection of a glucose solution (1 g/kg) and the evaluation of blood glucose levels at the indicated time points by a glucometer. (B) Area under the curve of GTT. (C) Fasting blood glucose levels as measured by a glucometer. (D) Fasting insulin levels as measured by ELISA. (E) HOMA-ratio was calculated according to the formula: fasting glucose (mg/dL) X fasting insulin (µU/mL) / 405. (F) Circulatory total cholesterol levels and (G) ALAT levels as measured by spectrophotometry. Data were combined from at least two independent experiments with the indicated mouse numbers and presented as mean ± SD. Statistical significance was calculated by two-way ANOVA and indicated as follows: *p ≤ 0.05, **p ≤ 0.01, ***p ≤ 0.001.

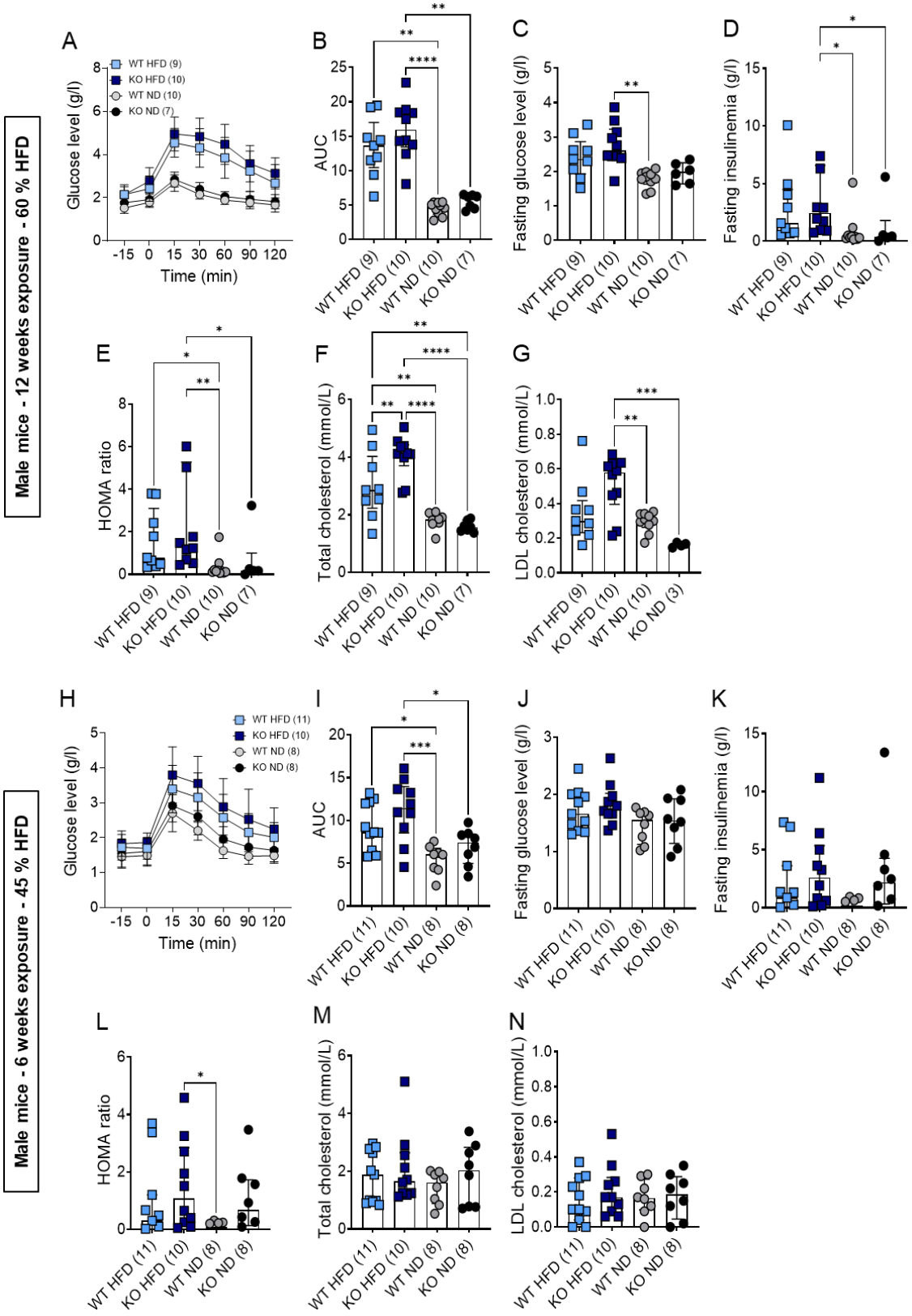

Supplementary Figure 3: *Dnase1l3* deficiency accelerates the development of metabolic syndrome induced by HFD

Metabolic profile of *Dnase1l3*-KO and WT male mice exposed during 12 weeks to a 60% HFD (A-G) and 6 weeks to a 45% HFD (H-N) and a chow diet as control. (A, H) Glucose tolerance test (GTT) were performed by an intraperitoneal (IP) injection of a glucose solution (1 g/kg) and the evaluation of blood glucose levels at the indicated time points by a glucometer. (B, I) Area under the curve of GTT. (C, J) Fasting blood glucose levels as evaluated by a glucometer. (D, K) Fasting insulin levels as measured by ELISA. (E, L) HOMA-ratio was calculated according to the formula: fasting glucose (mg/dL) X fasting insulin (µU/mL) / 405. (F, M) Circulatory total cholesterol levels and (H, N) LDL-cholesterol levels as measured by spectrophotometry. Data were combined from two independent experiments each time with the indicated mouse numbers and presented as mean ± SD. Statistical significance was calculated by two-way ANOVA and indicated as follows: *p ≤ 0.05, **p ≤ 0.01, ***p ≤ 0.001.

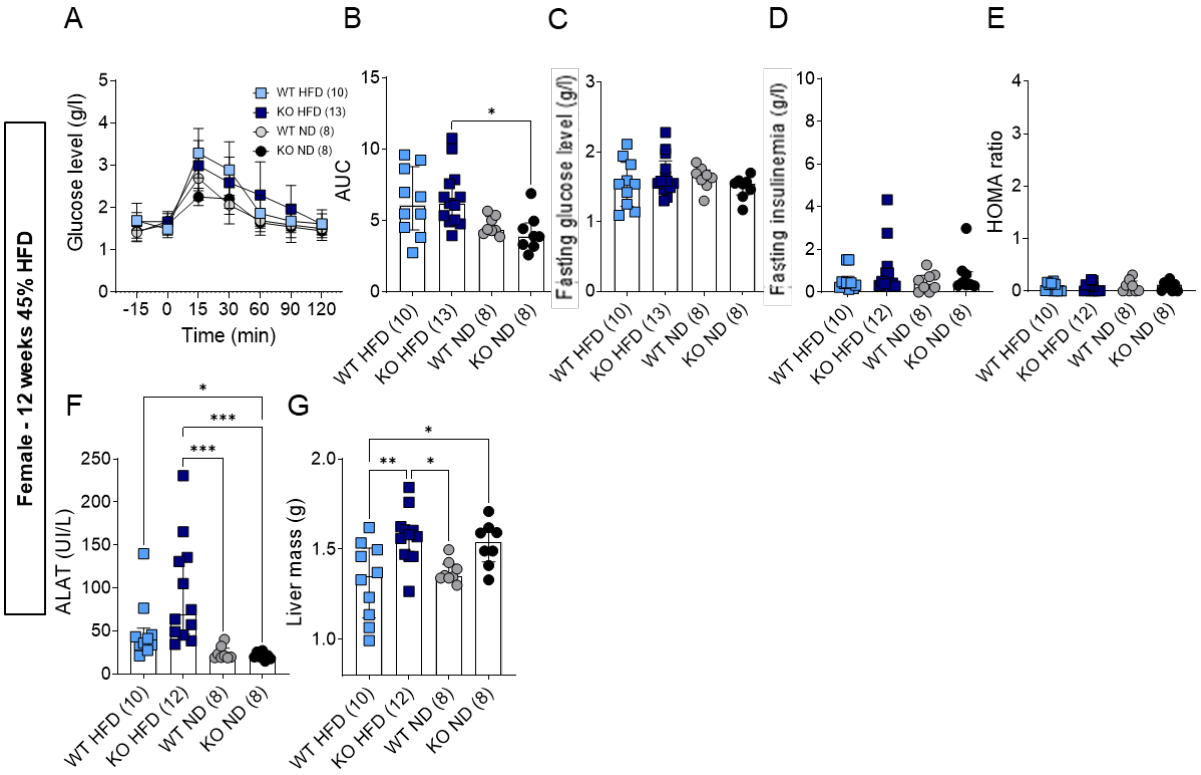

Supplementary Figure 4: *Dnase1l3* deficiency exacerbates the development of HFD-induced metabolic syndrome and steatosis in female mice

Metabolic profile of *Dnase1l3*-KO and WT female mice exposed during 12 weeks to a 45% HFD and a chow diet as control. (A) GTT (1 g/kg) and the evaluation of blood glucose levels at the indicated time points by a glucometer. (B) Area under the curve of GTT. (C) Fasting blood glucose levels as measured by a glucometer. (D) Fasting insulin levels as measured by ELISA. (E) HOMA-ratio. Liver pathology of *Dnase1l3*-KO and WT female mice exposed 12 weeks to 45% HFD (F) ALAT levels as measured by spectrophotometry. (G) Individual liver mass. Data were combined from two independent experiments with the indicated mouse numbers and presented as mean ± SD. Statistical significance was calculated by two-way ANOVA and indicated as follows: *$p \leq 0.05$, **$p \leq 0.01$, ***$p \leq 0.001$.

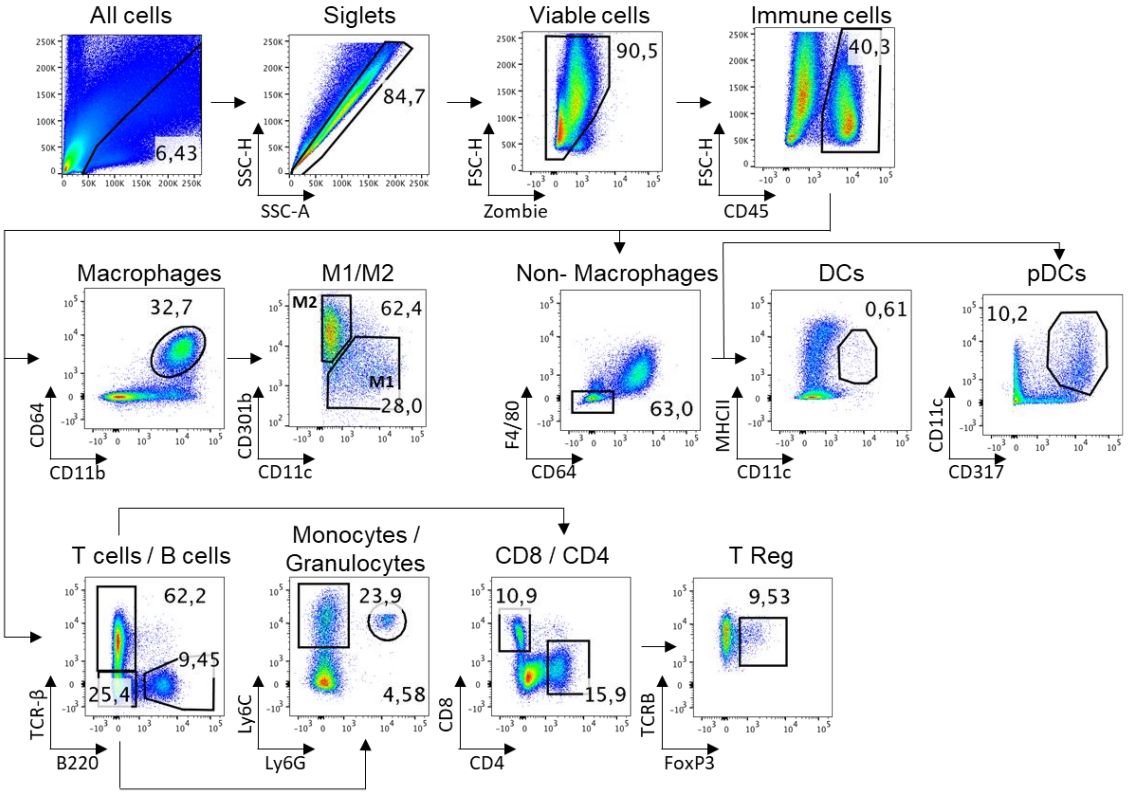

Supplementary Figure 5: Flow cytometry gating strategy of the visceral adipose tissue SVF

Representative plots indicating the gating strategy for the analysis of immune cells infiltrating the SVF of the VAT. All cells were gated according to their morphology (FSC and SSC). Doublet and dead cells were then eliminated based on their SSC-Height/SSC-Area parameters and their expression of the fixable viability Zombie dye, respectively. Then immune cells were isolated as cell expressing CD45. Among immune cells, macrophages were identified as CD11b^{+} and CD64^{+} cells and further separated into M1-like (CD11c^{+}) and M2-like (CD301b^{+}) macrophages. Conventional DCs (MHC II^{+} and CD11c^{+}) and plasmacytoid dendritic cells (pDCs, CD11c^{+} CD317^{+}) were identified among immune cells negative for macrophage markers CD64 and F4/80. Monocyte (Ly6C^{+}) and granulocytes (Ly6C^{+} and Ly6G^{+}) were identified among total immune cells (CD45^{+}) cells lacking B^{-} (B220) and T^{-} (TCRβ^{-}) cell markers. Finally, CD4 and CD8 T cells were identified among total T cells (TCRβ^{+}) and regulatory T cells (Tregs, FoxP3^{+}) were identified within CD4 T cells.

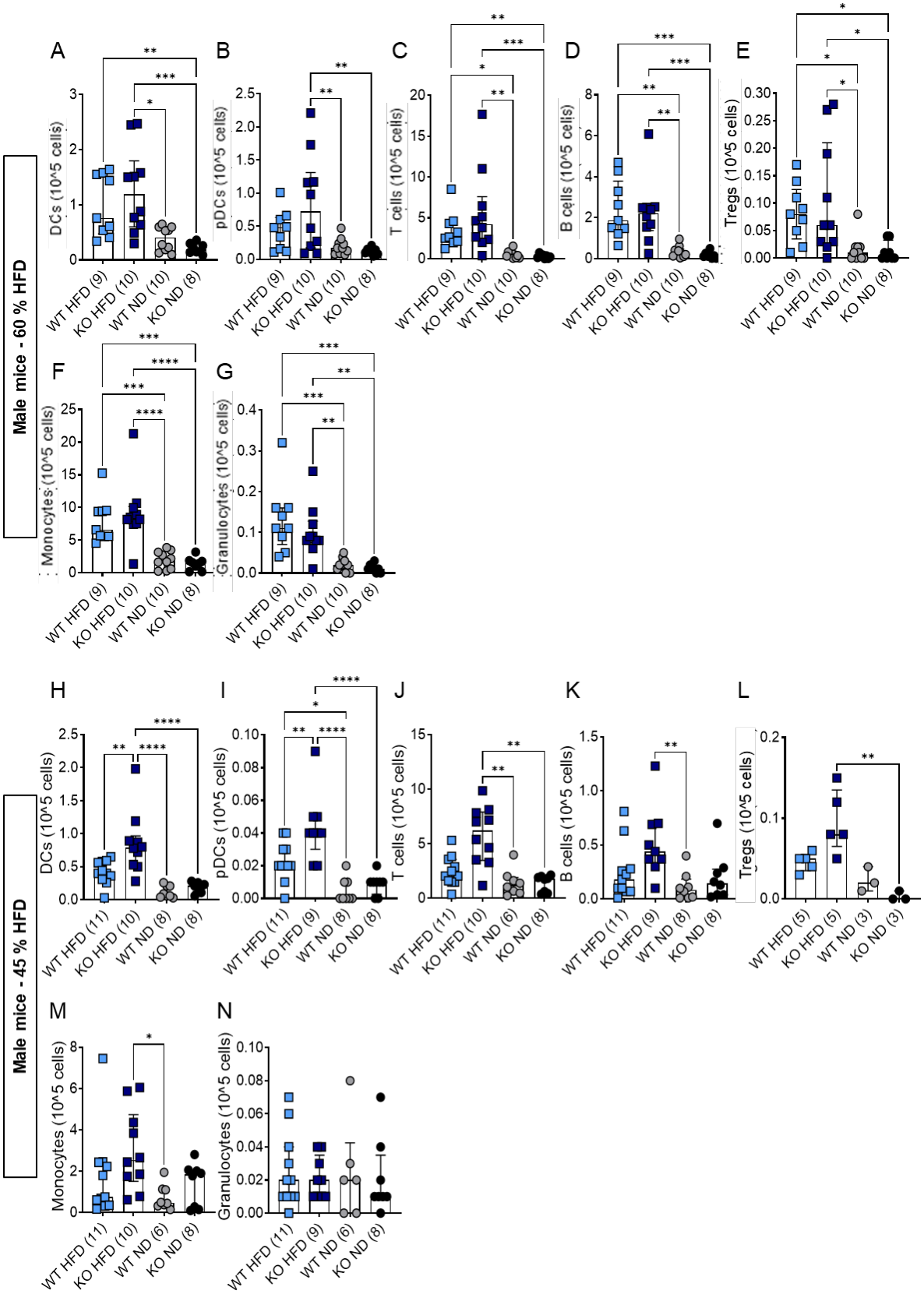

Supplementary Figure 6: Immune cells populations are enriched in the visceral adipose tissue SVF of obese mice.

Mice were fed with 60% HFD (A-G), 45% HFD (H-N) or standard diet as controls. After 12 weeks mice were euthanized and leucocytes from the stromal vascular fraction (SVF) of the VAT of obese (square) and lean (circle) WT and *Dnase1l3*-KO mice were analyzed by flow cytometry. (A, H) Absolute number of conventional dendritic cells (CD64- MHCII$^+$ CD11c$^+$ cells). (B, I) Absolute numbers of plasmacytoid dendritic cells (CD64$^-$ CD317$^+$ CD11c$^+$ cells). (C,J) Absolute numbers of T cells (TCRβ$^+$ B220$^-$ cells). (D, K) Absolute numbers of B cells (TCRβ$^-$ B220$^+$ cells). (E, L) Absolute numbers of regulatory in T cells (TCRβ$^+$, CD4$^+$, FoxP3$^+$ cells). (F, M) Absolute numbers of granulocytes (TCRβ$^-$, B220$^-$, Ly6C$^+$, Ly6G$^+$ cells). (G, N) Absolute numbers of granulocytes (TCRβ$^-$, B220$^-$, Ly6C$^+$, Ly6G$^-$ cells). Data were combined from two independent experiments with the indicated mouse numbers and presented as mean ± SD. Statistical significance was calculated by two-way ANOVA and indicated as follows: *$p \leq 0.05$, **$p \leq 0.01$, ***$p \leq 0.001$.

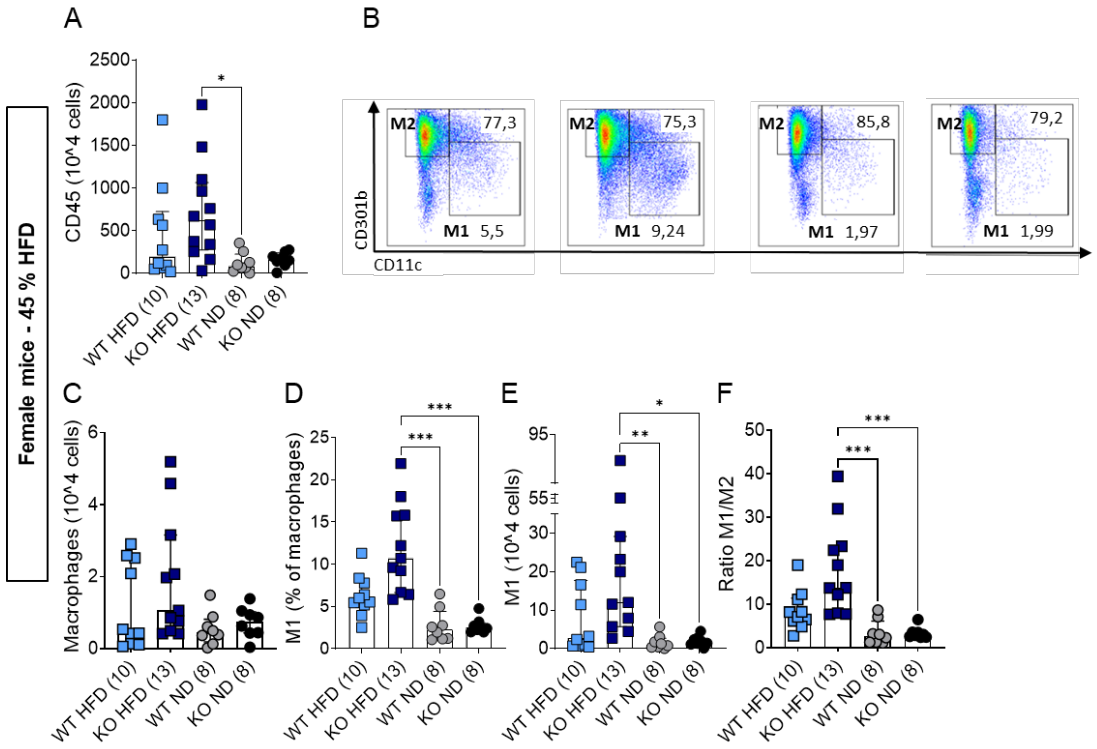

Supplementary Figure 7: *Dnase1l3* deficiency increases macrophages infiltration and their switch toward and M1 pro-inflammatory profile in the white adipose tissue of female obese mice

Female mice were fed with 45% HFD or standard diet as controls. After 12 weeks mice were euthanized and leucocytes from the stromal vascular fraction of the VAT of obese (square) and lean (circle) WT and *Dnase1l3*-KO mice were analysed by flow cytometry. (A) Absolute numbers of viable $CD45^+$. (B) Representative plots and frequency of macrophages ($CD45^+$ $CD11b^+$ $CD64^+$ cells) showing either the proinflammatory M1-like ($CD11c^+$ cells) or the anti-inflammatory M2 like ($CD301b^+$ cells) phenotype. (C) Absolute number of viable total macrophages identified as $CD45^+$ $CD64^+$ and $CD11b^+$ cells. (D) Percentage of M1-like macrophages identified as $CD45^+$ $CD64^+$ $CD11b^+$ and $CD11c^+$ cells out of total macrophages. (E) Absolute numbers of M1-like macrophages. (F, L) Ratio of the percentage of M1 to M2-like macrophages. Data were combined from two independent experiments with the indicated mouse numbers and presented as mean ± SD. Statistical significance was calculated by two-way ANOVA and indicated as follows: *$p \leq 0.05$, **$p \leq 0.01$, ***$p \leq 0.001$.

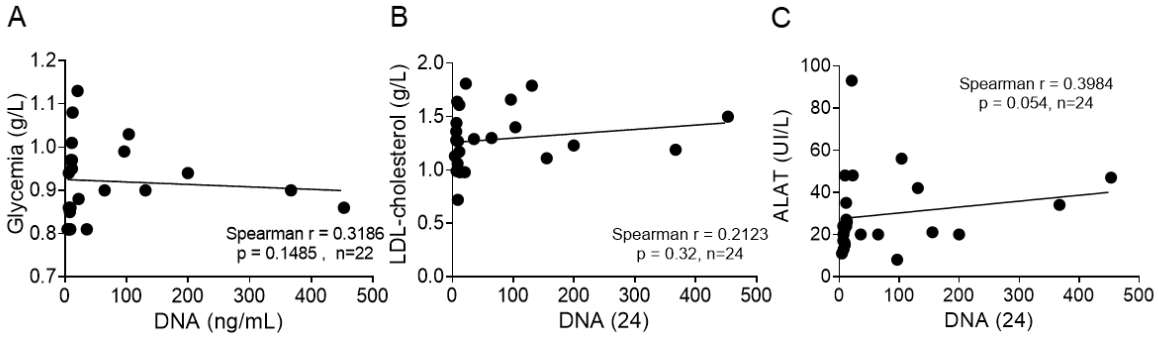

Supplementary Figure 8: Obese patients show an accumulation of circulatory cell-free (cf)DNA

Correlation between cfDNA isolated from peripheral blood mononuclear cells (PBMCs) of obese patients and their fasting glycemia (A), LDL-cholesterol level (B) or ALAT level (C). Data were presented as mean ± SD. The samples number (n) was indicated for each analysis. Spearman rank correlation was used in data analysis and significance was indicated as follows: *p ≤ 0.05, **p ≤ 0.01, ***p ≤ 0.001.

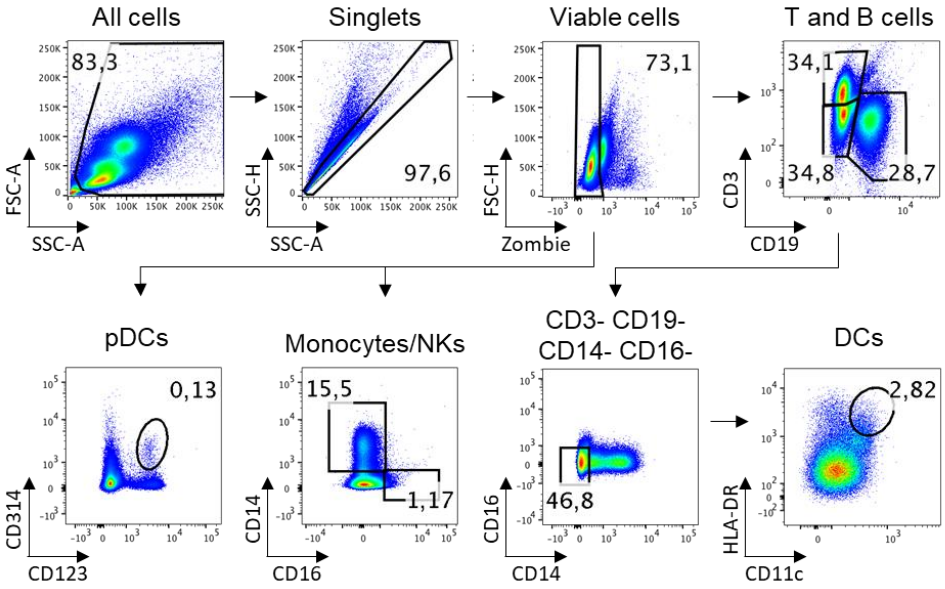

Supplementary Figure 9: Gating strategy for the Flow Fish analysis

Representative plots indicating the gating strategy for the analysis of immune cells in peripheral blood mononuclear cells (PBMCs) of obese patients (OB) and healthy donors (HD). All cells were gated according to their morphology (FSC and SSC). Doublet and dead cells were then eliminated based on their SSC-Height/SSC-Area parameters and their expression of the fixable viability Zombie dye, respectively. T cells ($CD3^+$), B cells ($CD19^+$), monocytes ($CD14^+$), NK cells ($CD16^+$), pDCs ($CD304^+$ and $CD123^+$) were identified among viable cells. DCs ($MHCII^+$ and $CD11c^+$) were identified among $CD3^-$, $CD19^-$, $CD14^-$, $CD16^-$ cells.

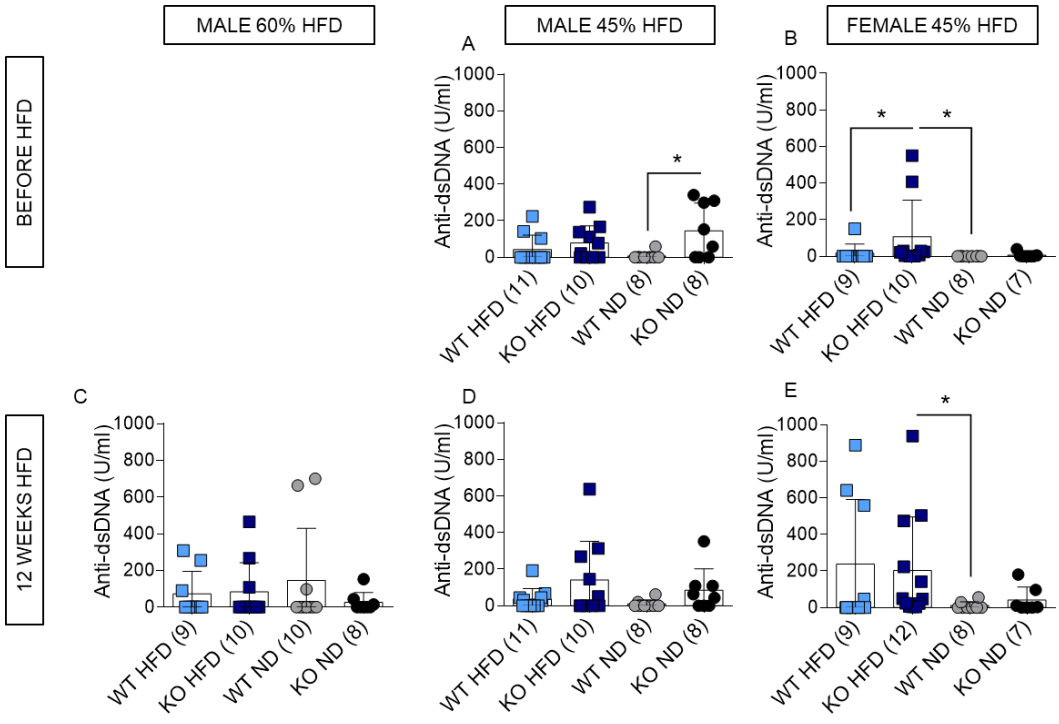

Supplementary Figure 10: Anti-dsDNA levels in male and female mice

Anti-DNA levels as measured by ELISA in male and female mice before (A, B) and after 12 weeks of HFD (C, D, E) feeding. Data were combined from two independent experiments with the indicated mouse numbers and presented as mean ± SD. Statistical significance was calculated by two-way ANOVA and indicated as follows: *$p \leq 0.05$, **$p \leq 0.01$, ***$p \leq 0.001$.

Supplementary table 1: Key ressources table

REAGENT or RESOURCE	SOURCE	IDENTIFIER	CONCENTRATION (µg/mL)
Animals Diets			
Standard Diet A03	SAFE	SAFE® DIET A03	
AIN93G AMF butter	SAFE	SAFE® U8978 v177	
260HF	SAFE	SAFE®U8978 v19	
246HF	SAFE	SAFE®U8955 v19	
Antibodies			
zombie Aqua dye AmCyan	BIOLEGEND	Cat# 423102	NA
Anti-mouse CD16/32 (93)	FISHER SCIENTIFIC	Cat# 15246827	5
Anti-mouse CD8 APC (53-6.7)	BD BIOSCIENCES	Cat# 561093	1
Anti-mouse CD11B APC Cy7 (M1/70)	FISHER SCIENTIFIC	Cat# A15390	0,25
Anti-mouse TCR-β APC-eFluor 780 (H57-597)	FISHER SCIENTIFIC	Cat# 47-5961-82	1,33
Anti-mouse CD64 BV605 (X54-5/7.1)	BIOLEGEND	Cat# 139323	1
Anti-mouse CD 317 BV711 (BST2) (927)	BD BIOSCIENCES	Cat# 747604	1
Anti-mouse LY6G BV711 (1A8)	BIOLEGEND	Cat# 127643	0,5
Anti-mouse F4/80 FITC (BM8)	BIOLEGEND	Cat# 123108	5
Anti-mouse CD4 FITC (1/200)	BIOLEGEND	Cat# 116004	2,5
Anti-mouse MHCII PB (1/400)	BIOLEGEND	Cat# 116422	1,25
Anti-mouse Ly6C PB (HK1.4)	BIOLEGEND	Cat# 128014	5
Anti-mouse FOXP3 PE (150D)	BIOLEGEND	Cat# 320008	NA
Anti-mouse CD11c PE (N418)	BIOLEGEND	Cat# 117308	0,4
Anti-mouse B220 PE CF584 (RA3-6B2)	BD BIOSCIENCES	Cat# 562313	0,5
Anti-mouse CD301B PECy7 (URA-1)	BIOLEGEND	Cat# 146808	2
Anti-mouse CD45 PerCP Cy5,5 (30-F11)	BD BIOSCIENCES	Cat# 550994	0,25
Anti-human CD19 PB (HIB-19)	BIOLEGEND	Cat# 302224	1,25
Anti-human CD4 SuperBright 600 (SK3)	FISHER SCIENTIFIC	Cat# 63-0047-42	0,06
Anti-human CD3 SuperBright 645 (UCHT1)	FISHER SCIENTIFIC	Cat# 64-0038-42	0,25
Anti-human CD304 BV711 (12C2)	BIOLEGEND	Cat# 354534	0,5
Anti-human HLA-DR BV785 (L243)	BIOLEGEND	Cat# 307642	0,4
Anti-human CD123 FITC (6H6)	BIOLEGEND	Cat# 306014	1
Anti-human CD16 PE-EF610 (CB16)	FISHER SCIENTIFIC	Cat# 61-0168-42	0,25
Anti-human CD11c PE (CB16)	BD BIOSCIENCES	Cat# 555392	NA
Anti-human CD141 (BDCA3) PECy7 (JAA17)	FISHER SCIENTIFIC	Cat# 25-1419-42	0,25
Anti-human CD14 AF700 (61D3)	FISHER SCIENTIFIC	Cat# 56-0149-42	0,5
Anti-human CD1c (BDCA1) APC-Cy7 (L161)	BIOLEGEND	Cat# 331520	1
Anti-human CD41 APC-Cy7 (HIP8)	BIOLEGEND	Cat# 303710	NA
Anti-human CD235a APC (REA175)	MILTENYI BIOTEC	Cat# 130-118-356	NA
Chemicals, Peptides, and Recombinant Proteins			
D-(+)-Glucose	SIGMA-ALDRICH	Cat# D7528	1g/kg
Insulin Asparte - NOVORAPID	NOVO NORDISK France		0,75UI/L
ISO-VET 100%	OSALIA		1000 MG/G
Collagenase from Clostridium histolyticum	SIGMA-ALDRICH	Cat# C5138	4mg/ml
Percoll® (Cytiva)	SIGMA-ALDRICH	Cat# GE17-0891-01	80% / 40%
Formalin solution, neutral buffered, 10%	SIGMA-ALDRICH	Cat# HT501128	0,1
RNAlater®	SIGMA-ALDRICH	Cat# R0901-500ML	NA
Foxp3 Staining Buffer Set	FISHER SCIENTIFIC	Cat# 00-5523-00	NA
Double-stranded genomic DNA from E. coli K1	INVIVOGEN	Cat# tlrl-ecdna	0.1µg/mL
ssPolyU Naked	INVIVOGEN	Cat# tlrl-sspu	1µg/mL
Stimulatory CpG ODN2395, Class C	INVIVOGEN	Cat# tlrl-2395	3µg/mL
DOTAP Liposomal Transfection Reagent	SIGMA-ALDRICH	Cat# 11202375001	10 U/µl
Gibco™ RPMI 1640 Medium	FISHER SCIENTIFIC	Cat# 15460564	NA
ClearSight DNA Stain	EUROMEDEX-BM	Cat# EUH40501	NA
Calf Thymus DNA	VWR	Cat# J64400.03	1mg/ml
GoScript Reverse Transcription	PROMEGA	Cat# A5001	NA
GoTaq Master Mix	PROMEGA	Cat# M7132	NA
Critical Commercial Assays			
Ultra Sensitive Mouse Insulin ELISA Kit	CRYSTAL CHEM INC	Cat# 90080	
RNeasy Lipid Tissue Mini Kit	QUIAGEN	Cat# 74804	
RNeasy Kits	QUIAGEN	Cat# 74004	
QIAamp DNA Blood Mini Kit	QUIAGEN	Cat# 51104	
ELISA MAX™ Deluxe Set Mouse TNF-α	BIOLEGEND	Cat# 430915	
QuantiT™-PicoGreen™ dsDNA assay	FISHER SCIENTIFIC	Cat# P11496	
Software and Algorithms			
FlowJo	TREESTAR		
GraphPad Prism	GRAPH PAD SOFTWARE		
NDP View2Plus	HAMAMATSU PHOTONICS		
QuPath	UNIVERSITY OF EDINBURGH		
Bio-Rad TM CFX Manager software	BIO-RAD TM		
ImageJ sofware	MACBIOPHOTONICS		

Supplementary table 2: Obese patients and Healthy donors' characteristics

	Patients (n=26)		Controls (n=25)	
Variables	**N (%) / x(SD)**	**Range**	**N (%) / x(SD)**	**Range**
Age	41.2 (10.39)	23.0 - 56.0	38.7 (12.7)	18.0 - 61.0
Gender				
Female	21 (80.8)		20 (74.1)	
Male	5 (19.2)		5 (25.9)	
BMI	41.4 (4.8)	33.8 - 52.3	24.2 (0.7)***	18.7 - 29.3
BMI max	44.1 (5.3)	37.0 - 53.0		
Glycemia (g/dL)	0.9 (0.09)	0.8 - 1.1		
Insulinemia	22.1 (11.7)	8.4 - 55.3		
HOMA-IR	4.2 (3.0)	0 - 11.7		
NASH	6 (26)			
CRP (mg/dL)	7.7 (5.5)	1.5 - 21.8		
				*** **p<0.001**

Supplementary table 3: Longitudinal cohort's characteristics

	Patients (n=20)		Controls (n=14)	
Variables	**N / x(SD)**	**Range**	**N / x(SD)**	**Range**
BMI before surgery (kg/m²)	41.8 (1.3)	35.2 - 42.8	21.5 (1.1)	19.6 - 23.8
BMI after surgery (kg/m²)	30.5 (1.3)	22.8 - 33.2		
Weight loss (%)	-27.1 (1.8)	-15.2 - -40.0		
Time to follow-up (months)	7.7 (0.7)	3.0 - 12.0		